NATO Science for Peace and Security Series - C:
Environmental Security

# Air Pollution Modeling and its Application XX

Edited by
Douw G. Steyn
S. Trivikrama Rao

Springer

NATO OTAN

*This publication is supported by:*

The NATO Science for Peace and Security Programme

Air Pollution Modeling and Its Application XX

# NATO Science for Peace and Security Series

This Series presents the results of scientific meetings supported under the NATO Programme: Science for Peace and Security (SPS).

The NATO SPS Programme supports meetings in the following Key Priority areas: (1) Defence Against Terrorism; (2) Countering other Threats to Security and (3) NATO, Partner and Mediterranean Dialogue Country Priorities. The types of meeting supported are generally "Advanced Study Institutes" and "Advanced Research Workshops". The NATO SPS Series collects together the results of these meetings. The meetings are co-organized by scientists from NATO countries and scientists from NATO's "Partner" or "Mediterranean Dialogue" countries. The observations and recommendations made at the meetings, as well as the contents of the volumes in the Series, reflect those of participants and contributors only; they should not necessarily be regarded as reflecting NATO views or policy.

**Advanced Study Institutes (ASI)** are high-level tutorial courses intended to convey the latest developments in a subject to an advanced-level audience

**Advanced Research Workshops (ARW)** are expert meetings where an intense but informal exchange of views at the frontiers of a subject aims at identifying directions for future action

Following a transformation of the programme in 2006 the Series has been re-named and re-organised. Recent volumes on topics not related to security, which result from meetings supported under the programme earlier, may be found in the NATO Science Series.

The Series is published by IOS Press, Amsterdam, and Springer, Dordrecht, in conjunction with the NATO Public Diplomacy Division.

**Sub-Series**

| | | |
|---|---|---|
| A. | Chemistry and Biology | Springer |
| B. | Physics and Biophysics | Springer |
| C. | Environmental Security | Springer |
| D. | Information and Communication Security | IOS Press |
| E. | Human and Societal Dynamics | IOS Press |

http://www.nato.int/science
http://www.springer.com
http://www.iospress.nl

**Series C: Environmental Security**

# Air Pollution Modeling and Its Application XX

edited by

Douw G. Steyn
University of British Columbia
Canada

and

S. Trivikrama Rao
U.S. Environmental Protection Agency
U.S.A.

Published in cooperation with NATO Public Diplomacy Division

Proceedings of the 30th NATO/SPS International Technical Meeting on
Air Pollution Modelling and Its Application
San Francisco, California, U.S.A.
18–22 May 2009

Library of Congress Control Number: 2010921300

ISBN 978-90-481-3811-1 (PB)
ISBN 978-90-481-3810-4 (HB)
ISBN 978-90-481-3812-8 (e-book)

Published by Springer,
P.O. Box 17, 3300 AA Dordrecht, The Netherlands.

*www.springer.com*

*Printed on acid-free paper*

## Previous Volumes in this Mini-Series

Volumes I–XII were included in the NATO Challenges of Modern Society Series

AIR POLLUTION MODELING AND ITS APPLICATIONS I
Edited by C. De Wispelaere

AIR POLLUTION MODELING AND ITS APPLICATIONS II
Edited by C. De Wispelaere

AIR POLLUTION MODELING AND ITS APPLICATIONS III
Edited by C. De Wispelaere

AIR POLLUTION MODELING AND ITS APPLICATIONS IV
Edited by C. De Wispelaere

AIR POLLUTION MODELING AND ITS APPLICATIONS V
Edited by C. De Wispelaere, Francis A. Schiermeier, and Noor V. Gllani

AIR POLLUTION MODELING AND ITS APPLICATIONS VI
Edited by Han van Dop

AIR POLLUTION MODELING AND ITS APPLICATIONS VII
Edited by Han van Dop

AIR POLLUTION MODELING AND ITS APPLICATIONS VIII
Edited by Han van Dop and Douw G. Steyn

AIR POLLUTION MODELING AND ITS APPLICATIONS IX
Edited by Han van Dop and George Kallos

AIR POLLUTION MODELING AND ITS APPLICATIONS X
Edited by Sven-Erik Gryning and Millán M. Millán

AIR POLLUTION MODELING AND ITS APPLICATIONS XI
Edited by Sven-Erik Gryning and Francis A. Schiermeier

AIR POLLUTION MODELING AND ITS APPLICATIONS XII
Edited by Sven-Erik Gryning and Nadine Chaumerliac

AIR POLLUTION MODELING AND ITS APPLICATIONS XIII
Edited by Sven-Erik Gryning and Ekaterina Batchvarova

AIR POLLUTION MODELING AND ITS APPLICATIONS XIV
Edited by Sven-Erik Gryning and Francis A. Schiermeier

AIR POLLUTION MODELING AND ITS APPLICATIONS XV
Edited by Carlos Borrego and Guy Schayes

AIR POLLUTION MODELING AND ITS APPLICATIONS XVI
Edited by Carlos Borrego and Selahattin Incecik

AIR POLLUTION MODELING AND ITS APPLICATIONS XVII
Edited by Carlos Borrego and Ann-Lise Norman

AIR POLLUTION MODELING AND ITS APPLICATIONS XVIII
Edited by Carlos Borrego and Eberhard Renner

AIR POLLUTION MODELING AND ITS APPLICATIONS XIX
Edited by Carlos Borrego and Ana Isabel Miranda

AIR POLLUTION MODELING AND ITS APPLICATIONS XX
Edited by Douw G. Steyn and S. Trivikrama Rao

# Preface

In 1969, the North Atlantic Treaty Organization (NATO) established the Committee on Challenges of Modern Society (CCMS). From inception, the subject of air pollution was established as one of the priority problems for study within the framework of various pilot studies undertaken by this committee. The main activity within the pilot study relating to air pollution is the periodic organization of a major international conference dealing with air pollution modeling and its application. The first five international conferences were organized by the United States of America as the pilot country, the second five by the Federal Republic of Germany, the third five by Belgium, the fourth five by the Netherlands, the fifth five by Denmark, the sixth five by Portugal, and currently by Canada.

This volume contains the abstracts of papers and posters presented at the 30th NATO/SPS International Technical Meeting on Air Pollution Modelling and Its Applications, held in San Francisco, California, during May 18–22, 2009. This ITM was supported by the Environmental Protection Agency, United States of America (Host Country) and The University of British Columbia, Canada (Pilot Country).

The key topics distinguished at this ITM included: Local and urban scale modelling; Regional and intercontinental modelling; Data assimilation and air quality forecasting; Model assessment and verification; Aerosols in the atmosphere; Interactions between climate change and air quality; Air quality and human health; and a Special Session on the California 2000 field study.

The ITM was attended by 156 participants representing 36 countries. Invited papers were presented by Hiram Levy, USA (Interactions between climate and air quality), Bert Brunekreef, the Netherlands (Air pollution and human health: from local to global issues), Robert Vautard, France (Regional air quality modelling: a few examples of recent progresses and remaining questions) and Spyros Pandis, Greece (Atmospheric organic particulate matter: revisiting its sources, properties and impacts).

On behalf of the ITM Scientific Committee and as organizers and editors, we would like to thank all the participants who contributed to the success of the 30th meeting. Among the participants, we especially recognize the efforts of the chairpersons and rapporteurs. Finally, special thanks to the sponsoring institutions: U.S. Environmental Protection Agency and The University of British Columbia, Canada, and the sponsoring organizations NATO Science for Peace and Security, Environment Canada, National Oceanic and Atmospheric Administration, California Air resources Board, European Association for the Science of Air Pollution (EURSAP), and the American Meteorological Society.

A special grant was given by EURASAP to award prizes to young researchers for the best paper or poster. The next meeting will be held in September 2010 in Torino, Italy. The views presented in this book are those of the authors and do not reflect the views and policies of the U.S. Environmental Protection Agency, University of British Columbia, or other co-sponsors.

S.T. Rao (Local Conference Organizer)
D.G. Steyn (Scientific Committee Chair)

**Members of the Scientific Committee for the 30th NATO/SPS International Technical Meeting (ITM) on Air Pollution Modelling and Its Application**

Ana Isabel Miranda (Portugal)
Guy Schayes (Belgium)
Dimiter Syrakov (Bulgaria)
Douw Steyn (Canada, Chair)
Sven-Erik Gryning (Denmark)
Nadine Chaumerliac (France)
Eberhard Renner (Germany)
George Kallos (Greece)
Domenico Anfossi (Italy)
Trond Iversen (Norway)
Carlos Borrego (Portugal)
Jose Baldasano (Spain)
Peter Builtjes (The Netherlands)
Selahattin Incecik (Turkey)
Bernard Fisher (United Kingdom)
S. Trivikrama Rao (USA)

Werner Klug (Germany, Honorary Life Member)
Han van Dop (The Netherlands, Honorary Life Member)
Frank Schiermeier (United States of America, Honorary Life Member)

# History of NATO/CCMS (SPS) Air Pollution Pilot Studies

## Pilot Studies on Air Pollution International Technical Meetings (ITM) on Air Pollution Modelling and Its Application

### Dates and Locations of Completed Pilot Studies

| | |
|---|---|
| 1969–1974 | Air Pollution Pilot Study (*Pilot Country – United States of America*) |
| 1975–1979 | Air Pollution Assessment Methodology and Modelling (*Pilot Country – Germany*) |
| 1980–1984 | Air Pollution Control strategies and Impact Modelling (*Pilot Country – Germany*) |

### Dates and Locations of Pilot Follow-Up Meetings

*Pilot Country – United States of America* (*R.A. McCormick, L.E. Niemeyer*)

| | | | |
|---|---|---|---|
| February | 1971 | Eindhoven, The Netherlands | First Conference on Low Pollution Power Systems Development |
| July | 1971 | Paris, France | Second Meeting of the Expert Panel on Air Pollution Modelling |

All subsequent meetings were supported by the NATO Committee for Challenges to Modern Society, and were designated NATO/CCMS International Technical Meetings (ITM) on Air Pollution Modelling and its Application, until 2007 when the designation changed to NATO/SPS with the creation of the NATO Committee on Science for Peace and Security.

| | | | |
|---|---|---|---|
| October | 1972 | Paris, France | 3rd ITM |
| May | 1973 | Oberursel, Federal Republic of Germany | 4th ITM |
| June | 1974 | Roskilde, Denmark | 5th ITM |

*Pilot Country – Germany* (*Erich Weber*)

| | | | |
|---|---|---|---|
| September | 1975 | Frankfurt, Federal Republic of Germany | 6th ITM |
| September | 1976 | Airlie House, USA | 7th ITM |
| September | 1977 | Louvain-la-Neuve, Belgium | 8th ITM |
| August | 1978 | Toronto, Canada | 9th ITM |
| October | 1979 | Rome, Italy | 10th ITM |

*Pilot Country – Belgium* (*C. De Wispelaere*)

| | | | |
|---|---|---|---|
| November | 1980 | Amsterdam, The Netherlands | 11th ITM |
| September | 1981 | Menlo Park, California, USA | 12th ITM |

| | | | |
|---|---|---|---|
| September | 1982 | Ile des Embiez, France | 13th ITM |
| September | 1983 | Copenhagen, Denmark | 14th ITM |
| April | 1985 | St. Louis, Missouri, USA | 15th ITM |
| *Pilot Country – The Netherlands* (*H. van Dop*) | | | |
| April | 1987 | Lindau, Federal Republic of Germany | 16th ITM |
| September | 1988 | Cambridge, United Kingdom | 17th ITM |
| May | 1990 | Vancouver, BC, Canada | 18th ITM |
| September | 1991 | Ierapetra, Greece | 19th ITM |
| *Pilot Country – Denmark* (*Sven-Erik Gryning*) | | | |
| November | 1993 | Valencia, Spain | 20th ITM |
| November | 1995 | Baltimore, Maryland, USA | 21st ITM |
| May | 1997 | Clermont-Ferrand, France | 22nd ITM |
| September | 1998 | Varna, Bulgaria | 23rd ITM |
| May | 2000 | Boulder, Colorado, USA | 24th ITM |
| *Pilot Country – Portugal* (*Carlos Borrego*) | | | |
| September | 2001 | Louvain-la-Neuve, Belgium | 25th ITM |
| May | 2003 | Istanbul, Turkey | 26th ITM |
| October | 2004 | Banff, Canada | 27th ITM |
| May | 2006 | Leipzig, Germany | 28th ITM |
| September | 2007 | Aveiro, Portugal | 29th ITM |
| *Pilot Country – Canada* (*Douw Steyn*) | | | |
| May | 2009 | San Francisco, California, USA | 30th ITM |

# List of Participants

The 30th NATO/CCMS International Technical Meeting on Air Pollution Modeling and Its Application, San Francisco, California, USA, May

**Argentina**

*Berri, Guillermo J.*

University of Buenos Aires
Department of Atmospheric and Oceanic Sciences
Pabellon 2, piso 2
Ciudad Universitaria
Buenos Aires, Argentina 1428
berri@at.fcen.uba.ar

**Australia**

*Lee, Sunhee*

CSIRO Marine and Atmospheric Research
PMB 1
Aspendale, Australia
sunhee.lee@csiro.au

*Physick, William Lloyd*

CSIRO
Marine and Atmospheric Research
PB 1
Aspendale, Victoria Australia 3195
bill.physick@csiro.au

**Austria**

*Fedra, Kurt*

Environmental Software & Services
P.O. Box 100
Gumpoldskirchen, Austria 2352
kurt@ess.co.at

**Belgium**

*Lefebvre, Wouter*
Vlaams Instituut voor
Technologisch Onderzoek
Boeretang 200
MOL, Belgium 2400
Wouter.lefebvre@vito.be

*Mensink, Clemens*
VITO NV
Boeretang 200
MOL, Belgium 2400
clemens.mensink@vito.be

**Bulgaria**

*Batchvarova, Ekaterina A.*
National Institute of Meteorology
and Hydrology
66 Tzarigzadsko Chaussee
Sofia, Bulgaria 1784
ekaterina.batachvarova@meteo.bg

**Canada**

*Antonopoulos, Stavros*
Environment Canada
2121 Transcanada Rd.
Dorval, QC Canada H9P 1J3
stavros.antonopoulos@ec.gc.ca

*Chtcherbakov, Andrei*
Doctor
125 Resources Road
Toronto, Ontario, Canada M9P 3V6
andrei.chtcherbakov@ontario.ca

*Gong, Wanmin*
Environment Canada
4905 Dufferin Street
Toronto, Ontario M3H 5T4
wanmin.gong@ec.gc.ca

*Menard, Sylvain*
Environmnet Canada
2121 TransCanada Highway
Dorval, Canada
sylvain.menard@ec.gc.ca

*Moran, Michael David*
Environment Canada
Air Quality Research Division
4905 Dufferin Street
Toronto, Ontario M3H 5T4
mike.moran@ec.gc.ca

*Reuten, Christian*
The University of British Columbia
8871 Dorval Rd.
Richmond
British Columbia V7C 5A5
creuten@eos.ubc.ca

*Sloan, James Joseph*
University of Waterloo
Department of Earth and
Environmental Science
200 University Ave. W.
Waterloo, Ontario Canada
N2L3G1
sloanj@uwaterloo.ca

*Steyn, Douw G.*
The University of British Columbia
Earth and Ocean Sciences
6339 Stores Road
Vancouver, British Columbia
Canada V6T 1Z4
dsteyn@eos.ubc.ca

**China**

*Fung, Christopher*
Environmental Protection
Department
33/f, Revenue Tower
5 Gloucester Road, Wanchai
Hong Kong, China
cfung@epd.gov.hk

**Croatia**

*Spoler Canic, Kornelija*
Meteorological and Hydrological
Service of Croatia
Gric 3
Zagreb, Croatia 10000
spoler@cirus.dhz.hr

**Cyprus**

*Astitha, Marina*

The Cyprus Institute
Athalassa Campus
Guy Ourisson Building
Nicosia, Cyprus 1645
m.astitha@cyi.ac.cy

**Czech Republic**

*Halenka, Tomas*

Charles University
Department of Meteorology and
Environment Protection
V Holesovickach 2
Prague, Czech Republic 180 00
tomas.halenka@mff.cuni.cz

**Denmark**

*Gryning, Sven-Erik*

Risoe DTU
Wind Energy Division
Frederiksborgvej 399
Roskilde, Denmark DK-4000
sveg.risoe.dtu.dk

**Estonia**

*Kerner, Eva-Stina*

University of Tartu
Institute of Physics
Tähe 4
Tartu, Estonia 51010
stinkin@ut.ee

**Finland**

*Prank, Marje*

FMI
Erik Palmenin Aukio 1
Helsinki, Finland
marje.prank@fmi.fi

*Siljamo, Pilvi*
Finnish Meteorological Institute
Research and Development/
Meteorology
P.O. Box 503
(Erik Palmenin Aukio 1)
Helsinki, Finland FI-00101
Pilvi.siljamo@fmi.fi

*Soares, Joana Raquel Alves*
Finnish Meteorological Institute
P.O. Box 503
Helsinki, Finland FI-00101
joana.soares@fmi.fi

*Sofiev, Mikhail A.*
Finnish Meteorological Insitute
Air Quality
Erik Palmenin Aukio 1
Helsinki, Finland 00560
mikhail.sofiev@fmi.fi

*Vira, Julius*
Finnish Meteorological Institute
PL 503
Helsinki, Finland FI-00101
julius.vira@fmi.fi

**France**

*Armand, Patrick Pierre*
French Atomic Energy Commission
DIF/DASE/SRCE - Batiment G
Bruyeres-le-Chatel
Arpajon, France 91297
patrick.armand@cea.fr

*Chaumerliac, Nadine*
CNRS
Universite Blaise Pascal 12
24 avenue des landais
Aubiere, France 63177
N.Chaumerliac@opgc.univ-
bpclermont.fr

*Deguillaume, Laurent*
Laboratoire de Météorologie Physique
CNRS
24 avenue des Landais
Aubière, France 63170
L.Deguillaume@opgc.univ-bpclermont.fr

*Valari, Myrto*
Laboratoire de Meteorologie Dynamique
Ecole Polytechnique
91128 Palaiseau Cedex
myrto.valari@lmd.polytechnique.fr

*Vautard, Robert*
IPSL
CSCE
91191 Gif sur Yvette
Paris, France
robert.vautard@cea.fr

**Germany**

*Banzhaf, Sabine*
Free University
Carl-Heinrich-Becker Weg
6-10
Berlin, Germany 12165
sabine.banzhaf@met.fu-berlin.de

*Kerschbaumer, Andreas*
Free University
Carl-Heinrick-Becker-Weg
6-10
Berlin, Germany D-12165
Andreas.kerschbaumer@fu-berlin.de

*Martens, Reinhard*
Gesellschaft f. Anlagen- u. Reaktorsicherheit mbH
Department of Radiation Protection
Schwertnergasse 1
Cologne, NRW Germany 50667
Reinhard.Martens@grs.de

*Renner, Eberhard*
Insitute for Tropospheric Research
Modelling Department
Permoserstraße 15
Leipzig, Germany 04318
renner@tropos.de

*Thielen, Harald*
Gesellschaft f. Anlagen- u.
Reaktorsicherheit mbH
Department of Radiation Protection
Schwertnergasse 1
Cologne, NRW Germany 50667
Harald.Thielen@grs.de

*Wolke, Ralf*
Leibniz Institute for Tropospheric
Research
Permoserstr. 15
Leipzig, Germany 04318
wolke@tropos.de

**Greece**

*Barmpas, Fotios*
Aristotle University of Thessaloniki
University Campus
Laboratory of Heat Transfer and
Environmental Engineering
Thessaloniki, 54 124
fotisb@aiz.meng.auth.gr

*Kallos, George*
University of Athens
School of Physics, Division of
Applied Physics
University Campus Bldg PHYS-5
Athens, Greece 15784
kallos@mg.uoa.gr

*Katragkou, Eleni*
Aristotle University of Thessaloniki
Laboratory of Atmospheric Physics
P.O. Box 149
Thessaloniki, Greece 54124
katragou@auth.gr

**Israel**

*Haikin, Nitsa*
Nuclear Research Center
Negev
D.O.B. 9001
Beer-Sheva, Israel 84190
nitsah@nrcn.org.il

*Kishcha, Pavel*
Tel-Aviv University
Ramat Aviv
Tel-Aviv, Israel
Pavel@cyclone.tau.ac.il

*Reisin, Tamir Gustavo*
SOREQ NRC
81800
Yavne, Israel
tgreisin@gmail.com

**Italy**

*Alessandrini, Stefano*
ERSE
Via Rubattino 54
Milano, Italy
stefano.alessandrini@cesiricerca.it

*Anfossi, Domenico*
CNR-ISAC
Corso Fiume 4
Torino, Italy 10133
anfossi@to.infn.it

*de Meij, Alexander*
Joint Research Centre
Transport and Air Quality Unit
Via E. Fermi
Ispra, Varese Italy 21020
alexander.de-meij@jrc.it

*Ferrero, Enrico*
University of Piemonte Orientale
Viale Teresa Michel, 11
Alessandria, Italy I-15100
enrico.ferrero@unipmn.it

*Galmarini, Stefano*
European Commission Joint Research Center
TP 441
Ispra, Varese Italy 21020
stefano.galmarini@jrc.it

*Mortarini, Luca*
CNR-ISAC
Corso Fiome 4
Torino, Italy
l.mortarini@isac.cnr.it

*Trini-Castelli, Silvia*
Instituto Di Cosmoaeofisica/CNR
Corso FUIME 4
Torino, Italy I-10133
s.trinicastelli@isac.cnr.it

**Japan**

*Bao, Linfa*
Saitama University
Department of Environmental Science and Technology
932-7 Shimo-okubo, Sakura-ku
Saitama City, Saitama Japan
338-8570
bolin8@gmail.com

*Ortiz Ramirez, Ricardo*
Saitama University
Graduate School of Science and Engineering
255 Shimo-okubo, Sakura, Saitama
338-8570
Saitama, Japan
ricardo@env.gse.saitama-u.ac.jp

**Luxembourg**

*Buchholz, Saskia*
Centre de Recherche Public - Gabriel Lippmann
41, rue du Brill
Belvaux, Luxembourg 4422
buchholz@lippmann.lu

**The Netherlands**

*Brunekreef, Bert*
Uttrecht University
IRAS
P.O. Box 80176
Utrecht, The Netherlands 3508TD
b.brunekreef@uu.nl

*Builtjes, Peter*
TNO
Department of Air Quality and Climate
P.O. Box 80015
Utrecht, The Netherlands 3508 TA
peter.builtjes@tno.nl

*Sauter, Ferol J*
RIVM
P.O. Box 1
Bilthoven, The Netherlands
3720 BA
ferd.sauter@rivm.nl

*Schaap, Martijn*
TNO
Princetonlaan 6
Utrecht, The Netherlands 3508TA
martijn.schaap@tno.nl

**New Zealand**

*Lucas, Vicky*
Environment Canterbury
58 Kilmore Street
Christchurch, New Zealand
vicky.lucas@ecan.govt.nz

**Norway**

*Bartnicki, Jerzy*
Norwegian Meteorological Institute
Research and Development
P.O. Box 43 Blindern
Oslo, Norway NO-0313
Jerzy.bartnicki@met.no

*Cassiani, Massimo*
Norwegian Institute for Air Research
P.O. Box 100
Instituttveien 18
Kjeller, Norway NO-2027
mc@nilu.no

*Iversen, Trond*
Norwegian Met. Inst.
P.O. Box 43, Blindern
Niels Henrik Abels Vei 40
Oslo, Norway N-0313
trond.iversen@met.no

*Saltbones, Jorgen*
Norwegian Meteorological Institute
P.O. Box 43, Blindern
Oslo, Norway
NO-0313
jorgen.saltbones@met.no

**Poland**

*Juda-Rezler, Katarzyna*
Warsaw University of Technology
Faculty of Environmental Engineering
Air Pollution Control Group
Nowowiejska 20
Warsaw, Poland 00-653
katarzyna.juda-rezler@is.pw.edu.pl

**Portugal**

*Miranda, Ana Isabel*
University of Aveiro
Department of Environment and Planning
Campus Universitário
Aveiro, Portugal
3810-193 Aveiro
miranda@ua.pt

**South Korea**

*Choi, Yongsuk*

Seoul Government Institute of
Health and Environment
Sechogu-Yangjaedong 202-3
Seoul, South Korea 137-130
hozer87@seoul.go.kr

**Spain**

*Baldasano, Jose M.*

Barcelona Supercomputing Center
Earth Science
Jordi Girona nº 29
Barcelona, Spain 08034
jose.baldasano@bsc.es

**Switzerland**

*Andreani-Aksoyoglu, Sebnem*

Paul Scherrer Institute
Laboratory of Atmospheric
Chemistry
Paul Scherrer Institut
Villigen, Switzerland 5232
sebnem.andreani@psi.ch

**Turkey**

*Incecik, Salahattin*

Istanbul Technical University
Department of Meteorology
Maslak
Istanbul, Turkey
incecik@itu.edu.tr

*Yenigun, Orhan*

Bogazici University
Institute of Environmental Sciences
Bebek, Istanbul Turkey 34342
yeniguno@boun.edu.tr

**United Kingdom**

*Dore, Anthony James*

Centre for Ecology and Hydrology
Bush Estate
Penicuik, Midlothian
United Kingdom EH26 OQB

*Fisher, Bernard*
Environment Agency
Kings Meadow House
Kings Meadow Road
Reading, United Kingdom
RG1 8DQ
benard.fisher@environment-agency.gov.uk

*Hallsworth, Stephen*
CEH
Bush Estate
Penicuik, Midlothian
United Kingdom EH26 OQB

*Pavlidis, Dimitrios*
Imperial College London
Earth Science and Engineering
Royal School of Mines
Prince Constort Road
London,
United Kingdom SW7 2BP
dimitrios.pavlidis@imperial.ac.uk

**USA**

*Anderson, Bret A.*
US Environmental Protection Agency
901 N 5th Street
Kansas City, KS 66101
ba05700@navix.net

*Arunachalam, Saravanan*
University of North Carolina
Institute for the Environment
137 E Franklin St, #656
Bank of America Plaza, CB #6116
Chapel Hill, NC 27599-6116
sarav@email.unc.edu

*Avise, Jeremy*
California Air Resources Board
1001 I Street, P.O. Box 2815
Sacramento, CA 95812
javise@arb.ca.gov

*Beaver, Scott*
Bay Area Air Quality Management District
939 Ellis St
San Francisco, CA 94109
sbeaver@baaqmd.gov

*Blanchard, Charles Lloyd*
Envair
526 Cornell Avenue
Albany, CA 94706
cbenvair@pacbell.net

*Bohnenkamp, Carol*
Federal Government
US Environmental Protection Agency
75 Hawthorne Street, 17th Floor
San Francisco, CA 94105
bohnenkamp.carol@epa.gov

*Clawson, Kirk L.*
National Oceanic and Atmospheric Administration/ARL
Field Research Division
1750 Foote Dr.
Idaho Falls, ID 83402
kirk.clawson@Noaa.agov

*Cohan, Daniel S.*
Rice University
Department of Civil and Environmental Engineering
6100 Main St MS 317
Houston, TX 77005
cohan@rice.edu

*Cohen, Ronald C.*
University of California
Hildebrand Hall
Berkeley, CA 94720-1460
rccohen@berkley.edu

*Coleman, Beverly*
Chevron Energy Technology Co.
1450 Marina Way South
RIC 145/1033B)
Richmond, CA 94804
bevcoleman@chevron.com

*Douglas, Sharon G.*
ICF International
101 Lucas Valley Rd
Suite 260
San Rafael, CA 94903
sdoublas@icfi.com

*Emery, Christopher A.*
ENVIRON International Corporation
773 San Marin Drive
Suite 2115
Novato, CA 94998
cemery@environcorp.com

*Fovell, Robert G.*
UCLA
Department of Atmospheric and Oceanic Sciences
405 Hilgard Ave
Los Angeles, CA 90095-1565
rfovell@ucla.edu

*Garcia, Valerie*
US Environmental Protection Agency
MD-E243-02
109 TW Alexander Drive
Research Triangle Park, NC 27711
garcia.val@epa.gov

*Ghosh, Saikat*
Texas A&M University-Kingsville
MSC 213, 700 University Blvd
Kingsville, TX 78363
saikat1985@hotmail.com

*Godowitch, James M.*
US Environmental Protection Agency/ORD/NERL/AMAD
MD E243-04
109 TW Alexander Drive
Research Triangle Park, NC 27711
godowitch.james@epa.gov

*Hammond, Davyda*
US Environmental Protection Agency
109 TW Alexander Dr
Durham, NC 27711
hammond.davyda@epa.gov

*Hanna, Steven R.*
Hanna Consultants
7 Crescent Ave.
Kennebunkport, ME 04046
hannaconsult@adelphia.net

*Kaduwela, Ajith*
Air Resources Board
California Environmental
Protection Agency
1001 I Street
Sacramento, CA 95814
akaduwel@arb.ca.gov

*Kang, Daiwen*
Computer Science Corporation
P.O. Box 14665
Research Triangle Park, NC 27709
kang.daiwen@epa.gov

*Kelly, James*
California Air Resources Board
1001 I Street
Sacramento, CA 95814
jkelly@arb.ca.gov

*Kemball-Cook, Sue*
ENVIRON International
Corporation
773 San Marin Drive
Suite 2115
Novato, CA 94998
skemballcook@environcorp.com

*Kleeman, Mike*
University of California
1 Shields Ave
Davis, CA 95616

*LaFranchi, Brian W.*
University of California at Berkeley
Chemistry
B76 Hildebrand
Berkeley, CA 94720
lafranchi@berkeley.edu

*Lee, Pius C.*
Air Resource laboratory
Ocean and Atmospheric research
1315 East West Hwy, Rm 3438
Silver Spring, MD 20910
pius.lee@noaaa.gov

*Levy II, Hiram*
GFDL/NOAA
P.O. Box 308
Princeton, USA
hiram.levy@noaa.gov

*Lin, Hsin-mu*
National Oceanic and Atmospheric Administration
EPA/NERL/AMAD
Mail Stop E243-03
Research Triangle Park, NC 27711
hsin-mu.lin@noaa.gov

*Lu, Sarah*
National Oceanic and Atmospheric Administration/NCEP EMC
5200 Auth Road
Camp Springs, MD 20746
Sarah.Lu@noaa.gov

*Martien, Philip*
BAAQMD
939 Ellis Street
San Francisco, CA 94109
pmartien@baaqmd.gov

*Mathur, Rohit*
U.S. Environmental Protection Agency
MD E243-03
109 TW Alexander Drive
Research Triangle Park, NC 27711
mathur.rohit@epa.gov

*Mobley, David*
US Environmental Protection Agency/ORD/NERL/AMAD
Mail Stop E243-02
Research Triangle Park, NC 27711
mobley.david@epa.gov

*Napelenok, Sergey L.*
US Environmental Protection Agency/ORD/NERL/AMAD
MD E243-01
109 TW Alexander Drive
Research Triangle Park, NC 27711
napelenok.sergey@epa.gov

*Odman, Mehmet T.*
Georgia Institute of Technology
Environmental Engineering
311 Ferst Drive
ES&T Building
Atlanta, GA 30332-0512
Talat.odman@ce.gatech.edu

*Osterman, Gregory B.*
Jet Propulsion Laborartory
4800 Oak Grove Drive
MS 183-601
Pasadena, CA 91109
Gregory.Osterman@jpl.nasa.gov

*Palazoglu, Ahmet*
University of California, Davis
Chemical Engineering and
Materials Science
One Shields Avenue
Davis, CA 95616
anpalazoglu@ucdavis.edu

*Pandis, Spyros*
Carnegie Mellon University
Chemical Engineering
5000 Forbes Avenue
Pittsburgh, PA 15213
spyros@andrew.cmu.edu

*Pleim, Jonathan E.*
US Environmental Protection
Agency
MD E243-03
109 TW Alexander Drive
Research Triangle Park, NC 27711
pleim.jon@epa.gov

*Porter, P. Steven*
University of Idaho
Department of Civil Engineering
1776 Science Center, Suite 306
Idaho Falls, ID 83402
porter@if.uidaho.edu

*Ran, Limei*
Institute for the Environment
University of North Carolina at
Chapel Hill
137 E. Franklin, Room 661
Chapel Hill, NC 27599
lran@unc.edu

*Rao, ST*
US Environmental Protection Agency/ORD/NERL/AMAD
109 TW Alexander Drive
MD E243-02
Research Triangle Park, NC 27711
rao.st@epa.gov

*Reynolds, Steven*
Envair
12 Palm Ave
San Rafael, CA, USA
steve@sreynolds.com

*Russell, Ashley*
University of California
1347 Hildebrand Hall
Berkeley, CA 94720
arrussell@berkeley.edu

*Sarwar, Golam*
US Environmental Protection Agency/ORD/NERL/AMAD
Mail Drop E243-03
109 TW Alexander Drive
Research Triangle Park, NC 27711
sarwar.golam@epa.gov

*Schiermeier, Francis A.*
NOAA/EPA (Retired)
303 Glasgow Road
Cary, NC 27511
schiermeier@msn.com

*Singh, Angadh*
University of California, Davis
Chemical Engineering and Materials Science
3086 Bainer Hall
One shields Avenue
Davis, CA 95616
angadh.singh@gmail.com

*Soong, Su-Tzai*
Bay Area Air Quality Management District
939 Ellis Street
San Francisco, CA 94109
ssoong@baaqmd.gov

*Tanrikulu, Saffet*
BAAQMD
939 Ellis Street
San Francisco, CA 94109
stanrikulu@baaqmd.gov

*Timin, Brian*
US Environmental Protection Agency/OAQPS
MD C439-01
109 TW Alexander Drive
Research Trianle Park, NC 27711
timin.brian@epa.gov

*Tremback, Craig J.*
ATMET
P.O. Box 19195
Boulder, CO 80308-2195
tremback@amet.com

*Valin, Lukas C.*
University of California
1347 Hildebrand Hall
Berkeley, CA 94720
lukevalin@gmail.com

*Wesson, Karen*
US Environmental Protection Agency
MC C439-01
109 TW Alexander Drive
Research Triangle Park, NC 27711
wesson.karen@epa.gov

*Wheeler, Neil J.*
Sonoma Technology, Inc.
1455 N. McDowell Blvd, Suite D
Petaluma, CA 94954
neil@sonomatech.com

*Wilczak, James M.*
NOAA/ESRL/PSD
325 Broadway
R/PSD
Boulder, CO 80305
james.m.wilczak@noaa.gov

*Xu, Kuan-Man*
NASA Langley Research Center
Mail Stop 420
Hampton, VA 23681
Kuan-Man.Xu@nasa.gov

*Yin, Dazhong*

California Air Resources Board
1001 I Street, P.O. Box 2815
Sacramento, CA 95812
dyin@arb.ca.gov

*Zhang, Yang*

North Carolina State University
Department of Marine Earth and
Atmospheric Science
Campus Box 8208
Raleigh, NC 27695
yang_zhang@ncsu.edu

*Zhou, Wei*

Rice University
Department of Civil and
Environmental Engineering
MS-317
6100 Main Street
Houston, TX 77005
zhouwei@rice.edu

# Contents

# Chapter 1 Local and urban scale modeling

Chairpersons: B. Fisher
D. Anfossi

Rapporteurs: M. Astitha
M. Valari

D.G. Steyn and S.T. Rao (eds.), *Air Pollution Modeling and Its Application XX*,
DOI 10.1007/978-90-481-3812-8_1, © Springer Science + Business Media B.V. 2010

# 1.1 Impact of High Resolution Land-Use Data in Meteorology and Air Quality Modeling Systems

**Limei Ran[1], Jonathan Pleim[2], and Robert Gilliam[2]**

[1]Institute for the Environment, University of North Carolina, Chapel Hill, NC, USA

[2]United States Environmental Protection Agency, Atmospheric Model Development Branch, Atmospheric Modeling and Analysis Division USEPA/ORD/NERL Research Triangle Park, NC 27711

**Abstract** Accurate land use information is important in meteorology for land surface exchanges, in emission modeling for emission spatial allocation, and in air quality modeling for chemical surface fluxes. Currently, meteorology, emission, and air quality models often use outdated USGS Global Land Cover Characterization (GLCC) 30-s (around 1 km) resolution land cover data. With the release of the 2001 National Land Cover Data (NLCD) products at 30 m cell resolution for the United States and 2001 NASA Moderate Resolution Imaging Spectroradiometer (MODIS) land cover data at 1 km cell resolution for the globe, meteorology and air quality modelers want to use these more current and accurate land cover data sets. In the Spatial Allocator, C++ programs were developed with the Geospatial Data Abstraction Library (GDAL) to compute modeling domain gridded land cover information based on input image data of the 2001 NLCD and MODIS land cover data. The programs output gridded fractional coverage of each land category for use in the Weather Research and Forecast (WRF) and Community Multiscale Air Quality (CMAQ) models. The land use data are used to specify vegetation and surface related parameters that are needed in land surface models (LSM) and dry deposition models. We have incorporated the gridded 2001 NLCD and MODIS land cover data in the WRF and CMAQ modeling for the CONUS and east US 12 km resolution domains. Preliminary WRF results show slight improvement and CMAQ runs show largest difference in the bi-directional $NH_3$ surface flux. We believe that these new land cover data should have more effects on both meteorological and air quality model simulations for higher resolution modeling.

**Keywords** NLCD, MODIS, WRF, CMAQ, LSM, landuse, land surface model, meteorology model, air quality model

D.G. Steyn and S.T. Rao (eds.), *Air Pollution Modeling and Its Application XX*,
DOI 10.1007/978-90-481-3812-8, © Springer Science + Business Media B.V. 2010

## 1. Introduction

Land cover data are used in meteorology, emission, and air quality modeling. In meteorology modeling land surface exchange processes are based on land cover categories within each modeling grid (e.g. Xiu and Pleim, 2001). In emission modeling, land cover data are used to spatially allocate some county-based emission inventories to modeling grids and to compute biogenic, dust, and fire emissions. In air quality modeling chemical surface fluxes are modeled based on different land cover categories (e.g. Pleim et al., 2001). Meteorology, emission, and air quality models often use land cover data created in the early 1990s. The land cover data that comes with WRF are USGS Global Land Cover Characteristics (GLCC) 30-s (~1 km) land use data which were developed from 1 km Advanced Very High Resolution Radiometer (AVHRR) satellite images obtained in 1992–1993. Currently, there are two new land cover data sets available for the US and Globe. One is the 2001 National Land Cover Data (NLCD) at 30 m resolution generated from Landsat 7 and 5 Thematic Mapper (TM) images for the entire U.S. (Homer et al., 2004) and the other is the 2001 NASA Moderate Resolution Imaging Spectro-radiometer (MODIS) land cover data at 1 km resolution generated from TERRA MODIS satellite images for the Globe (Friedl et al., 2001). We have developed programs to process the 2001 NLCD (for U.S. areas) and MODIS data (for areas outside U.S.) into fractional coverage of each land category for use in the Weather Research and Forecast (WRF) and Community Multiscale Air Quality (CMAQ) models. The gridded land use data are used to specify vegetation and surface related parameters that are needed by land surface models (LSM), dry deposition models, and biogenic emission model.

## 2. Data and Methods

The NLCD data base was developed by a group of federal agencies under the Multi-Resolution Land Characteristics (MRLC) Consortium since 1992. The NLCD 2001 data from MRLC includes 21 classes of land cover, tree canopy percent, and imperviousness percent at each 30-m pixel. NOAA Coastal Services Center Coastal Change Analysis Program (C-CAP) NLCD data has 30 land cover classes which includes detailed costal wetland classes in addition to MRLC NLCD 21 classes. NASA MODIS land cover data includes 20 International Geosphere-Biosphere Programme (IGBP) classes.

Those land cover data are stored in pixel-based format, which is often called raster data. We developed C++ raster tools using the Geospatial Data Abstraction Library (GDAL) in the Spatial Allocator (SA, http://www.ie.unc.edu/cempd/projects/mims/spatial/) to compute gridded land cover information from MRLC 2001 NLCD (including land cover, imperviousness, and canopy), NOAA coastal 2001–2006 NLCD land cover, and NASA 2001 MODIS land cover data (for areas

outside the US). There are two steps (run by two script files) in processing those new land use data sets. The first step is to pre-process downloaded NLCD data sets to get rid of spatial overlaps among data sets. The second step is to compute the gridded land cover fraction of each land use category for user-defined modeling grids from pre-processed NLCD data sets and MODIS data. The program outputs gridded fractional coverage of each land category stored in a WRF-ready NetCDF file. Figure 1 shows the 30 m NLCD (top) and the WRF GLCC land cover data (bottom) for deciduous forest processed for 1, 4, and 12 km resolution grids. For the higher resolution grid domains (1 and 4 km), gridded NLCD data have much finer gradation and better representation of deciduous forest distribution. Gridded GLCC land use data tend to underestimate or overestimate percent of deciduous forest coverage.

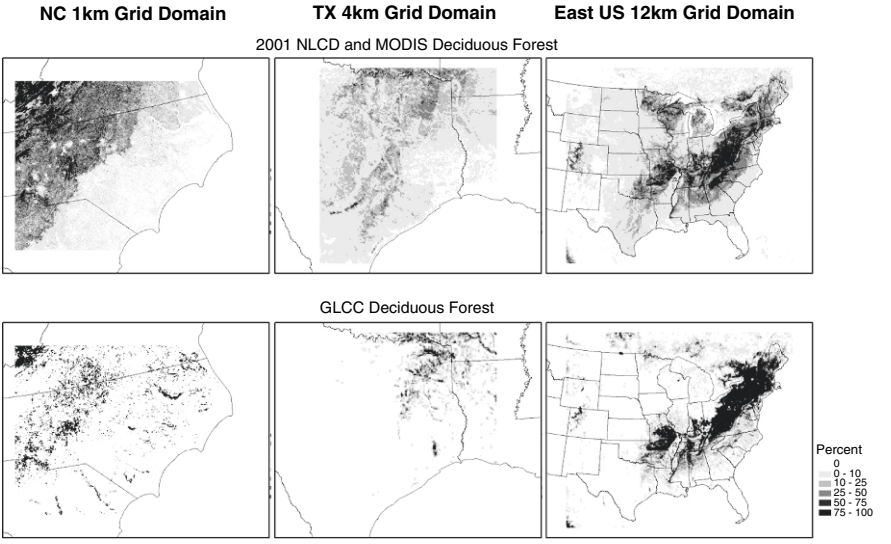


**Fig. 1.** Gridded land cover – deciduous forest at different grid scales

Vegetation and surface related parameter tables for the Pleim-Xiu land surface model (PX SLM) were modified based on NLCD and MODIS land cover categories. Then, we ran the WRF and CMAQ models for August 2006 on the continental US 12 km grid domain using both USGS GLCC and the new NLCD/ MODIS land cover data sets. We used WRF – ARW v3.0 with analysis nudging winds for all levels, and T, and $q_v$ above PBL and indirect soil moisture and temperature nudging in PX LSM. CMAQ v4.7 with CB05 gas-phase chemistry, AE5 modal aerosols, M3dry dry deposition w/ preliminary bidirectional NH3, and ACM2 were used for this study. 2006 emissions and Biogenic Emissions Landuse Database, version 3 (BELD3) data were emission inputs to CMAQ.

## 3. Results and Analysis

Preliminary WRF output comparisons show small differences in mean absolute error (MAE) at the 12 km grid resolution domain (Fig. 2) with the WRF/NLCD run slightly better in most of the eastern part of the domain but slightly worse in the middle part where shrublands and grasslands dominate. Note that these differences are very small due, in part, to the soil moisture nudging scheme in the PX LSM that minimizes biases in 2-m temperature and mixing ratio. Largest difference between CMAQ outputs is in the bi-directional NH3 surface flux because this is closely related to landuse, especially crops which results in a significant difference in $NH_3$ air concentrations (Fig. 2 right panel).

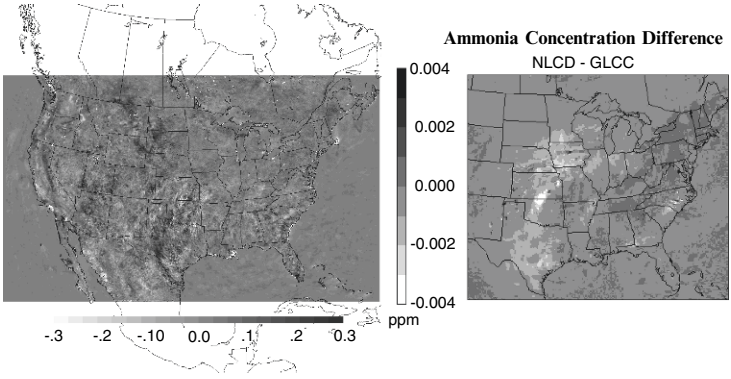


**Fig. 2.** WRF and CMAQ comparisons. Difference in 15-day mean absolute error in 2-m temperature for WRF/NLCD – WRF/GLCC (left) and difference in ammonia concentration at 20 UTC on August 20, 2006 for CMAQ/NLCD – CMAQ/GLCC (right)

## 4. Conclusions and Future Studies

The preliminary model results from WRF and CMAQ with the new high resolution land cover data are encouraging. We expect much greater improvement for higher grid resolution model runs (4 and 1 km). We are also developing Biogenic Emission Landcover Data version 4 (BELD4) land use data from 2001 30 m NLCD, 2001 1 km MODIS, USDA FIA data, and USDA National Agricultural Statistics (NASS) crop data, which are planned to be the input to estimate biogenic emissions from both the Model for Gaseous and Aerosols from Natural (MEGAN) sources and the Biogenic Emission Inventory System (BEIS).

## References

Friedl, M.A., D.K. McIver, X.Y. Zhang, J.C.F. Hodges, A. Schnieder, A. Bacinni, A.H. Strahler, A. Cooper, F. Gao, C. Schaaf, W. Liu, 2001: Global land cover classification results from MODIS. Geoscience and Remote Sensing Symposium, IGARSS apos; 01. IEEE 2001 International 2, pp.733–735.

Homer, C, Huang, C, Yang, L, Wylie, B. and Coan, M. 2004: Development of a 2001 National Land-cover Database for the United States. *Photogrammetric Engineering and Remote Sensing*, **70**:829–840.

Pleim, J. E., Xiu, A., Finkelstein, P. L., Otte, T. L., 2001. A coupled land-surface and dry deposition model and comparison to field measurements of surface heat, moisture, and ozone fluxes. Water, Air, & Soil Pollution: Focus 1, 243–252.

Xiu, A., and J.E. Pleim, 2001: Development of a Land Surface Model. Part I: Application in a Mesoscale Meteorological Model. *J. Appl. Meteor*., **40**, 192–209.

## 5. Questions and Answers

**Question 1:** How is the bi-directional ammonia surface flux modeled in relation to land use?

**Answer 1:** Currently, the ammonia bi-directional model specifies the gamma values ($NH4^+/H^+$) for soil and stomata according to land-use category such that cropland uses gamma = 1,000 and all other vegetated LU categories use gamma = 100. This is a prototype. We are developing methods to derive more realistic gamma values from data on crop types and fertilizer application.

**Question 2:** Nowadays land use data is available on a very detailed scale, but it depends on the algorithms used to extract information from the signal. Do we know the accuracy of this procedure and how it has been tested?

**Answer 2:** Land use data is normally generated from satellite images with digital signals based on classification algorithms, such as cluster algorithms. The 2001 National Land Cover Database (NLCD) has been developed under the Multi-Resolution Land Characteristics (MRLC) Consortium which is a group of US federal agencies. It is well documented database with detailed accuracy assessments. 1992 NLCD land cover dataset was first developed in the early 1990s from Landsat 5 TM images. 2001 NLCD data was developed in the recent years mostly from Landsat 7 TM images. This new 30 m resolution land cover data set is well documented and evaluated based on ground truth field information by different agencies. The data set has been created from an improved classification algorithm in comparison with the 1992 NLCD land cover data. The technical methods and algorithms used to generate the 2001 NLCD data set is published in a journal article.

# 1.2 Application of the Atmospheric Model RAMS to Simulate High Resolution Urban Flow: Validation with the MUST Case

**T.G. Reisin[1] and S. Trini Castelli[2]**

[1]Soreq Nuclear Research Center, Yavne, Israel

[2]Institute of Atmospheric Sciences and Climate, National Research Council, Torino, Italy

**Abstract** The latest version of RAMS regional model has been modified and applied to describe the flow circulation and tracer dispersion in an idealized urban environment at high resolution. A particular attention was dedicated to the critical role played by the turbulence closure, considering two alternative versions of the k-ε scheme. Here, the model performance and the effect of the two turbulence closures on flow and dispersion are tested for the MUST Experiment Case. Results of flow and concentration patterns and sensitivity to the turbulence closures are presented and discussed.

**Keywords** Meteorology modelling, urban flow, turbulence parameterization, MUST experiment

## 1. Description of the Case Study

In the frame of COST732 Action, the last version of the atmospheric model RAMS (RAMS6) has been tested on the MUST Field Experiment. RAMS is a well known atmospheric model, which simulates atmospheric processes on scales from an entire hemisphere down to the microphysics in the planetary boundary layer (Cotton et al., 2003). The goal of this study is to evaluate the possibility of using a regional meteorological modeling system to describe the flow and pollutant dispersion in an urban environment, characterized by short time (min) and space (hundreds of meters) scales, and by the presence of obstacles. More specifically, the aim here is to test the RAMS model, configured in a CFD-like mode and high resolution grid (~1 m grid space), in simulating the flow dynamics and tracer dispersion in the presence of obstacles.

The RAMS model originally uses turbulence parameterisations that are suitable to atmospheric flow. In past years, a standard version of the k-∑ turbulence closure (Trini Castelli et al., 2001) and the renormalization group (RNG) k-∑ turbulence model (Reisin et al., 2007; Trini Castelli and Reisin, 2008) were implemented and tested in RAMS. These closures belong to the type typically used in CFD models.

D.G. Steyn and S.T. Rao (eds.), *Air Pollution Modeling and Its Application XX*,
DOI 10.1007/978-90-481-3812-8, © Springer Science + Business Media B.V. 2010

Since the primary interest in this work is testing the applicability of our modified version of RAMS6 (RAMS6-mod hereafter) in real conditions, we focus on the MUST field experiment. From all the available cases we chose case n. 2681829, and considered the observations fields averaged over a reference period 300–500 s after the start of the observational period, as suggested in experiment's documentation (Yee and Biltoft, 2004). In the following, the flow, turbulence and concentration fields and profiles computed by RAMS6-mod are compared to observations collected in the above case.

The Mock Urban Setting Test – MUST data set provides flow and dispersion data measured within an idealized urban roughness, composed by an array of 120 containers (12.2 m long, 2.42 m wide, 2.54 m high), during an extensive field test carried out on a test site in the Great Basin Desert in 2001 (for details see Yee and Biltoft, 2004). The terrain of the field site is characterized as 'flat open terrain' with an horizontally homogenous roughness, 0.5–1 m high. Other orographical structures, present in the field, were assumed to have no significant effect on the approach flow conditions at the test site.

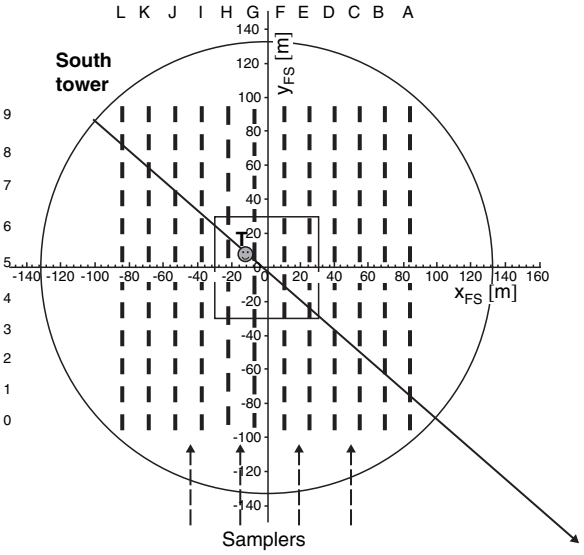


**Fig. 1.** Geometry of MUST experiment (c.o. B. Leitl), showing the direction of the incoming flow (arrow), the T tower location, the 119 containers and the service van. Note the labeling of the obstacles rows where samplers were placed

RAMS6-mod simulation domain extends 265 m in the longitudinal with a grid size of 0.8 and 321 m in the latitudinal direction with a grid size of 1.6 m. In the vertical there are 35 stretched levels with a resolution of 0.2 m up to 3.3 m, with a total height of 36 m. The size and locations of the 120 containers followed the data information provided for the MUST case. The mean wind profile for the inflow

was logarithmically extrapolated from the measured data available at three levels up to 16 m from the South tower. No initial profile was set for the turbulent kinetic energy. In all the simulations the timestep was $4 \times 10^{-3}$ s.

We recall that RAMS, as a meteorological model, was not designed to produce steady-state conditions. However, we set the boundary conditions so to approach as close as possible a steady state solution, verifying that a quasi-steady flow was reached after 4 min of simulation. The dispersion simulation was conducted using a passive tracer, released after the model reached its quasi-steady condition. The source in RAMS6-mod corresponded to a grid point at x = –77.46 m, y = 67.47 m and z = 1.8 m; the emission was continuous.

## 2. Results and Summary

In the following, some simulations results for MUST field case n. 2681829 are presented, exemplifying RAMS6-mod performance, and compared with observed data. We note that the only difference between the simulations presented here is in the turbulence closure. With respect to horizontal and vertical contour plots of tracer concentrations (not shown here) we notice that the turbulence closure scheme has a significant impact on the concentration pattern, both in the distribution and the shape of the plume. We found out that k-∑ scheme produces larger vertical spreads, while RNG-k∑ shows a slightly narrower and smoother horizontal distribution of the plume. The deflection of the plume's centerline with respect to the direction of the upstream wind was reproduced by both closure models in a similar way.

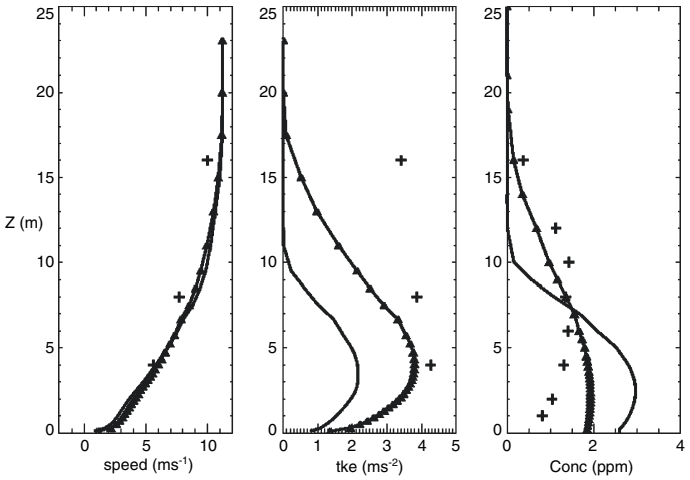


**Fig. 2.** Wind speed, turbulence and concentration profiles at T tower. Crosses: observations; line and triangles: k-∑ run; solid line: RNG-k∑ run

In Fig. 2 an example of the vertical profiles of speed, turbulent kinetic energy (t.k.e.) and concentration is plotted for tower T (see location in Fig. 1). In the present case the standard k-∑ and RNG-k∑ closures produce similar wind speeds, showing relatively small differences. In general, both schemes predict values that compare well with the few observed values. However, the standard k-∑ scheme produces always higher t.k.e. values than RNG-k ∑ and better reproduces the few observed values at the lower levels. Above 10 m height, the measured t.k.e. at T tower is not captured and the k-∑ simulated profiles slowly reach their minimum values. The predicted concentrations have similar values to the observed one, but the shapes of their profiles are different and the maximum is found at different heights. Comparisons with field concentration data are also presented in Fig. 3, where predictions are plotted versus the observations at the sensors displaced along the rows of the container arrays, at 1.6 m height. In general, simulations better match the observed data at the surface samplers than at the vertical profiles. The agreement between RAMS6-mod and observed fields is better with k-ε standard scheme close to the source, rows JI and HG, while at the farthest row, DC, RNG-k∑ run is superior. The location and magnitude of the maximum value is generally captured, while the spread of the plume is not well reproduced, especially at the southern part of the domain (negative Y values). This can be explained by a deviation of the plume centerline with respect to the upwind direction that is larger in the reality than in the simulation. This means that the RAMS6-mod meteorological wind and turbulence fields may have not fully reproduced the characteristics of the correspondent observed fields in the obstacles array.

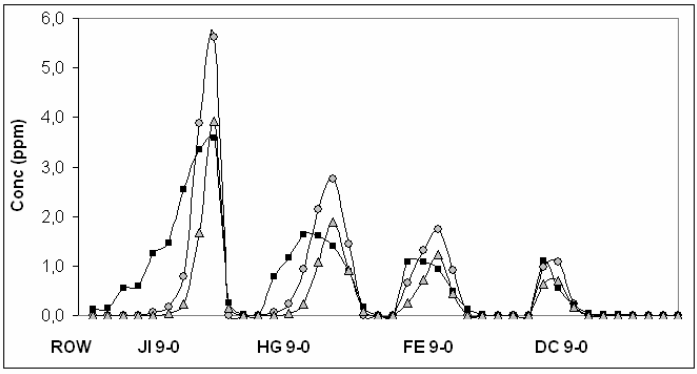


**Fig. 3.** Concentration at the samplers along the obstacles array rows. Line + squares: observations, line + triangles: k-∑ run; line + circles: RNG-k∑ run

## References

Cotton, W.R., R.A. Pielke, Sr., R. Walko, G.E. Liston, C.J. Tremback, H. Jiang, R.L. McAnelly, J.Y. Harrington, and M.E. Nicholls, 2003: RAMS 2001 – Current status and future directions. Meteor. Atmos. Phys, 82, 5–29.

Reisin, T., Altaratz Stollar, O. and Trini Castelli, S., 2007: Numerical simulations of microscale urban flow using the RAMS model. Air Pollution Modeling and its Applications XVIII. Developments in Environmental Science, Borrego C. and Renner E. Eds, vol. 6, 32–44.

Trini Castelli, S., Ferrero, E., Anfossi, D., 2001: Turbulence closures in neutral boundary layers over complex terrain. Boundary-Layer Meteorology, 100, 405–419.

Trini Castelli, S. and Reisin, T.G., 2008. Application of a modified version of RAMS model to 100 simulate the flow and turbulence in presence of buildings: the MUST COST732 exercise. Int. J. of Env. and Poll., accepted in 2008, in press in 2010.

Yee, E., Biltoft, C.A., 2004: Concentration fluctuation measurements in a plume dispersing through a regular array of obstacles. Boundary Layer Meteorology 111, 363–415.

## 3. Questions and Answers

**Steven Hanna:** Do you think that the model could be improved by including a parameterization scheme to increase the turbulence in the urban canopy and to account for mesoscale meandering?

**Answer:** Including a urban-canopy parameterization might help, since at least in the simulations presented for this case the calculated turbulence was lower than the measured one. However, a specific parameterization has to go together both with the turbulence closure and the boundary conditions around the obstacles, thus it is not a trivial task to pursue. The mesoscale meandering definitely cannot be simulated with the present setup of the model: we are considering a single grid domain of $265 \times 320$ m$^2$ with a single input wind profile, thus the mesoscale forcing is not solved. It should be remembered that the purpose of the present study was to test if RAMS model is able, at all, to simulate the flow at these scales and in the presence of obstacles. The next steps might be focused in the direction pointed out in the question.

**Bernard Fisher:** The comment is often made that finescale features of buildings have an important effect on flow and dispersion. Would the speaker like to comment (especially in relation to the COST 732 study)?

**Answer:** This point was only partly a focus of the COST 732 Action, and it was addressed by some participants using CFD (Computational Fluid Dynamics) models. Since the evaluation of the importance of these effects was not conducted in a fully systematic way, it is difficult to draw a generic conclusion. In cases with a very complex geometry like in the Oklahoma City case, certain finescale features of the buildings (e.g. garage openings) were found to have a non negligible effect on the flow and dispersion. Again, this was a specific example.

# 1.3 Simulation of Dense and Light Gas Dispersion in Presence of Obstacles

**D. Anfossi[1], G. Tinarelli[2], M. Nibar[3], J. Commanay[4], F. Ganci[5], S. Trini Castelli[1], L. Mortarini[1], and P.A. Bretonnière[4]**

[1]C.N.R.-ISAC, Torino, Italy

[2]ARIANET, Milano, Italy

[3]ARIA, Paris, France

[4]JAPSYS-EADS, Suresnes, France; MATMECA, University Bordeaux 1, France

[5]Politecnico di Torino, Italy

**Abstract** A new version of the Lagrangian Particle Dispersion Model SPRAY, developed to silmulate the dispersion of dense and light emissions at microscale, named MicroSpray is introduced. The first validation tests are presented.

**Keywords** Lagrangian Dispersion Model, microscale, buoyancy effects

## 1. Introduction

Hazardous toxic gases and vapours are produced and transported in modern industry. In case of accidents the release and dispersion of hazardous substances may cause severe problems to the populations living where such materials are handled. In general, these hazardous clouds may be emitted initially denser or less dense than the ambient air and, in some cases, because of high storage pressure, may possess a very high initial speed. In particular, dense clouds disperse quite differently from a neutral gas and, for instance, a significant upwind spread is observed for near ground level sources. Thus, it is important to have a model able to correctly estimate the area of critical concentration levels, in which population might be seriously injured. Furthermore, in many cases, such as fast emergency response or scenarios in complex terrain and obstacles, it is also important that the model is fast. In this work we present an intercomparison of MSS (which include the updated version of MicroSpray) with a CFD model (Mercure) in presence of an obstacle, and a simulation of the Kit Fox experiments.

D.G. Steyn and S.T. Rao (eds.), *Air Pollution Modeling and Its Application XX*,
DOI 10.1007/978-90-481-3812-8, © Springer Science + Business Media B.V. 2010

## 2. Brief Outline of the Models

MicroSpray is part of the model system MSS (Tinarelli et al., 2007; Moussafir et al., 2004) that comprises MicroSwift (it is an analytically modified mass consistent interpolator over complex terrain, able to derive a diagnostic turbulence inside the flow zones modified by obstacles) and MicroSpray (it is a Lagrangian Particle Dispersion model derived from SPRAY, able to account for the presence of obstacles). The new MicroSpray version is oriented to deal with dense and light gas dispersion in urban environment and industrial sites. It includes new algorithms to simulate dense and light gas dispersion in the following cases: plume with initial momentum in any direction, plume without initial momentum and plume spread at the ground due to gravity.

The Mercure model (Carissimo et al., 1997) includes: 3-D flow simulation, influence of terrain and obstacles, multiple fluids and full non-hydrostatic formulation. Mercure solves the classic Navier-Stokes equations system with adaptations for multiple fluids and for passive scalar tracer variables. A conservation relation for thermodynamic energy (enthalpy or virtual potential temperature) is optionally solved. Solving the thermal energy equation implies that thermal buoyancy (or dense) effects are included in the solution. Turbulence closure is by means of supplementary equations for the conservation of turbulent kinetic energy and dissipation using the k-e model. Important aspects of the Mercure setup for this study include: (1) ideal gas equation of state, (2) Boussinesq approximation is used, implying that density variations only affect the flow through buoyancy (or dense) terms, (3) gravity is the only retained volume force (Coriolis effects are ignored), (4) thermal forcing due to radiative flux divergence is negligible.

## 3. Intercomparison Mercure/MSS

Simulations with Mercure and MSS have been performed in several different flow conditions. Here we propose a case of a high horizontal momentum jet, characterized by 50 m/s of gas speed at the source, released in neutral stability conditions. The wind velocity of the environment flow is 5 m/s at a height of 10 m The emission stack is 10 m high. A regular obstacle (Lx = 26.2 m, Ly = 23.3 m and H = 47 m), whose base centre was located 50 m downwind the source, was included in the domain. In order to verify that the two models behave similarly in a base case, both Mercure and MSS have firstly considered a continuous emission without dense gas effects. Then the two models simulated an emission two times denser than air. Figure 1 shows the iso-surface of 0.01 kg/kg for the mixing ratio of concentration obtained for the neutral gas by the two models. Figure 2 shows instead the comparison of the dense emission case.

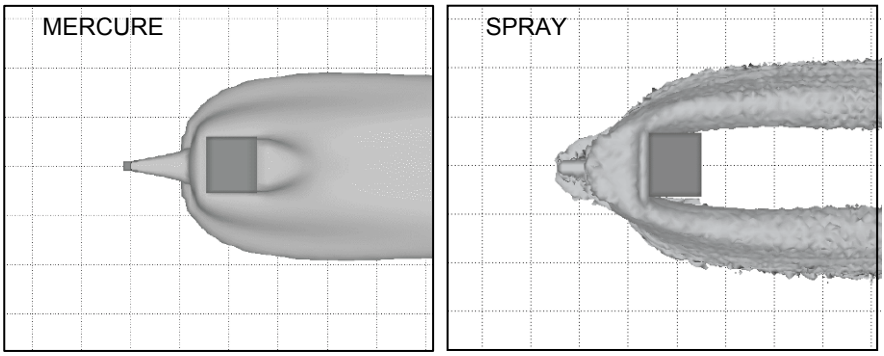


**Fig. 1.** Neutral gas: concentration mixing ratio, iso-surface 0.01 kg/kg obtained by Mercure (left) and MSS (right)

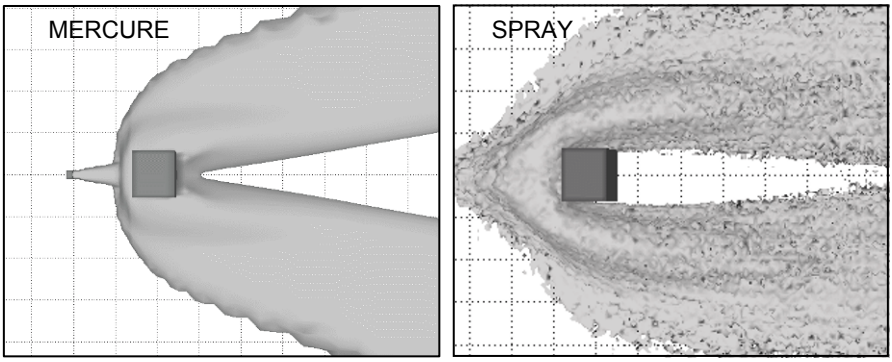


**Fig. 2.** Dense plume: concentration mixing ratio, iso-surface 0.01 kg/kg obtained by Mercure (left) and MSS (right)

MSS estimates more 'counterflow' motion than Mercure in both cases, but the effect of the ground spread is more enhanced with dense gas, as expected. In the neutral gas emission, the plume in MSS splits downwind the obstacle, while the same iso-surface keeps non-zero values for Mercure, due to the different level of turbulence Generated by the CFD model in the lee of the obstacle. In the dense gas emission experiment both Mercure and MSS show an evident splitting of the plume at ground, and a large horizontal spread due to the gravity effects. Qualitatively, the two models show a similar behaviour of the plume. Analogous numerical experiments are under process for jet emission of light gases.

## 4. KIT FOX Simulations

The 1995 Kit Fox dense gas field data set (Hanna et al., 1991) consists of 52 trials where $CO_2$ was releases from a 1.5 × 1.5 m ground level source over a rough

surface during neutral to stable conditions, with a relative emission density, $\rho_e/\rho_a$, equal to 1.52. Both puffs or continuous plumes were performed. 84 fast-response samplers were located on four downwind arrays (25, 50, 100 and 225 m). Wind speeds and directions at 2 m levels, friction velocities and Monin-Obukhov lengths were provided for each of the 52 trials. Moreover, two sets of artificial roughness arrays were used: Uniform Roughness Array (URA) with a roughness length of about 0.01–0.02 m and Equivalent Roughness Pattern (ERP) with a roughness length of about 0.12–0.24 m.

A computation domain of 400 × 240 × 100 m was considered. MicroSwift had horizontal grid spacing of 2 m and a stretched grid in the vertical. 10,000 particles were released per second from the area source, whatever the duration of release. Concentration at sampler locations was computed. Roughness lengths of 0.015 m and 0.18 m were considered for the two sets of artificial arrays, that is to say respectively URA and ERP. Maximum predicted concentrations and observations have been compared, for a 20 s averaging times, at the different downwind distances. Kit Fox trials can be split into four groups, that is to say URA – continuous (12 trials), URA – puff (21 trials), ERP – continuous (6 trials) and ERP – puff (13 trials).

At the moment, only comparisons related to URA – puff and ERP – puff have been performed. Each of these two last groups has been statistically evaluated in order to determine the accuracy of MicroSpray model predictions with the observed data. Geometric mean bias (MG), geometric variance (VG), as well as factor of 2 (FA2) are presented in the Table 1.

**Table 1.** Statistical indexes related to maximum concentrations (20 s averaging time)

| Kit Fox experiment | URA – puff | ERP – puff |
|---|---|---|
| | 21 Experiments | 13 Experiments |
| MG | 1.11 | 1.11 |
| VG | 1.20 | 1.22 |
| FAC2 | 92.9% | 84.6% |

These results are quite encouraging and, in particular, well agree with those obtained by three different versions of the model HEGADAS (Hanna and Chang, 2001), and the CFD code FLACS (Hanna et al., 2004).

## References

Carissimo, B., Dupont, E., Musson-Genon, L., and Marchand, O., 1997. Note de Principe du Code MERCURE. Version 3.1, Electricité de France, EDF HE-33/97/001, EDF publications, France

Hanna, S.R., Strimaitis, D.G., and Chang, J.C. (1991) Hazard response modeling uncertainty (a quantitative method). Vol. 2, *Evaluation of commonly used hazardous gas dispersion models.* Sigma Research Corporation for AFESC, Tyndall AFB, FL, and API, Report Nos. 4545, 4546, and 4547, 338 pp

Hanna, S.R., Chang, J.C., 2001. Use of the Kit Fox Field data to analyze dense gas dispersion modeling issues, *Atmospheric Environment* 35, 2231–2242

Hanna, S.R., Olav, R. Hansen and Seshu Dharmavaram: 2004. FLACS CFD air quality model performance evaluation with Kit Fox, MUST, Prairie Grass, and EMU observations. Atmospheric *Environment*, **38**, Pages 4675–4687

Moussafir, J., Oldrini, O., Tinarelli, G., Sontowski, J., and Dougherty, C., 2004. A new operational approach to deal with dispersion around obstacles: the MSS (Micro-Swift-Spray) software suite, 9th International Conference on Harmonisation within Atmospheric Dispersion Modelling for Regulatory Purposes Garmisch 1–4 June 2004

Tinarelli, G., Brusasca, G., Oldrini, O., Anfossi, D., Trini Castelli, S., Moussafir J., (2007) "Micro-Swift-Spray (MSS) a new modelling system for the simulation of dispersion at microscale. General description and validation". Air Pollution Modelling and its Applications XVII, C. Borrego and A.N. Norman eds., Springer, 449–458

## 5. Questions and Answers

**Question (by Peter Builtjes):** Are there any H2-dispersion field experiments available do evaluate your model results?

**Answer:** For what we could find so far there are many experiments but, generally, carried out by Private Company. These experiments are presented in Meetings and the complete set of data (at least the data necessary as input to the models) is not provided.

# 1.4 Estimating Toxic Industrial Chemical (TIC) Source Emissions and the Hand-Off to Dispersion Models

**S. Hanna[1], R. Britter[2], J. Weil[3], O.R. Hansen[4], R.I. Sykes[5], J. Leung[6], P. Drivas[7], and G. Lee[8]**

[1]Hanna Consultants, Kennebunkport, ME, USA

[2]Boston, MA, USA

[3]University of Colorado, Boulder, USA

[4]GexCon, Bergen, Norway

[5]Sage Mgmt, Princeton, NJ, USA

[6]Leung, Inc., Rancho Palos Verdes, CA, USA

[7]Bedford, MA, USA

[8]BakerRisk, San Antonio, TX, USA

**Abstract** The literature on toxic industrial chemical (TIC) source emissions formulations has been reviewed and specific equations suggested and evaluated with observations. The main focus is on pressurized liquefied gases where the concerns are foaming (level swell) and flashing in the vessel, amount of superheat, length of pipe to flashing, size and location of hole, phase of release, and aerosol drop size (rainout vs. entrained small aerosol drops). For high-priority TICs such as chlorine, the release could be all-liquid, all-gas, or two phase depending on the storage temperature and pressure. The two phase case is difficult and has been under study for decades. Evaporation of boiling liquid pools are also discussed. Relevant field and laboratory experiments have been reviewed and a subset used for source emission model evaluation. General methods for the transition from the source model to the dispersion model SCIPUFF are described. It is concluded that the current dimensional criteria could be improved by having the transition criteria based on fundamental physics relations expressed as non-dimensional criteria.

**Keywords** Toxic industrial chemicals, source emissions of hazardous chemicals, chlorine releases

D.G. Steyn and S.T. Rao (eds.), *Air Pollution Modeling and Its Application XX*,
DOI 10.1007/978-90-481-3812-8, © Springer Science + Business Media B.V. 2010

## 1. Objectives and Background

The authors have been studying Toxic Industrial Chemical (TIC) source emissions models and dispersion models for several years. Hanna et al. (2008) applied linked source emissions and dispersion models to three scenarios involving large chlorine releases from railcar accidents, and concluded that a major source of uncertainty in the estimation of health and environmental impacts was the source emission uncertainty. In the current project, the source emissions model improvements have been under study for 2 years, and the main objective is to suggest improvements for the (TIC) source emissions models in the Hazard Prediction Assessment Capability (HPAC) model system (DTRA, 2008). The study team is making use of TIC emissions models suggested by the chemical industry (Hanna et al., 1996) and detailed field experiments such as those involving two-phase jets (CCPS, 1999; Witlox et al., 2007). The highest priority scenarios concern releases of many tons of pressurized liquefied gases such as chlorine, anhydrous ammonia, and sulfur dioxide. In most cases, these releases become dense due to their high molecular weight, their cold temperature, and or/their imbedded liquid droplets. For most scenarios, the worst case will be when all of the released material quickly ends up in the gas phase or as a fine aerosol as it is transported downwind.

## 2. Source Emissions Models

Specific methodologies and the steps and equations for each category of TIC source type are given in the detailed project report by Britter et al. (2009), plus definitions and suggested input requirements and output formats, so that the steps can be directly implemented in HPAC. Because of page limits in the current paper, the equations are not listed here. The various modeling requirements have been categorized as: fluid property information; release rate and exit thermodynamic conditions; vessel response; flow after exit from the storage vessel; linkage or hand-off to HPAC's transport and dispersion model, SCIPUFF (Sykes et al., 2007); and liquid pool spreading and evaporation

A common source of fluid property information is required to ensure consistent model usage and performance. The National Institute of Standards and Technology (NIST) database is currently used in HPAC for many materials. Other chemical data sources are also used by DTRA, such as the widely used DIPPR database. Either NIST or DIPPR would be able to provide sufficient property data for source-term models.

For most cases with a rupture of a container full of pressurized liquefied gas the mass release rate will vary strongly with time. The optimum input for a dispersion model is the release rate as a function of time with a resolution of a few seconds. However, many dispersion models cannot use that much detail, and some models can take only a constant release rate (although perhaps for a finite duration)

or a single total mass released. The thermodynamic state of the material at the exit of the rupture is required as an input to the subsequent jet and dispersion modeling. Also because the flow may be choked at the exit the pressure at the exit may be above atmospheric pressure, and consequently the jet material will accelerate after the exit. This requires the calculation of the momentum flow rate of the jet including any acceleration due to an elevated pressure at the exit plane.

Because of the many possible release scenarios that could develop, a suite of six model equations is suggested. These allow for gas, two phase or liquid storage and release through ruptures of various types including sharp edged and "pipe-like" ruptures. A major change from previous reports has been the adoption of the ω–method as developed by Leung and Grolmes (1988).

Following a rupture of a storage vessel there will be a mass flow rate from the vessel and this may be gas, liquid or a mixture of gas and liquid depending upon the contents, their disposition and the rupture position. The vessel response (called blowdown in the chemical engineering community) will depend upon the fundamental equations for mass, momentum, enthalpy and entropy including heat transfer to or from the vessel contents, transfers between different phases within the storage vessel and the thermodynamic equilibrium or not of the vessel contents. These changes will lead to a change in the phase fractions in the vessel and the temperatures and pressure within the vessel and these will allow vapor, two-phase or liquid material to exit the vessel. A simple model of vessel blowdown is presented.

Model equations for jet depressurization and phase change due to flashing are summarized in Britter et al. (2009). The breakup of the jet into fine droplets and their subsequent suspension and evaporation, or rain out, is still a significant uncertainty in the overall modeling process. Two models for drop formation are the most widely used – the RELEASE model (CCPS, 1999; Johnson and Woodward, 1999) and the model by Witlox et al. (2007). The Witlox et al. (2007) JIP model is suggested though its uncertainty must be kept in mind.

An important scenario is a tank failure that results in the formation of a liquid pool and subsequent evaporation of the pool. The major liquid pool hazard, with the most rapid boiling, would occur for large spills of cryogenic TICs, whose boiling points are less than the ambient air and the ground temperature. Our review shows that the current pool evaporation models, such in SCIPUFF (Section 8.3 of Sykes et al., 2007), do agree fairly well with limited available data.

Some of the recommended source emission models have been evaluated with data from TIC field experiments, in particular recent experiments with pressurized liquefied gases. The experiments used for model evaluation include CCPS (1999) RELEASE (flashing jets and droplet sizes), FLIE, DNV JIP flashing jet studies (Witlox et al., 2007), and those from Richardson et al. (2006). Figure 1 provides an example of the comparisons of droplet diameter, D, model predictions with the RELEASE and JIP observations. The two models are the RELEASE model and the Witlox et al. (2007) JIP model, which are associated with the experiments with the same names. It should be mentioned, though, that the JIP data contain direct observations of droplet diameter, while the CCPS RELEASE data use their model to back-calculate the droplet diameters from observations of the rate of deposition

of liquid on the ground surface. The vertical axis in the figure is the ratio of predicted to observed droplet diameter, $D_{pred}/D_{obs}$.

Figure 1 (left side) shows the $D_{pred}/D_{obs}$ ratios for the JIP and the RELEASE model as a function of the superheat, $\Delta T_{SH}$. Overall, the JIP model exhibits a trend of over-prediction (up to a factor of 3) at the lower superheats ($\Delta T_{SH} < 30$ K) and under-prediction for the higher superheats, with the RELEASE model showing a similar trend. The dependence of these trends on the orifice velocity, $U_o$, is investigated in the right side of Fig. 1. For both models, a trend of over-prediction at lower velocities and under-prediction at higher $U_o$'s is seen, and may be caused by a deficiency in the model physics concerning the treatment of $U_o$, a difference in the measurement methods for the two datasets, and/or a difference between the methods for determining D.

In most of these and other comparisons of source emission model estimates with observations there is typically a factor of 2 error in models compared with research-grade observations. Of course, in a real accident or terrorist action, the source conditions (e.g., hole size and shape, and location on the vessel; storage temperature and pressure; wind speed and direction; locations of nearby obstacles) will be poorly known and thus there will be source emission uncertainties of more than a factor of 2.

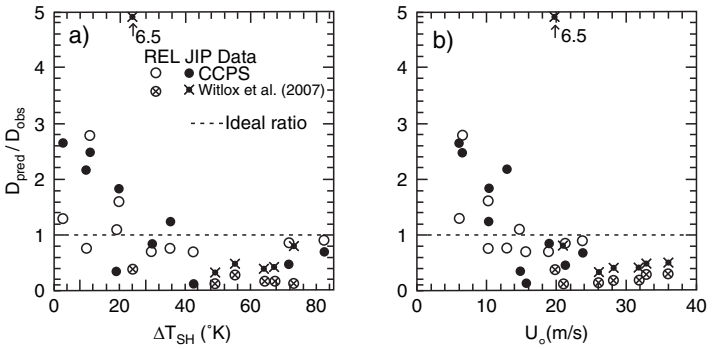


**Fig. 1.** Predicted-to-observed droplet diameter as a function of liquid superheat and orifice velocity for the JIP and RELEASE (REL) models

## 3. Hand-Off to the SCIPUFF Transport and Dispersion Model

The dispersion model SCIPUFF currently has some restrictions on what source emission model input data it can accept during the "hand-off" process. The principal limitation is that non-vertical jets cannot be accommodated. This restriction is currently being removed by the SCIPUFF developers. Britter et al. (2009) review general methods for the hand-off or transition (mostly based on physics-based

dimensionless criteria), as well as a review of the methods in HPAC/SCIPUFF (mostly based on arbitrary criteria concerning jet velocity and excess temperature). It is concluded that, while the current methods in HPAC/SCIPUFF are adequate, they are subjective in many places, and could be improved by having the transition criteria based on the fundamental physics relations.

**Acknowledgments** This research has been sponsored by the Defense Threat Reduction Agency (DTRA). The DTRA program manager is Rick Fry.

## References

Britter, R.E., Leung, J., Weil, J., Sykes, R.I., Hanna, S.R.: Toxic Industrial Chemical Source Emission Model Improvements; Task 4: Recommendations of Improved Source Emission Models, Draft Rep. No. P098-04 to DTRA, Ft. Belvoir, VA. 122 pp (Feb 2009)

CCPS/AIChE: RELEASE: A Model with Data to Predict Aerosol Rainout in Accidental Releases, ISBN No: 0-8169-0745-5, 184 pp (1999)

DTRA: HPAC Version 5.0 SP1 (DVD Containing Model and Accompanying Data Files), DTRA, 8725 John J. Kingman Rd, Ft. Belvoir, VA 22060 (2008)

Hanna, S., Dharmavaram, S., Zhang, J., Sykes, R.I., Witlox, H., Khajehnajafi, S., Koslan, K.: Comparison of six widely-used dense gas dispersion models for three actual chlorine railcar accidents. Process Safety Progress **27**, 248–259 (2008)

Hanna, S.R., Drivas, P.J., Chang, J.C.: Guidelines for Use of Vapor Cloud Dispersion Models (Second Edition). AIChE/CCPS, 345 East 47th St., New York, NY 10017, 285 pp + disk (1996)

Johnson, D.W., Woodward, J.L.: RELEASE: A Model with Data to Predict Aerosol Rainout in Accidental Releases, AIChE/CCPS, 345 East 47th St., New York, NY 10017, 184 pp (1999)

Leung, J.C., Grolmes, M.A.: A generalized correlation for flashing choked flow of initially subcooled liquid. AIChE J. **34**, 688–691 (1988)

Richardson, S.M., Saville, G., Fisher, S.A., Meredith, A.J., Dix, M.J.: Experimental determination of two-phase flow rates of hydrocarbons through restrictions, Process Safety Environ. Prot. **84,** 40–53 (2006)

Sykes, R.I., Parker, S.F., Henn, D.S., Chowdhury, B.: SCIPUFF 2.3 Technical Documentation, DRAFT Tech. Rep. for Co # DTRA01-03-D-0013, L-3 Titan Corp., Princeton, NJ, 336 pp (2007)

Witlox, H., Harper, M., Brown, P., Cleary, V.: Flashing liquid jets and two-phase droplet dispersion - II. Comparison and validation of drop size and rainout formulas. J. Haz. Mat. **142**, 797–808 (2007)

## 4. Questions and Answers

**Tamir Reisin:** What is the typical size of the drops measured and predicted?
**Answer:** The median drop size is about 10 or 20 μm in a strongly flashing jet.

# 1.5 NOAA EPA Near-Roadway Sound Barrier Atmospheric Tracer Study 2008

**Kirk L. Clawson[1], Dennis Finn[1], Roger G. Carter[1], Jason D. Rich[1], Richard M. Eckman[1], Steven G. Perry[2], Vlad Isakov[2], David K. Heist[2], and Thomas Pierce[2]**

[1]Air Resources Laboratory, Field Research Division, National Oceanic and Atmospheric Administration, Idaho Falls, ID, USA

[2]Atmospheric Modeling and Analysis Division, U.S. Environmental Protection Agency, Research Triangle Park, NC, USA

**Abstract** A roadway toxics dispersion study was conducted at the Idaho National Laboratory to document the effects on concentrations of roadway emissions behind a roadside sound barrier in various conditions of atmospheric stability. The key finding was that reduced concentrations were measured behind the barrier in all stability conditions. It was also found that the magnitude of the concentration footprint behind the barrier was tied to atmospheric stability and that the roadway tended to trap high concentrations during light wind speed conditions.

**Keywords** Wake zone, traffic emissions, pollutant dispersion near roadways, concentration deficits, atmospheric tracer, atmospheric stability

## 1. Introduction

Numerous studies have found that living and working near roadways are associated with a wide range of pathologies arising from the elevated levels of pollution associated with vehicular emissions (e.g. Baldauf et al., 2008a). Given that noise barriers and vegetation are now common roadside features it is pertinent to ask what effect they might have on pollution levels adjacent to roadways. Many studies have examined this issue. Some of these studies suggest that a barrier results in a well-mixed zone with lower concentration extending downwind behind the barrier (e.g. Baldauf et al., 2008b; Nokes and Benson, 1984; Bowker et al., 2007).

Some uncertainties persist, however, regarding the effects of roadside noise barriers on pollutant concentrations in surrounding areas. Specifically, the role of atmospheric stability has not been investigated in any systematic manner. Wind tunnel studies are done in neutral stability conditions and most of the field experimental work has been done during the daytime. Furthermore, much of the field work has been done in "natural" settings featuring moving traffic and the associated

D.G. Steyn and S.T. Rao (eds.), *Air Pollution Modeling and Its Application XX*,
DOI 10.1007/978-90-481-3812-8, © Springer Science + Business Media B.V. 2010

turbulence, potential variation in source strength, and irregular distribu-tions of canopy elements and flow obstructions. All of these can considerably complicate the interpretation of results.

The Field Research Division (FRD) of the Air Resources Laboratory (ARL) of the National Oceanic Atmospheric Administration (NOAA) conducted the Near Roadway Tracer Study (NRTS08) experiment during October 2008. NRTS08 was designed to quantify the effects of roadside barriers on the downwind dispersion of atmospheric pollutants emitted by roadway sources (e.g. vehicular transport). Pollutant transport and dispersion were measured during the field tests using sulfur hexafluoride ($SF_6$) tracer gas as a pollutant surrogate. The goal of the study was to produce a roadside barrier dataset that (1) covered a range of atmospheric stabilities, (2) minimized factors that could complicate data interpretation, and (3) could be used to guide model development.

## 2. Methods

Roadway emissions were simulated by release of an atmospheric tracer ($SF_6$) from two 54 m long line sources in unstable, neutral, and stable conditions. A 90 m long, 6 m high mock sound barrier constructed of straw bales (Fig. 1) was installed on one grid while the other grid had no barrier. Simultaneous tracer concentration measurements were made with real-time and bag samplers on the identical sampling grids downwind from the line sources at 1.5 m above ground level. An array of six sonic anemometers was employed to measure the barrier-induced turbulence. The pristine environment of the INL enabled a clearer and less ambiguous interpretation of the data.

**Fig. 1.** Straw bale mock roadside sound barrier

## 3. Results

Figure 2 compares barrier and non-barrier normalized tracer concentrations for a 15-min period in neutral conditions. Figure 3 is a contour map of the ratio between barrier and non-barrier concentrations at corresponding grid locations for the same neutral case. The barrier had the effect of reducing downwind concentrations by more than 50%. This pattern was repeated consistently in all stability conditions.

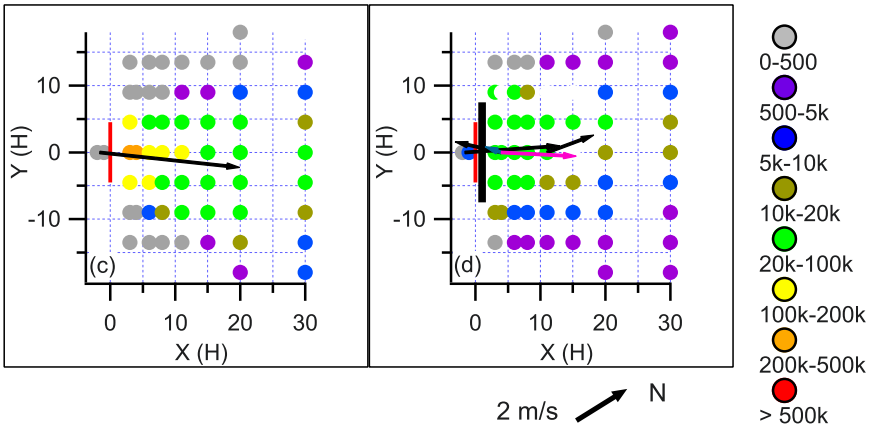


**Fig. 2.** Corresponding non-barrier (left) and barrier (right) normalized concentration/wind vector maps for an example neutral stability case. The tracer release line is indicated in bright red; the barrier in bold black

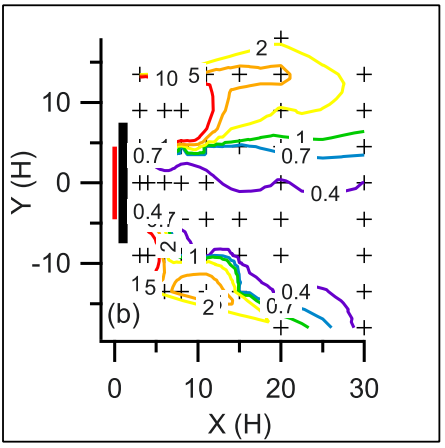


**Fig. 3.** Contour map of the ratio between barrier and non-barrier concentrations at corresponding grid locations for the neutral stability case shown in Fig. 2

Briefly, other key findings of the study include: (1) the magnitude of the concentration footprint expanded or contracted in stable and unstable conditions, respectively, and (2) very high concentrations were measured in the roadway upwind of the barrier in stable, light wind speed conditions.

**Acknowledgments and Disclaimer** We wish to thank Alan Vette and S.T. Rao from the EPA and Shane Beard, Tom Strong, and Neil Hukari from FRD for the contributions they made to the study. This work was completed under Interagency Agreement DW-13-92274201-0 between the National Oceanic and Atmospheric Administration and the U.S. Environmental Protection Agency. Although it has been reviewed by EPA and NOAA and approved for publication, it does not necessarily reflect their policies or views. U.S. Government right to retain a non-exclusive royalty-free license in and to any copyright is acknowledged.

## References

Baldauf., RW., Thoma, E., Hays, M., Shores, R., Kinsey, J., Gullett, B., Kimbrough, S., Isakov, V., Long, T., Snow, R., Khlystov, A., Weinstein, J., Chen, F., Seila, R., Olson, D., Gilmour, I., Cho, S., Watkins, N., Rowley, P., Bang, J., 2008a. Traffic and meteorological impacts on near-road air quality: summary of methods and trends from the Raleigh near road study. Journal of the Air and Waste Management Association 58, 865–878.

Baldauf, R.W., Thoma, E., Khlystov, A., Isakov, V., Bowker, G., Long, T., Snow, R., 2008b. Impacts of noise barriers on near-road air quality. Atmospheric Environment 42, 7502–7507.

Bowker, G.E., Baldauf, R., Isakov, V., Khlystov, A., Petersen, A., 2007. The effects of roadside structures on the transport and dispersion of ultrafine particles from highways. Atmospheric Environment 41, 8128–8139.

Nokes, W.A., Benson, P.E., 1984. Carbon monoxide concentrations adjacent to sound barriers. Office of Transportation Laboratory, California Department of Transportation, Report FHWA/CA/TL-84/04.

## 4. Questions and Answers

**Steve Hanna:** How did you decide on how long the barrier would be, and wouldn't the results depend on this length? Was this investigated by the EPA wind tunnel tests?

**Answer:** We were concerned about having a barrier long enough to ensure that edge effects would be minimal or nonexistent. We used the EPA wind tunnel study to guide us in determining the length of the barrier. Obviously, an infinite length barrier would have been ideal. Construction costs ultimately limited the length to 90 m. In some of the test periods, edge effects were visible when the data were plotted as shown in Fig. 2 above. However, in the majority of individual tests periods, which is when the wind was essentially perpendicular to barrier, edge effects were usually negligible. This is demonstrated by the fact that the areas of peak concentrations were located behind the barrier, even if not directly centered. It was when the peak concentrations were clearly located

outside the y-bounds of the barrier that edge effects became more of a factor. In summary, the barrier proved to be long enough that several sampler locations on each crosswind sampling line in the direct downwind influence of the barrier did not show edge effects. The next step is to knit the concentration fields together to produce a result that would be expected from an infinitely long barrier. Our EPA colleagues demonstrated this technique in the wind tunnel study report.

**Peter Builtjes:** The effect found of the barrier is larger than I recall from CFD calculations. What is your experience with that?

**Answer:** The decreases in tracer concentration we measured behind the barrier were in the upper range of decreases reported in previous field studies, which was typically 50–60%. In some of our individual experiments we observed decreases greater than that although this was often associated with clear edge effects. We commonly observed decreases of 50–60% even when there was little evidence of any significant edge effects. The EPA wind tunnel results were also similar to our results. Therefore, it seems reasonable to conclude that the tracer concentrations from our field study are accurate.

**Clemens Mensink:** Some CFD models do show an increase of concentrations in the vertical direction behind the barrier. Do you have any information on the concentration distribution in the vertical direction?

**Answer:** We desired to investigate the tracer concentration distribution in the vertical direction, but were limited by funding constraints to only ground-level concentrations, i.e., 1.5 m AGL.

# 1.6 Implementation of Efficient Two-Way Mesoscale-Microscale Coupling Using Interpolating Metamodels

**G. Tsegas, Ph. Barmpas, I. Douros, and N. Moussiopoulos**

Laboratory of Heat Transfer and Environmental Engineering, Aristotle University, Greece

**Abstract** Coupling between prognostic mesoscale and microscale flow models has been suggested as a way to improve the accuracy of calculated flows around artificial structures and over densely-built areas. Nevertheless, implementations of full two-way mesoscale-microscale coupling are burdened by large scale mismatches as well as the formidable computational cost of on-line microscale calculations. In the present work, an efficient implementation of an effective two-way coupling between the mesoscale model MEMO and the microscale model MIMO, based on interpolating metamodels, is introduced. The performance of two different meta-model formulations is assessed using vertical flow profiles obtained from a two-way coupled mesoscale-microscale calculation in the urban area of Athens, Greece.

**Keywords** Metamodelling, urbanisation, mesoscale, microscale, two-way coupling

## 1. Introduction

The main obstacles for an efficient implementation of two-way coupling between mesoscale and CFD flow models are the large gap of spatial and temporal scales as well as the prohibitive chasm between the execution speeds of the two classes of models. Metamodelling techniques (Piñeros Garcet et al., 2006) offer a potential solution by approximating numerically expensive physical modelling with multi-dimensional interpolators. As part of a mesoscale-microscale coupling scheme, a metamodel's function is to approximate the area-averaged outflow response of each microscale domain for various inflow conditions without performing a full microscale calculation at each timestep. In the present work, two metamodel-based schemes for implementing two-way coupling of the mesoscale model MEMO (Moussiopoulos et al., 1993) and the microscale model MIMO (Ehrhard et al., 2000) are developed and evaluated using a mesoscale test case.

D.G. Steyn and S.T. Rao (eds.), *Air Pollution Modeling and Its Application XX*,
DOI 10.1007/978-90-481-3812-8, © Springer Science + Business Media B.V. 2010

## 2. Methodology

Two multi-dimensional interpolating formulations are considered: the first one is based on the well-known inverse-squared distance weighting (ISD) interpolator while the second one is implemented using a radial basis functions (RBF) neural network (Nabney, 2001). In both formulations, the metamodel can be viewed as a multi-dimensional interpolation scheme that given a state of "input" conditions $\mathbf{x} = (u_{\text{in1,2}}, \alpha_{\text{in1,2}}, E_{\text{in1,2}})$ provides the "output" state $\mathbf{y} = (u_{\text{out1,2}}, \alpha_{\text{out1,2}}, E_{\text{out1,2}})$ consisting of the wind velocity ($u$), wind direction ($a$) and TKE ($E$) vertical profiles, averaged over the two inflow and outflow lateral boundaries of a given microscale computational domain. For each metamodel, a calibration set of input and output states $(\mathbf{x}_k, \mathbf{y}_k)$, $k = 1..N_{\text{cal}}$ has to be determined by explicitly simulating $N_{\text{cal}}$ microscale cases during the initialisation stage.

The calibration set is constructed starting from a small number of urban areas, with linear dimensions of the order of a few hundred meters, which are selected as representative of the urban geometry and subsequently simulated with MIMO for specific sampling periods. Area-averaged inflow and outflow profiles are extracted from the calculated fields for each period and used as the actual calibration points for each metamodel class. Following appropriate discretisation and classification of the entire urban area, metamodel instances are associated to the rest of the urban cells of the mesoscale grid, after rotations and vertical scaling are applied to account for differences in street geometry, orientation and average building height in each cell. During the coupled operation of the model, each metamodel instance receives input from the inflow boundaries of the corresponding mesoscale cell and in turn produces the extra forcing terms, approximating the effect of local urban structures. These are introduced back into the mesoscale domain by means of Newtonian relaxation terms.

## 3. Applications: The Athens Case

The performance of the coupled MEMO-MIMO model system was assessed using a 5-day case between 8 May and 12 May 2002 for the greater Athens area. A set of four calibration cases, subsequently labelled (1)–(4), was constructed based on microscale simulations of two representative urban areas, located near the shore of Piraeus and over Patision and Fokionos Negri streets, respectively. High-resolution microscale computational grids were constructed from three-dimensional Geographical Information System (GIS) data of the building and road structure. An example of calculated two-dimensional flow field at a horizontal level of 15 m over the sample area of Patision, is shown in Fig. 1a.

The differences between the wind speed and TKE fields calculated by the coupled system and the corresponding fields of the standard MEMO simulation are illustrated in Fig. 1b and c. A significant reduction of the predicted wind speed

of about 0.5–1.0 $ms^{-1}$ is evident over the entire domain where the extra forcing was applied. A corresponding significant increase of the TKE production is observed in the first three computational levels. A detailed discussion of the coupled model performance can be found in Tsegas et al. (2008).

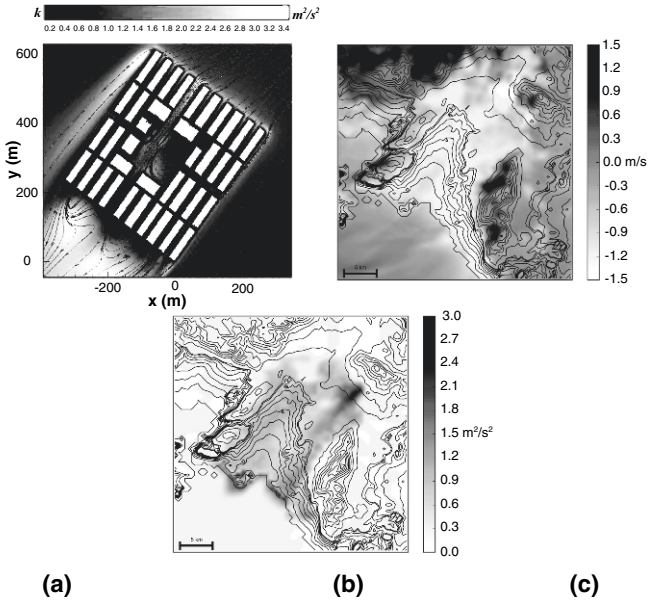


**Fig. 1.** Numerically predicted flow field and TKE (a) calculated for the Patision microscale domain for 08/05/2002:11:00 LST, and difference maps of the calculated wind velocities (b) and TKE (c) for the Athens mesoscale case

As a benchmark of the performance of the metamodels under study, their response was observed while the input state was linearly varied from the calibration state (1) (minimum inflow angle) to calibration case (3) (maximum inflow angle) for the Patision domain. As evident from the response curves in Fig. 2a, the RBF metamodel not only approximates the two intermediate calibration points better than ISD but effectively provides a better interpretation of the physical model's behaviour throughout the input range. The angular response calculated for an input vertical profile (dotted black line), obtained by averaging the MIMO inflow profiles of cases (1) and (3) for the Patision domain, is shown in Fig. 2b. The corresponding output profiles produced by RBF and ISD are indicated by solid black and violet lines. The superior performance of the RBF metamodel is indicated by the obvious similarity of its lower-level response (up to the average building height of ~20 m) with the one calculated by MIMO for the nearby profile (3) (red). Moreover, the deflection of the outgoing flow towards 190°, which is the principal direction of street canyons in the Patision domain, is better approximated.

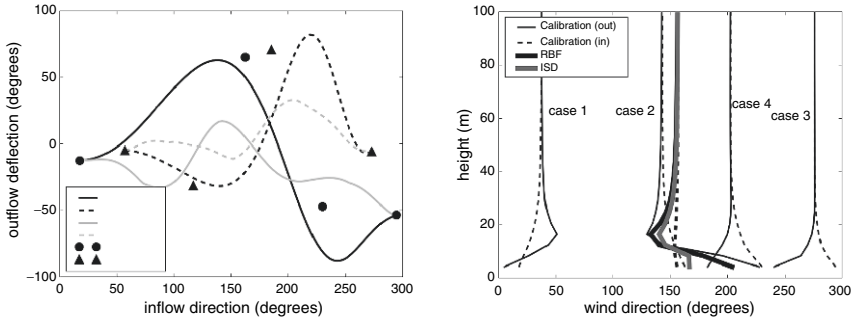


**Fig. 2.** Lowest-layer angular response (a) and vertical profiles of the angular response (b) of the RBF and ISD metamodels

## 4. Conclusions

A two-way coupled mesoscale-microscale model system was implemented using two alternative formulations of interpolating metamodels for simulating the effect of local forcings on the mesoscale field. The system was evaluated in calculations of the flow fields in the urban area of Athens, Greece. The performance of two metamodelling formulations was evaluated by observing their response to input conditions extracted from microscale simulations of a densely-built downtown location. The performance of the RBF neural network metamodel was found to be superior to that of the ISD interpolator both in terms of accuracy and predictive ability.

## References

Ehrhard, J., Khatib, I.A., Winkler, C., Kunz, R., Moussiopoulos, N., Ernst, G.: The microscale model MIMO: Development and assessment. J. Wind Eng. Ind. Aerod. **85**, 163–176 (2000)

Moussiopoulos, N., Flassak, Th., Berlowitz, D., Sahm, P.: Simulations of the wind field in Athens with the nonhydrostatic mesoscale model MEMO. Environ. Softw. **8**, 29–42 (1993)

Nabney, I.T.: Netlab: Algorithms for Pattern Recognition. Springer-Verlag, New York (2001)

Piñeros Garcet, J.D., Ordoñez, A., Roosen, J., Vanclooster, M.: Metamodelling: Theory, concepts and application to nitrate leaching modelling. Ecol. Model. **193**, 629–644 (2006)

Tsegas, G., Barmpas, Ph., Douros, I., Moussiopoulos, N.: A metamodelling implementation of a two-way coupled mesoscale-microscale flow model for urban area simulations. In: Đuričić, V. (ed.) Proceedings of the 12th International Conference on Harmonisation within Atmospheric Dispersion Modelling for Regulatory Purposes, Cavtat, Croatia, 6–9 October 2008, pp. 181–186, CD-ROM edition.

## 5. Questions and Answers

**Question 1:** Is it worthwhile to set up such a complicated model system, given the little differences obtained with respect to the original model version? (Stefano Galmarini, JRC)

**Answer:** In cases of such complex model setups, it is indeed important to weigh the prospective benefits with the effort expended to set up and process individual application cases. Nevertheless, one of the features of our system is that the setup effort is largely restricted to the initial configuration- and calibration phase, which mainly consists of microscale simulations. Once the metamodel library is prepared, the cost of running additional cases becomes minimal. Furthermore, the observed differences with the original mesoscale fields do reveal a strong modification of the flow field on the two lowest layers (see, e.g. Fig. 2b), which is expected to have a significant effect on pollutant dispersion calculations within urban cells.

**Question 2:** You have demonstrated micro and mesoscale coupling of the dynamics. How do you expect the coupling to behave when one is trying to model air quality, especially $NO_2$ or $PM_{10}$? (Bernard Fisher, University of Greenwich School of Earth and Environmental Sciences)

**Answer:** Qualitatively, we can expect the modification of the mesoscale fields as caused by the two-way coupling to influence dispersion calculations in two significant ways: the first is an overall increase of the average pollutant concentrations in densely built areas, due to the reduced average wind speeds as calculated in these areas. The second one is the amplification of turbulent mixing in the first two computational layers resulting from the introduction of additional shear and TKE production by the coupling process. A quantitative assessment of both effects on the dispersion of various pollutants (including $NO_2$ and $PM_{10}$) is the subject of ongoing work.

# 1.7 Four Diagnostic Urban Wind Flow and Dispersion Models Tested with Joint Urban 2003 Field Data

**S. Hanna[1], J. White[2], J. Trolier[3], R. Vernot[3], M. Brown[4], H. Kaplan[5], Y. Alexander[5], J. Moussafir[6], Y. Wang[7], J. Hannan[8], R. Fry[8], C. Kiley[8], and E. Hendrick[9]**

[1] Hanna Consultants, Kennebunkport, ME, USA

[2] US Army Test and Evaluation Command, Dugway Proving Ground, UT, USA

[3] Science Applications International Corporation, Allentown, PA, USA

[4] Los Alamos National Laboratory, Los Alamos, NM, USA

[5] IIBR, Tel Aviv, Israel

[6] ARIA Tech., Paris, France

[7] US Army Research Laboratory, Adelphi, MD, USA

[8] US Defense Threat Reduction Agency, Alexandria, VA, USA

[9] Epsilon Assoc., Maynard, MA, USA

**Abstract** There are several diagnostic wind flow models available for urban areas. Mass-consistent principles are used to solve for the mean wind flow on an approximate 1 km domain, within which detailed 3-D building geometries are defined. To initialize the models, simple vortex structures are parameterized behind and around buildings and in street canyons. An upwind wind profile must be prescribed. The wind flow results are used as inputs to a Lagrangian particle dispersion model, where turbulent velocities and time scales are parameterized based on the mean wind solution and the 3-D building geometry. The developers of four of these models are collaborating in a study where their models are run for two tracer releases (one daytime and one nighttime) during the Joint Urban 2003 (JU2003) field experiment. The four models are: Microswift/Spray (MSS) by SAIC, QUIC by LANL, the urban Lagrangian model by the Israel Institute for Biological Research, and 3DWind by the Army Research Laboratory. Nearly identical domains and grid systems are used, and model outputs are produced at agreed-upon horizontal and vertical cross-section locations and monitoring sites. All models use the same input wind profile. The simulated patterns of wind fields and tracer contours are in good qualitative agreement. For wind speed near the surface, the mean model biases are less than about 20% and RMS errors are about 1–2 m/s. The tracer concentrations also show low bias but much scatter.

**Keywords** Air quality model evaluation, mass consistent wind models, urban dispersion, emergency response, JU2003 field experiment

D.G. Steyn and S.T. Rao (eds.), *Air Pollution Modeling and Its Application XX*,
DOI 10.1007/978-90-481-3812-8, © Springer Science + Business Media B.V. 2010

## 1. Introduction

Atmospheric transport and dispersion models are used to predict downwind hazards associated with the release of hazardous materials. In urban areas, concentration patterns may be spread out and distorted because wind flows are variable due to vortices and channeling forced by the buildings. Three-dimensional wind fields accounting for urban effects can be constructed through a variety of methods ranging from simple urban canopy parameterizations to complex computational fluid dynamics (CFD) models. In an attempt to strike a balance between model speed and complexity, several groups have developed urban diagnostic wind flow models based on the Röckle (1990) approach, which initializes the system by parameterizing the geometric shapes of recirculating wakes and their flow patterns behind, over, and around buildings. The approach requires a detailed representation of the 3-D building geometry (with resolution of about 1–5 m). Kaplan and Dinar (1996) were the first to implement this method in an operational urban wind flow and dispersion model. Subsequently, several other groups have modified the basic model and coupled it with mass consistency algorithms to generate detailed flow fields within the urban environment within a matter of minutes. Dispersion models (usually Lagrangian particle dispersion models, or LPDMs) can then be used to quickly predict concentrations of hazardous substances.

In this paper, simulations from four such models are compared using a subset of the observations from the Joint Urban 2003 (JU2003) field study in Oklahoma City, OK, USA (see Allwine et al., 2004; Clawson et al., 2005). Data from continuous release 1 during IOP 2 (day) and continuous release 2 during IOP 8 (night) are used, and the release location was near the downtown Westin hotel.

The four models are the Los Alamos National Laboratory's (LANL) QUIC model suite (Williams et al., 2004; Gowardhan et al., 2008; Singh et al., 2008), the Science Applications International Corporation (SAIC)–ARIA MicroSwift/Spray (MSS) model (Moussafir et al., 2004); the US Army Research Laboratory's (ARL) three-dimensional Wind Field (3DWF) model (Wang et al., 2005), and the Israel Institute of Biological Research (IIBR) Kaplan and Dinar (1996) model. All models implement Röckle's original 1990 methodology but have been modified based on observations from a number of recent urban tracer studies and wind/water tunnel experiments. Because the Rockle models produce only simulations of the wind field and not the turbulence, it is necessary to parameterize the turbulent speeds and Lagrangian time scales for use in the LPDM.

## 2. Meteorological Inputs

The wind data used for model inputs in this study are 15-min average vertical wind profiles collected with the Pacific Northwest National Laboratory (PNNL) SODAR, located in a suburban area approximately 3 km S/SW of downtown

Oklahoma City. Wind directions averaged about 210° during IOP 02 and ~157° during IOP 08. The vertical resolution of the SODAR was 10 m from 30 to 500 m above ground level. Due to problems with the lower level data, only the SODAR observations at and above 100 m were used. Below 100 m, wind speeds were estimated using a neutral logarithmic profile: $u(z) = u(100\ m)\ \ln(z/z_o)/\ln(100\ m/z_o)$, where $z_o$ is the roughness length (assumed to be 0.5 m), z is the height, and $u_{100\ m}$ is the SODAR wind velocity at z = 100 m. A displacement length of zero is assumed in this suburban area and wind directions at z < 100 m are set equal to the value at 100 m. For each IOP, five 15-min average profiles were constructed beginning 15 min prior to the tracer release to 1 h after the beginning of the tracer release (e.g., 1545–1700 UTC for IOP 02.)

## 3. Comparison of Model Results

The simulated wind speeds and directions, turbulent kinetic energy (TKE), and concentrations are assessed by a combination of qualitative and quantitative comparisons. For example, qualitative analyses of contour plots (not shown here) may show that the model can correctly simulate the channeling of wind down a side street. Quantitative comparisons look at whether the model can match the observed mean wind speed or concentration and the degree of scatter. Examples of scatter plots of the near-surface wind outputs and concentration outputs for IOP 2 for the four models are shown in Figs. 1 and 2. Plots are available for all models and time periods, but the current manuscript has page limits. The figures illustrate the general finding that there is little mean bias but much scatter, and that there is not much

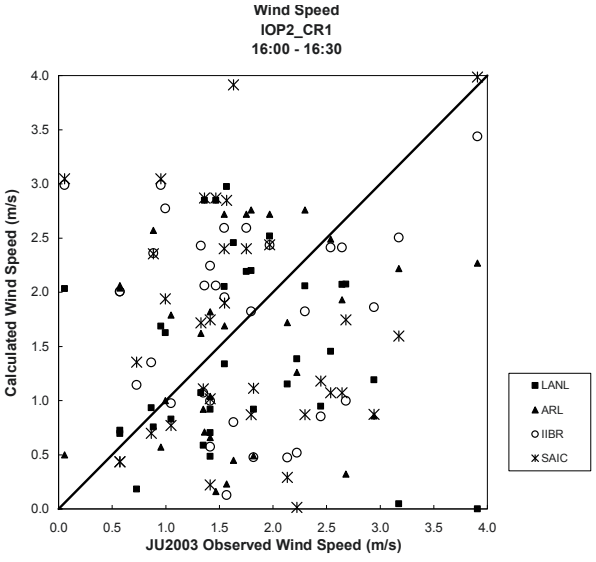


**Fig. 1.** Wind speed scatter plot for IOP02 (day) for the four models

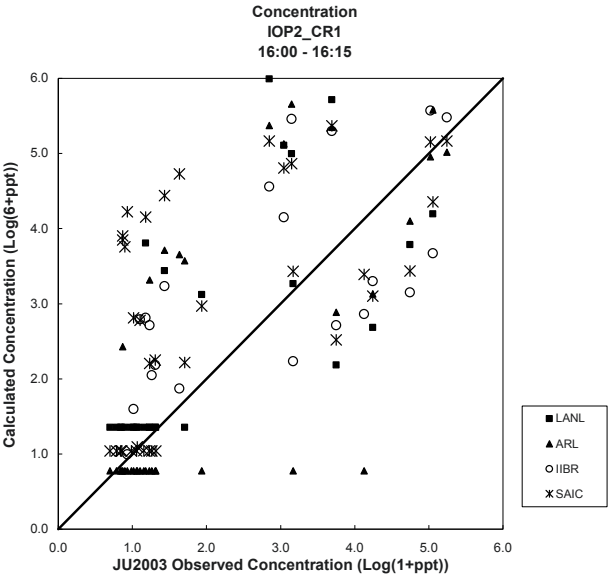


**Fig. 2.** Concentration scatter plot for IOP02 (day) for the four models

difference between the four models' performance. The calculated relative mean bias (e.g., the relative difference between the mean observed and predicted wind speed or concentration) is found to be usually less than about ±20% to 40%. However, the scatter is relatively large (about 60% for wind speed and a factor of 5–10 for concentration.

**Acknowledgments** This research was supported by the U.S. Defense Threat Reduction Agency (DTRA), with Dr. John Hannan as Project Manager. The QUIC model runs were supported by LANL, the 3DWF model runs were supported by the U.S. Army Research Laboratory, and the IIBR model runs were supported by that agency.

## References

Allwine, K.J., Leach, M., Stockham, L., Shinn, J., Hosker, R., Bowers, J., Pace, J.: Overview of Joint Urban 2003 – An atmospheric dispersion study in Oklahoma City, Preprints, Symposium on Planning, Nowcasting and Forecasting in the Urban Zone, American Meteorological Society, January (2004)

Clawson, K.L., Carter, R.G., Lacroix, D.J., Biltoft, C.J., Hukari, N.F., Johnson, R.C., Rich, J.D., Beard, S.A., Strong, T.: Joint Urban 2003 (JU03) SF6 Atmospheric Tracer Field Tests, NOAA Tech Memo OAR ARL-254, Air Resources Lab., Silver Spring, MD (2005)

Gowardhan, A., Brown, M., Pardjyak, E.: Evaluation of a fast response pressure solver for flow around an isolated cube. Environ. Fluid Mech. DOI 10.1007/s10652-009-9152-5 (2009)

Kaplan, H., Dinar, N.: A Lagrangian dispersion model for calculating concentration distribution within a built-up domain., Atmos. Environ. **30**, 4197–4207 (1996)

Moussafir, J., Oldrini, O., Tinarelli, G., Sontowski, J., Dougherty, C.M.: A new operational approach to deal with dispersion around obstacles: the MSS (Micro SWIFT SPRAY) software suite, 9th International Conference on Harmonization within Atmospheric Dispersion for Regulatory Purposes, June 1–4, 2004, Garmisch, Germany (2004)

Röckle, R.,: Bestimmung der stomungsverhaltnisse im Bereich Komplexer Bebauugsstruckturen, Ph.D. thesis, Vom Fachbereich Mechanik, der Technischen Hochschule Darmstadt, Germany (1990)

Singh, B., Hansen, B. Brown, M., Pardyjak, E.: Evaluation of the QUIC-URB fast response urban wind model for a cubical building array and wide building street canyon, Env. Fluid Mech., v 8, pp 281–312 (2008)

Wang, Y., Williamson, C., Garvey, D., Chang, S., Cogan, J.: Application of a multigrid method to a mass-consistent diagnostic wind model, J. Appl. Meteorol. **44**, 1078–1089 (2005)

Williams, M., Brown, M., Singh, B., Boswell, D.: QUIC-PLUME Theory Guide, LA-UR-04-0561, 22 pp. (2004)

## 4. Questions and Answers

**Domenico Anfossi:** Is there a difference in CPU time among the four models?

**Answer:** We did not check that aspect of the models because this type of model is designed to run quickly. A single run for one tracer release on the JU2003 domain takes 1 or 2 min, at most, on a standard laptop.

**R. Vautard:** Since the flow is turbulent, don't you expect to have large scatter in wind fields? Does scatter still exist in stable conditions?

**Answer:** The observed wind field is of course reflecting turbulent eddies of all scales. The models all use the same inflow wind profile, which is assumed constant during a given 15 min period. Any one model will give exactly the same wind field solution each time that it is run with this wind input. The differences between the four models' predicted wind fields is due to differences in the way that each model parameterizes the recirculating wake geometries and the logic used by that model to account for smaller wakes that intersect larger wakes. Concerning stable conditions, our results for IOP08 are from a nighttime period and show about the same amount of scatter as for the daytime IOP02. In the downtown domain being studied, the stability is less than in the upwind rural area due to the presence of mechanical mixing caused by the buildings and also due to anthropogenic heat inputs.

# 1.8 Atmospheric Boundary Layer Modeling for Combined Meteorology and Air Quality Systems

**Jonathan Pleim[1], Robert Gilliam[1], and Shaocai Yu[2]**

[1]United States Environmental Protection Agency, RTP, NC, USA

[2]Science and Technology Corporation, Hampton, VA, USA

**Abstract** Atmospheric Eulerian grid models for mesoscale and larger applications require sub-grid models for turbulent vertical exchange processes, particularly within the Planetary Boundary Layer (PBL). In combined meteorology and air quality modeling systems consistent PBL modeling of winds, temperature, humidity, and chemical concentrations is necessary for accurate simulation of chemical transport through the 3-d grid and accurate simulation of gas-phase and aerosol chemistry. A recently developed PBL model, known as the Asymmetric Convective Model version 2 (ACM2), has been designed to represent realistic turbulent transport of atmospheric constituents. The ACM2 has local and non-local components for transport in convective boundary layers. Evaluation of the ACM2 involves comparisons to observed vertical profiles of meteorology and chemistry. For example, simulations of the Weather Research and Forecast (WRF) model and the Community Multiscale Air Quality (CMAQ) model are compared to vertical profiles of potential temperature, water vapor mixing ratio, and several trace chemical species from aircraft and balloon soundings. The modeled vertical structures of chemical and meteorological parameters are consistent with observations.

**Keywords** Boundary layer, non-local closure, WRF, CMAQ

## 1. Introduction

Parameterizations of the Planetary Boundary Layer (PBL) are important components in meteorology models and even more critical for air quality models where ground-level concentrations of pollutants are largely determined by the extent of vertical mixing. Thus, accurate and consistent simulation of the diurnal evolution and vertical mixing of meteorological and chemical species is essential for realistic simulation of these atmospheric variables. Simple closure for the turbulent flux terms of the Reynolds averaged equations, such as eddy diffusion, are reasonable when the scale of the turbulent motions is smaller than the vertical grid spacing of the model as is usually the case in stable or neutral conditions, but these assumptions

D.G. Steyn and S.T. Rao (eds.), *Air Pollution Modeling and Its Application XX*,
DOI 10.1007/978-90-481-3812-8, 

break down in the convective boundary layer (CBL) where convective eddies often form in the atmospheric surface layer and rise through the entire depth of the CBL. Under such conditions, vertical fluxes can be counter to local gradients. To account for such large-scale transport, several models have been developed to include non-local components. Many of these models, which are commonly used in meteorology models, are based on gradient adjustments that are parameterized according to the surface heat flux. Thus, these models are most valid for modeling heat fluxes and are not easily adapted for chemical transport modeling. The Asymmetric Convective Model version 2 (ACM2) is a hybrid model that combines local and non-local components for comprehensive treatment of all stability conditions. However, unlike the gradient adjustment schemes, the ACM2's non-local component is equally valid for any atmospheric quantity because it is a simple transilient matrix scheme that describes the mass flux exchange between non-adjacent grid layers. The basic formulation, 1-D testing against large eddy simulations and field experiments, and evaluation within a mesoscale meteorology model are described in detail by Pleim (2007a, b). This paper provides preliminary evaluation of combined meteorology and air quality modeling using the ACM2 in the Weather Research and Forecast (WRF) and Community Multiscale Air Qualilty (CMAQ) models based on field data from the Texas Air Quality Study 2 (TexAQS II).

## 2. Modeling

The Advance Research WRF (ARW) version 3 was run for the TexAQS II period (August 1–October 15, 2006) with 12 km grid cell size and 34 vertical layers on a domain that covers the eastern 2/3 of the continental US. The WRF simulations include the Pleim-Xiu LSM and the ACM2. Details of the model configuration and a comprehensive model evaluation are presented by Gilliam and Pleim (2009). WRF model simulations were used to drive CMAQ modeling for the same period. Note that these air quality simulations are considered preliminary because they do not yet include the more detailed emission inventory for Texas that has been prepared by the Texas Commission on Environmental Quality. To ensure consistency between meteorology and air chemistry, the CMAQ was configured to use the ACM2 for turbulent transport of chemical species and to use land surface parameters from the PX LSM for calculation of chemical dry deposition.

## 3. PBL Heights

The TexAQS II field experiment included eleven radar wind profilers in East Texas during the study period. Reliable techniques have been developed to estimate the PBL height for daytime hours from the radar raw data (Bianco et al., 2008). These derived PBL height data have been paired in time at each profiler site with

the PBL heights estimated by the ACM2 in the WRF model simulations. Figure 1 shows modeled and observed values for four of these profilers. The lines represent the median values at each hour of the day for the simulation period (August 1–October 15) and the bars indicate the 25% and 75% values for each model and observed distribution. For three out the four sites shown the model overpredicts the median PBL height by about 100–300 m for most of the day. The interquartile ranges, however, almost always overlap. It is not clear how much of these differences are due to model error and how much is due to differences in technique. For example, the late afternoon collapse of the model PBL heights that often leads to underprediction is probably an artifact of the model's PBL height algorithm that is very sensitive to the near surface temperature and surface heat flux. The profiler PBL height algorithm, on the other hand, is more sensitive to indicators of ambient turbulent intensities. Thus, residual turbulence can lead to gradual declines in observed PBL height while the model algorithm senses the initial stabilization of the lowest layers resulting in very low PBL heights. It is conceivable that the mid-day overpredictions could have a similar algorithmic cause.

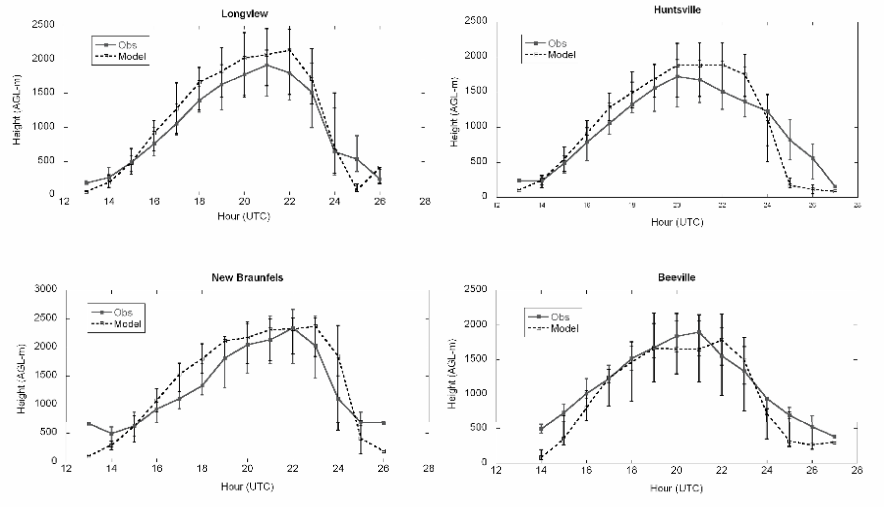


**Fig. 1.** Comparison of modeled and observed PBL height for August 1–October 15, 2006

## 4. Aircraft Measurements

Aircraft measurements were important components of the TexAQS II experiment. The NOAA WP-3D Lockheed Orion aircraft (P3) made flights over the east Texas region during September 11–October 12, 2006. On several occasions the P3 flew a spiral flight path that extended well above the PBL. These sections of the flight

measurements gave valuable evidence of the vertical structure of meteorological and chemical parameters within and above the PBL. Figure 2 shows an example of vertical profiles for potential temperature, water vapor mixing ratio, and $NO_y$ for a P3 spiral about 120 km SE of Dallas at 19 UTC on 9/25/2006 compared to the model simulations from the WRF-CMAQ system. Although the $NO_y$ concentration and water vapor mixing ratio are underpredicted in the PBL, the PBL structure is quite accurate for both meteorological and chemical parameters.

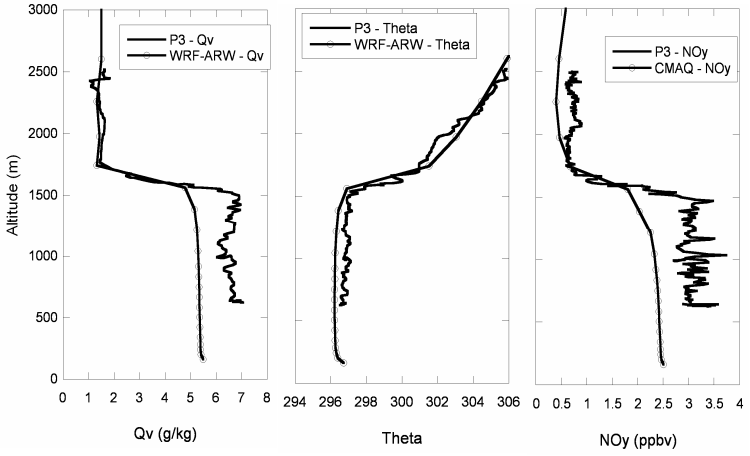


**Fig. 2.** Modeled and observed profiles from P3 spiral at 19 UTC on 9/25/2006

## 5. Next Steps

New CMAQ runs that include the special Texas emissions inventory and a 4 km horizontal nested grid domain centered on Houston are underway. Meteorology and chemistry model results will be compared to all of the P3 flight measurements with particular emphasis on the vertical spirals. Balloon data and aircraft lidar data will also be used to evaluate the vertical structure of meteorological and chemical fields**.**

**Dislaimer** Although this paper has been reviewed by EPA and approved for publication, it does not necessarily reflect EPA's policies or views.

## References

Bianco, L., J. M. Wilczak, and A. B. White, 2008, Convective Boundary Layer Depth estimation from wind profilers: Statistical comparison between an automated algorithm and expert estimations, J. Atmos. Occean. Tech., 25, 1397–1413.

Gilliam, R.C. and J.E. Pleim, 2009: An evaluation of the Pleim-Xiu land surface model, surface-layer and asymmetric convective model in version 3.0 of WRF ARW. J. Appl. Meteor. Climatol, in press.

Pleim, J.E., 2007a: A Combined Local and Nonlocal Closure Model for the Atmospheric Boundary Layer. Part I: Model Description and Testing. J. Appl. Meteor. Climatol., 46, 1383–1395.

Pleim, J.E., 2007b: A Combined Local and Nonlocal Closure Model for the Atmospheric Boundary Layer. Part II: Application and Evaluation in a Mesoscale Meteorological Model. J. Appl. Meteor. Climatol., 46, 1396–1409.

# 1.9 The Impact of MM5 and WRF Meteorology over Complex Terrain on CHIMERE Model Calculations

**A. de Meij[1], A. Gzella[1], C. Cuvelier[1], P. Thunis[1], B. Bessagnet[2], J.F. Vinuesa[1], L. Menut[3], and H. Kelder[4]**

[1]European Commission – DG Joint Research Centre, Institute for Environment and Sustainability, I-21020 Ispra, Italy

[2]INERIS, Institut National de l'Environnement industriel et des Risques, Parc Technologique ALATA, F-60550 Verneuil-en-Halatte, France

[3]Laboratoire de Météorologie Dynamique, Institut Pierre-Simon Laplace, Ecole Polytechnique, Palaiseau, France

[4]Department of Applied Physics, Eindhoven University of Technology, Eindhoven, The Netherlands

**Abstract** The objective of this study is to evaluate the impact of meteorological input data on calculated gas and aerosol concentrations. We use two different meteorological models (MM5 and WRF) together with the chemistry transport model CHIMERE. We focus on the Po valley area (Italy) for January and June 2005.

Firstly we evaluate the meteorological parameters with observations. The analysis shows that the performance of both models in calculating surface parameters is similar, however differences are still observed.

Secondly, we analyze the impact of using MM5 and WRF on calculated PM10 and $O_3$ concentrations. In general CHIMERE/MM5 and CHIMERE/WRF underestimate the PM10 concentrations for January. The difference in PM10 concentrations for January between CHIMERE/MM5 and CHIMERE/WRF is around a factor 1.6 (PM10 higher for CHIMERE/MM5). This difference and the larger underestimation in PM10 concentrations by CHIMERE/WRF are related to the differences in heat fluxes and the resulting PBL heights calculated by WRF.

**Keywords** MM5, WRF, meteorology, aerosol, sensitivity analysis, chemical transport model.

## 1. Introduction

Aerosols play an important role in health effects (respiratory and cardiovascular disease, Moshammer and Neuberger, 2003), pollution, eutrophication / acidification

D.G. Steyn and S.T. Rao (eds.), *Air Pollution Modeling and Its Application XX*,
DOI 10.1007/978-90-481-3812-8, © Springer Science + Business Media B.V. 2010

of aquatic and terrestrial ecosystems and radiative forcing (absorbing and scattering of solar radiation, Kaufman et al., 2002). The CTMs are used to assess the effects of future changes in gas, aerosol and aerosol precursor emissions and to study the impact of source pollutants on air quality elsewhere. Uncertainties in the emission inventories (De Meij et al., 2006), aerosol dynamics, meteorological factors, the impact of horizontal resolution of meteorology on model calculations (Menut et al., 2005) and the fact that the formation of aerosols are known to be nonlinearly dependent on meteorological parameters (Haywood and Ramaswamy, 1998), all contribute to uncertainties in the calculated gas and aerosol concentrations. A good estimate of meteorological variables in the meteorological datasets is therefore crucial for calculating gas and aerosol impacts on air quality and climate change, and evaluating coherent reduction strategies. The objective of this study is to evaluate the impact of meteorological input data on calculated gas and aerosol concentrations. We use two different meteorological models (MM5 and WRF) together with the chemistry transport model CHIMERE. We focus on the Po valley area (Italy) for January and June 2005.

## 2. Method

The CHIMERE model (Bessagnet et al., 2004) is used to simulate air quality over the Po valley area for January and June 2005 based on the meteorological data sets provided by MM5 and WRF. We start our study by evaluating the meteorological parameters T, RH, wind direction and wind speed by comparing them with meteorological observations for the year 2005. Then we evaluate the calculated aerosol (PM10) and ozone ($O_3$) concentrations, using the CHIMERE model with MM5 and WRF results as input data, by comparing the model calculated concentrations with measurements.

## 3. Results

Summarizing the analysis of the annual averaged statistics shows that the Ts are mainly underestimated (less by WRF) and RHs are in general overestimated by WRF and underestimated by MM5. WRF output follows better the hourly pattern of RH. The Po valley is characterized by low wind speeds, which makes it difficult to simulate the wind field with the prognostic meteorological models. This has been confirmed with our study. The wind speed is overestimated by both models. Both models reproduce well the prevailing wind direction. The rainfall is in general overestimated however the MM5 output shows lower rainfall values. The hit rate statistics are in general better for WRF.

In Fig. 1 we compare the potential temperature gradient (ptg) profile between 10 and 200 m at the hours 0.00, 06.00, 12.00 and 18.00 h for the whole year.

Positive values indicate that the atmospheric layer between 10 and 200 m is stable, negative values indicates that the layer is unstable, values around 0 indicates neutral conditions of this layer (Stull 1988). We see that the ptg profile by MM5 and WRF is in good agreement with the observations. In general the potential temperature gradient by WRF is better than by MM5.

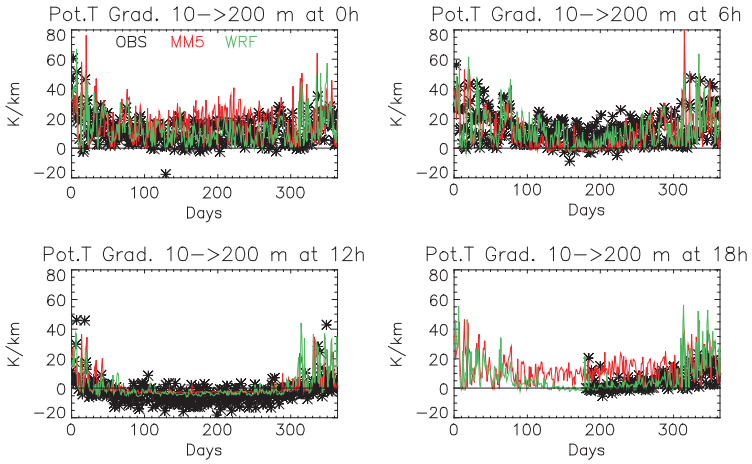


**Fig. 1.** Vertical potential temperature gradient profiles between 10 and 200 m by WRF, MM5 for the Linate airport, together with the observations for 0.00, 06.00, 12.00 and 18.00 h for the whole year

Secondly, we analyze the impact of using MM5 and WRF on calculated PM10 and $O_3$ concentrations. In general CHIMERE/MM5 and CHIMERE/WRF underestimate the PM10 concentrations for January. The difference in PM10 concentrations for January between CHIMERE/MM5 and CHIMERE/WRF is around a factor 1.6 (PM10 higher for CHIMERE/MM5), see Fig. 2. This difference and the larger underestimation in PM10 concentrations by CHIMERE/WRF are related to the differences in heat fluxes and the resulting PBL heights calculated by WRF. In general the PBL height by WRF meteorology is a factor 2.8 higher at noon in January than calculated by MM5. This study showed that the difference in microphysics scheme has an impact on the profile of cloud liquid water (CLW) calculated by the meteorological driver and therefore on the production of $SO_4$ aerosol.

A sensitivity analysis shows that changing the Noah Land Surface Model (LSM) for the 5-layer soil temperature model, the calculated monthly mean PM10 concentrations increase by 30%, due to the change in the heat fluxes and the resulting PBL heights, see Fig. 2c. For June, PM10 calculated concentrations by CHIMERE/MM5 and CHIMERE/WRF are similar and agree with the observations. Calculated $O_3$ values for June are in general overestimated by a factor 1.3 by CHIMERE/MM5 and CHIMRE/WRF.

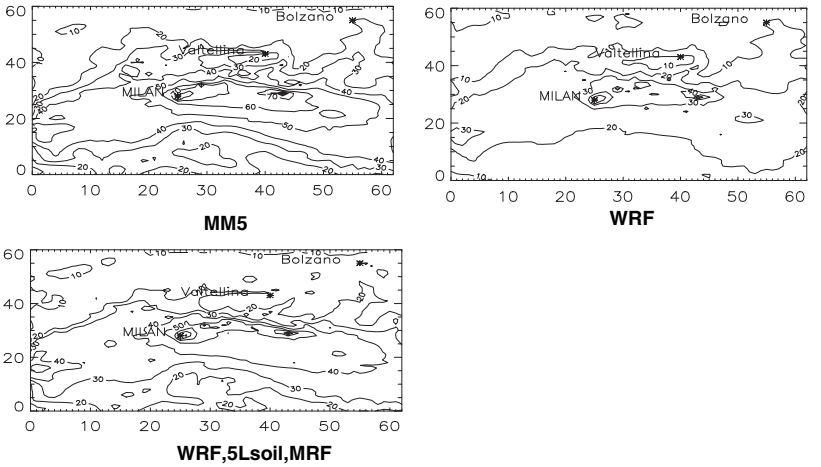


**Fig. 2.** Monthly mean PM10 concentrations for January by CHIMERE using the MM5 meteorology (a), WRF meteorology (b) and WRF meteorology using the five-layer soil temperature model + MRF PBL scheme (c)

## 4. Conclusions

The difference in PM10 concentrations for January between CHIMERE/MM5 and CHIMERE/WRF is around a factor 1.6 (PM10 higher for CHIMERE/MM5). This difference and the larger underestimation in PM10 concentrations by CHIMERE/WRF are related to the differences in heat fluxes and the resulting PBL heights calculated by WRF. In general the PBL height by WRF meteorology is a factor 2.8 higher at noon in January than calculated by MM5, which affect the vertical mixing of the aerosols. Changing the Noah LSM scheme in our WRF pre-processing for the 5-layer soil temperature model, calculated PM10 concentrations for January 2005 increase by 30% with respect to the simulation using Noah LSM. This study also showed that the difference in microphysics scheme has an impact on the profile of cloud liquid water (CLW) calculated by the meteorological driver and therefore on the production and removal of $SO_4^=$ aerosol. For June the differences in PM10 (and $O_3$) concentrations between the model simulations using MM5 and WRF are small.

## References

Bessagnet, B., Hodzic, A., Vautard, R., Beekman, M., Cheinet, S., Honeré, C., Liousse, C., Rouil, L., Aerosol modeling with CHIMERE – preliminary evaluation at the continental scale, Atmos. Environ., 38, 2004.

De Meij, A., Krol, M., Dentener, F., Vignati, E., Cuvelier, C., and Thunis, P., The sensitivity of aerosol in Europe to two different emission inventories and temporal distribution of emissions, Atmos. Chem. Phys., 6, 4287–4309, 2006.

Haywood, J.M., Ramaswamy, V., Global sensitivity studies of the direct radiative forcing due to anthropogenic sulfate and black carbon aerosols. J. Geophys. Res. 103, 6043–6058, 1998.

Kaufman, Y.J., Tanré, D., and Boucher, O., A satellite view of aerosols in the climate system, Nature, Vol. 419, 12 September 2002.

Menut L., I. Coll and S. Cautenet, Impact of meteorological data resolution on the forecasted ozone concentrations during the ESCOMPTE IOP 2a and 2b, Atmospheric Research - ESCOMPTE Special Issue, 74, 139–159, 2005.

Moshammer, H., Neuberger, M., The active surface of suspended particles as a predictor of lung function and pulmonary symptoms in Austrian school children. Atmos. Environ., 37, 1737–1744, 2003.

Stull, R., An Introduction to Boundary Layer Meteorology, Kluwer Academic Publishers, 1988.

## 5. Questions and Answers

**Sven-Erik Gryning:** The measurements did have a different wind rose than the model locations. The measurements represent local conditions only and model results a representation of the grid average. At low wind speeds for an area as Varese, the wind characteristics can be expected to very geographically and the meteorological stations will represent local conditions only.

**Answer:** It is very true that the modeled calculated meteorological parameters represent the average of a grid cell (5 × 5 km in this study) and that the meteorological measurements represents the reality of that location and time. However, when the observations are influenced by tunneling effects (buildings) and large trees, one can should be careful in using this data for model comparisons. The wind roses presented in the presentation for Ispra are taken from two measurement stations at the Joint Research Centre premises (300 m distant) and show complete different results. One set of data was clearly influenced by the tunneling effects and was therefore not representative for the area and not useful for model comparison.

**S. Andreani-Aksoyoglu:** Are PM10 results with CHIMERE/MM5 always higher than CHIMERE/WRF in January, when you look at individual days?

**Answer:** Yes, however the differences for other days is around a factor 1.3. The monthly mean difference between CHIMERE/MM5 and CHIMERE/WRF is higher (1.6), because between 14 and 18 January much more NO3- aerosol by MM5 is formed due to the lack of cloud liquid water, which causes higher peak of NO3- than by WRF.

**Peter Builtjes:** Is the conclusion valid that for this case the combination CHIMERE/MM5 is superior to the combination CHIMERE/WRF?

**Answer:** Yes, for the calculated aerosol concentrations CHIMERE/MM5 is showing a better agreement with the observations than CHIMERE/WRF. However, for the meteorological parameters calculated by MM5 and WRF (T, RH, precipitation, wind speed and wind direction), we see a slightly better agreement with the observations for WRF.

# 1.10 New Boundary Conditions for Positive and Negative Skewed Turbulence in Fluctuating Plume Models

**Luca Mortarini[1], Enrico Ferrero[2], and Pasquale Franzese[3]**

[1]Institute of Atmospheric Sciences and Climate, CNR, 10100 Torino, Italy

[2]Dipartimento di Scienze e Tecnologie Avanzate, Università del Piemonte Orientale, Alessandria, 15100, Italy

[3]Center for Earth Observing and Space Research, George Mason University, Fairfax, VA, 22030, USA

**Abstract** An analytical function is found and is used as boundary condition for the barycentre trajectories in a fluctuating plume model. The skewness profile in the fluctuating plume model is accounted for at two levels: in the reflections at the boundaries and in the concentration PDF relative to the centroid position. The model is tested in convective (positively skewed) and canopy (negatively skewed) turbulence. The mean and fluctuations of the concentration field in canopy turbulence are compared to experimental data showing the important improvements determined by the inclusion of the skewness effects close to the ground.

**Keywords** Lagrangian stochastic model, Fluctuating plume, Meandering, Relative dispersion, Concentration fluctuations, Canopy flow

## 1. Introduction

The fluctuating plume model is especially suited for simulating the concentration field statistics in the planetary boundary layer with its large-scale turbulent motions.

The model derives from Gifford's (1959) meandering plume model, where turbulent dispersion is partitioned into meandering motion and relative-diffusion components. Yee and Wilson (2000) added in-plume fluctuations by parameterizing the relative concentration using a Gamma PDF. Luhar et al. (2000), Franzese (2003), and Mortarini et al. (2009) extended the model to non-homogenous conditions in convective and plant canopy boundary layers using Lagrangian stochastic models to simulate the plume barycenter trajectories.

D.G. Steyn and S.T. Rao (eds.), *Air Pollution Modeling and Its Application XX*,
DOI 10.1007/978-90-481-3812-8, 

Within a Lagrangian particle modeling framework, the behavior of the model close to the boundaries and the correct estimation of the skewness of the velocity field are of crucial importance to predict the concentration field close to the ground (Dosio and Vilà-Guerau de Arellano, 2006). For instance, it is well known that perfect reflection at the boundaries cannot be applied in non-Gaussian turbulence, as the well-mixed condition requires that the distribution of particle velocities crossing any level in a fixed time interval must be preserved. Thomson and Montgomery (1994) proposed an exact solution for the case of positive turbu lent velocity skewness observed in the convective boundary layer. Dosio and Vilà-Guerau de Arellano (2006), and Mortarini et al. (2009) found that the skewness of the relative mean concentration PDF is important to correctly predict the concentration field inside the canopy. Recently, Gailis et al. (2007) provided useful parameterizations for fluctuating plume models inside a canopy, and suggested a new analytical form for the relative intensity of concentration fluctuations.

We will analyze the influence of boundary conditions and skewness of the particle relative mean distribution on a fluctuating plume model and a new reflection condition which avoids over-estimation of the centroid PDF close to the ground will be derived.

## 2. The Fluctuating Plume Model

The fluctuating plume model is based on the idea that absolute dispersion can be divided in two different components: dispersion of the barycenter of the plume and relative dispersion of the plume around its barycenter. The concentration moments can be expressed as (Franzese, 2003):

$$\left\langle c^n \right\rangle = \int \left\langle c_r^n \right\rangle p_m dz_m \tag{1}$$

where $p_m$ is the barycentre PDF and $\left\langle c_r^n \right\rangle$ are the concentration moments relative to the centroid position. Equation 1 is derived by writing the concentration PDF, $p\left(c|x,z\right)$, as the product of the barycentre position PDF, $p_m\left(z,z_m\right)$, and the PDF of concentration relative to $z_m$, $p_{cr}\left(c|x,z,z_m\right)$, and using the definition $\left\langle c_r^n \right\rangle = \int c^n p_{cr}\left(c|x,z,z_m\right)dc$, where $x$ is the downwind distance, $z$ is the vertical coordinate, and the subscript $m$ refers to the barycentre. We use a Lagrangian stochastich model to predict $p_m\left(z,z_m\right)$ and we parametrise $p_{cr}\left(c|x,z,z_m\right)$.

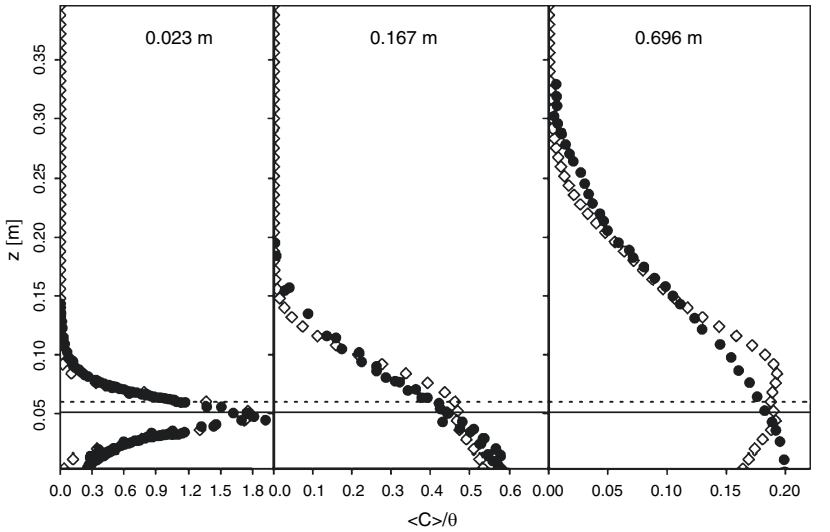


**Fig. 1.** Normalized mean concentration. Black points, Coppin et al. (1986) data. Diamonds, model results. The number at the top of each plot refers to the distance from the source

## 3. The Lagrangian Stochastic Model

We assume that the evolution of the centroid velocity is a Markov process (Luhar et al., 2000), hence the plume meandering motion can be described by:

$$\begin{aligned} dx_m &= U(z_m)dt \\ dz_m &= w_m dt \\ dw_m &= a_m(t,w_m,z_m)dt + b_m(t,z_m)dW(t) \end{aligned} \tag{2}$$

where $U(z_m)$ is the mean wind vertical profile. The Langevin equation diffusion parameter $b_m = \sqrt{2\langle w_m^2 \rangle / T_m}$, where $T_m$ is the Lagrangian time-scale. The drift coefficient $a_m$ can be derived using a quadratic functional form (Franzese, 2003; Mortarini et al., 2009):

$$a_m = \mathrm{A}_m w_m^2 + \mathrm{B}_m w_m + \Delta_m \tag{3}$$

with $\mathrm{A}_m$, $\mathrm{B}_m$ and $\Delta_m$ depending on the first fourth moments of the velocity PDF. An energy filter based on the partition of the turbulent kinetik energy is

applied to extract, from the measured data, only the length-scales involved in the meandering motion.

When the distance between centroid vertical position and a boundary is smaller than the characteristic radius of the plume bulk, the barycentre is reflected. Franzese (2003) and Mortarini et al. (2009) used perfect reflection, in this work, not to over-estimate the centroid PDF near the ground, we extend the Thomson and Montgomery (1994) boundary conditions to negative skewness, typical of canopy flows. In good agreement with the results of Anfossi et al. (1997) in convective turbulence, our numerical integration of the velocity PDF shows that the reflected barycentre velocity is a function of the incident velocity and of the velocity skewness. Thus an analytical function is found and is used as boundary condition for the barycentre trajectories.

## 4. The PDF of Concentration in the Relative Frame

Yee et al. (1994) proposed the following form for $p_{cr}$, which has been used in several other studies (e.g., Yee and Wilson, 2000; Luhar et al., 2000; Dosio and Vilà-Guerau de Arellano, 2006; Gailis et al., 2007; Mortarini et al., 2009):

$$p_{cr}\left(c|z,z_m\right)=\frac{c^{\alpha-1}}{\Gamma(\alpha)\beta^{\alpha}}\exp\left(-\frac{c}{\beta}\right) \tag{4}$$

with $\alpha=1/i_r^2$ and $\beta=\langle c_r\rangle/\alpha$, where $\langle c_r\rangle$ is the mean concentration in the relative frame and $i_r$ the intensity of concentration fluctuations. Substituting Eq. 4 in the definition of $\langle c_r^n\rangle$ gives:

$$\langle c_r^n\rangle=\frac{\Gamma(n+\alpha)}{\Gamma(\alpha)}\beta^{\alpha}\langle c_r\rangle \tag{5}$$

and finally substituting Eq. 5 in Eq. 1:

$$\langle c^n\rangle=\frac{\Gamma(n+\alpha)}{\Gamma(\alpha)}\beta^{\alpha}\int_0^H\langle c_r^n\rangle p_m dz_m \tag{6}$$

Providing a functional form that express $\alpha$ and $\beta$ as functions of the mean concentration and intensity of concentration fluctuations in the relative frame, the fluctuating plume model is able to reproduce all the concentration moments. A simple parametrisation of $i_r$ has been given by Gailis et al. (2007):

$$i_r^2 = (1 + i_{r0}^2)\left(\frac{\langle c_r \rangle}{\langle c_{r0} \rangle}\right)^{-\xi} - 1 \tag{7}$$

where $i_{r0}$ and $\langle c_{r0} \rangle$ are the plume centerline values and $0 < \xi < 1$.

We use a skewed PDF obtained as the sum of two reflected Gaussians for $\langle c_r \rangle$ (Luhar et al., 2000):

$$\langle c_r \rangle = \frac{Q}{U} \sum_{j=1}^{2} \sum_{n=-N}^{N} \frac{a_j}{\sqrt{2\pi}\sigma_j} \left( e^{-\frac{\left(z - z_m + 2nz_i - \bar{z}_j\right)^2}{2\sigma_j^2}} + e^{-\frac{\left(-z - z_m + 2nz_i - \bar{z}_j\right)^2}{2\sigma_j^2}} \right) \tag{8}$$

where $a_j$, $\sigma_j$, $\bar{z}_j$ depend on the skewness of the vertical relative coordinate.

## 5. Results

Figures 1 and 2 show the first two moments of the concentration field evaluated by the fluctuating plume model compared with the measurements by Coppin et al. (1986) in a simulated plant canopy.

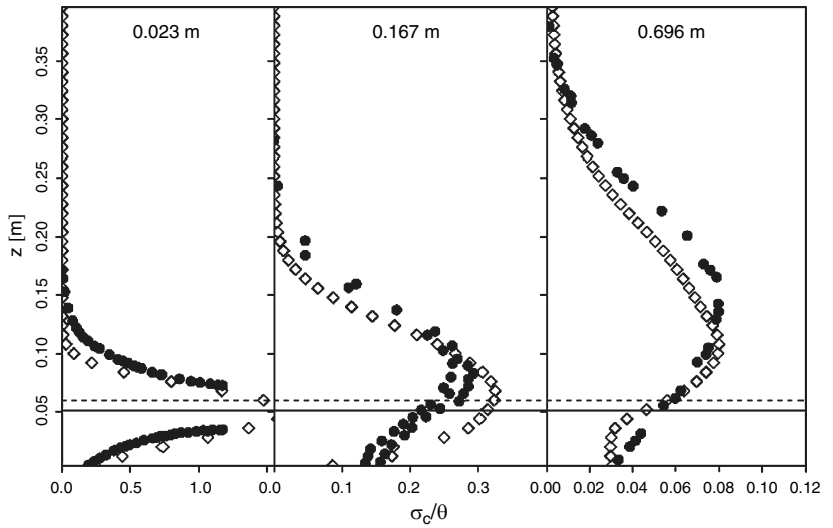


**Fig. 2.** Normalized concentration fluctuations. Black points, Coppin et al. (1986) data. Diamonds, model results. The number at the top of each plot refers to the distance from the source

## References

Coppin, P., Raupach, M., Legg, B., 1986. Experiments on scalar dispersion within a plant canopy, part II: the turbulence structure. Boundary-Layer Meteorol. 35, 167–191.

Dosio, A., Vila`-Guerau de Arellano, J., April 2006. Statistics of absolute and relative dispersion in the atmospheric convective boundary layer: a large-eddy simulation study. J. Atmos. Sci. 63(4), 1253–1272.

Franzese, P., 2003. Lagrangian stochastic modeling of a fluctuating plume in the convective boundary layer. Atmos. Environ. 37, 1691–1701.

Gailis, R.M., Hill, A., Yee, E., Hilderman, T., 2007. Extension of a fluctuating plume model of tracer dispersion to a sheared boundary layer and to a large array of obstacles. Boundary-Layer Meteorol. 122, 577–607.

Gifford, F.,1959. Statistical properties of a fluctuating plume dispersion model. Adv. Geophys. 6, 117–137.

Luhar, A., Hibberd, M., Borgas, M., 2000. A skewed meandering-plume model for concentration statistics in the convective boundary layer. Atmos. Environ. 34, 3599–3616.

Mortarini, L., Franzese, P., Ferrero, E., 2009. A fluctuating plume model for concentration fluctuations in a plant canopy. Atmos. Environ. 43, 921–927.

Thomson, D.J., 1987. Criteria for the selection of stochastic models of particle trajectories in turbulent flows. J. Fluid Mech. 180, 529–556.

Yee, E., Chan, R., Kosteniuk, P.R., Chandler, G.M., Biltoft, C.A., Bowers, J.F., 1994. Incorporation of internal fluctuations in a meandering plume model of concentration fluctuations. Boundary-Layer Meteorol. 67, 11–39.

Yee, E., Wilson, D.J., 2000. A comparison of the detailed structure in dispersing tracer plumes measured in grid-generated turbulence with a meandering plume model incorporating internal fluctuations. Boundary-Layer Meteorol. 94, 253–296.

# 1.11 Novel Mesh Adaptive LES Simulations for Multi-Scale Atmospheric Flows: Application to the Urban Environment

**D. Pavlidis[1], J.L.M.A. Gomes[1], G.J. Gorman[1], E. Aristodemou[1], C.C. Pain[1], H. ApSimon[2], and A.G. Robins[3]**

[1]Applied Modelling and Computation Group, Dept. Earth Science and Engineering, Imperial College London

[2]Centre for Environmental Policy, Imperial College London

[3]Fluids Research Centre, School of Engineering, University of Surrey

## 1. Introduction

Effective air quality management necessitates the implementation and validation of multi-scale models that are able to capture adequate spatial and temporal variability of urban pollution dispersion patterns. A new LES approach is implemented in a general purpose CFD model (Fluidity) with anisotropic mesh adaptivity for simulating turbulent airflows within complex urban environments. The model is compared to field and wind tunnel data considering a passive tracer dispersion scenario.

## 2. Methodology

Fluidity is capable of numerically solving the Navier-Stokes and accompanying field equations on arbitrary unstructured finite element meshes (Mansoorzadeh et al., 1998). It uses a moving finite element/spectral element methods which allow arbitrary movement of the mesh with time dependent problems (Pain et al., 2001). The LES model used to calculate the eddy viscosity is a variation of the Smagorinsky model developed by (Bentham, 2003). The advantage of the SGS model used here over the original Smagorinsky model is that the length-scale is related directly to the local length-scale of the flow, and is allowed to vary in space and direction, rather than being fixed and predetermined. For the generation of turbulent inlet boundary conditions the method described and validated in (Pavlidis et al., 2009) is used. It is based upon the view of turbulence as a superposition of

D.G. Steyn and S.T. Rao (eds.), *Air Pollution Modeling and Its Application XX*,
DOI 10.1007/978-90-481-3812-8, © Springer Science + Business Media B.V. 2010

coherent structures and is able to reproduce prescribed first and secondary order one point statistics and turbulence length-scales. The overall performance of the model used to simulate turbulent wall bounded flows has been evaluated using a channel flow numerical simulation and a flow past a bluff body physical simulation (see Pavlidis et al., 2009). Transport of pollutant concentrations is determined by a high resolution method, which is globally high order accurate in space and time.

## 3. Results

The area of study is the intersection of Marylebone Rd. and Gloucester Place, in Central London, UK. A large number of field and wind tunnel experiments (scale 1/200) have been undertaken for this site for the DAPPLE project (Arnold et al., 2004). The area of interest is 800 × 600 m² and includes 48 buildings. Available data include mean and turbulent quantities of flow and concentration from a number of tracer releases for a number of receptors. At low ambient wind speeds (~3 m/s at average roof-top height) the wind tunnel data deviate from the field data. In this study this low ambient wind speed scenario is reproduced numerically. The simulation models the dispersion of a 15 min release of a passive tracer from a fixed source for 30 min.

A schematic of the area under study along with the mean flow direction, the tracer source and receptors locations considered are given in Fig. 1. The lateral and vertical extents of the computational domain have been kept identical to those of the wind tunnel leading to a 200 m deep boundary layer. An anisotropic adaptive mesh with a maximum of 750,000 nodes is used. The mesh is adapted every 15 time-steps. For the generation of realistic inflow boundary conditions the synthetic eddy method (Pavlidis et al., 2009) is employed, the inflow plane is placed two boundary layer depths upwind of the built-up area to allow the flow to develop. Data used to prescribe the inlet boundary conditions come from the wind tunnel. No-slip boundary conditions are applied on all solid walls. An adaptive time-stepping scheme is employed to satisfy a CFL number equal to four. A snapshot of the surface mesh and tracer concentration at the end of the simulation (30 min) is shown in Fig. 3.

Comparison of total normalized (with velocity at roof-top height, $\boldsymbol{U}$, roof-top height, $\boldsymbol{H}$, and emission rate, $\boldsymbol{Q}$) concentration, at the sampling points between field, two (identical) physical model simulations and Fluidity is given in Fig. 2. Note that there are no data for receptor R2 for the field and receptor R3 for Fluidity. It is evident that the wind tunnel tends to over-predict the concentrations, while Fluidity is closer to the field data.

In particular, the solution obtained from the receptor at roof-top height (R5) agrees with field data, while one of the wind tunnel simulations is very close as

well. For receptors within the canopy numerical data slightly under-predict but in principal follow the same trend as the field data. On the other hand wind tunnel data present two peaks at receptors R3 and R6. All models present a peak at receptor R10. This is due to the fact that the modeled flow is over-estimated at that region because of no upwind blockage. Other discrepancies within the canopy could be associated with the absence of traffic induced turbulence which can dominate local flow patterns at these low ambient wind speed conditions. For this reason a two-fluid approach has been adopted to account for traffic induced turbulence. The model is able to explicitly model individual vehicles whose movement is controlled by a traffic micro-simulation code.

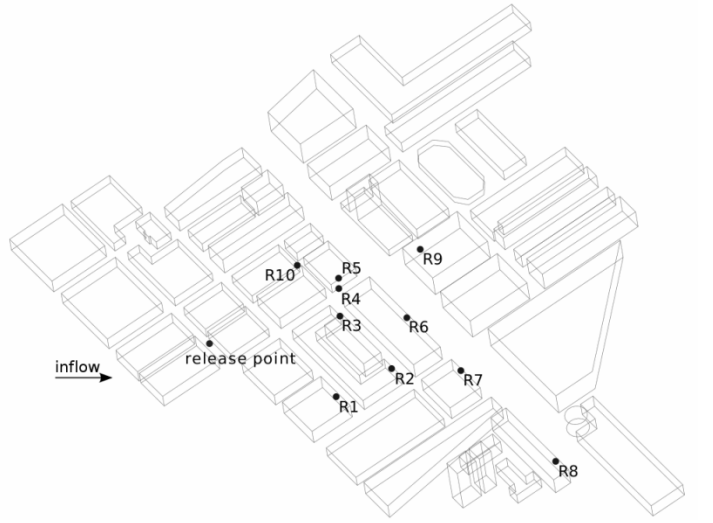


**Fig. 1.** Schematic of the computational domain, including the tracer source and receptor locations. Note: release point and all receptors are placed at ~1.8 m above ground level, except for R5 which is placed at roof-top

## 4. Conclusions

A novel LES method with anisotropic mesh adaptivity is implemented and compared against field and physical model data. Results are comparable to field data (5–10% error). Discrepancies are considered to have originated mainly from the lack of traffic induced turbulence. Future work includes simulating the same problem including traffic induced turbulence.

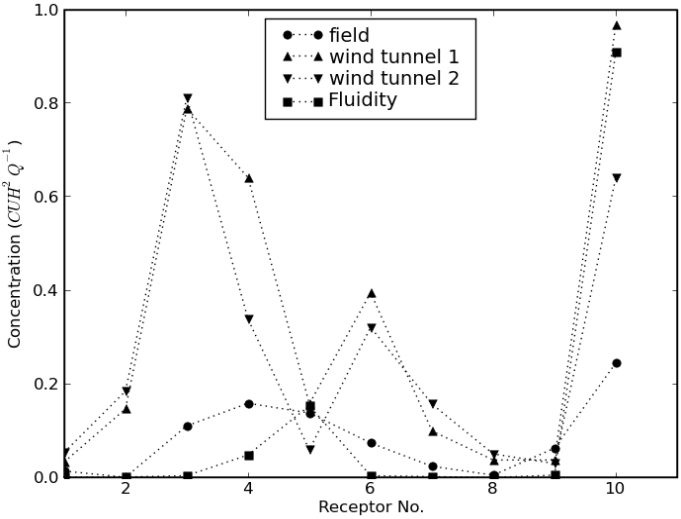


**Fig. 2.** Comparison of total normalised concentrations between field, two wind tunnel and Fluidity data for ten receptors, receptor R2 data for field and receptor R3 data for Fluidity are not available

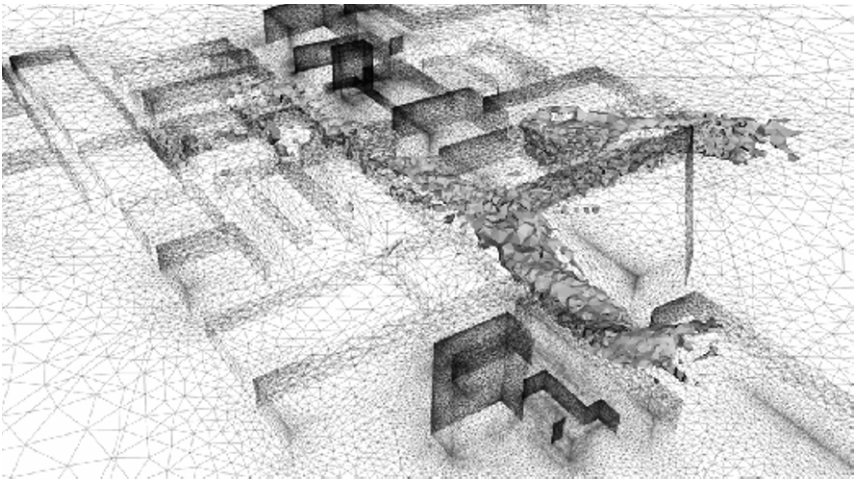

**Fig. 3.** Instantaneous mesh and normalized concentration iso-surface ($\boldsymbol{C}$ = 3.e-5) at the end of the simulation (30 min)

## References

Arnold, S. J., et al. 2004. Introduction to the DAPPLE Air Pollution Project. *Science of The Total Environment.* 2004, Vol. 332, pp. 139–153.

Bentham, T. 2003. Microscale modelling of air flow and pollutant dispersion in the urban environment. *Imperial College London Thesis.* 2003.

Mansoorzadeh, S., et al. 1998. Finite element simulations of incompressible flow past a heated/cooled sphere. *International Journal for Numerical Methods in Fluids.* 1998, Vol. 28, pp. 903–915.

Pain, C. C., et al. 2001. Tetrahedral mesh optimisation and adaptivity for steady-state for transient finite element calculations. *Computer methods in applied mechanics and engineering.* 2001, Vol. 190, pp. 3771–3796.

Pavlidis, D., et al. 2009. Synthetic Eddy Method for Regional Atmospheric Flows. *Boundary Layer Meteorology.* 2009, Vol. In preparation.

## 5. Questions and Answers

**Question:** One feature of your model is to include traffic induced turbulence. For very busy roads the traffic is not steady, but stops and starts in a complex way. Can this be included in your model?

**Answer:** Yes, it can be and it is included. Traffic induced turbulence is modeled through a two-fluid approach. Individual vehicles are explicitly modeled. Their movement is controlled by a traffic micro-simulation model. An interface between Fluidity and PTV-VISSIM has been built. Depending on the scenario considered each time, the traffic can be steady or, complex and vehicle clustering is evident.

**Question:** The title of your presentation was LES but you conclude that you presented a CFD model. The difference in the naming is not clear since LES and CFD are not always the same. (Tamir Reisin)

**Answser:** LES is just a closure technique for high Reynolds number flows for the Navier-Stokes equations. LES is a CFD method.

**Question:** Please clarify whether you have been using a RANS-CFD or an LES approach for your study. (Silvia Trini Castelli)

**Answer:** I have been using LES. As I mentioned earlier, LES is a scheme for efficiently solving the Navier-Stokes equations for turbulent flows, thus the LES method is a CFD method.

# 1.12 High-Resolution Air-Quality Modelling of the Windsor-Detroit Area Using Two Models: Comparisons to BAQSMet Data

**P.A. Makar[1], J. Zhang[1], W. Gong[1], M.D. Moran[1], C. Stroud[1], S. Gong[1], S. Gravel[1], J. Brook[1], K. Hayden[1], C. Mihele[1], S. Ménard[2], D. Talbot[2], H. Landry[1], M. Sassi[2], A. Kallaur[3], D. Sills[4], J. Abbatt[5], and J. Slowik[5]**

[1]Air Quality Research Division, Environment Canada, Toronto, ON, Canada, paul.makar@ec.gc.ca

[2]Air Quality Modelling Applications Section, Environment Canada, Montreal, QC, Canada

[3]Air Quality Research Division, Environment Canada, Montreal, QC, Canada

[4]Meteorological Research Division, Environment Canada, Toronto, ON, Canada

[5]Chemistry Department, University of Toronto, Toronto, ON, Canada

The Border Air-Quality Study and Meteorology Study (BAQS-Met) was conducted in the region between Lakes Huron, St. Clair, and Erie, with the aim of studying the impact of lake breezes on local air-quality and long-range-transported chemistry. The study comprised a measurement-intensive field campaign from June 22 to July 10, 2007 as well as a local monitoring network that operated from the months of June through August. Aerodyne Aerosol Mass Spectrometers (AMS) were used at two supersites (Bear Creek and Harrow) and on board the NRC Twin Otter aircraft and Environment Canada (EC)'s CRUISER mobile laboratory as part of the study. Also measured aboard the aircraft were $O_3$, CO, $SO_2$, $NO/NO_2$, particle size distribution and number. CRUISER observations also included CO, $O_3$, $SO_2$, $NO/NO_2$, NOy, $CO_2$, selected VOCs, Black Carbon, and particle number.

EC's A Unified Regional Air-Quality Modelling System (AURAMS, cf. Cho et al., 2009; Gong et al., 2006) was used for in-field forecastting, and for subsequent analysis using a three-level nested system (42 km/15 min resolution North American domain driving a 15 km/15 min. Eastern North America hence a 2.5 km/2 min study domain). AURAMS is a 3D gas and speciated/size-resolved (bin approach) regional transport model which makes use of meteorology provided by the 15 and 2.5 km versions of the Global Environment Multiscale (GEM) model (Côté et al., 1998). Each of the AURAMS simulations makes use of a 12 size bin, eight chemical species particulate module (sulphate, nitrate, ammonium, primary organic carbon, secondary organic carbon, elemental carbon, crustal material, sea-salt).

GEM-MACH is a new model being developed at Environment Canada primarily for operational AQ forecasting, following from earlier work with both AURAMS (Gong et al., 2006) and GEM-AQ (Kaminski et al., 2008), incorporating much of the process science of AURAMS "on-line" into GEM. The configuration used

D.G. Steyn and S.T. Rao (eds.), *Air Pollution Modeling and Its Application XX*,
DOI 10.1007/978-90-481-3812-8, 

here was the GEM-MACH North American 15 km/7.5 min forecast grid (GEM-MACH15), with the same eight species as AURAMS but only two bins (fine and coarse modes) in order to maintain computational efficiency. It should be noted that GEM-MACH is currently under development; the model results shown here are taken from an intermediate developmental version of the model (version AGY).

The 42 and 15 km AURAMS simulations were compared to North American monitoring data for hourly $PM_{2.5}$ and $O_3$ (Airnow network) for the 3 months simulated including the simulation period. The 2.5 km AURAMS simulations were compared to detailed observations made during individual flights and CRUISER drives during the measurement intensive.

GEM-MACH15 simulations were compared to monitoring networks for hourly $PM_{2.5}$ and $O_3$ for the time period simulated (see Table 1). The 15 km AURAMS and 15 km GEM-MACH results for $PM_{2.5}$ and $O_3$ give an approximation of the relative performance of the two models (different start and end times were employed for operational reasons, and the extent of the model domains differ). The numbers thus allow a rough comparison of model performance; further work will be required for a more robust comparison.

**Table 1.** Comparison of AURAMS42 km, AURAMS15 km, GEM-MACH15 kmAGY to observations during the BAQS-Met period

| Model | Species | Corr. coeff | Mean bias | RMS error |
|---|---|---|---|---|
| AURAMS-42 km | $O_3/PM_{2.5}$ | 0.47/0.42 | 14.0/–1.0 | 17.5/7.7 |
| AURAMS-15 km | $O_3/PM_{2.5}$ | 0.48/0.57 | 6.7/0.2 | 13.1/8.4 |
| GEM-MACH15 | $O_3/PM_{2.5}$ | 0.61/0.18 | –1.7/0.9 | 13.1/24.8 |

$O_3$ units ppbv, $PM_{2.5}$ units $\mu g/m^3$

GEM-MACH15 performance is better than AURAMS for ozone, with higher correlation coefficient, lower magnitude biases, and the same or lower RMSE. AURAMS has better performance than this version of GEM-MACH15 for $PM_{2.5}$. The latter errors relate to the two-bin approach used in GEM-MACH15; sub-binning was used to improve mass transfer between bins, but further investigation is required to determine the cause of the lower correlation coefficient and higher RMS values in GEM-MACH than in AURAMS15 km.

The Harrow super-site ozone time series (Fig. 1) is in accord with Table 1; the time series show several instances (e.g. 6/10/2007 8:00, 6/11/2007 6:00, 6/13/2007 17:00, 6/18/2007 16:00, 6/20/2007 9:00, 6/20/2007 18:00) where the GEM-MACH maximum or minimum ozone prediction is much closer to observations than that of AURAMS15. A significant GEM-MACH15 over-prediction occurs at 26/0:00 and 26/22:00.

The PM time series at Harrow (Fig. 2) is also in accord with Table 1. $PM_{2.5}$ $SO_4$ is given as an example, and the GEM-MACH values are considerably higher than

the AURAMS15 values, while the latter are close to the observations. The small difference between the AURAMS15 $PM_1$ $SO_4$ and $PM_{2.5}$ $SO_4$ suggests that most of the $PM_{2.5}$ mass is contained within $PM_1$. The GEM-MACH15 $PM_{2.5}$ $SO_4$ is therefore biased high. The reason for the GEM-MACH15 $PM_{2.5}$ $SO_4$ positive biases is currently under investigation and may relate to the simplified size distribution employed in the model. The size distribution of only two bins was employed in GEM-MACH15 due to operational constraints: using a minimum number of size bins is necessary to reduce the cpu-time required to create an operational air-quality forecast.

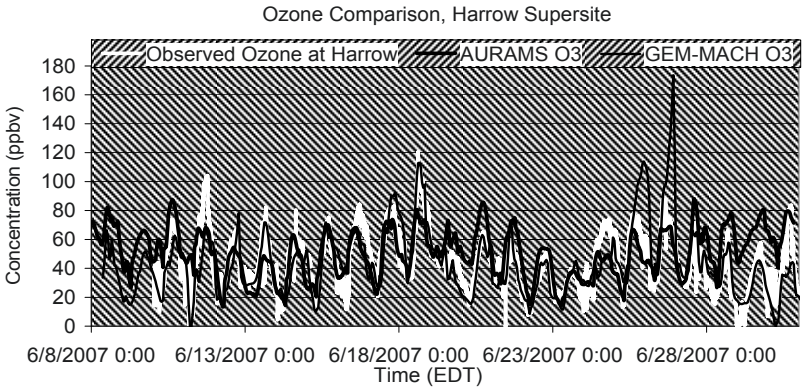


**Fig. 1.** Ozone at Harrow, AURAMS15, GEM-MACH15, Observations

The use of only two bins for the aerosol size distribution can result in errors in mass transfer between bins: too much $PM_{2.5}$ mass can be transferred to $PM_{10}$. Similarly, the two bin size distribution can result in too little mass removal due to settling and deposition of particles. The GEM-MACH15 simulations shown here correct for the inter-bin transfer by temporarily subdividing the two bins to a finer resolution for both particle inter-bin growth/shrinkage, and for deposition/settling.

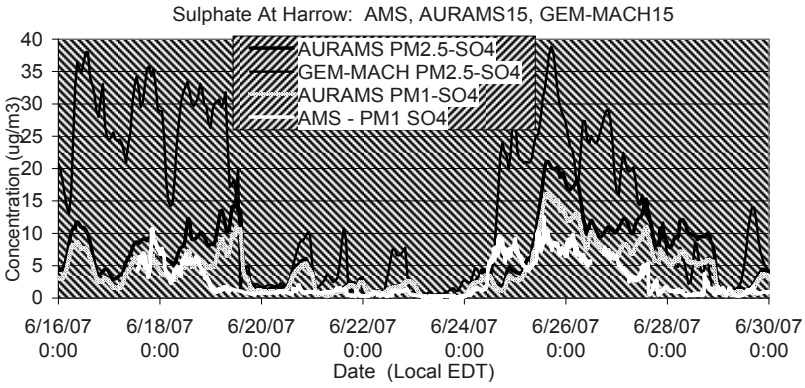


**Fig. 2.** PM-SO4 at Harrow

Figure 3 shows two examples of the AURAMS2.5 km simulations compared to observations. Figure 3a shows a comparison between $NO_2$ predictions and 2 min averaged $NO_2$ observations on board the NRC Twin Otter on July 7. The model captures the timing of three plumes of $NO_2$ observed in the measurement record, associated with major point source emissions in the city of Sarnia. Figure 3b shows a comparison between AURAMS2.5 km $SO_2$ and observations taken aboard the CRUISER mobile laboratory on July 3, while CRUISER was circumnavigating the city of Windsor. The model captures the magnitude of the $SO_2$ plume, but misses some of the fine structure present in the measurement record.

The AURAMS analysis of BAQS-Met and the development of GEM-MACH15 are both on-going projects, and the above results give the state of progress of these projects at the time of writing. Further updates and improvements to both models are underway; updated and revised results will be presented at the NATO-ITM itself. From the work to date, GEM-MACH15 outperforms AURAMS15 for ozone prediction accuracy, while the reverse is true for PM2.5, by correlation coefficient. Current work with GEM-MACH15 is focused on determining the cause of the $PM_{2.5}$ $SO_4$ over-predictions. Both models show a good ability to predict the timing of ozone and PM events.

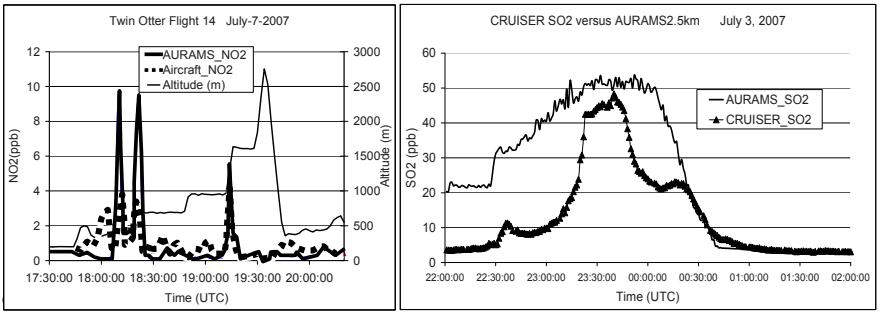


**Fig. 3.** (a): Twin Otter $NO_2$ observations versus AURAMS2.5 km, (b): CRUISER SO2 observations versus AURAMS2.5 km

## References

Cho, S., Makar, P.A., Lee, W.S., Herage, T., Liggio, J., Li, S.-M., Wiens, B., Graham, L., Evaluation of A Unified Regional Air-quality Modeling System (AURAMS) using PrAIRie2005 field study data: the effects of emissions data accuracy on particle sulphate predictions Atmospheric Environment 43 (2009) 1864–1877.

Côté, J., S. Gravel, A. Méthot, A. Patoine, M. Roch, and A. Staniforth, The operational CMC-MRB Global Environmental Multiscale (GEM) model. Part 1: Design considerations and formulation. *Monthly Weather Review*, **126**, 1373–1395 (1998).

Gong, W., A.P. Dastoor, V.S. Bouchet, S.L. Gong, P.A. Makar, M.D. Moran, B. Pabla, S. Menard, L-P. Crevier, S. Cousineau and S. Venkatesh, Cloud processing of gases and aerosols in a regional air quality model (AURAMS), *Atmospheric Research* (82): 248–275, 2006.

Kaminski, J.W., Neary, L., Struzewska, J., McConnell, J.C., Lupu, A., Jarosz, J., Toyota, K., Gong, S.L., Cote, J., Liu, X., Chance, K, Richter, A., GEM-AQ, an on-line global multiscale chemical weather modelling system: Model description and evaluation of gas phase chemistry processes. Atm. Chem. Phys., 8, 3255–3281, 2008.

## Questions and Answers

**S. Andreani-Aksoyoglu:** What is the collection efficiency of the AMS measurements?

**Answer:** About 0.5 (that is, the *raw* AMS data are 0.5 of the correct values). The AMS measurements were compared to laser scattering probes in order to determine the net collection efficiency, with the correction factor of 2 being the recommended change.

# 1.13 A High Resolution Study of Atmospheric Dispersion over a Coastal Urban Area with Complex Terrain

**N. Haikin[1*], Y. Mahrer[2], T.G. Reisin[3], E. Galanti[1], and P. Alpert[1]**

[1]Department of Geophysics and Planetary Science, Tel Aviv University, Israel

[2]The Hebrew University of Jerusalem, Rehovot, Israel

[3]Soreq Nuclear Research Center, Yavne, Israel

**Abstract** High resolution simulations were conducted to address the combined influence of meteorological conditions, topography and pollution sources on air quality. In this study we apply the Regional Atmospheric Modeling System (RAMS) nested down to a resolution of 0.5 km, to analyze the atmospheric behavior over the Haifa Bay Area in Israel. This area is characterized by a complex terrain adjacent to the Mediterranean Sea. Simulations were carried out for a time period of 48 h, and for different synoptic conditions. In order to validate the model performance, a special high resolution radiosonde campaign was conducted and data from ground stations was collected. Results show a fair agreement between the model and ground stations, and similar trends for observed and simulated profiles. However, systematic differences between the model results and the measurements for specific features require further improvements of the simulations.

**Keywords** RAMS, Model validation, complex topography, urban scale

## 1. Introduction

Haifa region in Israel, has an environmental challenging combination of heavy industry located next to a large urban area, all embedded in a coastal complex terrain. Episodes with high levels of air pollution are occasionally monitored by the local network and the occurrence of some of them is difficult to explain. In our study we implement the RAMS model (Pielke et al., 1992) to better understand the 3D atmospheric flow in that region and the air pollution patterns. Due to its complexity, very few modeling works were conducted on that area (Mahrer and Weinroth, 2007), being the present work the one with the highest resolution of

*On Sabbatical leave from Nuclear Research Center Negev, Israel

D.G. Steyn and S.T. Rao (eds.), *Air Pollution Modeling and Its Application XX*,
DOI 10.1007/978-90-481-3812-8, © Springer Science + Business Media B.V. 2010

0.5 km horizontal grid spacing. In this study we consider several typical synoptic conditions for Israel (Alpert et al., 2004; Osetinsky, 2006); a summer case will be discussed in this abstract. On August 2008 a campaign of high resolution upper air measurements was conducted. The purpose of the campaign was to obtain upper air data for validating the model results, along with ground stations data. GPS radiosondes were launched from three sites: two in Haifa Bay and one on Mt Carmel at different hours (up to three times a day). Results of RAMS simulations were compared with these measurements.

## 2. Methodology

The high resolution radiosondes were tracked up to 5,000 m, recording temperature, pressure, relative humidity and wind. Data was averaged over 50 m layers, reducing some noise of the measurements (especially of the wind). RAMS was run with four nested grids (Fig. 1), ranging from the synoptic scale initiated with NCEP reanalysis data, down to the urban scale. The model was tested for several configurations; some of the current results are shown here.

The model results were compared with data from the monitoring network observations of the Israeli Meteorological Service, as well as with observations from Haifa District Municipal Association for the Environment ("Igud") and with the measured high-resolution upper air profiles.

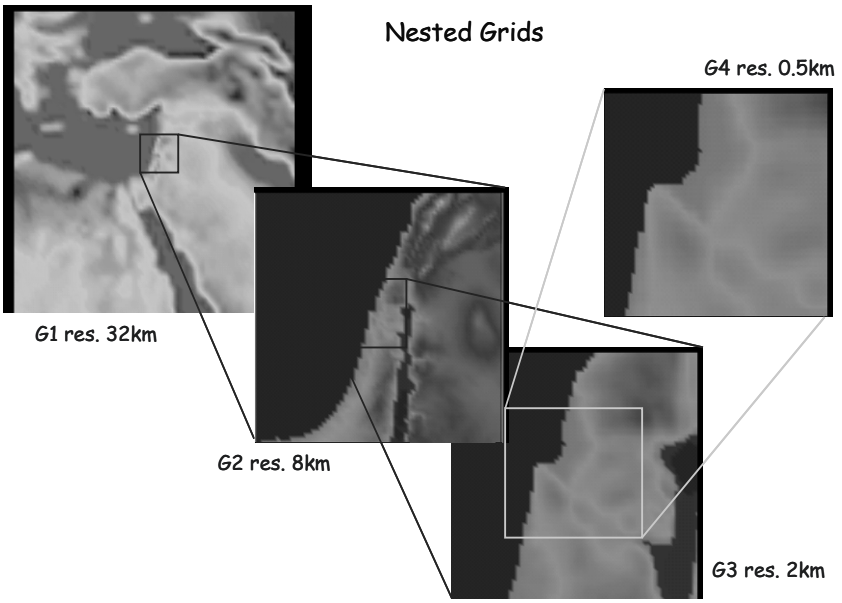


**Fig. 1.** RAMS four nested grids used for the simulations

## 3. Results

Observations from several surface stations were available for the summer campaign. Some of them are located within the inner model domain, thus, we could compare them with more than one grid of the model. "Igud station" (main municipal's station) results are presented in Fig. 2, showing a relatively good agreement for wind speed. However, the model predicted lower temperatures and longer periods of south-east winds at night (probably land breeze) than observed. The reason for this disagreement has still to be elaborated. Both discrepancies seem to be related since southeasterlies at night are associated with cooler air (by about 5–6°C).

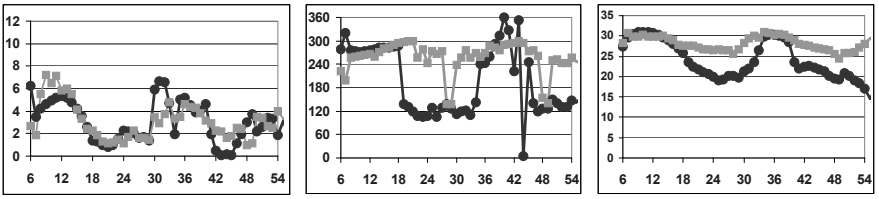


**Fig. 2.** "Igud" station located in Haifa Bay, was one of the launching sites. Model results compared with observations are shown on a 48 h time scale (GMT); wind speed (m/s) (a), wind direction (deg) (b), Temperature (°C) (c); model results in black ● observations in gray ■

Radiosonde profiles showed no ground inversion in the morning, while the model predicted one, as well as cooler temperatures at ground level. The profile demonstrated in Fig. 3 shows a case where the model managed to predict the marine inversion based at about 1,000 m height, though not as strong as the measured one. A higher inversion measured at about 2,400 m was not predicted by the model. This one was probably a subsidence inversion, which did not appear in the NCEP reanalysis used for initializing the model, and the coarse vertical resolution of the model at this height could be another reason for the disagreement. The wind direction profile in Fig. 3 shows a good agreement between the radiosonde and the model up to 2,000 m, while above that height the model and observations depart from each other even higher than 30° which is beyond the noise uncertainty (±30°).

## 4. Summary

Upper air and surface data were collected during a special observation campaign at the Haifa Bay region at the north of Israel. This area is characterized by a complex topography, vicinity to the Mediterranean Sea, heavy industry and periods of high air pollution. The data was used to validate high resolution simulations conducted with the RAMS model. In general, results showed good agreements, suggesting the model calculates realistic fields. However, comparisons in the

above case, of both ground and upper air, show deviations between the model and observations for ground level winds and temperatures in the morning, where the model predicted easterly winds for longer periods along the surface inversion. Further improvements are required, especially at the lower levels before starting the dispersion simulations. Following these improvements, the calculated meteorological fields will be used to drive a dispersion model such as HYPACT. Local air pollution sources and air pollutants monitoring data will be used for that stage.

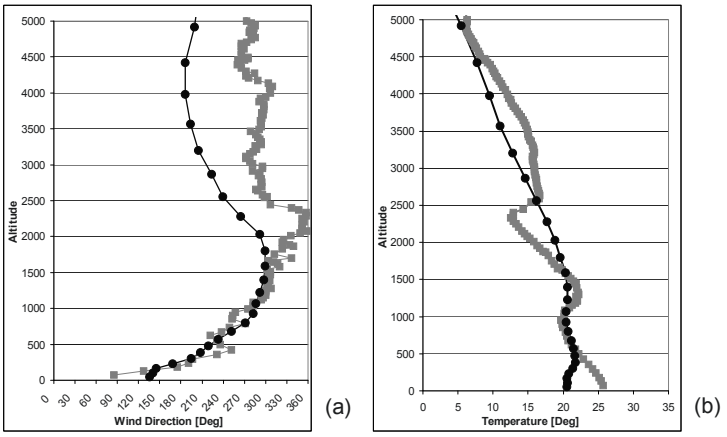


**Fig. 3.** Profiles at "Igud" station, located in the Haifa Bay. Profiles of wind direction (a) and temperature (b) are shown; model results in black ● observations in gray ■

**Acknowledgments** This work was supported by the joint VATAT-IAEC common lab foundation. We would like to thank the following for their help with data, time and good advise: Israel Meteorological Service; Haifa District Municipal Association for the Environment; Israel Electric Company – Environmental Dept; Ministry of Environment Protection.

## References

Alpert P, Osetinsky I, Ziv B, Shafir H, 2004. Semi-objective classification for daily synoptic systems: application to the eastern Mediterranean climate change. International Journal of Climatology, 24, 1001–1011.

Mahrer Y., Weinroth E., 2007, Merging of Meteorological and Photochemical Models for the Asessment of Air Quality in Israel. 6th International Conf. on Urban Air Quality, Cyprus.

Osetinsky I, 2006, Climate Changes over the E. Mediterranean –A Synoptic Systems Classification Approach. PhD thesis Tel Aviv University, Israel.

Pielke R. A., Cotton W. R., Tremback C. J., Lyons W. A., Grasso L. D., Nicholls M. E., Moran M. D., Wesley D. A., Lee T. J. & Copeland J. H. 1992. A comprehensive meteorological modeling system, Met. and Atm. Phys, Vol. 49, p. 69–91.

NCEP Reanalysis data was used for initiating RAMS. This data was provided by the NOAA, Boulder, Colorado, USA, from their Web site at: *http://nomad3.ncep.noaa.gov/ncep_data/*

## 5. Questions and Answers

**Douw Steyn**: Most of your simulated flows are thermally driven by surface temperatures.

1. Did you allow sea-surface-temperatures to evolve through the day?
2. Did you allow sea-surface-temperatures to be spatially variable?

**Answer**: At the beginning we used sea-surface-temperature (SST) from global data as input to the model, kept fixed in time along the simulation. Next, we tried fixed in time and space, and last – we let the SST evolve through the day. With the last option we had some noticeable improvements in the lower part of temperature profiles that could show the presence of the marine inversion. Thank you for pointing out that issue.

**Bill Physick**: My experience too has been that if the marine inversion is not in the initial large-scale analysis, then the mesoscale model won't produce it. It is virtually never in the large-scale analysis because the vertical resolution of the analysis is too coarse. It is a frustrating problem.

**Answer**: Indeed, we checked that and the synoptic grid did not reflect the presence of the inversions, though in one profile there was a mild inversion based at 500 m (just at about the observed marine inversion base). We tried to assimilate some of our measured profiles, in order to give the model the information about the inversions, but so far it didn't have a major impact on the results of the simulations.

**Sven-Erik Gryning**: What is the explanation for the upper inversion at 2 km height?

**Answer**: All the upper air measurements of August campaign showed a persisting inversion around 2–2.5 km height, which we related to subsidence. This subsidence is supposedly due to upper air ridge above our area, and the Hadley cell downward section located over our region in summertime. Again, this inversion did not appear in the initial large-scale analysis.

# 1.14 Comparing Models/Methods for Estimating Multi-pollutant Fine-Scale Air Quality Concentrations

**Karen Wesson[1], Kirk Baker[1], Uarporn Nopmongcol[2], Greg Yarwood[2], Tanarit Sakulyanontvittaya[2], Madeleine Strum[1], James Thurman[1], Louise Camalier[1], Darrell Ensley[3], Brian Timin[1], Sharon Phillips[1], and Tyler Fox[1]**

[1]U.S. Environmental Protection Agency, RTP, NC, USA

[2]ENVIRON International Corporation, Novato, CA, USA

[3]Computer Science Corporation, RTP, NC, USA

**Abstract** Photochemical models are commonly used in regulatory and policy assessments to estimate pollutant concentrations and deposition of both inert and chemically reactive pollutants over large spatial scales. These models are generally run for horizontal grid resolutions of 36 and 12 km. However, several recent assessments have revealed the need for air quality predictions at resolutions finer than 12 km to resolve important local-scale gradients in pollutant concentrations. Given this need, we are undertaking a study to investigate several methods that can be used to obtain local-scale air quality concentrations. This study looks at the application and evaluation of a variety of models including CMAQ, CAMx and AERMOD. In addition, we will also evaluate the use of a new method called the Multiplicative Approach to the Hybrid Method (MAHM), which combines CMAQ and AERMOD predicted concentrations to generate local-scale air quality predictions. To do this, these models/methods are applied at ≤ 4 km resolution for both a winter and summer month in the same local area: Detroit, MI. The study looks at model/method performance of $PM_{2.5}$, $O_3$, and several toxic pollutants by comparing modeled versus ambient measured concentrations. Resources for implementation of each model/method are also evaluated.

## 1. Modeling Applications

All model runs were performed for a summer month (July) and a winter month (January) in 2002. The multi-pollutant versions of CMAQ v4.6.1i (Byun et al., 1999) and CAMx v4.5 (Environ, 2008) were both run for three domains centered on the Detroit urban core: a large Midwest domain at 12 km horizontal resolution (114 × 117 grid cells), a 4 km domain (36 × 45 grid cells) and 1 km domain (72 × 108 grid cells). AERMOD was run for $PM_{2.5}$ and several toxics with a receptor do-main that was slightly smaller than the 1 km photochemical domain and was also centered on the Detroit urban core. The emissions data for these runs were

D.G. Steyn and S.T. Rao (eds.), *Air Pollution Modeling and Its Application XX*,
DOI 10.1007/978-90-481-3812-8, © Springer Science + Business Media B.V. 2010

from EPA's 2002 Multi-pollutant Modeling Platform, updated for fine-scale modeling (Tooly and Wesson, 2009). These emissions were processed using SMOKE, and the Surrogate Tool was used to provide spatial surrogates for gridding the emissions for the 4 and 1 km domain. More information about the meteorological data and emissions data can be found at EPA, 2008.

CMAQ v4.6.1i was run in a one-way nest. The meteorological inputs were processed through MCIP for the 12 km domain. For the 4 and 1 km domains, meteorological data were provided by disaggregating the 12 km MCIP output meteorology to 4 and 1 km modeling domains.

CAMx v4.5 was run for the same three domains as CMAQ, using the two-way nested grid structure and flexi-nesting features. The 1 km domain was run nested within the 4 km domain, which was nested within the 12 km domain. The 12 km MM5 meteorological data were processed using MM5CAMx and provided to the 4 and 1 km domains using flexi-nesting (Environ, 2008). The emissions, however, were provided for each of the three domains at the appropriate resolution.

As part of this study, the EPA's AERMOD dispersion model (EPA, 2004a) was exercised over a 36 by 48 km grid of receptors spaced 1 km apart centered in the urban Detroit core. SMOKE was used to generate temporalized and speciated emissions, which were then formatted for input into AERMOD. Meteorological data for AERMOD was extracted from the 2002 MM5 12 km data for the grid cell over the Detroit Metropolitan Airport and were processed using the MM5AERMOD tool.

To provide subgrid cell texture for multiple pollutants, AERMOD estimated concentrations were then combined with CMAQ 12 km concentrations using a post-processing technique called the Multiplicative Approach to the Hybrid Method (MAHM).[1]

Model outputs are compared with ambient measurements for a variety of pollutants. Total $PM_{2.5}$ monitoring data was extracted from the Federal Reference Monitor (FRM) Network, speciated PM data were taken from the Speciation Trends Network, $O_3$ data was used from AIRS, and toxics data were used from the state toxic monitoring sites and the Detroit Air Toxics Initiative Study (DATI).

## 2. Model Evaluation and Results

The CMAQ and CAMx modeled concentrations from the 12, 4, and 1 km domains were compared against monitoring results for $O_3$ and total $PM_{2.5}$. All data were extracted from the 1 km photochemical domain for comparison. Table 1 shows the

[1]The MAHM equation is C=CMAQ_primary* (AERMOD_rec/AERMOD_gridavg) + CMAQ_secondary where CMAQ_primary and CMAQ_secondary are the primary and secondary CMAQ emissions of a pollutant within the relevant CMAQ grid cell; AERMOD_rec is the concentration of a pollutant at an AERMOD receptor; and AERMOD_gridavg is the average concentration of a pollutant for all the AERMOD receptors located within the relevant CMAQ grid cell.

model performance evaluation statistics (bias and error) for these comparisons. For $PM_{2.5}$, CAMx tended to show less bias and error than CMAQ and for $O_3$, CMAQ tended to show better performance. However, for both $O_3$ (8 h max) and total $PM_{2.5}$, there were only slight differences in model performance between the three horizontal resolutions for each model.

**Table 1.** Model Performance Evaluation Statistics for CMAQ and CAMx for $O_3$ and total PM2.5 Modeled at Various Horizontal Grid Resolutions

| | N | 12 km | | 4 km | | 1 km | |
|---|---|---|---|---|---|---|---|
| | | **Bias** | **Error** | **Bias** | **Error** | **Bias** | **Error** |
| CMAQ $O_3$ 8 h Max (ppb) | ***93*** | 1.001 | 8.527 | –0.685 | 8.917 | –1.526 | 8.949 |
| CAMx $O_3$ 8 h Max (ppb) | ***93*** | –0.884 | 9.260 | –2.956 | 10.230 | –3.200 | 10.313 |
| CMAQ $PM_{2.5}$ (μg/m$^3$) | ***259*** | 3.990 | 8.217 | 4.512 | 8.182 | 4.932 | 8.760 |
| CAMx $PM_{2.5}$ (μg/m$^3$) | ***259*** | –0.053 | 6.315 | 0.344 | 5.247 | 0.483 | 6.583 |

In this study, we also compared the MAHM to the CMAQ and CAMx modeled concentrations for 1 km horizontal resolutions. Table 2 shows the model performance evaluation statistics (bias and error) for the MAHM, CMAQ and CAMx. The CMAQ and CAMx concentrations were only extracted for the AERMOD domain for this evaluation. For the toxics species, the EPA Initial Screening Risk

**Table 2.** Model Performance Evaluation Statistics for the MAHM and CMAQ and CAMx for 1 km horizontal resolution

| | N | ISRL | MAHM | | CMAQ 1 km | | CAMx 1 km | |
|---|---|---|---|---|---|---|---|---|
| | | | **Bias** | **Error** | **Bias** | **Error** | **Bias** | **Error** |
| **$PM_{2.5}$ (μg/m$^3$)** | 185 | | –2.222 | 6.083 | 6.213 | 9.318 | 0.896 | 6.375 |
| **EC+OC (μg/m$^3$)** | *25* | | –1.173 | 3.125 | –1.098 | 2.340 | –3.760 | 3.765 |
| **Benzene (μg/m$^3$)** | *36* | *0.1* | –1.049 | 3.203 | –0.797 | 2.739 | –1.974 | 3.075 |
| **Formaldehyde (μg/m$^3$)** | *32* | *181.8* | –3.112 | 4.520 | –3.150 | 4.491 | –3.323 | 4.600 |
| **Acetaldehyde (μg/m$^3$)** | *32* | *0.5* | 0.353 | 1.117 | 0.321 | 1.164 | –0.259 | 1.097 |
| **1,3-Butadiene (μg/m$^3$)** | *36* | *0.03* | 0.044 | 0.144 | 0.045 | 0.137 | –0.017 | 0.115 |
| **Dichlorobenzene (μg/m$^3$)** | *46* | *0.14* | –0.081 | 0.107 | –0.072 | 0.107 | –0.099 | 0.113 |

Level (IRSL) is included to help determine the relative importance of the magnitude of the bias and error. For total $PM_{2.5}$, CAMx showed the best model performance, with little or no bias while CMAQ was biased high and the MAHM was biased low. For EC+OC, all three models/methods were biased low, with CMAQ showing the best model performance overall. For the five toxics species analyzed, all three models/methods showed similar model performance, with small error and bias. Overall, CMAQ showed slightly less bias and error for most of these toxics species.

When comparing models/methods, it is also important to have an understanding of the time and resources required for implementation. Both the CMAQ and CAMx model runs were performed using 2 cores of an Intel Xeon E5440 CPU at 2.83 GHz. The run time for CMAQ for a 1-day run for all three grids (12, 4 and 1 km) was 4 h and 45 min or approximately 13.5 days for the 2 months. The run time for CAMx for a 1-day run for all three grids was 2 h and 50 min or approximately 8 days for the 2 months. In comparison, the MAHM, which requires both CMAQ and AERMOD concentrations, took more resources and time to implement. The AERMOD runs were performed using 19 compute nodes that were comprised of dual AMD 2800+ CPUs at 4 GB. It took approximately 3 months to complete these model runs for the 2 months. The CMAQ 12 km domain (implemented as described above) took 1 h and 50 min for a 1-day run or approximately 5.2 days for the 2 months. It also took several weeks to post-process the AERMOD and CMAQ concentrations using the Hybrid Approach and to quality assure the data. Therefore, it took approximately 4 months time to implement the MAHM for the 2 months. This comparison shows the time and resources required for the MAHM (4 months, 19 compute nodes, dual core) to be much greater than those needed to run the photochemical models of CMAQ (13.5 days, 2 core CPU) or CAMx (8 days, 2 core CPU).

## 3. Conclusions

This study demonstrates that CMAQ and CAMx can be used for multi-pollutant modeling of an urban area with fine spatial resolution. These photochemical models can treat photochemically reactive toxics (e.g., formaldehyde, acetaldehyde, 1,3-butadiene) as well as toxics with secondary sources (e.g., formaldehyde, acetaldehyde). Model performance evaluation statistics showed that both CMAQ and CAMx performed as well at finer scales (4 and 1 km) as at a 12 km horizontal resolution. There were small differences between CMAQ and CAMx model performance at 1 km horizontal resolution compared to the Hybrid Approach for $PM_{2.5}$ and several toxic species. Overall, this study shows that a single modeling system can be used for ozone, particulate matter, gaseous toxics and particulate toxics thus avoiding the need for the more complicated Hybrid Approach which requires more time and resources for implementation.

## References

Byun, D.W., Ching, J.K.S., 1999. Science Algorithms of the EPA Models-3 Community Multiscale Air Quality (CMAQ) Modeling System, EPA Report 600/R-99/030, Washington DC, Office of Research and Development, US Environmental Protection Agency.

ENVIRON. 2008. "User's Guide – Comprehensive Air-quality Model with extensions, Version 4.5." ENVIRON International Corporation, Novato, California. EPA, 2004. User's Guide for the AMS/EPA Regulatory Model – AERMOD. EPA-454/B-03- 001. U.S. Environmental Protection Agency, Research Triangle Park, NC.

EPA, 2008. Technical Support Document for the Final Locomotive/Marine Rule: Air Quality Modeling Analyses, EPA-454/R-08-002, U.S. Environmental Protection Agency, Research Triangle Park, NC.

Tooly, R.L., Wesson, K.H., 2009. Importance of Local-Scale Emissions Inventories. 18th International Emission Inventory Conference. Baltimore, Maryland.

# 1.15 Evaluation of Four Lagrangian Models Against the Cross-Appalachian and European Tracer Experiments

**B.A. Anderson[1] and R.W. Brode[2]**

[1]U S Environmental Protection Agency, Kansas City, KS, USA

[2]U S Environmental Protection Agency, Research Triangle Park, NC, USA

## 1. Introduction

In this study, a comparison of model performance of four state-of-the practice Lagrangian dispersion models: CALPUFF, SCIPUFF, HYSPLIT, and FLEXPART is presented. These models were used to simulate the dispersion of the tracer cloud for the European Tracer Experiment (ETEX) and the Cross-Appalachian Tracer Experiment (CAPTEX). Dispersion simulations for each of the modeling systems were done using a common meteorological dataset derived from the NCAR/PSU MM5 model. Statistical evaluation procedures used for model verification follow a hybrid approach based upon the procedures used in the second Atmospheric Transport Model Evaluation Study (ATMES-II) and the NOAA Data Archive of Tracer Experiments and Meteorology (DATEM) project. Verification scores show that the NOAA HYSPLIT model performed best overall, followed by the SCIPUFF and FLEXPART models. CALPUFF performance was significantly poorer than the other three models in the ETEX experiment and improved in CAPTEX, but will require additional analysis to diagnose possible causes of predicted tracer advection errors noted in the ETEX experiment.

## 2. Models and Methods

### 2.1. Mesoscale tracer experiments

This study focuses upon the evaluation of models against two major mesoscale tracer experiments conducted during the 1980s and 1990s widely used for long range transport model design and evaluation efforts. The Cross-Appalachian Tracer Experiment (CAPTEX) consisted of seven releases of a perflourocarbon tracer called perfluromonomethylcyclohexane (PMCH) in September and October 1983 from Dayton, Ohio and Sudbury, Ontario. Air sampling was conducted at 84 monitoring sites in the United States and Canada, with sampling frequencies of

D.G. Steyn and S.T. Rao (eds.), *Air Pollution Modeling and Its Application XX*,
DOI 10.1007/978-90-481-3812-8, 

both 3 and 6 h. The European Tracer Experiment (ETEX) consisted of two releases of PMCH were made in October and November 1994 from near Monterfil, France. Air concentrations were sampled at 168 monitoring sites in 17 European countries with a sampling frequency of every 3 h for approximately 90 h. For this study, model simulations were focused upon CAPTEX releases 1–5 and 7 and upon ETEX release 1 (Fig. 1).

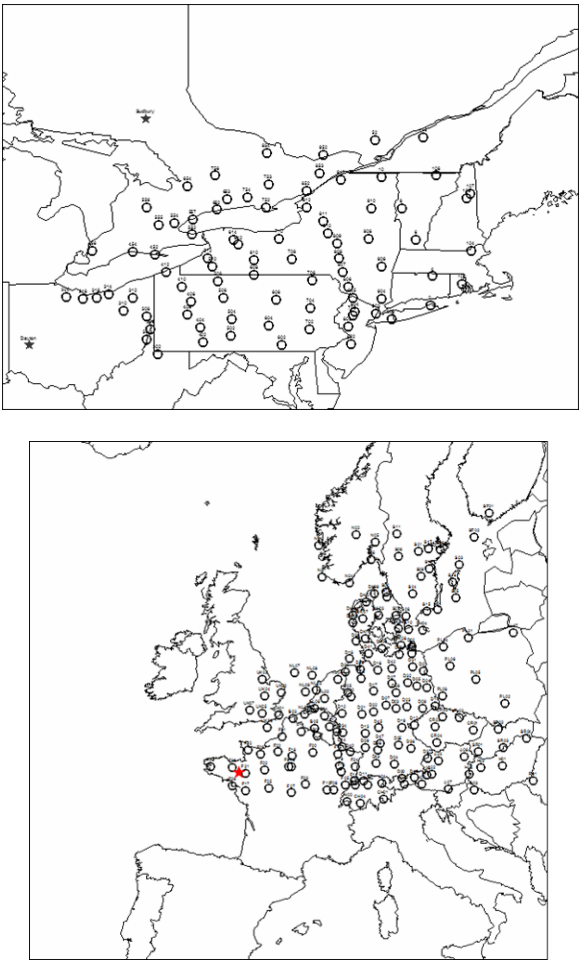

**Fig. 1.** Release and monitoring sites for CAPTEX (left) and ETEX (right) mesoscale tracer experiments. Release sites are denoted by star(s)

## 2.2. Long range transport modeling systems

This model evaluation exercise includes the following state-of-the-practice Lagrangian dispersion models: (1) the California Puff Model (CALPUFF) (Scire et al., 2000); (2) the Second-order Closure Integrated Puff Model (SCIPUFF) (Sykes et al.,

1998); (3) the beta version of the MM5-FLEXPART model (Stohl et al., 2006); and (4) the NOAA HYSPLIT model (Draxler, 1997). CALPUFF is a puff model that is currently recommended by the U.S. Environmental Protection Agency (EPA) to satisfy regulatory permitting requirements involving long range transport under EPA's *Guideline on Air Quality Models*, and SCIPUFF is a puff model that serves as the dispersion model core of the Hazard Prediction Assessment Capability (HPAC) developed for the Defense Threat Reduction Agency. HYSPLIT is a particle model developed by the National Oceanic and Atmospheric Administration's Air Research Laboratory (NOAA/ARL), and FLEXPART is a particle dispersion model developed and maintained by the Norwegian Institute for Air Research (NILU).

Meteorological fields were developed using MM5-v3.7.2 for CAPTEX releases 1–5, and 7 and ETEX release 1. MM5 was initialized with NCEP/NCAR Reanalysis data available on 2.5º × 2.5º grid every 6 h. For the CAPTEX releases, 3 nested domains of 108, 36, and 12 km were used. A single domain of 36 km was used for the ETEX simulations. Output from the finest resolution nest was used for each simulation.

### 2.3. Model experiment design

Intermodel comparisons can be challenging due to the inherent differences in model technical formulations. Chang et al. (2003) conducted an evaluation of three Lagrangian puff models. While based upon Gaussian puff formulation, these models varied significantly in terms of the level of sophistication of their technical formulation. Cheng et al. (2003) correctly opined that it is necessary to set up a proper framework to perform an objective and meaningful evaluation when such models vary significantly in their formulation. A primary focus of their model evaluation framework centered upon the use of the same observed meteorological data and similar modeling domains. To the extent practical, default model options were selected for all models in their evaluation.

Reflecting this evaluation paradigm, a major focus of this study was to provide a common source of meteorological fields to each of the dispersion models evaluated. Each of the four models in this exercise requires three-dimensional meteorological fields as input to the model. For the majority of these models, meteorological fields from prognostic meteorological models are the primary source. The MM5 simulations discussed in Section 2.2 were used to supply three-dimensional prognostic fields for each of the models. However, both CALPUFF and SCIPUFF typically rely upon its own diagnostic meteorological model (CALMET and MC-SCIPUFF respectively) to provide three-dimensional meteorological fields to the dispersion model. Even though MM5 data is ingested as the initial guess field into CALMET, much of the original MM5 data is not preserved, and key boundary layer parameters are recomputed. This compromises the evaluation paradigm – a common meteorological database. In 2008–2009, EPA developed software to facilitate direct ingestion of prognostic meteorological model data by the dispersion model with no changes to many of the boundary layer parameters

important to dispersion modeling simulations, effectively overcoming the challenge to this evaluation paradigm. Similarly, MM5SCIPUFF software developed by the Pennsylvania State University was used to directly couple MM5 to the SCIPUFF model.

### 2.4. Statistical evaluation methodology

Another major focus of this study was to develop an evaluation framework which provided a consistent, analytical method for determining how well modeled and observed concentrations fit. Previous EPA evaluations of long range transport models (USEPA, 1998) largely were subjective in nature and lacked a common foundation for model performance comparisons. The statistical framework developed for the ATMES-II experiment (Mosca et al., 1998), as implemented by Draxler et al. (2001) was chosen as the basis for this evaluation. The metrics for the global statistical analysis are divided into four broad categories: (1) scatter correlation in Eq. 1, (2) bias fractional bias in Eq. 2, (3) spatial coverage (figure of merit in space in Eq. 3), and (4) the unpaired distribution (Kolmogorov-Smirnov parameter in Eq. 4).

$$R = \frac{\sum_i \left(M_i - \overline{M}\right) \bullet \left(P_i - \overline{P}\right)}{\left[\sqrt{\sum \left(M_i - \overline{M}\right)^2}\right]\left[\sqrt{\sum \left(P_i - \overline{P}\right)^2}\right]} \tag{1}$$

$$FB = 2\overline{B} \Big/ \left(\overline{P} + \overline{M}\right) \tag{2}$$

$$FMS = \frac{A_M \cap A_P}{A_M \cup A_P} \times 100\% \tag{3}$$

$$KS = Max\left|C\left(M_k\right) - C\left(P_k\right)\right| \tag{4}$$

The final score, model rank (*RANK*), provides a combined measure to facilitate model intercomparison (Eq. 5). *RANK* is the sum of four statistical measures for scatter, bias, spatial coverage, and the unpaired distribution (Draxler et al., 2001). *RANK* scores range between 0 and 4 with 4 representing the best model ranking.

$$RANK = \left|R\right| + \left(1 - \left|FB/2\right|\right) + FMS/100 + \left(1 - KS/100\right) \tag{5}$$

## 3. Results and Discussion

### 3.1. Overall results

Results from the global statistical analysis are presented in the Table 1. These results show that overall HYSPLIT was the best performing model, exhibiting the highest model composite *RANK* of 2.00 and the highest individual *RANK* in 5 of 7 tracer simulations. By contrast, the lowest performing model was CALPUFF, with a composite *RANK* score of 1.47. Overall, SCIPUFF and FLEXPART exhibited similar behavior with composite *RANKs* of 1.78 and 1.72 respectively.

**Table 1**

| *Tracer Study* | SCIPUFF | CALPUFF | FLEXPART | HYSPLIT |
|---|---|---|---|---|
| CAPTEX-1 | 2.23 | 1.81 | 2.54 | 2.35 |
| CAPTEX-2 | 1.92 | 1.59 | 1.65 | 2.10 |
| CAPTEX-3 | 1.25 | 1.10 | 1.49 | 1.83 |
| CAPTEX-4 | 1.82 | 1.69 | 1.53 | 1.88 |
| CAPTEX-5 | 1.30 | 1.20 | 1.81 | 1.93 |
| CAPTEX-7 | 2.40 | 2.06 | 1.76 | 1.90 |
| ETEX-1 | 1.51 | 0.87 | 1.24 | 1.98 |
| *Overall RANK* | 1.78 | 1.47 | 1.72 | 2.00 |

### 3.2. European tracer experiment at a glance

Results from the ETEX-1 experiment significantly influence the overall RANK score for the CALPUFF modeling system (Table 1) and warrants further examination. Figure 2 displays the time series of the FMS scores over each of the 30 sampling intervals. CALPUFF exhibits marginal agreement during the first 36 h of the simulation, with the FMS scores varying between 8% and 22%. CALPUFF performance deteriorates rapidly after 36 h, with the FMS dropping to the 2–4%

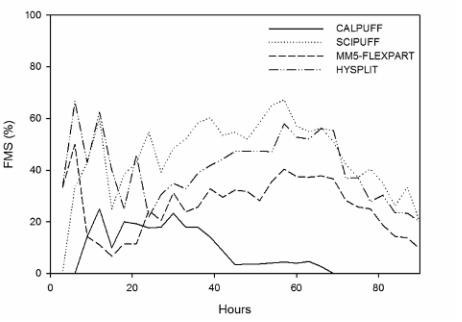


**Fig. 2.** Time series of figure of merit in space (FMS) for ETEX-1

range until hour 69 where the FMS drops to 0%. Both HYSPLIT and SCIPUFF exhibit very similar behavior, with the FMS ranging between ~22% and 60% through the first 60 h of the simulation.

The time series at times T+24, +36, +48, and +60 of both observed concentrations (Fig. 3) and CALPUFF predicted (Fig. 4) denote significant advection errors in the CALPUFF predicted evolution of the tracer cloud position. Advection error accounts for the poorer model performance during the ETEX-1 simulation. Additional investigation is necessary to understand the source of advection error in the CALPUFF modeling system.

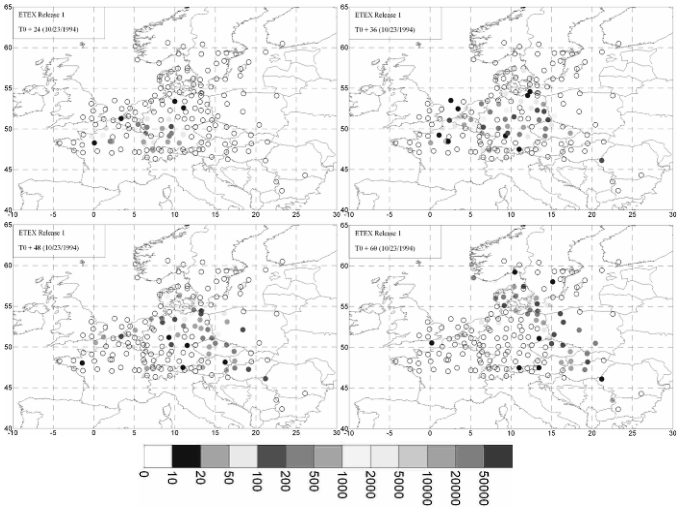


**Fig. 3.** Time series of observed concentrations for ETEX-1

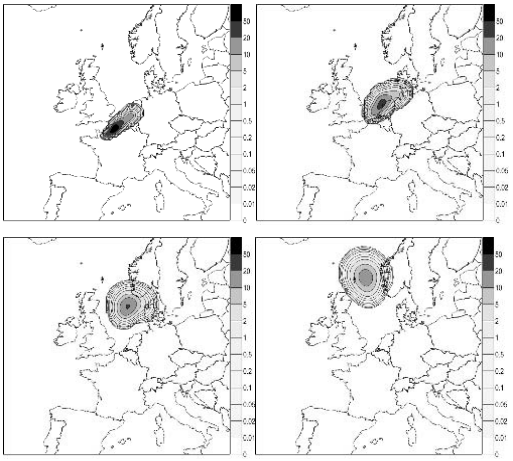

**Fig. 4.** Time series of predicted concentrations for the CALPUFF modeling system for ETEX-1

## 4. Summary

The results from the CAPTEX and ETEX simulations provide useful information about model performance for state-of-the-practice Lagrangian models as well as insight into the strengths and weaknesses in the technical formulations of the modeling systems under review. The overall model *RANK* scores show that the NOAA HYSPLIT model consistently performs the best of the seven simulations conducted as part of this study, followed closely by SCIPUFF and the beta version of the MM5-FLEXPART model. ETEX-1 results identify a potential issue with the advection predictions of CALPUFF that warrant further investigation.

**Acknowledgments and Disclaimer** The authors gratefully acknowledge Roland Draxler of the National Oceanic and Atmospheric Administration for his assistance with the HYSPLIT model and Mr. Douglas Henn of Sage Management, Inc. and Dr. Aijun Deng of the Pennsylvania State University for their assistance with the SCIPUFF modeling system. This research presented here has been performed as part of a joint research effort between EPA Region 7 and EPA's Office of Air Quality Planning and Standards. This work constitutes a contribution to the EPA Air Quality Program. Although it has been reviewed by EPA and approved for publication, it does not necessarily reflect their policies or views.

## References

Chang, J.C., K. Chayantrakom, and S.R. Hanna, 2003: Evaluation of CALPUFF, HPAC, and VLSTRACK with Two Mesoscale Field Datasets. *J. App. Meteor.*, 42, 453–466.

Draxler, R.R., and G.D. Hess, 1997: Description of the Hysplit_4 modeling system, Tech. Rep. NOAA Tech Memo ERL ARL-224, National Oceanic and Atmospheric Administration, Silver Springs, MD, 24 pp.

Draxler, R.R., J.L. Heffter, and G.D. Rolph, 2001: DATEM: Data Archive of Tracer Experiments and Meteorology, National Oceanic and Atmospheric Administration, Silver Springs, MD, 27 pp.

Mosca, S., G. Graziani, W. Klug, R. Ballasio, and R. Bianconi, 1998: A Statistical Methodology for the Evaluation of Long-Range Dispersion Models: An Application to the ETEX Exercise. *Atmos. Environ.*, 32, 4307- 4324.

Scire, J.S., D.G. Strimaitis, and R.J. Yamartino, 2000: A User's Guide for the CALPUFF Dispersion Model (Version 5), Tech. Rep., Earth Tech, Inc., Concord, MA, 521 pp.

Stohl, A., C. Forster, A. Frank, P. Seibert, and G. Wotawa, 2005: Technical Note: The Lagrangian particle dispersion model FLEXPART version 6.2. *Atmos. Chem. Phys*. 5, 2461–2474.

Sykes, R.I., S.F. Parker, D.S. Henn, C.P. Cerasoli, and L.P. Santos, 1998: PC-SCIPUFF Version 1.2PD, Technical Documentation. ARAP Report 718, Titan Research and Technology Division, Titan Corp., Princeton, NJ, 172 pp.

USEPA, 1998: Interagency Workgroup on Air Quality Modeling (IWAQM) Phase 2 Summary Report and Recommendations for Modeling Long Range Transport Impacts. Tech Rep., EPA-454/R-98-009, Research Triangle Park, NC, 160 pp.

# 1.16 Towards an Improved Characterization of Dispersion near Major Roadways

**Thomas Pierce[1], David Heist[1], Vlad Isakov[1], Steven Perry[1], Kirk Clawson[2], and Richard Eckman[2]**

[1]U.S. Environmental Protection Agency/Office of Research and Development

[2]National Atmospheric and Oceanic Administration/Air Resources Laboratory

**Abstract** Since the 1980s, there have been few improvements to line-source dispersion parameterizations in operational dispersion models. Under EPA's Near-Roadway Research Initiative, research to characterize dispersion near major roadways has experienced a resurgence. This paper summarizes an integrated study involving wind tunnel experiments, ambient field measurements, an $SF_6$ tracer field study, and numerical model development and application. The focus of the study has been to assess the impact of common roadway configurations, such as road cuts and noise barriers. In particular, the impact of noise barriers, which are common features along major roadways in the United States, is being examined. Results to date indicate that noise barriers significantly enhance dispersion of pollutants near major roadways.

## 1. Introduction

Over 36 million people in the U.S. live within 100 m of a major highway. A number of studies have identified adverse effects, including respiratory disease, cancer, and even mortality, for populations living, working, and/or attending schools near major roadways. EPA's Clean Air Research Program is emphasizing the need to characterize atmospheric transport and dispersion of emissions within the first few hundred meters of roadways, locales often characterized by complex flow patterns induced by noise barriers, road cuts, buildings and vegetation. This paper summarizes some of the research activities that are examining this phenomenon.

## 2. Approach and Results

The approach planned for understanding the spatial distribution of traffic-related pollutants and for improving tools for simulating the effects of roadside structures includes the following: (1) Examining existing tools – reviewing and evaluating

D.G. Steyn and S.T. Rao (eds.), *Air Pollution Modeling and Its Application XX*,
DOI 10.1007/978-90-481-3812-8, © Springer Science + Business Media B.V. 2010

existing models and data bases related to near road dispersion; (2) Developing measurement methods – developing methods for measuring near-road concentration distributions in both the laboratory and in actual urban situations; (3) Performing new studies – collecting and analyzing field, tracer, and wind tunnel measurements, as well as CFD results to understand the basic structure of flow and dispersion; and (4) Improving algorithms and modeling methodologies – developing and evaluating improved algorithms and incorporating them into a selected near-field modeling platform (e.g. AERMOD) and as a sub-grid algorithm within CMAQ.

**Examining existing tools:** An exhaustive review of 21 available dispersion models that simulate line-type sources was completed (Pierce et al., 2008). Based on the findings and recommendations of this report, AERMOD (Cimorelli et al., 2005; Perry et al., 2005) was chosen as the best platform for further development for roadway scenarios. AERMOD is the current near-field and urban scale model recommended by the EPA for regulatory assessments.

**Developing measurement methods:** Isakov et al. (2007) describe and demonstrate a methodology using mobile platform measurements in Wilmington, Delaware to characterize fine particulate and formaldehyde concentrations. This methodology has been adopted by EPA and is being used with an electric mobile sampling vehicle in a series of intensive field studies in Las Vegas, Detroit, and Durham (NC) for examining the impact of roadside barriers on local air quality and their potential use for pollution mitigation.

**Performing new studies:** Experiments in EPA's meteorological wind tunnel have examined the flow and dispersion around a variety of roadway features (e.g. barriers, road cuts). Clawson et al. in this issue report on a tracer study of line-source emissions upwind of a single 6-m high wall typical for a road noise barrier. Also, field measurements have been made along an eight-lane expressway in Raleigh, NC, examining the concentration gradient in a clearing and behind a noise barrier that showed the substantial influence of the barrier on concentration distributions.

**Improving algorithms and modeling methodologies:** Cook et al. (2008) describe an approach for developing detailed highway emission inventories based on emission factors and traffic inventories for individual road links. Applying a line-source model of Venkatram et al. (2007, 2009), the eight-lane expressway in the Raleigh 2006 field study was simulated for an area with no terrain changes or obstructions to the flow. The concentration gradient for benzene was matched well. Results of EPA wind tunnel studies provide initial indications that for distances beyond the cavity zone of the barrier, the effects of noise barriers can be simulated with a no- barrier model by adjusting the effective source location upwind by a distance of 5–10 barrier heights (Heist et al., 2008). Based on previous wind tunnel studies, an algorithm is being developed for inclusion into AERMOD for

simulating the influence of depressed roadways. Figure 1 compares the modeled concentration gradient with newly-collected independent wind tunnel data.

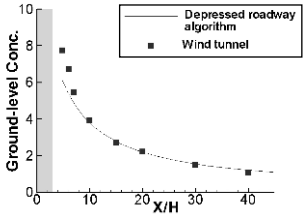


**Fig. 1.** Comparison of normalized ground-level concentrations downwind of a depressed roadway from wind tunnel observations and algorithm predictions

## 3. Conclusions and Future Directions

As this work continues to build on our understanding of the relationships between mobile emissions and adverse health effects and begins to yield tools to assess roadway impacts and mitigation strategies, it should inform decision making within EPA and Federal Highway regulatory programs such as the National Environmental Policy Act, the Conformity rule, and enforcement of the NAAQS. Additionally, programs within the Departments of Health and Human Services, Education, and Housing and Urban Development and the Centers for Disease Control and Prevention will benefit from this research in developing guidelines for the location of schools, hospitals, and residential housing.

Future plans related to research on dispersion near roadways include the following: (1) continued improvement of line-source type algorithms for the AERMOD and hybrid modeling for regulatory applications; (2) further wind tunnel studies and possible tracer studies to examine boundary layer characteristics, wind direction and atmospheric stability influences; (3) collaboration with other EPA laboratories and the FHWA on field campaigns in Las Vegas, Detroit, and Raleigh to better understand the relationship between traffic emissions and roadway-related air pollution concentration gradients; (4) computational fluid dynamics modeling of near-road dispersion to complement wind tunnel and tracer studies; and (5) use of the improved near-road dispersion models to support planned environmental health studies in Atlanta as part of an air pollution exposure and health study with Emory University.

**Acknowledgments and Disclaimer** We greatly appreciate collaborations with A. Vette (EPA/NERL), R. Baldauf (EPA/NRMRL), C. Bailey and R. Cook (EPA/OTAG), and A. Venkatram (U. Calfornia-Riverside). Although this paper has been reviewed and accepted for publication by the U.S. Environmental Protection Agency, it does not necessarily reflect its views or policies.

## References

Cook, R., V. Isakov, J. Touma, W. Benjey, J. Thurman, E. Kinnee, D. Ensley, 2008: Resolving local- scale emissions for modeling air quality near roadways. *J. Air and Waste Manage. Assoc.*, 58, 451–461.

Cimorelli, A., S. Perry, A. Venkatram, J. Weil, R. Paine, R. Wilson, R. Lee, W. Peters, R. Brode, 2005: AERMOD: A dispersion model for industrial source applications Part I: General model formulation and boundary layer characterization. *J.Appl.Meteor*., 44, 682–693.

Heist, D., S. Perry, L. Brixey, 2009: The effect of roadway configurations on the dispersion of traffic-related pollution: a wind-tunnel study. Submitted to *Atmospheric Environment*.

Isakov, V., J. Touma, A. Khlystov, 2007: A method of assessing air toxics concentrations in urban areas using mobile platform measurements. *J. Air and Waste Manage. Assoc.*, 57, 12861295.

Perry, S., A. Cimorelli, J. Weil, A. Venkatram, R. Paine, R. Wilson, R. Lee, W. Peters, 2005:, AERMOD: A dispersion model for industrial source applications II: Model performance against seventeen field-study databases. *J.Appl.Meteor*., 44, 694–708.

Pierce, T, V. Isakov, B. Haneke, J. Paumier, 2008: *Emission and Air Quality Modeling Tools for Near-Roadway Application*, EPA/600/R-09/001, U.S. Environmental Protection Agency, 40 pp., Available at http://www.epa.gov/amad/pdf/Pierceetal_EPA2008.pdf.

Venkatram, A., V. Isakov, E. Thoma, R. Baldauf, 2007: Analysis of air quality data near roadways using a dispersion model. *Atmospheric Environment,* 41, 9481–9497.

Venkatram, A., V. Isakov, R. Seila, R. Baldauf, 2009: Modeling the impacts of traffic emissions to air toxics concentration near roadways. *Atmospheric Environment* (in press).

# 1.17 Evaluation of RAMS6.0 Boundary-Layer Simulation over Sofia (Bulgaria)

**E. Batchvarova[1], E. Pisoni[2], and G. Finzi[2]**

[1]NIMH, Bulgaria Academy of Sciences, Sofia, Bulgaria

[2]Department of Electronics for Automation, Faculty of Engineering, University of Brescia, Italy

**Abstract** The horizontal and vertical structure of the atmospheric boundary layer over specific areas in Europe have been computed using appropriate high resolution runs of RAMS6.0 mesoscale model for short periods. The areas and periods were selected based on the availability of complex boundary layer experiments' data, so that different parametrisations within model runs could be validated.

This paper discusses comparison of model results and measurements for the city of Sofia, Bulgaria. The RAMS6.0 prediction for sensible heat flux during the intensive campaign (28 September–3 October 2003) were very close to measurements, while the 10 m wind speed was highly overestimated. The results showed further that the diurnal variation of wind speed in the model is quite idealized and the simulation cannot reflect the complex mountain-valley circulation pattern typical for the city and the measurements site.

The results showed that even well validated over complex terrain models when applied for "new" complex terrain conditions, do not ensure a success. Measurements for model initial conditions, data assimilation and model validation are needed for all applications of mesoscale models.

**Keywords** Atmospheric boundary layer, Models' evaluation, Sofia experiment, RAMS6.0, Urban meteorology

## 1. Introduction

Different meteorological models are available in the scientific community to be used for weather forecast downscaling and drivers for Air Quality Models, as i.e. MM5 (Grell et al., 1995), RAMS (Pielke et al., 1992), WRF (Grell et al., 2005). Here RAMS was chosen as known for the successful simulations of meteorology and turbulence over complex terrain (Batchvarova et al., 1999).

Presently, a worldwide effort is going on for better validation procedures and philosophy. The well developed statistics for point by point comparisons is not effective for validation of 3-D meteorological fields. Further studies are needed to

D.G. Steyn and S.T. Rao (eds.), *Air Pollution Modeling and Its Application XX*,
DOI 10.1007/978-90-481-3812-8, © Springer Science + Business Media B.V. 2010

elucidate the problems of natural variability, representativeness of measuring site and model grid averages, etc. A method for validation of models based on estimates of the variability of measured atmospheric parameters was suggested by Batchvarova and Gryning (2010) and was tested here as well.

Following an applied method of Sreenivasan et al. (1978) for estimation of the standard deviation of the wind speed and sensible heat flux for a given averaging time, T, was expressed as:

$$\sigma_{u,T} = \sqrt{12}\sqrt{\frac{z}{Tu}}u \text{ and } \sigma_{w\theta,T} = 8\sqrt{\frac{z}{Tu}}w'\theta'.$$

It can be seen that the standard deviation $\sigma_u$ increases with height, z, and wind speed, u, and decreases with averaging time. The standard deviation $\sigma_{w\theta}$ increases with height and sensible heat flux, $w'\theta'$ and decreases with averaging time and wind speed.

## 2. Sofia Experiment and RAMS6.0 Simulations

In the autumn of 2003, a boundary layer experiment was carried out in Sofia, comprising turbulence measurements at 20 and 40 m above ground and high resolution (both in space and time) vertical profiles of temperature, humidity and wind fields (Batchvarova et al., 2004, 2007) based on radio soundings. Therefore runs of RAMS6.0 were performed for specific days in September and October 2003 with horizontal resolution up to 1 km for part of Bulgaria. This task required powerful computing facilities, as the complex topography of the area did not allow choosing very small innermost grid (Table 1). The CINECA (Bologna, Italy) computing facilities were used as part of visiting project within HPC Europe ERA FP6 project. Even with these facilities, a compromise was needed between high vertical resolution near the ground and high horizontal resolution. Simulations were performed with three configurations of RAMS6.0 model.

**Table 1.** RAMS6.0 configurations for Sofia Experiment 2003

| Configuration code | Simulation period | Number of grid points in nested grids | Resolution of nested grids, time step for outer grid and time step ratio | Number of vertical levels, height of first level and increase factor |
|---|---|---|---|---|
| Case 1 | 28/09–4/10 2003 start at 0000 GMT | 62, 132, 202 | 25, 5, 1 km t step 30 s, ratio 1,5,3 | 42 Levels, start 50 m increase factor 1.15 |
| Case 2 | 27/09–30/09 2003 start at 0000 GMT | 42, 132, 252 | 25, 5, 1 km t step 10 s, ratio 1,5,4 | 56 Levels, start at 10 m increase factor 1.15 |
| Case 3 | 30/09–04/10 2003 start at 0600 GMT | 72, 202 | 25, 5 km t step 10 s, ratio 1,5 | 50 Levels, start at 20 m increase factor 1.15 |

## 3. Results

The simulations provided a vast data base for different studies, such as validation of the model performance on measured meteorological data; sensitivity tests for the influence of the resolution, boundary conditions and surface parametrisations on the simulations. Example of the modeled (Case 1, Table 1) and measured surface sensible heat flux and 10 m wind speed are shown in Figs. 1 and 2. Most difficult is to simulate correctly the exchange processes during night time and transition periods (morning and evening) when the atmosphere is stably stratified. The model predicts the daytime sensible heat flux within the limits given by measured data variability, Fig. 1. Still, it has to be noted that the model predicts the surface sensible heat flux (2 m), while the acoustic anemometers were mounted at 20 and 40 m above ground.

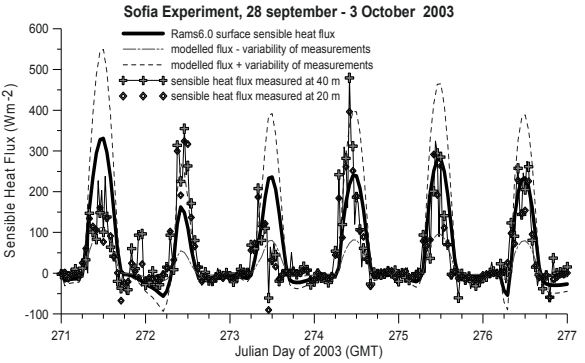


**Fig. 1.** Sensible heat flux (modeled surface values, measured at 20 and 40 m height, standard deviations)

The measured wind speed at 20 and 40 m above ground is considerably lower the modeled wind speed at 10 m height and lies outside the large variability interval estimated on those measurements (Fig. 2). The measured wind shows complex diurnal variation caused by the mountain-valley circulations typical for Sofia. The measuring site is relatively close to Vitosha Mountain.

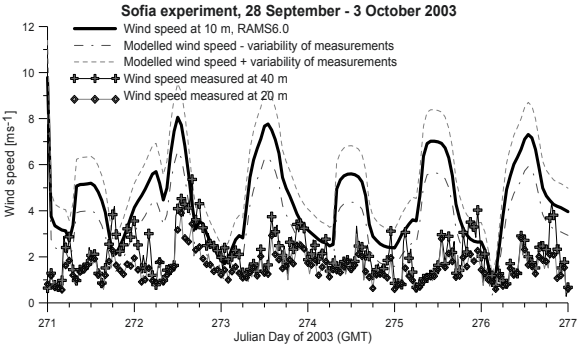


**Fig. 2.** Wind speed (modeled at 10 m height and measured at 20 and 40 m height)

The model predicts quite idealized symmetric diurnal variability of the wind speed, despite the high horizontal resolution of 1 km. The vertical resolution of minimum 50 m (which is standard for Numerical Weather Prediction models) is course for Boundary Layer studies in complex terrain.

## 4. Conclusions

The predictions of RAMS for the surface heat flux are in good agreement with measurements during the Sofia Experiment of 2003, while the surface wind speed is largely over predicted. The measured complex diurnal variation pattern reflects the mountain-valley circulation which is not captured by the model for this site.

RAMS is validated and performs well in many complex terrain conditions. A problem to evaluate all models (RAMS, MM5, WRF, ALADIN) over Bulgaria is the limited information from standard automatic meteorological stations, the existence of only one aerological station in the country and the lack of Boundary layer measuring campaigns with spatial coverage for scales above 2–3 km.

**Acknowledgments** The work has been performed under the Project HPC-EUROPA (RII3-CT-2003-506079), with the support of the European Community - Research Infrastructure Action under the FP6 "Structuring the European Research Area" Programme. It is also part of collaboration within COST Action 728 and supported by the Danish Council for Strategic Research, Sagsnr 2104-08-0025 and the EU FP7 Marie Curie Fellowship VSABLA.

## References

Batchvarova E. and S.-E Gryning, 2010. The ability of mesoscale models to predict vertical profiles, D.G. Steyn and S.T. Rao (eds.), *Air Pollution Modeling and Its Application XX*, 103 DOI 10.1007/978-90-481-3812-8, 375–379.

Batchvarova E., X. Cai, S.-E. Gryning and D. Steyn, 1999: Modelling internal boundary layer development in a region with complex coastline. Boundary-Layer Meteorology, 90, 1–20.

Batchvarova, E.; Gryning, S.-E.; Rotach, M.W.; Christen, A., Modelled aggregated turbulent fluxes compared to urban turbulence measurements at different heights. In: Proceedings. 9th International conference on harmonisation within atmospheric dispersion modelling for regulatory purposes, Garmisch-Partenkirchen (DE), 1–4 June 2004. Suppan, P. (ed.), (Forschungszentrum Karlsruhe GmbH, Karlsruhe, 2004), Vol. 2, 7–11.

Batchvarova, E, Gryning, S.-E., Rotach, M.W and Christen, A., 2007: Comparison of aggregated and measured turbulent fluxes in an urban area, In: Air pollution modeling and its application XVII. 27th. NATO/CCMS international technical meeting, 25–29 October 2004, Banff, Canada, Borrego, C. and Norman, A.-L. (eds), Springer, 363–370.

Grell, G. A., Dudhia, J. and Stauffer, D. R., 1995. A description of the fifth generation Penn State/NCAR mesoscale model (MM5). Technical report, National Centre for Atmospheric Research, Boulder, Colorado, USA. NCAR/TN-398+STR.

Grell G. A., Steven E. Peckham, R. Schmitz, S. A. McKeen, G. Frost, W. C. Skamarock and B. Eder, 2005. Fully coupled "online" chemistry within the WRF model. Atmospheric Environment, 39, 6957–6975.

Gryning, S.-E.; Batchvarova, E., Turbulence, atmospheric dispersion and mixing height in the urban area, recent experimental findings. In: Air Pollution modeling and its application 18. 28. NATO/CCMS international technical meeting, Leipzig (DE), 15–19 May 2006. Borrego, C.; Renner, E. (eds.), (Elsevier, Amsterdam, 2007) (Developments in Environmental Science, 6) p. 12–20.

Pielke, R.A., W.R. Cotton, R.L. Walko, C.J. Tremback, W.A. Lyons, L.D. Grasso, M.E. Nicholls, M.D. Moran, D.A. Wesley, T.J. Lee, and J.H. Copeland, 1992: A comprehensive meteorological modeling system – RAMS. Meteor. Atmos. Phys., 49, 69–91.

Sreenivasan K.R., Chambers A.J. and R.A. Antonia, 1978: Accuracy of moments of velocity and scalar fluctuations in the atmospheric surface layer, *Boundary-Layer Meteorology, 14, 341–359.*

# 1.18 An Updated Method for Estimating of Surface-Layer Scaling Parameters from Routine Ground-Based Meteorological Data

**Marko Kaasik and Eva-Stina Kerner**

Institute of Physics, University of Tartu, Estonia

**Abstract** There is presented a method for rough estimation of Monin-Obukhov length from meteorological measurements made routinely in ground-based stations. The independent variables are wind velocity, cloud amount and solar elevation. The method is based on bilateral relations of Pasquill stability classes with (1) wind and insolation and with (2) surface roughness and Monin-Obukhov length on the other hand. The result enables us to build up entire surface-layer scaling for a local dispersion model. Resulting atmospheric stratification estimations are validated in a case study based on radiosounding profiles and mast data collected during 3 years in Tallinn, Estonia.

## 1. Introduction

Although advanced numerical air quality models have far more realistic dynamics and physics included and thus, are theoretically capable to predict the dispersion of airborne ingredients with much higher precision and accuracy, the simple Gaussian models are still widely in use for local and urban scale applications (Air4EU, 2005). Due to lack of meteorological and emission data, the numerical models don't perform significantly better, but consume much more computer resources. Often the entire condition of surface layer must be still estimated from the surface-based mean flow wind and other routine meteorological station data, as neither flux- nor gradient-based micrometeorological measurements are available.

There is presented a technically new method for rough estimation of Monin-Obukhov length and building up the surface-layer scaling for local air pollution dispersion computations. Practical need for that method appeared due to pre-processing of meteorological data series for a bi-Gaussian model AERMOD (Cimorelli et al., 2005), version 6, for environmental impact assessment purposes.

D.G. Steyn and S.T. Rao (eds.), *Air Pollution Modeling and Its Application XX*,
DOI 10.1007/978-90-481-3812-8, 

## 2. Methods

The calculation scheme is based on two classical relationships: (i) definition of Pasquill stability classes through wind speed and net radiation index (Turner, 1964) and (ii) Pasquill classes as a discrete empirical function of surface roughness $z_o$ and Monin-Obukhov length $L$ (Golder, 1972; Myrup and Ranzieri, 1976). Both relations (i, ii) are made continuous through an interpolation procedure as well as the discrete net radiation index (NRI) is replaced with a continuous function of solar elevation, corrected with cloud cover. As the first step, NRI is expressed as a continuous function of solar elevation and corrected with cloud amount. Then the Pasquill class is expressed as a continuous "Pasquill function" $P$ of NRI and wind speed $u$. Then $L$ is expressed as a function of $P$ and $z_o$.

The friction velocity is expressed from modified-logarithmic wind profile law through 10-m wind speed, surface roughness and $L$; then the surface heat flux through $L$ and friction velocity. Surface roughness $z_o$ should be in such cases typically estimated from information on landscape (classification provided, e.g. by Stull, 1997).

As a validation case study, the frequency of night-time stable atmospheric conditions was studied for Tallinn, Estonia for years 2005–2007:

1. Based on the method developed here and two alternative criteria of stable stratification: (a) $P > 0.5$, (b) $L < 100$ m
2. Potential temperature inversions from radio sounding profile, 00 GMT
3. From a meteorological mast located in outskirts of Tallinn – measured potential temperatures Q at heights of 8 and 22 m

## 3. Results and Discussion

Clear-sky NRI, originally ranging from 0 to 4, is approximated as a function of solar elevation $h_O$:

$$\mathrm{NRI}_\mathrm{o} = 0.0914h_o - 0.0005h_o^2 \tag{1}$$

Corrected NRI for cloud amount $C$ (tenths) is

$$\mathrm{NRI} = \mathrm{NRI}_\mathrm{o} / \left(1 + 0.01C^2\right) \qquad \text{(daytime)} \tag{2}$$

$$\mathrm{NRI} = 0.02C^2 - 2 \qquad \text{(night-time)} \tag{3}$$

Approximations (1) – (3) are based on the algorithm by Turner (1964).

We derived a continuous counterpart of Pasquill stability classes, here denounced as $P$, depending on NRI and 10 m wind velocity $u$ (m/s). A polynomial fit according to discrete presentation by Turner (1964) is:

$$P = B_{00} + B_{01}\,u + B_{02}\,u^2 + B_{03}\,u^2 + B_{10}\mathrm{NRI} + B_{20}\mathrm{NRI}^2 + B_{30}\mathrm{NRI}^3 + B_{11}\mathrm{NRI}\,u + B_{12}\mathrm{NRI}\,u^2 + B_{21}\mathrm{NRI}^2\,u \quad (4)$$

Values –3, –2, –1, 0, 1, 2 of $P$ correspond respectively to discrete classes A, B, C, D, E and F; $P$ = –2.5 corresponds to transition between classes A and B *etc*. Regression coefficients in Eq. 4 are given in Table 1.

**Table 1.** Regression coefficients in Eq. 4

| | | | |
|---|---|---|---|
| $B_{00}$ | 0.444109 | $B_{20}$ | 0.095300 |
| $B_{01}$ | –0.177258 | $B_{30}$ | –0.008333 |
| $B_{02}$ | 0.019689 | $B_{11}$ | 0.266387 |
| $B_{03}$ | –0.000486 | $B_{12}$ | –0.011147 |
| $B_{10}$ | –1.343386 | $B_{21}$ | –0.014444 |

To avoid inconsistent and too extreme unstability, the stability function $P$ is set zero, if u > 7 m/s and values higher than 2.5 (appearing at low wind and negative NRI) are set to 2.5. From graphical representation by Myrup and Ranzieri (1976) we derive the polynomial fit for Monin-Obukhov length $L$:

$$L^{-1} = A_{00} + A_{01}\,Z + A_{02}\,Z^2 + A_{10}\,Z + A_{11}\,PZ + A_{12}\,PZ^2 + + A_{20}\,Z^2 + A_{21}\,P^2Z + A_{22}\,P^2Z^2, \quad (5)$$

where $Z$ = -log $z_0$ (m). Regression coefficients are given separately for unstable ($P$<0, $L$<0) and stable stratification ($P$ > 0, $L$ > 0) in Table 2.

**Table 2.** Regression coefficients in Eq. 5

| *Coefficient* | *Unstable* | *Stable* | *Coefficient* | *Unstable* | *Stable* |
|---|---|---|---|---|---|
| $A_{00}$ | *–0.002107* | *0.002309* | $A_{12}$ | *0.004600* | *0.009098* |
| $A_{01}$ | *0.001128* | *–0.001385* | $A_{20}$ | *–0.015660* | *0.023065* |
| $A_{02}$ | *–0.000379* | *0.000166* | $A_{21}$ | *–0.001540* | *0.004786* |
| $A_{10}$ | *–0.014491* | *–0.022966* | $A_{22}$ | *0.002279* | *–0.004117* |
| $A_{11}$ | *0.011234* | *0.006258* | | | |

Polynomial fit (5) produces a non-physical maximum of $L^{-1}$ in unstable stratification and minimum in stable stratification for $z_0$ > 0.5 m and Pasquill stability close to neutral. These false extremums are removed, using linear interpolation for $L^{-1}$ between values 0 and –0.0015 for unstable stratification and between values 0 and 0.001 for stable stratification.

Comparison of monthly average frequencies of night-time stable conditions for Tallinn by three different methods is given in Fig. 1. The frequencies agree well with sounding- and mast-based estimations, except the lower mast level, which obviously includes all shallow inversions entirely in suburban canopy layer. A sharp maximum at this graph most probably corresponds to snowmelt inversions. In general, surface inversions are more frequent in summertime, when diurnal temperature variations are larger.

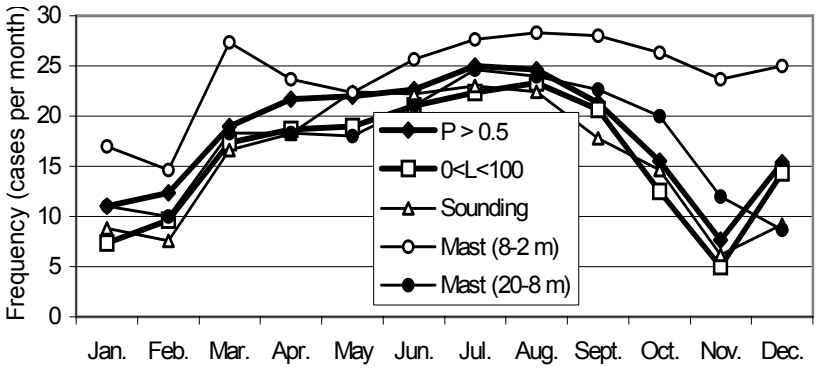


**Fig. 1.** Frequencies of stable meteorological conditions estimated by different methods

## 4. Conclusions

Although the statistics presented in Fig. 1 are neither strictly comparable nor comprehensive, they constitute a rough proof that the developed method is applicable in practice for diagnosing the night-time stagnating conditions in surface layer.

However, due to surface-based initial data and definition of NRI, this method is in principle not able to predict neither elevated inversions nor relatively infrequent daytime inversions.

**Acknowledgments** Elaboration of the method was funded by AS Steiger. Investigation of inversions based on radiosounding data was supported by Estonian Science Foundation, research grants No 7005 and 7478.

## References

Air4EU (2005) *Air Quality Assessment for Europe: from local to continental scale*. Report on workshop 29th June 2005, Athens.

Cimorelli A. J., S. G. Perry A. Venkatram J. C. Weil R. J. Paine R. B. Wilson R. F. Lee W. D. Peters and R. W. Brode (2005) AERMOD: A dispersion model for industrial source applications Part I: General model formulation and boundary layer characterization. *J Appl Meteor*, 44: 682–693.

Golder D. (1972) Relations among stability parameters in the surface layer. *Boundary Layer Meteor.*, 3: 47–58.

Myrup, L.O., Ranzieri, A.J. (1976) A consistent scheme for estimating diffusivities to be used in air quality models. *Caltrans*, FHWA-CA-TL-7169-76-32.

Stull, R.B. (1997) *An introduction to boundary layer meteorology*. Kluwer, 670.

# Chapter 2 Regional and intercontinental modelling

Chairpersons: W. Gong
P. Builtjes
E. Batchvarova

Rapporteurs: J. Godowitch
B. Timin
P. Siljamo

D.G. Steyn and S.T. Rao (eds.), *Air Pollution Modeling and Its Application XX*,
DOI 10.1007/978-90-481-3812-8_2, © Springer Science + Business Media B.V. 2010

# 2.1 Regional Air Quality Modelling: A Few Examples of Recent Progresses and Remaining Questions

**Robert Vautard**

LSCE/IPSL, Laboratoire CEA/CNRS/UVSQ

**Abstract** The rising concern of health impacts of atmospheric pollution necessitates an increasing need of acute understanding, accurate description and prediction of air quality. Major progresses in knowledge and techniques over several fronts have been achieved in the last decade or so (Monks et al., 2009). More chemical species have been characterized, with increased accuracy, and over larger and finer spatial scales. These progresses have been obtained through observations made during intensive campaigns and routine monitoring. Many progresses have also been obtained through regional-scale modelling, taking into account intercontinental transport and global-scale atmospheric composition changes. The objective of this paper is to give an overview of the contribution of regional-scale modelling to these progresses. It focuses on a selected sample of results obtained at the Institute Pierre-Simon Laplace (IPSL) in collaborative projects with INERIS, Meteo-France and the TNO in the Netherlands, among others.

## 1. Patterns of Air Quality

For more than 10 years now, the Institute Pierre-Simon Laplace (IPSL) has been developing research on atmospheric chemistry through observations and modelling. At global scale, the online and offline aerosol/chemistry LMDz-INCA model has been developed and used in many studies (Hauglustaine et al., 2004). At regional to urban scale, IPSL and INERIS teams gathered their efforts to develop the CHIMERE model (Schmidt et al., 2001; Vautard et al., 2003; Bessagnet et al., 2004), which has now worldwide applications. These tools have been used basically to complement atmospheric composition and air pollution observations in order to understand their interaction with transport, meteorology or climate, for instance in severe episodes, and also in operational air quality forecasting or emission control scenario analysis. The models work together, LMDzINCA feeding boundary conditions of CHIMERE (see, e.g. Szopa et al., 2006). The chain of models and the respective spatial is summarized in Fig. 1. The models were designed to allow long-term, multi-seasonal, multi-annual or multi-decadal simulations.

D.G. Steyn and S.T. Rao (eds.), *Air Pollution Modeling and Its Application XX*,
DOI 10.1007/978-90-481-3812-8, © Springer Science + Business Media B.V. 2010

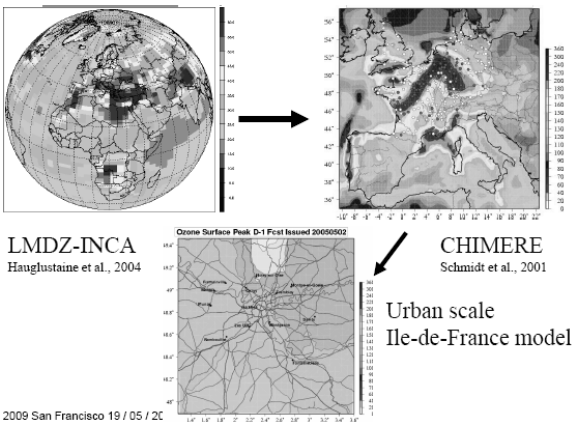


**Fig. 1.** The chain of models (LMDz-INCA and CHIMERE) used at IPSL

One of the major advances regional modelling has brought is the description of patterns of air pollutants such as city plumes, large-scale episodes and transport, which helps explaining the time evolution observed of concentrations at individual sites. The development of European-scale photochemical smog episode in several connected large-scale plumes built from the aggregation of individual city plumes was particularly clear in simulations of the August 2003 episode using CHIMERE (Vautard et al., 2005). By contrast the pointwise representation provided by observations only could not clearly identify the dynamical build-up of the episode (see Fig. 2). What was also demonstrated is that during such episodes several weakly connected "air basins" could be identified in Europe. For instance the region between Marseille and Northern Italy appears connected, but disconnected from Northern Europe.

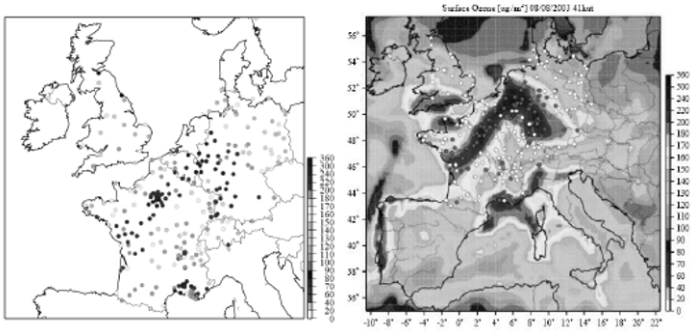

**Fig. 2.** Observations (left panel) and simulation (right panel) from the CHIMERE model for August 8 2003, 14:00 UT. The right panel figure is taken from Vautard et al. (2005). Observations were taken from several monitorinig networks in Europe

At city scale, the development of the urban Paris ozone plume was studied during the ESQUIF field campaign (Menut et al., 2001) that has taken place during three consecutive summer periods (1998–2000). The use of CHIMERE and the campaign measurements allowed to identify the areas around Paris most exposed to ozone pollution and the sensitivity to emissions (Sillman et al., 2003; Beekmann and Derognat, 2003).

The description of patterns of pollutant concentrations also progressed concerning mineral dust due to Aeolian erosion. A "dust" version of the CHIMERE model has been developed (Menut et al., 2009), that was able to describe several episodes of mineral aerosol elevated concentrations (see, e.g. Bessagnet et al., 2008).

## 2. Synergetic Use of Oservations with Model Simulations

A major progress in the use of observations and model simulations in synergy is the development of methods for spatial representation of air quality pollutant concentrations. The deal is that surface observations are more accurate than model simulations but model simulations cover areas uncovered by observations. Several advanced methods have been devised such as four-dimensional variationnal assimilation (Elbern and Schmidt, 2001). At IPSL a geostatistical approach has been developed, tested over several real cases (Blond et al., 2003), and used in operational real-time ozone and PM10 analyses within the PREV'AIR system (Honoré et al., 2008).

Data assimilation of satellite data may also help describing the three-dimensional structure of the regional atmospheric composition. For instance an ensemble Kalman filter approach has been tested in idealized experiments conducted to evaluate the added value of satellite data to PM2.5 forecasts (Timmermans et al., 2009). These applications are presently preliminary. However, a general result that was found in other studies was confirmed: air quality forecasts are weakly sensitive to initial conditions beyond a lead time of about 24 h (Elbern and Schmidt, 2001; Blond and Vautard, 2004; Timmermans et al., 2009).

Another important use of models and data has been demonstrated in several attempts to improve emission inventories by the use of observations. Results are often difficult to interpret because of the bad handling of model errors. However striking reliable results were obtained by the synergetic use of CHIMERE decadal simulations and satellite observations of $NO_2$ columns from the GOME and SCIAMACHY platforms (Konovalov et al., 2008). This study showed in particular European regions where observed $NO_2$ column decadal changes are compatible with emission inventories as provided by countries.

## 3. Operational Purposes: Forecasting and Emission Control Scenario Analysis

The use of regional air quality models for forecasting has evolved from a prototypal stage, about 10 years ago, to a currently fully operational stage. Several centres now produce routine forecasts of air pollutants. The evaluation of the forecast skill of prototype (Tilmes et al., 2002) or operational systems (Honoré et al., 2008) has been made. A common platform of air quality has been set up within the integrated GEMS/MACC European projects.

As an example, daily operational forecasts have been carried out since 2004, using the models MOCAGE and CHIMERE within the PREV'AIR forecasting platform, on the request of the French ministry of environment. This system is evaluated on an annual basis and results for the first 3 years of operations are now published (Honoré et al., 2008). The results (see Fig. 3) indicate in particular that the fair skill of ozone forecasts slowly decreases with lead time, showing that the accuracy of weather forecasts are not a major limitation to ozone forecasts.

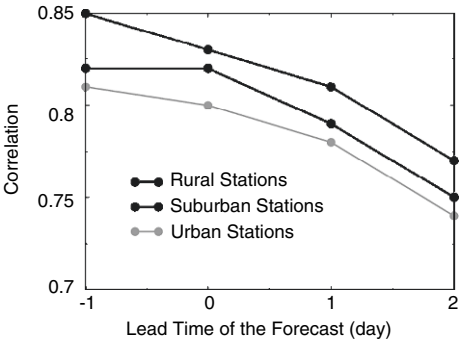


**Fig. 3.** Mean correlation between observed and predicted ozone daily maxima over most ozone monitoring stations in France, as a function of lead time. Negative lead times stand for hindcasts. The skill is calculated using the operational forecasts over three summer seasons

In the beginning of last decade a prospective vision of long-term emission control has been built and models have been used to predict the expected air quality improvement in 2010. This prediction has been coordinated at the European level, within the Clean Air For Europe strategy, through the CITYDELTA and EURODELTA projects (Cuvelier et al., 2007; van Loon et al., 2007), by the use of several models.

The characterization of uncertainty in our knowledge is reflected in the spread of the simulations carried out by an ensemble of air quality models for the same weather conditions. The extent to which model ensembles spread correctly characterize uncertainty has been discussed (Vautard et al., 2006). Ensembles have also been used for producing improved forecasts or simulations of air pollutants, by the use of advanced statistical techniques (Riccio et al., 2007).

## 4. Air Quality and Climate Change

The 2007 IPCC confirmation of the anthropogenic nature of climate change has brought up key questions about the interaction between air quality and climate change. Several recent studies attempt to quantify the impact of climate change on regional air quality (see, e.g. Forkel and Knoche, 2006). Among the expected consequences of climate change, heat waves have been the focus for air quality and its impact on health, especially in the wake of the August 2003 heat wave (Vautard et al., 2005). Using Summer 2003 as a prototype for air quality in future summers is not obvious (Vautard et al., 2007) as the evolution of regional and global emissions are expected to have a large effect, at least in the next 2 decades (Szopa et al., 2006).

The significant contribution of air quality in regional climate change through the direct and indirect effects of aerosols also has been identified, for instance from statistical links between radiation, aerosol optical depth or visibility and temperature changes (Norris and Wild, 2008; Philipona et al., 2009; Vautard et al., 2009). However most regional air quality models do not yet include the key feedback processes on climate through direct and indirect aerosol effects. Moreover the current skill of simulation of aerosol concentrations is poor, at least for Europe (Stern et al., 2008). In order to quantify this effect an effort should be made to improve aerosol models and develop coupled approaches.

## 5. Future Directions

It is clear that the development of comprehensive models has brought a lot to our understanding of air quality. But a lot more is still ahead. Improved simulation of aerosols at regional scales is needed, together with their radiative and microphysical feedback processes. More progresses are expected from inverse modelling in order to improve emission inventories and their changes over years or decades. For that purpose the use of satellite data should be essential. Air quality models should also be used in conjunction with regional climate models in order to simulate impacts on human and ecosystems exposure, and to evaluate possible emission control scenarios that would preserve both climate and air quality.

## References

Beekmann M., C. Derognat, Monte Carlo uncertainty analysis of a regional-scale transport chemistry model constrained by measurements from the Atmospheric Pollution Over the Paris Area (ESQUIF) campaign, J. Geophys. Res., 108 (D17), 8559, doi:10.1029/2003JD003391, 2003.

Bessagnet, B., A. Hodzic, R. Vautard, M. Beekmann, S. Cheinet, C. Honoré, C. Liousse and L. Rouil, 2004, Aerosol modeling with CHIMERE: preliminary evaluation at the continental scale. *Atmospheric Environment*, **38**, 2803–2817.

Bessagnet, B., Menut, L., Aymoz, G., Chepfer, H., and Vautard, R., 2008: Modelling dust emissions and transport within Europe: the Ukraine March 2007 event. J. Geophys. Res., 113, D15202, doi:10.1029/2007JD009541.

Blond, N., Bel, L. and Vautard, R., 2003: Three-dimensional ozone data analysis with an air quality model over the Paris area. J. Geophys. Res., 108, D17, 8564.

Blond, N., and R. Vautard, 2004: Three-dimensional ozone analyses and their use for short-term ozone forecasts, J. Geophys. Res., doi:10.1029/2004JD004515.

Cuvelier, C., Thunis, P., Vautard, R., Amann, M., Bessagnet, B., Bedogni, M., Berkowicz, R., Brandt, J., Brocheton, F., Builtjes, P., Coppalle, A., Denby, B., Douros G., Graf, A., Hellmuth, O., Honoré, C., Hodzic, A., Jonson, J., Kerschbaumer, A., de Leeuw, F., Minguzzi, E., Moussiopoulos, N., Pertot, C., Pirovano, G., Rouil, L., Schaap, M., Stern, R., Tarrason, L., Vignati, E., Volta, M., White, L., Wind, P., Zuber, A., 2007: CityDelta: A model inter-comparison to explore the impact of emission reductions in 2010 in European cities in 2010, Atmospheric Environment, 41, 189–207.

Elbern, H., and H. Schmidt, 2001, Ozone episode analysis by four-dimensional variational chemistry data assimilation, *J. Geophys. Res., 106,* 3569–3590.

Forkel, R. and R. Knoche, 2006, Regional climate change and its impact on photooxidant concentrations in southern Germany: Simulations with a coupled regional climate-chemistry model, J. Geophys. Res., 111, D12302.

Hauglustaine, D. A., F. Hourdin, L. Jourdain, M.-A. Filiberti, S. Walters, J.-F. Lamarque, and E. A. Holland (2004), Interactive chemistry in the Laboratoire de Météorologie Dynamique general circulation model: Description and background tropospheric chemistry evaluation, J. Geophys. Res., 109, D04314, doi:10.1029/2003JD003957.

Honoré, C., Rouil, L., Vautard, R., Beekmann, M., Bessagnet, B., Dufour, A., Elichegaray, C., Flaud, J.-M., Malherbe, L., Meleux, F., Menut, L., Martin, D., Peuch, A., Peuch, V.-H., Poisson, N., 2008. Predictability of European air quality: The assessment of three years of operational forecasts and analyses. J. Geophys. Res., 113, D04301, doi:10.1029/2007JD008761.

Konovalov, I. B., M. Beekmann, J.P. Burrows and A. Richter, Satellite measurement based estimates of decadal changes in European nitrogen oxides emissions., *Atmos. Chem. Phys.*, **8**, 2623–2641.

Menut, L., R. Vautard, C. Flamant, C. Abonnel, M. Beekmann, P. Chazette, P. H. Flamant, D. Gombert, D. Guedalia, D. Kley, M.-P. Lefebvre, B. Lossec, D. Martin, G. Mégie, P. Perros, M. Sicard, G. Toupance, 2000: Measurements and modelling of atmospheric pollution over the Paris area: An overview of the ESQUIF project. Annales Geophysicae, 18, 1467–1481.

Menut L., I. Chiapello, C. Moulin 2009, Predictability of mineral dust concentrations: The African Monsoon Multidisciplinary Analysis first short observation period forecasted with CHIMERE-DUST, J. Geophys. Res., 114, D07202, doi:10.1029/2008JD010523.

Monks, P. S., C. Granier, S. Fuzzi, A. Stohl, M. Williams, H. Akimoto, M. Amman, A. Baklanov, U. Baltensperger, I. Bey, N. Blake, R.S. Blake, K. Carslaw, O.R. Cooper, F. Dentener, E. Fragkou, G. Frost, S. Generoso, P. Ginoux, V. Grewe, A. Guenther, H.C., Hansson, S. Henne, J. Hjorth, A. Hofzumahaus, H. Huntrieser, M.E. Jenkin, J. Kaiser, M. Kanakidou, Z. Klimont, M. Kulmala, M.G. Lawrence, J.D. Lee, C. Liousse, G. McFiggans, A. Metzger, A. Mieville, N. Moussiopoulos, J.J. Orlando, P.I. Palmer, D. Parrish, A. Petzold, U. Platt, U. Poeschl, A.S.H. Prévôt, C.E. Reeves, S. Reiman, Y. Rudich, K. Sellegri, R. Steinbrecher, D. Simpson, H. ten Brink, J. Theloke, G. van der Werf, R. Vautard, V. Vestreng, Ch. Vlachokostas, R. vonGlasow, 2009, Atmospheric composition change – global and regional air quality, Atmospheric Environment, Submitted.

Norris, J. R., M. Wild, Trends in aerosol radiative effects over Europe inferred from observed cloud cover, solar "dimming," and solar "brightening", *J. Geophys. Res. Atmospheres* 112, doi:10.1029/2006JD007794 (Apr 26, 2007).

Philipona, R., K. Behrens, and C. Ruckstuhl (2009), How declining aerosols and rising greenhouse gases forced rapid warming in Europe since the 1980s, *Geophys. Res. Lett.*, *36*, L02806, doi:10.1029/2008GL036350.

Riccio, A., Giunta, G and S. Galmarini, Seeking for the rational basis of the Median Model: the optimal combination of multi-model ensemble results. Atmospheric Chemistry and Physics, 7, 6085–6098.

Schmidt, H., Derognat, C., Vautard, R., and Beekmann, M., 2001. A comparison of simulated and observed ozone mixing ratios for the summer of 1998 in Western Europe. *Atmospheric Environment,* **36**, 6277–6297.

Sillman, S., R. Vautard, L. Menut and D. Kley, 2003: O3-NOx-VOC sensitivity and NOx –VOC indicators in Paris: results from models and ESQUIF measurements, J. Geophys. Res., 108, D17, 8563.

Stern, R., P. Builtjes, M. Schaap, R. Timmermans, R. Vautard, A. Hodzic, M. Memmesheimer, H. Feldmann, E. Renner, R. Wolke, and A. Kerschbaumer, 2008 : A model inter-comparison study focusing on episodes with elevated PM10 concentrations. Atmos. Environ, 42, 4567–4588.

Szopa, S., Hauglustaine, D. A., Vautard, R., Menut, L., 2006 : Future global tropospheric ozone changes and impact on European air quality. Geophys. Res. Lett., 33, L14805, doi:10.1029/2006GL025860.

Tilmes, S., Brandt, J., Flatoy, F., Bergrstrom, R., Flemming, J., Langner, J., Christensen, J.H., Frohn, L.M., Hov, O., Jacobsen, I., Reimer, E., Stern, R., Zimmermann, J., 2002. Comparison of five Eulerian air pollution forecasting systems for the summer of 1999 using the German ozone monitoring data. Journal of Atmospheric Chemistry 42, 91–121.

Timmermans, R. M. A., Segers, A. J., Builtjes, P. H. J., Vautard, R., Siddans, R., Elbern, H., Tjemkes, S. A. T., and M. Schaap, 2009, The added value of a proposed satellite imager for ground-level particulate matter analyses and forecasts. IEEE J-STARS, submitted.

Van Loon, M., R. Vautard, M. Schaap, R. Bergström, B. Bessagnet, J. Brandt, P.J.H. Builtjes, J. H. Christensen, K. Cuvelier, A. Graf, J.E. Jonson, M. Krol, J. Langner, P. Roberts, L. Rouil, R. Stern, L. Tarrasón, P. Thunis, E. Vignati, L. White, P. Wind, 2007: Evaluation of long-term ozone simulations from seven regional air quality models and their ensemble average. Atmos. Environ., 41, 2083–2097.

Vautard, R., Martin, D, Beekmann, M. Drobinski, P., Friedrich, R., Jaubertie, A., Kley, D., Lattuati, M., Moral, P., Neininger, B., Theloke, J., 2003, Paris emission inventory diagnostics from ESQUIF airborne measurements and a chemistry transport model, J. Geophys. Res. 108, D17, 8564.

Vautard, R., Honoré, C., Beekmann, M. and L. Rouil, 2005: Simulation of ozone during the August 2003 heat wave and emission control scenarios. Atmospheric Environment, 39, 2957–2967.

Vautard, R., M. Van Loon, M. Schaap, R. Bergström, B. Bessagnet, J. Brandt, P.J.H. Builtjes, J. H. Christensen, K. Cuvelier, A. Graf, J.E. Jonson, M. Krol, J. Langner, P. Roberts, L. Rouil, R. Stern, L. Tarrasón, P. Thunis, E. Vignati, L. White, P. Wind, 2006: Is regional air quality model diversity representative of uncertainty for ozone simulation ? Geophys. Res. Lett., 33, L24818, doi:10.1029/2006GL027610.

Vautard, R., M. Beekmann, J. Desplats, A. Hodzic, S. Morel, 2007. Air quality in Europe during the summer of 2003: a prototype of air quality in a warmer climate. CR Geoscience, 339, 747–763.

Vautard, R., Yiou, P., and G. J. van Oldenborgh, 2009: Decline of fog, mist and haze in Europe over the past 30 years, Nature Geoscience, 2, 115–119.

## 6. Questions and Answers

**S. Galmarini:** Which are your research priorities in AQ modeling and can you comment on the role of subgrid scale processes (not necessarily emissions) in regional AQ modeling?

**Answer:** More detailed measurements are needed to understand chemistry and more specifically aerosol processes. I would give first priority to detailed aerosol measurements. Then for modeling, long-term regional climate-air quality coupled simulations must be carried out requiring model development, and computer power for regional simulations. Subgrid scale processes are very important because they are the missing link between regional air quality and exposure. Several methods are currently being developed to account for subgrid scale variability.

**Douw Steyn:** Can you comment on the ability of existing climate models to capture frequencies of occurrence of synoptic conditions conducive of episodes with degraded air quality?

**Answer:** This is a key question. Climate models do not presently have the resolution to represent air flows conducive to episodes. It is not clear whether they are representing, even for present climate, the correct frequency of such weather regimes. Even so this does not prevent predicted climate to have the right frequencies. This question should be investigated in the future.

# 2.2 Application of CAMx Model in Switzerland with the New SOA Mechanism

**Ş. Andreani-Aksoyoğlu, D. Oderbolz, J. Keller, I. Barmpadimos, A.S.H. Prévôt, and U. Baltensperger**

Laboratory of Atmospheric Chemistry (LAC), Paul Scherrer Institute, Switzerland

**Abstract** In this study, we report the preliminary results of the CAMx (Comprehensive Air quality Model with eXtensions) application in Switzerland using a new secondary organic aerosol (SOA) module. The latest CAMx version includes polymerization of SOA in addition to partitioning mechanism as well as other SOA formation pathways such as from isoprene and sesquiterpenes. The aerosol parameters were updated as well. The model was tested for two different periods in winter and summer 2006. We compared the model results with the Aerosol Mass Spectrometer (AMS) measurements. Simulations with earlier model version underestimated organic aerosols and contradicted the measurements about the fractions of SOA and POA (primary organic aerosols). A significant improvement (20%) was achieved in SOA formation in winter using the new version. The SOA concentrations increased by 11% for the summer episode. The improvements are due to increased SOA production and polymerization from biogenic precursors.

**Keywords** SOA, CAMx, aerosols, polymerization, biogenic emissions

## 1. Introduction

The current models often underestimate SOA concentrations (Volkamer et al., 2006; Andreani-Aksoyoğlu et al., 2008). A recent model study by Morris et al. (2006) showed that including mechanisms such as polymerization, SOA formation from isoprene and sesquiterpenes led to increased SOA yields. Robinson et al. (2007) indicated another pathway to SOA formation from primary organic-particulate emissions. The authors showed experimentally that photo-oxidation of diesel emissions rapidly generates organic aerosol, greatly exceeding the contribution from known secondary organic-aerosol precursors. There were several measurements in northern Switzerland during winter and summer 2006 investigating the chemical composition of particles. In this study, winter and summer episodes were simulated by two CAMx versions.

D.G. Steyn and S.T. Rao (eds.), *Air Pollution Modeling and Its Application XX*,
DOI 10.1007/978-90-481-3812-8, 

## 2. Method

In this study, we used the CAMx version 4.42 and 4.51 (Environ, 2008). We calculated the meteorological parameters using the MM5 model (PSU/NCAR, 2004). There were three domains with resolutions of 27 × 27 km (Europe), 9 × 9 km (central Europe) and 3 × 3 km (Switzerland). We used 14 σ-layers in a terrain-following Lambert Conic Conformal coordinate system in CAMx. The initial and boundary conditions were extracted from the output of the global model MOZART for similar periods (Horowitz et al., 2003). The simulated episodes are January and June 2006. The concentrations of particles smaller than 2.5 μm in diameter were calculated using CAMx. The main changes in the new version (4.51) are CB05 gas-phase mechanism (instead of CB4), SOA formation from isoprene and sesquiterpenes (in addition to monoterpenes), polymerization of anthropogenic and biogenic SOA. In addition, the saturation concentrations and values of enthalpy of vaporization were updated as well.

## 3. Results and Discussion

Both measurements and model results suggest that the main components of the winter aerosols in Zurich are particulate nitrate and organic aerosols. The organic aerosols calculated by the previous model version were mainly primary organic aerosols whereas the measurements suggested that more than half of the particulate organic mass was oxygenated organic aerosols (OOA), mostly representing secondary organic aerosols (Lanz et al., 2008). Calculations with the new model version improved the organic aerosol fraction by 20% mainly due to increased SOA formation from biogenic precursors and their polymerization. Model predicted 45% of OA as secondary (Fig. 1). In spite of the improvements in SOA modeling, the predicted total organic aerosol concentrations are still lower than the measurements (Fig. 2).

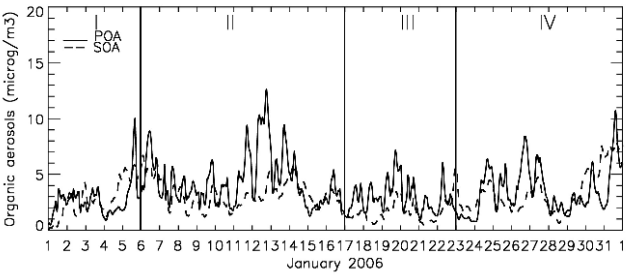


**Fig. 1.** Predicted organic aerosol (OA) concentrations with new model version (CAMx4.51) in January 2006. I and III: high-wind, II and IV: low-wind periods

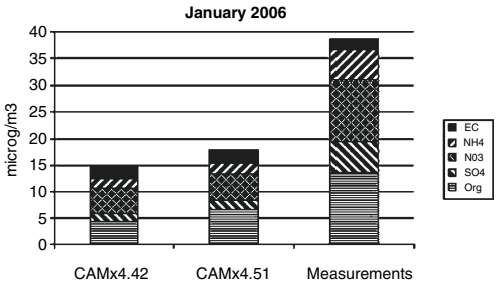


**Fig. 2.** Predicted aerosol concentrations with two model versions (CAMx4.42 and CAMx4.51) as well as measurements at Zurich in January 2006

The calculations for the summer episode suggested an increase in OA by 11%. Model results indicate that SOA fraction in summer is about 70% and comes mainly from biogenic precursors. In spite of the improvements, predicted OA concentrations are still lower than the measurements (Fig. 3). The highest fraction of SOA in winter is predicted to come from monoterpenes. On the other hand, sesquiterpenes are the main source of SOA in summer.

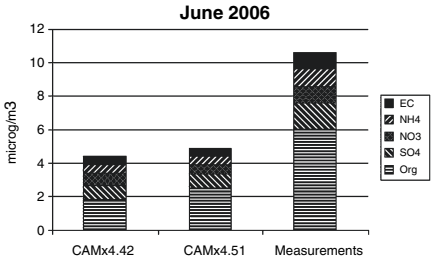


**Fig. 3.** Predicted aerosol concentrations with two model versions (CAMx4.42 and CAMx4.51) as well as measurements at Payerne in June 2006

## 4. Conclusions

We compared the results of aerosol simulations with two CAMx versions (v4.42 and v4.51) for winter and summer episodes in Switzerland. The organic aerosols predicted by the earlier version in winter were mainly primary, however, analysis of AMS data suggested that about half of the particulate organic mass in winter was oxygenated organic aerosols (OOA), mostly representing SOA. The new version with updated SOA module led to improved SOA concentrations (20%) due to polymerization and updated SOA parameterization. Results indicate a similar trend about the POA and SOA fractions as measurements suggest. On the other hand, improvement in SOA was less in summer (11%). Both model predictions and measurements suggest that the main component of aerosols is the

organic aerosol fraction in summer and it is mostly secondary. The preliminary model results indicate that secondary organic aerosols are produced mainly from the biogenic precursors. Another approach using Volatility Basis Set will be tested in the near future as well (Robinson et al., 2007; Donahue et al., 2009).

**Acknowledgments** This study was financially supported by the Federal Office of Environment (FOEN). We thank Environ, MeteoSwiss, FUB, UBA, TNO, INFRAS, METEOTEST, EMPA, ACCENT, M.R. Alfarra, J. Sandradewi, M. Schultz and S. Pandis.

## References

Andreani-Aksoyoğlu, S., J. Keller, A. S. H. Prévôt, U. Baltensperger, and J. Flemming (2008), Secondary aerosols in Switzerland and northern Italy: Modeling and sensitivity studies for summer 2003, *Journal of Geophysical Research*, *113*, D06303, doi:06310.01029/02007JD009053.

Donahue, N. M., A. L. Robinson, and S. N. Pandis (2009), Atmospheric organic particulate matter: From smoke to secondary organic aerosol, *Atmospheric Environment*, *43*, 94–106.

Environ (2008), User's Guide, Comprehensive Air Quality Model with Extensions (CAMx), Version 4.50, Environ International Corporation, California.

Horowitz, L. W., S. Walters, D. L. Mauzerall, L. K. Emmons, P. J. Rasch, C. Granier, X. Tie, J.-F. Lamarque, M. G. Schultz, G. S. Tyndall, J. J. Orlando, and G. P. Brasseur (2003), A global simulation of tropospheric ozone and related tracers: Description and evaluation of MOZART, version 2. , *J. Geophys. Res.*, *108*, 4784, doi:4710.1029/2002JD002853.

Lanz, V. A., M. R. Alfarra, U. Baltensperger, B. Buchmann, C. Hueglin, S. Szidat, M. N. Wehrli, L. Wacker, S. Weimer, A. Caseiro, H. Puxbaum, and A. S. H. Prevot (2008), Source Attribution of Submicron Organic Aerosols during Wintertime Inversions by Advanced Factor Analysis of Aerosol Mass Spectra, *Environ. Sci. Technol.*, *42*, 214–220.

Morris, R. E., B. Koo, A. Guenther, G. Yarwood, D. McNally, T. W. Tesche, G. Tonnesen, J. Boylan, and P. Brewer (2006), Model sensitivity evaluation for organic carbon using two multi-pollutant air quality models that simulate regional haze in the southeastern United States, *Atmospheric Environment*, *40*, 4960–4972.

PSU/NCAR (2004), MM5 Version 3 Tutorial Presentations.

Robinson, A. L., N. M. Donahue, M. K. Shrivastava, E. A. Weitkamp, A. M. Sage, A. P. Grieshop, T. E. lane, J. R. Pierce, and S. N. Pandis (2007), Rethinking Organic Aerosols: Semivolatile emissions and photochemical aging *Science*, *315*, 1259–1262.

Volkamer, R., J. L. Jimenez, F. S. Martini, K. Dzepina, Q. Zhang, D. Salcedo, L. T. Molina, D. R. Worsnop, and M. J. Molina (2006), Secondary organic aerosol formation from anthropogenic air pollution: Rapid and higher than expected, *Geophysical Research Letters*, *33*, doi:10.1029/2006GL026899.

## 5. Questions and Answers

**M. Sofiev:** Apart from differences in chemistry and formation mechanisms emission of pre-cursors is of importance, in particular, bio-VOC. Could you please go into some details of your bio-VOC emissions?

**Answer:** We are using our own emission inventory. The European land use is used for the mother domain and then the data inside Swiss borders are replaced by our own detailed data. More than 70% of our forests are coniferous. We have ten different tree species in the inventory. Most abundant ones are Norway Spruce and fir. We calculate the emission rates using temperature and irradiance data from MM5 output.

**W. Gong:** You showed that SOA from isoprene has very small contribution. You do consider isoprene as SOA precursor in your mechanism, don't you?

**Answer:** Yes, SOA formation mechanism from isoprene is included in the mechanism. However, isoprene emissions are very low with respect to monoterpene emissions in Switzerland. Terpenes dominate biogenic emissions. There are relatively low isoprene emissions coming from oak trees in southern Switzerland.

# 2.3 Nonlinear Formation of Ozone in Power Plant Plumes in Texas

**Wei Zhou and Daniel S. Cohan**

Department of Civil and Environmental Engineering, Rice University, Houston, TX 77005, USA

**Abstract** Six Texas power plants are simulated in a photochemical model with higher-order direct sensitivity analysis to investigate the nonlinear ozone formation of power plant plumes. Power plants with largest $NO_x$ emissions had the largest spatial extent of ozone impact. Ozone production tended to occur sooner in small $NO_x$ plumes, but overall ozone production efficiency was similar for plumes. Ozone formation was most nonlinear near power facilities but became a nearly linear function of emissions as plumes dispersed downwind.

## 1. Introduction

Power plants are the largest point source emitters of nitrogen oxides ($NO_x$ = NO and $NO_2$), yet emit very little volatile organic compounds (VOC). Ozone formation in power plant plumes thus exhibits distinct features from that in other industrial or urban plumes. Numerous modeling and observational studies have characterized ozone formation in power plant plumes and its dependence on factors such as $NO_x$ emissions intensity and the extent of nearby VOC emissions (Luria et al., 2003; Nunnermacker et al., 2000; Ryerson et al., 2001; Sillman, 2000; Springston et al., 2005).

In this study, six power plants in Texas, three of which have the largest NOx emissions in the state, are simulated with a high-order direct sensitivity method to examine how the nonlinearity of ozone formation evolves as plumes disperse.

## 2. Methodology

The Comprehensive Air Quality Model with Extensions (CAMx) is applied with the CB-05 chemical mechanism to simulate air quality during the period June 1–15, 2006. The modeling domain covers eastern Texas and surrounding states with 12-km resolution (Fig. 1). Emissions and meteorology inputs were provided by the Texas Commission on Environmental Quality (TCEQ, 2008). Model performance was evaluated by comparison with ambient monitoring of ozone and other pollutants.

D.G. Steyn and S.T. Rao (eds.), *Air Pollution Modeling and Its Application XX*,
DOI 10.1007/978-90-481-3812-8, © Springer Science + Business Media B.V. 2010

In addition to baseline modeling, brute force "zero-out" simulations and high-order decoupled direct method (HDDM) sensitivity analysis (Dunker, 1984; Hakami et al., 2003; Koo et al., 2007) were conducted to simulate the impacts of each of six power plants (Table 1). Four of the facilities (Martin Lake, Limestone, Monticello, and Welsh) are among the largest $NO_x$ emitters in Texas and located amidst dense biogenic emissions of isoprene (Fig. 1). The other two, Deepwater and Parish, are in the Houston metropolitan region.

The zero-out source contributions (ZOC) of the facilities were computed by differencing concentrations from the baseline and zero-out simulations:

$$ZOC_{i,j} = C_i(base) - C_i(zero\ out\ j) \tag{1}$$

where $C_i$ is concentration of species $i$, and $j$ is the facility. The HDDM first- and second-order sensitivity coefficients, defined as the first- and second-order derivatives of concentration to emissions respectively, characterize the responsiveness of concentrations to small changes in emissions.

The zero-out and HDDM results were used to develop metrics characterizing the efficiency, spatial extent, and nonlinearity of ozone formation in each plume. Ozone production efficiency (OPE) is the number of ozone molecules produced per $NO_x$ molecule lost and is a key metric of pollutant formation in a plume (Liu et al., 1987). Here, we approximate OPE by the ratio of ozone to $NO_z$ ($NO_z$ = reactive nitrogen ($NO_y$) – $NO_x$) contributed by the plume:

$$OPE = \frac{ZOC_{O_3,j}}{ZOC_{NO_z,j}} \tag{2}$$

This equation assumes that all ozone formed and $NO_x$ lost in a plume remain as ozone and $NO_z$, respectively. Over time, deposition of nitric acid and ozone can influence the ratio (Neuman et al., 2004; Nunnermacker et al., 2000).

To characterize the spatial extent of ozone formation, we define a Distance of Ozone Impact metric by the following equation.

$$DI = \frac{\sum_x d_j(x) \cdot ZOC^+_{O3,j}(x)}{\sum_x ZOC^+_{O3,j}(x)} \tag{3}$$

Here, $d_j(x)$ is the distance from power plant j to cell x, and $ZOC^+_{O3,j(x)}$ is the contribution of $NO_x$ emissions from j to ozone at x (excluding cells with negative source contributions).

A final metric, the nonlinearity index (α), characterizes the nonlinearity of pollutant responsiveness to emissions changes (Cohan et al., 2005).

$$\alpha_{i,j} = \left| \frac{S^{(2)}_{i,j}}{2S^{(1)}_{i,j}} \right| \tag{4}$$

High levels of α typically indicate that a large reduction in a $NO_x$ source would yield more ozone reduction per ton than a small reduction, whereas a small α indicates that the ozone impact scales linearly with the amount of emissions reduction.

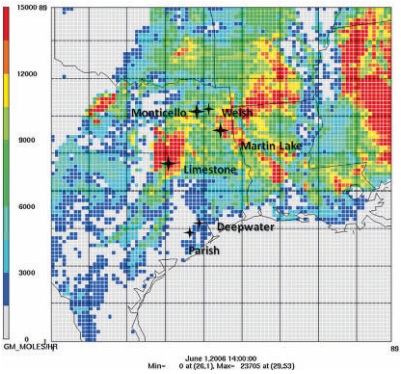


**Fig. 1.** Isoprene emissions (mol/h) and the locations of power plants studied here

## 3. Results

The DI metric (Eq. 3) was computed for each power plant plume on each afternoon at 2:00 pm. DI tended to be largest at the plants with the largest $NO_x$ emissions, likely reflecting a longer time for ozone to form as these more intense plumes disperse. For most days of the episode, Martin Lake and Limestone were the two power plants with largest DI and Parish had the smallest DI (Table 1).

**Table 1.** Locations, emission, electrical generation of power plants studied

| Plant name | $NO_x$ emissions (tons/day)[a] | Annual electrical generation (GWh)[b] | Height of stacks (m) | Distance of ozone impact (km)[c] |
|---|---|---|---|---|
| Deepwater | 11.6 | 1,209 | 145 | 112 |
| Limestone | 40.9 | 13,017 | 137 | 140 |
| Martin | 48.5 | 17,239 | 137 | 138 |
| Monticello | 33.8 | 14,048 | 137 | 132 |
| Parish | 16.6 | 19,144 | 51–180 | 77 |
| Welsh | 26.9 | 10,395 | 92 | 107 |

[a]From TCEQ, 2008. [b]eGRID. [c]At 2:00 pm

For each distance from each power plant, maximal $ZOC_{NOy}$ was used to diagnose which cell was at the plume center. For large power plants, ozone production efficiency tends to increase asymptotical with distance (a proxy for plume age) as the plume dilutes and more ozone forms. The smaller power plants tended to reach their maximal OPE at first due to more rapidly dilution to $NO_x$ limited conditions.

The nonlinearity index (α) decreases dramatically with distance downwind of the power plant, as the magnitude of $S^{(2)}$ declines much more quickly than $S^{(1)}$ (Fig. 2). This is consistent with the findings of Cohan et al. (2005), who showed that α increased with the intensity of a $NO_x$ plume.

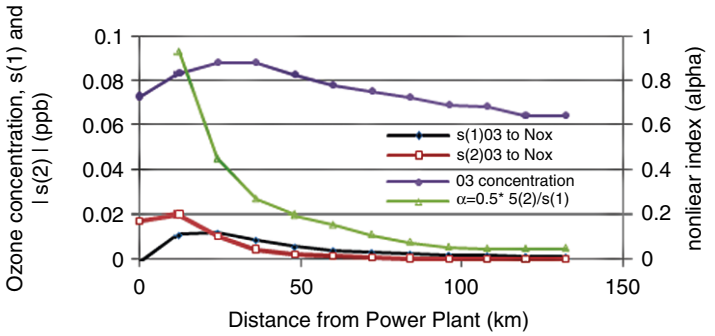


**Fig. 2.** Surface layer baseline ozone concentration and its first- and second-order sensitivity to Martin Lake $NO_x$ at the center of the plume (defined by maximal $ZOC_{NOy}$ ) on June 4, 2006, at 14:00 ($S^{(2)}$ is negative, plot shows $|S^{(2)}|$)

## 4. Conclusion

The nonlinear formation of ozone from six Texas power plants has been characterized for a summertime air pollution episode. The spatial extent of the ozone impacts tends to increase with the size of the $NO_x$ source, as ozone production occurred more quickly in the smaller $NO_x$ plumes. However, the large power plant plumes considered here achieved relatively high OPE's downwind, likely reflecting the rich biogenic emissions near those facilities.

The nonlinearity of ozone impact tended to be greatest for the largest $NO_x$ emitters and to sharply decrease with time as each plume dispersed downwind. This suggests that while power plant impacts are highly nonlinear near the facility, responsiveness to controls will be nearly linear at large distances downwind.

One limitation of this study is the use of 12-km resolution, which may unrealistically dilute the initial intensity of the $NO_x$ plumes and thus fail to capture ozone titration near the facilities. Future work could apply finer resolution or plume-in-grid modeling to better resolve the near-facility features of ozone formation.

## References

Cohan DS, Hakami A, et al. (2005) Nonlinear response of ozone to emissions: Source apportionment and sensitivity analysis, *Environ Sci Technol*, *39*(17), 6739–6748.

Dunker AM (1984) The decoupled direct method for calculating sensitivity coefficients in chemical kinetics, *J. Chem. Phys.*, *81*(5), 2385–2393.

Hakami A, Odman MT, et al. (2003) High-order, direct sensitivity analysis of multidimensional air quality models, *Environ Sci Technol*, *37*(11), 2442–2452.

Koo B, Yarwood G, et al. (2007) Incorporation of High-order Decoupled Direct Method (HDDM) Sensitivity Analysis Capability into CAMx, Prepared for Texas Commission on Environmental Quality.

Liu SC, Trainer M, et al. (1987) Ozone production in the rural troposphere and the implications for regional and global ozone distributions, *J Geophys Res-Atmos*, *92*(D4), 4191–4207.
Luria M, Imhoff RE, et al. (2003) Ozone yields and production efficiencies in a large power plant plume, *Atmos Environ*, *37*(25), 3593–3603.
Neuman JA, Parrish DD, et al. (2004) Nitric acid loss rates measured in power plant plumes, *J Geophys Res-Atmos*, *109*(D23), 13.
Nunnermacker LJ, Kleinman LI, et al. (2000) NOy lifetimes and O-3 production efficiencies in urban and power plant plumes: Analysis of field data, *J Geophys Res-Atmos*, *105*(D7), 9165–9176.
Ryerson TB, Trainer M, et al. (2001) Observations of ozone formation in power plant plumes and implications for ozone control strategies, *Science*, *292*(5517), 719–723.
Sillman S (2000) Ozone production efficiency and loss of NOx in power plant plumes: Photochemical model and interpretation of measurements in Tennessee, *J Geophys Res-Atmos*, *105*(D7), 9189–9202.
Springston SR, Kleinman LI, et al. (2005) Chemical evolution of an isolated power plant plume during the TexAQS 2000 study, *Atmos Environ*, *39*(19), 3431–3443.
Texas Commission on Environmental Quality (TCEQ) (2006) Houston-Galveston-Brazoria Eight-Hour Ozone SIP Modeling.

## 5. Questions and Answers

**Stefano Galmarini:** Turbulent mixing can significantly affect chemical reactions of species as the time scale of turbulent mixing is comparable to that of chemical reactions. Did you take them into account in your model?

**Answer:** We have not taken sub-gridscale turbulent mixing into account in our model and analysis.

**S.T. Rao:** Have you considered plume_in_grid option in your modeling? Have you analyzed the impact of transport of power plant plumes overnight?

**Answer:** In our CAMx base model, we did not use the plume_in_grid options. We modeled a multi-day episode including daytime and nighttime, but our analysis to date focuses on impacts on afternoon ozone.

# 2.4 Real-Time Air Quality Assessment and Management: Cascading Models in a Web Based Implementation

**K. Fedra[1], Y. Rashidi[2], and T. Kim[3]**

[1] Environmental Software and Services GmbH, Austria

[2] Air Quality Control Company, Tehran, Iran

[3] BioTel, Seoul, South Korea

**Abstract** For the assessment of regional to local air quality in urban and industrial areas, a system of coupled models (AirWare) that cover several levels of nesting from regional (several hundred kilometers) to city level and street canyons has been developed in EUREKA E!3266 WEBAIR. The main objectives are to support regulatory tasks, compliance monitoring, and public information, and to provide a reliable basis for the multi-criteria optimization of emission control strategies to effectively and efficiently meet a range of environmental standards. Examples from Tehran, Iran, and Seoul/Gyeonggi-do, South Korea are used to demonstrate the system operation and performance. We compare two very large cities with different physiographical and socio-economic structures, management objectives, and policy options, yet a common problem. A web based implementation where all functions are accessed by a standard web browser provides ease of use for all major actors and stakeholders including public information functions. The system includes daily forecasts (meteorology and air quality) for 3–7 days, and hourly now-casts with data assimilation. In parallel to forecast and now-cast runs, the system supports interactive scenario analysis for EIA and emission control optimization tasks. The simulation tools include MM5 and WRF for meteorological forecasts based on downscaling global (GFS) weather forecasts, and dynamic emission modeling. The models are linked to several data bases (monitoring data and emission inventory) and an embedded GIS. CAMx is used for photochemistry and particulates, AERMOD for conservative substances. A high-resolution convolution model with a near-field mixing zone is based on AERMOD as a computational kernel for city-wide line sources and local concentration gradients with allows for near real-time simulation of thousands of road segments. Additional models include a 3D FD code for street canyons with explicit building obstacles for selected hot-spots, and a stochastic implementation of CAMx for probabilistic ozone forecasts.

D.G. Steyn and S.T. Rao (eds.), *Air Pollution Modeling and Its Application XX*,
DOI 10.1007/978-90-481-3812-8, © Springer Science + Business Media B.V. 2010

## 1. Objectives and Functions

A central objective of the AirWare system is to support monitoring and regulatory compliance (e.g., with the European Union Air Quality Framework Directive 96/62/EEC); this includes an important public information component that is extended by daily forecast of up to 7 days, as well as probabilistic forecasts using the 3D photochemical code CAMx both with an ensemble of meteorological forecasts, and assumed PDF around the major emission sources and their dynamics. Results are shown as color coded map overlays for current or forecast ambient concentrations, or air quality indices such as PSI, CAI, APMI, incorporating moving averages and maxima for several substances over longer periods. The series of multi-day forecasts at any given date is also available as an animation of hourly ambient concentration plots over the background map, formatted as an mpeg movie. Beyond monitoring and forecasts, AirWare includes tools for data analysis (emissions, monitoring) and several analytical functions. These support scenario analysis (WHAT IF … questions), direct comparison of scenarios, and impact assessment, as well as optimization task (HOW BEST TO …): for each emission source or class of emission sources one or more alternative or additive emission control technologies can be assigned with it respective (piecewise linear) costs functions for annualized investment and operational costs. A combination of Monte Carlo, adaptive heuristics and machine learning, and genetic algorithms, and a discrete multi-criteria DSS as post-processing tool then allocates and scales technologies to design a set of pareto-optimal solutions given a set of user defined constraints on environmental and economic performance criteria. A similar tool finds optimal location for monitoring stations given a series of long-term (annual) model runs at hourly resolution and a preference structure for the monitoring.

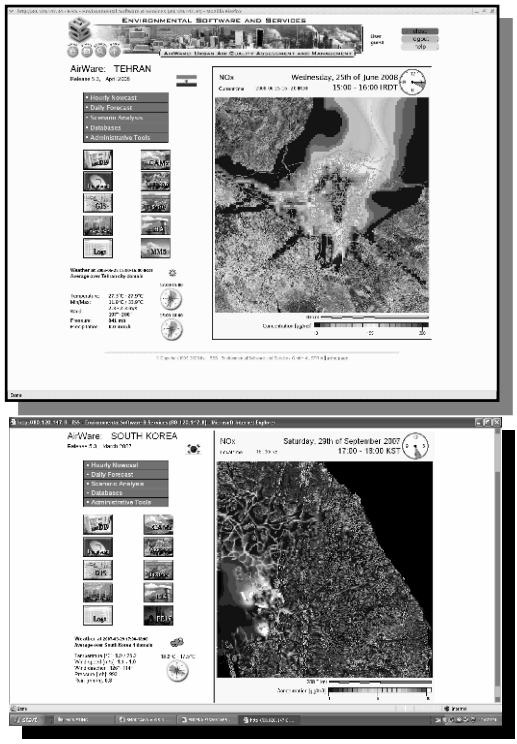

## 2. Components and Implementation

Beside the model supported monitoring and public information, AirWare offers data bases and analysis tools for emission sources, including dynamic emission modeling; monitoring data analysis for both historical data sets and the real-time data acquisitions; a data base of emission control technologies used for the optimization; and an embedded GIS that manages distributed models input data such as DEM, land cover, but also population distribution for exposure analysis. The primary models in AirWare are the prognostic meteorological models MM5 and WRF, that generate high-resolution meteorological fields to drive the air quality models. The central model is the 3D nested-grid photochemical code CAMx (in Korea, Anyang University uses CMAQ in parallel), and AERMOD for regulatory applications, long-term (annual) impacts assessment, and a high-resolution convolution version with a mixing zone representation of streets and the near-field gradients from traffic sources. For larger individual point sources under transient conditions and very short time steps (e.g., boiler start-up), we use a version of (multi)PUFF, Lagrangian transport of a Gaussian plume. Finally, for very high-resolution near field representation where building obstacles have to be treated explicitly, a CFD code (TIMES-URBAN) developed in collaboration with the Russian Academy of Sciences, Institute for Mathematical Modeling, is used. These models obtain their input data "automatically" from dynamic emission models. The models in turn use an emission data base and emission scenarios, generated for any arbitrary spatial model domain and model period, using historical data, data observed in real-time, or data generated (forecasted) with temporal patterns from average emission values. AirWare is implemented as a distributed client-server system, that uses the Internet protocol TCP/IP to connect several "logical application servers", remote information resources (monitoring networks as well as high-performance cluster computing for demanding simulations and forecasts), and its users through any networked device that supports standard web browsers or the MMS/WAP protocol for mobile clients such as smart phones or PDAs.

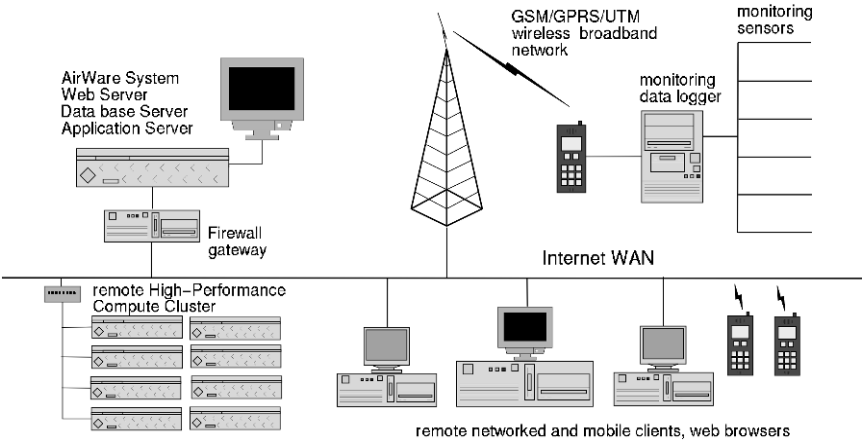

## 3. Test Application Examples

Within the international EUREKA E!3266 WEBAIR development project (http://www.ess.co.at/WEBAIR), several parallel test cases are used to develop and validate the system. They include: the Island Republic of Cyprus and a several urban scale case studies including Limassol. Cyprus has comparatively low emissions, but complex meteorology due to its island nature; the Korean peninsula, with a central case study of Seoul metropolitan area and the surrounding heavily industrialized province Gyeonggi-do; the Greater Tehran Area around the capital city of Iran, a case that is dominated by traffic sources; the industrial city of Sisak in Croatia; and selected industrial development zones along the Arabian Gulf, United Arab Emirates. Experiments with real-time data assimilation are just starting, but the comparison with historical data shows very good correspondence of model results with observational data for both meteorological and photochemical air quality model results.

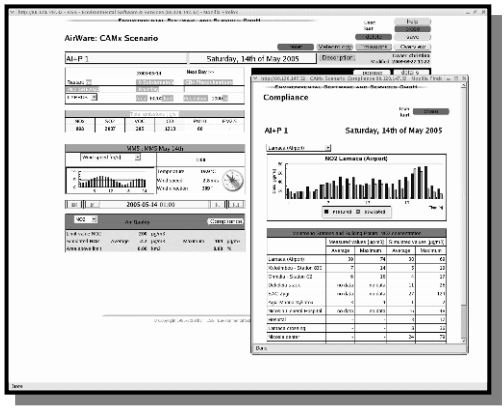


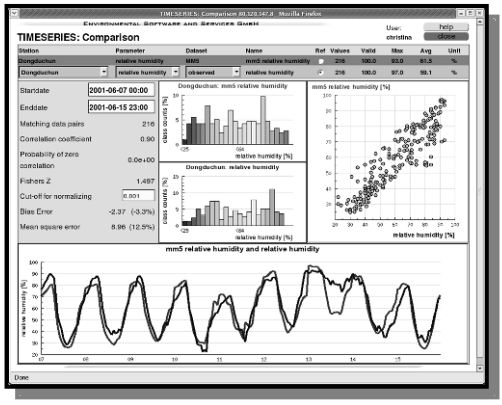


The on-line pilot systems and operational forecasts are accessible from http://www.ess.co.at/DEMOS#air, and the WEBAIR and AirWare project sites: http://www.ess.co.at/WEBAIR and http://www.ess.co.at/AIRWARE

## 4. Questions and Answers

**Peter Builtjes:** Did you consider improving your air quality forecasting by improving – trying – the emission "forecasting" ?

**Kurt Fedra**: Yes, we try to tune both the temporal patterns used (analyzing the residuals) as well as for individual monitoring stations where the wind-direction dependent contributions can be well identified (apportionment) by adjusting sectoral emission scaling factors if the bias is "consistent".

# 2.5 Sea-Salt Aerosol Forecasts over the Mediterranean Sea

**P. Kishcha[1], S. Nickovic[2], A. Luvchik[1], Z. Janjic[3], N. Pérez[4], M. Viana[4], N. Mihalopoulos[5], Mamane[6], O. Yossef[6], and P. Alpert[1]**

[1]Department of Geophysics and Planetary Sciences, Tel-Aviv University, 69978 Tel-Aviv, Israel,

[2]World Meteorological Organization, Geneva, Switzerland,

[3]NCEP/UCAR, Washington, DC, USA,

[4]Institute for Environmental Assessment and Water Research (IDAEA-CSIC), Barcelona, Spain,

[5]University of Crete, Heraklion, Crete, Greece,

[6]Faculty of Civil and Environmental Engineering, Technion, Haifa, Israel

**Abstract** Numerical simulations of sea-salt aerosol (SSA) over the Mediterranean were conducted and compared with sea-salt ground-based measurements taken at the following three sites: Barcelona, Spain, a 2-year data set (2006–2007); Tel-Aviv, Israel, from March 12 to April 9, 2006; and Finokalia, Crete, Greece, from May 2 to 30, 2008. The comparison showed that the model was capable of producing reasonable sea-salt concentrations. We found that specific features of the monitoring site located over the land could contribute to some discrepancy between model data and measurements. In summer, the model underestimated SSA-measurements when actual sea-wave height did not correspond to observed surface sea winds. In winter, winds which do not blow from sea to land create sea-salt aerosols over the sea in the vicinity of Barcelona: these aerosols are not transported inland. Under these circumstances, the model overestimated sea-salt measurements.

## 1. Introduction

SSA scatters solar radiation and thereby plays an important role in the atmospheric radiation budget. Acting as cloud condensation nuclei, sea-salt could affect cloud formation in the marine boundary layer. The Mediterranean Sea is of specific interest as it is a crossroad where natural aerosols and anthropogenic aerosols from different sources are superimposed. Because of the lack of in situ ground-based sea-salt measurements, model-based 24-h forecasts of SSA could be helpful, providing valuable information about space and time distributions of sea-salt aerosols in the Mediterranean region. This study was aimed at comparing quantitatively madel-predicted sea-salt aerosol concentrations with sea-salt ground-based

D.G. Steyn and S.T. Rao (eds.), *Air Pollution Modeling and Its Application XX*,
DOI 10.1007/978-90-481-3812-8, © Springer Science + Business Media B.V. 2010

measurements at the following three Mediterranean sites: Barce-lona, Spain; Tel-Aviv Israel; and Finokalia, Crete, Greece. It is known from previous studies that there are some discrepancies between model data and SSA-measurements. We found that specific features of the monitoring sites, located over the land, could contribute to the discrepancies between model data and measurements. The full description of this study has been previously submitted for publication to the Journal of Geophysical Research (Kishcha et al., 2009).

## 2. Methodology

Numerical simulations of the sea-salt aerosols were conducted using the first version of the DREAM-Salt prediction model. This model is based on the DREAM dust aerosol model (Nickovic et al., 2001), which was adapted to function not only for mineral dust but also for sea salt aerosols (Nickovic et al., 2007). In operational use in Tel-Aviv University, DREAM-Salt produces daily forecasts of 3-D distribution of sea-salt aerosol concentration over the Mediterranean model domain 20W–45E, 15N–50N (http://wind.tau.ac.il/salt-ina/salt.html). The model has 0.3° horizontal resolution, and 24 vertical levels. Forecasts are made once every day, starting from the 12:00 UTC objective analyses and providing forecasts up to 72 h ahead. The NCEP/Eta regional atmospheric model (Janjic, 1994) drives the aerosol. The aerosol emission scheme is based on the viscous sub-layer model (Janjic, 1994), in which energy and mass transfers above the air-sea interface critically depend on turbulent conditions. The aerosol concentration at the top of the viscous sub-layer is used as the lower boundary condition. The sea-salt emission scheme defines the lower boundary condition using the source function of Erickson et al. (1986). Eight particle categories with sizes ranging from 1 to 8 μm are used in the model. DREAM-Salt incorporates parameterizations of all other major phases of atmospheric sea-salt aerosol life such as: diffusion, advection, gravitational settling, and wet removal of sea-salt aerosols (Nickovic et al., 2001).

In Barcelona, the sea-salt measurements were taken 2 days/week during the 2-year period, 2006–2007. In Tel-Aviv, a special sampling campaign was arranged, which resulted in the collection of sea salt measurements from March 12 to April 9, 2006. Both in Barcelona and in Tel-Aviv, samples were collected over 24 h with the usual start time of 0900 LT. In Finokalia, Crete, 6-h-averaged measurements were taken from May 2–30, 2008.

## 3. Results and Discussion

Shown in Fig. 1a, a model-vs.-measurements comparison in Finokalia shows similarities between model data and 6-h measurements. Some overestimation can be partly explained by the fact that, in the sea, sea-salt aerosols are produced under

any wind direction. However, sea-salt transport inland, to the monitoring site, depends on a specific wind component directed from sea to land. Because of coarse resolution, the model produced the same sea-salt concentration over the monitoring site as over the adjacent sea area. This is correct for all sites located over the land, except for those located at very small islands.

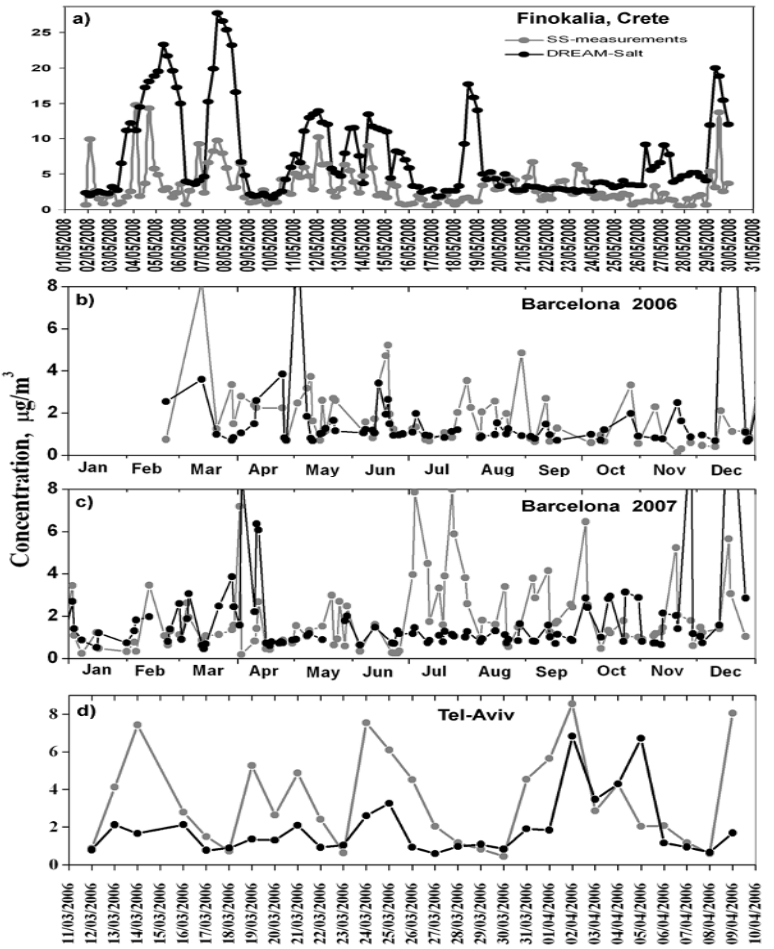


**Fig. 1.** Comparison between modeled sea-salt concentrations (the black lines) and measurements (the grey lines) in (a) Finokalia, Crete, (b,c) Barcelona, Spain, and (d) Tel-Aviv, Israel (Adapted from Kishcha et al. (2009))

The model-vs.-measurement comparison in Barcelona showed that for the majority of days, the model produced quite realistic sea-salt concentrations (Fig. 1b and c). An average simulated aerosol concentration (±standard deviation) ranged within the same interval as the measurements did $2 \pm 2$ μg/m$^3$. The relatively high standard deviation indicates strong variability of sea-salt aerosol concentrations

due to strong variability of wind speed and wind direction. Although sometimes the model fit measurements quite well, a correlation between model data and measurements in Barcelona over the 2 year period, 2006 –2007, was rather low (~0.2). Possible reasons for the discrepancy are discussed in detail by Kishcha et al. (2009). In particular, it was found that specific features of the chosen monitoring site could contribute to low correlation between model data and measurements. In summer, the model underestimated SSA-measurements when actual sea-wave height did not correspond to observed surface sea winds. In winter, winds which do not blow from sea to land create sea-salt aerosols over the sea in the vicinity of Barcelona: these aerosols are not transported inland. Under these circumstances, the model overestimated sea-salt measurements.

In contrast to Barcelona, Tel-Aviv is located on the east coast of the Mediterranean and is not surrounded by mountains. The direction of sea-salt aerosol transport from sea to land is the same as the direction of prevailing winds, from west to east. So it is much easier to predict SSA in Tel-Aviv than in Barcelona. As seen in Fig. 1d, some similarity exists between model data and measurements. The averaged measured SSA concentrations over the sampling period ranged within approximately the same intervals: $3 \pm 3$ $\mu g/m^3$ for measurements and $2 \pm 2$ $\mu g/m^3$ for model data. We found (Kishcha et al., 2009) that model errors are mainly positive, indicating that the model tends to underestimate observations. A possible reason is that the model does not take into consideration SSA which is produced by breaking waves in the surf zone.

**Acknowledgments** We gratefully acknowledge B. Starobinets for helpful discussion. This study was supported by the BMBF (Germany) – MOST (Israel) grant number 1946 on global change.

## References

Erickson, D.J., Merril, J.T. and Duce, R.A. 1986. Seasonal estimates of global atmospheric sea-salt distribution, J. Geophys. Res., 91, 1067–1072.

Janjic, Z. I. 1994. The step-mountain eta coordinate model: further developments of the convection, viscous sublayer and turbulence closure schemes. Monthly Weather Review, Vol. 122, 927–945.

Kishcha, P., Nickovic, S., Luvchik, A., Starobinets, B., Janjic, Z., Perez, N., Viana, M., Mihalopoulos, N., Mamane, Y., Agnon, Y., Alpert, P. 2009. Comparison between sea-salt aerosol forecasts and Mediterranean coastal measurements. Atmos. Environment, submitted.

Nickovic, S., Kallos, G., Papadopoulos, A., and Kakaliagou, O. 2001. A model for prediction of desert dust cycle in the atmosphere. J. Geophys. Res., 106, D16, 18113–18129.

Nickovic, S., Janjic, Z.I., Kishsha, P. and Alpert, P. 2007. Model for simulation of the sea salt aerosol atmospheric cycle. Research Activities in Atmospheric and Oceanic Modelling, WMO, Geneva, CAS/JSC WGNE, Sect. 20, 19–20.

## 4. Questions and Answers

**A. Kerschbaumer:** Did you take into account deposition processes in the model?

**Answer:** Both gravitation settling and wet removal of sea-salt aerosols were included in the model. Our analysis of sea-salt measurements in Finokalia, Crete, shows that southerly winds, blowing across the island, do not contribute to sea-salt measurements at the monitoring site due to sea-salt deposition (Kishcha et al., 2009). In particular, we detected that the majority of sea-salt aerosols was not transported over land more than 50–60 km under moderate surface wind speeds ~7 m/s. In accordance with model sea-salt simulations in Tel-Aviv, under summer light breeze conditions with surface wind speeds less than 4 m/s, the majority of SSA is transported up to 30 km inland. During the transit of cyclones across the Mediterranean, when surface wind speeds exceed 10 m/s, sea-salt aerosols could be transported over ~70 km.

**J. Casares:** Was any work done on size distributions of sea-salt measurements?

**Answer:** A detailed set of eight particle size classes with effective size between 1 and 8 μm (1, 2, 3, 4, 5, 6, 7, and 8 μm) was used in our model.

**M. Astitha:** Sea-salt aerosol production depends on relative humidity, especially with respect to the size distribution of generated aerosols. Was that taken into account in your emission scheme?

**Answer:** In the current study, we used a sea-salt model with no dependence of sea-salt production on relative humidity. The purpose of our study was to demonstrate that specific features of the chosen monitoring site located over the land could contribute to some discrepancy between model data and measurements, no matter how sophisticated the sea-salt source function is. In the future, our sea-salt forecasts may be further improved on sea-salt hygroscopic properties.

# 2.6 Constraining the Potential Source Strength of Various Soil Dust Sources Contributing to Atmospheric PM10 Concentrations in Europe

**E.C.J. Hendriks, H.A.C. Denier van der Gon, and M. Schaap**

TNO Environment and Geosciences, Utrecht, The Netherlands

**Abstract** Crustal material makes up 5–20% of the ambient PM10 mass. Despite the importance of crustal material in total PM10 mass, the sources are still poorly understood and not well-represented in emission inventories or air quality models. In this paper we present a methodology to check first order estimates of the various source strengths in Europe using the LOTOS-EUROS model. We have implemented simple and therefore transparent emission functions for wind erosion, (re-)suspension by traffic and agricultural land management as well as boundary conditions for desert dust. First results indicate that the emissions as a result from agricultural land management contribute most to the total modelled mineral dust concentration followed by those from traffic and wind erosion. The total mineral dust concentration is underestimated by the present model approaches. The large uncertainties involved in the modelling of mineral dust are discussed.

## 1. Introduction

Crustal material (CM) typically contributes 5–20% to the ambient PM10 mass. In certain regions and/or specific meteorological conditions the contribution may be higher. Despite the importance of crustal material in total PM10 mass, the sources are still poorly understood and not (well) represented in emission inventories or air quality models. Crustal material may originate from distinctly different sources e.g., *wind erosion of bare soils, agricultural land management, resuspension of road dust, road wear*, driving on unpaved roads, handling of materials and building and construction activities. Here, we aim to develop a methodology to check first order estimates of the various source strengths in Europe. For this purpose we will implement simple and therefore transparent emission functions in the chemistry transport model LOTOS-EUROS for the processes indicated in italics as they are thought to give the highest source contributions in Europe.

D.G. Steyn and S.T. Rao (eds.), *Air Pollution Modeling and Its Application XX*,
DOI 10.1007/978-90-481-3812-8, © Springer Science + Business Media B.V. 2010

## 2. Model Description

The LOTOS-EUROS model (Schaap et al., 2008) is used to calculate the PM10 distributions over Europe for 2005. The LOTOS-EUROS model is a 3D chemistry transport model aimed to simulate air pollution in the lower troposphere. In the vertical the model has four layers up to 3.5 km following the dynamic mixing layer approach. The horizontal resolution used here is 0.5° × 0.25°. The model is suitable to calculate the transport of primary (combustion) particles (EC, OC), sea salt and secondary inorganic aerosols (SIA: SO4, NO3, NH4). In this study, we incorporated the description of crustal material for the following emission sources: wind-abrasion, resuspension by traffic, and resuspension by agricultural-activities (see below). In addition, the inflow of desert dust originating from large deserts residing outside the LOTOS-EUROS model domain is included by applying concentration data of the TM5 global transport model at all boundaries.

### 2.1. Wind-blown dust emission

The emission of wind-blown dust (wind-induced abrasion) was included following the work of Marticorena and Bergametti (1995, 1997), Gomes et al. (2003) and Alfaro et al. (2004). The applied methods are based on well-know relations for saltation induced dust production in desert area and take into account information on soil texture.

### 2.2. Resuspension by traffic

A pragmatic approach is followed to calculate of traffic related resuspension emission with the LOTOS-EUROS model:

$$F_{trs} = C_{c\lim} C_{rs} \sum_{veh} \sum_{road} EF_{veh,road} D_{veh,road},$$

The method is based upon a vehicle driven kilometre map ($D_{veh,road}$ ) over Europe, typified for light duty (LDV) and heavy duty (HDV) traffic and three road type classes (rural roads, urban roads and highways), with corresponding emission factors ($EF_{veh,road}$). The first order estimates for the applied emission factors for $PM_{2.5\text{-}10}$, based upon literature (Ketzel et al., 2007; Thorpe et al., 2007 a.o.) are listed in Table 1. $C_{clim}$ and $C_{rs}$ are factors to account for variability of traffic resuspension due to the variability of climate conditions (parameterised using soil water content) and road sanding activities. During precipitation traffic resuspension is neglected.

**Table 1.** PM2.5-10 emission factor ($mg.vkt^{-1}$) for traffic related resuspension as a function of road type for light and heavy duty traffic applied in the LOTOS-EUROS model

| | Road type | | |
|---|---|---|---|
| | HW | RUR | URB |
| HDV | 198 | 432 | 432 |
| LDV | 22 | 48 | 48 |

### 2.3. Resuspension by agricultural activities

Despite the poor knowledge and availability of observations, a first approach to calculate the resuspension emission related to agricultural activities with the LOTOS-EUROS model is made. The source function describes emission of mineral dust from agricultural land based on the agricultural activity calendar. The emission flux $F_{ars}$ is defined as follows:

$$F_{ars} = \sum_{operation} C_{operation} EF_{operation} A$$

where $EF_{operation}$ ($mg.m^{-2}$) is the emission factor for a specific agricultural operation and A ($m^2$) is the arable surface area over which the emission occurs. $C_{operation}$ ($h^{-1}$) is a factor that accounts for the timing of each activity and its duration. For now, we distinguish between land preparation activities (harrowing, discing, cultivating and ploughing) using emission factor estimates by Öttl et al. (2007) and harvesting activities using a corn harvesting emission factor (Gaffney et al., 2003). Regional dependency is neglected in the present model setup. We account for the effect by precipitation by neglecting emissions during rain events.

## 3. Results

The modelled annual average contribution of crustal material to PM10 is about 2 $\mu g\ m^{-3}$ over Europe (Fig. 1). Concentrations exceeding 3 $\mu g\ m^{-3}$ are modelled in densely populated area and over relatively dry and arid environments. The contribution by wind erosion is generally less than 0.1 $\mu g.m^{-3}$ and is less important than the other modelled crustal material sources. Traffic resuspension contributes 0.3 $\mu g.m^{-3}$ in rural area and up to 5 $\mu g.m^{-3}$ or more in cities reflecting car use The presently modelled contribution by agricultural activities is 2–3 $\mu g.m^{-3}$ and exceeds that of traffic resuspension over rural area. More details on these results and a comparison with compiled set of observations will be presented at the conference.

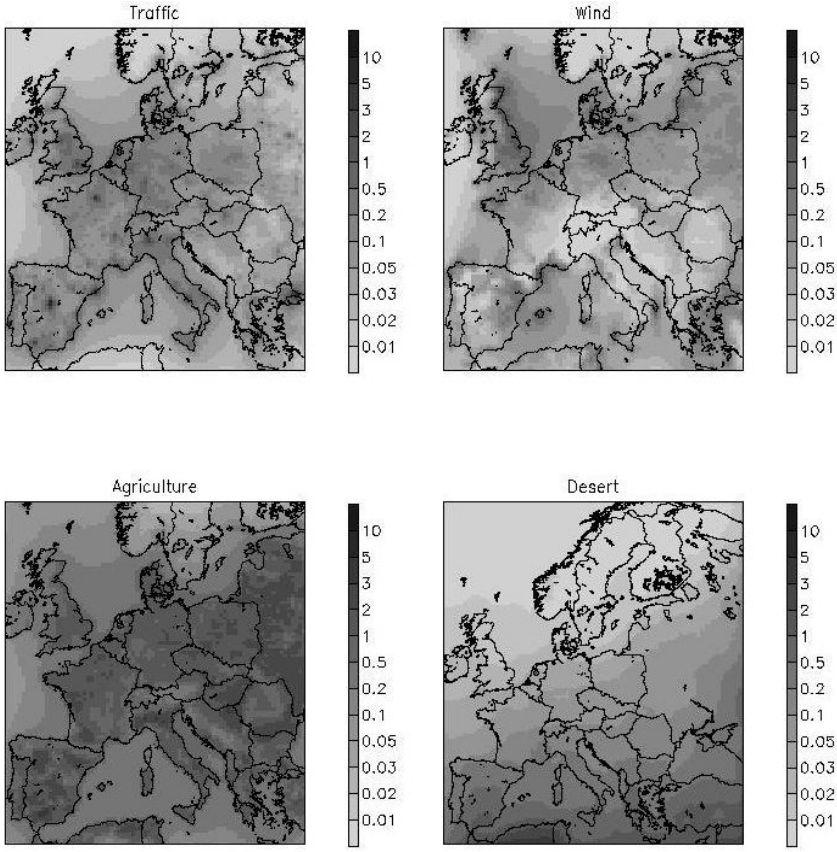


**Fig. 1.** Modelled CM contributions to PM10 (μg $m^{-2}$ $a^{-1}$) as a result of resuspension by traffic (top left), by wind (top right), by agriculture (bottom left), and trans-boundary entrainment of desert dust (bottom right) for 2005

## 4. Uncertainties

In general, the emission factors used here are based on a very limited knowledge basis, which is not representative for the full range of European conditions. Hence, the modelled contributions to mineral PM10 of the different resuspension sources are a crude approximation of reality and associated with a large uncertainty.

Based upon the applied methods, we presume an overall uncertainty of a factor 2–3 for the modelled traffic resuspension and a factor 10 or more for wind resuspension. Largest uncertainties are expected for resuspension by agricultural activity.

## 5. Conclusions

- Agricultural land management contributes most to the total modelled mineral dust concentration followed by traffic and wind erosion.
- The uncertainties are generally large (>300%).
- Limited availability of observations hampers a thorough evaluation of the results.
- The model overestimates the impact of ploughing emissions.
- It appears that with the present set up we can not explain the observed concentrations of mineral dust.

## References

Alfaro, S.C., Gomes, L., 2001. Modelling mineral aerosol production by wind erosion: emission intensities and aerosol distributions in source areas. J. Geophys. Res. 106, 18075–18084.

Ketzel, M., Omstedt, G., Johansson, C., Düring, I., Pohjola, M., Öttl, D., Gidhagen, J., Wåhlin, P., Lohmeyer, A., Haakana, M., Berkowicz, R., Estimation and validation of PM2.5/PM10 exhaust and non-exhaust emission factors for practical street pollution modeling, Atmospheric Environment 41, pp. 9370–9385, doi:10.1016/j.atmosenv.2007.09.005, 2007.

Gaffney, P, Yu, H. Computing Agricultural PM10 Fugitive Dust Emissions Using Process Specific Emission Rates and GIS, Dust Conference 2007, Maastricht, The Netherlands, 2007.

Gomes, L., Arrue, J.L., Lopez, M.V., Sterk, G., Richard, D., Gracia, R., Sabre, M., Gaudichet, A., Frangi, J.P., 2003. Wind erosion in a semi-arid agricultural area of Spain: the WELSONS project. Catena 52, 235–256.

Marticorena, B., Bergametti, G., Gillette, D.A., Belnap, J., 1997. Factors controlling threshold friction velocity in semiarid and arid areas of the United States. J. Geophys. Res. 102, 23277–23287.

Öttl, D, Funk, R., PM emission factors for farming activities by means of dispersion modeling, Landbauforshung Völkenrode Special Issue 308, pp. 173–177, 2008.

Schaap, M., Timmermans, R.M.A., Sauter, F.J., Roemer, M., Velders, G.J.M., Boersen, G.A.C., Beck, J.P., Builtjes, P.J.H., The LOTOS-EUROS model: description, validation and latest developments. International Journal of Environment and Pollution 32, 270–289, 2008.

Thorpe, A., R. M. Harrison, P.G. Boulter, I.S. McCrae, Estimation of particle resuspension source strength on a major London Road, Atmospheric Environment 41, pp. 8007–8020, doi: 10.1016/j.atmosenv.2007.07.006, 2007

# 2.7 Meso-to-global Modeling of Atmospheric Transport: Numerical Recipies, Tests and Applications

**M. Galperin, E. Genikhovich[1], M. Sofiev[2], I. Gracheva[1], J. Vira[2], and J. Soares[2]**

[1]Voeikov Main Geophysical Observatory, St. Petersburg, Russia

[2] Finnish Meteorological Institute, Helsinki, Finland

## 1. Introduction

This paper outlines some nuances of numerical algorithms applied in chemical transport models (CTMs). The splitting technique nowadays is considered more-or-less as *a must*, hence our description will be centered on the parabolic 1D transport equation written in the following form:

$$\mathrm{L}\varphi=\mathrm{E},\quad \mathrm{L}\equiv\frac{\partial}{\partial \mathrm{t}}+\mathrm{a}\frac{\partial}{\partial \mathrm{x}}-\frac{\partial}{\partial \mathrm{x}}\mu\frac{\partial}{\partial \mathrm{x}}-\xi \tag{1}$$

with corresponding initial and boundary conditions. Here, $\varphi$ is the solution sought (e.g., concentration of the pollutant), E is the emission term (that could include also non-linear terms describing, for example, atmospheric chemical reactions), "a" is a component of the advection or "convection + gravitational settling" velocity, $\mu$ is the "eddy diffusivity" along the x-axis. This axis can be oriented along any of the axes of the coordinate system in use. It should be also noted that the results presented for Eq. 1 can be used in solution of both, direct and inverse (adjoint) problems.

## 2. Modelling Dynamics: Advection Scheme

One of the main problems for existing schemes is substantial numerical diffusion (or numerical viscosity) originating from finite-step discretization algorithms. Seemingly inevitable, this phenomenon, however, does not exist in Lagrangian advection schemes, which operate in continuous space rather than in predefined grid meshes. As a result, their numerical viscosity is zero – at a price of very high non-monotonicity of the concentration fields, which originate from limited spatial representativeness of a single Lagrangian particle.

D.G. Steyn and S.T. Rao (eds.), *Air Pollution Modeling and Its Application XX*,
DOI 10.1007/978-90-481-3812-8, © Springer Science + Business Media B.V. 2010

In a series of works (Galperin et al., 1994, 1995a, b, 1996a, b; Galperin, 1999, 2000) it was shown by Michael Galperin that the advantages of Lagrangian and Eulerian approaches can be combined successfully into a non-diffusive positively defined and reasonably monotonic advection scheme, which versions were presented by Galperin (1999, 2000), Galperin et al. (1996a), and Sofiev (2000). The procedure mainly follows the methodology suggested in Galperin (2000), which can be qualified as a pseudo-Lagrangian finite volume approach.

When deriving the Galperin's scheme, one should re-write the advection term in Eq. 1 in the divergent form using the continuity equation with boundary conditions defined separately for in- and outflow boundaries. Simulation grid is defined as a set of $N$ grid cells ($\mathrm{i}=\overline{1,\mathrm{N}}$). Centre of the *i-th* grid cell has a co-ordinate equal to $x_i$, its left- and right-hand borders have co-ordinates $x_{i-0.5}$ and $x_{i+0.5}$, respectively. The 1-D cell volume is then $V_i = x_{i+0.5} - x_{i-0.5}$. The advected field is described by the total mass $\mathrm{M_i}$ and position of the centre of mass $\mathrm{X_i}$, $\mathrm{X_i} \in [\mathrm{x_{i-0.5}}, \mathrm{x_{i+0.5}}]$ in each grid cell $i$. Initially, a piecewise constant mass concentration $\varphi_\mathrm{I} = \mathrm{M_i}/\mathrm{V_i}$ is defined and $\mathrm{X_i}$ is set equal to the center-point of each grid cell: $X_i = x_i$. At time step $k$, the mass distribution inside *i-th* cell is defined as a rectangular pulse equal to 0 outside $\omega_\mathrm{i}$ and equal to $0.5\mathrm{M_i}/\omega_\mathrm{i}$ inside $\omega_\mathrm{i}$, where $\omega_i = \min\left(\left|X_i - x_{i-0.5}\right|, \left|X_i - x_{i+0.5}\right|\right)$ is the distance from the centre of mass position $X_i$ to the nearest border of the cell. Advection of the pulse does not change its shape within the time step $\delta t$ assuming locally constant velocity field "a": $\varphi_\mathrm{i}^{\mathrm{k+1}}(\mathrm{x}) = \varphi_\mathrm{i}^{\mathrm{k+1}}(\mathrm{x} - \mathrm{a}(\mathrm{X_i}, \mathrm{t_k})\delta t)$. The global concentration distribution at $k+1$ step is considered as a sum of pulses $\varphi(\mathrm{x}, \mathrm{t}^{\mathrm{k+1}}) = \sum_\mathrm{i} \varphi_\mathrm{i}^{\mathrm{k+1}}(\mathrm{x}), \quad \mathrm{x} \in [-\infty, \infty]$.

Finally, for each grid cell new mass and its position are computed following the mass and momentum conservation equations

$$\mathrm{M_i} = \int_{\mathrm{x_{i-0.5}}}^{\mathrm{x_{i+0.5}}} \varphi(\mathrm{x})\mathrm{dx}\,, \quad \mathrm{X_i} = \int_{\mathrm{x_{i-0.5}}}^{\mathrm{x_{i+0.5}}} \mathrm{x}\varphi(\mathrm{x})\mathrm{dx}$$

The Galperin's scheme is mass conservative, can operate at practically any wind speed, in particular with Courant number exceeding 1, and its generalization to 2D and 3D versions is trivial. It should be stressed that the algorithm is free from any filtration, which is a pre-requisite for zero numerical viscosity (not necessarily sufficient in general).

## 3. Diffusion Algorithms

There are several well-known finite-difference substitutes for the diffusion term, $\partial/\partial x(\mu\partial\varphi/\partial x)$, which are usually of second order of accuracy and differ one from another in methods for calculating the values $\mu_{i+1/2}$ corresponding to "half-integer" grid points. Some of them do not work well in dispersion applications because of strong variations of the eddy diffusivity $\mu$ as a function of x (especially, in case of vertical diffusion). In particular, $\mu$ could be close to zero near the underlying surface and inside the layers with very stable thermal stratifications. As a result, derivatives of $\varphi$ and the error of approximation equation (1) with finite differences could be very high. To avoid corresponding problems, Marchuck (1961), Samarski (1971), and independently (actually, his work was published in Russian in 1961) Berlyand (1982) introduced a so called "balance method for constructing finite-difference schemes". Practical applications of this method are discussed by Genikhovich et al. (1995).

Using this method, one can derive the following expressions for $\mu_{i\pm1/2}$:

$$\mu_{i+1/2}=(x_{i+1}-x_i)/\int_{x_i}^{x_{i+1}}dx/\mu\,;\quad \mu_{i-1/2}=(x_i-x_{i-1})/\int_{x_{i-1}}^{x_i}dx/\mu\,; \tag{2}$$

It was proven by Samarski (1961) that, when using Eq. 2, the solution of the finite-difference scheme approaches the exact solution of Eq. 1 even for sharply varying $\mu$. In addition, Marchuck (1961) introduced the following discrete approximation for the right-hand term, E, in Eq. 1:

$$E_i=2[\frac{\mu_{i+1/2}}{x_{i+1}-x_i}\int_{x_i}^{x_{i+1}}\frac{1}{\mu}\int_{x_i}^{x}Edtdx+\frac{\mu_{i-1/2}}{x_i-x_{i-1}}\int_{x_{i-1}}^{x_i}\frac{1}{\mu}\int_{x}^{x_i}Edtdx\,]/(x_{i+1}-x_{i-1}] \tag{3}$$

As shown by Marchuck, asymptotically the finite-difference scheme, which uses Eqs. 2, 3, has an "infinite order of approximation", i.e. its solution coincide with the solution of Eq. 1 (assuming a = 0). It should be noted that, with certain corrections, a similar approach can be used in the case with $a \neq 0$ (e.g. to account for the gravitational settling). Actually, Eq. 2 provides expressions for the "turbulent resistance". In this sense, this finite-difference scheme is analogues to the schemes introduced later by Erisman et al. (1994) and Sofiev (2002).

**Acknowledgments** This paper is dedicated to the memory of the outstanding scientist, our close friend and long-lasting colleague, late Prof. Michael Galperin.

## References

Berlyand, M.E. (1982) Moderne Problemen der atmospharischen Diffusion und der Verschmutzung der Atmosphare, Academie-Verlag, Berlin. 435 s.

Erisman J.W., A. van Pul, P.Wyers (1994) Parameterization of the surface resistences for the quantification of atmospheric deposition of acidifying pollutants and ozone. *Atmosph. Environ.,* **28**, 2595–2607.

Galperin, M. (1999) Approaches for improving the numerical solution of the advection equation. In Z. Zlatev, J. Dongarra, I. Dimov, J. Brandt, and P. J. Builtjes, (Eds), *Large Scale Computations in Air Pollution Modelling*, pages 161–172. Kluwer Academic Publishers, 1999.

Galperin M.V. (2000) The Approaches to Correct Computation of Airborne Pollution Advection. In: *Problems of Ecological Monitoring and Ecosystem Modelling*. **XVII**, St. Petersburg, Gidrometeoizdat, 2000, pp. 54–68 (in Russian)

Galperin, M., Afinogenova, O., Grigoryan, S., Sofiev, M. (1995a) "Long-range model for the evaluation of Airborne Pb, Cd, As and Zn Pollution", in Proc. of the International Conference Heavy Metals in the Environment, Eds. R-D.Wilken, V.Forstner, A.Knochel, Hamburg, pp. 212–215

Galperin, M., Maslyaev, A., Pekar, M., Sofiev, M. (1996a) The development of HM model in 1996. *EMEP / MSC-E Report 5/96*, Moscow, July 1996, 62 p

Galperin, M., Sofiev, M., Erdman, L., Chechukina, T. (1994) Model evaluation of airborne Trace Metal transport and deposition. Short model description and preliminary results. *EMEP/ MSC-E Report 3/94*, Moscow, March 1994.

Galperin, M., Sofiev, M., Gusev, A., Afinogenova, O. (1995b) The approaches to modelling of heavy metals transboundary and long-range airborne transport and deposition in Europe. *EMEP / MSC-E Report 7/95*, Moscow, June 1995 28 p

Galperin, M., Sofiev M., Mantseva E. (1996b) A model of the chemical transformation of mercury and its long-range atmospheric transport. *Global and Regional Mercury cycles: Sources, Fluxes and Mass Balances, eds. Bayens W., R.Ebinghaus, O.Vasiliev, NATO ASI Series 2: Environment*- **21**, Kluwer Academic Publishers, The Netherlands, pp. 219–227.

Genikhovich E.L, Berlyand M.E., Onikul R.I (1999) Progress in the theory of atmospheric diffusion as a basis for development of the air pollution prevention policy. In: Modern Studies at Main Geophysical Observatory. v. 1. Hydrometeorological Publ, St. Petersburg.- p. 99–126 (in Russian)

Marchuck, G.I. (1961) Methods for calculating nuclear reactors. Atomic Energy Publ., Moscow (in Russian)

Samarski, A.A. (1971) Introduction in the theory of finite-difference schemes. Fizmatgiz Publ., Moscow, 533 p. (in Russian)

Sofiev, M. (2000) A model for the evaluation of long-term airborne pollution transport at regional and continental scales. *Atmospheric Environment.* **34**, No.15, pp. 2481–2493

Sofiev, M. (2002) Extended resistance analogy for construction of the vertical diffusion scheme for dispersion models. *J. of Geophys.Research – Atmosphere*, **107**, D12, doi: 10.1029/ 2001JD001233

# 2.8 Development and Application of the CMAQ Ozone and Particle Precursor Tagging Methodologies (OPTM and PPTM)

**Sharon G. Douglas, Thomas C. Myers, Jay L. Haney, and Yihua Wei**

ICF International, San Rafael, California, USA

## 1. Introduction

The Community Multiscale Air Quality (CMAQ) model is a state-of-the-science, regional air quality modeling system that is designed to simulate the physical and chemical processes that govern the formation, transport, and deposition of gaseous and particulate species in the atmosphere. This paper describes the recent enhancement of the CMAQ model to include source attribution capabilities for ozone and particulate matter. The Ozone and Precursor Tagging Methodology (OPTM) and the Particle and Precursor Tagging Methodology (PPTM) are designed to provide detailed, quantitative information about the *contribution* of selected sources, source categories, and/or source regions to simulated ozone and fine particulate ($PM_{2.5}$) concentrations, respectively. Emissions of precursor pollutants from selected sources, source categories, or source regions are (numerically) tagged and then tracked throughout a simulation. The contribution from each tag to the resulting simulated concentration of ozone, $PM_{2.5}$, or any of the $PM_{2.5}$ component species for any given location within the CMAQ modeling domain can be quantified.

## 2. Overview of OPTM and PPTM

The CMAQ simulation processes include advection, dispersion (or turbulent mixing), chemical transformation, cloud processes, and wet and dry deposition. Within the model, tagging is accomplished by the addition of duplicate model species variables for each source, source category, or source region that is to be tagged. For OPTM, the duplicated modeled species are ozone, oxides of nitrogen ($NO_x$), and volatile organic compounds (VOCs). For PPTM, the duplicated species include all PM-related sulfur, nitrogen, and secondary organic compounds, as well as primary organic carbon, elemental carbon, and other inorganic particulates. PPTM can also be applied for mercury. The tagged species have the same properties and are subjected to the ssameprocesses (e.g., advection, chemical transformation, deposition) as the actual (or base) species. Because the tagged species are separate from the base species, tagging does not alter or affect the base simulation results. OPTM and PPTM have been implemented in versions 4.5, 4.6 and 4.7 of CMAQ.

D.G. Steyn and S.T. Rao (eds.), *Air Pollution Modeling and Its Application XX*,
DOI 10.1007/978-90-481-3812-8, © Springer Science + Business Media B.V. 2010

At each time step in the simulation, the effects of linear processes, such as advection and dry deposition, are calculated directly for all tagged species. Potentially non-linear processes, such as gas-phase chemistry, aqueous chemistry, and particle dynamics are calculated for the overall (base) species and apportioned to the tagged species. The results for the tagged species are not normalized to ensure that their sum equals the total. Thus, the difference between the sum of all tags and the overall concentration gives an estimate of the numerical uncertainty in the contribution estimates. The tagged species are included as additional species in the model output files.

The OPTM and PPTM techniques can be used by air quality planners to identify the contributors to a particular air pollution problem. The tagging methodology differs from typical air quality model sensitivity simulations in which the emissions are modified or omitted. Sensitivity simulations provide information on the effects of changes in emissions on the simulation results. In contrast, OPTM and PPTM provide information about the contribution of emissions from the tagged sources, relative to the unmodified simulated conditions.

## 3. OPTM Results

Figure 1 presents example results for the application of CMAQ/OPTM to examine the contribution of emissions from selected source areas to 8-h average ozone concentrations in Milwaukee, WI and the surrounding area. For this application, OPTM tags were applied to anthropogenic emissions sources in selected counties. This is an example of the use of OPTM to quantifying the contribution of emissions from selected geographical regions to regional ozone concentrations and ozone concentrations in specific (e.g., nonattainment) areas. Figure 1 displays the

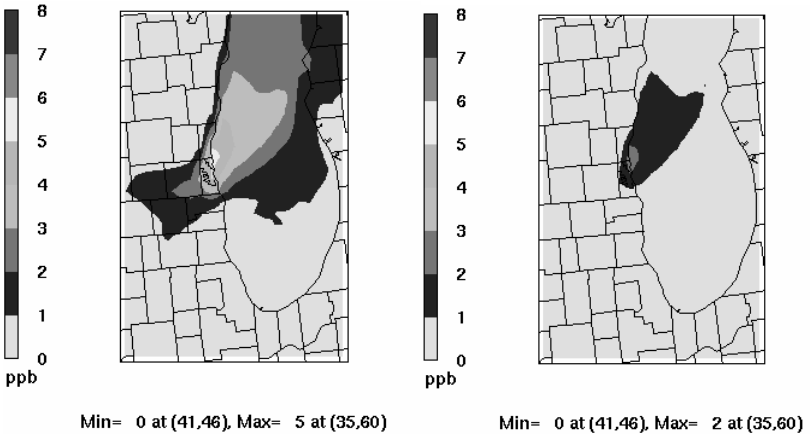


**Fig. 1.** OPTM-derived monthly average contributions to 8-h average ozone from NOx (left) and VOC (right) emissions for Milwaukee County, WI

monthly average contribution from $NO_x$ and VOC emissions from sources located in Milwaukee County to 8-h ozone concentrations in the Lake Michigan area for a 1-month simulation period for July 2002.

Examples of other applications for OPTM include: quantifying the contribution of NOx and VOC emissions from source sectors (e.g., non-road mobile, biogenic) or specific types of facilities; and quantifying the contribution from estimated boundary conditions.

## 4. PPTM Results

Figure 2 presents example results for the application of CMAQ/PPTM to examine the contribution of emissions from selected source categories to annual average $PM_{2.5}$ concentrations in the U.S. For this application, PPTM was used to examine the contributions to simulated PM for the following major emissions source categories: electric generating unit (EGU) sources, non-EGU point sources, on-road

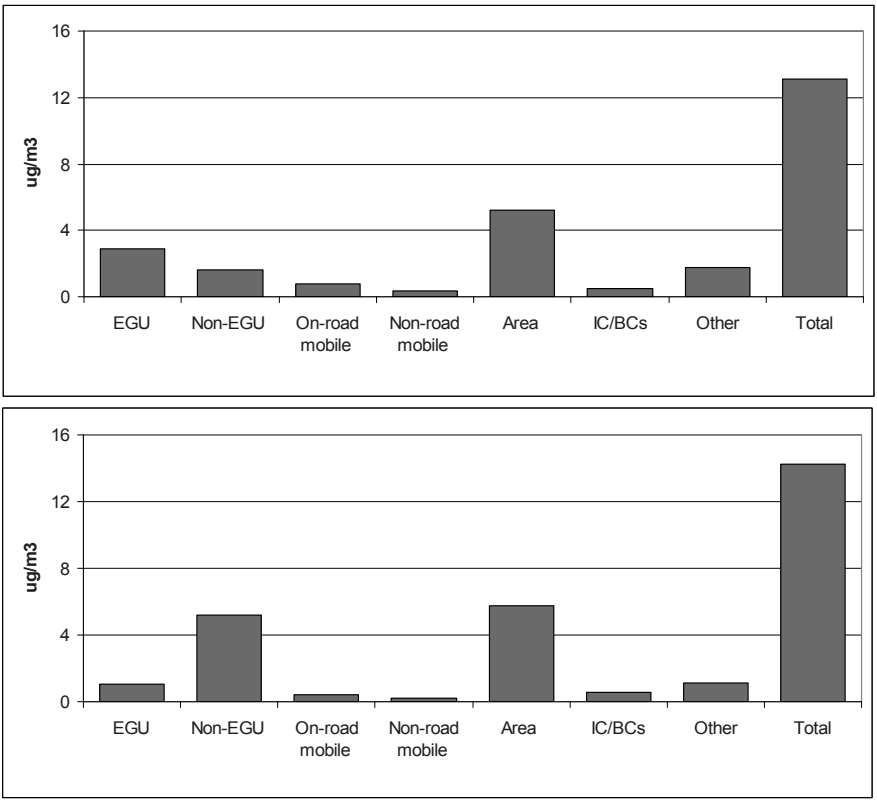


**Fig. 2.** PPTM-derived contributions to annual average PM2.5 from selected source categories and regions for Pittsburgh (top) and Houston (bottom)

mobile sources, non-road sources, area (non-point, non-mobile), initial/boundary conditions (IC/BCs), and all other sources (including natural emissions and offshore sources. Figure 2 displays the contribution to annual average $PM_{2.5}$ concentrations for Pittsburgh, PA and Houston, TX for the projection-year 2010.

Examples of other applications for PPTM include: quantifying the contribution of emissions from other source sectors or geographical regions; tracking the fate of emissions from specific facilities to estimate their range of influence and contribution to $PM_{2.5}$ concentrations, and quantifying the contribution of emissions from selected sources or source categories to atmospheric deposition (e.g., mercury) or visibility impairment.

**Acknowledgments** Tom Braverman and Kirk Baker of the U.S. PA, Office of Air Quality Planning and Standards (OAQPS) are gratefully acknowledged for theEir upport of this work.

# 2.9 The WRF-CMAQ Integrated On-line Modeling System: Development, Testing, and Initial Applications

**Rohit Mathur[1], Jonathan Pleim[1], David Wong[1], Tanya Otte[1], Robert Gilliam[1], Shawn Roselle[1], Jeffrey Young[1], Francis Binkowski[2], and Aijun Xiu[2]**

[1]United States Environmental Protection Agency

[2]University of North Carolina, Chapel Hill, NC, USA

**Abstract** Traditionally, atmospheric chemistry-transport and meteorology models have been applied in an off-line paradigm, in which archived output on the dynamical state of the atmosphere simulated using the meteorology model is used to drive transport and chemistry calculations of atmospheric chemistry transport model (CTM). A modeling framework that facilitates coupled on-line calculations is desirable since it (1) provides consistent treatment of dynamical processes and reduces redundant calculations, (2) provides ability to couple dynamical and chemical calculations at finer time-steps and thus facilitates consistent use of data, (3) reduces the disk-storage requirements typically associated with off-line applications, and (4) provides opportunities to represent and assess the potentially important radiative effects of pollutant loading on simulated dynamical features. A coupled on-line atmospheric modeling system is developed based on the Weather Research and Forecasting (WRF) meteorological model and the Community Multiscale Air Quality (CMAQ) air quality modeling system. The flexible design of the system facilitates consistent configurations for both on-line and off-line modeling paradigms as well as the systematic investigation of the impacts of frequency of data exchange between the dynamical and chemical calculations as well as feedback effects of chemical concentrations on meteorological process.

## 1. Introduction

While the role of long-lived greenhouse gases on modulating the Earth's radiative budget has long been recognized, it is now well acknowledged that the increased tropospheric loading of aerosols can also affect climate in multiple ways. Aerosols can enhance reflection of solar radiation both directly, by scattering light in clear air and indirectly by increasing the reflectivity of clouds. On the other hand, organic aerosols and soot absorb radiation, thus warming the atmosphere. Current estimates of aerosol radiative forcing are, however, quite uncertain. The major sources

D.G. Steyn and S.T. Rao (eds.), *Air Pollution Modeling and Its Application XX*,
DOI 10.1007/978-90-481-3812-8, © Springer Science + Business Media B.V. 2010

of this uncertainty are related to the accurate characterization of atmospheric loading of aerosols, the chemical composition and source attribution of which is highly variable both spatially and temporally. The accurate regional characterization of aerosol composition and size distribution is critical for estimating their optical and radiative properties and thus in quantifying their impacts on radiation budgets of the earth-atmosphere system. Hence, coupled regional meteorology and atomspheric chemistry models are needed to properly characterize the spatial heterogeneity in radiative forcing associated with short-lived aerosol and gases, and, consequently to better understand their aggregate influence on the earth's radiation budgets. Coupling the modeling systems provides means for finer scale applications, wherein higher frequency of data exchange between meteorological and chemistry-transport calculations is necessary to better represent the effects of meteorological variability on modeled concentrations.

## 2. Design of the WRF-CMAQ Coupled Modeling System

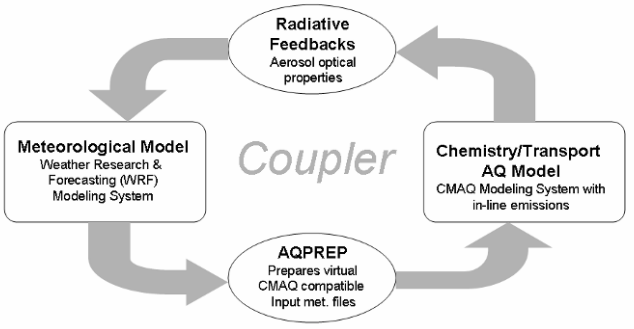


**Fig. 1.** The coupled WRF-CMAQ modeling system

The design of the coupled WRF-CMAQ system was based on a number of desired structural attributes: (1) maintain integrity of the WRF and CMAQ (Byun and Schere, 2006) models, so that both models can evolve independently benefitting from their respective user and development communities, (2) support both coupled and the traditional uncoupled modeling paradigms within the same modeling framework to assess their relative benefits for both research and regulatory applications, (3) maintain flexibility in design to add feedback process representations, and (4) ensure efficiency in coupling to enable applications from urban to hemispheric scales. A schematic the coupling of the WRF and CMAQ modeling systems is shown in Fig. 1. In this design, the WRF and CMAQ modeling systems are coupled through the use of memory resident buffer data files. CMAQ is called from the main "Solve"

routine in WRF. The coupler (Wong et al., 2009) allows for flexibility in time stepping between the two models; CMAQ can be called every WRF time step or any user defined multiple. Additionally, simple switching of the buffer files to disk files allows for identical uncoupled simulation (without feedback). Both models use the same map projections, coordinate systems, and grid structures, thereby ensuring consistent data use across both models. CMAQ has been modified to include meteorology-dependent processes: biogenic emissions, point source plume-rise, and dry deposition velocity estimation, previously calculated upstream of the CMAQ model. Simulated aerosol composition and size distributions are used to estimate the optical properties of aerosols which are then used in the radiation calculations in WRF. Thus, direct radiative effects of scattering and absorbing aerosols in the troposphere estimated from the spatially and temporally varying simulated aerosol distributions, can be fed-back to the WRF radiation calculations, resulting in "2-way" coupling between the atmospheric dynamical and chemical modeling components. Though both WRF and CMAQ are designed to run on parallel computing environments, the details of domain decomposition, i.e., mapping of sub-domains and processors, is quite different. The coupler is designed such that these differences in the parallelization and coupling of the models, is transparent to the user.

## 3. Results and Discussion

Pleim et al. (2008) previously analyzed the impact of different frequency of coupling between the dynamical and chemical calculations in the coupled WRF-CMAQ system and demonstrated that relatively large differences in simulated instantaneous values compared to an off-line simulation. Figure 2 presents an illustration of the direct aerosol feedbacks simulated by the coupled WRF-CMAQ modeling system over the eastern U.S. In general relatively high aerosol optical depths are noted in regions of high surface and boundary-layer particulate matter pollution. Aerosol direct radiative effects associated with scattering and absorption of incoming radiation, result in a reduction of short-wave radiation reaching the surface, which then translate to reduction in temperature at the surface as well as a reduction in planetary boundary layer (PBL) height. For the moderate pollution levels illustrated in Fig. 2, the noted impacts on short-wave reduction and subsequent suppression in boundary-layer heights are relatively modest. As illustrated in Fig. 3, the inclusion of direct radiative effects of aerosol loading lead to slight cooling and slightly better agreement with measured values. Application of the modeling system to cases characterized by higher tropospheric $PM_{2.5}$ burden and detailed comparisons with available measurements of short-wave radiation are underway.

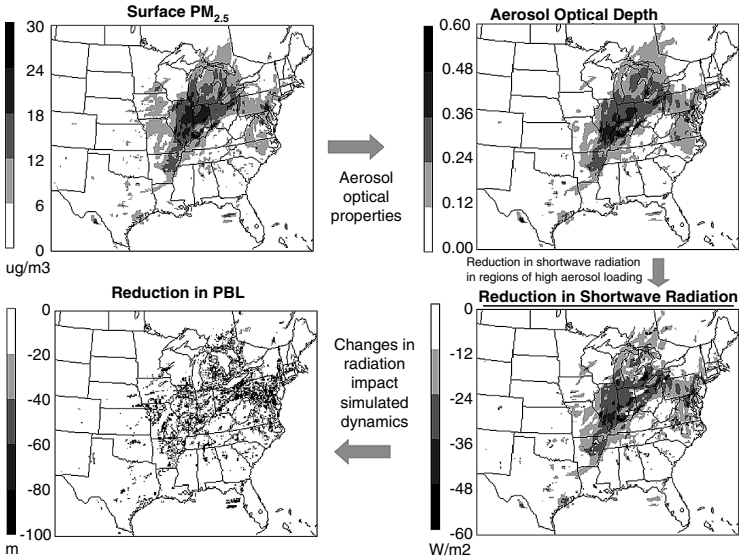


**Fig. 2.** Illustration of the direct radiative effects of aerosol simulated by the WRF-CMAQ coupled model at 22 UTC on August 6, 2006

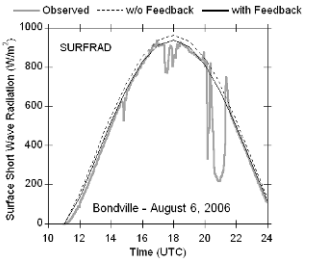


**Fig. 3.** Comparison of simulated shortwave radiation at the surface with and without direct aerosol feedbacks with measurements at Bondville on August 6, 2006

**Disclaimer** Although this paper has been reviewed by EPA and approved for publication, it does not necessarily reflect EPA's policies or views.

## References

Byun, D.W., Schere, K.L., 2006. Review of the governing equations, computational algorithms, and other components of the Models-3 Community Multiscale Air Quality (CMAQ) modeling system. *Appl. Mech. Rev.*, 59, 51–77.

Pleim, J., J. Young, D. Wong, R. Gilliam, T. Otte, and R. Mathur, 2008, Two-Way Coupled Meteorology and Air Quality Modeling, *Air Pollution Modeling and Its Application XIX*,

C. Borrego and A.I. Miranda (Eds.), 496–504, ISBN 978-1-4020-8452-2, Springer, The Netherlands.

Wong, D., J. Pleim, R. Mathur, F. Binkowski, A. Xiu, T. Otte, J. Young, and R. Gilliam, 2009, WRF-CMAQ Two-way coupling system: overview, *Environ. Modeling Softw*., submitted.

## 4. Questions and Answers

**C. Emery:** Regarding the ozone impacts from the western fires, were only aerosol emissions added from fires to capture the AOD-SW-PBL-⊗$O_3$ effect, or did you also add the fire NOx and VOC to include the chemistry impact of fires on O3? If latter, how did you "tease" out just the aerosol effect?

**Answer:** Yes, we did include emissions of NOx and VOCs from the fires in our simulations. We conducted two sets of simulations with these emissions: one with the radiative feedback effects of aerosol and the other without. The difference between these simulations was then used to estimate the impacts on short-wave radiation, PBL heights, and subsequent effects on $O_3$.

**G Kallos:** You mentioned PBL effects due to short-wave radiation, but did not mention effects from long-wave radiation.

**Answer:** In limited early experiments, we have included effects of tropospheric $O_3$ burden on the long-wave radiation, but have not found a significant modulation of simulated PBL. Clearly, additional testing and verification is warranted.

**S. Lu:** Will EPA consider using the Earth System Modeling Framework (ESMF) that has been used at NOAA and NASA?

**Answer:** In our initial design of the WRF-CMAQ system we did explore the potential use of ESMF as a means to couple the two models; at that time the framework did not appear to be ready to facilitate the level of coupling that was needed between WRF and CMAQ models. We look forward to learning more about the recent developments with ESMF from our NOAA and NASA colleagues, and could consider using it in future versions of the model.

# 2.10 Integrated Modelling of Allergenic Pollen: Phenological Stages, Pollen Release and Transport for Different Species

**Pilvi Siljamo[1], Mikhail Sofiev[1], Hanna Ranta[2], Tapio Linkosalo[3], Siegfried Jaeger[4], Regula Gehrig[5], Alix Rassmussen[6], Elena Severova[7], Ari Karppinen[1], and Jaakko Kukkonen[1]**

[1]Finnish Meteorological Institute, Finland,

[2]University of Turku, Aerobiological Unit, Finland,

[3]Finnish Forest Research Institute, Finland,

[4]NHO Klinik der Medizinischen Universitaet Wien, Austria,

[5]Meteo Swiss, Switzerland,

[6]Danish Meteorological Institute, Denmark,

[7]Moscow State University, Russia

**Abstract** Pollen can be considered as one of types of atmospheric natural "pollution" with direct health impact. There are many different pollen grains in the atmosphere during spring and summer. Some of them are harmless but some other, like birch, olive, alder, grasses and ragweed, can have remarkable allergenic impacts. Pollen grains of wind pollinated species can be transported from tens of kilometres (e.g., some grass species and mugwort) to thousands of kilometres (e.g., birch and ragweed) depending on size and other features of the pollen grain. In all cases, pollen prediction is not a local problem but rather requires an integrated modelling system, which would include both numerical weather prediction and dispersion models, as well as models for start and end of flowering and pollen release characterization. Current paper presents such a system developed in Finnish Meteorological Institute, which has been used and evaluated over Europe since 2005.

**Keywords** Birch, grass, long-range transport, phenological model, pollen

## 1. Introduction

Some species, such as many types of trees, start their flowering when a certain level of accumulated heat, often expressed as a daily temperature sum (the corresponding model is often referred as thermal-type model) is reached. For some

D.G. Steyn and S.T. Rao (eds.), *Air Pollution Modeling and Its Application XX*,
DOI 10.1007/978-90-481-3812-8, © Springer Science + Business Media B.V. 2010

other species the length of day or ground moisture are the important factors. In the current work, we consider the forecasting of birch and grass pollen concentrations. Birch is a tree, which has got light pollen grain and its flowering is well described by the thermal time type model. Usually, birch flowering lasts a couple of weeks.

Grasses include many different species and thus the flowering period of a "general grass" lasts for several weeks or even months. In case of grass pollen the source is near the ground and grains themselves are usually heavier than those of birch. Thus, grass pollen is rarely transported over very long distances.

In the current work we compare the quality of the forecasts for different type of pollen grains and analyse the sensitivity of the model performance to its parameters: low versus high source assumption, short versus long flowering period, light versus heavy pollen grain and also an ability of the model to use fixed starting time of flowering in real-life situations. We will also highlight the weather parameters, which have the most important role in numerical pollen forecasts.

## 2. Material and Methods

Pollen long-range transport forecasts are performed with the dispersion modelling system SILAM (Sofiev et al., 2006b). It is capable of both forward and inverse simulations, for which Lagrangian random-walk particle model and Eulerian dynamic cores are available. Current pollen simulations use SILAM v4.2.1 with Eulerian dynamics. The system is based on input flow of meteorological information obtained from numerical weather prediction (NWP) models. Here we have used ECMWF data with 3 h resolution.

In case of birch, both phenological models for the starting and ending date of flowering and a pollen release model itself need information from the NWP model. This information controls also transport with wind, mixing due to turbulence, and sink processes removing the pollen grains from the air. Release of pollen grains, as presented in our model, is a complex system, which uses a map of the fraction of birch forests in European landscape (Sofiev et al., 2006a), and computes the starting date of flowering using Thermal Time-type phenological model (e.g., Häkkinen et al., 1998; Linkosalo, 2000). The emission module also utilizes the number of catkins per tree (relative to normal for each specific region). Dynamics of the emission is driven by the pollen release model. More details about the SILAM pollen forecasting system can be found from Siljamo et al. (2008).

In case of grass, maps of fixed calendar dates for starting and ending the flowering was computed from grass pollen observations of the European Aeroallergen Network (EAN). Pollen release model is similar to that of birch. Birch and grass pollen observations used for the model evaluation were available from EAN(European Aeroallergen Network) database, which receives the data from about 35 countries and about 300 sites. Pollen observations began in 1974 but the bulk of data is after 1985.

## 3. Results and Discussion

Figures 1a and 1b show observed and predicted pollen counts in Moscow together with the most important weather factors: Rain, relative humidity, 2 m temperature and wind speed. It should be kept in mind that all meteorological parameters are taken from the weather prediction model and, consequently, are prone to errors.

Relative humidity and especially rain are very important for pollen concentrations both in grass and birch case and not only in Moscow. If it is raining or relative humidity is too high, pollen concentrations become low or zero. Because of the systems sensitivity to rain and humidity, it can sometimes explain negative correlation in observed and predicted pollen counts, such as those presented in Fig. 1a on the 2 May or in Fig. 1b on the 9 June.

Grass pollen concentration correlates clearly with 2 m temperature in several places in Europe especially in the model output, but also in the observations. This is not always held since rain and humidity can prevent high pollen counts even if temperature is high but in general the relation is strong. Positive correlation between temperature and birch pollen counts can also be seen, but it is not as clear as in grass pollen case, because observed/modelled birch pollen represent pollen from larger area.

Wind speed does not seem to correlate with pollen counts at all, at least at daily level. Since the diurnal variability is very large, averaging over 24 h may appear far too long to detect the link. It can also be masked by other factors, such as temperature, rain and humidity.

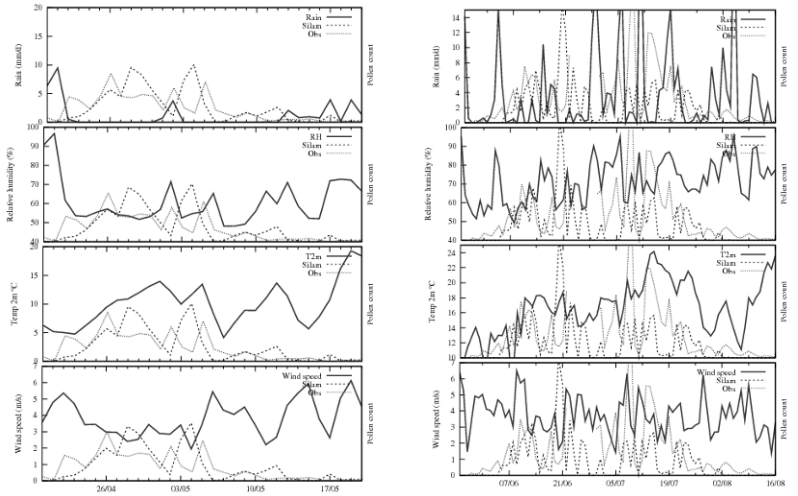


**(a)** **(b)**

**Fig. 1. (**a) Birch (b) grass pollen concentrations in Moscow in spring 2008. Dash line: SILAM pollen concentrations, dotted line: observed pollen concentrations, solid line: daily averages of weather parameters (rain, relative humidity, 2 m temperature or wind speed)

Grass pollen concentration seems to be more difficult to predict than that of birch pollen. Present system uses the same pollen release model and dynamic threshold values for birch and grass, but most probably there should be something different for grasses. Grass pollen concentration is a more local phenomenon, hence the local and microscale factors are more important, such as a fraction of grass, local rain showers and micro climate.

Grass pollen season is long, weeks or months, hence a few days of mis-predicted starting and ending of flowering are not as disturbing as for birch, where the whole flowering is much shorter. Therefore, the prescribed map of calendar dates of the start of pollination seems to work surprisingly well, while the end of the season appeared more problematic, especially in the southern Europe, where drought can interrupt the flowering. However, in temperate climate (e.g., Moscow, Fig. 1b) the whole season can be prescribed reasonably well.

For birch, the Thermal Time-type phenological model predicted starting dates of flowering in 2008 surprisingly well in most part of Europe, as well as the ending of the season with typical long tail (e.g., Fig. 1a).

## 4. Conclusions

Grass pollen concentrations seem to be more difficult to predict than birch pollen concentrations. Grass pollen grains is heavier and sources locate near ground. Thus grass pollen represents smaller area than birch pollen and is more sensitive to local factors, like fraction of grass, rain showers and micro climate.

Rain and high humidity prevent high pollen concentrations, while high 2 m temperature correlates well with high pollen counts. Instead effect of wind speed does not shown in pollen concentration forecasts.

**Acknowledgments** The work and the presentation at ITM-2009 have been supported by COST Action ES0603, ESA-PROMOTE project, and FP-7 project HIALINE. The data have been provided by the European Aeroallergen Network EAN.

## References

Häkkinen R, Linkosalo T, Hari P (1998) Effects of dormancy completion and the environmental factors on timing of bud burst in *Betula pendula*, Tree Physiology 18, 707–712.

Linkosalo T (2000) Mutual regularity of spring phenology of some boreal tree species: predicting with other species and phenological models, Canadian Journal of Forest Research 30, 667–673

Siljamo P, Sofiev M, Linkosalo T, Ranta H, Kukkonen J (2008) Development and applications of biogenic emission term as a basis of long-range transport of allergenic pollen in Air Pollution Modeling and its Application XIX (eds. C. Borrego and A. I. Miranda), NATO Science for Peace and Security Series –C: Environmental Security, Springer, 154–162

Sofiev M, Siljamo P, Ranta H, Rantio-Lehtimäki A (2006a) Towards numerical forecasting of long-range air transport of birch pollen: theoretical consideration and a feasibility study, International Journal of Biometeorology 50, 392–402

Sofiev M, Siljamo P, Valkama I, Ilvonen M, Kukkonen J, (2006b) A dispersion system SILAM and its evaluation against ETEX data, Atmospheric Environment, 40, 674–685

## 5. Questions and Answers

**Question:** One can expect close relationships between pollen appearance and allergic diseases. Did you compare your pollen forecasts with allergic diseases? (P. Kishcha)

**Answer:** No, we have not, since they are not as easily available as pollen counts. But it is true that pollen counts do not explain allergic rhinitis alone. Different human populations are sensitized to different pollen concentrations and also pollen grain can be empty from tiny allergen particle, which is a real reason for allergic diseases.

**Question:** Will the pollen problem increase with climate change? (P. Builtjes)

**Answer:** Warming climate seems to increase pollen counts already now. But, of course, pollen production and concentrations do not depend only on air temperature, but also e.g., land use and soil moisture.

# 2.11 AMFIC: Air Quality Modeling and Forecasting in China

**Wouter Lefebvre[1], Karen Van de Vel[1], Koen De Ridder[1], Joachim Maes[1,2], Clemens Mensink[1], Bas Mijling[3], Ronald van der A[3], Nele Veldeman[1], Peter Viaene[1], and Jo Vliegen[1,4]**

[1]Flemish Institute for Technological Research (VITO), Mol, Belgium

[2]Now at Joint Research Center, Ispra, Italy

[3]Royal Netherlands Meteorological Institute (KNMI), De Bilt, The Netherlands

[4] Now at Katholieke Hogeschool Limburg (KHLIM), Hasselt, Belgium

**Abstract** The AMFIC project (http://www.knmi.nl/samenw/amfic/) develops an integrated information system for monitoring and forecasting tropospheric pollutants over China. The system uses satellite and in situ air quality measurements together with air quality modelling to generate consistent and continuous air quality information. In this way it supplements and broadens the existing ground-level monitoring and air quality assessment activities in China.

Within AMFIC, the AURORA air quality model is applied to zoom in to the urban scale in order to identify hot spots of air pollution, to assess population exposure and the impact of emission reduction strategies at the city level. In this contribution we present our contribution to AMFIC (ESA Dragon Programme) and focus on the megacity of Shenyang.

Here the AURORA model is used to investigate the impact of urban vegetation abundance on air quality. First of all, some base runs were made and validated using local measurement data. It is shown that the model results are close to the measurements for most cases, especially taking into account the limited emission data available for this region. Thereafter, urban greening scenarios were implemented by artificially increasing and decreasing the percentage urban green vegetation cover. Both the amount and the spatial distribution of green vegetation cover were specified using a remotely sensed vegetation index.

This paper discusses both the methodology used to create high resolution emission data over China as the results of the dispersion modelling.

**Keywords** Modelling, air quality, China, urban greening, emission disaggregation

## 1. Introduction

China has one of the world's fastest-growing economies, but major cities such as Beijing, Shanghai and Shenyang have problems with choking pollution levels. In

D.G. Steyn and S.T. Rao (eds.), *Air Pollution Modeling and Its Application XX*,
DOI 10.1007/978-90-481-3812-8, © Springer Science + Business Media B.V. 2010

order to assess the problem and in order to be capable of taking effective measures against the pollution, it is necessary to get a better understanding of the local pollution distribution. The National People's Congress in China asked to work on developing clean energy sources and changing energy use patterns, in order to try to bring the air quality in most Chinese cities up to the international standards.

The AMFIC project (www.amfic.eu) aims to combine satellite observations, ground-based measurements and modelling techniques in order to assess air quality. Within AMFIC the AURORA regional-scale air-quality model is used in order to assess air-quality levels at the city level. Besides retrospective analyses, air-quality models can also be used to forecast air-pollution levels and to investigate the effect of mitigation strategies on air quality. In this contribution we present AURORA results for the city of Shenyang as well as a tool to derive high-resolution emission maps for air pollutants.

## 2. Methodology

Crucial input to air-quality models are the emission data for both gaseous and particulate pollutants. When applying models at the city level at high resolution, it is of paramount importance that the geographical information of the emissions has the same scale as the level on which the concentration levels need to be calculated.

For this reason, E-MAP, which is a tool developed by VITO, is used to spatially distribute emissions (Maes et al., 2009). It is based on a top-down methodology where total emissions, known for large regions (for instance, a country), are spread by making use of additional geo-information such as population density, the road network, land use, … Also time-variable data like the day-night rhythm can be used to disaggregate the date.

The disaggregation of emission data uses so-called substitute or surrogate variables, in order to weight statistical emission data. The most simple system to calculate the local emission out of a more global dataset is to use the following equation:

$$E_L = E_T * V_L / V_T$$

in which $E_L$ is the local emission, $E_T$ the total emission, $V_L$ the local value of the substitute variable and $V_T$ the total value of the substitute value. Examples of substitute variables are population density, fuel use, traffic volumes. In short, variables that represent the real local emissions fairly well but are easier to measure than the real emissions. The E-MAP tool is optimized by picking the most suitable substitute variables, which of course is a crucial step in the process.

In order to derive high-resolution maps for Chinese cities we start with the ACESS (Ace-Asia and Trace-P Modelling and Emission Support System) emission database. ACESS estimates anthropogenic emissions of the gaseous pollutants SO2, NOx, CO, NMVOC, as well as for PM10 and PM2.5 for Asia, broken down over four economic sectors (industry, transport, power plants and residential heating

(Woo et al., 2003). The emissions are provided on a 0.5° by 0.5° grid. The reference year is 2006 and emissions are given in ton per year (http://www.cgrer.uiowa.edu/people/carmichael/ACESS/Emission-data_main.html).

Meteorological fields, required as input for AURORA, were simulated using the Advanced Regional Prediction System (ARPS), a non-hydrostatic mesoscale atmospheric model developed by the University of Oklahoma (Xue et al., 2000, 2001). The equations of this model are finite-difference on a Arakawa C-grid. Terrain-following coordinates are employed in the vertical direction. Leapfrog time stepping in a fourth order central differencing scheme is used to solve the advection, while the turbulence is represented by a 1.5 order TKE model with the Sun and Chang (1986) parameterization for the convective boundary layer. Furthermore, ARPS contains detailed parameterizations for the cloud microphysics, cumulus convection and radiation transfer. Thanks to its nesting capacities, large-scale atmospheric features are allowed to enter the domain through the lateral boundaries. A detailed land surface scheme was also incorporated in ARPS, with an improved land surface model for urban surfaces (De Ridder and Schayes (1997); De Ridder (2006)).

The air quality model used in this study is AURORA (Air quality modelling in urban regions using an optimal resolution approach, Mensink et al. (2001)). In this model, the vertical diffusion is calculated with the Crank-Nicholson method (De Ridder and Mensink, 2002), while the horizontal diffusion uses a Walcek (2000) scheme. The gas phase chemistry is treated by the Carbon-Bond IV scheme (Gery et al., 1989), which has been enhanced to take into account biogenic isoprene emissions. For particulate matter ($PM_{10}$ and $PM_{2.5}$), a distinction has been made between primary and secondary particles. These secondary particles are simulated in a simple fashion using constant gas-to-particle conversion rates for both the transitions between $SO_2$ and sulphate aerosols and between $HNO_3$ and nitrate aerosols.

Both the amount and distribution of green vegetation cover are taken from the SPOT-VEGETATION satellite. Terrain height is taken from the Global 30 Arc-second Elevation Data Set, distributed by the U.S. Geological Survey.

The model effort is centered on the city of Shenyang, one of the ten largest cities of China and capital of the Liaoning Province, in North-Eastern China. Together with its neighboring cities it forms one of the most important industrial centers of China. Within the AMFIC program we obtained measurements of air pollution data in Shenyang which makes it an interesting area to test the performance of the our AURORA model.

The measurement data comes from eight stations in and around the city of Shenyang and measures three distinct pollutants, TSP (Total Suspended Particles), $NO_2$ and $SO_2$, which therefore will be in our focus in this paper. The simulations have been made on resolutions of 30, 10, 3 and 1 km (with in each case $51 \times 51$ horizontal grid points and 35 vertical levels) centered on the city of Shenyang, in which the runs on a finer resolution are nested in the runs with a coarser resolution. The 30 km run has been nested for the meteorology in the GFS-FNL (Global Forecast System-Final) model of the NCEP (National Centers for Environmental

Prediction) whereas the air quality run has been nested in the results of the CHIMERE chemical transport model, provided by the KNMI. The left panel of Fig. 1. shows the map for the city of Shenyang for July 2007. By artificially increasing or decreasing the percentage urban green vegetation cover, one can investigate its impact on air quality. The middle and right panels show artificial vegetation cover maps by decreasing and increasing the real maps, respectively. The effect of the vegetation change on the air pollution can be very interesting for the local government when they define abatement measures for air pollution.

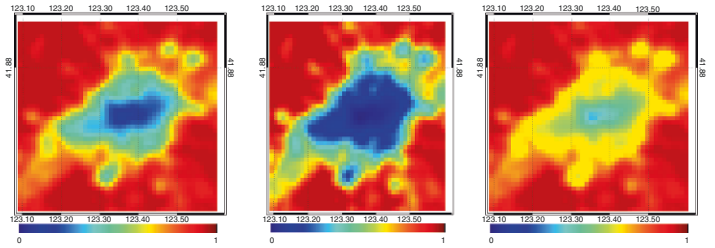


**Fig. 1.** Map of fractional vegetation for the city of Shenyang: satellite-derived data for July 2007 (left panel); artificially decrease in vegetation (middle panel); and artificially increase in vegetation abundance (right panel)

## 3. Results

In Fig. 2 the validation results for $SO_2$ and TSP/$PM_{10}$ can be found. All in all, the validation gives good results with positive correlations between measurements and modeled results in almost all stations, periods and discussed pollutants. It is also clear that the January pollution levels are much higher than the October pollution levels, especially for $SO_2$. Looking specifically at January 2004, we can see that the model has too high peak concentrations for both $SO_2$ and $PM_{10}$. However, the correlation and regression of the model on the measurements are quite good (correlation[1] of $SO_2$ = 0.46 with the slope of the regression[1] = 0.92; correlation[1] of $PM_{10}$ = 0.58 with the slope of the regression[1] = 1.21). This shows that our model is quite capable of reproducing the winter time variability of the Shenyang pollution. The modelled pollution is more important in stations where the measured pollution is higher, giving confidence in the spatial variability of the model.

For the October results, the same conclusions as for January can be made for $PM_{10}$, although the correlation is slightly lower (correlation[1] of $PM_{10}$ = 0.52 with the slope of the regression[1] = 0.67) and the spatial spread in the concentrations is strongly underestimated in the model. This underestimation can also be found in January but is less clear there. The October $SO_2$ concentrations are much less well represented in the model than the previous discussed pollutants and months (correlation[1] of $SO_2$ = 0.20 with the slope of the regression[1] = 0.40). This is pro-

[1] Using measurements and model results averaged over all the available stations.

bably due to the small spread in measurements during the month of October for $SO_2$. In January, a lot of $SO_2$ is emitted due to the heating of the houses, while this is not the case in October. This is both seen in the measured concentrations and in the modelled concentrations.

Furthermore, by using the vegetation maps of Fig. 1. we assess the effect on ozone concentration levels in the city centre.

## 4. Conclusions

High-resolution emission maps were produced for the city of Shenyang by using downscaling techniques employing spatial surrogate data (from $0.5° \times 0.5°$ to $1 \times 1\,km^2$ resolution). Afterwards, the AURORA model is used to investigate the impact of urban vegetation abundance on air quality. For both periods, the results of the AURORA model are in good agreement with the local measurements, increasing our confidence in the E-MAP tool as well as in the results of AURORA. However, the correlation between the observations and measurements of $SO_2$ for October 2004 are low.

**Acknowledgments** This research has been funded by the EU-FP6 project AMFIC. The ARPS meteorological model was made available by the Center for Analysis and Prediction of Storms at the University of Oklahoma. We would also like to acknowledge the U.S. Geological Survey for the GTOPO30 data set, the Jet Propulsion Laboratory for the SST imagery, VITO for the SPOT-VEGETATION NDVI imagery).

## References

De Ridder, K. 2006: Testing Brutsaert's temperature roughness parametrization for representing urban surfaces in atmospheric models. *Geophys. Res. Lett.,* **33**, L13403, doi:10.1029/2006GL026572.

De Ridder, K. and C. Mensink, 2002. Improved algorithms for advection and vertical diffusion in AURORA. In: Borrego and Schayes (eds.), *Air pollution modeling and its Application XV*, Kluwer Academic/Plenum Publishers, New York, 395–401.

De Ridder K. and G. Schayes, 1997. The IAGL land surface model. *Journal of Applied Meteorology*, **36**, 167–182.

Gery, M.W., G.Z. Whitten, J.P. Killius and M.C. Dodge, 1989. A Photochemical Kinetics Mechanism for Urban and Regional Scale Computer Modeling. *J. Geophys. Res.,*, **94**, 925–956.

Maes J., J. Vliegen, K. Van de Vel, S. Janssen, F. Deutsch, K. De Ridder, C. Mensink (2009), Spatial surrogates for the disaggregation of CORINAIR emission inventories, *Atmospheric Environment*, Volume 43, Issue 6, February 2009, Pages 1246–1254.

Mensink C., K. De Ridder, N. Lewyckyj, L. Delobbe, L. Janssen, P. Van Haver, 2001. Computational aspects of air quality modelling in urban regions using an optimal resolution approach (AURORA). Large-scale scientific computing – lecture notes in computer science, **2179**1, 299–308.

Sun, W.Y., and C.z. Chang, 1986: Diffusion model for a convective layer. Part I: Numerical simulation of convective layer. *J. Climate Appl. Meteor.*, **25**, 1445–1453.

Walcek, C.J. (2000). Minor flux adjustment near mixing ratio extremes for simplified yet highly accurate monotonic calculation of tracer advection. *Journal of Geophysical Research,* **105**, 9335–9348.

Xue, M., K. K. Droegemeier, and V. Wong, 2000. The Advanced Regional Prediction System (ARPS) – A multiscale non-hydrostatic atmospheric simulation and prediction tool. Part I: Model dynamics and verification. *Meteor. Atmos. Physics*., **75**, 161–193.

Xue, M., K. K. Droegemeier, V. Wong, A. Shapiro, K. Brewster, F. Carr, D. Weber, Y. Liu, and D.-H. Wang, 2001. The Advanced Regional Prediction System (ARPS) – A multiscale non-hydrostatic atmospheric simulation and prediction tool. Part II: Model physics and applications. *Meteor. Atmos. Physics*., **76**, 134–165.

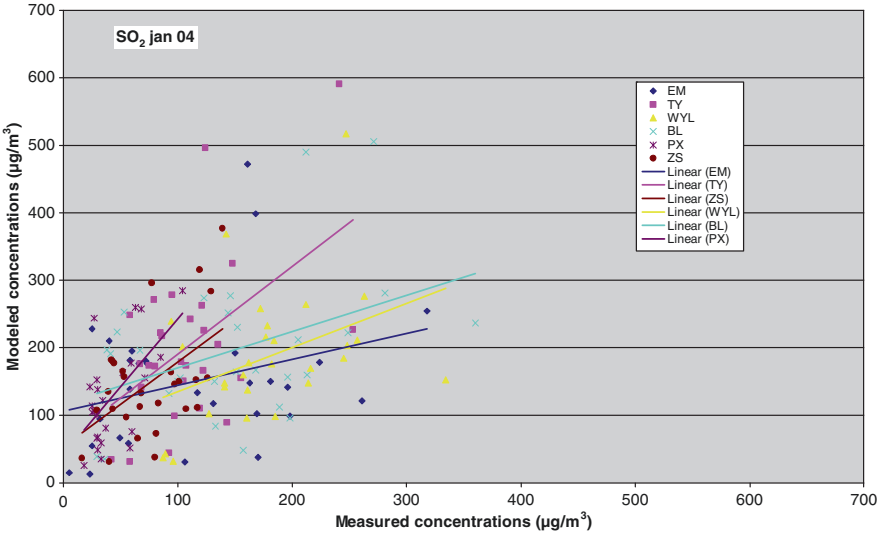


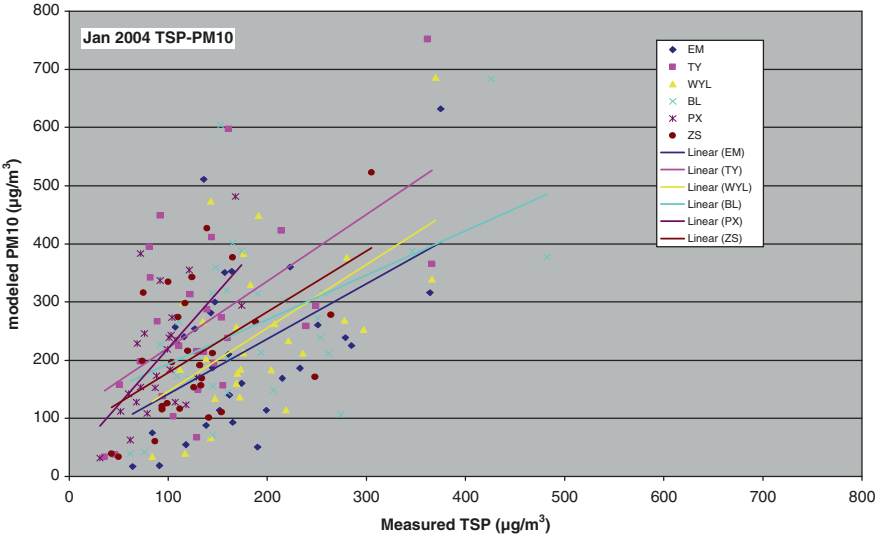

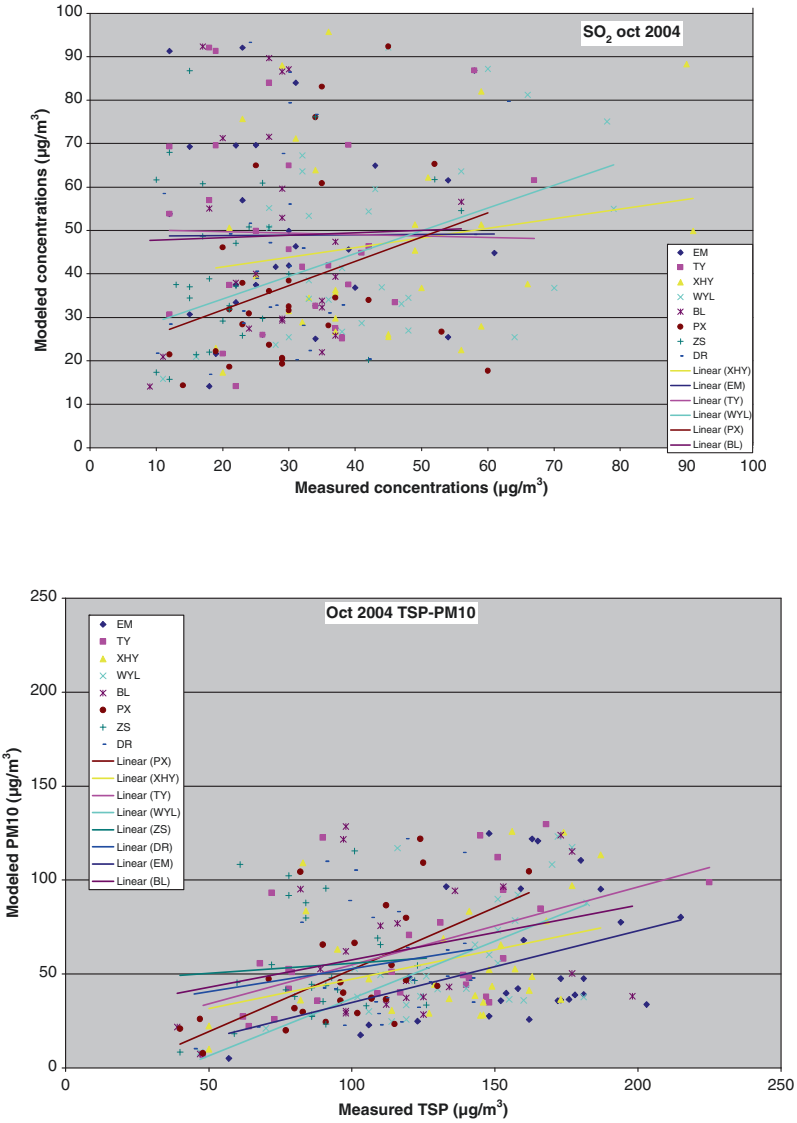


**Fig. 2.** Comparison between the measured and the modeled data. On the X-axis: the measured pollutant concentratins. On the Y-axis: the modeled pollutant concentrations. Each color represents a different station, for which the line of the same color represents the regression of the modeled concentrations on the measurements. In the left column of figures, the plots for $SO_2$ are shown. In the right column, those for TSP (measurements)/PM10 (modeled) are shown. Above: the results for January 2004. Below: the results for October 2004. Each point represents 1 day for which both measurements and model data were available

## 5. Questions and Answers

**Question:** The PM emission zoom on map of Shenyang is not much larger (if not even less) than its eastern neighbour of Fushun. Why is a smaller city to the East has compatible if not larger PM emissions? Question: Pius Lee (Air Resource Lab, NOAA, Silver Spring, MD, USA).

**Answer:** This is due to the EMAP methodology and to the available proxy data. Our proxy data shows that the region of Fushun is much more industrialized than the city of Shenyang. This results in a repartition of a major part of the regional industrial emissions to Fushun, and barely none to Shenyang.

**Question:** On the Validation January $SO_2$ plots (modeled versus manual) EM, TY, ZS have different regression slopes (Fig. 2, left above). Do you have any insight in that? Question: Pius Lee (Air Resource Lab, NOAA, Silver Spring, MD, USA).

**Answer:** Unfortunately, it is impossible to obtain further insight on that for the moment. In order to be able to answer this, it would be necessary to have data on the relative location of the stations to the various sources. As the emissions are not based in this case on local data but on a scaling of low resolution data using proxies, no data on this can be provided. Furthermore, one has to take into account that the measurements at one specific point are being compared to the model values in a grid cell of $1 \times 1$ km². This induces also errors.

# 2.12 Application of Model and Ambient Data Fusion Techniques to Predict Current and Future Year PM2.5 Concentrations in Unmonitored Areas

**Brian Timin, Karen Wesson, and James Thurman**

U.S. Environmental Protection Agency

## 1. Introduction

States with nonattainment areas for ozone and/or $PM_{2.5}$ must attain the ambient air quality standards by their respective attainment dates. The majority of areas use photochemical models to estimate future year pollutant concentrations to show how they will meet and/or maintain the standards. The EPA photochemical modeling guidance (U.S. EPA 2007) recommends an ambient monitor based relative attainment test. Since the test examines future year concentrations at monitor locations, it does not evaluate the likelihood of violations in unmonitored areas. To account for unmonitored areas, the modeling guidance also recommends an "unmonitored areas analysis" to examine future year concentrations of ozone and/or $PM_{2.5}$ in locations without nearby monitors. For the unmonitored area analysis, the guidance recommends using data fusion techniques to combine spatially interpolated ambient data with gridded photochemical model output to produce a "fused" surface of spatial fields. These fused spatial fields can be produced for both current years and also combined with future year modeling output to produce future year fields. Because they utilize both ambient data and model outputs, the fused spatial fields should provide an improved concentration estimate in unmonitored areas. In this application, we attempt to examine the performance of fused spatial fields compared to a simple ambient data interpolation technique.

## 2. Methods

The focus of this analysis is on annual average PM2.5 predictions. Using EPA's Model Attainment Test Software (MATS) (Abt, 2009) we created several sets of gridded spatial fields for a domain which covers the Eastern ~2/3 of the United States. The domain consists of 279 × 240 grid cells, 12 km on a side. In all cases, concentrations were interpolated to the center of each grid cell. The "basic" interpolation technique used for all interpolations was Voronoi Neighbor Averaging (VNA). This technique identifies the set of monitors that are nearest to the center

D.G. Steyn and S.T. Rao (eds.), *Air Pollution Modeling and Its Application XX*,
DOI 10.1007/978-90-481-3812-8, 

of each grid cell, and then takes an inverse distance squared weighted average of the monitor concentrations. The "fused" spatial fields are calculated by adjusting the interpolated ambient data (in each grid cell) up or down by a multiplicative factor calculated as the ratio of the modeled concentration at the grid cell divided by the modeled concentration at the nearest neighbor monitor locations (weighted by distance). Equation 1 shows the calculation of the fused concentrations.

$$Species_{E,\,baseline} = \sum_{i=1}^{n} Weight_i \cdot Monitor_i \cdot \frac{Model_{E,\,baseline}}{Model_{i,\,baseline}}$$

The concentration of Species E (which can be PM2.5, ozone, or any PM2.5 species component) is calculated as the sum of the weighted concentrations at each neighbor monitor. The multiplicative model adjustment factor, which is the last term in the equation, is only used in the fused data fields calculation.

## 3. Spatial Fields Performance

In order to test the performance of the interpolated and fused interpolated spatial fields, we employed a cross validation technique. Using MATS, we produced several sets of fields which were developed using various sets of ambient data and photochemical model outputs. The "control" case spatial fields were run for the Eastern 12 km domain using all available PM2.5 ambient data for 2002. The data was derived from the Federal Reference Method (FRM) and IMPROVE monitoring networks. Within the domain, there were 855 sites which had complete data[2] for all 4 quarters of 2002. A set of annual average spatial fields for 2002 were created using the data from all 855 sites. This was designated the "control case". Additionally, the control case interpolations were combined with photochemical model output for 2002[3] to create a "fused control case" (using the calculations from Eq. 1). Table 1 shows the performance statistics for these two spatial fields. As expected, the performance at the monitors is excellent.[4]

[2] Complete data was defined as having ≥11 samples per quarter.

[3] The analysis used output from the CMAQ photochemical model. Documentation of the 2002 modeling platform that was used can be found here: http://www.epa.gov/scram001/reports/Emissions%20TSD%20Vol1_02-28-08.pdf.

[4] The bias and error is not zero because the data is interpolated to the center of the 12km grid cells, and not to the actual monitor locations.

**Table 1.** Spatial field performance statistics

| Spatial field | Number of monitors | R-squared | Mean bias ($\mu g/m^3$) | RMSE ($\mu g/m^3$) |
|---|---|---|---|---|
| Control case | 855 | 0.98 | –0.025 | 0.43 |
| Fused control case | 855 | 0.97 | –0.026 | 0.51 |

In the control cases, the performance statistics between the fused and the standard interpolation are almost identical. This is expected because data fusion should have very little impact in grid cells where monitors are located.

## 4. Cross Validation

Additional sets of interpolated and fused interpolated spatial fields were created in order to examine interpolation performance in unmonitored areas. These new spatial fields were created using an abbreviated set of monitors, in which monitors were removed from the ambient datasets based on distance to the nearest neighbor monitor. This allowed us to simulate unmonitored areas by removing monitors from the ambient datasets feeding the spatial fields. Performance for both the interpolated and fused interpolated spatial field methods was examined by comparing the interpolated concentration in the grid cell where the removed monitors were located to the ambient measured concentration of the removed monitors.

We prepared and ran three sets of cross validation cases. Since we were interested in examining interpolation performance in unmonitored areas, we chose to remove monitors that were relatively isolated from all other monitors. We calculated the distance between monitors and removed all monitors in the domain whose closest neighbor monitor was >60, >40, and >20 km from the monitor. This led to the removal of 116, 218, and 589 monitoring sites in the three cases, respectively.

Table 2 shows the performance statistics for the "40 km" Interpolated and fused interpolation cases. The performance statistics were calculated for the grid cells where the monitors were *removed*.

**Table 2.** Interpolation performance for the "40 km" case in the grid cells where monitors were removed

| Spatial field | Number of monitors removed | R-squared | Mean bias ($\mu g/m^3$) | RMSE ($\mu g/m^3$) |
|---|---|---|---|---|
| 40 km interpolation | 218 | 0.72 | 0.57 | 1.62 |
| Fused 40 km interpolation | 218 | 0.72 | –0.64 | 1.62 |

As shown by Table 2, the performance statistics for both cases are similar. However, there is a clear over-prediction bias in the interpolation case and an under-prediction bias in the fused interpolation case. This bias can be seen more clearly in a scatterplot of the 40 km cases versus the observed data (Fig. 1).

The general over-prediction of the simple interpolated fields was expected. Most of the non-cross validation PM2.5 monitors are in urban areas and the simple interpolation technique cannot estimate relatively lower PM2.5 concentration in rural areas. The fused data technique was employed precisely for that reason. The additional information from the photochemical model output should, in theory, improve the interpolation results. In some locations, the data fusion does indeed improve the interpolation. For example, in mountainous areas such as Central West Virginia, the fused interpolation results accurately lower the PM2.5 concentrations (compared to the interpolation results) due to accurate model predictions of relatively low PM2.5 concentrations. However, the data fusion is only as good as the underlying photochemical model output. In some locations, the fused data severely overestimates the observed concentrations. In general, these are locations where the model predicted a large gradient in PM2.5 concentrations which apparently was not accurate.[5]

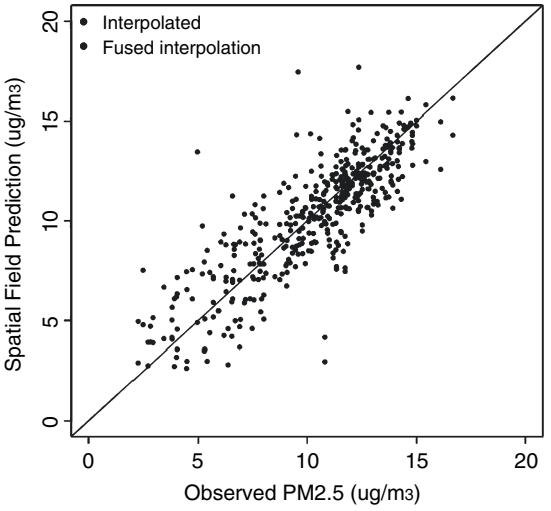


**Fig. 1.** Annual average PM2.5 concentrations of interpolated fields compared to observed data

[5] The 2002 CMAQ model output used to derive the fused interpolated fields has a known over-prediction bias due to mishandling of fugitive dust emissions. A correction factor (to lower the emissions) was not correctly applied. This may lead to performance issues in the fused data fields.

## 5. Conclusion

Spatial fields can be used for several purposes. Base year fields can be used to help site new monitors and future year fields can be used to examine potential future ambient standard violations as well as to calculate health benefits. Cross validation of interpolated and fused interpolated fields shows that in this application, interpolated fields suffer from an over-estimation bias and the fused fields have an under-estimation bias. In some cases, the fused fields are an improvement over the non-fused fields. More accurate model estimates of PM2.5 should lead to more accurate fused fields. Additional applications and performance evaluation of fused fields should be completed using more recent model outputs that have adequate PM2.5 performance.

## References

Abt Associates, 2009. User's Guide- Modeled Attainment Test Software. http://www.epa.gov/scram001/modelingapps_mats.htm

U.S. EPA, 2007. Guidance on the Use of Models and Other Analyses for Demonstrating Attainment of Air Quality Goals for Ozone, PM2.5, and Regional Haze. http://www.epa.gov/scram001/guidance/guide/final-03-pm-rh-guidance.pdf

## 6. Questions and Answers

**Question:** How does your data fusion approach compare to the approach used in the BenMAP model?

**Answer:** The PM2.5 results shown in this paper use the identical approach found in BenMAP (VNA based interpolation). However, the MATS software uses a more sophisticated routine for projecting PM2.5 concentration to future years. BenMAP projects PM2.5 based on the modeled relative change in total PM2.5 mass. MATS projects PM2.5 based on the modeled relative change in individual PM2.5 species components and then adds the components together to get future year total PM2.5 mass.

# 2.13 A Regional Multimedia Modelling System for the Simulation of the Long Range Transport, Chemistry and Deposition of Semi-Volatile Pollutants

**Rong Li[1], M. Trevor Scholtz[2], Fuquan Yang[1], and James J. Sloan[1]**

[1]Waterloo Centre for Atmospheric Sciences, University of Waterloo, Waterloo, ON, Canada

[2] Canadian ORTECH Environmental, Mississauga, ON, Canada

**Abstract** We will report the development and application of a multimedia regional chemical transport model designed to investigate the long range transport and deposition of semi-volatile organic materials (SVOMs). The model was built by combining the US EPA MM5/MCIP/SMOKE/CMAQ modelling system with a dynamic air-soil exchange model, PEM (Pesticide Emission Model), which was developed by Canadian ORTECH Environmental Ltd. The combined model accounts for the important physical and chemical processes governing the behaviour of the SVOM in both the soil and the atmosphere. Hourly outputs from the modelling system include SVOM emission from the soil, its concentrations in both the gas phase and on atmospheric particulate matter and its wet and dry deposition to terrestrial and water surfaces. The CMAQ system used the CB4 mechanism and simulated common pollutants such as $NO_X$, VOCs and $SO_2$, which interacted with the SVOM.

The model was tested by simulating the emission, transport, chemical reactions and deposition of toxaphene, a persistent, bio-accumulative, toxic pesticide. Although banned more than 20 years ago in North America, significant residues remain in the soil and these continue to be emitted slowly into the atmosphere. The model was evaluated from January 1 to December 31, 2000 in a domain that covers most of North America. Satisfactory agreement was obtained between the model predictions and measurements for: (a) daily-average toxaphene air concentrations, (b) fraction on atmospheric particulate matter, and (c) annual wet and dry deposition into Lake Ontario and the seasonal variations of these depositions.

**Keywords** Multimedia, chemical transport model, semi-volatile pollutant, pesticide

## 1. Introduction

Toxaphene, a mixture of chlorinated bornanes, is an effective pesticide for cotton, soybean and corn. Beginning in the 1940s, it was used heavily in the United States

D.G. Steyn and S.T. Rao (eds.), *Air Pollution Modeling and Its Application XX*,
DOI 10.1007/978-90-481-3812-8, © Springer Science + Business Media B.V. 2010

and Mexico, but it was banned in 1982 due to its toxicity to animals and all usage stopped by 1986. A total of about 490 kt (kt = $10^6$ kg) was used in the United states from 1947 to 1986 (Li, 2001) and about 10–100 kt were used in Mexico during the same time. No toxaphene was used in Canada.

Despite the fact that toxaphene has not been used in North America for nearly 3 decades, significant concentrations are found in the atmosphere, soil, lakes, fish, and animals at locations far from the regions where it was used. Although virtually all toxaphene use was in the southern US and Mexico, it is found in the upper Great Lakes in such high concentrations that restrictions have been placed on the consumption of fish caught there. Thus it is clear that this pesticide continues to be emitted from soils where it was used, transported over long distances and deposited at locations many hundreds or even thousands of km from the location of its original application.

The slow emission and gradual dispersion over great distances is a general characteristic of a wide range of semi-volatile organic materials (SVOMs) that have been dispersed into the soil and water. In order to quantify this behaviour and thereby assess the dangers to human populations posed by such materials, we have developed a modelling system consisting of the US EPA's MM5/SMOKE/CMAQ regional chemical transport model (CTM), which is coupled in-line with an air-soil exchange Pesticide Emission Model (PEM). The resulting system is capable of simulating the transport of heat, moisture and SVOM in the soil; SVOM emission from the soil to the atmosphere; transport and chemical reaction of the SVOM in the atmosphere and its deposition to terrestrial and water surfaces. In this report, we describe its application to the pesticide toxaphene, but with suitable modification of certain physical parameters, the model is also capable of simulating the behaviour of a wide range of other SVOMs.

## 2. Modelling Details and Simulations

The SMOKE/CMAQ regional CTM includes all relevant atmospheric species such as ozone, OH radicals and aerosols. Thus it accounts for the chemical removal of the SVOM by reaction with OH as well as its physical partitioning between the gas phase and three aerosol size modes. The PEM soil model uses 17 soil texture classes having different hydraulic properties and tillage characteristics, all of which affect the rate of volatilization to the atmosphere. PEM is driven by the same meteorology as the CTM, so it is capable of simulating the diurnal and seasonal emission variations realistically. The combined system has high vertical resolution: 22 sigma layers in the atmosphere up to a pressure level of 100 mb and 49 layers in the soil down to a depth of 1 m.

The 1999 US and 1995 Canadian criteria emission inventories were used directly in the SMOKE emissions processor. The pesticide emissions calculated by PEM were also introduced into SMOKE through an interface developed for this purpose and combined with the other atmospheric species.

Simulations of toxaphene were done for 18 months from 1 January 2000 to 30 June 2001 on the domain shown in Fig. 1 at a spatial resolution of 36 × 36 km. In this figure, the colour scale shows the toxaphene emissions for the year 2000 calculated by the PEM emission model from residues that were determined from the known toxaphene usage and an assumed soil half-life of 4 years (James and Hites, 2002). The residues were allocated to the model domain using the gridded percentage of cropland (Environment Canada, 2002) as a surrogate for spatial distribution.

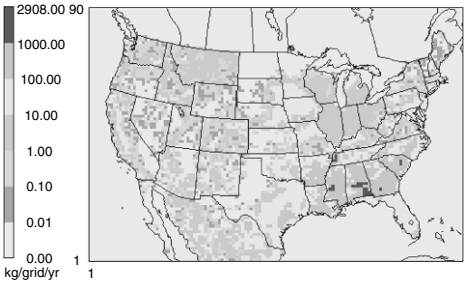


**Fig. 1.** Toxaphene emissions for the year 2000 in the model domain

## 3. Results and Discussion

The simulated average surface gas phase concentrations of toxaphene for the year 2000 are shown in Fig. 2. The highest gas phase concentrations coincide with the regions of highest emission, but it is clear that they extend into regions where there were no residues and hence no emission. (There are, for example, high gas phase concentrations over the Atlantic Ocean and the Gulf of Mexico.)

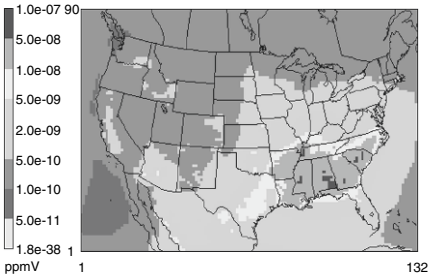


**Fig. 2** Gas phase toxaphene concentrations in the lowest atmospheric layer (depth of 35 m)

Because of the semi-volatile nature of toxaphene, the surface gas phase concentrations are dominated by the emission, which is highest in the summer. The transport, however, is reflected by the spatial distributions of deposition fluxes. The dry depositions are also dominated by the surface concentrations, but depositions of particulate matter and wet depositions are more dependent on the meteorology.

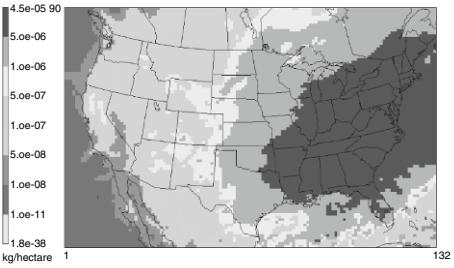


**Fig. 3** Averaged wet deposition of toxaphene for the year 2002

The wet deposition pattern of the gas phase material is shown in Fig. 3. This illustrates clearly that the prevailing meteorology transports the material in a north-westerly direction and also that a significant amount (averaged over 1 year) is deposited far from where it was originally applied. This represents one yearly cycle of emission, transport and deposition. Obviously the same qualitative behaviour occurs every year, with the material deposited in 1 year being re-emitted and transported further during the next.

**Acknowledgments** We are pleased to acknowledge financial support from the Province of Ontario, The Natural Sciences and Engineering Research Council of Canada, Ontario Power Generation Ltd. and Canadian Ortech Environmental Ltd.

## References

Environment Canada, Global Pesticides Release Database, http://www.msc.ec.gc.ca/data/gloperd/emission_e.cfm, (2002).

James, R.R. and Hites, R.A., 2002. Atmospheric transport of toxaphene from the southern united states to the great lakes region. Environmental Science & Technology 36, 3474–3481.

Li, Y.F., 2001. Toxaphene in the United States 1. usage gridding. Journal of Geophysical Research-Atmospheres 106, 17919–17927.

# 2.14 A Comparison of Multiple Ozone and Particulate Matter Source Apportionment Models

**Kirk Baker and Brian Timin**

U.S. Environmental Protection Agency

## 1. Introduction

It is useful to understand what types of sources or regions are contributing to ozone estimated by photochemical grid models. Understanding the contribution from particular sources to specific geographic receptor locations helps regulators develop effective emissions control strategies. Source apportionment is an alternative approach to zero-out modeling and has the advantage of being much more efficient with computational resources. The incremental run-time associated with the additional source region tracking is far less than performing numerous iterative zero-out simulations.

Ozone source apportionment tracks the contribution to model ozone estimates from pre-cursor emissions of nitrogen oxides (NOX) and volatile organic compounds (VOC). Particulate source apportionment tracks contributions to particulate species from pre-cursor emissions. Ozone and particulate source apportionment are implemented in state of the science photochemical grid models CMAQ and CAMx.

The Milwaukee metropolitan area was chosen for an exercise comparing absolute model predictions and source contribution estimates using CAMx and CMAQ source apportionment. The source apportionment estimates are compared for 11 specific geographic tags, all other sources that were not tagged, and boundary conditions at monitors located in Milwaukee and Waukesha counties in Wisconsin. The 11 tags constitute the emissions from all source sectors in entire counties or groups of counties.

## 2. Methods

Each model was applied with particulate source apportionment to a modeling domain covering the Midwest United States with 12 km sized grid cells over 4 months in 2002: January, April, July, and October. Ozone source apportionment is only applied for the month of July 2002. The SMOKE emissions model was run separately for each source region to ensure that each geographic region tag only contains emissions for that specific area. Ozone source apportionment in CAMx

D.G. Steyn and S.T. Rao (eds.), *Air Pollution Modeling and Its Application XX*,
DOI 10.1007/978-90-481-3812-8, © Springer Science + Business Media B.V. 2010

(OSAT and APCA) tracks the contributions to each grid cell from emissions source groups, emissions source regions, initial conditions, and boundary conditions with reactive tracer species. APCA recognizes that there are source categories such as biogenics that can not be controlled so the model only attributes ozone to biogenics when it is due to the interaction of biogenic VOC + biogenic NOx. Ozone and particulate matter source apportionment technology (PSAT) has been implemented into the most recent version of the CAMx model (v4.5) and is publicly available (ENVIRON, 2008). PSAT estimates the contribution from specific emissions source groups, emissions source regions, initial conditions, and boundary conditions to PM2.5 using reactive tracers.

The Ozone and Precursor Tagging Methodology (OPTM) and Particle and Precursor Tagging Methodology (PPTM) have been implemented in CMAQ v4.6 (ICF International 2007a, b). OPTM estimates contributions from emissions source groups, emissions source regions, initial conditions, and boundary conditions to ozone by tracking total oxidant (defined for this purpose as $\{NO_2 + NO_3 + 2*N_2O_5 + O_3\}$) formation from duplicate model species for each contributing source. PPTM estimates contributions from emissions source groups, emissions source regions, initial conditions, and boundary conditions to PM2.5 by adding duplicate model species for each contributing source.

## 3. Results and Discussion

Both models tend to over-predict the lowest ozone concentrations and under-predict the highest ozone concentrations. PM2.5 model performance is similar for both models. CMAQ tends to predict higher concentrations of ammonium nitrate at this location. Both models show the best agreement with observations for PM2.5 sulfate ion.

In general, CMAQ/OPTM tends to predict higher contributions for the boundary conditions and less contribution to more local regions. The CAMx/APCA approach estimates the highest contribution from local sources. This is in part due to APCA switching contribution to local NOX emissions during conditions where local NOX mixes with biogenic VOC under VOC limited ozone formation. CMAQ and CAMx contribution estimates are well correlated ($r^2 = .9$) and have a RMSE less than 2.55. Most of the error between CAMx and CMAQ estimates is from the contributions from the boundary and all other non-tagged sources.

CMAQ/OPTM tends to predict higher contributions from the boundary than the CAMx ozone source apportionment implementations. CAMx tends to estimate higher contributions from the non-tagged emissions inside the modeling domain than CMAQ/OPTM. CMAQ has higher estimates of local contributions. A comparison of DDM sensitivity to CAMx ozone source apportionment indicates ozone source apportionment may overstate the contribution from the boundaries (Dunker et al., 2003). The spatial pattern of contribution from the sources regions tracked in each model slightly different. CAMx/APCA tends to have the highest contributions

to ozone closer to the source region. In general, the spatial patterns are very similar between the various implementations.

The CAMx and CMAQ estimated PM2.5 contribution from each source region to the Milwaukee/Waukesha area is consistent. The total PM2.5 contribution can also be examined at each receptor location by chemical composition. This type of evaluation suggests that the contribution from more distance source regions tends to be from secondarily formed species like nitrate and sulfate and local contribution tends to be dominated by primarily emitted species.

CMAQ and CAMx show the best agreement for species dominated by primary emissions like elemental carbon and primary organic carbon. The poorest agreement is for PM2.5 nitrate ion, which is likely due to differences in model formulation for nitrate aerosol formation and exacerbated by differences in advection and deposition as it tends to be secondarily formed specie that is more likely to transport in from nearby source regions.

Source apportionment also tracks the contribution from initial conditions, which allows for an evaluation about how long initial concentrations remain an important contribution to model estimates. The domain peak ozone contribution from initial conditions decreases to approximately 1 ppb by the seventh day of the modeling episode. Total 24-h averaged PM2.5 concentrations from initial conditions reduce below 1.0 $\mu g/m^3$ after four simulation days in each quarter. This suggests that four to five simulation days would be necessary to remove the influence of start-up conditions on model estimates of PM2.5 and a week to remove ozone initial concentrations.

## 4. Conclusions

Both models tend to under-predict ozone greater than 75 ppb. The relationship between estimated ozone contribution over all receptors from all source regions is strong between CAMx and CMAQ. Most of the variability in the error is due to differences in contribution estimates from the boundary and the group consisting of all other emissions in the modeling domain that were not tagged. CAMx and CMAQ are fairly consistent with absolute model estimates of PM2.5 species, with the exception of nitrate ion, of which CMAQ tends to predict higher concentrations. The modeling systems also tend to have strong relationships in predicted source contributions. Again, nitrate ion source contribution between models has the weakest relationship of the species examined in this study. The largest contributing species on the top 10% of modeled days include primarily emitted species including primary organic carbon and elemental carbon. Contributions from source areas furthest away from the Milwaukee/Waukesha area tend to be dominated by secondarily formed species such as nitrate ion and sulfate ion. Despite differences in model formulations, the source contributions estimated by each modeling system compare well with each other. This increases the confidence that each is appropriately implemented and suitable for the estimation of source contribution.

## References

ENVIRON International Corporation. 2008. User's Guide Comprehensive Air Quality Model with Extensions (CAMx4) Version 4.50. ENVIRON International Corporation, Novato, California. www.camx.com

ICF International, 2007a. Implementation of Sulfur and Nitrogen Tagging in the Community Multiscale Air Quality (CMAQ) Model: Technical Description and Users' Guide. January 15, 2007.

ICF International, 2007b. Implementation of Ozone and Particle Precursor Tagging Methodologies in the Community Multiscale Air Quality (CMAQ) Model: Technical Description and User's Guide. November 20, 2007.

# 2.15 Predicting the Regional Air Quality Impacts of Prescribed Burns

**M. Talat Odman[1*], Yongtao Hu[1], D. Scott McRae[2], Scott L. Goodrick[3], Yongqiang Liu[3], Gary L. Achtemeier[3], and Luke P. Naeher[4]**

[1]School of Civil and Environmental Engineering, Georgia Institute of Technology, Atlanta, GA 30332-0512, USA

[2]Department of Mechanical and Aerospace Engineering, North Carolina State University, Raleigh, NC 27695-7910, USA

[3]Forestry Sciences Laboratory, USDA Forest Service, Athens, GA, 30602-2044, USA

[4]College of Public Health, University of Georgia, Athens, GA 30602-7396, USA

**Abstract** Prescribed burning plumes are not sufficiently resolved in current modeling systems; therefore, their regional impacts cannot be accurately predicted. A modeling system is being developed to better characterize the emissions from the burns and the dispersion and chemical transformation of the smoke plumes. Adaptive grids are used to increase the resolution of regional-scale models and a Lagrangian plume model is employed to model the sub-grid scale plume dynamics. Simulations of a prescribed burn conducted at Fort Benning, Georgia on 9 April 2008 show that the new system significantly improves the predictions of downwind pollutant levels over conventional modeling systems.

**Keywords** Adaptive grid, sub-grid scales, coupled models, particulate matter

## 1. Introduction

Prescribed burning (PB) is an economical way of maintaining and improving the ecosystem and reducing wildfire risk. However, pollutants emitted from the fires may be transported long distances, mix with emissions from other sources, and contribute to air quality problems in downwind urban areas. Accurate predictions of PB impacts can help land managers continue their operations without endangering public health.

Biomass burning plumes are not well resolved in current air quality modeling systems due to insufficient grid resolution and inadequate sub-grid scale treatments. A modeling system is being developed to address these weaknesses. The

* Phone: 404-894-2783, Fax: 404-894-8266, E-mail: talat.odman@ce.gatech.edu

D.G. Steyn and S.T. Rao (eds.), *Air Pollution Modeling and Its Application XX*,
DOI 10.1007/978-90-481-3812-8, © Springer Science + Business Media B.V. 2010

objectives of this system are to better characterize the emissions from the fires, to accurately simulate the dispersion of the smoke plumes, and to increase the resolution of regional-scale models so that the impacts of PB emissions can be discerned from other pollution sources in the region. The approach taken is to utilize a dynamic, solution-adaptive grid algorithm to increase grid resolution locally around the PB plume. Turbulence parameterization is being revised in view of the refined grid scales, and Daysmoke, a plume model specifically designed for PB plumes, is being used as the sub-grid model.

## 2. Adaptive Grid Models

An adaptive grid version of MM5 was developed to predict the occurrence and extent of optical scale turbulence [1]. Using a dynamic adaptive grid algorithm, it is possible to resolve gravity waves, shear or optical turbulence sufficiently to provide accurate predictions. The standard MM5 turbulence parameterization was replaced with a physically based, four equation, LES/RANS turbulence model that outputs directly the dissipation rates needed to calculate optical turbulence without parameterization.

The adaptive grid air quality modeling methodology of Odman et al. [2] was implemented in CMAQ. The grid adaptation is restricted to the horizontal plane. A 2-D weight function, consisting of the Laplacian of the ground-level $PM_{2.5}$ concentration field, determines where grid nodes are to be clustered for a more accurate solution. The concentrations are then interpolated to the new grid positions. Owing to the equivalence of interpolation to numerical advection, a higher order advection scheme is used for interpolation. Emissions and meteorological data are also processed to the new grid.

The grid becomes non-uniform after adaptation but, for easy computation of the solution, a coordinate transformation reestablishes the uniform grid. The Jacobian of the coordinate transformation from the physical ($x$, $y$, $z$) space to the computational $(\xi, \eta, \sigma)$ space is calculated as

$$J = \frac{1}{m^2}\frac{\partial z}{\partial \sigma}\left(\frac{\partial x}{\partial \xi}\frac{\partial y}{\partial \eta} - \frac{\partial y}{\partial \xi}\frac{\partial x}{\partial \eta}\right).$$

The governing equation of the CMAQ model is modified as

$$\frac{\partial (Jc_n)}{\partial t} + \frac{\partial \left(Jv^{\xi} c_n\right)}{\partial \xi} + \frac{\partial \left(Jv^{\eta} c_n\right)}{\partial \eta} + \frac{\partial \left(Jv^{\sigma} c_n\right)}{\partial \sigma} + \frac{\partial}{\partial \xi}\left(JK^{\xi\xi}\frac{\partial c_n}{\partial \xi}\right)$$
$$+ \frac{\partial}{\partial \eta}\left(JK^{\eta\eta}\frac{\partial c_n}{\partial \eta}\right) + \frac{\partial}{\partial \sigma}\left(JK^{\sigma\sigma}\frac{\partial c_n}{\partial \sigma}\right) = JR_n + JS_n$$

where the superscripts denote contravariant components of the velocity vector and diffusivity tensor. Since the grid is uniform in the computational space, the same numerical solution algorithms used in CMAQ can be used directly.

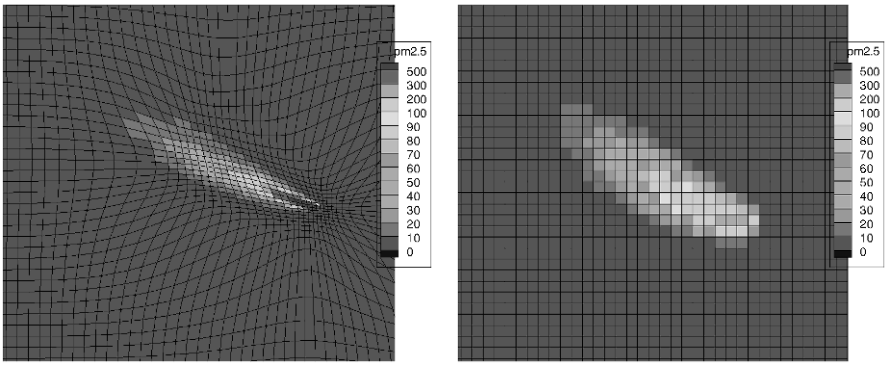


**Fig. 1.** Comparison of $PM_{2.5}$ concentrations ($\mu g\ m^{-3}$) at Fort Benning, GA during a prescribed burn on April 9, 2008: (a) standard CMAQ with 1.33 km grid resolution, (b) adaptive CMAQ with dynamically adapting mesh. Boxes shown are cutouts of the Fort Benning area from the model domain

The adaptive grid provides significant improvement of the PB plume simulation over the standard CMAQ (Fig. 1).

## 3. Sub-grid Scale Plume Model

The dynamics of smoke plumes from PB are often far more complex than the dynamics of plumes from industrial stacks. Daysmoke, a dynamical-stochastic plume model, was developed specifically to simulate smoke from PB in a manner consistent with how the burns are engineered by land managers. It is an extension of a plume model developed to simulate deposition of ash from sugar cane fires [3]. Daysmoke employs a dynamic plume-rise algorithm and a large eddy parameterization to describe the plume boundaries; a stochastic turbulence model diffuses the particles through the boundaries of the plume. Its predictions of smoke concentrations generally agreed with ground-level measurements at several locations beneath the plumes (Fig. 2) and were also confirmed with lidar observations.

The major task ahead is the development of a suitable coupling technique that can inject Daysmoke particles into the CMAQ grid cells without significant loss of accuracy. For this, a Fourier analysis technique is being explored. First, the smoke particle concentrations predicted by Daysmoke are represented as spectra of waves with different frequencies. Then, the waves whose frequencies cannot be supported by the adaptive CMAQ grid are identified. If the amplitudes of those waves are negligible, then the plume is handed over to CMAQ; otherwise the plume is

continued to be followed by Daysmoke. A particle-in-grid method is also being explored for modeling the chemistry of currently nonreactive Daysmoke particles prior to mixing with the contents of CMAQ grid cells. This is expected to enable accurate representation of plume dynamics and chemistry at local scales as well as accurate prediction of impacts over regional scales.

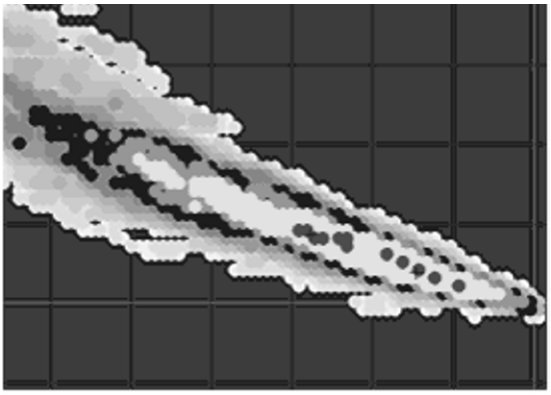

**Fig. 2.** Daysmoke predictions of ground-level $PM_{2.5}$ concentrations at Fort Benning, GA during a prescribed burn on April 9, 2008. The predictions were confirmed with measurements at locations marked by cross hatches

## 4. Future Directions

The next step will be to have MM5 and CMAQ operate on the same adaptive grid. This can be achieved immediately in 2-D by using an adaptive weight function of smoke concentrations and dynamic variables such as vorticity, so that both the wind field and the PB plumes are resolved. The models will be time stepped parallel to each other so that there is no need for interpolating the variables from one model to another. This will be followed by the development of the 3-D adaptation capability in CMAQ. The ultimate goal is a fully merged interactive model where any feedbacks of PB plumes on dynamics and vice versa are fully resolved.

**Acknowledgments** This work is supported by the Strategic Environmental Research Program with substantial cost sharing from the US Forest Service.

## References

Xiao, X., D. S. McRae, and H. A. Hassan: A new dynamically adaptive mesoscale atmospheric model, Proceedings, AMS 11th Conference on Mesoscale Processes, Albuquerque, NM, October 2005

Odman, M. T., M. N. Khan, R. K. Srivastava, and D. S. McRae, 2002: Initial application of the adaptive grid air pollution model. *Air Pollution Modeling and its Application XV* (C. Borrego and Guy Schayes, Eds., Kluwer Academic/Plenum publishers, New York), 319–328.

Achtemeier, G.L., 1998: Predicting dispersion and deposition of ash from burning cane. *Sugar Cane*, **1,** 17–22.

## 5. Questions and Answers

**S.T. Rao:** How do you ensure that the adaptive grid structures of MM5 with that of CMAQ where different dynamical forcings dictate the adaptive grid requirements in met and AQ models?

**Answer:** The grid adaptation is performed by means of a weight function. This weight function can be a linear combination of functions of different variables. The determination of the most relevant meteorology and air quality variables, and their weights in the combination, is part of our research. For optimum resolution of the feedbacks between the dynamics and the plume, we propose the combination of smoke concentration, as the major air quality variable in a prescribed burn, with vorticity, as an important dynamic variable.

# 2.16 Emulating Complex Calculations for Regulatory Decisions

**Bernard Fisher[1], Charles Chemel[2], Rong-Ming Hu[2], and Ranjeet Sokhi[2]**

[1]Environment Agency, UK

[2]University of Hertfordshire, UK

**Abstract** The application of Gaussian process emulators to air pollution models of low and intermediate complexity is demonstrated using the health impact of a power station footprint as an illustrative example. In the future it is planned to apply the emulator approach to more complex models such as CMAQ.

**Keywords** Emulator, Gaussian process, complex models, TAPM model, CMAQ model, life years, simulator, decisions

## 1. Introduction to Model Emulators

Complex models are built to simulate the behaviour of real-world systems. These models may be empirical or represent detailed scientific understanding of the real-world process. They are usually implemented in computer programs, which can run to many thousands of lines of code and can take from a fraction of a second to several weeks to run. Such a simulator can be regarded as a mathematical function *f(x)*, that takes a vector *x* of inputs and produces an output vector *y = f(x)*. The outputs *y* of a simulator are a prediction of the real-world phenomena that are simulated by the model, though there will be uncertainty about how close the true real-world quantities will be to the outputs *y*. This uncertainty arises from many sources, particularly uncertainty in the correct values to give the inputs x and uncertainty about the correctness of the model *f(x)* in representing the real-world system.

An emulator is a statistical representation of a simulator. A Gaussian process emulator makes use of Gaussian stochastic processes which have convenient mathematical properties to approximate the simulator and to describe the uncertainty associated with the simulator (Kennedy and O'Hagan, 2001). These authors have also provided a freely available code for calibrating Gaussian process emulators and for producing a free standing representation. These tools are available from: http://www.tonyohagan.co.uk/academic/GEM/GEM-SA1_1.zip. For additional explanation, see Rasmussen and Williams (1996). The purpose of

D.G. Steyn and S.T. Rao (eds.), *Air Pollution Modeling and Its Application XX*,
DOI 10.1007/978-90-481-3812-8, © Springer Science + Business Media B.V. 2010

building an emulator is to facilitate other calculations that would not be practical to do using the simulator itself. An emulator provides an entire probability distribution for *f'(x)*. The formula representing the emulator is

$$f'(x) \sim GP(m(x), k(x, x'))$$

where $x$ is a vector of input parameters (where for our purposes $x$ consists of, say, the deposition velocity, scavenging coefficient, transformation rate *etc.* and is potentially of high dimension) each of which is uncertain. We can consider a randomly chosen sequence of values of $x$ which has the properties of a Gaussian process, namely $m(x')$ the mean function and $k(x, x')$ the covariance function are the only non-zero correlations between values of vectors $x$ and $x'$. The Gaussian process has simple properties determined by $m(x)$ and $k(x, x')$, such that

$$m(x) = \overline{f'(x)} \text{ and } k(x, x') = \overline{(f'(x) - m(x))(f'(x') - m(x'))}$$

and all other moments are zero. The symbol ~ in the equation for *f'(x)* denotes that the Gaussian process approximation is not a single valued function, but a probability distribution determined by values chosen randomly from the probability distribution of $x$ and $x'$. One can imagine a number of training points $x_i$ where the complex model has been run, giving the output $y_i$ so the emulator should return $GP(m(x_i), k(x_i, x')) = y_i$ with no uncertainty. The convenient properties of the Gaussian emulator mean that it is possible to evaluate the mean and standard deviation in an exact closed form, so that $GP(m(x), k(x, x')$ can be very easily evaluated and code written to evaluate *f'(x)*. From this code *f'(x)* can be evaluated at points which are not training points. The probability distribution for *f'(x)* should give a mean value $m(x)$ that represents a plausible interpolation of the training data, and the probability distribution around this mean should be a realistic expression of uncertainty about how the simulator might interpolate. Some similar approaches to emulation that may be familiar include fitting regression models to data, krigging, data assimilation or neural networks.

## 2. Examples of Applying a Gaussian Process Emulator

A power station footprint with typical 'new build' coal emission factors, using a simple analytical model with emissions scaled by 100, to give particulate matter (PM) concentrations at various locations, illustrates how GEM can be applied to a multidimensional example. The analytical model is based on 2 × 2 matrix solutions for the primary $G$ and secondary $S$ concentrations of particulate matter components surviving during wet and dry periods of average duration $t_0$ and $t_1$. $G$ and $S$ are solutions of equations of the type:

$$\begin{pmatrix} u\frac{\partial}{\partial x} - D\frac{\partial^2}{\partial z^2} + \lambda_0 + \frac{1}{t_0} & -\frac{1}{t_1} \\ -\frac{1}{t_0} & u\frac{\partial}{\partial x} - D\frac{\partial^2}{\partial z^2} + \lambda_1 + \Lambda_{pri} + \frac{1}{t_1} \end{pmatrix} \begin{pmatrix} G_{00} & G_{01} \\ G_{10} & G_{11} \end{pmatrix} = \begin{pmatrix} 0 & 0 \\ 0 & 0 \end{pmatrix}$$

$$\begin{pmatrix} u\frac{\partial}{\partial x} + \frac{v_{g\,sec}}{a} + \frac{1}{t_0} & -\frac{1}{t_1} \\ -\frac{1}{t_0} & u\frac{\partial}{\partial x} + \frac{v_{g\,sec}}{a} + \Lambda_{sec} + \frac{1}{t_1} \end{pmatrix} \begin{pmatrix} S_{00} & S_{01} \\ S_{10} & S_{11} \end{pmatrix} = \begin{pmatrix} \lambda_0 G_{00} & \lambda_0 G_{01} \\ \lambda_1 G_{10} & \lambda_1 G_{11} \end{pmatrix}$$

The parameters $\lambda_0$ and $\lambda_1$ describe the conversion of primary to secondary forms of a particular species during wet and dry periods, $\Lambda_{pri}$ and $\Lambda_{sec}$, washout rates for primary and secondary species and $v_{g\,pri}$ and $v_{g\,sec}$, deposition velocities. There are enough of these parameters (at least of order 30 assuming four primary components of particulate matter: sulphate, nitrate, ammonium and primary particulate matter) apart from the meteorological uncertainty, to make a sensitivity analysis for this analytical model fairly complex. By integrating the footprint over population one can remove the spatial variability and concern oneself with the number of extra years of life lost due to exposure from 1 year of notional emissions (the numbers are not realistic due to the scaling of emissions). One can estimate the population exposure *f(x)* which is a function of the input parameters $x = (v_{g\,pri}, v_{g\,sec}, \Lambda_{pri}, \Lambda_{sec}, \lambda_0, \lambda_1 ...)$. The main uncertainty is the health impact factor relating the PM concentration to the number of life years lost, but this parameter is not included as it dominates over the uncertainty in the atmospheric processes.

GEM has been applied to this analytical model with components $SO_4$, $NO_3$ and PM and the impact factor fixed, by varying the following eight parameters: $SO_2$: $v_{g\,pri}$ (m $s^{-1}$), $\Lambda_{pri}$ ($s^{-1}$), $\lambda_0$ and $\lambda_1$ ($s^{-1}$), NOx: $v_{g\,pri}$, $\Lambda_{pri}$, $\lambda_0$ and $\lambda_1$ (0.00002–0.00004), PM: $v_g$ (0.005–0.02), $\Lambda$. Using the Latin Hypercube option in GEM, one is able to select a limited number of possible values of input parameters within expected ranges. It turns out that the health outcome is clearly dependent on the transformation rate of primary NOx and the deposition velocity of the sum of primary and secondary PM. The lives lost and the uncertainty, as a function of these parameters, are plotted in Fig. 1.

This example of an emulator, based on an analytical solution, is artificial. The benefits of an emulator arise when applied to complex atmospheric models. To illustrate this case, we use The Air Pollution Model TAPM (http://www.csiro.au/products/ps1gu.html) of intermediate complexity, for its convenience in generating results. Again we consider the footprint from a major new point source subject to current emission controls. Two parameter values are varied, corresponding to the total emission strength (kg $s^{-1}$) of the source (in the range 0.3–10 kg $s^{-1}$ applying a fixed PM:NOx:$SO_2$ ratio) and the smog concentration (reactivity weighted background VOC concentration ppb), which determines the reactivity of the air into

which the plume is discharged. TAPM uses a simplified chemical scheme and the smog parameter largely determines the oxidation rates of $NO_2$ and $SO_2$ $\lambda_0, \lambda_1$. The external emulator from 8 runs of the model generates the health impact and uncertainty shown in Fig. 2. The uncertainty is large and with realistic emissions one would anticipate much lower numbers of life years lost (of order of a few hundred) corresponding to values close to the origin. Larger values were used in the calculation to avoid rounding errors in the code and to investigate the functional dependence on the smog parameter. This represents a preliminary application illustrating how the emulator can be used to investigate the behaviour of a complex code. In future trials it is planned to generate an emulator from runs of the more complex chemical transport model CMAQ (Yu et al., 2008).

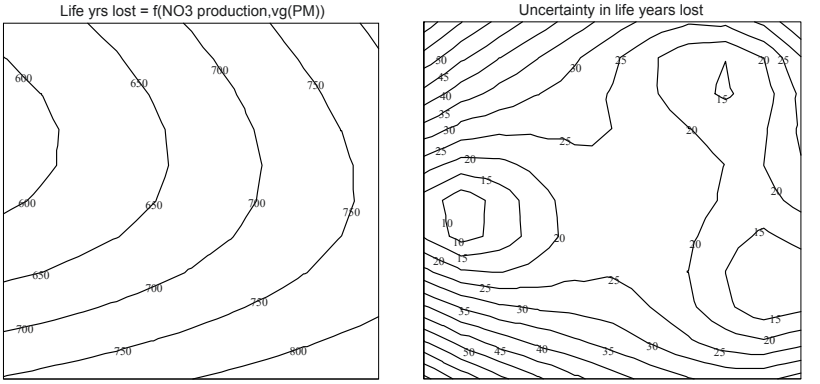


**Fig. 1.** Life years lost and uncertainty (standard deviation of probability distribution) as function of oxidation rate of NOx (x-axis) and the deposition velocity of particulate matter (y-axis) for an analytical footprint model

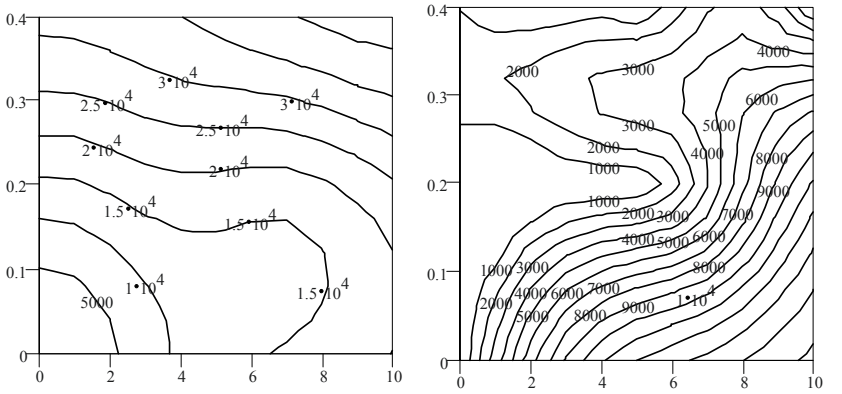

**Fig. 2.** Life years lost and uncertainty (standard deviation of probability distribution) as a function of emission rate (x-axis) and smog (y-axis) for the TAPM simulation

## References

Kennedy M.C. and O'Hagan A.: Bayesian calibration of computer models. J. R. Stat. Soc. Ser. B Stat. Methodology, 63, 425–464 (2001)

Rasmussen C.E. and Williams C.K.L.: Gaussian Processes for Machine Learning. MIT Press, ISBN 026218253X www.GaussianProcess.org/gpml (1996)

Yu Y., Sokhi R.S., Kitwiroon N., Middleton D.R., Fisher B.: Performance characteristics of MM5–SMOKE–CMAQ for a summer photochemical episode in southeast England, United Kingdom. Atmospheric Environment, 42, 4870–4883 (2008)

## 3. Questions and Answers

**Ferd Aauter (RIVM):** Is it possible to use this type of analysis when you are dealing with spatially distributed uncertain parameters and complex, time-consuming models?

**Answer:** The purpose of an emulator is to make an uncertainty analysis possible and practical when one is dealing with a complex model containing many distributed uncertain parameters. In this case a full Monte-Carlo analysis is not possible and alternative efficient methods need to be tried.

# 2.17 Use of the CAMx Model to Assess the Air Quality Impacts of Proposed Oil and Gas Production Projects in the Western U.S.: Simulation of Winter High Ozone Events

**Susan Kemball-Cook, Ralph Morris, Bonyoung Koo, Uarporn Nopmongcol, Jeremiah Johnson, and Tejas Shah***

ENVIRON International Corporation, 773 San Marin Drive, Suite 2115, Novato, CA 94998, USA

**Abstract** The CAMx photochemical grid model is used to evaluate air quality impacts of a proposed natural gas development project in the Western U.S. CAMx is shown to simulate observed high winter ozone events in a region of intensive oil and gas development.

**Keywords** Winter ozone, CAMx, oil and gas development

## 1. Introduction

Oil and gas production in the western states has increased as demand for domestic sources of energy has risen. Under the National Environmental Policy Act (NEPA), the development of an oil and gas production project on Federal land usually involves the preparation of an Environmental Impact Statement (EIS) or Environmental Assessment (EA) that discloses the potential environment effects of the project. Such environmental effects include the potential impacts of emissions from oil and gas production on air quality (AQ) and air quality-related values (AQRVs) including visibility and acid deposition. High wintertime ozone concentrations have recently been observed in otherwise rural regions of the U.S. where intensive oil and gas production activity is occurring [1, 2]. Therefore, recent oil and gas EISs [3] have applied photochemical grid models (PGMs) to address potential ozone impacts as well as AQ and AQRV impacts.

The basic modeling strategy used in an EIS that employs a PGM is to first simulate a current year base case without the proposed Project using a comprehensive regional emission inventory of actual emissions from all sources (motor

* E-mail: skemballcook@environcorp.com

D.G. Steyn and S.T. Rao (eds.), *Air Pollution Modeling and Its Application XX*,
DOI 10.1007/978-90-481-3812-8, © Springer Science + Business Media B.V. 2010

vehicles, power plants, biogenic sources, etc.). The base case simulation is evaluated with respect to ambient air quality measurements. If the base case simulation reproduces concentrations of observed species with reasonable fidelity, then the model can be used in a future year assessment of Project impacts. The future year modeling involves development of a future year Project emission inventory as well as a future year regional emission inventory. Project AQ and AQRV impacts are determined from the future year PGM simulations.

This paper presents the use of the Comprehensive Air Quality Model with Extensions (CAMx) [4] PGM to estimate the potential ozone, AQ, and AQRV impacts due to a proposed natural gas production project in southwest Wyoming. We briefly describe the model application and then focus on the CAMx simulation of winter high ozone events in southwest Wyoming.

## 2. CAMx Model Configuration

To assess the AQ and AQRV impacts of the proposed oil and gas Project located in southwest Wyoming, CAMx is applied for both base year and future year simulations on a 36/12/4 km nested-grid modeling domain. The 36 km grid covers the continental United States and serves to provide boundary conditions to the finer grids. The main study area lies within the 12/4 km modeling domain shown in Fig. 1.

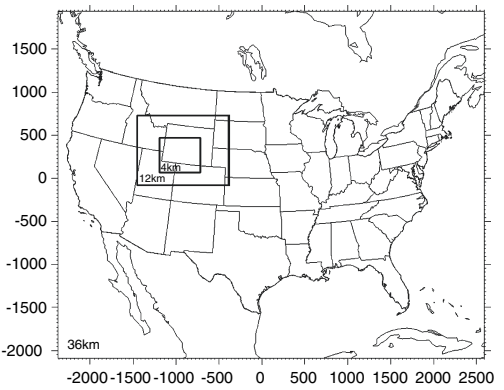


**Fig. 1.** 36/12/4 km Nested CAMx Modeling Domain

CAMx was applied for the calendar years of 2005 and 2006 using actual emissions of NOx, $SO_2$, $PM_{10}$, $PM_{2.5}$, VOC and CO from all sources for those years. Detailed emission inventories of oil and gas production sources in the 12/4 km domain have been compiled for these periods, and a comprehensive regional emission inventory has been prepared. CAMx output gas and particle phase model concentrations were compared against observed values for the two modeled base years.

## 3. Winter Ozone Model Performance Evaluation

As part of the model performance evaluation of the 2005–2006 base year simulations, the model's ability to simulate observed winter high ozone events in southwestern Wyoming during February 2006 was assessed. CAMx sensitivity tests were conducted that were guided by field study data collected by the Wyoming Department of Environmental Quality (WDEQ) during the winters of 2007 and 2008 and analyzed by WDEQ and their contractors [1]. The field study data indicate that the following conditions are necessary in order for high wintertime ozone events to occur in southwestern Wyoming: shallow inversion (limited mixing), white snow on ground (high albedo), few or no clouds, stagnant and/or re-circulating slow surface winds, high morning total non-methane hydrocarbon (TNMHC) concentrations (e.g., ~4,000 ppbC), and high morning TNMHC/NOx ratios (e.g., 90:1).

The sensitivity of the CAMx modeling system to each of the components of the above conceptual model of wintertime ozone formation was tested. In these sensitivity tests, several changes were made to model inputs to adapt the model for the simulation of conditions typical of high winter ozone days. For snow-covered surfaces in Southwest Wyoming, the CAMx snow albedo was increased from its default value of 0.5–0.75 based on UV up/down radiometer measurements at the Boulder monitoring site in southwestern Wyoming from the WDEQ field study. In the region where high ozone was observed, a thin cloud deck was removed, PBL heights were capped at 100 m on high ozone days in accord with observations [2], and the oil and gas emission inventory TNMHC emissions were adjusted upward so that the inventory matches the observed TNMHC/NOx ratio. The average TNMHC/NOx ratio in the Jonah-Boulder area in the oil and gas emission inventory was approximately 13:1, compared to the observed ratio of 90:1 (note that this is a comparison of observed ozone precursor levels with the emission inventory). The adjustment to the oil and gas emission inventory had by far the

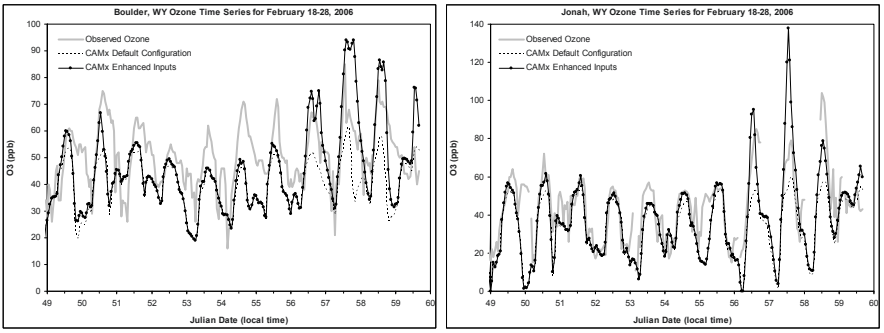


**Fig. 2.** CAMx winter ozone sensitivity test. Ozone time series for Boulder (left) and Jonah (right) Wyoming for CAMx run in default configuration suitable for modeling summer ozone episodes and with enhanced inputs indicated by results of WDEQ field study

largest impact of any of the changes to the model inputs. The sensitivity tests showed that when all of the above factors were accounted for in the CAMx inputs, the model was able to produce high wintertime ozone concentrations in southwestern Wyoming that are comparable to the observed values (Fig. 2).

**Acknowledgments** Much of the photochemical modeling presented in this paper was funded by BP America. We acknowledge the work of BP America and Sage Consulting, who developed the detailed 2006 oil and gas emissions inventory for southwest Wyoming used in the modeling. We also acknowledge the use of the field study data collected by the Wyoming Department of Environmental Quality and their contractors that formed the basis for the conceptual model of winter ozone formation in southwestern Wyoming.

## References

ENVIRON International Corporation, T&B Systems Inc. and Meteorological Solutions Inc. 2008. "2008 Upper Green River Ozone Study". Prepared for Cara Keslar, Air Quality Division, Wyoming Department of Environmental Quality. October.

Schnell, R., S. Oltmans, R. Neely, M. Endres, J. Molenar, and A. White. 2009. Rapid photochemical production of ozone at high concentrations at a rural site during winter. *Nature Geoscience* **2**, 120–122.

Bureau of Land Management (BLM). 2006. Draft Supplemental EIS for the Pinedale Anticline Oil and Gas Exploration and Development Project, Sublette County, WY.

ENVIRON International Corporation. 2008. "User's Guide Comprehensive Air Quality Model with Extensions (CAMx) Version 4.50." Novato, CA. (www.camx.com).

## 4. Questions and Answers

**Question:** How will CAMx performance if you do not update albedo for the snowy days? (Question rendered as written)

**Answer:** The effects of increased albedo and photolysis rates over snow-covered surfaces were accounted for in CAMx.

**Question:** Did field studies show evidence for increased secondary organic aerosols. This might be expected from high VOCs in oxidizing conditions.

**Answer:** The field study did not examine this question, but this would be an interesting issue for future field studies to explore.

**Question:** In Houston, where the chemical industry is a major source of VOC, the inventory is also ten times too low. Is there a common error in how we are developing VOC inventories for industrial facilities? Asked by Ron Cohen.

**Answer:** It is unclear at present whether there are similar underestimates of VOCs in emission inventories for Houston chemical facilities and oil and gas production facilities in Wyoming. It is likely that fugitive VOC emissions are

underestimated in both inventories. Other oil and gas sources may be underestimated, have temporal allocation profiles which are not well-represented in the model, or are simply not present in currently available emission inventories (e.g., evaporation from produced water ponds).

**Comment:** The WDEQ campaign was ended earlier this year. Bob Baxter et al. was showing real-time measurements of the Wyoming monitors. A few monitors showed 120 ppb peak ozone. So no doubt it was widespread. But between February 15 and 28 (when campaign ended on February 28) no such high readings at the monitors. So looked like the high ozone reading at the monitors did reflect sporadic occurrence. A very specific set of conditions must concurrently happening in order to produce such a scenario.

Conditions associated with high winter ozone in Southwest Wyoming during the WDEQ 2007–8 field study are noted above on page 3. When the model inputs reflect these conditions, CAMx simulates these high winter ozone events.

**Comment:** The low bias of CAMx not capturing the surface ozone peaks are perhaps due to (a) strong albedo that added to photolytic rates were not accounted for and (b) dry depositional velocity over different kind of snow may not be well captured by the model. Comments 4 and 5 by Pius Lee (NOAA ARL).

Snow albedo effects and their feedbacks on photolysis rates are accounted for in CAMx, as are the effects of snow on the dry deposition velocity.

# 2.18 Modelling the Individual Contributions of Gaseous Emissions Sources to the Deposition of Sulphur and Nitrogen in the UK

**Anthony J. Dore[1*], Bill Bealey[1], Maciej Kryza[2], Massimo Vieno[3], and Mark A. Sutton[1]**

[1]Centre for Ecology and Hydrology, UK

[2]Department of Meteorology and Climatology, University of Wrocław, Poland

[3]Institute of Atmospheric and Environmental Science, University of Edinburgh, UK

**Abstract** An important application of atmospheric transport models is to estimate the contribution of different sources of emissions to pollutant deposition. This can rarely be achieved by measurement. A simple Lagrangian atmospheric transport model, FRAME, was employed to assess the contribution to sulphur and nitrogen deposition in the UK from 160 different point and area sources in the UK as well as European emissions and international shipping. For the year 2005, the largest emissions sources for dry deposition of $SO_x$, $NO_y$ and $NH_x$ were power stations, road transport and livestock respectively, comprising 29%, 42% and 52% of the totals. For wet deposition, European emissions were important, comprising 31%, 35% and 41% of total deposition for $SO_x$, $NO_y$ and $NH_x$ respectively. International shipping emissions of $SO_2$ and $NO_x$ were also significant, contributing 21% and 17% of wet deposition of $SO_x$ and $NO_y$.

**Keywords** Atmospheric transport model, acidification, sulphur, nitrogen, emissions

## 1. Introduction

In order to develop an effective strategy to combat the effects of acidification and eutrophication, regulators and policy makers need to know not just the magnitude and spatial variation of nitrogen and sulphur deposition but also the relative contributions of different emissions sources. Long range chemical transport models are required to calculate aerosol and gas concentrations and their contribution to wet and dry deposition of pollutants. Examples of such data sets include the EMEP source-receptor matrices (Tarrasón and Nyiri, 2008) which show the contribution of emissions from individual countries in Europe to deposition in other countries.

* Corresponding author: Tel: +0131 445 4343; E-mail: todo@ceh.ac.uk

D.G. Steyn and S.T. Rao (eds.), *Air Pollution Modeling and Its Application XX*,
DOI 10.1007/978-90-481-3812-8, © Springer Science + Business Media B.V. 2010

The present study focuses on the UK and considers the individual contribution of emissions from a number of major point sources (power stations), distributed sources as well as international shipping and import from European sources.

## 2. Description of Model and Input Data

The FRAME model (Dore et al., 2007) is a Lagrangian atmospheric transport model employing annually averaged statistical meteorology. It's main features include: 5 km horizontal resolution covering the British Isles; vertical resolution varying from 1 m at the surface to 100 m near the top of the boundary layer; vertical diffusion calculated with k-theory eddy diffusion; dry phase and aqueous phase chemistry of sulphur and nitrogen; wet removal calculated by constant drizzle using scavenging coefficients driven by a map of annual rainfall for the UK; gaseous dry deposition calculated using a canopy resistance parameterisation; a plume rise module to calculate 'effective stack height' of point source emissions; boundary concentrations generated from a European scale simulation on the EMEP 50 km grid. The model was found to give a good representation of aerosol and gas concentrations of nitrogen and sulphur compounds as well as wet deposition when compared with measurements from the UK national monitoring networks (Dore et al., 2007).

A detailed data base of emissions for the year 2005 including stack parameters for point sources was compiled for the UK. Distributed emissions were obtained from the National Atmospheric Emissions Inventory (www.naei.org.uk). The model was applied to perform 160 individual simulations, each with a different point source or area emissions source abated. The sources comprised: 100 individual point sources, 21 groups of combined minor point sources, 37 sources of area emissions disaggregated according to region and emission classification as well as international shipping and import from other European countries.

## 3. Discussion and Conclusion

The results of the simulations were used to apportion deposition in the UK to emissions from UK sources, European sources and international shipping. The results from FRAME showed good agreement with the EMEP source-receptor matrices. FRAME estimated that international shipping contributed 18% and 15% respectively to total sulphur and oxidised nitrogen deposition in the UK, compared with 19% and 18% for EMEP. FRAME calculated that emissions from the UK contributed 59% of sulphur, 58% of oxidised nitrogen and 70% of reduced nitrogen deposition, as compared with 56%, 42% and 73% for EMEP. Total deposition to the UK was dominated by wet deposition with reduced and oxidised nitrogen making similar contributions to total nitrogen deposition.

**Table 1.** Relative contributions to total wet and dry deposition of $NH_x$, $NO_y$ and $SO_x$ in the UK from different emissions sources (%)

| | $NH_x$ dry | $NO_y$ dry | $SO_x$ dry | $NH_x$ wet | $NO_y$ wet | $SO_x$ wet |
|---|---|---|---|---|---|---|
| Power stations (%) | – | 9 | 29 | – | 14 | 45 |
| Road transport (%) | – | 42 | – | – | 12 | – |
| Livestock (%) | 52 | – | – | 26 | – | – |
| Shipping (%) | – | 10 | 11 | – | 17 | 21 |
| Import (%) | 6 | 9 | 0 | 41 | 35 | 31 |
| Total deposition (Gg) | 66 | 66 | 51 | 105 | 82 | 106 |

Following enforcement of the International Maritime Organisation agreement to reduce the sulphur content in marine fuel from 2.7% to 0.5%, the contribution of international shipping emissions to sulphur deposition will be significantly reduced by the year 2020. A number of sample deposition 'footprints' are illustrated in Figs. 1 and 2. These include: dry deposition of sulphur from international shipping emissions (with deposition highest in the south-east near the busy shipping lanes of the English Channel); dry deposition of oxidised nitrogen from road transport emissions in England (with deposition highest near the major motorways and urban areas); wet deposition of sulphur from European sources (with deposition highest over the high rainfall upland regions of Wales and the Pennines) and dry deposition of $SO_x$ from a single power station (with dry deposition highest within a few tens of km from the point source). Analysis of the contribution of UK and international sources to the national wet and dry deposition budgets for nitrogen and sulphur is illustrated in Table 1. This reveals that the power generating industry continues to make a significant contribution to sulphur deposition, accounting for 29% of dry deposited and 45% of wet deposited sulphur. Emissions of $NO_x$ from road transport in the UK account for 42% of dry deposited and 12% of wet deposited $NO_y$. Emissions of ammonia from livestock make a major contribution to deposition of reduced nitrogen, accounting for 52% of dry and 26% of wet deposition.

These summary statistics illustrate that whilst national policy to abate emissions of low level sources (i.e. $NO_x$ and $NH_3$) can be effective in reducing dry deposition of nitrogen in the local area, efforts to control wet deposition in sensitive upland regions require international cooperation due to the trans-boundary transport of aerosol with emissions sources originating in Europe and from international shipping (Fig. 2, right hand plot).

Further work will employ these maps to estimate the contribution of the emissions sources to exceedance of critical loads for acid deposition and nitrogen deposition as well as cost effective abatement measures to protect the environment using the UK Integrated Assessment Model (Oxley et al., 2003). In addition a comparison between footprints of deposition from point sources will be undertaken between FRAME and more complex Eulerian models.

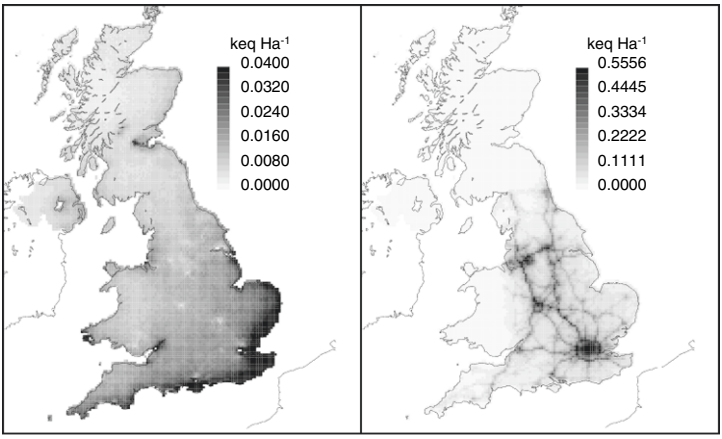


**Fig. 1.** Dry Deposition of $SO_x$ from international international shipping emissions (left); dry deposition of $NO_x$ from road transport emissions in England (right)

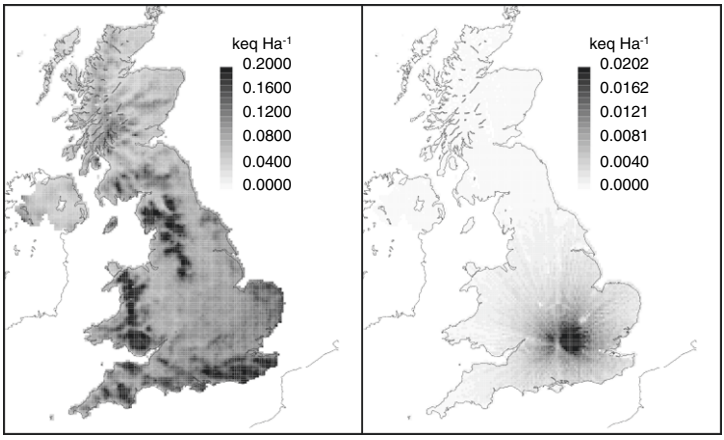


**Fig. 2.** Wet deposition of $NO_y$ from European emissions (left); dry deposition of $SO_2$ from a single power station (right)

## References

Dore, A.J., M. Vieno, Y.S. Tang, U. Dragosits, A. Dosio, K.J. Weston and M.A. Sutton (2007) Modelling the atmospheric transport and deposition of sulphur and nitrogen over the United Kingdom and assessment of the influence of $SO_2$ emissions from international shipping. *Atmos. Env.* **41**, 2355–2367.

Oxley, T., H. ApSimon, A.J. Dore, M.A. Sutton, J. Hall, E. Heywood, T. Gonzales del Campo and R. Warren (2003) The UK Integrated Assessment Model, UKIAM: A National Scale Approach to the analysis of strategies for abatement of atmospheric pollutants under the convention on long-range transboundary air pollution *Integrated Assessment*, **4**, 236–249.

Tarrasón, L. and Nyiri, A. (2008) Transboundary Acidification, Eutrofication and Ground Level Ozone in Europe in 2006. EMEP Status Report 1/200.

## 4. Questions and Answers

**Peter Builtjes:** You showed that the FRAME model results for wet deposition compare favourably with observations. Does that mean that your rain intensity data are correct?

**Answer:** Yes. The rainfall intensity data can be considered to be reliable. The map of annual rainfall driving the washout rate in the FRAME model is calculated from interpolation of measurements from the UK Met Office national rain gauge network. This simple approach of using measured annual rainfall has certain advantages, as annual precipitation can be measured accurately but presents challenges to be well represented by meteorological models. However, complex Eulerian models do have the advantage of an event based approach to representing precipitation whereas FRAME assumes constant drizzle.

**Christian Reuter:** Projections of 2020 acid deposition showed exceedances over mountainous areas with high precipitation. Are the sources of $SO_2$ therefore located outside the UK? If so, how did you account for future $SO_2$ emissions outside the UK?

**Answer:** The boundary conditions for the UK model simulation were generated from a European scale simulation. Emissions from the UK and Europe are projected to fall significantly by 2020. Major reductions in $SO_2$ emissions from international shipping will also take place by 2020 due to imposition of Annex VI of the MARPOL convention resulting in large reductions in the sulphur content of bunker fuel. Trans-continental import and 'background concentrations' are considered to make a relatively small contribution, though hemispherical modelling will be required to better quantify their importance. In the future, nitrogen will become a more significant driver for acidification, through deposition of both oxidised and reduced nitrogen. The latter can contribute via in-soil oxidation.

# 2.19 A Perspective on Development of Effective Ozone Control Strategies in Urban Regions of South and Central Texas

**M. Zuber Farooqui[1], Jhumoor Biswas[2], Kuruvilla John[3], and Saikat Ghosh[4]**

[1]University of North Carolina–Chapel Hill, Chapel Hill, NC, USA

[2]Indian Institute of Social Welfare and Business Management, Kolkata, India

[3]University of North Texas-Denton, Denton, TX, USA

[4]Texas A&M University–Kingsville, Kingsville, TX, USA

**Abstract** A regional photochemical modeling system is applied to multiple high ozone episodes of September 13–20, 1999 and September 8–16, 2002 over urban South and Central Texas to assess the relative impact of emissions on ozone levels. Overall $NO_x$ emission reductions produced greater ozone benefits. The cities of Austin and San Antonio exhibited greater sensitivity towards $NO_x$ emissions and were affected most by on-road mobile emissions with zero-out emission simulations. The coastal urban area of Corpus Christi indicated no significant bias towards $NO_x$ or VOC emissions and was most affected by non-road mobile emissions. The city of Victoria demonstrated greater sensitivity towards point sources. Emission reduction strategies needed for maintaining air quality within any urban airshed must be based on multiple ozone episodes in order to reduce episode-episode variability in the effectiveness of emission control strategies.

**Keywords** Ozone, photochemical modeling, multiepisode, emission sensitivity runs, exceedances

## 1. Introduction

Ozone abatement strategies based mostly on regional scale photochemical modeling simulations of single ozone episodes have been a vital part of the State Implementation Plans submitted to the United States Environmental Protection Agency (EPA) by individual states. The model sensitivity to emission controls is contingent on key input parameters of the models: meteorology and emissions. The impact of meteorology on ozone processes has been well established (Brônnimann et al., 2002). Emission control requirements based on one episode may be different from the emissions controls based on another episode due to the impact of meteorological

D.G. Steyn and S.T. Rao (eds.), *Air Pollution Modeling and Its Application XX*,
DOI 10.1007/978-90-481-3812-8, © Springer Science + Business Media B.V. 2010

variability on VOC/$NO_x$ sensitivity (Bärtsch-Ritter et al., 2004) and the variability in emissions. The ozone changes on weekly and long-term scales are caused primarily by anthropogenic emission changes, while changes at the hourly, diurnal, synoptic and seasonal scales are mainly influenced by meteorology. Investigative methods such as "zeroing out" approaches of specific sources of emissions can serve as a preliminary guide for the development of control strategies. This methodology is applied in this study to inter-compare impact of relative emission distribution patterns in the four ozone near non-attainment areas (Austin, San Antonio, Corpus Christi and Victoria), which have had several high ozone days in recent times despite being in attainment of the federal air quality standards. The study will also evaluate the fluctuations in the impact on air quality for two separate high ozone episodes. Ozone exceedances are extremely important from the standpoint of human health. Impact assessment of emissions was evaluated on both the number of exceedances and their spatial extent based on EPA's new standards for ozone. The results from these preliminary investigations depict ozone benefits arising from emissions controls exhibit substantial episode-episode fluctuations thus reiterating the need to consider multiple ozone episodes in order to reduce uncertainties while developing effective emission control strategies.

## 2. Model Setup

The photochemical model (CAMx) version 3.1 and 4.1 was applied in a nested mode (36, 12 and 4) km with the innermost grid encompassing all the near non-attainment areas (NNA) of south and central Texas for 1999 and 2002 respectively. Hourly meteorological data from MM5 simulations were used for both the episodes. Emissions processor EPS version 2 and 3 was employed to generate hourly CAMx ready gridded emissions input files for the two ozone episodes September 13–20, 1999 and September 8–16, 2002, respectively, over south and central Texas. Details of the September 1999 model set up are provided by Emery et al. (2003) and that of September 2002 are provided by Farooqui M.Z. (2008).

## 3. Methodology

The index of improvement of modeled $O_3$ concentrations was computed for n25v50 (25% $NO_x$ emission reduction and 50% VOC emission reduction) and n50v25 (50% $NO_x$ emission reduction and 25% VOC emission reduction) emission control runs relative to the base case (n00v00) run. "Zero-out emission runs" from area, on-road mobile, non-road mobile, point, anthropogenic, and biogenic emission sources were conducted. The impact of emission sensitivity runs on ozone exceedances was assessed by computing the reduction in the number of exceedances and in spatial extent of exceedances within the study domain.

## 4. Results and Discussions

The base case model evaluations for both episodes are within USEPA's recommended statistical limits. Both episodes display greater sensitivity to $NO_x$ emission reductions with maximum improvement of 9–13% in San Antonio and Austin for the 1999 episode, while a similar analysis for the 2002 episode demonstrated over 15% improvement using the n50v25 control run (Fig. 1). The maximum impact from n25v50 reduction simulation is about 3–10% for both episodes in these urban areas. Corpus Christi exhibits comparable ozone benefit from both $NO_x$ and VOC emission reductions.

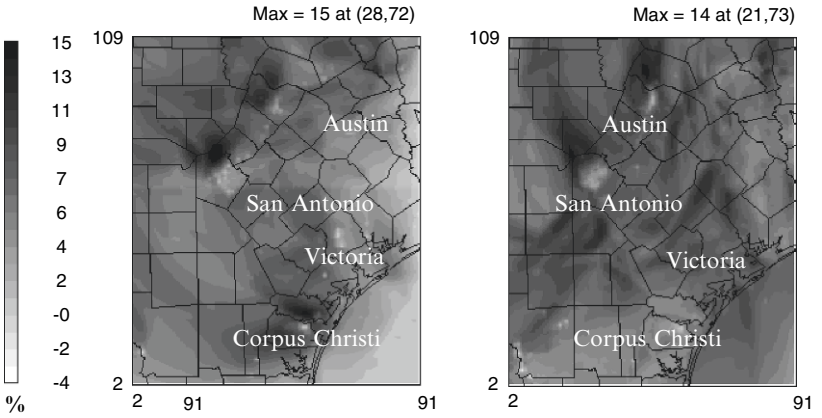


(a) 1999 (b) 2002

**Fig. 1.** Index of Improvement with n50v25 control (a) 1999 episode and (b) 2002 episode

### 4.1. Impact of zero-out emission control runs on peak concentrations (ppb)

There are marked differences in episode-episode peak reductions with zero out runs (Table 1). San Antonio and Austin are affected mostly by mobile on-road emissions with reductions of 15.5 and 9.8 ppb as demonstrated in the 1999 episode and 21.5 and 23.4 ppb respectively for the 2002 episode. The biogenic VOC emissions have increased by nearly 100 and 133 t in San Antonio and Austin respectively in 2002. As the on-road mobile emissions in these two areas are dominated more by $NO_x$ emissions, peak concentrations also tend to be more sensitive to $NO_x$ control. It is seen from Table 1 that Corpus Christi is most affected by non-road emissions and Victoria was affected by point sources. Marine emissions in coastal Corpus Christi have reduced in 2002 (Farooqui et al., 2008) and in Victoria there was a net decline of the total anthropogenic emissions.

**Table 1.** Reduction of peak ozone concentrations (ppb)

| Urban areas | Area | | Point | | On-road | | Non-road | |
|---|---|---|---|---|---|---|---|---|
| | *99* | *02* | *99* | *02* | *99* | *02* | *99* | *02* |
| Austin | 3.4 | 3.7 | 8.3 | 7.2 | 9.8 | 23.4 | 3.5 | 3.8 |
| San Antonio | <1 | <1 | 8 | 7.9 | 15.5 | 21.5 | 6.5 | 3.2 |
| Corpus Christi | 1.5 | <1 | 1.4 | 3.3 | 1.6 | 2.5 | 17 | 3.9 |
| Victoria | 1.4 | <1 | 3.0 | 6.0 | 9.8 | 3.4 | 1.2 | <1 |

### 4.2. Impact of zero out emissions on ozone exceedances (>75 ppb)

The number of exceedances is greater in 2002 especially in Victoria and Corpus Christi indicating higher average ozone concentrations (Table 2). These two regions are neither $NO_x$ nor VOC sensitive and the model is less responsive to emission reductions in these areas in 2002 with further decrease in total $NO_x$ and VOC emissions. The uncertainty in response of modeled ozone to controls is enhanced by meteorological variability. San Antonio and Austin are more responsive to mobile emissions reductions in 2002 due to increased $NO_x$ sensitivity as explained earlier. Pattern of spatial extent of exceedances is similar. The relatively low impact area emissions have not been considered in this study.

**Table 2.** Number of ozone exceedances (>75 ppb)

| Urban areas | Base Case | | Point | | On-road | | Non-road | |
|---|---|---|---|---|---|---|---|---|
| | *99* | *02* | *99* | *02* | *99* | *02* | *99* | *02* |
| Austin | 1112 | 2019 | 870 | 1647 | 397 | 117 | 870 | 1486 |
| San Antonio | 1013 | 1708 | 620 | 1276 | 395 | 503 | 787 | 1514 |
| Corpus Christi | 325 | 1252 | 273 | 1252 | 285 | 1252 | 0 | 1252 |
| Victoria | 136 | 4585 | 101 | 4432 | 133 | 4517 | 133 | 4559 |

## 5. Summary

The preliminary results clearly depict the importance of considering multiple ozone episodes in devising effective emission control strategies. There are substantial spatial differences in the effectiveness of control strategies with San Antonio and Austin being most responsive to mobile emissions, Corpus Christi to non-road and Victoria to point sources. Biogenic VOC emissions play a crucial role in model sensitivity to controls. The study also reveals the challenge to reduce exceedances under EPA's revised standards. The non-linear response of ozone to $NO_x$-VOC chemistry coupled with meteorological variations makes it imperative that emission strategies be based on averaged response of model to multiple episodes.

**Acknowledgments** This material is based upon work supported by CREST-RESSACA at Texas A&M University – Kingsville through a Cooperative Agreement No. HRD-0734850 from the National Science Foundation.

## References

Brônnimann S, Buchmann B, Wanner H (2002) Trends in near-surface ozone concentrations in near-surface in Switzerland: the 1990s. *Atmos. Environ.* 36: 2841–2852.

Bärtsch-Ritter N, Keller J, Dommen J, Prévôt ASH (2004) Effects of various meteorological conditions and spatial emission resolutions on the ozone concentration and ROG/NOx limitationin the Milan area (I). *Atmos. Chem. Phys. Discussion*. 4: 423–438.

Emery CA, Tai E, Wilson GM, Yarwood G (2002) Report from ENVIRON International Corporation, 101 Rowland Way, Novato, CA, 94945.

Farooqui MZ (2008) Development of a comprehensive air quality modeling framework for a coastal urban airshed in South Texas. PhD Dissertation. Texas A&M University-Kingsville, Kingsville, TX 78363, USA.

Farooqui MZ, John K, Gupta AK (2010) Evaluation of the impact of marine vessels on ambient air quality in a coastal urban airshed of South Texas. *Int. J. of Environ. and Waste Management* (In Press).

## 6. Questions and Answers

**Ronald C. Cohen:** Is the observed $O_3$ decrease on weekends the same as predicted? Weekend $NO_x$ is approximately 25% lower than weekday $NO_x$, therefore observations can provide a direct comparison.

**Answer:** The observed ozone data shows a 2–26% decrease during weekend days at the monitoring sites possibly due to a decrease in the $NO_x$ emissions. The model also captured this similar trend of decrease in ozone from weekday to weekend. The total modeled $NO_x$ showed a net decrease of less than 10% during weekend days in the near non-attainment areas of Texas during the high ozone episode in September 2002. This is also borne out by our findings that most of the region is $NO_x$ limited. However for the high ozone episode of 1999 there is no discernible trend between weekday and weekend ozone concentrations even though the $NO_x$ emissions reveal a decrease from weekday to weekend. This demonstrates the importance of meteorology and regional transport for the 1999 ozone episode. This study thus reemphasizes the importance of considering multiple episodes to develop effective emission control strategies.

# 2.20 Background Ozone in Regional-Scale Modelling over North America

**A. Chtcherbakov[1], R. Bloxam[1], N. Reid[2], and Y. Hall[1]**

[1]Ontario Ministry of the Environment, Toronto, Canada

[2]Smeraldo Environmental, Toronto, Canada

**Abstract** This study estimates background ozone concentrations over Eastern North America for the year 2005 based on analysis of CMAQ (the Community Multiscale Air Quality model) simulations with all anthropogenic emissions set to zero.

Influences of inflow boundary conditions, land use characteristics, meteorological conditions, and dry deposition on the background ozone concentrations were analyzed. The spatial distributions and temporal peculiarities of ozone background concentrations were examined with statistical analysis applied and results presented.

**Keywords** Ozone, background concentrations, CMAQ simulations

Background ozone may form a significant part of the daily 8 h maximum ozone concentrations. This can be extremely important, since the background concentration is the level below which concentrations can not be reduced by local/regional efforts alone.

It is essential how the background ozone concentration is defined. In this study we consider background ozone as concentration of ozone advected into the modelling domain as a result of anthropogenic and biogenic emissions anywhere outside the domain (including stratospheric ozone intrusions) plus ozone generated from emissions from natural, biogenic sources only, excluding anthropogenic sources inside the domain.

To estimate the impacts of background ozone, CMAQ v4.6 (the Community Multiscale Air Quality Model) was run for the May–September 2005 period with all anthropogenic emissions set to zero over the domain which covers Eastern North America (Fig. 1) Meteorological data to run CMAQ was obtained from WRF v 2.2 (Weather Research and Forecast model) runs.

In this run the southern and western boundaries of the domain (usually inflow) have ozone concentrations of 35 ppb near the surface increasing to 40, 45, 50, 60 and 70 ppb in five layers to the model top (100 mbars). The eastern and northern boundaries (frequently outflow) have 30 ppb in the lowest layer. These values are based on average observed ozone profiles.

D.G. Steyn and S.T. Rao (eds.), *Air Pollution Modeling and Its Application XX*,
DOI 10.1007/978-90-481-3812-8, © Springer Science + Business Media B.V. 2010

Figure 1 shows the average modelled 8 h maximum background ozone concentrations across the model domain. Near the boundaries the ground level ozone concentrations are high because they have not had time to adjust to the balance between vertical mixing and dry deposition processes which affect the impacts in the inner part of the model domain. The 5 month average background 8 h maxima are in the 30–34 ppb range in the inner portion of the model domain. Note that over large water bodies (such as the Great Lakes) higher background concentrations are modelled likely because the dry deposition rates are lower over water.

Meteorology can have significant impacts on background concentrations due to the balance between mixing higher concentrations to ground level and dry deposition of ozone under different weather conditions. As an example Fig. 2 shows the frequency distribution of the background 8 h ozone maxima concentration for South Western Ontario, Canada (sub region #5 shown in Fig. 1). It is a skewed distribution with the most frequently occurring maxima almost 3 ppb higher than the average value. The skewed distribution suggests that reducing concentrations at ground level by dry deposition more frequently dominates over miing higher concentrations to ground level. Table 1 summarizes the average and the distributions of the background concentrations for nine sub-domains shown in Fig. 1. The modelled highest concentrations and the standard deviations were similar in all sub-domains (Fig. 2).

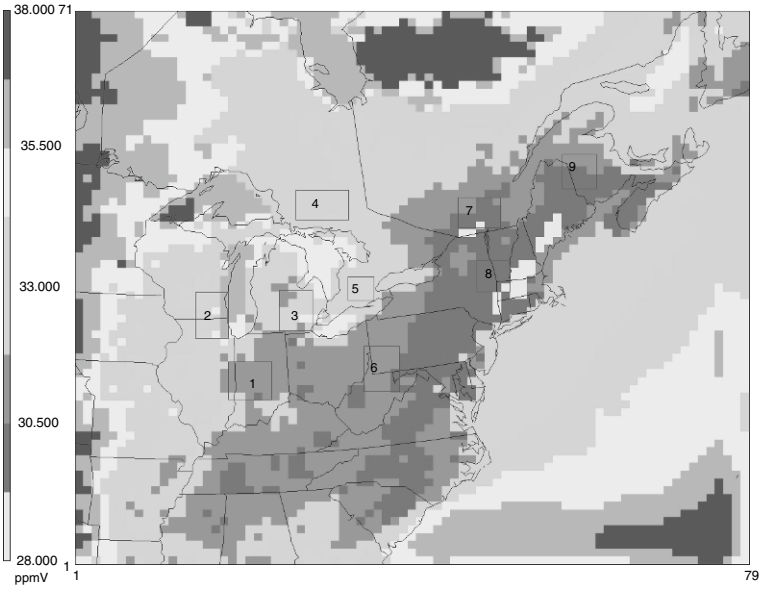


**Fig. 1.** Averaged background ozone concentration (ppb) for May–September 2005 and sub-domains' location

An additional analysis of background ozone concentrations was performed on selected days when the 8 h ozone concentrations, with anthropogenic emissions included, exceeded 70 ppb. Table 1 shows lower contributions from background ozone by typically 1–3 ppb. This could be caused by more dry deposition with slow moving high pressure systems that are typical during high ozone episodes.

**Table 1.** Background ozone concentration (ppb), May–September 2005

| Subdomain | Average | Max | Min | Standard deviation | Averaged on high concentration days |
|---|---|---|---|---|---|
| 1 | 31.2 | 44.0 | 21.1 | 4.4 | 30.0 |
| 2 | 34.0 | 43.9 | 23.1 | 4.2 | 32.7 |
| 3 | 32.3 | 43.2 | 19.3 | 4.2 | 29.5 |
| 4 | 33.1 | 46.0 | 21.9 | 4.3 | 32.4 |
| 5 | 32.4 | 42.8 | 16.8 | 4.6 | 29.9 |
| 6 | 30.8 | 43.3 | 16.5 | 4.4 | 28.4 |
| 7 | 30.3 | 45.3 | 18.2 | 4.3 | 27.7 |
| 8 | 29.6 | 44.7 | 18.7 | 4.6 | 25.1 |
| 9 | 30.4 | 44.3 | 18.5 | 4.1 | 23.7 |

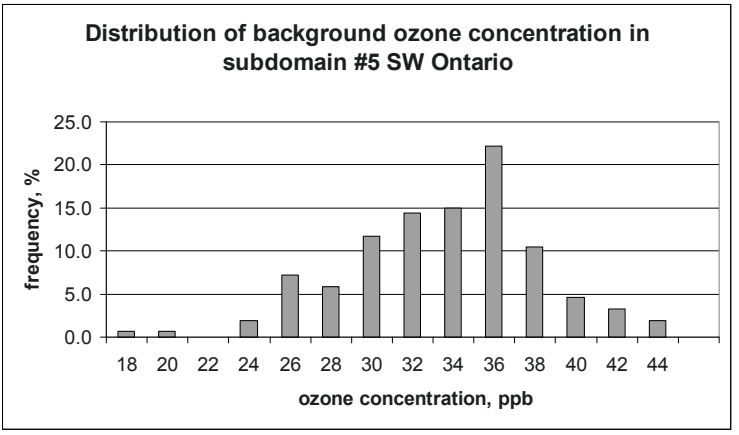


**Fig. 2.** Frequency distribution of background ozone concentration in South-Western Ontario for ozone season May–September 2005

# 2.21 Influence of Biogenic Emission Estimates on Ozone and PM10

**Andreas Kerschbaumer[1] and Peter J.H. Builtjes[1,2]**

[1]Institut für Meteorologie, FU-Berlin, Germany

[2]TNO, Utrecht, The Netherlands

**Abstract** In this study we report results of REM_Calgrid (RCG) runs with two different tree inventories over Europe. Both inventories are based on Corine-Landcover information, the first comprising only 3 surrogate forest types and the second specifying 126 individual tree species. Biogenic VOC and NO emissions were estimated and the model was tested for a summer 10 days period in 2005. Biggest differences in biogenic emissions were found in Northern Europe, Spain and the Alps. A significant improvement was achieved in Ozone simulations when biogenic emissions were derived from the comprehensive forest database. Also, secondary organic aerosol (SOA) production rate is enhanced especially in Scandinavia, Northern Russia and the Alps, giving more realistic SOA-contributions to the total PM10 concentrations.

**Keywords** SOA, RCG, aerosols, tree inventories, biogenic emissions

## 1. Introduction

Ozone and atmospheric aerosols (PM10) are known to have adverse health effects. While the formation of ozone and of secondary inorganic aerosols (SIA) is well understood, and thus modelled with satisfactory accuracy, there is still a lack of knowledge about secondary organic aerosols (SOA). Even the relative importance of secondary organic compounds in the total PM10 mass is not clear. It is generally accepted that biogenic emissions play an important role not only in the formation of ozone but also of SOA. The estimate of biogenic VOC including terpenes and isoprenes, and NOx, is still a challenging task and depends deeply on the availability of an accurate description of the land. Furthermore, geographical position, light availability and physiological situation of the plants may change enormously these factors. The Chemistry Transport Model REM_Calgrid (RCG) has been used to analyse the influence of different land-use-databases with differing quantities of information on O3 and SOA. The first database comprises 13 different land-use-classes, the second one is a detailed forest inventory with

D.G. Steyn and S.T. Rao (eds.), *Air Pollution Modeling and Its Application XX*,
DOI 10.1007/978-90-481-3812-8, © Springer Science + Business Media B.V. 2010

126 geo-referenced tree species over the most part of Europe. Chemistry transport models also allow to trace-back the origin of simulated secondary species by analysing the chemical production terms individually for relevant precursors. This has been done choosing a control volume for which simulated production terms have been examined.

## 2. Methods

The biogenic emissions have been estimated following the methods proposed by Simpson et al. (1999). The original land use dataset is based on CORINE-land-use-data – modified by Smiatek (1998). Only three forest classes were available: deciduous, coniferous and mixed forest. Emissions were estimated based on the biomass associated to six statistically distributed surrogate tree-species. A second land-use database has been constructed implementing information about tree-species from Köble et al. (2001) in the original land-use-database. They developed a tree species map mainly combining the site inventory information on 126 tree species from ICP Forests, CORINE land cover, satellite and statistical data for the EU. The Chemistry Transport Model REM_Calgrid (RCG) (Beekmann et al., 2007 and references therein) has been used for simulating $O_3$ and PM10. Secondary aerosols are divided into fine inorganic and organic aerosols. Organic particles are subdivided into aerosols stemming from biogenic and anthropogenic precursors. Production of secondary organic aerosol (SOA) from anthropogenic and biogenic VOC is treated with the SORGAM module. Simulations started on 20 July 2005 at 00:00 UTC and ended on 30 July 2005 at 00:00 UTC. Meteorological data were calculated based on observations. Anthropogenic emissions were based on EMEP information and spatially disaggregated by TNO.

## 3. Results and Discussion

The biggest differences in the biogenic precursor emissions were found in Scandinavia and over the North-Western Russian Area, in Spain and over the Alps. RCG was not able to capture ozone maxima over Spain. RCG-simulation with biogenic emissions derived from detailed tree information improved considerably. Especially in Spain, Italy and also between the Netherlands and the Ruhr-Area in Germany, up to 15% higher ozone values are modeled, when biogenic emissions were based on the detailed forest data-base.

Figure 1 shows the absolute values of the secondary organic aerosols simulated with RCG for the considered time-period. Biogenic emission estimates were based on land-use data without (Fig. 1a) and with (Fig. 1b) detailed tree information. While both integrations show spatially highest secondary organic aerosols over

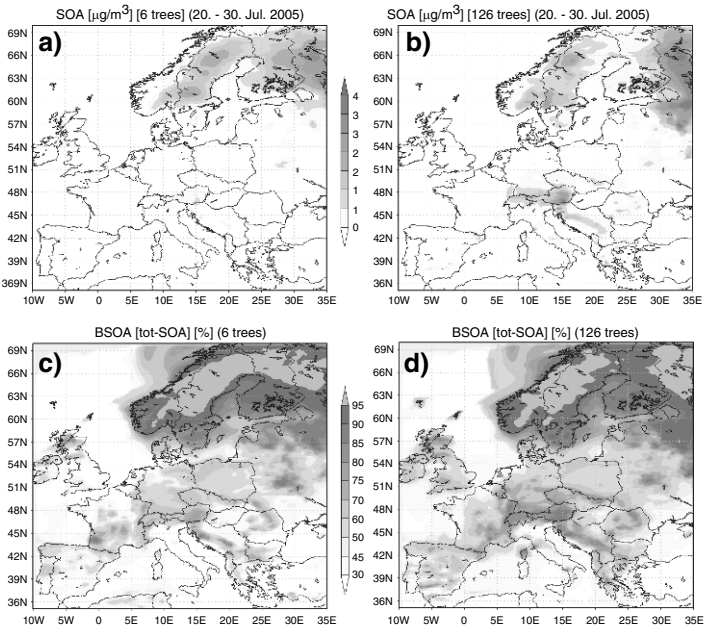


**Fig. 1.** Secondary organic aerosols. Average values over time-period from 20 to 30 July 2005 without (a) and with (b) detailed tree information in µg/m³. Biogenic to total secondary organic aerosol ratio expressed in percentages without (c) and with (d) detailed tree information

Sweden, Finland and North-Western-Russia, RCG with detailed tree information simulates considerably higher values of SOA over Austria (ca. 2 µg/m³), Balkans (ca. 1.5 µg/m³), Spain and Italy (up to 1 µg/m³) than without the detailed tree inventory. This becomes even more evident if the only biogenic part of the total secondary organic aerosol, with terpenes as gaseous precursors, is considered (Fig. 1c, d). Over 70% of total SOA concentrations stem from biogenic terpene emissions over Scandinavia, Russia, Switzerland, Austria, Balkans and Southern France, when only surrogate tree information is used. This percentage becomes considerably higher when detailed tree information is used, especially over Spain, the Alps and Corsica. During hot summer days RCG simulations with detailed biogenic emissions give higher ozone and secondary organic aerosol values than with emission estimates based only on aggregated forest information. Especially in Southern and Central Europe Secondary organic aerosols with origin in biogenic emissions may be determinant in reaching dangerous levels of ozone as well as of PM10.

Figure 2a shows the contribution to the total Ozone concentration of the RCG CBIV-Chemistry Module over a chosen domain in central Spain. Especially on 21 and 22 July 2005 RCG with the detailed biogenic emission estimates gives almost double ozone-production values than RCG with biogenic emissions derived from the aggregated forest information. Comparisons with observations show that this higher contribution to the overall $O_3$ concentration brings RCG with 126 tree species

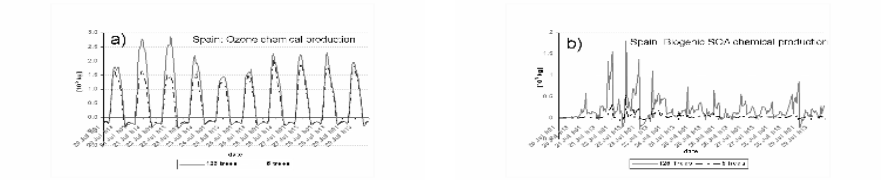


**Fig. 2.** Ozone (a) and SOA (b) Production (positive) and Destruction (negative) due to gas-phase chemistry simulated with RCG for a 120 × 120 km (area) × 3 km (height) chosen volume over central Spain. Units are $10^5$ kg; gray continuous line: detailed forest inventory; black dashed line: surrogate trees

to simulate the actual air pollution situation much better than with only the 6 surrogate tree species. During the rest of the period, the differences in the chemistry due to different amount of forest information is negligible because terpene emissions become less for lower temperatures and overcast sky. Figure 2b shows the hourly production of biogenic secondary organic carbons, simulated with RCG, with biogenic emissions estimated with a detailed tree data-base (gray continuous line) and with the six surrogate tree species data-base. The production rate in the considered period over the control volume in Spain is factor 3 higher when considering all available tree information. RCG with surrogate tree species is much less reactive and thus gives much less secondary organic aerosol production than with the full 126 tree data-set. The introduction of higher amounts of terpene, isoprene and thus in general of more volatile organic carbons into the model system not only produces more ozone and secondary organic aerosol concentrations, but it makes the whole chemistry more reactive. This influences also the production of inorganic secondary aerosols, for instance. The more detailed tree species database emission estimate is responsible for approximately 20% higher nitrate concentrations over the Milan metropolitan area and over the London-the Netherlands-German Ruhr belt for the considered period.

## 4. Conclusion

The comparison between simulations and observations of ozone in southern Europe has shown a better agreement when biogenic emissions are derived from a comprehensive forest database. This suggests that RCG describes the oxidation processes better. The model prediction of biogenic secondary organic aerosols especially over Northern Europe over the Alps and Balkans gives some 2 μg/m³ higher concentrations with all available tree information than with 6 surrogate tree information. Especially in these regions the contribution of biogenic secondary organic aerosols with biogenic VOC as direct precursors is more the 70%. It could be shown that the chemistry production process simulation in RCG is enhanced when all tree information is used. This holds for Ozone, and it could be proved

that this augmented chemistry production led to a better simulation of total ozone concentrations, especially in clear-sky and hot days. The production of secondary organic aerosols is determined by the biogenic precursors. Again, the chemical production is enhanced when more detailed tree information is used.

## References

Beekmann, M., A. Kerschbaumer, E. Reimer, R. Stern, and D. Möller (2007), PM measurement campaign HOVERT in the Greater Berlin area: model evaluation with chemically specified particulate matter observations for a one year period, Atmos. Chem. Phys., 7, 55–68.

Köble, R., and G. Seufert (2001), Novel maps for forest tree species in Europe, Proceedings of the 8th European Symposium on the Physico-Chemical Behaviour of Air Pollution: "A Changing Atmosphere!", Torino (IT), 17–20 September.

Simpson, D., W. Winiwarter, G. Börjesson, S. Cinderby, A. Ferreiro, A. Guenther, C. N. Hewitt, R. Janson, M. A. K. Khalil, S. Owen, T. E. Pierce, H. Puxbaum, M. Shearer, U. Skiba, R. Steinbrecher, L. Tarrason, and M. G. Öquist (1999), Inventorying emissions from nature in Europe, J. Geophys. Res., 104 (D7), 8113–8152.

Smiatek, G. (1998), Mapping land-use for modelling biogenic and anthropogenic emissions, Proceedings of the EUROTRAC2-Sypmosium, Garmisch-Partenkirchen.

## 5. Questions and Answers

**S. Andreani-Aksoyoglu:** What pathways are included in SOA mechanism? How does resolution (30 km in model, 2 km in land-use) affect the results?

**Answer:** SOA-simulation is base on SORGAM-module developed by B. Schell et al. and described in detail in Schell, B., Ackermann, I. J., Hass, H., Binkowski, F., and Ebel, A.: Modelling the formation of secondary organic aerosol within a comprehensive air quality model system, J. Geophys. Res., 106(D22), 28 275–28 293, 2001. SOA formation is done from the oxidation of alkanes, alkenes, cresol, aromatics and monoterpenes. All high-resolved information (2 km forest-associated biogenic VOC, for example) is maintained via percentages in the coarse resolution. So, virtually there is no information loss due to resolution.

**R. Vautard:** How does your inventory compare with emissions coming from the NATAIR – EU-project?

**Answer:** The uncertainty in the NATAIR-project is estimated to be between –100% and +200% for biogenic VOC emissions, thus our emission inventory based on different amount of tree information in Europe is within this uncertainty.

# 2.22 Air Quality Models Sensitivity to On-Road Traffic Speed Representation: Effects on Air Quality of 80 km $h^{-1}$ Speed Limit in the Barcelona Metropolitan Area

**José M. Baldasano[1,2], Pedro Jiménez-Guerrero[2], Eugeni López[2], María Gonçalves[1], and Albert Soret[2]**

[1]Environmental Modelling Laboratory, Technical University of Catalonia. Avda. Diagonal 647, Edificio H, Oficina 10.23, 08028 Barcelona, Spain

[2]Barcelona Supercomputing Center – Centro Nacional de Supercomputación (BSC-CNS). Earth Sciences Department. Jordi Girona 29, Edificio Nexus II, 08034 Barcelona, Spain

**Abstract** This work explores the changes in urban air quality caused by the introduction of a maximum speed limit to 80 km $h^{-1}$ on motorways in the Barcelona Metropolitan Area. The tool used is the WRF-ARW/HERMES/CMAQ modelling system. Simulations take into account the entire year 2008 versus the traffic conditions for the year 2007. This speed limitation has been implemented in the HERMES emissions model, which considers hourly variable speeds and hourly traffic intensity in the affected area, taken from measurement campaigns for the aforementioned years; it also permits to take into account the traffic congestion effect. Overall, for the whole metropolitan area, the emissions are reduced up to 4%; however the local effects of this reduction achieve an important impact for specific points of the domain under study, reaching 11%. In this sense, the speed limitation effects assessed represent improvements in air quality levels (5–7%) of primary pollutants over the area affected. Hence, limiting the circulation speed to 80 km $h^{-1}$ has been proved as a feasible traffic management strategy for air quality improvement in urban areas.

## 1. Introduction

Improving air quality in urban areas is nowadays an important environmental challenge (Baldasano et al., 2003). The public administrations are testing management strategies mainly addressed to reduce on road traffic emissions, because this sector is the largest contributor to anthropogenic pollutants emissions in the urban environments (Colvile et al., 2001; Querol et al., 2001; Ghose et al., 2004; Nagl et al., 2006). A way of reducing traffic emissions consists in changing the speed circulation patterns. The speed dependency of emissions varies as a function of the pollutant, depending on the vehicle age, weight and cubic capacity of the engine.

D.G. Steyn and S.T. Rao (eds.), *Air Pollution Modeling and Its Application XX*,
DOI 10.1007/978-90-481-3812-8, © Springer Science + Business Media B.V. 2010

Therefore a unique optimal speed circulation for atmospheric pollutants for the whole range of vehicles in an urban vehicles fleet does not exist. Nevertheless, it is a widely adopted traffic management strategy, because its benefits concern not only pollutants emissions, but also reduces congestion, noise and traffic accidents. In addition, the evaluation of air quality management strategies requires the use of air quality models to perform quantitative impact studies (Ponche and Vinuesa, 2005) and emission data (Baldasano et al., 2008).

This work explores the changes in urban air quality by using the WRF-ARW/HERMES/CMAQ modelling system, introducing a maximum speed limit to 80 km $h^{-1}$ in the access motorways of the Barcelona Metropolitan Area, which is planned by the regional administration to improve the air quality conditions. Simulations take into account the entire year 2008.

## 2. Methods

The Weather Research and Forecasting (WRF) model (Michalakes et al., 2005) provides the meteorology parameters as inputs to the Models-3 Community Multiscale Air Quality (CMAQ) model (Byun and Schere, 2006). The High Elective Resolution Emission Modeling System (HERMES) has been developed specifically for Spain with a high resolution (1 $km^2$ – 1 h) (Baldasano et al., 2008). The traffic emissions module of HERMES considers fundamentally a bottom-up approach and takes into account 72 diesel and petrol vehicles categories (including Euro II and Euro III emission standards) according to COPERT III-EEA-EMEP/CORINAIR methodology; divided by fuel type, vehicle weight, age of the vehicle and cubic capacity; each of them with its specific emissions factors, defined as a function of the circulation speed. The emissions account in HERMES traffic module considers hot exhaust, cold exhaust and evaporative emissions. It also estimates particulate matter produced by brakes abrasion, tire wear and pavement erosion. The vehicular fleet is defined for Spain and specifically for Barcelona in this case of study using data provided by DGT (2004), and distributed in the 72 aforementioned categories. The model includes the definition of the road network, dividing it in stretches (inside the 1 $km^2$ cells) with specific temporary disaggregating profiles (distinguishing day-type: weekday-holiday, and month), specific average speed, daily average traffic (number of vehicles per day), stretch length, route type (highway, road or urban) and circulation zones. For the implementation of the 80 km $h^{-1}$ limit, data coming from 125 measurement points have been assimilated within HERMES; these points are located in the access roads to the city of Barcelona and contain hourly detailed information of average circulation speed and hourly traffic intensity.

The WRF-ARW/HERMES/CMAQ was applied to the final study area with high spatial (1 $km^2$) and temporal (1 h) resolution (Fig. 1). Four one-way nested domains were defined for the simulations, centering the final domain in Barcelona (Fig. 1), which covers the north-eastern Iberian Peninsula (148 × 148 $km^2$), to

assess not only the effects in the urban area, but also to detect the urban plume behavior in downwind areas. The availability of the MareNostrum supercomputer hold in the BSC-CNS, together with the advances in the parallelization of air quality model codes, has allowed the high-resolution simulations.

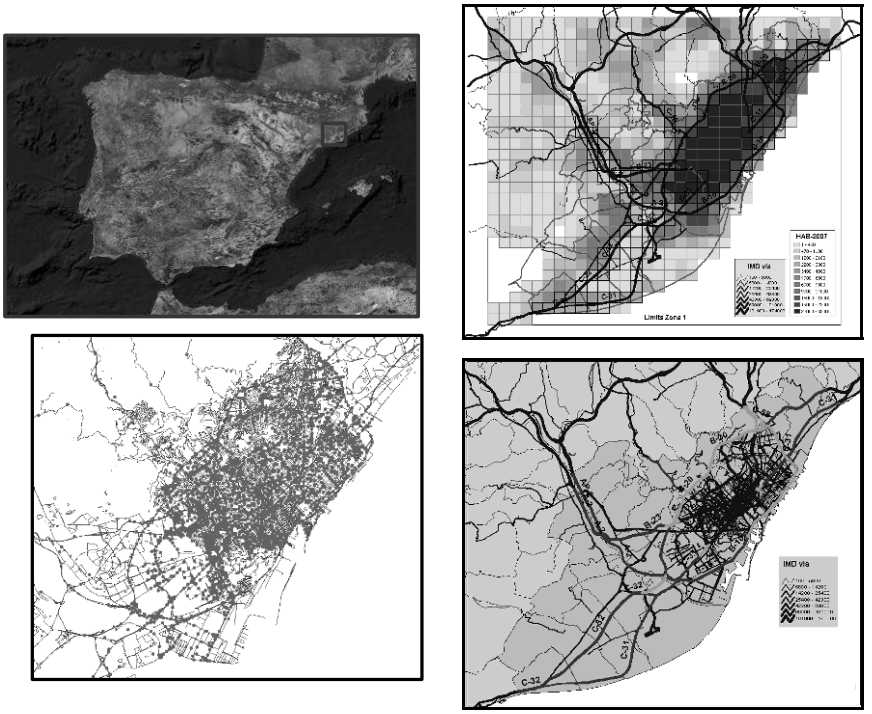


**Fig. 1.** (Left-up) Location of the domain of study; (right-up) population density in the areas affected by the 80 km $h^{-1}$ limit; (left-down) points with daily average traffic information in the city of Barcelona; (right-down) roads limited to 80 km $h^{-1}$ (red), roads with speed under 80 km $h^{-1}$ before the implementation of the limit (green) and not-affected roads (blue)

## 3. Results and Discussion

The measure of speed limitation (80 km $h^{-1}$) is applied to the access roads of the Barcelona Metropolitan Area (Fig. 1), formed by Barcelona and other 15 municipalities, with high levels of $NO_x$ and PM10 emissions (Costa and Baldasano, 1996; Baldasano et al., 2008). The maximum speed allowed in these roads was 100 km $h^{-1}$ (in 63.2% of affected stretches) and 120 km $h^{-1}$ in 20.4% of the considered stretches. The population directly affected by the measure (that is, city dwellers adjacent to the roads where the limit of 80 km $h^{-1}$ is implemented) is 1.35 million inhabitants, but 3.29 million dwellers are potentially benefited from the limitation of speed (Fig. 1). The measure involves the average reduction of speed

in the indicated roads from 92 to 78 km $h^{-1}$, that is, a difference of 14 km $h^{-1}$. On the contrary, the intensity of traffic has been similar for both years analysed (47,859 daily average traffic –DAT- during January–August 2007 and 47,606 DAT in the period January–August 2008). For September–November there is a decrease in DAT of 5.9% (49,795 vs. 46,883 DAT for the years 2007 and 2008, respectively). Therefore it should be highlighted that the differences in emissions and air quality are caused by the limitation of the speed and not because of modifications in the intensity of traffic. However, several monthly differences in the DAT are depicted (both increases and decreases) caused by the temporal variation of holidays (Eastern, summer holidays, etc.) and their corresponding special traffic patterns. The limitation of the speed together with the reduction in the congestion lead to a diminution in the fuel consumption. The fuel consumption is reduced in 40.8 t $day^{-1}$ for gasoline and 46.6 t $day^{-1}$ for diesel; that is, an annual reduction of 4% in the Barcelona Metropolitan Area (over 30,000 t of fuel/year). Since the $CO_2$ emissions are directly proportional to the fuel consumption, the reduction in the emission of this greenhouse gas is also around 4% (over 94,000 t/year). The variation in the fuel consumption leads to a reduction in the emissions of primary pollutants in the whole metropolitan area around 4% for $NO_x$, PM2.5, PM10, $SO_2$ and CO. As an example, for the nitrogen oxides, the emissions diminish in 1.85 t $day^{-1}$ (4.36%). For the particulate matter (PM10) emissions are reduced in 0.13 t $day^{-1}$ (3.95%). The main reductions of emissions are achieved over the access roads to the city of Barcelona. If we consider just the areas with control of the circulation speed to 80 km $h^{-1}$, the fuel consumption reduces about 10.4%. This also affects the emissions, which are reduced in a 14.81% for CO, 10.98% for nitrogen oxides, 12.47% for PM2.5 and 10.99% for PM10.

Regarding air quality implications, the speed limitation involves a reduction in ground levels of atmospheric pollutants in the whole area where the measure is implemented. Specifically, the improvement of air quality is especially effective in the areas close to the access roads. In this sense, several domains have been defined according to the name of the road where they have been implemented: inside the Barcelona city ring roads (IRR), A2-C32, AP2, C31 and C32 (Fig. 2). The measure takes importance in the domains A2-C32, AP2, C31 and C32 where the levels of $NO_x$ are reduced 5–8% on average. For the particulate matter the reduction is around 3%, with reductions for several days over 10–15%. Improvements for sulphur dioxide are lower (around 1%). The $NO_x$ emissions decrease in a VOCs limited area, such as the Barcelona city, and it produces local increases of $O_3$ concentrations, especially in the urban plume over the roads affected by the speed limit (up to 1–2%); nevertheless the $O_3$ concentrations in downwind areas remain practically constant. It is also noticeably how air quality is also improved in areas far from those roads where the speed limitation has not come into effect (IRR); here the air quality improvements are around 1%.

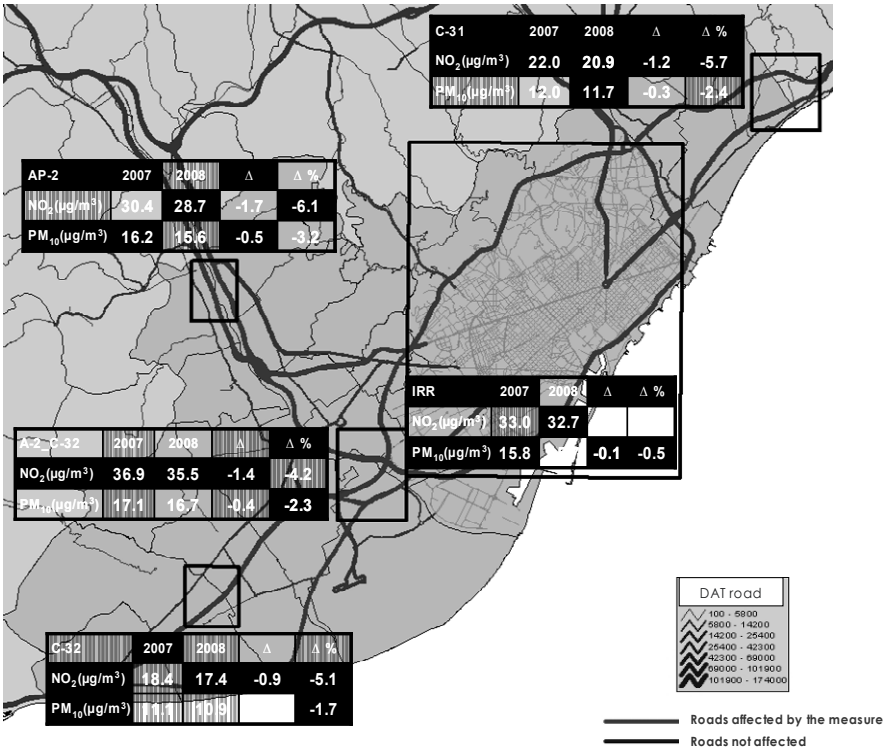


**Fig. 2.** Summary of the impacts on air quality ($NO_2$ and PM10) of the speed limitation measure for different areas of study within the Barcelona Metropolitan Area (in red, roads affected by the measure)

## 4. Conclusions

The WRF-ARW/HERMES/CMAQ modeling system was applied to assess the effects on air quality of the 80 km $h^{-1}$ speed restriction for the Barcelona Metropolitan area. The analysis of real circulation patterns shows that the changes in emissions estimates range from 4% to 11% depending on the area studied. Consequently, the effects on air quality predicted should focus in the Barcelona area, mainly over the affected roads, where the reductions on primary pollutants reach up to 5–8% on 24-h average concentration. The $NO_x$ emissions decrease in a VOCs limited area, such as Barcelona, produces local increases of $O_3$ concentrations, especially in the urban plume over the roads affected by the speed limit (lower than 1% in most cases); nevertheless the $O_3$ concentrations in downwind areas remain practically constant. The most positive effects of the management measure is observed for CO, $NO_x$ and PM2.5, with daily improvements in air quality reaching 10–15%. This work shows the importance of introducing speed limit scenarios in urban areas together with the necessity of using hourly traffic

data in emission model; they both strongly condition the changes in the air quality model predictions.

**Acknowledgments** The authors gratefully acknowledge Dr. Oriol Jorba for the meteorological information provided. This work was funded by Environmental Department of the Catalonia Government and CALIOPE project 157/PC08/3-12.0 of the Spanish Ministry of the Environment. Simulations were carried out in the MareNostrum supercomputer of the Barcelona Supercomputing Center – Centro Nacional de Supercomputación.

## References

Baldasano, J.M., Valera, E., Jiménez, P. (2003). Air quality data from large cities. The Science of the Total Environment 307, 141–165.

Baldasano, J.M., Güereca, P., López, E., Gassó, S., Jiménez-Guerrero, P. (2008). Development of a high resolution (1 km x 1 km, 1 h) emission model for Spain: the High-Elective Resolution Modelling Emission System (HERMES). Atmospheric Environment 42, 7215–7233.

Byun, D.W., Schere, K.L. (2006). Review of the governing equations, computational algorithms and other components of the Models-3 Community Multiscale Air Quality (CMAQ) Modeling System, Applied Mechanics Reviews 59(2), 51–77.

Carslaw, D., Beevers, S.D. (2005). Development of an urban inventory for road transport emissions of NO and comparison with estimates derived from ambient measurements. Atmospheric Environment 39, 2049–2059.

Colvile, R.N., Hutchinson, E.J., Mindell, J.S., Warren, R.F. (2001). The transport sector as a source of air pollution. Atmospheric Environment 35, 1537–1565.

Costa, M., Baldasano, J.M. (1996). Development of a source emission model for atmospheric pollutants in the Barcelona area. Atmospheric Environment, 30A, 2, 309–318.

DGT (2004). Spanish Department of Transportation, Statistical data in the number of vehicles and fuel used for the year 2004. http://www.dgt.es/portal/ (January, 2008)

Ghose, M.K., Paul, R., Banerjee, S.K. (2004). Assessment of the impacts of vehicular emissions on urban air quality and its management in Indian context: the case of Kolkata (Calcutta). Environmental Science & Policy 7, 345–351.

Michalakes, J., Dudhia, J., Gill, D., Henderson, T., Klemp, J., Skamarock, W., Wang, W. (2005). The Weather Research and Forecasting Model: Software architecture and performance, Proceedings of the Eleventh ECMWF Workshop on the Use of High Performance Computing in Meteorology, Zwiefhofer, W. and Mozdzynski, G. (Eds.), World Scientific, 156–168.

Nagl, C., Mossmann, L., Schneider, J. (2006). Assessment of plans and programmes reported under 1996/62/EC – Final Report. Report REP-0079. Viena, December 2006. European Commission. 139 pp. (http://ec.europa.eu/environment/air/ambient.htm, May, 2008)

Ponche, J.L., Vinuesa, J.F. (2005). Emission scenarios for air quality management and applications at local and regional scales including the effects of the future European emission regulation (2015) for the upper Rhine valley. Atmospheric Chemistry and Physics 5, 999–1014.

Querol, X., Alastuey, A., Rodríguez, S., Plana, F., Ruiz, C.R., Cots, N., Massague, G., Puig, O. (2001). PM10 and PM2.5 source apportionment in the Barcelona Metropolitan area, Catalonia, Spain. Atmospheric Environment 35, 6407–6419.

## 5. Questions and Answers

**Question:** The European limit value is expressed in terms of nitrogen dioxide. Increases in the regional concentration of ozone could therefore offset any reductions in the emissions of $NO_x$ (primarily NO) from road vehicles (Bernard Fisher).

**Answer:** The effects of the 80 km $h^{-1}$ speed limit are very local and conditioned by the specific location of the measure; our evaluation of the increase in ozone is only ranging between 1 and 2 $\mu g\ m^{-3}$.

**Question:** How significant is the reduction in PM10, which is approximately 2–4%, with respect to the accuracy of PM10 measurement? (Pavel Kishcha)

**Answer:** The reduction of PM10 is 4% for the whole Barcelona Metropolitan Area, but close to the highways is 10%, and this is the representative value. Also, according to the evaluation of the modelling system for PM10 in this area, as shown, the agreement with the measures from the air quality network is highly correlated.

# 2.23 Influence of Chlorine Emissions on Ozone Levels in the Troposphere

**Golam Sarwar[1], Ravi Joseph[2], and Rohit Mathur[1]**

[1]United States Environmental Protection Agency

[2]Austin Energy, Austin, TX, USA

**Abstract** Chlorine emissions from cooling towers are emitted mainly as hypochlorous acid, not as molecular chlorine. Chlorine emissions from cooling towers in electric utilities in the U.S. are estimated to be 4,400 t/year. On a molar basis, molecular chlorine results in a greater increase in tropospheric ozone than hypochlorous acid. However, hypochlorous acid produces more ozone than molecular chlorine when an equal amount of chlorine is present on a mass basis.

**Keywords** Emissions, molecular chlorine, hypochlorus acid, chlorine chemistry, ozone

## 1. Introduction

Recent studies suggest that chlorine chemistry can increase ozone ($O_3$) in the troposphere in some areas of the U.S. (Chang et al., 2002; Knipping and Dabdub, 2003; Chang and Allen, 2006; Sarwar and Bhave, 2007). While these studies suggest that chlorine may affect $O_3$ concentrations in the troposphere, information about chlorine emissions is sparse. Molecular chlorine ($Cl_2$) is a hazardous air pollutant; thus, the National Emissions Inventory (NEI) for hazardous air pollutants includes estimates of anthropogenic $Cl_2$ emissions in the U.S. However, both $Cl_2$ and hypochlorous acid (HOCl) can undergo photolysis to produce chlorine radical (Cl) which can enhance chemical production of $O_3$. Thus, emissions inventories for air quality study need to include estimates of both $Cl_2$ and HOCl emissions. This study develops an estimate of chlorine emissions from cooling towers in electric utilities and evaluates the relative impact of $Cl_2$ and HOCl on tropospheric $O_3$ formation.

D.G. Steyn and S.T. Rao (eds.), *Air Pollution Modeling and Its Application XX*,
DOI 10.1007/978-90-481-3812-8, © Springer Science + Business Media B.V. 2010

## 2. Method

Chlorine is used as a biocide to control the growth of microorganism in cooling water. When $Cl_2$ is added to cooling tower, following reactions can occur in water:

$$Cl_2 + H_2O \leftrightarrow HOCl + H^+ + Cl^- \quad (1)$$

$$HOCl \leftrightarrow H^+ + OCl^- \quad (2)$$

$$NH_3 + H_2O \rightarrow NH_4^+ + OH^- \quad (3)$$

$$HOCl + NH_3 \rightarrow NH_2Cl + H_2O \quad (4)$$

$$H_2O \rightarrow H^+ + OH^- \quad (5)$$

where, $NH_3$ is ammonia, $H_2O$ is water, and $NH_2Cl$ is monochloramine ($H^+$, $Cl^-$, $NH_4^+$, and $OCl^-$ are ions). Concentrations of these species are dependent on pH and temperature. Other competing reactions such as formation of other chloramines and reactions with metals, hydrogen sulfide were not accounted for in this study. In order to calculate the concentration of various chlorine species in water, mass balance based on the equilibrium constants was solved. Calculated distribution of chlorine compounds in water is shown in Table 1. Cooling towers are operated at a pH of 7.0 and greater. At such conditions, the amount of $Cl_2$ in water is negligible. The fraction of HOCl depends on pH. Thus, chlorine emissions from cooling tower can be emitted in the form of HOCl, not as $Cl_2$ and only a fraction of chlorine that is added to water is available for striping into the atmosphere.

**Table 1.** Percent distribution of chlorine compounds (as Cl) in cooling water

| pH | $Cl^-$ | $Cl_2$ | $NH_2Cl$ | HOCl | $OCl^-$ |
|---|---|---|---|---|---|
| 7.0 | 50.0 | Negligible | 0.1 | 38.7 | 11.2 |
| 7.5 | 50.0 | Negligible | 0.5 | 25.9 | 23.7 |
| 8.0 | 50.0 | Negligible | 1.4 | 12.5 | 36.2 |

Holzworth et al. (1984a) conducted experiments at a refinery cooling tower with a circulation rate of 60,000 gal/min that used 184,000 gm of $Cl_2$ per day. HOCl emissions for this cooling tower are estimated as follows:

$$\text{HOCl emissions (gm/day)} = 1.48 * TCl_2 * P_{HOCl} * F/100$$

The factor of 1.48 is the ratio of the molecular weight of HOCl to Cl, $TCl_2$ is the total $Cl_2$ added to the cooling tower (gm/day), $P_{HOCl}$ is the percent of total chlorine present as HOCl in water (%), and F is the flash-off factor for HOCl (-).

While the average pH of water at this cooling tower was 8.2, other cooling towers can be operated at lower or higher pH. For this study, a pH of 7.5 is used to estimate emissions. At this pH, only 25.9% of the total chlorine is present as HOCl in water. Flash-off factor determines the fraction of chlorine that can be stripped from the cooling tower into the atmosphere. Holzwarth et al. (1984b) determined flash-off factors for HOCl in laboratory. The highest flash-off factor was 0.1 which is used in this study to estimate the maximum possible emissions. Using these values, estimated HOCl emissions from this cooling tower are about

7,000 gm/day. Chlorine emissions of cooling towers in electric utilities are estimated by multiplying this value to the ratios of water circulating rates. Cooling tower data for electric utility were obtained from the Environmental Directory of U.S. Power Plants (Bergesen and Hull, 1996). More than 600 cooling towers are operated in electric utilities in the U.S. To our knowledge, chlorine emissions from these cooling towers have not been estimated before.

## 3. Results and Discussion

Annual HOCl emissions from cooling towers in electric utilities are estimated to be 4,400 t. This estimate is only a fraction of the 33,000 t of $Cl_2$ emissions in the 1999 NEI for hazardous air pollutants. The top five ranked states are: Pennsylvania, Texas, Georgia, Arizona, and Ohio.

A box model containing gas-phase chemical reactions was used to assess the relative impact of $Cl_2$ and HOCl on $O_3$. The 2005 version of the Carbon Bond (CB05) chemical mechanism was combined with chlorine chemistry and was used in the box model (Yarwood et al., 2005). While both $Cl_2$ and HOCl photolyze to produce Cl, photolysis rate of $Cl_2$ is about eight times faster than that of HOCl (9.0 $h^{-1}$ for $Cl_2$ vs. 1.1 $h^{-1}$ for HOCl at typical summer noon). The box model run was performed with prescribed initial conditions for urban conditions based on Gao et al. (1996). Model calculations were performed without and with initial chlorine. Three sets of initial chlorine were examined: 300 pptv of $Cl_2$, 300 pptv of HOCl, and 600 pptv of HOCl. The difference in predicted $O_3$ with and without chlorine is presented in Fig. 1.

When an equal amount of $Cl_2$ and HOCl is present on a mole basis (300 pptv), the increases in $O_3$ with $Cl_2$ are greater than those with HOCl. The rate of increase of

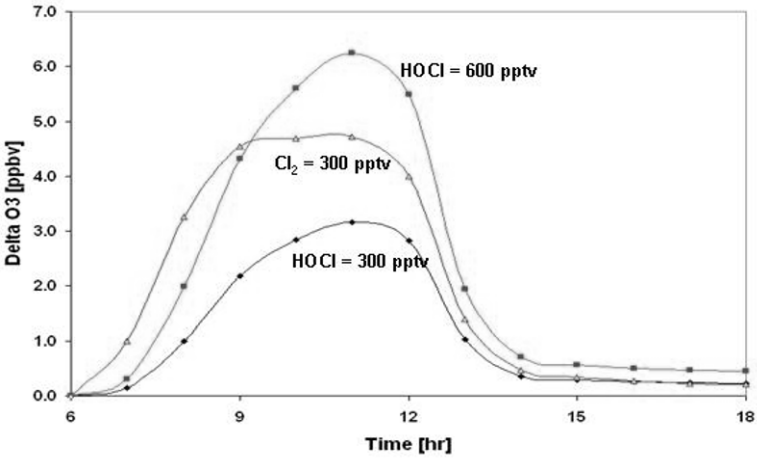


**Fig. 1.** The relative impact of $Cl_2$ and HOCl on $O_3$ in the troposphere

$O_3$ with $Cl_2$ is also greater than that with HOCl. When an equal amount of chlorine is present on a mass basis (300 pptv of $Cl_2$ vs. 600 pptv of HOCl), then the largest increase in $O_3$ obtained with HOCl is greater than that with $Cl_2$. However, the initial rate of increase of $O_3$ with $Cl_2$ is still greater than that with HOCl. Similar results were also obtained for rural conditions described in Gao et al. (1996).

## 4. Summary

These findings have important implications. First, it suggests that only a fraction of chlorine that is added to cooling tower water can be emitted into the atmosphere. Second, chlorine emissions from cooling towers are primarily emitted as HOCl, not as $Cl_2$. The chemical form of chlorine emissions is important since it affect $O_3$ differently. We plan to combine these estimates with other available estimates of chlorine emissions and evaluate their impacts on $O_3$ in the U.S. by using the Community Multiscale Air Quality (CMAQ) model (Byun and Schere, 2006).

**Disclaimer** Although this paper has been reviewed by EPA and approved for publication, it does not necessarily reflect EPA's policies or views.

## References

Bergessen, C.A.E. and Hull, V., 1996. Environmental Directory of US Power Plants, Edison Electric Institute, Washington DC.

Byun, D. and Schere, K.L., 2006. Review of the governing equations, computational algorithms, and other components of the Models-3 Community Multiscale Air Quality (CMAQ) modeling system, *Applied Mechanics Reviews*, 59, 51–77.

Chang, S., McDonald-Buller, E.C., Kimura, Y., Yarwood, G., Neece, J., Russel, M., Tanaka, P., and Allen, D., 2002. Sensitivity of urban ozone formation to chlorine emission estimates, *Atmospheric Environment*, 36, 4991–5003.

Chang, S. and Allen, D.T., 2006. Atmospheric chlorine chemistry in Southeast Texas: Impacts on ozone formation and control, *Environmental Science & Technology*, 40, 251–262.

Gao, D., Stockwell, W.R., and Milford, J.B., 1996. Global uncertainty analysis of a regional-scale gas-phase chemical mechanism, *Journal of Geophysical Research*, 101, C4, 9107–9119.

Holzwarth, G., Balmer, R.G., and Soni, L., 1984a. The fate of chlorine in recirculating in cooling towers. *Water Research*, 18, 1429–1435.

Holzwarth, G., Balmer, R.G., and Soni, L., 1984b. The fate of chlorine and chloramines in cooling towers. *Water Research*, 18, 1421–1427.

Knipping, E.M. and Dabdub, D., 2003. Impact of chlorine emissions from sea-salt aerosol on coastal urban ozone, *Environmental Science & Technology*, 37, 275–284.

Sarwar, G. and Bhave, P., 2007. Modeling the effect of chlorine emissions on atmospheric ozone across the eastern United States, Journal of *Applied Meteorology and Climatology*, 46, 1009–1019.

Yarwood, G., Rao, S., Yocke, M., and Whitten, G., 2005. Updates to the Carbon Bond Chemical Mechanism: CB05, Final Report to the US EPA, RT-0400675, Available at http://www.camx.com/publ/pdfs/CB05_Final_Report_120805.pdf.

# 2.24 Annual Dynamics and Statistical Evaluation of an Air Quality Forecasting System (CALIOPE) with High Resolution for Europe

**Matthias Piot[1], Maria Teresa Pay[1,2], Oriol Jorba[1], Pedro Jiménez-Guerrero[1], Eugeni Lopez[1], Santiago Gassó[1,2], and Jose Maria Baldasano[1,2]**

[1]Barcelona Supercomputing Center – Centro Nacional de Supercomputación (BSC-CNS). Earth Sciences Department. Jordi Girona 29, Edificio Nexus II, 08034 Barcelona, Spain

[2]Environmental Modelling Laboratory, Technical University of Catalonia. Avda. Diagonal 647, Edificio H, Oficina 10.23, 08028 Barcelona, Spain

**Abstract** The WRF-ARW/HERMES-EMEP/CMAQ/BSC-DREAM forecasting system was used to simulate the dynamics and chemistry over Europe for a reference year (2004). The present work describes a quantitative evaluation of gas phase species ($O_3$, $NO_2$, $SO_2$) as well as particulate matter ($PM_{10}$ and $PM_{2.5}$) in comparison to ground-based measurements from the EMEP network. Except various peaks overestimated, the model captures well the general dynamics for $SO_2$ with correlations between 0.44 and 0.56. The trend and daily variations of $SO_2$, $NO_2$, and $O_3$ are satisfactory, although we noted a recurrent underestimation of mean simulated $NO_2$ levels most likely caused by the disaggregation method of the emission model. Concentrations of ozone are well captured, with corresponding statistics ($13.1\% < MNGE < 23.5\%$, $-15.2\% < MNBE < 1.5\%$) lying within the ranges defined by the US-EPA guidelines. Mean levels of both $PM_{10}$ and $PM_{2.5}$ are systematically underestimated, but the trends are well reproduced ($0.53 < cor < 0.72$). Deficient levels of particulate matter are caused by the lack of sources implemented in the emission model.

**Keywords** BSC supercomputer, CALIOPE project, dynamical and statistical evaluation, forecasting system, gaseous pollutants, particulate matter

## 1. Introduction

In the frame of the CALIOPE project, funded by the Spanish Ministry of the Environment, a high-resolution air quality forecasting system, WRF-ARW/HERMES-EMEP/CMAQ/BSC-DREAM has been developed and applied to the

D.G. Steyn and S.T. Rao (eds.), *Air Pollution Modeling and Its Application XX*,
DOI 10.1007/978-90-481-3812-8, © Springer Science + Business Media B.V. 2010

European domain (see http://www.bsc.es/caliope/). This contribution describes the annual dynamics and the statistical performances of the model system for a reference year (2004). The analysis is centered on summer months, as the most severe ozone and other pollutant episodes mainly occur during warm and sunny periods. The evaluation comprises the inter-comparison of $O_3$, $NO_2$, and $SO_2$ in the gas phase and particulate matter $PM_{10}$ and $PM_{2.5}$, together with observations performed at EMEP measurement sites.

## 2. Methodology

The WRF-ARW meteorological model contains 38 vertical layers reaching up to 50 hPa. Initial and boundary conditions are obtained from the NCEP reanalysis data. The vertical resolution of the CMAQ chemistry-transport model (version 4.5; Byun and Schere, 2006) was increased from 8 to 15 layers in order to simulate vertical exchanges more accurately. The vertical sigma-p coordinates cover up to the lower stratosphere (5 hPa) with an increased resolution within the planetary boundary layer. Gas phase boundary conditions are provided by the LMDz-INCA2 global climate-chemistry model (see Hauglustaine et al., 2004). The aerosol module utilized is AERO4, in comparison to the AERO3 module used in previous simulations. The Dust REgional Atmospheric Model (DREAM, Nickovic et al., 2001) model simulates long-range transport of mineral dust from the African continent over the domain under study. For this European simulation (resolution: 12 km, 1 h), emissions are disaggregated from the EMEP expert emission inventory for 2004 to the utilized resolution using the criteria implemented in the HERMES emission model (Baldasano et al., 2008). In order to evaluate the performances of the CALIOPE system, model simulations were compared with ground-based measurements from the EMEP network which applied quality criteria and controls on the data (Fig. 1). Note that the months of March, April and May are referred to as "spring", and June, July and August as "summer", respectively. Note that only hourly data are discussed for gas phase species, while aerosol measurements are available on daily basis only. According to previous studies of single and inter-comparison model evaluations and to the US-EPA (1991, 2007) suggestions, a suite of discrete statistics has been used to characterize the model behaviour, such as the Mean Normalized Bias Error (MNBE) (%), Mean Normalized Gross Error (MNGE) (%), Root Mean Square Error (RMSE) ($\mu g\ m^{-3}$) and correlation (cor). Apart from the correlation, statistics are calculated using recommended thresholds ($O_3$: 80 $\mu g.m^{-3}$; $NO_2$: 5 $\mu g.m^{-3}$; $SO_2$: 3 $\mu g.m^{-3}$; $PM_{10/2.5}$: 10 $\mu g.m^{-3}$).

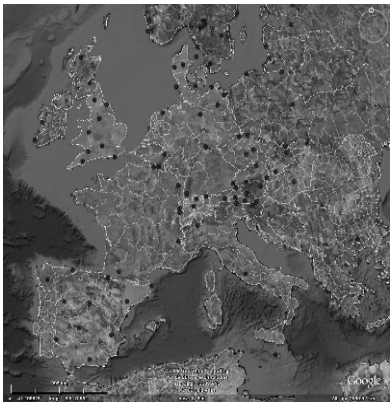

| | | HOURLY | | | DAILY | | | |
|---|---|---|---|---|---|---|---|---|
| | | $NO_2$ | $SO_2$ | $O_3$ | $NO_2$ | $SO_2$ | $PM_{10}$ | $PM_{2.5}$ |
| ***TOTAL*** | ***205*** | ***18*** | ***12*** | ***60*** | ***43*** | ***31*** | ***25*** | ***16*** |
| Austria | 19 | - | 2 | 11 | 1 | 2 | 2 | 1 |
| Belgium | 2 | 2 | - | - | - | - | - | - |
| Bulgaria | 1 | - | - | 1 | - | - | - | - |
| Czech. Replublic | 6 | - | - | 2 | 2 | 2 | - | - |
| Denmark | 5 | - | - | 1 | 1 | 2 | 1 | - |
| France | 13 | 2 | - | 5 | 2 | 4 | - | - |
| Germany | 14 | - | - | 4 | 1 | 1 | 6 | 2 |
| Great Britain | 16 | 3 | - | 10 | 3 | - | - | - |
| Hungary | 1 | - | - | - | 1 | - | - | - |
| Ireland | 3 | - | - | 2 | 1 | - | - | - |
| Italy | 6 | - | - | - | 2 | 1 | 2 | 1 |
| Latvia | 5 | - | - | 1 | 2 | 2 | - | - |
| Lithuania | 3 | - | - | 1 | 1 | 1 | - | - |
| Malta | 1 | - | - | 1 | - | - | - | - |
| Netherlands | 2 | 1 | - | - | 1 | - | - | - |
| Norway | 2 | - | - | 2 | - | - | - | - |
| Poland | 10 | - | - | 3 | 4 | 3 | - | - |
| Slovakia | 5 | - | - | - | 4 | 1 | - | - |
| Slovenia | 2 | - | - | 2 | - | - | - | - |
| Spain | 67 | 10 | 10 | 9 | 10 | 8 | 10 | 10 |
| Sweeden | 6 | - | - | 3 | 2 | 1 | - | - |
| Switzerland | 15 | - | - | 2 | 4 | 3 | 4 | 2 |
| Turkey | 1 | - | - | - | 1 | - | - | - |

**Fig. 1.** Location (left) and number (right) of EMEP stations with data availability for the year 2004

## 3. Results and Discussions

The temporal series over spring and summer of measured and simulated pollutant gases ($SO_2$, $NO_2$ and $O_3$) and particulate matter (only $PM_{10}$ is shown) at the EMEP stations are plotted in Fig. 2. The monthly statistics for gases and particulate matter are presented in Table 1. The $SO_2$ concentration tends to be well correlated throughout the period of study ($0.44 < cor < 0.56$). Background levels are well represented ($9.6\ \mu g\ m^{-3} < RMSE < 28.9\ \mu g\ m^{-3}$) but overestimations of peaks are detected mainly due to those stations directly affected by stack plumes of large coal power plants. All stations located in regions of very low $SO_2$ concentrations present systematic slight overestimations under anticyclonic situations. Background levels of $NO_2$ during both spring and summer are underestimated ($-55.6\% < MNBE < -49.7\%$), but high correlation values demonstrate the satisfactory mean variations ($0.41 < cor < 0.63$). The best modeled regions for $NO_2$ were identified to be the stations in the Iberian Peninsula. The worst simulated levels were found in Great Britain, most probably due to uncertainties in the description of the chemical boundary conditions. The general underestimation by the model is most likely due to country-to-country discrepancies within the EMEP emission inventory and partly to the "top-down" disaggregation method utilized to build the EMEP emission scheme with a resolution down to 12 km. The modeled $O_3$ is well characterized ($13.1\% < MNGE < 23.5\%$, $-15.2\% < MNBE < 1.5\%$) and presents high correlations ($0.48 < cor < 0.60$) and high daily variability in the warmest period. However, mean levels of nighttime $O_3$ are captured with low accuracy in summer. As regard to the US-EPA guidelines ($MNBE \leq 15\%$ and $MNGE \leq 35\%$) and a European Directive 2008/50/EC criterion (Uncertainty $\leq 50\%$, see European Community, 2008), the model presents a good behavior for the $O_3$ simulation. $PM_{10}$ background concentrations tend to be underestimated throughout the year

(–62.2% < MNBE < –54.8%, 57.6% < MNGE < 63.4%). However, the model presents a good correlation (0.53 < cor < 0.72) with the observations, the lowest correlations corresponding to spring where the DREAM model did not capture several dust outbreaks. Levels of $PM_{2.5}$ present similar tendency than $PM_{10}$, (–56% < MNBE < –35.4%, 55.1% < MNGE < 62.6%), although slightly lower correlations are obtained (0.44 < cor < 0.58). This problem is related to the uncertainty in our knowledge of the sources, and dynamical or chemical processes of secondary aerosol.

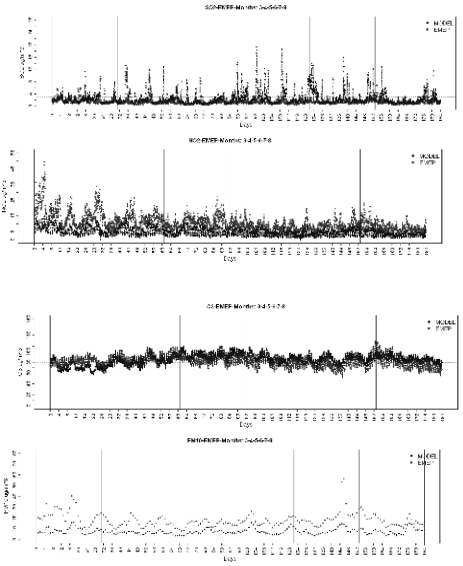

**Fig. 2.** Time series at EMEP stations over spring and summer (2004): $SO_2$, $NO_2$, and $O_3$ on hourly basis and $PM_{10}$ on daily basis

**Table 1.** Monthly statistics obtained with the CALIOPE system for gases at the EMEP stations (hourly data) and particulate matter (daily data): number of data (NDATA), cor, MNBE (%), MNGE (%), RMSE (μg $m^{-3}$).

| | $O_3$ | | | | | $NO_2$ | | | | | $SO_2$ | | | | |
|---|---|---|---|---|---|---|---|---|---|---|---|---|---|---|---|
| Period | NDATA | cor | MNBE | MNGE | RMSE | NDATA | cor | MNBE | MNGE | RMSE | NDATA | cor | MNBE | MNGE | RMSE |
| **Mar** | 23066 | 0.48 | -15.2 | 23.5 | 27.4 | 8180 | 0.63 | -53.7 | 63.7 | 26.9 | 1229 | 0.56 | -24.4 | 69.1 | 9.6 |
| **Apr** | 26964 | 0.45 | -10.1 | 17.5 | 21.9 | 6574 | 0.55 | -52.8 | 65.4 | 21.8 | 689 | 0.47 | 36.0 | 113.3 | 18.1 |
| **May** | 26087 | 0.55 | 1.5 | 16.6 | 19.9 | 6386 | 0.53 | -49.7 | 64.0 | 19.1 | 664 | 0.44 | 15.6 | 94.2 | 11.0 |
| **Jun** | 20387 | 0.58 | -1.0 | 14.9 | 19.3 | 6400 | 0.41 | -51.5 | 63.8 | 13.4 | 662 | 0.50 | 136.8 | 202.6 | 28.9 |
| **Jul** | 18931 | 0.61 | -5.1 | 14.7 | 20.9 | 6040 | 0.42 | -54.2 | 66.0 | 14.9 | 841 | 0.46 | 45.6 | 127.0 | 19.2 |
| **Aug** | 19697 | 0.60 | -4.5 | 13.1 | 18.6 | 6031 | 0.50 | -55.6 | 64.4 | 14.4 | 753 | 0.55 | 28.2 | 116.2 | 13.9 |

| | $PM_{10}$ | | | | | $PM_{2.5}$ | | | | |
|---|---|---|---|---|---|---|---|---|---|---|
| Period | NDATA | cor | MNBE | MNGE | RMSE | NDATA | cor | MNBE | MNGE | RMSE |
| **Mar** | 533 | 0.53 | -60.4 | 63.2 | 22.9 | 257 | 0.44 | -56.0 | 62.6 | 18.4 |
| **Apr** | 489 | 0.53 | -57.9 | 60.1 | 14.9 | 167 | 0.57 | -55.3 | 58.8 | 12.3 |
| **May** | 456 | 0.53 | -54.8 | 57.6 | 12.5 | 187 | 0.53 | -51.0 | 55.1 | 9.4 |
| **Jun** | 558 | 0.62 | -55.1 | 58.2 | 13.0 | 255 | 0.49 | -35.4 | 55.7 | 9.4 |
| **Jul** | 622 | 0.65 | -62.2 | 63.4 | 24.3 | 315 | 0.58 | -50.2 | 57.7 | 12.1 |
| **Aug** | 546 | 0.72 | -60.0 | 61.7 | 14.6 | 248 | 0.46 | -38.2 | 61.3 | 12.3 |

## 4. Summary and Conclusion

In general, the annual dynamics of gas phase species as well as of particulate matter was relatively well simulated. Note that the EMEP emission inventory needs improvements and constitutes a limitation in the accuracy of air quality modelling. The CALIOPE system complements the present network of air quality measurements managed by regional and local authorities, and in certain experimental measurement campaigns or air quality studies performed both in urban or background areas.

**Acknowledgments** The authors wish to thank Carlos Perez for providing us the DREAM mineral dust data from the African continent. This work is funded by the CALIOPE project of the Spanish Ministry of the Environment. All simulations were performed in the MareNostrum supercomputer hosted by the Barcelona Supercomputing Center.

## References

Baldasano J.M., P. Jiménez-Guerrero, O. Jorba, C. Pérez, E. López, P. Güereca, F. Martin, M. García-Vivanco, I. Palomino, X. Querol, M. Pandolfi, M.J. Sanz and J.J. Diéguez. CALIOPE: An operational air quality forecasting system for the Iberian Peninsula, Balearic Islands and Canary Islands-First annual evaluation and ongoing developments. Adv. Sci. and Res., 2: 89–98, 2008.

Byun, D. W. and K. L. Schere. Review of the governing equations, computational algorithms and other components of the Models-3 Community Multiscale Air Quality (CMAQ) Modeling System, Applied Mechanics Reviews, 59(2), 51–77, 2006.

European Community. Directive 2008/50/EC of the European Parliament and of the Council of 21 May 2008 on ambient air quality and cleaner air for Europe. Official Journal of the European Communities L 152, 01–44, 2008.

Hauglustaine, D.A., F. Hourdin, S. Walters, L. Jourdain, M.-A. Filiberti, J.-F. Larmarque, and E. A. Holland: Interactive chemistry in the Laboratoire de Météorologie Dynamique general circulation model: description and background tropospheric chemistry evaluation, Journal of Geophysical Research, 109, D04314, doi: 10.1029/2003JD003957, 2004.

Nickovic, S., A. Papadopoulos, O. Kakaliagou and G. Kallos: Model for prediciton of desert dust cycle in the atmosphere, Journal of Geophysical Research, 106 (D16), 18113–18130 2001.

USEPA. Guideline for Regulatory Application of the Urban Airshed Model. US EPA Report No. EPA-450/4-91-013. Office of Air and Radiation, Office of Air Quality Planning and Standards, Technical Support Division. Research Triangle Park, North Carolina, US, 1991.

USEPA. Guidance on the Use of Models and Other Analyses for Demonstrating Attaintment of Air Quality Goals for Ozone, PM2.5, and Regional Haze. US EPA Report No. EPA-454/B-07-002. Office of Air Quality Planning and Standards. Research Triangle Park, North Carolina, US, 2007.

# 2.25 Impact of Vegetation Along a Highway on Local Air Quality: A CFD Simulation Approach

**Stijn Janssen[1], Bart De Maerschalck[1], Jean Vankerkom[1], Wouter Lefebvre[1], Clemens Mensink[1], Aad van den Burg[2], and Paul Fortuin[2]**

[1]VITO – Flemish Institute for Technological Research, Boeretang 200, B-2400 Mol, Belgium

[2]Rijkswaterstaat – Centre for Transport and Navigation (RWS-DVS), Delft, The Netherlands

**Abstract** In this paper a CFD-based micro scale air quality model called ENVI-met is presented. ENVI-met distinguishes itself from other CFD-models due the implementation of a detailed vegetation model which describes the interaction of local vegetation, not only on the wind field, but also on the thermodynamic processes and the diffusion and deposition of gases and particulate matter. This makes the model particularly suitable for a recent research programme initiated by the Air Quality Innovation Programme (IPL), founded by the Dutch Ministry for Transport, Public Works and Water Management (Rijkswaterstaat) and the Ministry of Housing, Spatial Planning and the Environment (Ministry of VROM). One of the seven branches of the IPL-programme is to investigate both by measurements and modelling the effect of line vegetation along a motorway on local air quality. Recently the model results have been compared to a first measurement campaign.

**Keywords** Air quality, traffic emission, CFD, vegetation

## 1. Introduction

Computational Fluid Dynamics or CFD-based air quality models have the capability to describe the local atmospheric conditions over a complex domain in a detailed way. This makes them particularly useful for small scale air quality modelling in complex areas like an irregular street canyon with vegetation objects, multiple emission sources and chemical reactions.

ENVI-met is such a CFD-model. It was originally designed as a micro-climate model (Bruse, 1998). Later it has been extended with an air quality module for both quasi inert gases and particulate matter and recently the a chemical model was included for the photo-chemical reactions of ozone and nitrogen oxides. ENVI-met contains an extended vegetation module which not only describes the effect on the wind-field and turbulent kinetic energy, but also describes the thermodynamic effects of the vegetation on the ambient air, as well as the effects

D.G. Steyn and S.T. Rao (eds.), *Air Pollution Modeling and Its Application XX*,
DOI 10.1007/978-90-481-3812-8, © Springer Science + Business Media B.V. 2010

on the diffusion and deposition of gasses and particulate matter. For this, ENVI-met contains a plant physiologic model which calculates the stomata resistance based on the local radiation, leaf surface temperature, the ratio of leaf- to ambient air $CO_2$-concentrations and water content. For the latter one the CFD-model is coupled to a simplified soil model as well.

The model is applied within the framework of the Dutch Air Quality Innovation Program (IPL). The ambition of the programme is to come up with a strategy to improve local air quality in the vicinity of motorways and so called hot spots. One of the seven braches of the project is the investigation, both by the means of in situ measurements and by modelling, of the effect of line vegetation along a motorway. In this framework, the model results have been compared to a first measurement campaign which was executed before in the summer of 2006 along the A50 close to the village of Vaassen, The Netherlands (Weijers et al., 2007).

## 2. Model Setup

In order to perform a validation study between the measurement campaign and the ENVI-met model, a total area of 200 by 600 m and up to 50 m height has been modelled. The whole domain is subdivided into non-overlapping elements, 121,688 in total, with a spatial resolution of $6 \times 6 \times 2$ m with a vertical refinement in the lowest five cells. Five measurements days have been modelled (only 3 for PM). During these days the mean wind direction was mainly perpendicular to the motor way, but varies between plus and minus 45°.

The traffic emission are modelled as line sources, one line per lane. The emission rates are based on the local traffic counts by the Dutch Ministry of Transportation, multiplied by the Dutch emission factors defined by the Ministry of Housing, Spatial Planning and Environment.

## 3. Model Results

ENVI-met was capable of representing the measurement campaign quite well. Figures 1 and 2 show the normalized mean concentration for nitrogen oxides and fine particles at 2 m height. These are the mean concentrations averaged over 5 days of measurements (three measurement days for PM) and normalized with the value of the concentration just in front of the vegetation barrier. The plots show both the modelled concentrations, full lines, and the measured mean values, dots with error bars. The red dots and lines represent the measurements and model results in the reference field, while the green dots and lines represent the measurements and model results in front of and behind the vegetation. The green bar indicates the location of the vegetation barrier and the red blocks at the bottom the location of the traffic emissions.

Notice that the normalized model results and measurements fit best for $NO_2$. However, for $NO_2$ the model systematically shows a slight underestimation of the concentrations. At the moment it is not fully clear why and further research is necessary. For NO the model predicts a slightly faster decay of the concentrations behind the vegetation. For PM the model does not follow the measurements. The measurements even show an increase in the concentrations due to the vegetation while the model shows a pattern similar to those of the nitrogen oxides. Notice that for PM only a limited measurement data set was available. For this reason it would be to soon to draw hard conclusions on this and further research remains necessary.

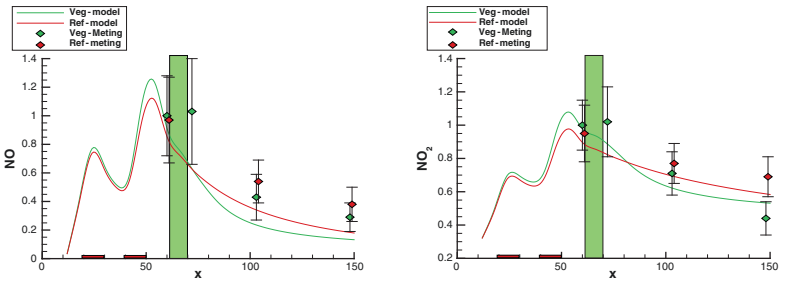


**Fig. 1.** Normalised mean nitrogen oxides concentrations (NO left, $NO_2$ right) at 2 m height. Green bar indicates the location of the vegetation, the red boxes the line sources. Green and red dots represent the ECN measurements, continuous lines: model results. Red: Along the reference measurement line, green: in front of and behind the vegetation barrier. Mean wind is blowing from the left

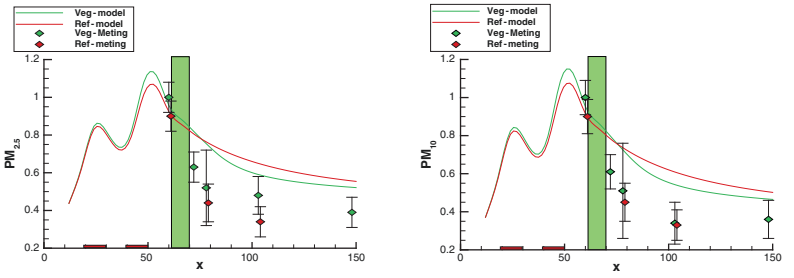


**Fig. 2.** Normalized mean PM concentrations ($PM_{2.5}$ left, $PM_{10}$ right) at 2 m height. Similar to Fig. 1

In all cases the model predicts an increase in concentration in front of and just behind the vegetation barrier. This is due to the decrease in wind speed at the location of the emission source. Further away from the vegetation a decrease of about 5% and for NO even more than 10% can be found (see Fig. 3).

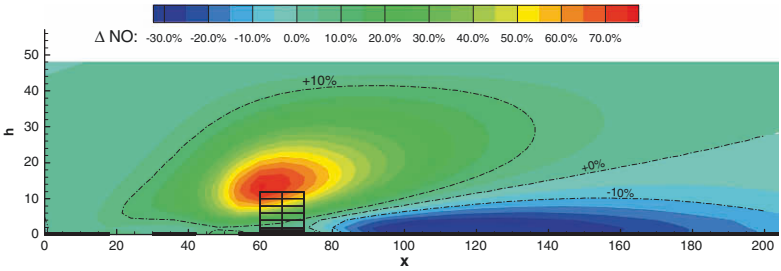


**Fig. 3.** Mean relative difference in the vertical plane in NO-concentrations with and without a vegetation barrier

## 4. Conclusions

Both the measurements and the ENVI-met model results show that a vegetation barrier along a motorway can have a local positive effect on the air quality at the downwind side of the motorway. For nitrogen oxides both the model and the measurements show similar relative effects caused by the vegetation. For PM, model results do not agree with the measurement campaign. However due to exceptional meteorological conditions, only limited measurement data for PM was available. It would be to premature to draw conclusions based on this limited data set.

Both the measurement campaign and the modelling are a first attempt to better understand the effect of a vegetation barrier along a motorway. A second and third measurement campaign are conducted and currently being analysed. Those results will help to give more insight in the processes and to improve the modelling.

## References

Bruse, M. and H. Fleer, (1998) Simulating surface–plant–air interactions inside urban environments with a three dimensional numerical model, Environmental Modelling and Software, 13, 373–384.

Weijers, E. P., G. P. A. Kos, W. C. M. van den Bulk and A. T. Vermeulen, (2007) Onderzoek naar de luchtkwaliteit rondom een vegetatiestrook langs de snelweg, Technical report ECN-E--07-011, Energy Research Center of the Netherlands.

# 2.26 Evaluation of Toxic Air Contaminants in the San Francisco Bay Area: Regional Emissions and Ambient Observations

**Philip T. Martien[1], David Fairley[1], Cuong Tran[1], Amir Fanai[1], Minh Nguyen[1], Eric Stevenson[1], Tirlochan Mangat[1], Saffet Tanrikulu[1], Gary Kendall[1], Henry Hilken[1], Stephen B. Reid[2], Dana C. Sullivan[2], Bryan M. Penfold[2], and Eric Fujita[3]**

[1]Bay Area Air Quality Management District, San Francisco, CA, USA

[2]Sonoma Technology, Inc., Santa Rosa, CA

[3]Desert Research Institute, Reno, NV, USA

## 1. Introduction

Emissions and concentrations of toxic air contaminants (TAC) have declined significantly in the past decade in the San Francisco Bay Area (Bay Area), a major metropolitan center of northern California. However, these contaminants continue to pose serious health concerns, particularly within urban and industrialized communities. To monitor ambient concentrations and track trends, the Bay Area Air Quality Management District (BAAQMD) has established a TAC monitoring network. Recently, the authors of this extended abstract have developed gridded estimates of TAC emissions in the Bay Area and used ambient measurements and fuel-use data to evaluate and improve these estimates. The resulting emissions inventory was used for developing inputs for regional air quality modeling (Martien et al., 2009) and for designing TAC mitigation measures as part of its Community Air Risk Evaluation (CARE) program.

## 2. Measured Trends in Ambient TAC

The BAAQMD and the California Air Resources Board (CARB) have measured selected toxic pollutants in the Bay Area since the late 1980s. There are no ambient standards for these pollutants, but there are known health risks for cancer and other acute or chronic health problems associated with them. Trends based on TAC measurements were estimated as the ratio of means of the 2001–2005 data with the earliest 5 years of available data.

D.G. Steyn and S.T. Rao (eds.), *Air Pollution Modeling and Its Application XX*,
DOI 10.1007/978-90-481-3812-8, © Springer Science + Business Media B.V. 2010

With some exceptions, ambient toxic compounds in the Bay Area have been reduced substantially. The introduction of reformulated fuels have been reduced concentrations of benzene and 1,3-butadiene. MTBE has been eliminated from gasoline. Perchloroethylene has been reduced dramatically because of BAAQMD and CARB dry cleaner rules. Cleaner-burning diesel engines and cleaner diesel fuel have reduced diesel concentrations over 50%. Carbon tetrachloride is one exception, showing essentially no change. This pollutant is no longer manufactured but is long-lived in the atmosphere and ubiquitous world-wide. A second exception is chloroform, which has shown a 16% increase since the late 1980s. Formaldehyde and acetaldehyde show reductions of 14% and 8% respectively from 1996–1998 to 2003–2005. It is not clear that these represent statistically significant reductions.

## 3. Emissions Inventory of TAC

For permitted stationary sources, an annual inventory of speciated TAC emissions and facility locations were available as a part of BAAQMD's routine records. For other source types, we applied a "top-down" approach, wherein source-specific chemical speciation profiles were applied to total organic gas (TOG) and particulate matter (PM) emissions to estimate the fractions released as TAC. In addition, county-level emissions were mapped to source-specific areas using representative geographic data. For example, ship emissions were mapped to shipping lanes in the bay and ocean.

Weighting factors were applied to scale the emissions of each TAC according to its toxicity for cancerous effects, non-cancerous chronic effects, and acute effects. The details of inventory preparation, as well as findings and caveats, are described elsewhere (Reid et al., 2006).

Comparison of various emission species revealed that diesel particulate matter (diesel PM) contributes more than 85% of the cancer-risk-weighted emissions (Fig. 1a). On-road vehicles and off-road mobile sources are the primary sources of diesel PM (Fig. 1b). The highest diesel PM emissions occur in core urban areas and along major freeways (Fig. 1c). The main contributor to chronic non-cancer and acute health effects in the Bay Area is acrolein (not shown) whose major sources include cars, trucks, and aircraft. Comparison of the maps of demographic and health data (not shown) to TAC emissions (Fig. 1c) reveals that high TAC emissions occur near areas with sensitive populations.

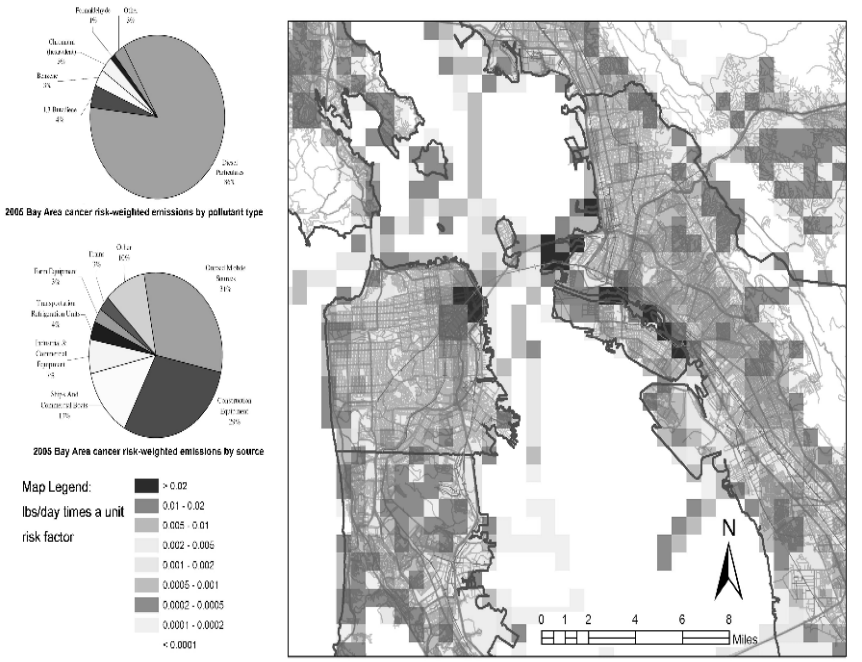


**Fig. 1.** Cancer-risk weighted emissions of toxic air contaminants are shown (a, top left) by pollutant type, (b, bottom left) by source type, and (c, right panel) mapped in the central Bay Area

## 4. Evaluation of the Inventory

To evaluate emissions estimates for on-road diesel emissions, we compared diesel fuel consumption from CARB's EMFAC2007 model with diesel fuel consumption from the California Department of Transportation's (Caltrans) California Motor Vehicle Stock, Travel and Fuel Forecast (MVSTAFF) model. The two methods provided similar estimates of diesel fuel consumption from on-road motor vehicles in the Bay Area in 2005 (about 1 million gal/day).

To evaluate emissions estimates for off-road diesel emissions, we compared CARB's OFFROAD2007 model fuel consumption estimates with Bay Area diesel fuel production used for off-road sources. (Diesel fuel sold in California for off-road use is tax exempt and dyed red to distinguish it from taxed fuel.) OFFROAD2007's diesel fuel consumption for the Bay Area – when tallied with estimates from other off-road categories (commercial boats, cargo-handling equipment, and trains) not included in OFFROAD2007 – totaled about 80% of on-road diesel fuel usage.

In 2005, non-taxed, red dye diesel fuel throughput for Bay Area refineries was found to be about 250,000 gal/day. State Board of Equalization tax refund records indicated that about 20% of clear diesel produced in California is used in off-road equipment. Assuming all red-dye diesel produced in the Bay Area is used locally, total off-road diesel consumption was estimated to be about 440,000 gal/day, or 45% of on-road usage, and roughly half the OFFROAD2007 estimate, a finding similar to that of a fuel-based study at the national level (Kean et al., 2000).

As an additional check of the inventory, we compared ratios of toxic compounds in the inventory with corresponding ratios measured in ambient air. Elemental carbon estimated via the IMPROVE method was used as a surrogate for diesel PM in this comparison. The relative mass and risk from various compounds in the emissions inventory was generally well correlated with ambient concentrations. Diesel emissions dominated the risk in both ambient samples and the emissions inventory, contributing about 75% in the ambient data and 85% in the inventory, followed by 1,3-butadiene and benzene, each contributing 7–11% in the ambient data and 3–7% in the inventory. The ambient data show a risk from carbon tetrachloride of about 4% but the inventory does not; this compound is no longer produced and measured concentrations reflect global background.

## 5. Summary

Analyses based on both measurements and emissions estimates suggest that diesel PM contributes the greatest cancer risk from TAC (between 75% and 85%) in the Bay Area. Regional maps of TAC emissions show that the highest risk weighted emissions occur in core urban areas and along major freeways. Such analyses have helped to inform and focus TAC mitigation measures at the Bay Area Air Quality Management District.

## References

Kean, A.J.; Sawyer, R.F.; Harley, R.A. (2000) *J. Air & Waste Manage. Assoc.* 50, 1929–1939.

Martien et al., (2009) Presented at the 30th NATO/SPS International Technical Meeting on Air Pollution Modelling and its Application, May 18–22.

Reid S.B.; Sullivan D.C.; and Penfold B.M. (2006) Preparation of emission inventories of toxic air contaminants for the Bay Area. Final report 2 prepared for the Bay Area Air Quality Management District, San Francisco, CA, by Sonoma Technology, Inc., Petaluma, CA, STI-906020.07-2771-FR2, July.

# 2.27 Closing the Peroxy Acetyl (PA) Radical Budget: Observations of Acyl Peroxy Nitrates (PAN, PPN, and MPAN) During BEARPEX 2007

**B.W. LaFranchi[1], G.M. Wolfe[2], J.A. Thornton[3], S.A. Harrold[3], E.C. Browne[1], K.E. Min[4], P.J. Wooldridge[1], J.B. Gilman[5], W.C. Kuster[5], P.D. Goldan[5], J.A. de Gouw[5], M. McKay[6*], A.H. Goldstein[6], X. Ren[7**], J. Mao[7***], and R.C. Cohen[1,4]**

[1]Department of Chemistry, University of California, Berkeley, Berkeley, CA, USA

[2]Department of Chemistry, University of Washington, Seattle, WA, USA

[3]Department of Atmospheric Sciences, University of Washington, Seattle, WA, USA

[4]Department of Earth and Planetary Science, University of California, Berkeley, CA, USA

[5]NOAA/ESRL Chemical Sciences Division, Boulder, CO, USA

[6]Department of Environmental Science, Policy, and Management, University of California, Berkeley, Berkeley, CA, USA

[7]Department of Meteorology, Penn State University, University Park, PA, USA

Acyl peroxy nitrates (APNs, also known as PANs) are an important class of reactive nitrogen species having the general structure: $RC(O)OONO_2$. In urban source regions, APN production acts as a net sink for $NO_x$ ($NO_x = NO + NO_2$). Under high $NO_x$ (VOC-limited) conditions this temporary sink results in increased ozone production rates by slowing the rate of OH reaction with $NO_2$, and thus extending the $HO_x$ ($HO_x = OH + HO_2$) chain length. Downwind of the source region, where total $NO_x$ levels have decreased, APN decomposition injects $NO_x$ into the atmosphere under low $NO_x$ conditions resulting in increased ozone prouction rates.

Acyl peroxy nitrates are formed from the oxidation of aldehydes and other oxygenated VOC (oVOC) in the presence of $NO_2$. There are both anthropogenic and biogenic oVOC precursors to APNs, but a detailed evaluation of their chemistry against observations has proven elusive. Here we describe measurements of PAN, PPN, and MPAN along with the majority of chemicals that participate in their production and loss, including OH, $HO_2$, numerous oVOC, and $NO_2$. Observations were made during the Biosphere Effects on AeRosols and Photochemistry Experiment (BEARPEX 2007) in the outflow of the Sacramento urban plume. BEARPEX 2007 took place at a site on a ponderosa pine plantation owned and managed by

* Now at California Air Resources Board, Sacramento, CA, USA
** Now at Rubenstein School of Marine and Atmospheric Science, University of Miami, Miami, FL, USA
*** Now at School of Engineering and Applied Sciences, Harvard University, Cambridge, MA, USA

D.G. Steyn and S.T. Rao (eds.), *Air Pollution Modeling and Its Application XX*,
DOI 10.1007/978-90-481-3812-8, © Springer Science + Business Media B.V. 2010

Sierra Pacific Industries and adjacent to the University of California Blodgett Forest Research Station (UC-BFRS). The site is located 75 km northeast of Sacramento, CA (1,315 m a.s.l., 38.9°N, 120.6°W). The experiment began on August 15, 2007 and ended on October 10, 2007.

In this analysis we use measurements of APNs, OH and $HO_2$, a suite of VOCs, and $NO_2$. These observations are used to evaluate a detailed chemical model of APN ratios and concentrations. We find the ratios of APNs are nearly independent of the loss mechanisms and thus an especially good test of our understanding of their sources. We show that oxidation of methylvinyl ketone, methacrolein, methyl glyoxal, biacetyl and acetaldehyde are all significant sources of the PAN + peroxy acetyl (PA) radical reservoir, with methylvinyl ketone (MVK) often being the primary non-acetaldehyde source. Figure 1 shows the relative contribution of the various PA radical sources to the total PA radical production rate. At high tempeatures, oxidation of non-acetaldehyde PA radical sources contributes over 60% to the total PA production rate.

**Acknowledgments** The authors thank the UC Blodgett Forest Research Station staff for logistical support and Sierra Pacific Industries for access to their land. This work was supported by the National Science Foundation (grants ATM-0639847 (Berkeley) and ATM-0633897 (UW)). B. LaFranchi acknowledges support from the Camille and Henry Dreyfus Postdoctoral Program in Environmental Chemistry. G. Wolfe acknowledges support from NASA ESSF NNG-05GP64H.

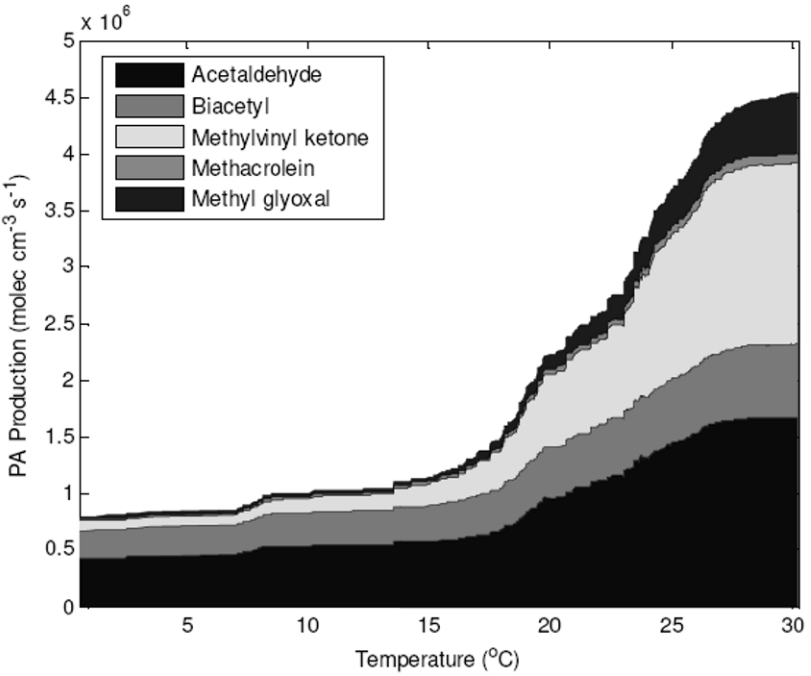


**Fig. 1.** Behavior of different PA production sources vs. temperature during BEARPEX 2007. This figure is obtained by using a running average with temperature of the calculated production rates from observations of oVOCs

# 2.28 Modeling Chemically Reactive Air Toxics with CAMx

**Chris Emery and Greg Yarwood**

ENVIRON International Corporation, Novato, CA, USA

**Abstract** Hazardous air pollutants (HAPs or "toxics") are of concern because they cause acute and/or chronic health impacts and may have sufficiently long atmospheric lifetimes that allow them to be transported and transformed over great distances. Traditional Gaussian plume and puff dispersion models are applicable for simulating primary pollutants (e.g., diesel particulate matter) over short scales. Such dispersion models are not suitable, however, for simulating chemically reactive pollutants (e.g., formaldehyde, 1,3-butadiene, acrolein) and secondary pollutants (e.g., acrolein, formaldehyde) over larger scales where variable chemical regimes and transport/removal processes are important aspects of the long-term distribution and ultimate fate of these compounds. On the other hand, photochemical grid models can address complex chemical transformation pathways for toxics, and simulate their three-dimensional dispersion and removal over wide areas and for long periods. ENVIRON has developed a highly flexible Reactive Tracer Chemical Mechanism Compiler (RTCMC) for the Comprehensive Air quality Model with extensions (CAMx; ENVIRON, 2008). CAMx is a regional photochemical/particulate grid model used for regulatory applications in the U.S. and is applied widely throughout the world to address complex air quality issues. The RTCMC module allows a user-defined toxic chemistry mechanism to run in parallel with, and to draw oxidant information from, a standard gas-phase photochemical simulation (i.e., Carbon Bond or SAPRC). In this paper we describe the RTCMC for modeling air toxics on regional and annual scales.

**Keywords** Hazardous air pollutants, toxics, air quality, grid modeling, dispersion, photochemistry, CAMx

## 1. RTCMC Overview

The RTCMC allows users to define, in an external text-based (ASCII) format, a set of chemical species and reactions (a mechanism) to be treated as "reactive tracers" within a CAMx photochemical simulation. The core model simulates photochemistry using standard oxidant mechanisms (e.g., CB05 or SAPRC99) and the reactive tracers simulate emission, dispersion, chemical decay/production and

D.G. Steyn and S.T. Rao (eds.), *Air Pollution Modeling and Its Application XX*,
DOI 10.1007/978-90-481-3812-8, 

deposition of other trace compounds within the photochemical environment provided by the core model. Upon startup, CAMx reads, checks and compiles the toxics mechanism and then configures the reactive tracer chemistry solver; hence no solver development or coding is necessary on the user's part. During the model simulation, the toxics chemistry receives oxidant information from the core model and uses this to calculate the decay and/or production of toxic species. The current implementation of RTCMC is for gas-phase reactions, i.e., gas-phase tracers reacting with each other and/or gas-phase host model species. A suitable application for RTCMC is simulating air toxic species that photolyze and/or decay according to ambient concentrations of ozone and radicals such as OH, $NO_3$, etc.

The format of the RTCMC input mechanism file is essentially the same as the "IMC" input file format of the SCICHEM Lagrangian puff model (Santos and Sykes, 2000). An example IMC format file is shown in Fig. 1.

```
#Control
    rate_species_units = 'ppm'
    rate_time_units = 'min'
    solver = 'dlsode'
    Jacobian = 'numeric'
#Species, Type, Ambient, Tolerance, deposition vel, wet scav
O3        A     1.0      1.0E-12    0.0             0.0
OH        A     1.0      1.0E-12    0.0             0.0
ATRAC     F     1.0      1.0E-12    0.010           0.0
BTRAC     F     1.0      1.0E-12    0.001           0.0
CTRAC     F     1.0      1.0E-12    0.020           0.0
DTRAC     F     1.0      1.0E-12    0.001           0.0
ETRAC     F     1.0      1.0E-12    0.030           0.0
FTRAC     F     1.0      1.0E-12    0.001           0.0
#Table
  0      0.     15.     30.     45.     60.     75.     80.     86.     87.     88.
  1 4.2E-04 4.1E-04 3.8E-04 3.3E-04 2.6E-04 9.5E-05 3.0E-05 4.9E-06 8.3E-08 1.0E-09
#Equations
  1 [ATRAC]              -> (2.0)[BTRAC] ; 0 0.000E-00
  2 (1.5)[CTRAC] + [OH]  -> (0.5)[DTRAC] ; 1 4.2000E+04
  3 [ETRAC] + [O3]       -> [FTRAC]      ; 1 1.8000E-02
```

**Fig. 1.** Example RTCMC chemistry input file

There are four sections in an IMC file that are identified by a keyword at the start of each section, as follows. The "#Control" section defines which chemistry solver to use (three are available), species and time units for chemical rates, solver error tolerances, and whether to determine the Jacobian matrix of first-order derivatives algebraically or numerically. The "#Species" section lists the chemical species and associated data, including type (from the core photochemical model [A] or independently solved [F]), species-specific error tolerances, and deposition velocity (ambient and wet scavenging parameters are not used). The "#Table" section provides photolysis rates as a function of solar zenith for any photolytic reactions in the RTCMC mechanism; this is the only section that is optional if there are no photolytic reactions defined. The "#Equations" section lists the chemical reactions and rate constants for the RTCMC reaction mechanism. All chemical species referred to in the equation section must appear in the species

section. CAMx supports numerous rate constant expression types; the format for specifying rate expressions is the integer expression type followed by a list of the numerical values required by that expression type. In the Fig. 1 example, reaction 1 is photolytic, where ATRAC photolyzes to 2 BTRAC molecules according to the rates given for reaction 1 in the "#Table" section. Oxidation reactions 2 and 3 are temperature dependent according to the parameters specified on their specific lines.

## 2. Demonstration Application

ENVIRON is assisting the San Francisco Bay Area Air Quality Management District (BAAQMD) in CAMx modeling of chemically reactive air toxics in the region. An RTCMC toxics chemistry file was developed for modeling formaldehyde, acetaldehyde, butadiene, acrolein and benzene. Formaldehyde and acrolein may be primary (emitted) or secondary (formed in the atmosphere from precursors) and the mechanism is configured to distinguish between the two for these species. However, the secondary formaldehyde in this mechanism comes only from acetaldehyde, butadiene and acrolein. Secondary acetaldehyde was not included in the mechanism because it is not formed from butadiene or acrolein.

A schematic of the detailed mechanism for modeling 1,3-butadiene (BUTD), acrolein (ACR) and secondary formaldehyde (SFRM) is shown in Fig. 1 and a schematic of the detailed mechanism for modeling acetaldehyde (ATAL) and secondary formaldehyde (SFRM) is shown in Fig. 2.

The BAAQMD is using this chemical mechanism in simulating HAPS distributions throughout the Bay Area. Modeling results are presented in a companion paper (Fig. 3) (Martien et al., 2009).

## References

ENVIRON (2008) Users' Guide: Comprehensive Air quality Model with Extensions (CAMx), Version 4.50 (May 2008). ENVIRON International Corporation, Novato, CA, USA. www.camx.com

Martien P, Tanrikulu S, Jia Y, Fairley D, Tran C, Matsuoka J, Hilken H, Emery C, Tai E, Yarwood G (2009) Evaluation of Toxic Air Contaminants in the San Francisco Bay Area: Regional Modeling. Presented at the 30th NATO/SPS International Technical Meeting on Air Pollution and its Application, San Francisco, CA, May 18–22, 2009.

Santos L, Sykes I (2000) SCICHEM Version 1.2 Technical Documentation. Prepared for EPRI, by Titan Corporation, Princeton, NJ.

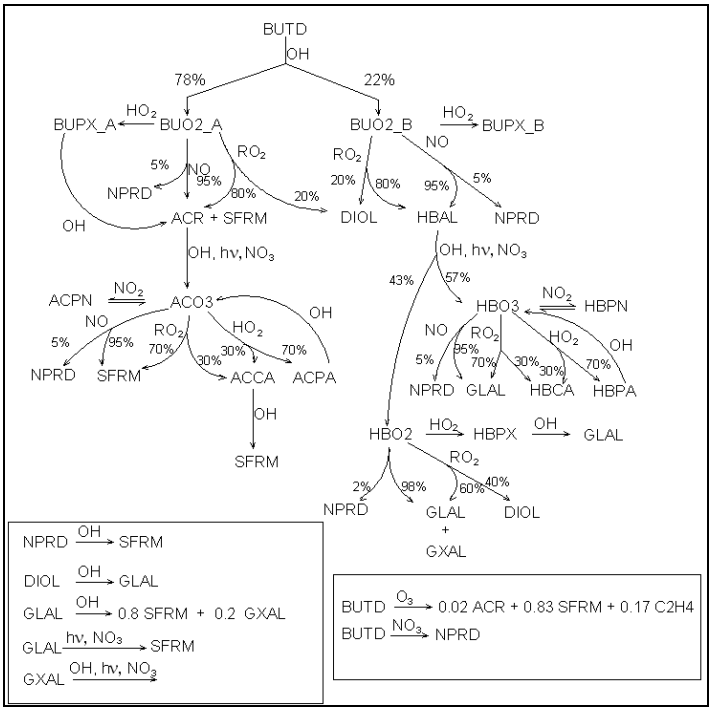


**Fig. 2.** Schematic of the BAAQMD mechanism for modeling 1,3-butadiene (BUTD), acrolein (ACR) and secondary formaldehyde (SFRM)

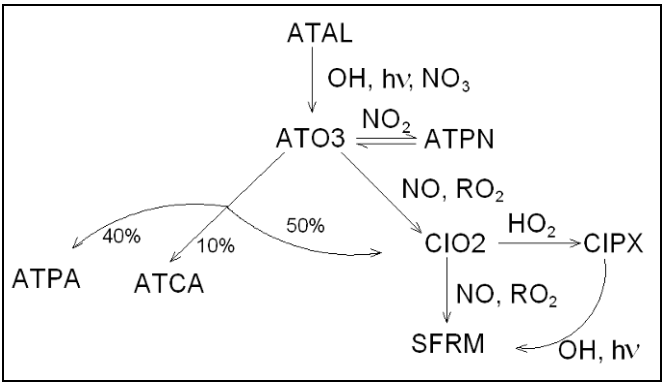


**Fig. 3.** Schematic of the BAAQMD mechanism for modeling acetaldehyde (ATAL) and secondary formaldehyde (SFRM)

# 2.29 Dispersion of Radioactive Debris from Nuclear Explosions in Novaya Zemlya in 1958: Results of the Model Simulations

**Jerzy Bartnicki, Jørgen Saltbones, Hilde Haakenstad, and Bjørn Røsting**

Norwegian Meteorological Institute, P.O. Box 43 Blindern, NO-0313 Oslo, Norway

**Abstract** In October 1958 a series of large nuclear explosions has been performed in the region of Novaya Zemlya in the former Soviet Union emitting a significant amount of radioactivity into the stratosphere. The Severe Nuclear Accident Program (SNAP) model has been used to simulate dispersion from each of three selected explosions and stratospheric intrusion for the episode of high measured activity in Bergen on 20 October 1958. Model simulations have shown that there was no direct transport of radioactivity from Novaya Zemlya to Bergen and strongly indicated that the stratospheric intrusion was the main mechanism responsible for measured high level of radioactivity.

## 1. Introduction

In October 1958 a series of large nuclear explosions was performed in the region of Novaya Zemlya in the former Soviet Union. All together 17 bombs were detonated in October 1958, but of special interest are three large atmospheric explosions which occurred on 12th, 15th and 18th October with the yield of 1.45, 1.5 and 2.9 Mt, respectively. These explosions emitted large amounts of radioactivity directly into the stratosphere.

Several days after the detonations, significantly elevated levels of radioactivity were measured at four stations of the Norwegian measurement network: Tromsø, Vaernes, Vadsø and Bergen. The highest level was measured on 20 October in Bergen, with a total beta activity in the air reaching 600 mBq $m^{-3}$ (Bergan et al., 2005).

The time of the detonations in Novaya Zemlya was carefully planned in this way that atmospheric transport of radioactive debris was mostly directed into the Soviet Union. However, the measurements indicated at first that some direct tropospheric transport from Novaya Zemlya to Norway could be responsible for high levels of measured radioactivity.

On the other hand, trajectory analysis based on the meteorological data for the time of explosions indicated that such a transport did not take place (Bartnicki et al., 2004a) and stratospheric intrusion is the most likely mechanism responsible

D.G. Steyn and S.T. Rao (eds.), *Air Pollution Modeling and Its Application XX*,
DOI 10.1007/978-90-481-3812-8, © Springer Science + Business Media B.V. 2010

for the high level of radioactivity measured at Norwegian measurement sites (Saltbones et al., 2007).

Here we discuss the model runs simulating dispersion of radioactive debris from three selected nuclear explosions, as well as the model run simulating stratospheric intrusion of radioactivity to the measurement site in Bergen.2. Model Simulations of Dispersion from Selected Nuclear.

The Severe Nuclear Accident Program (SNAP) model (Bartnicki et al., 2004b) has been used for simulating tropospheric and stratospheric dispersion of radioactive particles emitted from each of three selected explosions in Novaya Zemlya on 12.10.1958, 15.10.1958 and 18.10.1958. The results of the model simulation for 20 October at 16:00 UTC in the form of model particle locations are shown in Fig. 1.

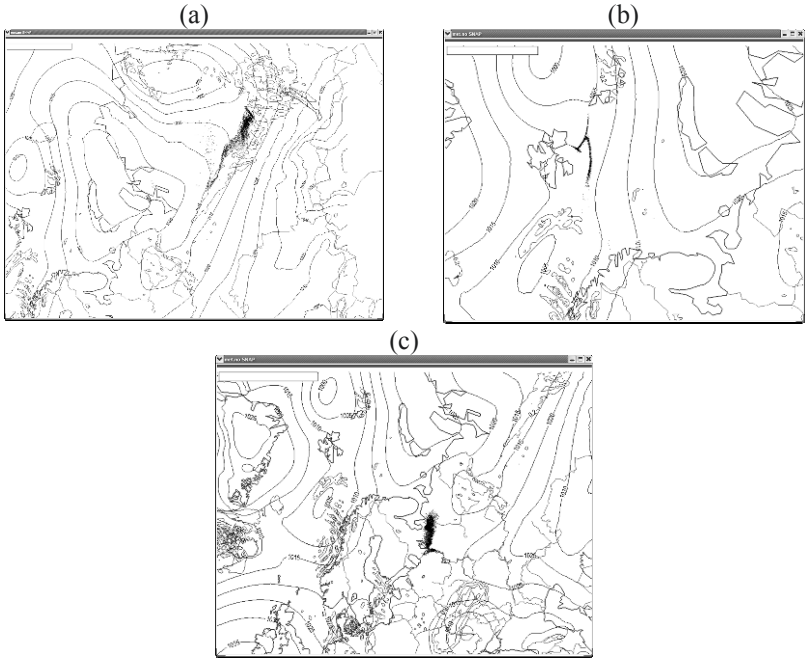


**Fig. 1.** The locations of model particles on 20 October 1958 released during three nuclear explosions: (a) On 12 October, (b) on 15 October, and (c) on 18 October 1958. Particles at all vertical levels are shown. The isolines of the Mean Sea Level Pressure and precipitation are also shown

The explosive yield for all three bombs was very high: 1.45, 1.5 and 2.9 Mt for the releases on 12th, 15th and 18th October, respectively. For all explosions, the initial shape of the radioactive cloud simulated in the model was of the form of mushroom formed by two cylinders. The radius of the lower cylinder was about 2.5 km and upper cylinder 17.5 km. The base of the upper cylinder was about 13.5 km and its top at approximately 21.5 m. Total released activity was assumed $2 \times 10^{22}$ Bq. The same parameters were used for all three explosions in the SNAP model simulations.

The model simulations for the three selected explosions have shown that the radioactive clouds of particles emitted during these explosions were located outside the Norwegian territory on 20 October 1958. However, the radioactive cloud from the second explosion (15.10.1958) passed the Northern Norway on the way to its final destination on 20 October. The model simulations once again confirmed that the direct transport from Novaya Zemlya to Bergen was not responsible for the high level of activity measured in Bergen on 20 October 1958.

As meteorological input for the model runs has been generated by running the high resolution limited area model HIRLAM version 7.1.3. (Unden et al., 2002). HIRLAM has been running on ERA40 data (Uppala et al., 2005), using a blending method (Yang, 2005).

## 2. Model Simulation of Stratospheric Intrusion

The SNAP model was also applied to simulate the stratospheric intrusion of radioactive particles for the episode of high measured activity on 20 October 1958, in the Norwegian territory close to Bergen. The case of stratospheric intrusion was strongly indicated by the analysis of potential vorticity shown in Fig. 2a. (Saltbones et al., 2007).

In order to simulate this affect with the SNAP model we placed a large cloud of the model particles in the stratosphere, in the range 1,000–2,000 km upwind from Bergen, as an initial condition for the model run. The results of the model simulation are shown in Fig. 2b in the form vertical cross-section with the model particle locations. They confirmed the earlier findings about the effect of stratospheric intrusion as the major mechanism leading to high level of radioactivity measured on 20 October 1958 in Bergen.

a) b)

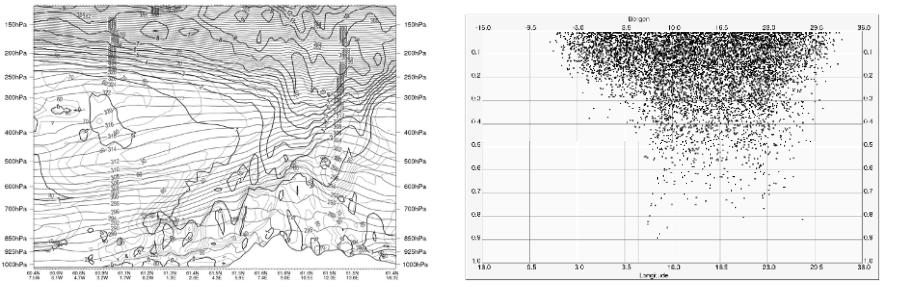

**Fig. 2. (**a) Vertical cross-section near Bergen showing potential vorticity, potential temperature and relative humidity for 20 October 12 UTC. (b) Vertical locations of model particles for the same cross-section as (a)

## 3. Conclusions

Numerical simulations performed with the SNAP model confirmed that the direct transport of radioactivity from Novaya Zemlya to Bergen, related to three large nuclear explosions on 12th, 15th and 18th October 1958 did not take place. Therefore, the elevated levels of radioactivity measured in Bergen on 20 October 1958 can not be explained in this way. On the other hand, analysis of potential vorticity together with the model simulation of stratospheric intrusion on 20 October 1958 strongly indicate, that this is the most likely mechanism causing high level of radioactivity measured in Bergen. This study is an example of the SNAP model application to historical simulations with the use of meteorological data from the ERA40 re-analysis.

## References

Bartnicki J., Foss A. and J. Saltbones, (2004a) Analysis of trajectories related to nuclear bomb tests performed in Novaya Zemlya. Met.no Note 9. Norwegian Meteorological Institute. Oslo, Norway.

Bartnicki J., B. Salbu, J. Saltbones, A. Foss and O. C. Lind (2004b) Long-range transport of large particles in case of nuclear accident or explosion. In: *Air Pollution Modelling and Its Application XVI* (C. Borrego and S. Incecik, eds). Kluwer Academic/Plenum Publishers. pp. 77–86.

Bergan D.T., Bartnicki J., Dowdal M., Foss A. and J. Saltbones, 2005, Analysis of trajectories related to nuclear bomb tests performed at Novaya Zemlya. In: Proceedings from The 6th International Conference on Environmental Radioactivity in the Arctic & Antarctic, 2–6 October 2005 in Nice, France (P. Strand, P. Børretzen and Torun Jølle, eds). Norwegian Radiation Protection Authority, Østeraas, Norway 2005. pp. 77–86.

Saltbones J., J. Bartnicki, T. Bergan, B. Salbu, B. Rosting, H. Haakenstad (2007) Analysis of atmospheric transport of radioactive debris related to nuclear bomb tests performed at Novay Zemlya. Proceedings of the 29th NATO/SPS INTERNATIONAL TECHNICAL MEETING ON AIR POLLUTION MODELLING AND ITS APPLICATION. 24–28 September 2007 Aveiro, Portugal.

Undén, P., Rontu, L., Järvinen, H., Lynch, P., Calvo, J., Cats, G., Cuaxart, J., Eerola, K., Fortelius, C., Garcia-Moya, J.A., Jones, C., Lenderlink, G., McDonald, A., McGrath, R., Navascues, B., Nielsen, N.W., Ødegaard, V., Rodriguez, E., Rummukainen, M., Rööm, R., Sattler, K., Sass, B.H., Savijärvi, H., Schreur, B.W., Sigg, R., The, H. and Tijm, A. (2002) HIRLAM-5 Scientific Documentation, HIRLAM-5 Project. Available from SMHI, S-601767 Norrköping, Sweden.

Uppala S.M. et al. (2005) The ERA40-reanalysis. Q.J.R. Meteorol. Soc. 131, pages 2761–2779.

Yang, X. (2005) Background blending using an incremental spatial filter, Hirlam Newsletter, 49, pages 3–11.

# 2.30 Experimental Determination of the Partition Coefficient for Bifunctional Carbonyls in the Atmosphere and in Smog Chamber

**Ricardo Ortiz, Kenji Enya, and Kazuhiko Sakamoto***

Graduate School of Science and Engineering, Saitama University, 255 Shimo-okubo, Sakura, Saitama 338-8570, Japan

**Abstract** Bifunctional carbonyls can undergo heterogeneous reactions producing species with lower vapor pressure and increase their abundance in the particulate phase. Hence, the predicted aerosol production by these compounds is sometimes underestimated. Atmospheric concentrations of bifunctional carbonyls in gaseous and particulate phases during summer from 2003 to 2006 in the Kanto region, Japan, were measured and their partition coefficients calculated. Additionally smog chamber experiments of toluene oxidation were carried out and the partition coefficient of bifunctional carbonyls experimentally determined. Our results showed that the distribution of these species to the particulate phase is higher in the atmosphere than in chamber experiments, and these values are higher than those predicted thermodynamically. In average, the Log *K*p values measured in the atmosphere were 3.73 times higher for glyoxal and 12.37 times higher for methylglyoxal than those measured in the smog chamber.

**Keywords** Bifunctional carbonyls, Field measurements, PFBHA derivatization, Partition coefficient

## 1. Introduction

The transformation and dynamics of aerosol particles complicate the description of the life and fate of particles. Temporal and geographical distribution of activities and sources in combination with climate and topography influence the aerosols composition. Organic carbon is a ubiquitous component in the aerosol, however, its aerosol-phase chemistry is not well understood yet and hence, it is not included in many atmospheric models (Molina et al., 2004). Partitioning of semi-volatile organics affect the evolution of organic aerosol, photochemical reactions generate compounds with lower vapor pressure that will be partially

* Corresponding author: Tel/Fax: +81-48-858-9542; E-mail: sakakazu@env.gse.saitama-u.ac.jp

D.G. Steyn and S.T. Rao (eds.), *Air Pollution Modeling and Its Application XX*,
DOI 10.1007/978-90-481-3812-8, 

adsorbed into particulate material forming secondary organic aerosol (SOA). Partitioning alters the composition of organic material in the aerosol by fresh emissions; dilution by fresh air masses; change in temperatures; and chemical reactions. If sufficient material is changed from high volatile into low volatile, these new material will tend to condense, increasing the aerosol phase (Donahue et al., 2006).

Kalberer et al. (2006) found compounds with molecular weights up to 700 Da in Zurich aerosol. Increasing molecular weight coincided with 6–8 h of absorption of low-molecular oxidized compounds from the gaseous phase. Organic layers in the aerosol phase are able to react with OH radical and even with $Cl^-$. Molina et al. (2004) found that organic layers react with $H_2O$, NO, $NO_2$, $O_2$, HONO, $HNO_3$ or mixtures of them when OH radical is present, these reactions in the aerosol interface can volatilize the aerosol.

Field species-resolved chemical evolution of aerosols is so complicated that reports of it are almost non-existent. Efforts on trying to describe such processes consist basically on air quality models development. It can be surmised in the fact that, it is necessary to understand the chemical and physical transformations in the atmosphere, but these processes are too complicated due to the movement of air masses. Therefore, it is common to find that, compared to actual atmospheric values, models under-predict aerosol formation. This work is focused on the measurement of concentrations of bifunctional carbonyls in gaseous and particulate phases to determine their partition coefficients in the urban atmosphere and surrounding areas, as well as in smog chamber experiments, in order to evaluate their variation and its correlation to the variation of atmospheric conditions and pollutants concentrations

## 2. Experimental

Atmospheric concentrations of bifunctional carbonyls in gaseous and particulate phases were measured during summer from 2003 to 2006 in the Kanto region, Japan, with a sampling system we developed and described elsewhere (Ortiz et al., 2009) and their partition coefficients were calculated. Additionally smog chamber experiments of toluene oxidation were carried out and the partition coefficients of bifunctional carbonyls experimentally determined. Samples were taken with a time resolution of 5.5 h in four periods a day, starting from 06:00. Analysis was carried out by a GC-MS after the bifunctional carbonyl compounds were double derivatized with O-(2,3,4,5,6-pentafluorobenzyl)hydroxylamine hydrochloride (PFBHA) (which was also used as sorbent in the sampling system) and N,O-bis(trimethylsilyl)-trifluoroacetamide (BSTFA).

## 3. Results

The partition coefficient was proposed by Pankow (1997) and he defined it as Log $K$p = Log ([F]/[A]) – Log [TSP] (where F represents the particulate concentration of a given compound, A represents its gaseous concentration, TSP represents the concentration of the total suspended particles). For field results, we calculated an approximation to this partition coefficient by using suspended particulate matter (SPM) instead of TSP (SPM is defined in this work as the particulate matter below 7 μm of aerodynamic diameter, and it is measured by the β-ray attenuation method) (Takahashi et al., 2007). For chamber experiments, TSP was evaluated by integration of particle size distributions, assuming an aerosol density of 1.5 g $cm^{-3}$ (Kostenidou et al., 2007). Table 1 shows the results for each compound at all sites and in the smog chamber, Meguro site (urban), is situated in the center of Tokyo, all the other sites were situated north of Meguro at different distances, Saitama site (suburban), at 30 km; Kisai site (rural), at 50 km; and Fukaya site (rural), at 70 km.

In the smog chamber, the Log $K$p values for glyoxal ranged from −1.72 to −4.88 and for methylglyoxal ranged from −2.96 to −4.87, while in the atmospheric measurements, Log $K$p value for glyoxal and methylglyoxal ranged from −0.082 to −3.27 and from −0.13 to −3.37, respectively.

**Table 1.** Log $K$p average values measured at different sites

| Compound | Meguro | Saitama | Kisai | Fukaya | Field average | Chamber |
|---|---|---|---|---|---|---|
| Glycolaldehyde | –1.552 | –1.146 | –1.696 | –2.470 | –1.644 | –3.479 |
| Hydroxyacetone | –1.309 | –1.054 | –1.584 | –2.559 | –1.700 | –3.514 |
| Glyoxilic acid | –1.231 | –1.318 | –1.774 | –2.571 | –1.723 | –2.336 |
| Pyruvic acid | –1.442 | –1.062 | –1.901 | –2.668 | –1.694 | –1.998 |
| Glyoxal | –1.512 | –1.184 | –1.938 | –2.279 | –1.630 | –2.946 |
| Methylglyoxal | –1.989 | –0.999 | –1.639 | –1.638 | –1.467 | –3.983 |

In the field, the highest Log $K$p average values were found at Saitama site, and the values were decreasing at longer distances from the city. In the chamber experiments the values found were the lowest. This indicates that the composition and real atmospheric conditions affect the partitioning of these compounds in different ways; therefore the compounds tend to be at higher concentrations in the particulate phase. For example, the presence of salts in the aerosol can make, even at relatively low acidities, some bifunctional carbonyls (e.g., glyoxal) to increase their solubility in water (Ervens and Kreidenweis 2007) or perhaps in the more polar organic compounds. Aerosols undergo a chemical evolution during their lifetime, including the possibility of being evaporated by oxidation reactions with radicals. This evolution also seems to affect the partitioning, as seen in the values on Table 1.

Regarding the effect of humidity on aerosols evolution, Figs. 1 and 2 show the change on the partitioning of glyoxal and methylglyoxal with photochemical age (1-NO/NOx) in the chamber and in the atmosphere respectively. The effect seen is that under high relative humidity (RH), the compounds will evaporate from the particle phase more slowly than under low RH as photochemical age increases.

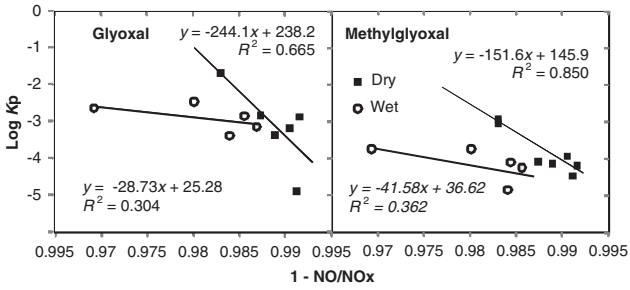


**Fig. 1.** Log *K*p under two different RH levels in the smog chamber

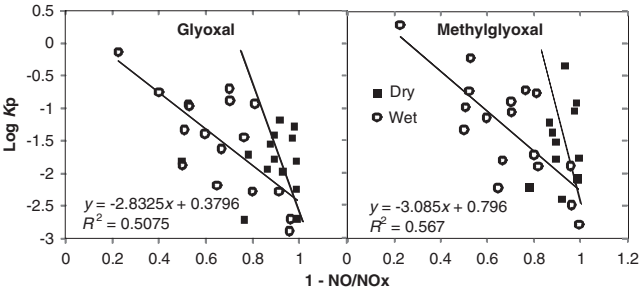


**Fig. 2.** Log *K*p under high and low RH levels in the field

In the chamber, the decrease of the log *K*p value for glyoxal was 8.3 times faster under dry conditions than under wet conditions, and only 3.6 times faster for methylglyoxal, which is according with their solubility in water. This fact also indicates that equilibrium between phases also depends on their evolution in time, if we consider that in the field the aerosol is transported from central Tokyo to its downwind regions, the results in Table 1 can be expected, since the age of transported aerosol increases at farther areas. Hence a different partitioning was found at the different sites under similar atmospheric conditions.

## 4. Concluding Remarks

The partition coefficient of six bifunctional carbonyl compounds was calculated from concentrations measured in the field, at an urban, a suburban and two rural sites. Our findings include that even if the effect of variables like humidity and

photochemical age are important on the partitioning of these compounds, the partitioning in the field still shows big differences with the partitioning in the chamber experiments (3.73 times higher for glyoxal and 12.37 times higher for methylglyoxal).

## References

Donahue, N.M., Robinson A.L., Stanier, C.O., Pandis, S.N.: Coupled partitioning, dilution and chemical aging of semivolatile organics. Environ. Sci. Technol. 40, 2635–2643 (2006)

Ervens, B., Kreidenweis, S.M.: SOA formation by biogenic and carbonyl compounds: Data evaluation and application. Environ. Sci. Technol. 41, 3904–3910 (2007)

Kalberer, M., Sax, M., Samburova, V.: Molecular size evolution of oligomers in organic aerosols collected in urban atmospheres and generated in a smog chamber. Environ. Sci. Technol. 40, 5917–5922 (2006)

Kostenidou, E., Pathak R.K., Pandis, S.N.:An algorithm for the calculation of secondary organic aerosol density combining AMS and SMPS data. Aerosol Sci. Technol. 41, 1002–1010 (2007)

Molina, M.J., Ivanov, A.V., Trakhtenberg, S., Molina, L.T.: Atmospheric evolution of organic aerosol. Geophys. Res. Lett. 31, L22104 (2004)

Ortiz, R., Enya, K., Sekiguchi, K., Sakamoto, K.: Experimental testing of an annular denuder and filter system to measure gas-particle partitioning of semivolatile bifunctional carbonyls in the atmosphere, Atmos. Environ. 43, 382–388 (2009)

Pankow, J.F.: Review and comparative analysis of the theories on partitioning between the gas and aerosol particulate phases in the atmosphere. Atmos. Environ. 21, 2275–2290 (1987)

Takahashi, K., Minoura, H., Sakamoto, K.: Examination of discrepancies between β-attenuation and gravimetric methods for the monitoring of PM. Atmos. Environ. 42, 5232–5240 (2008)

# 2.31 Forecasting Sulphur and Nitrogen Oxides, Ozone and Aerosols as Key Components of Chemical Weather

**J. Soares, M. Sofiev, M. Prank, and J. Kukkonen**

Finnish Meteorological Institute, FI-00101 Helsinki, Finland

**Abstract** Tropospheric aerosols and ozone are the key pollutants of the greatest concern for the public health. This paper presents the chemical modules in development in SILAM and to-date verification against observed concentrations in Europe and global remote-sensing optical information. The comparisons show that SILAM reproduces relatively well the concentrations of the main precursors for ozone production, and the concentration patterns of sea salt aerosol.

**Keywords** Modeling, SILAM, photochemistry, sea salt aerosol

## 1. Introduction

The focus on the short-term forecasting of the atmospheric chemical composition has posed several specific requirements to existing and developing chemical transport models. The goal of the current study is to describe the modules currently in development in SILAM: the photochemical and the sea salt emission module. We also discuss the model applications at regional and global scales and compare the model results with in situ measurements and global remote-sensing optical information for the years 2000 and 2001.

## 2. Methodology

### 2.1. Modelling tool and input data

The modelling tool used in this study is the Air Quality and Emergency Modelling System, SILAM (Sofiev et al., 2008a). SILAM incorporates a both Lagrangian and Eulerian advection-diffusion formulations. The Eulerian scheme (Galperin, 1999, 2000) combines horizontal diffusion with the advection module (the scheme itself has zero numerical viscosity) while the vertical exchange follows the extended resistance analogy scheme of Sofiev (2002). A physico-chemical module of SILAM includes basic SOx-NOx-NHx-VOC-O3 chemistry, a linearized scheme

D.G. Steyn and S.T. Rao (eds.), *Air Pollution Modeling and Its Application XX*,
DOI 10.1007/978-90-481-3812-8, 

for sulphur oxides, primary particles of various types, with flexible definition of the particle size spectrum, and about 500 radioactive nuclides.

### 2.2. Basic-chemistry scheme and sea salt emission parameterization

The current SILAM basic-chemistry scheme covers 21 transported and 5 short-lived substances, which are inter-related via ~60 chemical reactions. This mechanism covers the most important transformation chains for the photochemical smog formation (except for some of the VOC oxidation pathways that have been parameterized in a simplified manner) and takes into account the main reservoir substances. To reach a sufficient numerical efficiency of the scheme, all reactions are segregated in accordance with their actual rates (in relation to the model time step), split to day- and night-time processes and treated via forced-equilibrium, first-order explicit or third-order implicit numerical algorithms. Other matters such as: emission of biogenic ozone precursors, boundary conditions for long-living substances, and proper representation of the solar radiation are addressed.

Within this study, the "classical" parameterization of Monahan et al. (1986) was applied as the reference formulation and extrapolated towards fine particles following the laboratory results from Mårtensson et al. (2003). This resulted in a unified function for particle sizes from 20 nm to 10 μm, for a reference water temperature of 23°C and salinity 3.3%, and two correction functions for temperature/salinity with particle size dependency (Sofiev et al., 2010).

The chemical scheme development and evaluation was based on year 2000, with source emission provided by EMEP and TNO. Sea salt parameterization was evaluated based on the year 2000 for European and Northern Atlantic region, and 2001 for the globe. The water temperature was set constant for both regional and global run, 12°C, and salinity of the Ocean was set constant, 33‰. For the sea salt evaluation, five size bins were described with the following ranges: 20 nm to 0.1 μm, f 0.1 to 1 μm, 1–2.5 μm, 2.5–10 μm, and 10–30 μm. Depending on the particle size, mechanisms for dry deposition vary from primarily diffusion-driven removal characteristic (fine aerosols) to primarily gravitational settling (coarse particles). Wet deposition distinguished sub- and in-cloud scavenging by both rain and snow (Sofiev et al., 2006).

## 3. Results and Discussion

The evaluation of the basic chemistry scheme was based on information from the database of the European Monitoring and Evaluation Programme, EMEP (www.emep.int). The basic chemistry and transport mechanisms allow the system to follow fairly accurately the evolution of primary emitted and secondary pollutant concentrations throughout the year (Fig. 1).

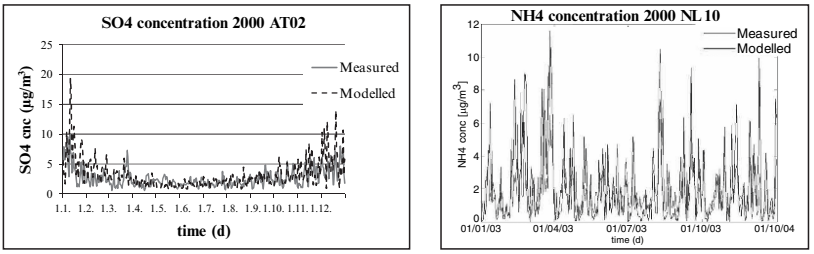


**Fig. 1.** SILAM hourly predictions vs. measurement data from EMEP stations, 2000. Left-hand panel: NO2 in air, Illmitz, Austria (AT02); Right-hand panel: NH4 in air, Vredepeel, The Netherlands (NL10) [µg $m^{-3}$].

Observations of sea salt, apart from dedicated experimental campaigns, are available in three forms: (a) a few sites of the EMEP network performing regular measurements of Na in aerosol (Fig. 2, left-hand panel); (b) several EMEP stations perform ion analysis of precipitation including Na+ (Fig. 2, right-hand panel); (c) satellite retrievals of aerosol optical depth in column (AOD) can be considered representative for sea salt in remote regions of the southern hemisphere (Gong et al., 1997, with care taken to distinguish sea salt AOD from that of e.g. biomass burning plumes, Fig. 4). The model predicted the temporal variation fairly well, but overestimates the concentrations by about a factor of 2 (on the annual average level). The correlation of the predicted and measured hourly time series was ~0.50 on the average for all stations.

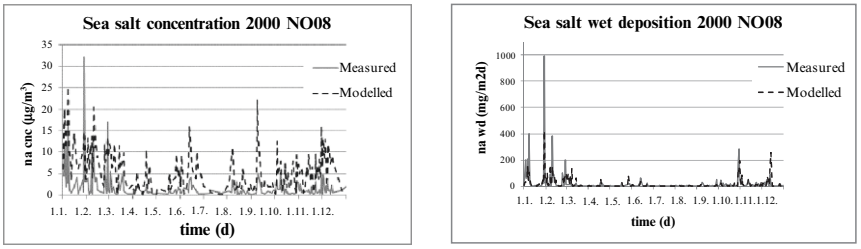


**Fig. 2.** SILAM hourly predictions vs. measurement data from EMEP stations, 2000. Left-hand panel: Na+ in aerosol (µg $m^{-3}$); right-hand panel Na+ wet deposition, Skreådalen, Norway (NO08) (mg $m^{-2}$ $day^{-1}$)

The global simulations were evaluated using the AOD observed by the MODIS instrument onboard the NASA satellites Aqua and Terra. AOD is a column-integrated optical parameter, which is more sensitive to number concentrations than to the mass of aerosols; therefore AOD-based comparison is complementary to the above analysis. This evaluation is only qualitative since we have not analysed non-sea salt PM constituents (Fig. 3).

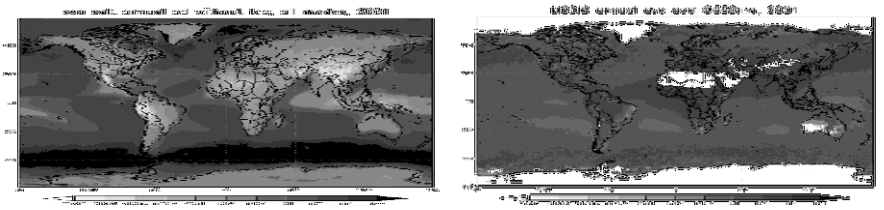

**Fig. 3.** Column-integrated predicted and measured AOD averaged over 2001. Left-hand panel: AOD caused by the sea salt concentrations predicted by SILAM; right-hand panel: observed by the NASA MODIS instrument

Higher predicted sea salt concentrations and measured AOD occurred in the southern hemisphere, where there is a larger fraction of sea area, and the wind velocities are higher. The comparisons with EMEP data show that SILAM tends to over-predict the sea-salt concentrations, in average, staying within a factor of 2 from the concentrations.

## 4. Conclusions

The basic chemical transformation scheme captures the main features of the inorganic species and their reactions. The ozone-formation mechanisms require further development. The sea salt emission parameterisation seems to predict fairly well the spatial and temporal variation for the considered particle size ranges. However, the new model for sea salt production over-estimates both near-surface concentrations, where the coarse mode plays the main role, and also the column-integrated optical density, which is primarily influenced by fine particles.

**Acknowledgments** The financial support by the GEMS and PROMOTE projects, the Maj and Tor Nessling Foundation and COST ES0602 is gratefully acknowledged.

## References

Galperin M.V. 1999. Approaches for improving the numerical solution of the advection equation. In: Large-Scale Computations in Air Pollution Modelling (ed. by Z. Zlatev et al.) Proc. NATO Advanced Research Workshop on Large Scale Computations in Air Pollution Modelling, Sofia, Bistritza, July 6–10, 1998, Kluiwer Academic Publishers, The Netherlands, pp. 161–172

Galperin M.V. 2000. The Approaches to Correct Computation of Airborne Pollution Advection. In: Problems of Ecological Monitoring and Ecosystem Modelling, vol. XVII, St. Petersburg, Gidrometeoizdat, pp. 54–68 (in Russian).

Gong, S.L., Prospero, J.M., Savoie, D. L., Ayers, G. P. Blanchet, J.-P. and Spacek, L. 1997. Modeling sea-salt aerosols in the atmosphere.2: Atmospheric concentration and fluxes. J. Geophys. Res. 102: 3819–3830.

Monahan, E. C., D. E. Spiel, and K. L. Davidson, 1986, A model of marine aerosol generation via whitecaps and wave disruption, in Oceanic Whitecaps, edited by E. C. Monahan and G. MacNiochaill, pp. 167–193, D. Reidel, Norwell, Mass.

Mårtensson, E.M., Nilsson, E.D., de Leeuw, G., Cohen, L.H, Hansson, H-C. 2003. Laboratory simulations and parameterization of the primary marine aerosol production. JGR, **108**, NO. D9, 4297, doi:10.1029/2002JD002263

Sofiev, M., 2002. Extended resistance analogy for construction of the vertical diffusion scheme for dispersion models. J. of Geophys.Research – Atmosphere, 107, D12, doi: 10.1029/2001JD001233.

Sofiev, M., Siljamo, P. Valkama, I., Ilvonen, M. and Kukkonen, J. 2006. A dispersion modeling system SILAM and its evaluation against ETEX data. Atmospheric Environment 40:674–685

Sofiev, M., Galperin, M., Genikhovich, E. 2008a. Construction and evaluation of Eulerian dynamic core for the air quality and emergency modeling system SILAM. NATO Science for piece and security Serties C: Environmental Security. Air pollution modelling and its application, **XIX**, Borrego, C., Miranda, A.I. (eds.), Springer, pp. 699–701

Sofiev, M., Soares, J., Prank, M., de Leeuw, G. and Kukkonen, J. 2010. A regional-to-large-scale model of emission and transport of sea salt particles in the atmosphere (in preparation)

# 2.32 Regional Background Fine Particulate Matter

**Sergey L. Napelenok[1], Jeffrey Arnold[1], Kristen M. Foley[1], and Daven K. Henze[2]**

[1]United States Environmental Protection Agency

[2]University of Colorado, Boulder, CO, USA

**Abstract** A modeling system composed of the global model GEOS-Chem providing hourly lateral boundary conditions to the regional model CMAQ was used to calculate the policy relevant background level of fine particulate matter. Simulations were performed for the full year of 2004 over the domain covering the continental United States. The influence on particulate matter from boundary conditions was quantified using the decoupled direct method in three dimensions. Similar to base CMAQ particulate concentrations themselves, background levels and the influence of the boundaries were found to be highly variable spatially and temporally in the domain. Particulate matter background levels were found to range between 0.62 and 1.72 μg/m$^3$ averaged annually with higher values in the southeastern part of the domain subject to high concentrations of organics from fire emissions and the formation of secondary organic aerosols. The influence from the boundary ranged 0.39–0.53 μg/m$^3$ averaged annually.

## 1. Introduction

Due to recent gains in scientific understanding of the processes governing formation and transport of air pollutants, as well as technological advances in pollutant control, ambient concentrations of ozone and particulate matter (PM) have decreased significantly over the past decade over the European and North American continents. However, further improvements in air quality are both feasible and necessary in order to reduce unhealthy levels of exposure and to improve visibility. As air quality standards tighten to target further reductions in PM, ozone, and other species, the concept of the background or natural concentration of pollutants becomes more important. This quantity is useful to the regulatory communities where it is also known as the policy relevant background (PRB). Here, the PRB of fine particulate matter ($PM_{2.5}$) is investigated by region in the United States for the full year of 2004. For the purposes of this analysis, PRB is defined as the pollutant concentrations resulting from non-anthropogenic emissions sources within North America and all emissions sources elsewhere.

D.G. Steyn and S.T. Rao (eds.), *Air Pollution Modeling and Its Application XX*,
DOI 10.1007/978-90-481-3812-8, © Springer Science + Business Media B.V. 2010

## 2. Method

The 2004 regional scale simulation was performed using the CMAQ model version 4.7 (Byun and Schere, 2006) instrumented with the decoupled direct method in three dimensions (DDM-3D) (Napelenok et al., 2008). Standard model configuration was used including the inverse donor-cell advection scheme, eddy diffusion, saprc99 chemical mechanism, and asymmetric convective cloud module. Regional meteorology was processed using MM5, and emissions were processed using SMOKE based on the National Emission Inventory (2002 NEI). Two emissions scenarios were considered and compared: one using a standard emissions inventory; and one with only "natural" emissions sources. The biogenic sources included processes such as volatile organic compounds (VOCs) emissions from plants, nitrogen oxide (NO) emissions from soil, various compounds from wildfires, etc. Emissions from prescribed non-agricultural burning are also included in the PRB calculation, because these are used for land management to prevent more devastating wildfires.

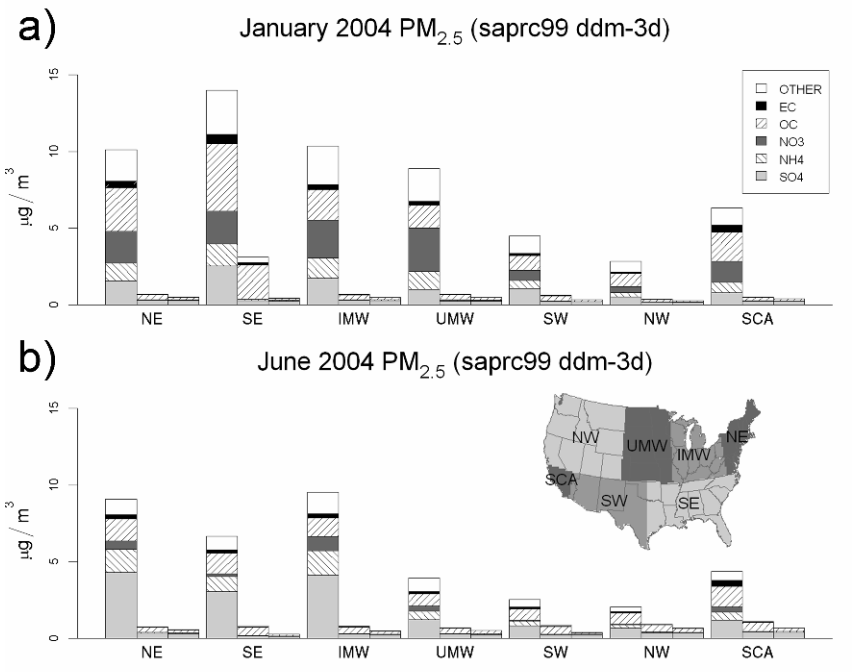


**Fig. 1.** Regional $PM_{2.5}$ concentrations in January and August, 2004 for base case, PRB, and the influence from the boundary for each region

To account for the influence of long-range transport on background $PM_{2.5}$ concentrations, the global chemical transport model, GEOS-Chem version 7-04-11, was used to provide hourly lateral boundary conditions for the full simulation

period. Recent improvements to processes governing the formation of secondary organic aerosols were included in this model version (Henze et al., 2008). Global emissions were developed using the Emission Database for Global Atmospheric Research (Olivier et al., 1999) supplemented with more detailed inventories where available, such as the European Monitoring and Evaluation Program (Auvray and Bey, 2005).

The domain was divided into seven regions for analysis (Fig. 1): Northeast (NE), Southeast (SE), Industrial Midwest (IMW), Upper Midwest (UMW), Southwest (SW), Northwest (NW), and Southern California (SCA). Influences on background particulate matter concentrations on each region were evaluated geographically (intercontinental transport or local) and by chemical precursor (primary, secondary organic and inorganic species, etc.) by calculating sensitivity coefficients using DDM-3D.

## 3. Results and Discussion

Both base $PM_{2.5}$ concentrations and the PRB show highly variable spatial and temporal patterns (Fig. 2). Wintertime $PM_{2.5}$ concentrations are composed of approximately equal parts of sulfate, ammonium, nitrate, organic carbon, and another nonreactive compounds (Fig. 1). In the summer, sulfate fraction becomes more dominant, while nitrate decreases. Total concentrations are higher in the winter months for all regions. Averaged PRB values are fairly constant throughout the domain at under 1.0 $\mu g/m^3$ except in Southeastern region (Table 1). In SE, organic PM from primary emissions from wild fires and secondary organic aerosol formation results in the highest modeled annual PRB of 1.72 $\mu g/m^3$. The influence from the boundaries manifests primarily in elevated sulfate and organic carbon concentrations with significant spatial and temporal variability (Table 1).

**Table 1.** Annually averaged $PM_{2.5}$ concentrations in $\mu g/m^3$ for the base run, PRB, and the boundary influence

| | Base | PRB | Boundary |
|---|---|---|---|
| Northeast | 9.76 | 0.74 | 0.52 |
| Southeast | 10.05 | 1.72 | 0.50 |
| Industrial Midwest | 11.38 | 0.86 | 0.51 |
| Upper Midwest | 6.70 | 0.84 | 0.54 |
| Southwest | 3.30 | 0.62 | 0.38 |
| Northwest | 2.72 | 1.01 | 0.46 |
| Southern California | 4.43 | 0.84 | 0.53 |

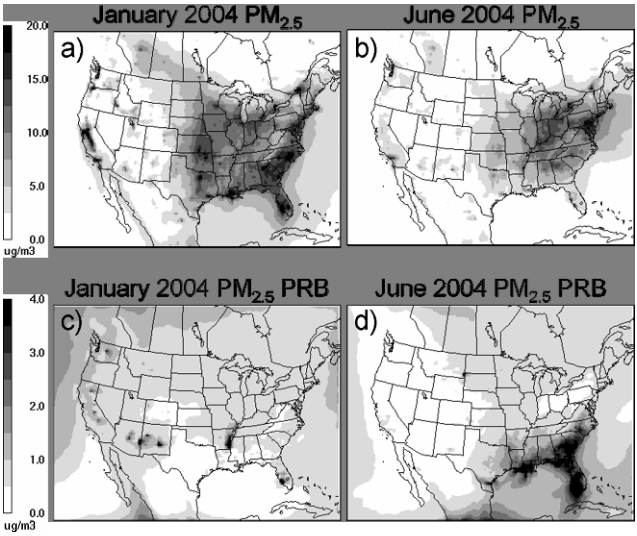


**Fig. 2.** Monthly averaged $PM_{2.5}$ concentration and PRB for January and June of 2004

## References

Auvray M., and Bey, I., 2005. Long-Range Transport to Europe: Seasonal Variations and Implications for the European Ozone Budget, *J. Geophys. Res*. 110, D11303.

Byun, D.W., Schere, K.L., 2006. Review of the governing equations, computational algorithms, and other components of the Models-3 Community Multiscale Air Quality (CMAQ) modeling system. *Appl. Mech. Rev*., 59, 51–77.

Henze, D.K., Seinfeld, J.H., Ng, N.L., Kroll, J.H., Fu, T.-M., Jacob, D.J., Heald, C.L., 2008. Global modeling of secondary organic aerosol formation from aromatic hydrocarbons: high- vs. low-yield pathways. *Atmos. Chem. Phys*., 8, 2405–2420.

Napelenok, S.L., Cohan, D.S., Odman, M.T., Tonse, S., 2008. Extension and evaluation of sensitivity analysis capabilities in a photochemical model. *Environ. Modell. Softw*., 23, 994–999.

Olivier, J.G.J., Bouwman, A.F., Berdowski, J.J.M., Veldt, C., Bloos, J.P.J., Visschedijk, A.J.H., Van der Maas, C.W.M., and Zandveld, P.Y.J., 1999. Sectoral emission inventories of greenhouse gases for 1990 on a per country basis as well as on 1 × 1 degree, *Environ. Sci. Policy*, 2, 241–264.

# Chapter 3 Data assimilation and air quality

Chairperson: G. Kallos

Rapporteur: B. Pun

D.G. Steyn and S.T. Rao (eds.), *Air Pollution Modeling and Its Application XX*,
DOI 10.1007/978-90-481-3812-8_3, © Springer Science + Business Media B.V. 2010

# 3.1 Implementation of Real-Time Bias-Corrected $O_3$ and $PM_{2.5}$ Air Quality Forecast and Their Performance Evaluations During 2008 over the Continental United States

**Daiwen Kang[1*], Rohit Mathur[2], and S. Trivikrama Rao[2]**

[1]Computer Science Corporation, Research Triangle Park, 79 T.W. Alexander Drive, NC 27709, USA

[2]Atmospheric Modeling Division, National Exposure Research Laboratory, U.S. Environmental Protection Agency, Research Triangle Park, NC, 27711, USA

**Abstract** Real-time bias-corrected $O_3$ and $PM_{2.5}$ forecast systems are implemented using the Kalman Filter, combining observations from AIRnow and outputs from the NOAA/EPA's NAM/CMAQ air quality forecast model. Bias-corrected $O_3$ and $PM_{2.5}$ forecasts are created at locations of the AIRNow monitoring network where report hourly concentrations of these species. Observations and model outputs from two previous consecutive days are required to produce bias-corrected model forecasts. The performance of these systems is examined on a daily basis using $O_3$ and $PM_{2.5}$ observations and the results are compared with raw model forecasts. The overall performance of the Kalman filtering technique and its capability to produce a real-time bias correction to improve the day-to-day forecast from the NAM-CMAQ modeling system during 2008 is investigated. Performance evaluation trough detailed time-series analysis and regional analysis will be presented. The ability of the technique in improving the prediction of daily 8-hr maximum $O_3$ and daily mean $PM_{2.5}$ as well as its impacts on false-alarms will be examined through the use of statistical categorical metrics.

**Keywords** Air quality forecast, Bias-adjustment, $O_3$, $PM_{2.5}$, Kalman filter

## 1. Introduction

Ozone ($O_3$) and fine particulate matter ($PM_{2.5}$; particles with aerodynamic diameters less than 2.5 μm) air pollution is of concern due to their adverse effect on human and ecosystem health. Ambient levels of $O_3$ and $PM_{2.5}$ are the two primary components used in the calculation of the Air Quality Index (AQI), a standardized

* E-mail: kang.daiwen@epa.gov; Voice (919) 541-2460, Fax (919) 541-1379

D.G. Steyn and S.T. Rao (eds.), *Air Pollution Modeling and Its Application XX*,
DOI 10.1007/978-90-481-3812-8, © Springer Science + Business Media B.V. 2010

indicator of air quality degradation at a given location. The National Oceanic and Atmospheric Administration (NOAA), in partnership with the United States Environmental Protection Agency (EPA), is operationally implementing an Air Quality Forecast (AQF) system. This program, which couples NOAA's North American Mesoscale (NAM) weather prediction model with EPA's Community Multiscale Air Quality (CMAQ) model, has provided forecasts of ozone ($O_3$) mixing ratios since 2004. Developmental $PM_{2.5}$ forecasts were initiated in 2005 (Mathur et al., 2008). The modeling domain for both the operational and developmental predictions currently covers the continental U.S. (CONUS).

Bias-adjustment techniques have been used to correct systematic biases in surface $O_3$ predictions (Delle Monache et al., 2006; Wilczak et al., 2006; Kang et al., 2008), and more recently have also been extended for $PM_{2.5}$ forecasts (Kang et al., 2009). Among these techniques, Kalman Filter (KF) predictor forecast method has shown the most improvement in forecast skill. To test the applicability of the methods in an operational real-time setting, during 2008 the KF bias-adjustment technique (Kang et al., 2008, 2009) was implemented in near real-time along with the NAM/CMAQ AQF system to provide daily bias-adjusted $O_3$ and $PM_{2.5}$ forecasts at all the locations where observations from EPA's AIRNOW network were available within the CONUS domain. The bias-adjusted $O_3$ forecasts were performed from the beginning of April to the middle of September covering the entire $O_3$ season, and the $PM_{2.5}$ bias-adjusted forecasts were conducted through the whole year. In this paper, the preliminary performance evaluations of the KF bias-adjusted $O_3$ and $PM_{2.5}$ forecasts are presented. To facilitate performance evaluations for $PM_{2.5}$, the study period is divided into cold season (from January to April 20 and from September to December) and warm season (from April 21 to August 31).

## 2. Implementation of the KF Bias-Adjustment Method

The KF predictor bias-adjustment algorithm is described in detail by Delle Monache et al. (2006). The adaptation and implementation of the technique in our applications is presented in Kang et al. (2008). Also in our previous study (Kang et al., 2008), the error ratio, a key parameter in the KF approach which determines the relative weighting of observed and forecast values, was investigated extensively with $O_3$ forecasts at over 1,000 monitoring locations. Even though the optimal error ratios inherent in the KF algorithm implementation were found to vary across space, the impact of using the optimal values on the resultant bias-adjusted predictions was insignificant when compared with using a reasonable single fixed value of this parameter for all the locations within the modeling domain. In this study, the same single fixed error ratio value of 0.06 was used to all the locations for the real-time bias-adjusted $O_3$ and $PM_{2.5}$ forecasts.

The KF bias-adjustment technique was implemented for $O_3$ and $PM_{2.5}$ forecasts separately. First, the KF was initialized with the initial estimates of KF parameters as outlined in Kang et al. (2008) and with 2 days of hourly observations and raw

model predictions. It then generated the third day's bias-adjusted forecasts by combining with the third day's raw model forecasts with the updated KF parameters. All the updated KF parameters for each hour and at each site were saved into a file for use in the next KF run. The KF runs then continued by reading the previous day's KF parameters and 2 preceding days' observations and raw model predictions to continuously generate the next day's bias-adjusted forecasts through combining with the next day's raw model forecasts. The KF simulations run daily when the preceding day's observations and the raw model forecasts for next day (issued on current day) were available. In our implementation, if 2 consecutive days' data were missing at a site, the method would automatically drop this site from future bias-adjustment forecasts; however, if a new site with 2 consecutive days' data appeared in the observation data set, the KF would initialize the site with initial values of KF parameters and generate bias-adjusted forecasts further on. This implementation is very adaptable to the variable nature of monitoring stations which report hourly observations to the AIRNOW network and can be easily combined with AQF system to perform real-time bias-adjusted forecasts. The bias-adjusted forecasts were initialized on January 4 and April 3 for $PM_{2.5}$ and $O_3$ forecasts, respectively, and the programs were run daily on a Linux system; it took less than 10 min of computation to create a bias adjusted forecast.

## 3. Performance Evaluations

Table 1 presents a summary of domain (Dom) and sub-regional mean discrete statistics for the raw model and the KF forecast daily maximum 8-h $O_3$ mixing ratios during the study period. Table 2 presents similar model performance statistics for daily mean PM2.5 concentrations for warm and cold seasons; in each cell, the value on the left of slash (/) is for warm season and the value on the right of the slash is for the cool season; the values in the rows with white background marked with "–mod" represent Table 1. Regional summary of discrete statistics for raw model and KF bias-adjusted daily maximum 8-h $O_3$ forecasts during 2008 summer season statistics associated with raw model forecasts, while those in the rows with shaded background and with the extension "–kf" represent the statistics associated with the KF bias-adjusted forecasts. As seen in Table 1, for daily maximum 8-h $O_3$ forecasts, the Root Mean Square Error (RMSE) values associated with raw model forecasts ranged from 10.4 to 16.0 ppb. The application of the KF bias-adjustment, reduced the RMSE to 8.5–10.5 ppb; on average, this corresponds to more than 25% reduction. Similar reduction was reflected by Normalized Mean Bias (NMB). More remarkable forecast improvement by the KF forecasts over raw model is reflected by the Mean Bias (MB) and Normalized Mean Bias (NMB); the MB values were reduced from several ppb to less than 1 ppb for all the regions, and NMB from as high as 17% to less than 2%. The correlation coefficients (r) also increased systematically from 0.5–0.7 for the raw model to 0.7–0.84 in the KF forecasts. Similar forecast skill improvement in $PM_{2.5}$ forecasts by the KF forecasts over

raw model is shown in Table 2, though compared to $O_3$ forecasts, the overall statistics for $PM_{2.5}$ forecasts still need to be improved due to the difficulty in simulating the complexity of $PM_{2.5}$ formation and distribution by the raw model.

**Table 1.** Regional summary of discrete statistics for raw model and KF bias-adjusted daily mean $PM_{2.5}$ forecasts during 2008 warm/cold season

| TYPE | RMSE (ppb) | NME (%) | MB (ppb) | NMB (%) | R |
|---|---|---|---|---|---|
| Dom-mod | 12.5 | 20.1 | 3.2 | 6.8 | 0.65 |
| Dom-kf | 9.1 | 14.5 | 0.6 | 1.3 | 0.81 |
| NE-mod | 10.6 | 16.9 | 2.7 | 5.6 | 0.70 |
| NE-kf | 8.9 | 13.8 | 0.7 | 1.4 | 0.78 |
| SE-mod | 12.2 | 20.1 | 5.8 | 12.2 | 0.70 |
| SE-kf | 9.1 | 14.7 | 0.5 | 1.1 | 0.80 |
| UM-mod | 10.4 | 17.5 | 2.5 | 5.4 | 0.59 |
| UM-kf | 8.5 | 13.7 | 0.7 | 1.5 | 0.72 |
| LM-mod | 13.6 | 27.0 | 7.0 | 16.9 | 0.64 |
| LM-kf | 9.8 | 17.7 | 0.8 | 1.9 | 0.77 |
| RM-mod | 11.4 | 16.4 | 2.7 | 5.1 | 0.50 |
| RM-kf | 8.9 | 12.8 | 0.7 | 1.3 | 0.70 |
| PC-mod | 16.0 | 21.9 | –3.2 | –5.9 | 0.60 |
| PC-kf | 10.5 | 14.5 | 0.2 | 0.3 | 0.84 |

**Table 2.** Regional summary of discrete statistics for raw model and KF bias-adjusted daily mean $PM_{2.5}$ forecasts during 2008 warm/cold season

| TYPE | RMSE ($\mu g/m^3$) | NME (%) | MB ($\mu g/m^3$) | NMB (%) | R |
|---|---|---|---|---|---|
| Dom-mod | 9.6/10.5 | 47.5/70.5 | –2.3/4.5 | –19.6/45.1 | 0.33/0.53 |
| Dom-kf | 6.6/6.4 | 32.9/42.5 | –0.1/1.7 | –0.4/16.5 | 0.71/0.68 |
| NE-mod | 7.5/12.3 | 39.5/76.1 | –2.4/6.6 | –17.8/59.9 | 0.56/0.63 |
| NE-kf | 5.5/7.3 | 29.1/44.7 | –0.4/2.4 | –2.7/22.1 | 0.76/0.72 |
| SE-mod | 7.8/9.1 | 41.5/62.1 | –3.9/4.6 | –27.5/43.8 | 0.40/0.47 |
| SE-kf | 5.3/5.4 | 27.1/37.2 | –0.4/1.3 | –2.7/12.8 | 0.63/0.58 |
| UM-mod | 6.0/10.7 | 36.6/68.3 | –0.7/6.5 | –6.0/57.4 | 0.58/0.62 |
| UM-kf | 5.0/6.1 | 30.7/37.3 | –0.2/1.7 | –1.7/15.2 | 0.69/0.73 |
| LM-mod | 8.7/9.4 | 52.4/67.7 | –4.0/3.6 | –32.9/36.8 | 0.17/0.32 |
| LM-kf | 5.8/5.9 | 34.9/42.5 | –0.2/1.2 | –1.5/12.2 | 0.37/0.49 |
| RM-mod | 6.4/9.3 | 50.5/75.7 | –1.5/3.5 | –17.2/43.1 | 0.18/0.37 |
| RM-kf | 4.6/5.6 | 33.5/44.4 | 0.0/1.3 | 0.2/16.2 | 0.57/0.62 |
| PC-mod | 15.3/10.2 | 57.9/60.2 | –3.4/1.8 | –30.6/15.8 | 0.23/0.53 |
| PC-kf | 10.5/7.0 | 39.0/40.9 | 0.2/1.2 | 1.9/10.4 | 0.73/0.72 |

It is important for an air quality forecast product to be able to accurately predict exceedance and non-exceedance events (categorical predictions). Categorical evaluations for the raw model and KF bias-adjusted forecasts for daily maximum $O_3$ and daily mean $PM_{2.5}$ concentrations have shown that the KF bias-adjusted forecasts were able to significantly reduce False Alarm Ratio (FAR) values and increase Hit rate (H) values for both daily maximum 8-h $O_3$ forecasts and daily mean $PM_{2.5}$ forecasts.

## 4. Summary

The near real-time KF bias-adjustment technique was applied to NAM-CMAQ $O_3$ and $PM_{2.5}$ air quality forecasts over the continental United States. These bias-adjustment forecasts were implemented to run daily for improving next-day forecasts. The bias-adjustment post-processing adds minimal computational burden; on a daily-basis, it required less than 10 min of CPU on a single processor Linux machine. Hourly $O_3$ and $PM_{2.5}$ bias-adjusted forecasts were provided at all the locations where the observations were available from the AIRNOW network. The performance evaluation of the bias-adjusted forecasts for both $O_3$ and $PM_{2.5}$ has shown significant improvement over the raw model forecasts for a variety of performance evaluation statistical measures. Specifically, errors and biases were systematically reduced, the correlation coefficients were increased, false alarm ratios went down, and hit rates went up. The robustness of this technique was also manifested through time and space and over all the concentration bins; the forecast skills were improved at all the locations within the domain during all the seasons.

## References

Delle Monache, L., T. Nipen, X. Deng, Y. Zhou, and R. Stull (2006), Ozone ensemble forecasts: 2. A Kalman filter predictor bias correction, J. Geophys. Res., 111, D05308, doi:10.1029/2005JD 006311.

Kang, D., B. Eder, A. Stein, G. Grell, S.Peckham, and J. McHenry (2005), The New England air quality forecasting pilot program: development of an evaluation protocol and performance benchmark. *J. Air & Waste Manage. Assoc.*, **55**, 1782–1796.

Kang, D., R. Mathur, S.T. Rao, and S. Yu (2008), Bias adjustment techniques for improving ozone air quality forecasts, *J. Geophys. Res., 113*, D23308, doi: 10.1029/2008JD010151.

Kang, D., R. Mathur, and S.T. Rao (2009), Assessment on bias-adjusted NAM-CMAQ $PM_{2.5}$ air quality forecasts over the continental United States during 2007, in preparation.

Mathur, R., S. Yu, D. Kang, and K. Schere (2008), Assessment of the Winter-time Performance of Developmental Particulate Matter Forecasts with the Eta-CMAQ Modeling System, *J. Geophys. Res.*, doi:10.1029/2007JD008580, 113, D02303.

Wilczak, J., S. McKeen, I. Djalalova, G. Grell, S. Peckham, W. Gong, V. Bouchet, R. Moffet, J. McHenry, P. Lee, Y. Tang, and G. R. Carmichael (2006), Bias-corrected ensemble and probabilistic forecasts of surface ozone over eastern North America during the summer of 2004, *J. Geophys. Res.*, *111*, D23S28, doi:10.1029/2006JD007598.

## 5. Questions and Answers

**Bernard Fisher:** Does the forecast system have to reach a certain level of performance (hit rate, false alarm rate) before the pollution forecasts are made public and operational?

**Answer:** There is official criterion for this. However the air quality forecast program generally requires of the accuracy of 90%.

# 3.2 Particulate-Matter Forecasting with GEM-MACH15, A New Canadian Air-Quality Forecast Model

**M.D. Moran[1], S. Ménard[2], D. Talbot[2], P. Huang[3], P.A. Makar[1], W. Gong[1], H. Landry[2], S. Gravel[1], S. Gong[1], L.-P. Crevier[2], A. Kallaur[4], and M. Sassi[2]**

[1]Air Quality Research Division, Environment Canada, Toronto, Ontario, Canada

[2]Air Quality Modelling Applications Section, Environment Canada, Montreal, Quebec, Canada

[3]Contractor, Toronto, Ontario, Canada

[4]Air Quality Research Division, Environment Canada, Montreal, Quebec, Canada

**Abstract** Operational AQ forecasting began in Canada in 2001 with the implementation by Environment Canada (EC) of a continental-scale, 21-km, ozone-only version of the CHRONOS off-line regional chemical transport model. Work to replace CHRONOS with a 15-km limited-area version of GEM-MACH, an in-line chemical transport model embedded within EC's operational weather forecast model, GEM, started in 2006. Like CHRONOS, GEM-MACH15 employs a simple 2-bin representation of the PM size distribution, but PM chemical composition is treated in more detail and additional processes affecting PM concentration have been included. This short paper focuses on PM forecasting with GEM-MACH15 and presents some preliminary evaluation results.

## 1. Introduction

Operational AQ forecasting began in Canada in 2001 with the implementation by Environment Canada (EC) of a continental-scale, 21-km, ozone-only version of the CHRONOS *off-line* regional chemical transport model (Pudykiewicz et al., 1997; Sirois et al., 1998). The meteorological driver used with CHRONOS was the regional configuration of EC's GEM operational weather forecast model (Côté et al., 1997a, b). Operational CHRONOS forecasts of $PM_{2.5}$ and $PM_{10}$ using a simple 2-bin sectional representation of the PM size distribution followed in 2003 (e.g., Fig. 1a).

A project to build a new operational AQ forecast modelling system started at EC in 2006 (Talbot et al., 2008). The goal of this project is to replace CHRONOS with a limited-area version of GEM-MACH (**G**lobal **E**nvironmental **M**ultiscale model - **M**odelling **A**ir quality and **CH**emistry), an *in-line* chemical transport model embedded within the GEM weather forecast model. A number of AQ process representations from EC's AURAMS chemical transport model (Gong et al.,

D.G. Steyn and S.T. Rao (eds.), *Air Pollution Modeling and Its Application XX*,
DOI 10.1007/978-90-481-3812-8, © Springer Science + Business Media B.V. 2010

2006; Smyth et al., 2009) have been implemented in GEM-MACH, including gas-phase, aqueous-phase, and heterogeneous chemistry and many aerosol processes.

GEM-MACH15 is a limited-area forecast configuration of GEM-MACH. It uses a continental-scale domain with 15-km horizontal grid spacing on a 348 × 465 rotated latitude-longitude grid (Fig. 1b). The 58 vertical levels extend to 0.1 hPa on a hybrid sigma-pressure vertical coordinate. Time-dependent meteorological lateral boundary conditions (LBCs) are provided hourly by GEM15, EC's global variable-mesh regional forecast model. Monthly-average concentration vertical profiles for different species are used to provide chemical LBCs. Version 1.3.0 of GEM-MACH has been used in this study.

The SMOKE emissions processing system (v2.5) was used to produce input anthropogenic emission files on the GEM-MACH15 rotated latitude-longitude grid from the 2006 Canadian, 2005 U.S., and 1999 Mexican national emissions inventories. Biogenic emissions are estimated on-line using the BEIS v3.09 algorithms.

## 2. Representation of PM Processes

Like CHRONOS, to reduce execution time GEM-MACH15 employs a simple 2-bin representation of the PM size distribution (Bin 1 is 0–2.5 μm aerodynamic diameter in size and Bin 2 is 2.5–10 μm), but PM chemical composition is treated in more detail in GEM-MACH15 and additional processes affecting PM concentrations have been included. CHRONOS considers six chemical components: $SO_4$; $NO_3$; $NH_4$; secondary organic carbon (sOC); $H_2O$; and "primary" PM. GEM-MACH15 considers nine chemical components, as it separates the CHRONOS "primary" component into elemental carbon (EC), primary organic carbon (pOC), crustal material (CM), and sea salt (SS).

Both models represent inorganic gas-particle partitioning, PM sedimentation and dry deposition, in-cloud scavenging, and secondary organic aerosol (SOA) formation (CHRONOS uses the Pandis et al. (1992) SOA scheme whereas GEM-MACH15 uses the Jiang (2004) scheme). In addition GEM-MACH15 considers sea-salt emissions, aerosol nucleation, condensation, coagulation, and below-cloud scavenging, and aerosol activation and aqueous-phase chemistry. To calculate inter-bin condensational/evaporative transfers, the two bins are subdivided into sub-bins to account for size dependence more accurately. The same approach is used to calculate dry deposition velocities.

## 3. Results

GEM-MACH15 and CHRONOS predictions of surface $O_3$ and $PM_{2.5}$ concentrations have been compared for a 36-day period during summer 2008. Initial chemical conditions were provided by running GEM-MACH15 in a series of 12-h

segments from a "cold start" from 3 June 2008 at 00 UTC to 19 June at 00 UTC. Seventy-two 48-h forecasts were then made 12 h apart from 19 June at 12 UTC to 24 July at 00 UTC, alternating between 12 and 00 UTC starts.

Figure 1 shows the mean Day-1 20-UTC $PM_{2.5}$ concentration fields for the period 20 June to 23 July predicted by CHRONOS and GEM-MACH15. The overall $PM_{2.5}$ spatial patterns are similar for the two models, but GEM-MACH15-predicted $PM_{2.5}$ magnitudes are generally higher, especially over eastern North America, and $PM_{2.5}$ transport over the Atlantic Ocean is greater.

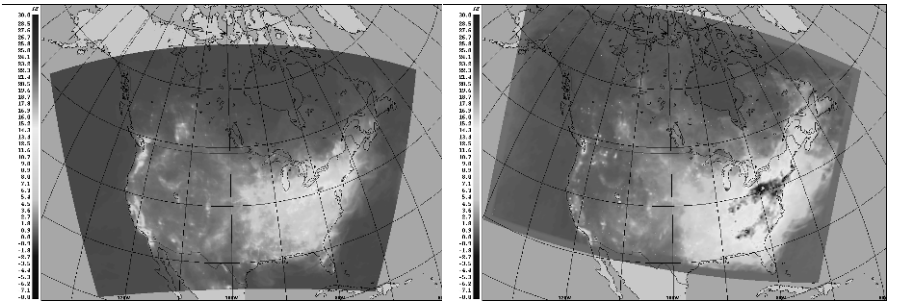

**Fig. 1.** Mean Day-1 20-UTC $PM_{2.5}$ concentration fields (μg $m^{-3}$) for the 20 June–23 July 2008 period from averaging 12 (left) CHRONOS and (right) GEM-MACH15 00-UTC runs

Table 1 presents some objective scores for both CHRONOS and GEM-MACH15 against measurements for a similar period. Canadian and U.S. $O_3$ and $PM_{2.5}$ ambient measurements were obtained in near-real time from Canadian stations and the AIRNow meta-network (see http://airnow.gov). For both $O_3$ and $PM_{2.5}$, CHRONOS predictions are on average biased low for this period whereas GEM-MACH15 predictions are biased high. Overall, the GEM-MACH15 scores for hourly $O_3$ are slightly better than those for CHRONOS. For hourly $PM_{2.5}$ the GEM-MACH15 mean bias and correlation coefficient (r) scores are better than the CHRONOS scores but the unbiased RMSE score is worse. Except for the $O_3$ correlation coefficient, all of these differences are statistically significant based on a bootstrapping calculation.

**Table 1.** Objective scores for 72 CHRONOS and GEM-MACH15 runs for all hours of period from 19 June (12 UTC) to 26 July 2008 (00 UTC)

| **Statistics** | **Hourly $O_3$ (ppbv)** | | **Hourly $PM_{2.5}$ (μg $m^{-3}$)** | |
|---|---|---|---|---|
| | **CHRONOS** | **GEM-MACH15** | **CHRONOS** | **GEM-MACH15** |
| Mean bias | –4.3 | 2.5 | –2.1 | 0.7 |
| Unbiased RMSE | 15.4 | 15.3 | 12.8 | 13.5 |
| R | 0.68 | 0.68 | 0.30 | 0.40 |

## 4. Discussion

The choice to use only two bins or sections to represent the PM size distribution was made in order to reduce the number of tracers being modelled, since nine chemical components must be considered for each additional bin. By contrast, in the AURAMS model we have used ten bins to represent the same PM size range (Gong et al., 2006). However, a recent model intercomparison of regional PM models suggested that CHRONOS performance for $PM_{2.5}$ was comparable to other models in spite of its "bulk" treatment of $PM_{2.5}$ (McKeen et al., 2007).

Numerical experiments with GEM-MACH15, on the other hand, have shown considerable sensitivity to the treatment of inter-bin mass transfer, which CHRONOS neglects. The choice of dry deposition velocity and sedimentation velocity, which are both size dependent, is also complicated by the consideration of only two PM size bins. We account for such size dependence in GEM-MACH15 by subdividing each bin into sub-bins in order to determine inter-bin mass transfer and dry-deposition and sedimentation velocities.

## References

Côté J, Desmarais J-G, Gravel S et al. (1998a) The operational CMC/MRB Global Environmental Multiscale (GEM) model. Part 1: Design considerations and formulation. Mon. Wea. Rev. 126:1373–1395.

Côté J, Desmarais J-G, Gravel S et al. (1998b) The operational CMC-MRB Global Environment Multiscale (GEM) model. Part II: Results. Mon. Wea. Rev. 126:1397–1418.

Gong W, Dastoor AP, Bouchet VS et al. (2006) Cloud processing of gases and aerosols in a regional air quality model (AURAMS). Atmos. Res. 82:248–275.

Jiang W (2004) Reply to the "Comment on 'Instantaneous secondary organic aerosol yields and their comparison with overall aerosol yields for aromatic and biogenic hydrocarbons'", by Knipping et al. (2004). Atmos. Environ. 38:2763–2767.

McKeen S., Chung SH, Wilczak J et al. (2007) Evaluation of several real-time PM2.5 forecast models using data collected during the ICARTT/NEAQS 2004 field study. J. Geophys. Res. doi:10.1029/2006JD007608.

Pandis SN, Harley RA, Cass GR et al. (1992) Secondary organic aerosol formation and transport. Atmos. Environ. 26A:2269–2282.

Pudykiewicz JA, Kallaur A, Smolarkiewicz PK (1997) Semi-Lagrangian modelling of tropospheric ozone. Tellus 49B:231–248.

Sirois A, Pudykiewicz JA, Kallaur A (1999) A comparison between simulated and observed ozone mixing ratios in eastern North America. J. Geophys. Res. 104:21, 397–21, 423.

Smyth SC, Jiang W, Roth H et al. (2009) A comparative performance evaluation of the AURAMS and CMAQ air quality modelling systems. Atmos. Environ. 43:1059–1070.

Talbot D, Moran MD, Bouchet V et al. (2008) Development of a new Canadian operational air quality forecast model. In: Borrego C, Miranda AI (eds) Air pollution modelling and its application XIX, Springer, Dordrecht, 470–478.

## 5. Questions and Answers

**S. Lu:** Have you run GEM-MACH for global resolutions, and if so, at what resolution?

**Answer:** Yes, we have run some global tests at 2° by 2°.

**S. Antonopoulos:** What differences were there between the emissions used for CHRONOS) and for GEM-MACH15)?

**Answer:** For CHRONOS, we have used the 2000 Canadian and 2001 U.S. national emissions inventories, with adjustments to U.S. NOx emissions from major point sources at the state level to account for emissions reductions associated with the U.S. NOx SIP Call. For GEM-MACH15, we have used the 2006 Canadian and 2005 U.S. national emissions inventories. Biogenic emissions are calculated for both models based on BEISv3.09.

# 3.3 Effect of Temporal Averaging of Vertical Eddy Diffusivity on the Forecast Quality of Surface Ozone Concentration of the National Air Quality Forecast

**Pius Lee[1], Daewon Byun[1], Ariel Stein[1], You-Hua Tang[2], Hsin-Mu Lin[3], Ho-Chun Huang[2], Sarah Lu[2], Marina Tsidulko[2], Jeff McQueen[4], Daniel Tong[3], Shaocai Yu[3], Tianfeng Chai[3], Dongchul Kim[2], Ivanka Stajner[5], and Paula Davidson[6]**

[1]Air Resource Lab., NOAA, 1315 East West Highway, Room 3316, Silver Spring, MD 20910, USA

[2]Scientific Applications International Corporation, Beltsville, MD, USA

[3]Science and Technology Corp., Hampton, VA, USA

[4]Environmental Modeling Center, National Centers for Environmental Prediction, NWS, MD, USA

[5]Noblis Inc. Fairfax, VA, USA

[6]Office of Science and Technology, NWS, Silver Spring, MD, USA

**Abstract** Air Quality forecast models are employed to provide numerical guidance for forecasters to issue timely ozone and particulate matter concentration forecast pertinent to human health exposures to the communities they serve. The National Centers for Environmental Prediction (NCEP), National Weather Service Weather Research and Forecasting Non-hydrostatic Mesoscale Model (WRF/NMM) has been coupled off-line with the EPA Community Multi-scale Air Quality (CMAQ) model in 2003 to form the National Air Quality Forecast Capability (NAQFC). Coupling of the turbulent mixing processes of the meteorological driver and CMAQ has been a challenge. WRF/NMM uses the Mellor-Yamada-Janjic (MYJ) turbulence mixing scheme in the boundary layer. The option of directly using MYJ provided vertical eddy diffusivity to calculate turbulent mixing of the atmospheric chemical constituents in CMAQ has been tested. This study investigated the effect of various temporal averaging treatments of vertical eddy diffusivity in redistributing ozone in the boundary layer. Model predicted concentration structures of ozone resulting from these various temporal treatments of vertical eddy diffusivity have been studied and verified using AIRNOW, an EPA surface ozone concentration network, and ozone-sonde data.

D.G. Steyn and S.T. Rao (eds.), *Air Pollution Modeling and Its Application XX*,
DOI 10.1007/978-90-481-3812-8, 

# 1. Introduction

Air Quality forecast models are employed to provide forecasters with numerical guidance to issue timely ozone and particulate matter concentration forecast pertinent to human health exposures to the communities they serve. The National Centers for Environmental Prediction (NCEP) North American Mesoscale Model (NAM) has been coupled with the EPA Community Multi-scale Air Quality (CMAQ) model to form the National Air Quality Forecast Capability (NAQFC). Coupling of the turbulent mixing processes of the meteorological driver and CMAQ has been a challenge. Both Eta and NAM use the Mellor-Yamada-Janjic (MYJ) turbulence mixing scheme in the boundary layer (Janjic, 2001). The option of directly using MYJ provided vertical eddy diffusivity to calculate turbulent mixing of the atmospheric constituents in CMAQ has been considered. This study investigated the redistribution of ozone by various temporal averaging treatments of vertical eddy diffusivity in the boundary layer. Model predicted concentration of ozone resulted from these various temporal treatments of vertical eddy diffusivity has been studied and verified using AIRNow, a surface ozone concentration observation network compiled by U.S. EPA, and ozone-sondes data. Observation sites representative of various geographic and chemical settings to reflect their effect on the diurnal cycle of the pollutant plumes are chosen, and the fidelity of vertical diffusivity thus successfully captured or not by the schemes was studied.

# 2. Verical Mixing Schemes Sensitivity

In 2006, NAQFC (Otte et al., 2005) used a version of CMAQ very similar to CMAQ version 4.5 (CMAQ-4.5) but customized computationally for NCEP production requirements. Beside this real time forecast, two sensitivity cases were run. They are stipulated hereby as Cases-*a*: Turbulence Kinetic Energy-Planetary Boundary Layer height (TKE-PBL) derived Vertical Eddie Diffusivity, $K_z$; or dubbed the (TKE-PBL Kz) Case – the baseline real time case; Case-b: (NAM-$K_z$); and Case-c: (NAM hrly $K_z$). The latter two cases parameterize turbulent mixing of tracer gases within CMAQ by using NAM predicted $K_z$.

## 2.1. RADM scheme with NAM TKE-based PBL height

The RADM (Regional Acid Deposition Model) scheme (Chang et al., 1987) addresses boundary layer mixing based on a parameterization of turbulent mixing in the surface and convective boundary layers using an application of the similarity theory. The scheme computes vertical mixing using the eddy diffusion formulation, the so-called K-theory. One benefit of the K-theory is the assumption of similar diffusivity characteristics between tracer species and potential temperature: namely

$K_z$=$K_h$, where $K_z$ is the eddy diffusivity for tracer species, and $K_h$ is the eddy diffusivity for heat. The *Kz* equations for the various stability regimes of the surface layer and layers above that and below the PBL top are repeated in (Lee et al., 2009).

### 2.2. Use NAM predicted Kz for CMAQ vertical mixing

The NAQFC had an important improvement in the vertical grid alignment between NAM and CMAQ in 2006. Both models are now using a common hybrid sigma-*P* vertical coordinate. NAM uses 61 interface levels and CMAQ in NAQFC selects a subset of 23 levels from them with coarser spacing near the model top at 100 hPa. In the NAM, *Kz* is defined at these interface surfaces from the Mellor-Yamada Level 2.5 turbulence closure scheme (Janjic, 2001). In accordance with Janjic, the Turbulent Kinetic Energy (TKE),

$$\frac{\partial}{\partial t}(\frac{q^2}{2})+\vec{V}\bullet\nabla\frac{q^2}{2}-\frac{\partial}{\partial z}[Kz\frac{\partial}{\partial z}(\frac{q^2}{2})]=P\,s+Pb-\varepsilon \qquad (1)$$

where $q^2$ is the sum of square of the wind turbulence fluctuations, $u'^2+v'^2+w'^2$; $\vec{V}$ is the mean wind; $Ps$ is the shear production; $Pb$ is production by buoyancy; and $\varepsilon$ represents rate of dissipation of turbulent energy. *Kz* is given by

$$Kz = {}_l\, qS_q \qquad (2)$$

where $l$ is the master length scale for turbulence, and $S_q$ is an empirical constant for which the numerical value of 0.2 was found (Mellor and Yamada 1982) to optimize agreement between model results and observed data.

### 2.3. Use hourly averaged NAM predicted Kz for CMAQ vertical mixing

NAQFC is an offline system. NAM feeds meteorological data to CMAQ hourly. A total of 12 3-D fields and 33 2-D fields were thus past. Most fields are instantaneous values, except for the following time-averaged 2-D fields: precipitation rate, shortwave and long-wave radiation fluxes, and latent and sensible heat fluxes. Within CMAQ, the Models-3 Input/Output Applications Programming Interface (I/O API) temporally interpolated all these 2-D, and 3-D fields between the full hours into the advection time steps which are typically 5 min. Ideally all fields fed should be hour-centered hourly averaged fields to match the temporal interpolation. To understand the impact of such considerable restructuring of the coupling interface, *Kz*, one the most influential fields in governing surface $O_3$ concentration is chosen to be studied. A β-version of NAM is used to feed CMAQ with hourly averaged *Kz* output at full hours for the duration of the previous hour. Therefore it

is still not the ideal situation of hour-centered fields, but rather staggered late by half an hour from the time stamps I/O API sees. This half-hour lagged hourly average *Kz* is used to drive turbulent mixing of tracer gases in CMAQ.

## 3. August 2–3, 2006 Episode and Verifications

A surface elevated $O_3$ concentration episode on August 2–3, 2006 is chosen. This episode provides opportunity to analyze the characteristics of the schemes at different locations. The episode is chosen to co-incide with the TexAQS campaign where a good set of ozonesonde data are available. All runs are daily 12 UTC cycle out-to 48 h forecast initialized by outputs from a previous cycle. A regionalized second-day daily 8 h maximum forecast verification dividing the CONUS into 6 regions: Pacific Coast, Rocky Mountains, Lower Midwest, Upper Midwest, Southeastern and Northeaster US, in terms of correlation and Root Mean Square Error (RMSE) for July 30–August 4, 2006, showed that there was no obvious dominant winner among the three schemes. Dependent on the region and the time of focus, all three schemes performed comparable in all six regions during the analyzed 6 days period. It is arguable that Cases b and c are superior to Case a for Lower Midwest (LM) and Northeastern (NE) regions; especially Case c has been consistently superior among all three schemes throughout the period.

## 4. Structures of $K_z$, TKE, $O_3$ and RH on August 2, 2006

The vertical structure of the $O_3$ field is further examined through using ozonesonde data made available through the ITEX-B campaign (Thompson et al., 2008). Four sites have been chosen: (1) Table Mountain, CA (34.4°N, 117.7°W) at elevation 2,285 m; Boulder, CO (40.3°N, 105.2°W) at elevation 1,745 m; Huntsville, AL (34.7°N, 86.5°W) at elevation 196 m, and Beltsville, MD (39.04°N, 76.52°W) at elevation 24 m. Figure 1a shows the *Kz* profiles predicted by the three schemes and then NAM predicted TKE profile at launching time of 20:52 UTC, on August 2, 2006 at the Table Mountain, CA site. Figure 1b shows ozonesonde data overlaid with the model-predicted $O_3$ concentrations by all three cases over the same site at 20:52 UTC. A measured moisture profile inferred PBL height at 1,200 m AGL is also indicated with overlaid of measured and NAM-predicted relative humidity (RH). Figures 2–4 repeated similar analyses from the above paragraph to Boulder, CO with ozonesonde launch time at 19:28 UTC on August 2, 2006; Huntsville, AL with ozonesonde launch time at 17:36 UTC on August 2, 2006; and Beltsville, MD with ozonesonde launch time at 19:18 UTC on August 2, 2006; respectively.

Over Boulder, CO, all three cases captured the PBL height, inferred at 1,750 m AGL, rather well with a relatively small overshot (Fig. 2). It is noted that both measured and model-predicted $O_3$ concentration profiles show a rather uniform

profile. Multiple local minima of the measured RH indicated co-location of various cloudy air-mass prevailed over the site. Therefore cloud mixing activities were speculated to have contributed to the rather uniform profiles.

Unlike the previous two sites, Huntsville, LA is a non-elevated site. The overshot of 250 m or larger in PBL height prediction was not uncommon during a developing PBL (Fig. 3). From measure RH profile, PBL height was inferred to be at 1,500 m AGL at launch time. In terms of instantaneous surface $O_3$ concentration, Cases b, and c performed slightly better than that by Case a. There is virtually no difference in vertical $O_3$ concentration profiles between Cases b and c.

At Beltsville, MD, there was an over-estimated PBL height. It was overshot by about 1,000 m. The inferred PBL height was 1,250 m (Fig. 4). The measured $O_3$ concentration showed well-mixed behavior below the PBL top as reflected rather well by Cases b and c. Cases b and c illustrated the capping of the mixing activity below the predicted PBL height by about 500 m as indicated by the inflexion points of model-predicted $O_3$ concentration profiles.

## References

Chang, J. S., R. A. Brost, I. S. A. Isaksen, S. Madronich, P. Middleton, W. R. Stockwell, and C. J. Walcek, 1987: A three-dimensional Eulerian acid deposition model: Physical concepts and formulation. J. Geophys. Res., 92, 14681–14700.

Janjic, Z. I., 2001: Nonsingular implementation of the Mellor-Yamada level 2.5 scheme in the NCEP meso-model, NCEP Office Note 437. [Available at http://www.emc.ncep.noaa.gov/officenotes/FullTOC.html]

Lee, P. and coauthors (2009): Impact of consistent boundary layer mixing approaches between NAM and CMAQ**,** Environmental Fluid Mechanics: Volume 9, Issue1, Page 23–42 DOI:10.1007/s10652-008-9089-0.

Mellor, G. L., and T. Yamada, 1982: Development of a turbulence closure model for geophysical fluid problems. *Rev. Geophys. Space Phys*., **20**, 851–871.

Otte, T.L., G. Pouliot, J. E. Pleim, J. O. Young, K. L. Schere, D. C. Wong, P. C. S. Lee, M. Tsidulko, J. T. McQueen, P. Davidson, R. Mathur, H.Y. Chuang, G. DiMego, and N. L. Seaman, 2005: Linking the Eta model with the Community Multiscale Air Quality (CMAQ) modeling system to build a national air quality forecasting system, *Wea. Forecasting*, 20 (No.3), 367–384.

Thompson A. M., J. E. Yorks, S. K. Miller, J. C. Witte, K. M. Dougherty, G. A. Morris, D. Baumgardner, L. Ladino, and B. Rappenglueck, (2008), Tropospheric ozone sources and wave activity over Mexico City and Houston during MILAGRO/Intercontinental Transport Experiment (INTEX-B) Ozonesonde Network Study, 2006 (IONS-06), Atmos. Chem. Phys. Discuss., 8, 5979–6007.

**Acknowledgments** The authors appreciate numerous valuable discussions with Drs. Rohit Mathur, Jon Pleim, David Wong, Tanya Otte, George Pouliot, Brian Eder, Jeff Young, and Ken Schere of the Atmospheric Modeling Division of the National Exposure Research Laboratory, U.S. EPA. The U.S. EPA AIRNow program staff provided the observations necessary for quantitative model evaluation. The authors are indebted to Mr. Jerry Gorline of Meteorological Development Laboratory of NOAA for providing Fig. 1b.

**Disclaimer** The research presented here was performed under the Memorandum of Understanding between the U.S. Environmental Protection Agency (EPA) and the U.S. Department of Commerce's National Oceanic and Atmospheric Administration (NOAA) and under agreement number DW13921548. Although it has been reviewed by NOAA and approved for publication, it does not necessarily reflect its policies or views.

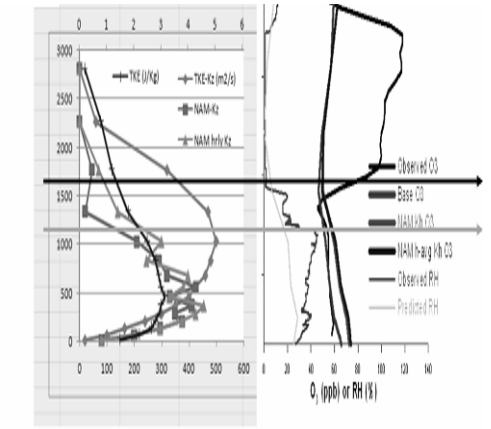


**Fig. 1.** Profiles at ozonesonde launch time at 20:52 UTC on August 2, 2006, at Table Mountain, CA for (a) *Kz* predicted by the three schemes and TKE predicted by the NAM model; and (b) measured and model-predicted $O_3$ and RH. Where black and grey horizontal lines indicate NAM predicted PBL height, and measure-RH inferred PBL height, respectively

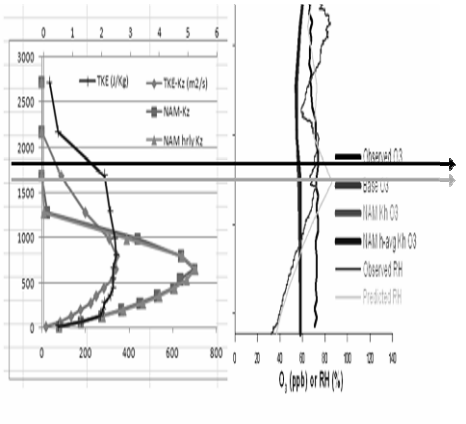


**Fig. 2.** Same as Fig. 1 but for launch time at 19:28 UTC on August 2, 2006, at Boulder, CO

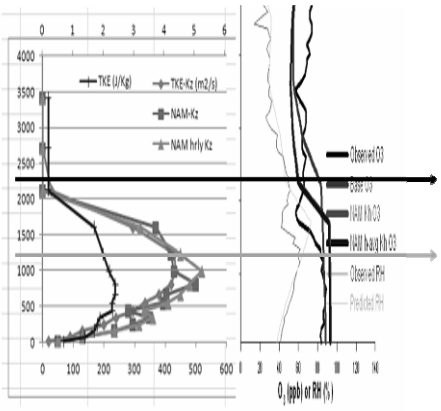


**Fig. 3.** Same as Fig. 1 but for launch time at 17:36 UTC on August 2, 2006, at Huntsville, AL

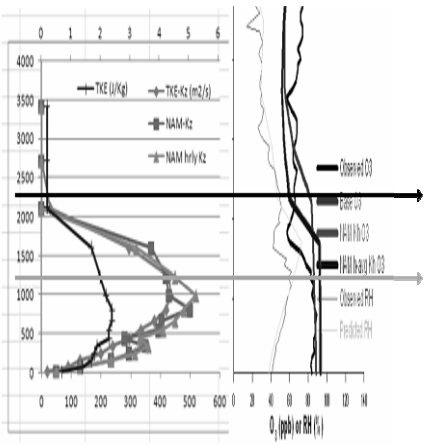


**Fig. 4.** Same as Fig. 1 but for launch time at 19:18 UTC on August 2, 2006, at Beltsville, MD

## 5. Questions and Answers

**Dr. Dazhong Yin, CA Environmental Protection Agency:** Standard CMAQ uses a sigma vertical co-ordinate. NAM uses a sigma-pressure hybrid vertical co-ordinate. Did you make any changes in CMAQ to use Kz directly from NAM?

**Answer:** Yes, the vertical grid structure of CMAQ for the NAQFC changed. It adapted to the implementation of vertical grid structure change in June 2006. Now the CMAQ model within the NAQFC has 22 sigma-lower and pressure-upper vertical grid structure. Since NMM has 61 levels, CMAQ picks 22 from that with denser spacing in the lower levels. The lowest 14 levels straddle a height of 2.5 km.

# 3.4 A Case Study of 4D-VAR Data Assimilation in Southern Europe

**Julius Vira, Marje Prank, and Mikhail Sofiev**

Finnish Meteorological Institute, P.O. Box 503, FI-00101 Helsinki, Finland

**Abstract** This paper describes a case study on variational data assimilation of in-situ measurements at 260 stations in Central and Southern Europe, using the SILAM chemistry-transport model. The aim of the experiment was to investigate the emission distribution, and both initial concentration and emission correction factor were included in estimated parameters. The main improvement in forecasts due to assimilation was seen at sites with the worst model-measurement agreement. Throughout the assimilation period, the estimated emission rates for Mt. Etna and the surrounding volcanic areas were substantially smaller than those derived from the emission inventory. Subtler emission corrections were obtained for industrialised areas in Central Europe.

**Keywords** Data assimilation, chemistry-transport models, sulphur dioxide, emissions

## 1. Introduction

Extending the concept and methods of data assimilation into atmospheric chemistry-transport models has been a topic of active research over the last decades. In addition to operational forecasting of air quality, data assimilation in air pollution modelling is closely related to atmospheric inverse problems for source localisation and apportionment. However, this requires using advanced variational or sequential assimilation methods.

The evolution of atmospheric pollutants is strongly affected by the distribution of emission sources, and consequently, estimating the emission sources through data assimilation has been the focus of recent studies including [1]. A common approach has been to consider an emission distribution derived from inventories, and use data assimilation to estimate a correction factor.

This paper describes an assimilation experiment based on in-situ measurements of $SO_2$ and the 4D variational method with the emission correction approach. In particular, we explore the potential of a dataset with limited geographic coverage in emission estimation and operational forecasting.

D.G. Steyn and S.T. Rao (eds.), *Air Pollution Modeling and Its Application XX*,
DOI 10.1007/978-90-481-3812-8, 

## 2. The Assimilation Experiment

The assimilation experiment covered a period of 2 weeks starting at February 8, 2006, representing typical winter conditions. The period was divided into assimilation windows of 24 h. The species included in the run were sulphur dioxide ($SO_2$) and sulphates $SO_4$.

The computations were performed using the SILAM chemistry-transport model and ECMWF meteorological fields. A description of the model and its evaluation against data from the European Tracer Experiment (ETEX) is given by [2]. Furthermore, the Eulerian dynamical core, based on a semi-Lagrangian advection scheme [3], was employed in this work. The discretisation of vertical diffusion follows the extended resistance analogy scheme described in [4]. Oxidation of SO2 to sulphates was computed using the linear parametrisation described in [5].

Adaptation of the 4D-VAR assimilation method in chemistry-transport modelling has been described in detail for instance in [1] and [6]. In this work, emission is used as a control variable by defining the emission rate as

$$E(x,t)=\alpha(x)E_0(x,t) \tag{1}$$

where α is the correction factor, and $E_0(x, t)$ is the a priori (background) value for emission. A standard quadratic cost function is used, with control variable being the pair $(\alpha\ (x),c_0(x))$, where $c_0(x)$ is the concentration field at $t = 0$. Given the solution $c(x, t)$ of the adjoint problem, the sensitivity of the cost function with respect to $\alpha$ is obtained by integrating $c(x, t)E_0(x, t)$ over the assimilation window.

The background covariance matrices for $c0$ and a were assumed to be constant and diagonal, with $\sigma^2_\alpha = 10.0$ (relative units) and $\sigma^2_{c0} = 10^{-12}$ mol m$^{-3}$.

### 2.1. Observations

The set of measurements used in assimilation consists of hourly concentrations of SO2 at total of 456 central European stations made available through the Air-basedatabase (www.eea.europa.eu) maintained by European Environmental Agency. For grid cells containing several monitoring stations, one was selected randomly. This limits the number of stations to 260, and consequently, the number of data points inside the 24 h assimilation window to ~6,200.

Furthermore, a control set of 50 stations located on the same region was chosen randomly to evaluate the performance of the assimilation system. Because of the difficulties in collecting accurate information on the measurement errors in the dataset, the measurement errors are in this study prescribed with a constant standard deviation $\sigma = 10^{-7}$ mol m$^{-3}$.

## 3. Results and Discussion

The iteration converged with typically 15–30 gradient evaluations. Examples of the estimated emission corrections are shown in Fig. 1. On certain areas, the corrections were consistent throughout the experiment, as reflected by the average emission correction in Fig. 1. Especially, the concentrations at stations near Mt. Etna were strongly overestimated in the reference run, which resulted in up to 100% reduction in some grid cells. Total emission of $SO_2$ from the area near the volcano was reduced by approximately 50–75% depending on the day. This suggests that the parametrisation of the volcano was, at least, not representative of the time period under consideration.

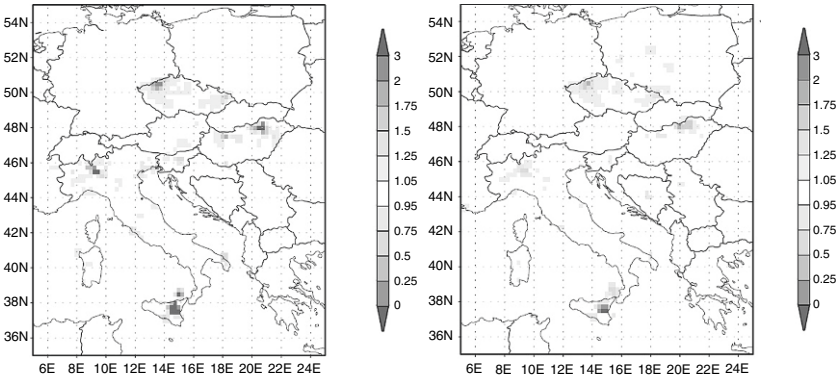


**Fig. 1.** Emission correction factors. Left: corrections for day 1. Right: average correction over the period of 14 days

### 3.1. Effect on forecasts

For the stations in the control set, the mean RMS forecast error for each day of the assimilation experiment is presented in Fig. 2. Compared to the background run, a substantial improvement is observed on average.

However, most of the improvement is concentrated on a small set of stations. This is illustrated by right panel of Fig. 2, which shows the median with 13th and 86th percentiles of the RMS errors. Here, the difference between the reference and assimilation runs is greatest in the upper percentile. It can therefore be concluded that for the present case, the main benefit of data assimilation was in improvement of the worst-case performance of the model.

A possible explanation for the uneven improvement across the stations is in the different contributions by local and remote sources. Obviously, only the emissions affecting the stations during the 24 h assimilation window can be adjusted by the assimilation. Hence, the possible discrepancies in remote transport only contribute to the optimised initial state, which in turn is likely to have only transient impact.

In conclusion, the results indicate that data assimilation can provide significant improvement at sites with strong contribution by a local source. Therefore, further improvement could be expected through utilisation of observations covering also major remote sources influencing the area of interest.

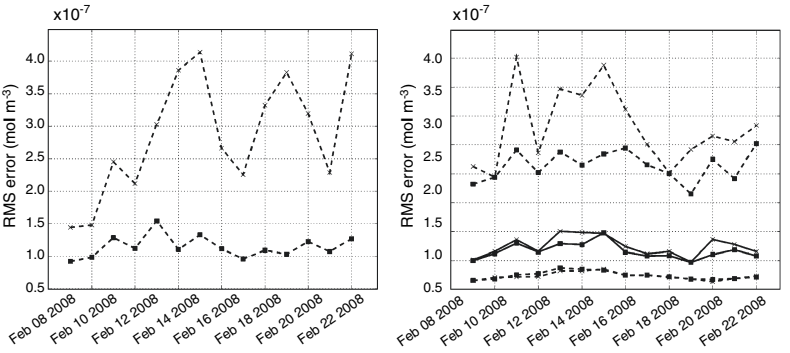


**Fig. 2.** RMS forecast errors for the reference (crosses) and assimilation runs (boxes). Left: mean RMS in the control set. Right: median (solid line), 13th and 86th percentiles (dashed lines)

## References

H. Elbern, A. Strunk, H. Schmidt, O. Talagrand, Atmospheric Chemistry and Physics **7**(14), 3749 (2007)

M. Sofiev, P. Siljamo, I. Valkama,M. Ilvonen, J. Kukkonen, Atmospheric Environment **40**, 674 (2006)

M. Galperin, in Large Scale Computations in Air Pollution Modelling, ed. By Z. Zlatev, J. Dongarra, I. Dimov, J. Brandt, P.J. Builtjes (Kluwer Academic Publishers, 1999), pp. 161–172

M. Sofiev, J. Geophys. Res. **107** (2002)

M. Sofiev, Atmospheric Environment **34**, 2481 (2000)

A. Sandu, D.N. Daescu, G.R. Carmichael, T. Chai, J. Comput. Phys. **204**(1), 222 (2004). DOI http://dx.doi.org/10.1016/j.jcp.2004.10.011

## 4. Questions and Answers

**M. Schaap:** Do you know what is the impact of assimilation of $SO_2$ on the performance for $SO_4$?

**Answer:** Due to the limited availability of $SO_4$ measurements we have so far been unable to analyse the effect of assimilation on $SO_4$.

**P. Builtjes:** Why do you keep the emission update constant over a day, and not on an hourly basis?

**Answer:** The 24 h assimilation window provides a natural time scale for the emission adjustments. Furthermore, trying to estimate the emission corrections in one hour steps would most probably lead into a severely underdetermined problem.

# 3.5 Daily Air Quality Predictions from the BlueSky Gateway

**Neil J.M. Wheeler[1], Sean M. Raffuse[1], Dana Coe Sullivan[1], Kenneth J. Craig[1], Stephen B. Reid[1], Robert Solomon[2], Tara Strand[2], and Sim Larkin[2]**

[1]Sonoma Technology, Inc., 1455 N. McDowell Blvd., Petaluma, CA 94954, USA

[2]U.S. Forest Service Pacific Northwest Research Station, 400 N. 34th St. #201, Seattle, WA 98103, USA

**Abstract** Smoke from biomass burning events, both large and small, contributes to air quality problems associated with elevated concentrations of particulate matter, ozone, and air toxics. Currently, real-time smoke predictions are via the BlueSky smoke modeling framework. BlueSky modularly links computer models of fuel consumption and emissions, fire, weather, and smoke dispersion into a system for predicting the cumulative impacts of smoke from prescribed fires, wildfires, and agricultural fires. The BlueSky smoke modeling framework has recently been upgraded in several key ways: satellite data are now incorporated, using the SMARTFIRE system, to provide information on the location and size of fires; the most recent fuel loading, fuel consumption, and emission models have been added; and the Community Multiscale Air Quality model (CMAQ) is being used to predict concentration fields of particulate matter and ozone nationally from both fire and anthropogenic emissions. A general overview of the BlueSky program and a description of its current features are provided. In particular, we focus on BlueSky products of interest to the air quality community, such as daily experimental predictions and how the products are being distributed through the BlueSky Gateway web portal.

**Keywords** Air quality, particulate matter, ozone, forecasting, satellite, wildfire, SMARTFIRE, BlueSky, CMAQ

## 1. Introduction

Smoke from biomass burning events, both large and small, contributes to air quality problems such as particulate matter, ozone, and air toxics. Currently, real-time smoke predictions are available across the coterminous United States via the BlueSky smoke modeling framework. BlueSky modularly links computer models of fuel consumption and emissions, fire, weather, and smoke dispersion into a system for predicting the cumulative impacts of smoke from prescribed fires,

D.G. Steyn and S.T. Rao (eds.), *Air Pollution Modeling and Its Application XX*,
DOI 10.1007/978-90-481-3812-8, © Springer Science + Business Media B.V. 2010

wildfires, and agricultural fires. The BlueSky smoke modeling framework has recently been upgraded in several key ways: satellite data are now incorporated to provide information on the location and size of fires; the most recent fuel loading, fuel consumption, and emission models have been added; and a photochemical grid model is used to predict concentration fields of $PM_{2.5}$ and ozone nationally from both fire and anthropogenic emissions.

## 2. Components of the BlueSky Gateway Modeling System

The BlueSky Gateway Modeling System consists of five component systems, each of which is described below.

**SMARTFIRE –** The Satellite Mapping Automated Reanalysis Tool for Fire Incident Reconciliation (Sullivan et al., 2008) combines satellite fire data from the National Oceanic and Atmospheric Administration (NOAA) Hazard Mapping System (HMS) (Ruminski et al., 2006) and ground-based reports into a unified geographic information system (GIS) database. SMARTFIRE then compiles a database of fire location information for use in retrospective analyses and provides fire location input to the BlueSky Framework.

**BlueSky Framework –** The BlueSky Framework (BSF) (Larkin et al., 2008) version 3.0 is a "modeling framework" that enables use of state-of-the-science models to simulate smoke impact, air quality, and emissions from fires. The BSF was developed by the U.S. Forest Service AirFIRE Team at the Pacific Northwest Research Station and re-engineered by Sonoma Technology, Inc. (STI) and the Air FIRE Team to provide real-time fire emissions estimates. These estimates are produced using Fuel Characterization Classification System (FCCS) fuel loading, the CONSUME 3.0 consumption, and the Fire Emission Production Simulator (FEPS) emissions models.

**MM5 –** The Pennsylvania State University/NCAR Mesoscale Model (MM5) (Grell et al., 1994) version 3.7 is applied on a national domain with 36-km horizontal grid spacing and 29 vertical layers. Initial and boundary conditions are derived from the North American Mesoscale (NAM) model's 40-km analyses and forecasts. The Meteorology-Chemistry interface Processor (MCIP) version 3.1 is used to prepare MM5 data for the emissions and air quality model.

**SMOKE –** The Sparse Matrix Operator Kernel Emissions (SMOKE) modeling system (Houyoux et al., 2000) version 2.3 is used to merge fire emissions from the BlueSky Framework with non-fire emissions. Non-fire emissions are derived from the 2002 NEI version 3 projected to the current year using EGAS version 4.0 (U.S. Environmental Protection Agency, 2004a). MM5 temperature predictions are used in the on-road (MOBILE6) (U.S. Environmental Protection Agency, 2005) and

biogenic (BEIS v3.09) emissions models (U.S. Environmental Protection Agency, 2004b).

**CMAQ –** The Community Multiscale Air Quality (CMAQ) model (National Exposure Research Laboratory, 1999) version 4.5.1 is used to predict the fate of airborne chemical species. Full gas-phase chemistry (CB-IV) and secondary aerosol formation (AERO3) are simulated. Simulations are initialized with carryover smoke from the previous day's prediction and several fire types are tracked for future use.

## 3. Real-Time System Work Flow

Two model simulations are performed each day. The workflow in the modeling system is described in Fig. 1. The early 1800 Coordinated Universal Time (UTC) run cycle relies on preliminary SMARTFIRE data to provide timely 2-day forecasts, while the main 0000 UTC run cycle relies on SMARTFIRE data supplemented with ground reports to provide 3-day forecasts. Current and carryover $PM_{2.5}$ are tracked separately to facilitate use within regional fire modeling systems.

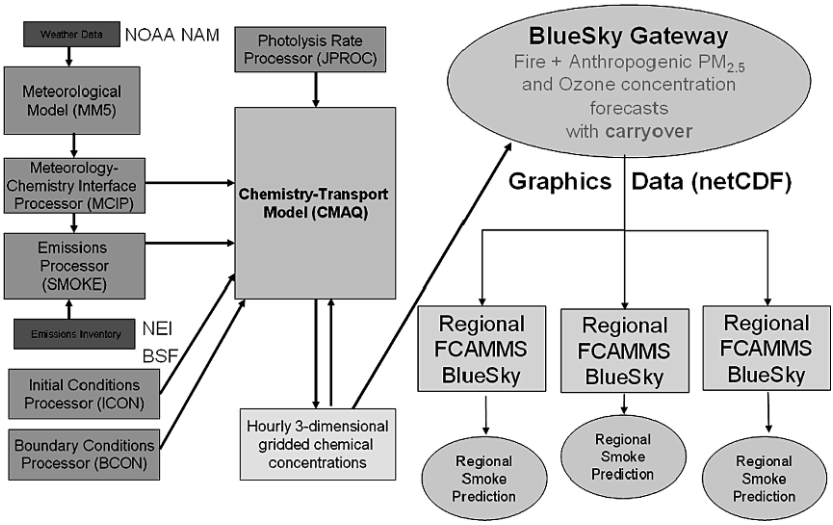


**Fig. 1.** Workflow in the BlueSky Gateway Modeling System

## 4. Products and Tools Available via the BlueSky Gateway

**Graphic Products –** Real-time graphical products from the BlueSky Gateway Modeling System include color contour plots of:

- Surface $PM_{2.5}$ (total, fire-only, and non-fire)
- Surface ozone due to all emission sources
- Visual range derived from CMAQ's estimated aerosol concentrations
- Surface wind speed, surface wind direction, and temperature; mixing depth and ventilation index

KML files for all model products will soon be available for visualization through Google Earth.

**Data Downloads –** Outputs from SMARTFIRE and the BlueSky Gateway Modeling System are available for FTP download. SMARTFIRE web services are also available. Data products include fire emissions and CMAQ predictions of $PM_{2.5}$ and ozone concentrations.

**SMARTFIRE Viewer –** The interactive SMARTFIRE viewer provides graphical access to real-time and historical fire location information with the ability to overlay trajectories from the NOAA Hybrid Single-Particle Lagrangian Integrated Trajectory (HYSPLIT) model. SMARTFIRE data are also available via FTP and web services technology.

**Smoke Forecast Products –** In addition to the experimental BlueSky Gateway predictions, the BlueSky Gateway Web Portal also provides access to other publicly available smoke prediction products. These products include National Weather Service operational forecasts of smoke impacts using the HYSPLIT dispersion model, an earlier version of the BlueSky emissions module, and smoke predictions produced by the Fire Consortia for the Advanced Modeling of Meteorology and Smoke (FCAMMS).

## 5. Access to the BlueSky Gateway

The BlueSky Gateway is accessible at: http://www.getbluesky.org

General access includes:

- Graphical products from the experimental BlueSky Gateway Modeling System
- Links to experimental graphical products from regional FCAMMS
- Links to operational smoke predictions from the NOAA Air Quality Forecast Model

Controlled access is available for:

- netCDF and CSV data from the experimental BlueSky Gateway Modeling System
- SMARTFIRE viewer

- SMARTFIRE data (FTP and web services)
- BlueSky Framework distribution

Access to controlled data is routinely granted upon request. Password protection is used to monitor and control the use of resources on experimental computing systems. To request an account, please email BlueSkyGateway@sonomatech.com.

**Acknowledgments** Support for SMARTFIRE and the BlueSky Framework was provided through a cooperative research agreement with National Aeronautics and Space Administration (NASA) under the direction of Lawrence Friedl, the U.S. Department of Agriculture – Forest Service, and the Joint Fire Science Program.

## References

Grell G.A., Dudhia J., and Stauffer D.R. (1994) A description of the fifth-generation Penn State/NCAR mesoscale model (MM5). Prepared by the National Center for Atmospheric Research, Boulder, CO, NCAR Technical Note-398.

Houyoux M., Vukovich J., and Brandmeyer J. (2000) Sparse Matrix Operator Kernel Emissions Modeling System (SMOKE) user manual. Prepared by MCNC-North Carolina Supercomputing Center, Environmental Programs, Research Triangle Park, NC.

Larkin N.K., O'Neill S.M., Solomon R., Krull C., Raffuse S.M., Rorig M., Peterson J., and Ferguson S.A. (2008) The BlueSky smoke modeling framework. *International Journal of Wildland Fire* **18**, 906–920 (8).

National Exposure Research Laboratory (1999) Science algorithms of the EPA Models-3 Community Multiscale Air Quality (CMAQ) modeling system. Report prepared by the National Exposure Research Laboratory, Research Triangle Park, NC, EPA/600/R-99/030 (peer reviewed), March.

Ruminski M., Kondragunta S., Draxler R.R., and Zeng J. (2006) Recent changes to the Hazard Mapping System. 15th International Emission Inventory Conference, New Orleans, LA. Available at http://www.epa.gov/ttn/chief/conferences.htm.

Sullivan D.C., Raffuse S.M., Pryden D.A., Craig K.J., Reid S.B., Wheeler N.J.M., Chinkin L.R., Larkin N.K., Solomon R., and Strand T. (2008) Development and applications of systems for modeling emissions and smoke from fires: the BlueSky smoke modeling framework and SMARTFIRE: 17th International Emissions Inventory Conference, Portland, OR, June 2–5.

U.S. Environmental Protection Agency (2004a) EGAS version 5.0 beta. Available at http://www.epa.gov/ttn/ecas/egas5.htm.

U.S. Environmental Protection Agency (2004b) Biogenic emissions inventory system (BEIS) modeling. Website prepared by the Atmospheric Sciences Modeling Division. Available at http://www.epa.gov/asmdnerl/biogen.html.

U.S. Environmental Protection Agency (2005) EPA's National Inventory Model (NMIM), a consolidated emissions modeling system for MOBILE6 and NONROAD. Prepared by the Office of Transportation and Air Quality, Research Triangle Park, NC, EPA 420-R-05-024, December.

# 3.6 On Integrated Modelling of Air Quality Using Information About Anthropogenic, Natural, and Biogenic Emission Sources

**M. Sofiev[1], P. Siljamo[1], M. Prank[1], J. Vira[1], J. Soares[1], R. Vankevich[2], M. Lotjonen[1], J. Koskinen[1], and J. Kukkonen[1]**

[1]Finnish Meteorological Institute

[2]Russian State Hydrometeorological University

**Abstract** The paper presents the current status of chemical composition modelling system SILAM. The system uses input information about anthropogenic, biogenic, natural, and complex sources, such as wild-land fires. The system is an attempt to combine the available knowledge on each of these terms in both retrospective and operational senses and use it for re-analysis and forecasting the atmospheric composition at various time scales. The three main inputs to the system are: the anthropogenic emission databases with simple temporal disaggregation, biogenic emission models for evaluating emission of natural aerosols and their precursors, and the Fire Assimilation System (FAS) jointly developed by Finnish Meteorological Institute and Russian State Hydrometeorological University. FAS converts the observed quantities – the pixel absolute temperature and radiative emissivity – to emission fluxes via empirical emission factors. Information from all three sources is consumed by the chemical transport model SILAM that is used in both forecasting and re-analysis modes.

## 1. Introduction

A large variety of models for simulating atmospheric tracer gases and aerosols are currently used in the areas, such as emergency preparedness, chemical composition, air quality, stratospheric ozone, etc. (Saltbones et al., 1996; Maryon et al., 1991; Stohl et al., 1998; Robertson et al., 1999; Sofiev et al., 2006, 2008; Damski et al., 2007). It is currently accepted that different types of species and processes are interconnected and have to be considered together and with the appropriate interactions with each other. However, the objective limitations of the current knowledge about these interactions, as well as high computational costs largely reduce the ability of the existing models to reflect the actual relations.

Current paper presents the status and capability of the atmospheric composition and emergency modelling system SILAM, which represents one of attempts to provide a unified platform for a wide variety of tasks.

D.G. Steyn and S.T. Rao (eds.), *Air Pollution Modeling and Its Application XX*,
DOI 10.1007/978-90-481-3812-8, © Springer Science + Business Media B.V. 2010

## 2. Methodology

The Atmospheric Composition and Emergency Modelling System SILAM was started as emergency model described by Sofiev et al. (2006) and then extended towards more general atmospheric composition problems. It has two parallel dynamic cores. The Lagrangian random-walk particle model is based on well-mixed boundary layer assumption while he other core uses the Eulerian scheme of M.Galperin (1999, 2000) and the extended resistive analogy for vertical exchange by Sofiev (2002). A physico-chemical module of SILAM includes basic SOx-NOx-NHx-VOC-O3 chemistry, the linearized scheme for sulphur oxides, primary particles of various types, covers up to 496 radioactive nuclides, and probability. Meteorological information and geophysical data are routinely taken from regional NWP models, such as the HIRLAM, and from global models, such as the ECMWF Integrated Forecasting System.

New module for the biogenic VOC is based on the Guenther et al. (1995) model where the emission flux is computed as a product of several factors reflecting the type of the vegetation, released species, and the external meteorological forcing. The module considers the temperature- and light-dependent fluxes of monoterpenes, hemi-terpenes represented by isoprene, while the list of other compounds includes formaldehyde and a few hydrocarbons.

The smoke emission fluxes for SILAM are produced by a standalone Fire Assimilation System (FAS) based on Level 2 MODIS Collection 4 and 5 Active Fire Products. FAS consists of two parallel branches based on semi-independent products: the Temperature Anomaly and Fire Radiative Power (Sofiev et al., 2009).

## 3. Examples of the Model Applications

At present, the transformation modules responsible for the classes of substances outlined above do not interact with each other. However, even without interaction, the model-measurement comparison or the estimation of the total aerosol concentrations in air requires considerations of all relevant substances groups.

For instance, spring of 2006 in Europe appeared to be tough for allergic people: during several days at the end of April and the beginning of May high concentrations of birch pollen were reported in several countries, in particular, in Northern Europe. Absolute levels of birch pollen concentrations in air (pollen counts) varied from a few hundred grains per cubic meter (Iceland, 8–11 May) to a few thousands in Russia, Denmark, Germany, Poland, etc (20 April–10 May) and up to more than 10,000 grains $m^{-3}$ in Finland (6–10 May). The weekly number of phone calls to Finnish Asthma and Allergy Association for advisory service from 24 April to 14 May 2006 was from double to triple, compared to the same period of previous years.

However, the amount of pollen was not record-breaking and the severity of the episode can hardly be explained by pollen counts alone. An extra complexity to

the case was added by the large-scale wild-land fires in Russia that started in the middle of April and lasted up to the middle of May. These fires are not unusual either – they take place nearly every year in western and central Russia. By end of April the remnants of leaves and grass from the previous year dry sufficiently to get burned. Due to limited fire fighting measures, once ignited, the fires can continue during several days affecting large agriculture and wild-land areas. In 2006, the dry and warm weather prevailed in Western Russia during the considered period, which particularly emboldened the fires. The third component – anthropogenic pollution – concludes the list of sources of the episode. The severity of the episode was a result of a combination of unfavorable atmospheric conditions and intensive emissions from all the above source types (Fig. 1).

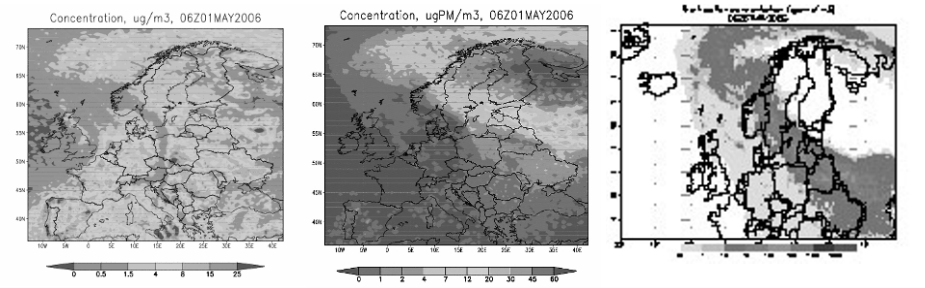


(a) Anthropogenic $PM_{10}$ μg PM $m^{-3}$ (b) Fire-induced $PM_{2.5}$ μg PM $m^{-3}$ (c) Birch pollen grains $m^{-3}$

**Fig. 1.** Concentrations of aerosols released from anthropogenic sources, wild-land fires and birch forests, forecast valid for 1.5.2006, 6:00 UTC

## 4. Summary

With growing understanding of multi-dimensional character of the atmospheric composition and air quality, it is important to include all the relevant species into consideration while evaluating environmental or health consequences of the atomspheric pollution. Current setup of the SILAM modelling system allowed inclusion of several main types of tropospheric aerosol and major reactive gases. The treatments for the types of aerosol currently being under development are the windblown mineral dust and secondary organic aerosol. The model applications showed that most of the recent strong air pollution events have originated from more than one source type, which are often synchronized and strengthened by unfavorable meteorological conditions.

## References

Damski, J., Thölix, L., Backman, L., Kaurola, J., Taalas, P., Austin, J., Butchart, N. and Kulmala, M. (2007) A Chemistry-Transport Model Simulation of Middle Atmospheric Ozone from 1980 to 2019 Using Coupled Chemistry GCM Winds and Temperatures, *Atmos. Chem. Phys*., 7, 2165–2181.

Galperin, M. (1999) Approaches for improving the numerical solution of the advection equation. In Z. Zlatev, J. Dongarra, I. Dimov, J. Brandt, and P. J. Builtjes, (Eds), *Large Scale Computations in Air Pollution Modelling*, pages 161–172. Kluwer Academic Publishers, 1999.

Galperin M.V. (2000) The Approaches to Correct Computation of Airborne Pollution Advection. In: *Problems of Ecological Monitoring and Ecosystem Modelling*. **XVII**, St. Petersburg, Gidrometeoizdat, 2000, pp. 54–68 (in Russian)

Guenther A., Hewitt N.C., Erickson D., Fall R., Geron C., Graedel T., Harley P., Klinger L., Lerdau M., McKay W. A, Pierce T., Scholes B., Steinbrecher R., Tallamraju R., Taylor J., Zimmerman P.A (1995): Global model of natural volatile organic compound emissions. J. Geophys. Res. 100, 8873–8892

Maryon, R.H., Smith, F.B., Conway, B.J., Goddard, D.M. (1991) The UK Nuclear Accident Model. *Progress in Nuclear Energy*, **26**, No 2, 85–104

Robertson, L., Langner, J. and Engardt, M. (1999) An Eulerian limited-area atmospheric transport model. *J. Appl. Meteor*. **38,** 190–210

Saltbones, J., Foss, A., Bartnicki, J. (1996) A real time dispersion model for severe nuclear accidents, tested in the European tracer experiment. *Syst. Anal. Modelling Simulat.* **25**, 263–279

Sofiev, M. (2002) Extended resistance analogy for construction of the vertical diffusion scheme for dispersion models. *J. of Geophys.Research – Atmosphere*, **107**, D12, doi: 10.10292001JD 001233.

Sofiev M., Siljamo, P., Valkama, I., Ilvonen, M., Kukkonen, J. (2006) A dispersion modelling system SILAM and its evaluation against ETEX data. *Atmosph. Environ.*, **40**, 674–685, doi:10.1016/j.atmosenv.2005.09.069.

Stohl, A., Hittenberger,M., and Wotawa,G. (1998): Validation of the Lagrangian particle dispersion model FLEXPART against large scale tracer experiments. *Atmosph. Envir.* **24**, 4245–4264.

# 3.7 Smog Forecasting in The Netherlands Using Assimilation of Ground-Based and Satellite Observations

**Astrid Manders[1,3], Suzanne Calabretta-Jongen[2], Henk Eskes[2], Martijn Schaap[1], Renske Timmermans[1], Arjo Segers[1], Ferd Sauter[3], and Daan Swart[3]**

[1] TNO Unit Environment, Health and Safety, P.O. Box 80015, 3508 TA Utrecht, The Netherlands

[2]KNMI , P.O. Box 201, 3730 AE De Bilt, The Netherlands

[3]RIVM, P.O. Box 1, 3720 BA Bilthoven, The Netherlands

**Abstract** The capability of the regional chemistry transport model LOTOS-EUROS to forecast air quality in the Netherlands has been tested. For PM10, the free-running LOTOS-EUROS model outperforms the time correlation of the Dutch operational statistical air quality forecasting model. But when a bias correction is applied also the abolute concentrations are modelled better than for the statistical model. For ozone, data assimilation of ground-level concentrations in The Netherlands, Belgium and Germany was applied using ensemble Kalman filtering. The data assimilation improved the initial conditions and the one-day forecast. However, the model has difficulties in forecasting extreme ozone concentrations. Work is under way to improve on this and to include ground-based PM observations and satellite observations of PM and NO2 in the assimilation process.

**Keywords** Air quality forecasting, data assimilation, ozone, PM10

## 1. Introduction

In the Netherlands, smog episodes due to enhanced concentrations of particulate matter or ozone occur occasionally. In such cases, the public is informed, so that people can adapt their behaviour. But already for modestly increased concentrations, sensitive people would like to be aware of the situation. Therefore, it is important to have an accurate smog forecast. Presently, two statistical models are used in the Netherlands. These models predict the daily average PM10 concentration and the ozone maximum concentration on observation locations, based on the weather and observed concentrations of the day before and on the weather prediction. The advantage of these models is that they are relatively simple, do not have a bias and

D.G. Steyn and S.T. Rao (eds.), *Air Pollution Modeling and Its Application XX*,
DOI 10.1007/978-90-481-3812-8, 

are good at predicting extreme values. But the limitation is that they do not include information about concentrations upstream, therefore they are often not so good in predicting the beginning and end of a smog episode. We have investigated the possibility to use the chemistry transport model LOTOS-EUROS to improve on the statistical models.

## 2. Model Description

LOTOS-EUROS is a Eulerian regional model (10W-40E, 35N-70N, grid resolution 0.5 × 0.25 lon × lat with zooming possibility) with three dynamical vertical layers and a surface layer, covering the lowest 3.5 km of the atmosphere. It uses an emission database with simple time-dependency, ECMWF meteorological fields and it includes chemistry for ozone formation (CBM-IV) and the formation of secondary inorganic aerosols. A complete description can be found in Schaap et al. (2008). Data assimilation with an ensemble Kalman filter (EnKF) is optional.

## 3. PM10 Forecasting

A test was done for 2004–2006, using LOTOS-EUROS on a zoom domain with nesting. The concentrations of secondary inorganic aerosols are in good agreement with observations, and also the concentrations of black carbon and sea salt aerosol can be predicted reasonably well, which gives the model credit (Manders et al., 2009). However, the model underestimated the total observed PM10 concentrations substantially, like most CTMs. This is caused by components for which the source processes are not well quantified, like mineral dust and secondary organic aerosols. To compensate for this, a simple bias correction was proposed, which depends on the season and the PM10 concentration:

PM10biascor = 1.54 * PM10 + 8.1 $R^2$ = 0.52 Winter (DJF)
PM10biascor = 1.42 * PM10 + 7.5 $R^2$ = 0.47 Spring (MAM)
PM10biascor = 0.76 * PM10 + 13.5 $R^2$ = 0.26 Summer (JJA)
PM10biascor = 1.31 * PM10 + 9.1 $R^2$ = 0.51 Fall (SON)

The model results are shown in Fig. 1 and Table 1, together with the observations and the results form the statistical model. The bias-corrected LOTOS-EUROS has a better time correlation than the statistical model, which is only marginally better than a persistence model. The drawback is that LOTOS-EUROS is still under-predicting the highest concentrations. This can be improved by using an alternative bias correction forced through the origin, which enhances the extremes, albeit this goes slightly at the expense of the general performance.

The free-running model is thus already better than the statistical model in a general sense. It could be improved further by using data-assimilation of ground-based PM10 observations from the Dutch air quality monitoring network and surrounding countries to improve the initial conditions. Furthermore, satellite data from for example MODIS could be used to detect and include the contribution of incidental sources like dust storms and forest fires, which cannot be included in emission databases. These possibilities will be investigated in the near future.

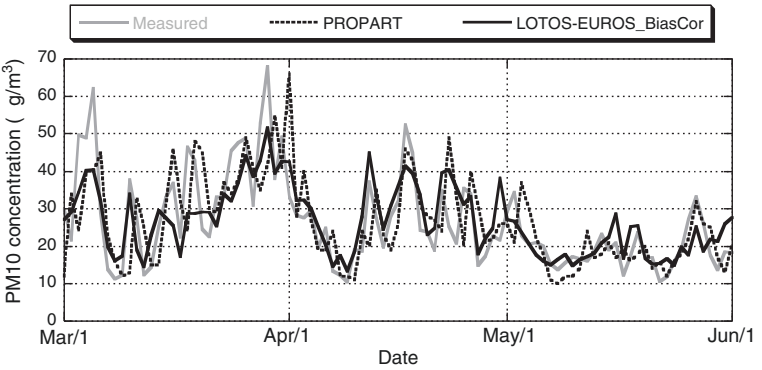


**Fig. 1.** Time series of observations, the bias-corrected LOTOS-EUROS and the statistical model PROPART for a station in the south-east of the Netherlands

**Table 1.** Performance of bias-corrected LOTOS-EUROS (LE_bc) as compared with persistence, the statistical model PROPART, LOTOS-EUROS without bias correction and LOTOS-EUROS with an alternative bias correction (LE_altbc)

| Parameter | LE_bc | Persist | PROPART | LE | LE_altbc |
|---|---|---|---|---|---|
| Mean (μg/m$^3$) | 26.45 | 26.51 | 27.22 | 13.25 | 25.21 |
| Bias (μg/m$^3$) | –0.03 | 0.02 | 0.82 | –13.23 | –1.28 |
| stde (μg/m$^3$) | 9.06 | 10.99 | 10.50 | 9.60 | 9.47 |
| Skillvariance | 0.70 | 1.00 | 0.99 | 0.50 | 0.89 |
| Correlation R | 0.70 | 0.63 | 0.66 | 0.68 | 0.70 |
| Residue (μg/m$^3$) | 6.49 | 7.64 | 7.53 | 13.40 | 6.94 |
| rmse (μg/m$^3$) | 9.06 | 10.99 | 10.54 | 16.34 | 9.56 |
| Hit rate | 49.21 | 46.32 | 45.43 | 8.30 | 44.47 |
| # Predicted 50–200 (μg/m$^3$) | 380 | 991 | 1047 | 1 | 725 |
| # Observed 50–200 (μg/m$^3$) | 1003 | 983 | 949 | 1003 | 1003 |
| %Correct 50–200 (μg/m$^3$) | 61.32 | 42.48 | 40.21 | 100.00 | 50.34 |

## 4. Ozone Forecasting

For ozone forecasting the operational statistical model performs well. But since it includes only temperature as meteorological variable, some situations cannot be handled well, for example when only part of the country is covered in cloud. LOTOS-EUROS is better equipped to include meteorological variables. Furthermore, it desrcibes the hour to hour development of the concentrations over the whole country and provides the timing of ozone maximum values which enhances the possibility to communicate the results to the general public.

The free-running LOTOS-EUROS model does not outperform the statistical ozone model for a 1-day forecast, but it does so for longer forecast times. Average concentrations are well modelled, but the variability of the model's extreme values is underestimated.

A data-assimilation procedure was set up, using hourly ground-based observations from the Dutch national air quality monitoring network and networks in Germany and Belgium, upwind of the Netherlands when conditions for smog are favourable. The emissions of NOx, VOC, the top ozone boundary conditions and deposition velocities were provided with random noise to create an ensemble. The EnKF was used with 15 ensemble members, which appeared to be the best trade-off between convergence and computational efforts. Indeed, the analysis was improved substantially (Fig. 2).

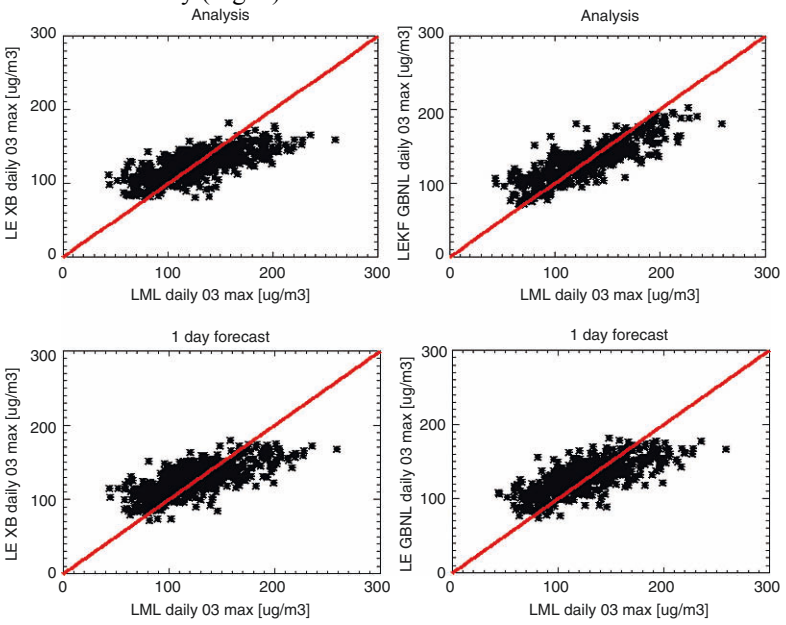


**Fig. 2.** Modelled (LE) versus observed (LML) daily ozone maxima. Upper panels: analyses of free-running model (left) and model with data assimilation (right). Lower panels: 1-day forecast of free-running model (left) and model with data assimilation (right)

When only initial conditions of the forecast are improved, the additional information from the assimilation is lost rapidly. Therefore, the noise settings from the analysis were used to adapt the emissions, boundary condition and deposition velocities also in the forecast. The noise settings from the time of the ozone maximum of the previous day appeared to give the best results for the 1 day forecast. For a longer forecast time, the free-running model was slightly better. This possibly relates to the question of how long the adapted emission settings are expected to be valid. Furthermore, since the free-running model is not able to reproduce the extremes, it is possible that the model is biased for high temperatures, which makes data assimilation effective in the sense that it improves the initial conditions but not in the sense that it compensates for inherent model uncertainties. Therefore, a temperature-dependent bias correction is being tested.

Further model improvements include the assimilation of NO2 column observations from OMI and the combination of the ground- and satellite-based data sets.

## 5. Conclusions

CTMs can be used successfully in forecasts during episodes of high concentrations of Particulate Matter and ozone. They are superior to statistical models when meteorological conditions change, especially at the beginning and end of the episode. Data assimilation of ground-based monitoring network data can improve the forecasts at least for 1 day ahead. Work is under way to include ground-based PM observations and satellite observations of PM and $NO_2$ in the assimilation process.

## References

Schaap et al.: The LOTOS-EUROS model: description, validation and latest developments. Int. J. Environment and Pollution **32** no 2. (2008)

Manders et al.: Testing the capability of the chemistry transport model LOTOS-EUROS to forecast PM10 levels in the Netherlands. Atmospheric Environment, **43** (2009)

# Chapter 4 Model assessment and verification

Chairpersons: T. Iversen
S.-E. Gryning

Rapporteurs: R. Jones
S. Galmarini

D.G. Steyn and S.T. Rao (eds.), *Air Pollution Modeling and Its Application XX*,
DOI 10.1007/978-90-481-3812-8_4, © Springer Science + Business Media B.V. 2010

# 4.1 Cluster Analysis and Classification of Wind Fields for Meteorological and Air Quality Model Validation

**Scott Beaver[1], Saffet Tanrikulu[1], Douw Steyn[2], Yiqin Jia[1], Su-Tzai Soong[1], Cuong Tran[1], Bruce Ainslie[2], Ahmet Palazoglu[3], and Angadh Singh[3]**

[1]Bay Area Air Quality Management District, San Francisco, CA, USA

[2]The University of British Columbia, Vancouver, BC, Canada

[3]University of California, Davis, CA, USA

**Abstract** Clustering of observed winds and classification of simulated winds were used for meteorological and air quality model evaluation. We simulated meteorology with MM5 and particulate matter (PM) with CMAQ for December to January 2000–2001 in the San Francisco Bay Area (SFBA). EOFs were used to classify simulated winds among the patterns identified by a previous clustering of observations. We investigated the match between the classification of the simulated winds and the original clustering. Agreement between the clustering of observed winds and the classification of simulated winds implies model validity. Disagreement serves as a diagnostic tool, indicating how inaccurately modeled winds may explain degraded air quality model performance. This novel framework complements traditional model validation methods.

**Keywords** Pattern matching, model evaluation, weather patterns, and wind field analysis

## 1. Introduction and Goal of Study

Accurate meteorological simulations are important for air quality modeling. Traditional model validation techniques include error and bias statistics calculated between simulated and observed fields [1]. Surface wind field accuracy is critical, especially for winter PM modeling. Here, a new validation technique is presented based on cluster analysis of observed winds and classification of simulated winds. Categorical evaluation is important for seasonal simulations, as the model must discriminate among different classes of conditions.

Clustering [2] is applied to wind field observations to group days sharing air flow patterns impacting air quality. A similar classification process is then applied to modeled wind fields. Agreement between the observation- and simulation-based groupings implies consistent spatial structures between the wind fields. Disagreement may indicate potential mismatches between the observed and simulated wind fields.

D.G. Steyn and S.T. Rao (eds.), *Air Pollution Modeling and Its Application XX*,
DOI 10.1007/978-90-481-3812-8, © Springer Science + Business Media B.V. 2010

Mismatches between observation- and simulation-based groupings can be used to explore the relationship between CMAQ model performance for PM and biases in the driving wind fields. This model validation approach is demonstrated for the winter PM season in the San Francisco Bay Area (SFBA) of California, USA.

## 2. SFBA Study Domain and Summary of Previous Cluster Analysis Results

SFBA is linked to Sacramento Valley (SV) and San Joaquin Valley (SJV) with connections at the Delta of the San Francisco Bay (Fig. 1). These basins share similar air quality characteristics due to similar emissions, meteorology and terrain. NAAQS 24-h $PM_{2.5}$ exceedances (>35 $\mu g/m^3$) occur mostly during anticyclonic weather conditions in December and January. Light, terrain-induced air flows influence PM buildup, allowing ample time for secondary PM to form.

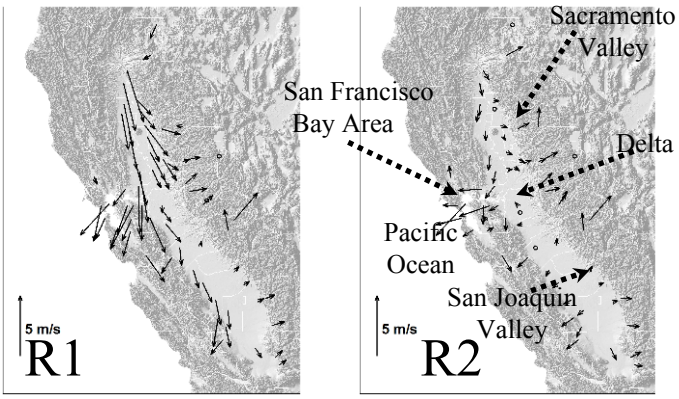


**Fig. 1.** Mean 1200 PST surface flow patterns for clusters R1 and R2. Arrow points along wind. Geography indicated using dashed arrows for the R2 pattern

Clustering 1996–2007 SFBA winter surface wind measurements identified five regional air flow patterns [2]. Three clusters (named R1, R2, and R3) are associated with anticyclonic conditions and elevated PM levels. ("R" denotes upper-level high pressure ridges.) R2 and R3 have weak large-scale pressure gradients, near calm SV and SJV conditions and shallow, localized flows through SFBA. R2 exhibits sustained SFBA easterly flows all day, whereas R3 SFBA flows may reverse to westerly in the afternoon. Over 80% of SFBA $PM_{2.5}$ exceedances occur under R2, and the rest are mostly under R3. R1 has a strong large-scale pressure gradient, high winds entering SFBA from the east, moderate mixing depth and moderate SFBA PM levels. Surface flows for R1 and R2 are shown in Fig. 1. Two other clusters (V-ventilated; Z-zonal, often with precipitation) exhibit strong large-scale pressure gradients, high SFBA westerly winds and low PM levels.

## 3. Classification of Simulated Winds

MM5 was used to simulate Central California meteorology for December to January 2000–2001 on a 4-km horizontal grid with 30 vertical layers. Simulated hourly winds were interpolated to 10 m AGL using the lowest modeled level for grid points closest to the SFBA monitors. Each day of model output was statistically classified among the five SFBA clusters (wind patterns) using EOFs.

Table 1 shows the correspondence of each pair of cluster (observation) and classification (simulation) labels using low- and high-order EOFs. Low-order EOF classifications reflect large-scale (synoptic) influences, and high-order EOF classifications reflect more localized winds. Several results are noted. First, MM5 could not produce the R3 flow pattern. Second, days with observations assigned to R2 were often simulated as R1. For low-order EOFs, nearly half (16 days) of the 33 R2 days were correctly classified. For high-order EOFs, the R2 days were usually classified as R1 (25 of 33 days). Third, for days with strong large-scale pressure gradients (clusters R1, V, or Z), simulation- and observation-based labels generally agreed. Three of five V days were classified as Z, the other cyclonic pattern.

**Table 1.** Observed cluster names and numbers of assigned days for December to January 2000–2001 (left panel). Numbers of simulated days classified to each pattern, using low- (middle panel) and high-order (right panel) EOFs

| Obs. clusters | | Model low-order classif. | | | | | Model high-order classif. | | | | |
|---|---|---|---|---|---|---|---|---|---|---|---|
| name | # days | R1 | R2 | R3 | Z | V | R1 | R2 | R3 | Z | V |
| R1 | 17 | 13 | 0 | 0 | 4 | 0 | 15 | 0 | 0 | 4 | 0 |
| R2 | 33 | 13 | 16 | 0 | 3 | 0 | 25 | 6 | 0 | 3 | 0 |
| R3 | 7 | 3 | 1 | 0 | 2 | 0 | 5 | 0 | 0 | 2 | 0 |
| Z | 11 | 1 | 0 | 0 | 11 | 0 | 2 | 0 | 0 | 11 | 0 |
| V | 5 | 1 | 0 | 0 | 3 | 2 | 1 | 0 | 0 | 3 | 1 |

The R2-R1 mismatch and the lack of R3 are consistent with MM5's tendency to exaggerate influences of the large-scale pressure gradient and understate localized flows. Anticyclonic conditions were generally simulated as R1, the anticyclonic pattern with the strongest synoptic forcing. R2 days were simulated with realistic low-order EOFs, but the model departed from reality at finer scales (high-order EOFs). As most PM episodes involve R2 (exceedances are rare under R1), the R2-R1 meteorological mismatch should result in CMAQ underestimating PM. Since MM5 distinguishes between anticyclonic and cyclonic conditions, it should reproduce the timings of the onsets and terminations of PM episodes.

## 4. Impacts of Meteorological Mismatch on Air Quality Simulation

The MM5 modeled winds were input to CMAQ using the SAPRC99-AE3aq chemical mechanism, a 4-km horizontal grid resolution and 16 vertical layers. Time series for 24-h observed and simulated PM levels are shown in Fig. 2.

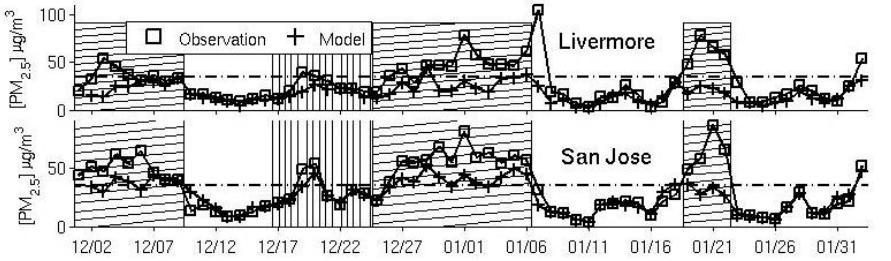


**Fig. 2.** Simulated and observed 24-h $PM_{2.5}$ levels for 2 SFBA PM monitors. Episodes highlighted: persistent R2-type (diagonal hatch), other (vertical hatch)

For three persistent R2-type episodes (Fig. 2), the R2-R1 mismatch occurred and PM levels were underestimated. Simulated winds were too strong in southern SV. Light overnight drainage (downslope) flows off the SV rims were observed, but MM5 winds were instead persistently downvalley. Simulated winds into the Bay Area from the east and in the northern SJV from the south agreed with the observations during the R2-R1 mismatch. Winds for another episode with rapidly evolving large-scale conditions (17–24 December) were realistically simulated, and modeled PM levels were reasonable.

## 5. Conclusions

The novel model validation technique indicates days for which a meteorological simulation cannot capture localized circulation patterns. It also suggests how air quality model performance may be adversely affected. This categorical model evaluation is useful for seasonal PM simulations that must distinguish between a variety of atmospheric conditions. The diagnosed MM5 shortcomings are consistent with MM5's documented problems of providing excessive synoptic push during periods of weak large-scale pressure gradients and light terrain-induced winds.

## References

Seaman, N.L., 2000. *Atmospheric Environment*, **34,** 2231–2259**.**
Beaver, S. et al., 2008. *A&WMA Ann. Conf. and Exh.*, #623, Portland, OR.

## 6. Questions and Answers

**Question:** In the SARMAP study for the Central Valley of California, the MM5 developers carried out many sensitivity studies. They found that a high vertical resolution was needed. Did you employ a high vertical resolution? Could the stated problem be due to model resolution? What was the grid resolution in your study (especially the lowest vertical grid)?

**Answer:** The MM5 configurations used in our study built upon a wealth of knowledge from previous modeling and field study efforts. The lowest modeled level in our MM5 simulations was around 24 m, and horizontal grid size was $4 \times 4$ km. We believe that this grid resolution is sufficiently fine to represent three dimensional PM transport and dispersion processes. The major deficiencies identified when validating the simulations related to localized flow features (slope flows and land/sea breezes) that could not be reproduced by MM5. The inability of this model to accurately simulate meteorological features at the intra-day time scale (less than about 12 h) has been documented by a number of researchers for various study domains.

**Question:** How much of the discrepancy in simulated PM levels was from meteorological insufficiency under stagnant conditions, and how much was from chemistry?

**Answer:** Our validation method only considers the fidelity with which meteorological conditions are simulated. The air quality simulation used the same chemistry model for every day, and only the meteorology was changed. Meteorology does affect PM precursor levels, which could indirectly affect the chemistry. The proposed method cannot apportion biases in simulated PM levels between these components.

**Question:** How is the "microscale" defined? Is it sub-grid scale, or defined physically based on monitoring network size? What is the exact cutoff value?

**Answer:** The scales are based on EOF modeling of surface wind monitoring network measurements. A large number of EOFs were estimated, and they could be ranked in order of decreasing scale. (This is not true of EOF modeling in general, but it has been verified for this particular study domain.) EOFs associated with the microscale appeared to capture random fluctuations. The fluctuations are not necessarily at the subgrid scale. The EOFs representing the fluctuations were ranked higher than the 14 EOFs retained for the model validation. There is no exact cutoff value based on the physical characteristics of the measured winds.

# 4.2 Measurement of Water-Soluble Organic Acids in Gaseous and Particulate Phases at a Suburban Site in Saitama, Japan

**Linfa Bao and Kazuhiko Sakamoto**

Department of Environmental Science and Technology, Graduate School of Science and Engineering, Saitama University, 255 Shimo-Okubo, Sakura, Saitama 338-8570, Japan

**Abstract** In summer, daily variation of water-soluble organic acids showed that gaseous and particulate phase concentrations reached the maximum in the daytime, and got down at deep night. The average abundances in gaseous phase to the total of organic acids ([G]/[P + G]) were 36%. The formation mechanism according to physical interactions was evaluated using a gas-particle sorption equilibrium model. It is suggested that the gas-to-particle sorption has occurred, but the sorption equilibrium has not reached yet. Gas-particle partitioning of organic acid depends not only on physical and chemical characteristics of organic acids, but also on other chemical compositions in aerosols.

**Keywords** Gas-particle partitioning, dicarboxylic acids, ketocarboxylic acids, oxygenated organic aerosol (OOA)

## 1. Introduction

Water-soluble dicarboxylic acids may affect aerosol's hygroscopic and cloud-nucleating properties (Peng et al., 2001; Abbatt et al., 2005), but the details of their secondary formation mechanisms and behaviors are still unclear. Dicarboxylic acids were considered to be principally associated with particle phase due to their relatively low vapour pressures and their hygroscopic behavior. However, recent investigations have shown that dicarboxylic acids display a semi-volatile behavior (Limbeck et al., 2001). A suitable approach for the correction of these semi-volatile compounds is the use of a denuder-filter-adsorbent system for sample collection (Limbeck et al., 2005). In this study, water-soluble organic acids (mainly dicarboxylic acids) in gaseous and particulate phases at a suburban site were investigated with an annular denuder-filter pack system.

D.G. Steyn and S.T. Rao (eds.), *Air Pollution Modeling and Its Application XX*,
DOI 10.1007/978-90-481-3812-8, 

## 2. Experimental

Two annular denuder-filter pack (AD-FP) systems were used for collecting of water-soluble organic acids in gaseous and particulate phases at a suburban site in Saitama, Japan. The AD-FP system consisted of a $PM_{2.5}$ cyclone (URG-2000-30EN), followed by two KOH-coated annular denuders (URG-2000-30B) in series, and a filter pack with a quartz filter (Pallflex 2500 QAT-UP) and a KOH-impregnated quartz filter. The sampler was operated at a flow rate of 16.7 $Lmin^{-1}$. The sampling was taken during July 29 to August 4, 2008 ($n$ = 48), with sampling intervals of 00:00−05:45, 03:00−08:45, 06:00−11:45, 09:00−14:45, 12:00−17:45, 15:00−20:45, 18:00−23:45, 21:00−02:45.

The Aerodyne aerosol mass spectrometer (Q-AMS, Aerodyne Research Inc.) was used to measure the compositions (water content, organics, sulfate, nitrate, chloride and ammonium etc.) of submicron aerosols ($PM_1$) during July 29 to August 4, 2008. The mass concentrations of hydrocarbon-like organic aerosol (HOA) and oxygenated organic aerosol (OOA) were further separated, using *m/z* 57 (mostly $C_4H_9^+$) and *m/z* 44 (mostly $CO_2^+$) as their tracers (Hagino et al., 2007).

Water-soluble dicarboxylic acids, ketocarboxylic acids, and dicarbonyls in denuder and filter samples were analyzed by means of $BF_3$/*n*-butanol derivatization to their esters followed by a gas chromatography/mass spectrometer (Shimadzu GCMS-QP 5050) determination (Kawamura and Yasui 2005). The target compounds were identified by comparison of GC retention times with mass chromatograms of authentic standards to contain quantities to 100, 250, 500, 1,000, 2,500, and 5,000 ng of each compound. These target compounds included seven saturated *n*-dicarboxylic acids ($C_2$: oxalic, $C_3$: malonic, $C_4$: succinic, $C_5$: glutaric, $C_6$: adipic, $C_7$: pimelic, and $C_9$: azelaic acid), three unsaturated dicarboxylic acids (M: maleic, F: fumaric, and Ph: phthalic acid), two ketocarboxylic acids (Pyr: pyruvic and $WC_2$: glyoxilic acid), and two dicarbonyls (Gly: glyoxal and MeGly: methylglyoxal).

## 3. Results and Discussion

In summer, the average total concentrations of target organic acids in gaseous and particulate phase were 496.2 and 1,076.6 $ng/m^3$, respectively. Oxalic acid ($C_2$), as the final product of photochemical reaction, was the most abundant species in gaseous and particulate phase. Longer chain *n*-dicarboxylic acids were less abundant in gaseous phase, except for malonic acid ($C_3$) and azelaic acid ($C_9$). $C_3$, glyoxilic ($WC_2$), and pyruvic acid (Pyr) have higher abundances in particulate phase.

Daily variation of gaseous and particulate phase concentrations together with OOA concentrations are showed in Fig. 1. Gaseous phase line showed multiple-peaks, and appeared the maximum in the afternoon (12:00−18:00) during July 29−31 and in the morning (06:00−12:00) during August 1−4, 2008, possibly due

to emission sources and different atmosphere state (including temperature, wind velocity, sunlight, relative humidity, oxidants, etc.). Particulate phase concentrations increased from lowest values at deep night (21:00−03:00) to the highest values in the afternoon (12:00−18:00). As the typical oxygenated organics, the total organic acids in particulate phase accounted for about 30% of OOA mass, and the concentration line exhibited a time trend similar to OOA in Fig. 1. The correlation between particulate organic acids and OOA was strong ($r$ = 0.93, $n$ = 48, $p$ < 0.001). In addition, Low-molecular-weight (LMW) dicarboxylic acids ($C_2$–$C_4$) in particles showed strong correlation with ambient oxidants ($r$ = 0.72 for $C_2$; $r$ = 0.74 for $C_3$, $r$ = 0.74 for $C_3$, $r$ = 0.67 for $C_4$, $n$ = 48, $p$ < 0.001), related to atmospheric oxidation processes.

Further, gas-particle partitioning of individual organic acid was shown in Fig. 2. The average abundances in gaseous phase to the total of organic acids ([G]/[P + G]) were 36%. LMW dicarboxylic acids ($C_2$–$C_4$) and ketocarboxylic acids ($WC_2$ and Pyr) had higher abundances in particulate phase (>61%), however unsaturated dicarboxylic acids (M and F) had higher abundances in gaseous phase (>87%). It is expected that compounds with decreasing vapor pressures will have increasing abundances in particulate phase. Interestingly, $C_4$–$C_6$ acids were observed with relative higher abundances in gaseous phase compared to $C_3$, though vapor pressures of $C_4$–$C_6$ are much lower (1.0E-05 mm Hg for $C_3$, 6.9E-07 mm Hg for $C_4$, 4.1E-06 mm Hg for $C_5$, 1.50E-07 mm Hg for $C_6$). $C_3$ has relatively higher acidity and solubility in water, and will be more efficiently scavenged from the gas phase into the particulate phase compared to $C_4$–$C_6$. It can be said that gas-particle partitioning depends not only on the vapor pressure, but also on other physical and chemical processes influencing the gaseous phase to particulate phase partition (Limbeck et al., 2005). For example adsorption onto available particle surfaces or absorption into a liquid phase of an individual compound will allow some gas to particle conversion to occur even when the gas phase pressure is below its saturation vapor pressure (Pankow 1994).

To discuss gas-to-particle sorption according to physical interactions, gas-particle sorption equilibrium constant $K$p was used (Pankow, 1994). The distribution of mass between gaseous and particulate phases at equilibrium can be described by $K$p:

$$K\mathrm{p} = [P]/([TSP]*[G]) \quad (1)$$

where [$TSP$] is the concentration of total suspended particles, [$G$] is the gaseous phase concentration for the target compound, and [P] is the particulate phase concentration. When we take the logarithm of the $K$p equation and put the log $K$p for $y$-axis and log [$TSP$] for $x$-axis, the curve is linear with a slope of −1:

$$\log K\mathrm{p} = -\log[TSP] + \log([P]/[G]) \quad (2)$$

During the sampling period, daily TSP concentrations were not available; instead we use the concentrations of $SO_4^{2-}$, $NO_3^-$, $NH_4^+$, organics, and water content in $PM_1$ instead of TSP as the sorption medium in the gas-particle sorption equilibrium. In summer, log [$K$p] showed relatively strong correction with log [*water content*] in the model (slope = −0.68, $r$ = 0.73, $n$ = 48, $p$ < 0.001) in Fig. 3, followed by log

[$SO_4^{2-}$] (slope = −0.61, $r$ = 0.70, $n$ = 48, $p$ < 0.001) and log [$NH_4^+$] (slope = −0.56, $r$ = 0.65, $n$ = 48, $p$ < 0.001). Good negative correlations indicate that the gas-to-particle sorption has occurred, and the slopes below −1 suggest that the sorption equilibrium has not reached yet. These results suggest that gas-particle partitioning of organic acid depends not only on physical and chemical characteristics of organic acid (vapor pressure, water solubility, Henry's law constant, acidity constant, etc.), but also on compositions in aerosols, such as water content (to affect aerosol hygroscopic), ammonium (to affect aerosol acidity and ammonium salt formation), and sulfate (to affect secondary particle formation).

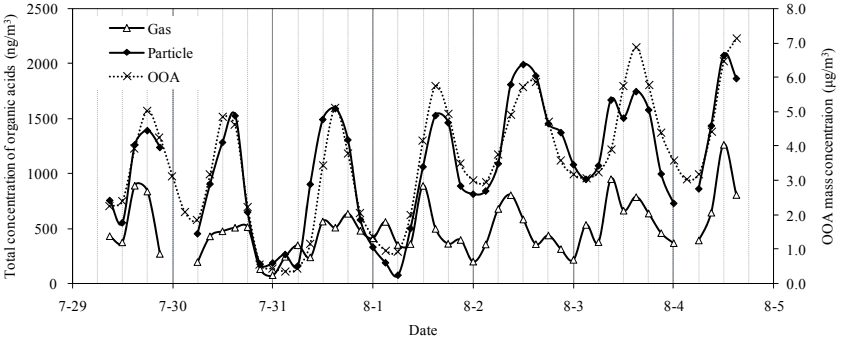


**Fig. 1.** Temporal variation of gaseous and particulate concentrations of total organic acids

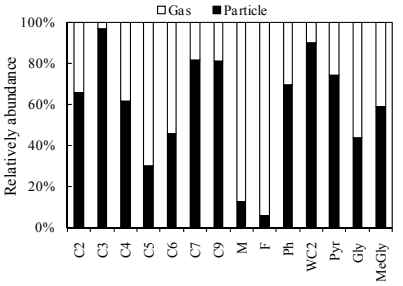


**Fig. 2.** Gas-particle partitioning of individual organic acid during July 29−August 4, 2008

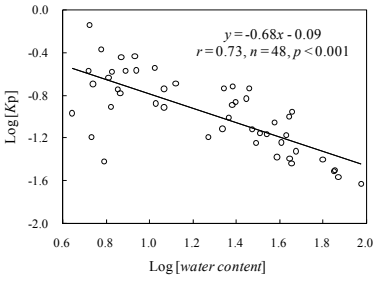


**Fig. 3.** Correlation between log [$K$p] and log [*water content*]; $K$p = [$P$]/([$G$]*[*water content*])

## References

Abbatt, J.P.D., Broekhuizen, K., Pradeep Kumar, P. (2005). Cloud condensation nucleus activity of internally mixed ammonium sulfate/organic acid aerosol particles. *Atmospheric Environment*, *39*, 4767–4778.

Hagino, H., Takada, T., Kunimi, H., Sakamoto, K. (2007). Characterization and source presumption of wintertime submicron organic aerosols at Saitama, Japan, using the Aerodyne aerosol mass spectrometer. *Atmospheric Environment*, *41*, 8834–8845.

Kawamura, K. and Yasui, O. (2005). Diurnal changes in the distribution of dicarboxylic acids, ketocarboxylic acids and dicarbonyls in the urban Tokyo atmosphere. *Atmospheric Environment*, *39*, 1945–1960.

Limbeck, A., Kraxner Y., Puxbaum, H. (2005). Gas to particle distribution of low molecular weight dicarboxylic acids at two different sites in central Europe (Austria). *Journal of Aerosol Science, 36*, 991–1005.

Limbeck, A., Puxbaum, H., Otter, L., Scholes, M.C. (2001). Semivolatile behavior of dicarboxylic acids and other polar organic species at a rural background site (Nylsvley, RSA). *Atmospheric Environment,* 31, 1853–1862.

Pankow J. F., 1994. An absorption model of the gas/particle partitioning of organic compounds in the atmosphere. *Atmospheric Environment, 28*, 185–188.

Peng, C., Chan, M.N., Chan, C.K. (2001). The hygroscopic properties of dicarboxylic and multifunctional acids: measurements and UNIFAC predictions. *Environmental Science and Technology, 35*, 4495–4501.

# 4.3 On the Use of a Dynamic Evaluation Approach to Assess Multi-year Change in Modeled and Observed Urban $NO_x$ Concentrations

**James M. Godowitch, George A. Pouliot, and S. Trivikrama Rao**

Atmospheric Modeling and Analysis Division, National Exposure Research Laboratory, United States Environmental Protection Agency, Research Triangle Park, NC, USA

**Abstract** Model results and measurements were analyzed to determine the extent of change in concentrations of nitrogen oxides ($NO_x$) during morning weekday high traffic periods from different summer seasons that could be related to change in mobile source emissions. The dynamic evaluation technique was applied to compare the relative (%) changes in modeled and observed 3-h morning $NO_x$ at numerous urban locations. The average changes in modeled and observed $NO_x$ levels between 2002 and 2005 were −16% and −15%, respectively, which are close to the decline (−17%) in $NO_x$ emissions estimated by a mobile emissions model.

**Keywords** Model evaluation, dynamic evaluation, $NO_x$ concentrations, $NO_x$ mobile emissions

## 1. Introduction

Since nitrogen oxides ($NO_x$ = NO + $NO_2$) are key precursor species in the photochemical production of tropospheric ozone, numerous control programs have been implemented to reduce $NO_x$ emissions from various source types (USEPA, 2005). The major source categories of anthropogenic $NO_x$ emissions include the electrical utility sector, industrial point sources, on-road and non-road mobile sources. However, in populated areas, on-road mobile emissions are the dominant source of $NO_x$. It is important from an accountability viewpoint to determine whether emission reductions achieve improvements in air quality. To investigate whether recent estimated reductions in mobile emissions have translated into changes in $NO_x$ concentrations, observed and modeled $NO_x$ concentrations during high traffic weekday 6:00–9:00 periods are analyzed from different summer years. The emerging dynamic evaluation approach was applied to focus on the model's ability to simulate concentration response to emission changes and how well it compares to changes in observations. In this regard, selected results of the relative (%) changes in modeled and observed morning $NO_x$ concentrations between the summers of 2002 and 2005 are highlighted.

D.G. Steyn and S.T. Rao (eds.), *Air Pollution Modeling and Its Application XX*,
DOI 10.1007/978-90-481-3812-8, © Springer Science + Business Media B.V. 2010

## 2. Study Description

### 2.1. Model overview and scenarios

The Community Multiscale Air Quality (CMAQv4.5) chemical transport model (Byun and Schere, 2006) was applied in this study using the CB-IV photochemical mechanism. Simulations were performed for the same 3-month summer period (June 1–August 31) in 2002, 2004, and 2005. The modeling domain covered the eastern United States (US) and southeastern Canada with a 12 km horizontal grid cell resolution. There were 14 vertical layers with a layer 1 thickness of 40 m. Gilliland et al. (2008) provides details about these model simulations and results of a prototype application of the dynamic evaluation approach involving an assessment of the impact on modeled maximum 8-h $O_3$ concentrations in the eastern US due to major point source $NO_x$ emission reductions over these periods.

Meteorological fields were generated by the Penn State/NCAR fifth-generation mesoscale model (MM5v3.6.3) with a four-dimensional data assimilation (FDDA) technique. The CMAQ Meteorology-Chemistry Interface Processor (MCIP v3.1) was exercised to post-process MM5 output into compatible input data sets with hourly 2-D and 3-D meteorological parameter fields for the CMAQ simulations. Specific details about the MM5 simulations are given in Gilliland et al. (2008).

The 3-D emissions were generated by the Sparse Matrix Operator Kernel Emissions (SMOKE v2.2) processing system. Anthropogenic emissions from the EPA 2001 National Emissions Inventory (NEIv3) were used to generate surface and elevated point source emissions with complete details in Gilliland et al. (2008). The MOBILE6 model generated gridded on-road vehicle emissions based on projections of vehicle-miles-traveled (VMT) and fleet factors for a reference county in each state for each summer period. The typical temporal variation in average weekday mobile emissions (Fig. 1) shows a rapid early morning ramp up due to increasing traffic with the peak rush period emissions from 7:00 to 8:00 AM. Figure 1 also indicates mobile $NO_x$ emissions declined between these two summer seasons in this grid cell encompassing Washington, DC. In fact, mobile $NO_x$ emissions in the modeling domain decreased by close to 18% between summers 2002 and 2005 from the MOBILE6 model (Gilliland et al., 2008).

### 2.2. Measurements

Hourly $NO_x$ measurements at numerous sites in the eastern US were analyzed in this study. Data for different years were obtained from US EPA's Air Quality System data base (http://www.epa.gov/ttn/airs/airsaqs/detaildata/).

## 3. Results and Discussion

The hourly average modeled $NO_x$ concentrations in the grid cell covering Washington, DC and at an urban monitoring site in Fig. 2 depict the typical temporal variation found at numerous locations with the highest concentrations occurring from 6:00 to 9:00 AM. Peak concentrations are clearly associated with the highest mobile emissions displayed in Fig. 1. The dramatic decrease in modeled and observed $NO_x$ concentrations during the late morning period is primarily attributed to a combination of meteorological processes, (i.e., greater vertical mixing and increasing horizontal transport) associated with the growth of the convective mixing layer and increasing photochemical activity which converts $NO_x$ to other nitrogen products. The temporal pattern of hourly modeled concentrations (Fig. 2a) closely resembles the observed results in Fig. 2b indicating CMAQ captures the dynamic and chemical processes governing concentrations during this time period. Modeled and observed results indicate lower $NO_x$ concentrations in summer 2005.

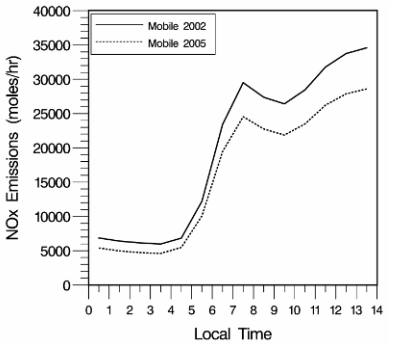


**Fig. 1.** Modeled mobile $NO_x$ emissions in the grid cell of Washington, DC during summers 2002 and 2005

Weekday morning periods from 6:00 to 9:00 are of particular interest since the high $NO_x$ concentrations are strongly governed by mobile emissions. Observed and modeled 3-h average $NO_x$ concentrations were computed from hourly concentrations for each weekday. Cumulative frequency distributions (CFDs) of modeled 3-h $NO_x$ concentrations from an urban grid cell displayed in Fig. 3 depict the range in concentrations and the differences between these two summer periods. A notable decrease in $NO_x$ is apparent across a broad range of concentrations which was also evident at other urban locations (not shown). A weekday mean concentration was computed from values over the 50th to 95th percentiles in each CFD to focus on change in the upper portion of the modeled and observed distributions for each urban site. A comparison of modeled results from summer 2002 versus summer 2005 in Fig. 4a reveals that, with few exceptions, $NO_x$ in 2005 was lower than in 2002 at sites exhibiting a broad range of $NO_x$ concentration levels. Figure 4b displays similar results from the urban measurement sites. These

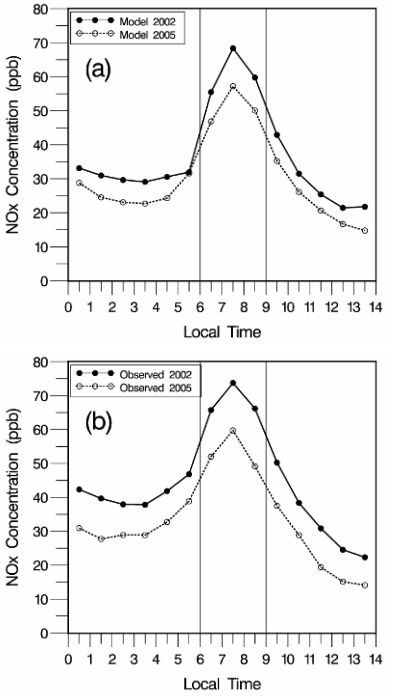


**Fig. 2.** Temporal variation of (a) modeled and (b) observed weekday average $NO_x$ concentrations at the same location as in Fig. 1

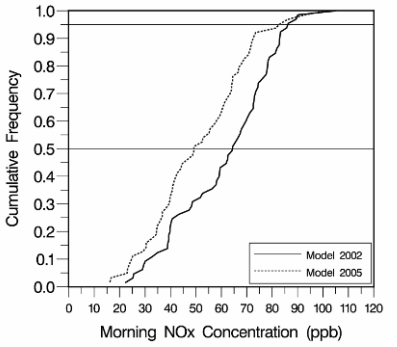


**Fig. 3.** Cumulative distributions of modeled morning $NO_x$ concentrations from summer 2002 and 2005 in the Washington, DC grid cell

results are also in agreement with the overall decline reported in 3-h average morning observed $NO_x$ concentrations in this region spanning a more extended set of years (NESCAUM, 2006). Results based on 34 urban sites reveal the average changes in modeled and observed weekday morning $NO_x$ concentrations between summers 2002 and 2005 were −16% ± 6% and −15% ± 9%, respectively, which are close to yet slightly less than the mobile $NO_x$ emissions decline of −17% ± 1%

generated by the MOBILE6 model at these locations. Although mobile emissions represent a majority (≈70% or more) of $NO_x$ emissions in the urban areas, variations in $NO_x$ emissions from other source categories are also likely impacting the relative change in concentrations.

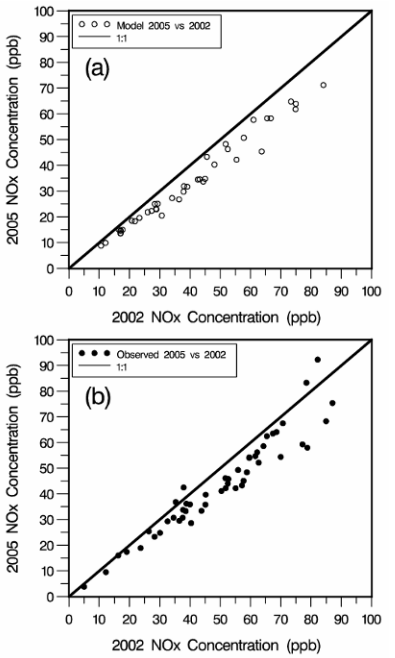


**Fig. 4.** Results of (a) modeled and (b) observed mean $NO_x$ concentrations averaged over the 50th to 95th percentiles of CFDs for the summer of 2002 versus 2005

**Disclaimer** Although this work was reviewed by EPA and approved for publication, it may not necessarily reflect official Agency policy.

## References

Byun, D., Schere, K.L., 2006. Review of the governing equations, computational algorithms, and other components of the Models-3 Community Multiscale Air Quality (CMAQ) modeling system. Appl. Mech. Rev., 59, 51–77.

Gilliland, A.B., C. Hogrefe, R.W. Pinder, et al., 2008. Dynamic evaluation of regional air quality models: Assessing changes in $O_3$ stemming from changes in emissions and meteorology. Atmos. Environ., 42, 5110–5123.

NESCAUM, 2006. The Nature of the Ozone Air Quality Problem in the North east: A Conceptual Description. October 2006, Boston, MA. (http://www.nescaum.org/topics/air-pollution-transport )

USEPA, 2005. Evaluating Ozone Control Programs in the Eastern United States:Focus on the NOx Budget Trading Program, 2004, EPA454-K-05-001. (http://www.epa.gov/airmarkets/progress/progress-reports.html)

# 4.4 Evaluation of the Air Quality Forecasting System Using Satellite and In-situ Data

**Marje Prank, Milla Lotjonen, Joana Soares, and Mikhail Sofiev**

Finnish Meteorological Institute, Erik Palmenin Aukio 1, Helsinki, Finland

**Abstract** The paper presents the evaluation of the regional air quality forecasting system based on chemical transport model SILAM, using three pollution cases selected in the CO ST Action 728 – a heavy PM episode in Central Europe during January–April 2003, mainly fire-induced multi-pollutant episode in April–May 2006, and another fire- and anthropogenic- emission induced episode in August 2006. Modelling results for these cases were compared with both in-situ and satellite measurements. Comparison with in-situ data shows the model well reproducing or over-estimating PM concentrations while under-estimating most of gases. Comparison with AOD data from MODIS shows that the model correctly reproduces the overall spatial patterns being in most cases within a factor of 1.5 from the total spatially-averaged AOD. For total modelled AOD at 550 nm, the largest contributions came from sulphates, nitrates and primary PM2.5, while coarse particles and sea salt contributions were negligible.

**Keywords** Model evaluation, model inter-comparison

## 1. Introduction and Setup of the Evaluation Exercise

The current paper presents model evaluation exercises performed within the scope of the COST Action 728 "Enhancing mesoscale meteorological modelling capabilities for air pollution and dispersion applications". A specific exercise performed within the Action was the multi-model evaluation and inter-comparison using three selected challenging pollution cases: a set of heavy PM episodes in Central Europe, February–March 2003; multi-pollutant episode in April–May 2006, largely created by wild-land fires in western Russia, and fire- and anthropogenic- emission induced episode in August 2006.

There were up to seven models performing the specific episode analysis. This multi-model ensemble was evaluated against in-situ and remote-sensing observations as shown in Fig. 1. Additionally, the individual models were compared with each other and the ensemble average was computed with the Joint Research Centre Ispra ENSEMBLE software.

D.G. Steyn and S.T. Rao (eds.), *Air Pollution Modeling and Its Application XX*,
DOI 10.1007/978-90-481-3812-8, © Springer Science + Business Media B.V. 2010

One of the goals of the evaluation was to test the ability of the multi-model ensemble to (a) reproduce the specifics of the episodes (the actual level of concentrations), preferably, better than the individual models do, (b) reflect the uncertainty of the predictions represented via an ensemble spread.

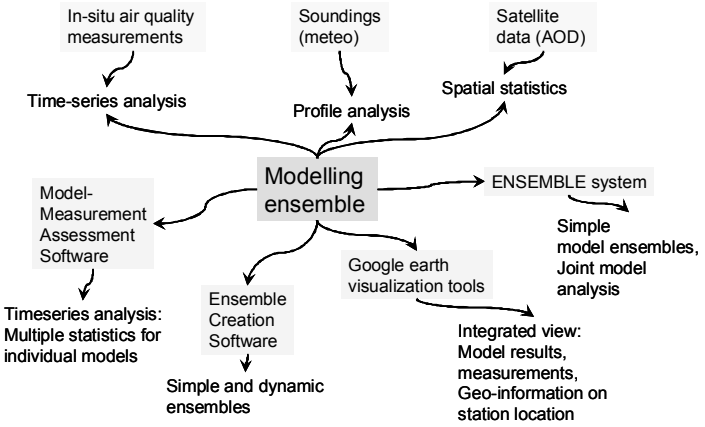


**Fig. 1.** A scheme of evaluation of the model ensemble

The current paper presents the details of evaluation of the SILAM model, which was one of the members of the multi-model ensemble.

For the SILAM model (Sofiev et al., 2006, 2008) evaluation, the input meteorological data were taken from ECMWF operational archives for the case of 2003 and from FMI-HIRLAM v.6 for both 2006 cases. Anthropogenic emissions of CO, NH3, NOx, SOx and primary PM from TNO and EMEP emission inventories were used. The wild-land fire emissions were derived from the MODIS fire radiative power product using FMI Fire Assimilation System FAS-FRP. Separate computations were also performed for sea salt. For 2006 cases daily MODIS Collection 5 AOD (Kaufman et al., 1997) was generated at Giovanni website http://disc.sci.gsfc.nasa.gov/techlab/giovanni/. Hourly in-situ observations of a few main pollutants were collected from the Airbase archive of European Environment Agency and included about 150 sites in 2003 and over 300 for 2006.

## 2. Results of the Computations and Comparison with Observations

The episode of February–March 2003 was a continuation of long-lasting poor air quality conditions (Fig. 2), with the bulk of pollution seemingly originating from the anthropogenic sources (Stern et al., 2008). The end of the series was put by a frontal precipitation 7.3.2003, which cleaned the air and promoted better ventilation due to substantially increased wind speed.

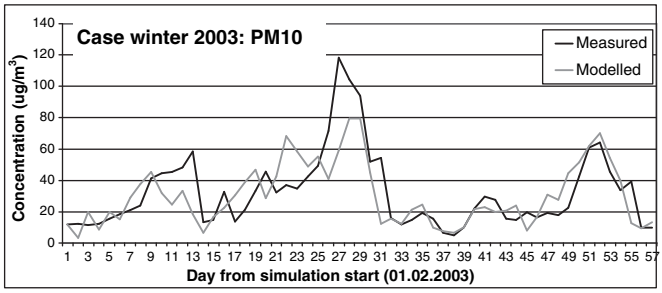


**Fig. 2.** Predicted PM-10 time series (μg $m^{-3}$) for Melpitz site (Germany), 2003

The spring episode in 2006 started in mid-April when high temperatures over most of Eastern Europe dried the soil, leading to a significant risk of fires. The low wind speed resulted in poor ventilation. After a few days of accumulation, a "cloud" of pollutants about 1,000 km in diameter was blown north-westwards reaching Iceland and Spitsbergen (Fig. 3). The development of this multi-pollution episode was strongly driven by the meteorology, which synchronised otherwise uncorrelated phenomena – birch flowering, forest fires, and accumulation of anthropogenic pollutants.

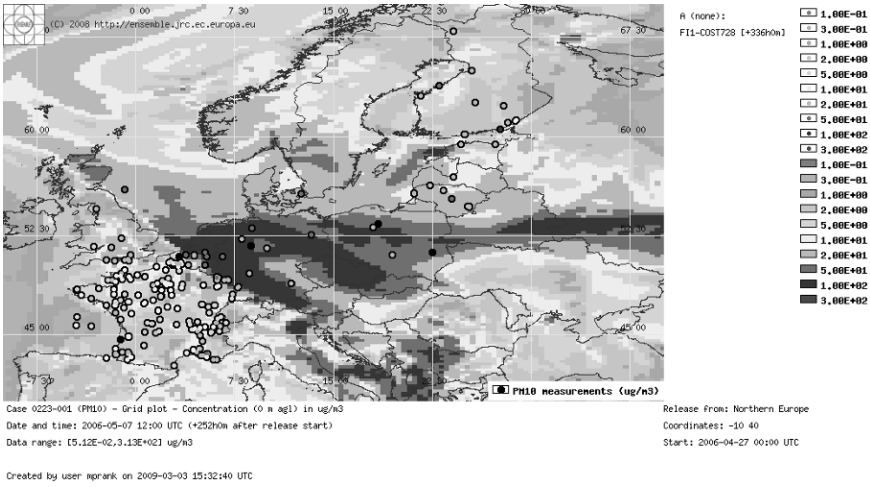


**Fig. 3.** Predicted PM-10 pattern (μg $m^{-3}$) for 7.5.2006, 12:00. Observations for the same hour are plotted on top of the model map using the same color scale

Total aerosol optical depth at 550 nm computed by SILAM was compared with AOD measured by MODIS The spatial correlation coefficient between SILAM and MODIS maps computed for each day of the episode ranges from ~0.5 to over 0.7, being highest during days with the highest mean modelled concentrations, when the wind is blowing from the large emission sources, such as fires in Russia,

and lowest in the opposite case – wind from areas, such as Atlantic ocean, with low and also partly missing emissions.

The main contributions to modelled AOD at 550 nm averaged over the whole period of computations, come from sulphates (47%), nitrates (30%), and fine-mode primary particles (16%) while the contributions of sea salt and coarse primary particles are negligible. The contribution of fire emissions gives about one fourth of the total AOD raising up to 30% for specific periods.

## 3. Conclusions

Selected cases by-construction evaluate the model ability to work in complicated conditions sayng little about the standard situations.

The model tends to fit well or over-estimate PM under-estimating most of gases (except for the highest PM-10 peak 27.2.2003). PM also has the highest correlation at hourly averaging. Comparison with MODIS AOD showed that the model correctly reproduces the overall spatial pattern being in most cases within a factor of 1.5 from the total spatially-averaged AOD.

The pattern was sensitive to chemical composition of the emission. In spring-2006, the visibility degradation was largely driven by sulphates, nitrates and primary PM-2.5, while PM-10 and sea salt contributions were negligible. Wild-land fires were the major contributor of both PM and reactive gases.

Synchronization by meteorological conditions was found between the plumes from different sources, such as anthropogenic emitters and biomass burning.

## References

Kaufman, Y. J., Tanre D., Remer L. A., Vermote E. F., Chu A., Holben B. N. (1997) Operational remote sensing of tropospheric aerosol over land from EOS moderate resolution imaging spectroradiometer, *J. Geophys. Res*, **102**, *D14.* 17,051–17,067.

Sofiev, M., Galperin, M., Genikhovich, E. (2008) Construction and evaluation of Eulerian dynamic core for the air quality and emergency modeling system SILAM. *NATO Science for piece and security Serties C: Environmental Security. Air pollution modelling and its application*, **XIX**, Borrego, C., Miranda, A.I. (eds.), Springer, pp. 699–701.

Sofiev, M., Siljamo, P., Valkama, I., Ilvonen, M., Kukkonen, J. (2006) A dispersion modelling system SILAM and its evaluation against ETEX data. *Atmosph.Environ.*, **40**, 674–685, DOI:10.1016/j.atmosenv.2005.09.069.

Stern, R., Builtjes P., Schaap M., Timmermans R., Vautard R., Hodzic A., Memmesheimer M., Feldmann H., Renner E., Wolke R., Kerschbaumer A. (2008) A model inter-comparison study focussing on episodes with elevated PM10 concentrations *Atmosph. Environ.*, **42***, 19*, 4567–4588.

## 4. Questions and Answers

**Question:** We have no theory for ensemble dispersion modeling, you are already developing a tool, this means standardization of the practice. Can you comment on that?

**Answer:** The "no theory" statement sounds too bold for me. In fact, a complete theory is indeed lacking, while some of the pieces are at hands: perturbational analysis, adjoint sensitivity estimation, singularity vectors, etc. These items are not fully utilized in daily practice of AQ or emergency ensembles, which are indeed more based on hand waving than rigorous derivations. But the more reasons to develop tools based on these approaches. Also, developing a tool is a way to facilitate the advance of theory: by making a "toy to play with". I would not also be afraid of "standardization" of practice: all depends on how to use the particular instrument and what to include in it as basic formulations.

**Question:** Are you sure that ANY model should be admitted to the ensemble or minimum requirement should be set?

**Answer:** Well, rather yes than no. Every modern model passes certain evaluation during the development and applications, so it should not deliver outright wrong computations to the ensemble – not as a rule, at least. But each model is allowed to have "bad days" and it is the task for ensemble generation methodology to eliminate the influence of problems of individual members. With more advanced approaches, there has to be a segregation of the models introduced as a result of their evaluation during the ensemble building.

# 4.5 Est modus in Rebus: Thoughts on Ensemble Modeling from Darwin to Horace

**S. Galmarini and S. Potempski**

European Commission – DG Joint Research Centre, Institute for Environment and Sustainability, Via E. Fermi 2749, 21027, Ispra, VA, Italy

**Abstract** The use of multi-model ensembles in atmospheric dispersion applications is becoming more and more popular. Methodologies for the combination of model results explored in the past are being adopted even in the operational or pre-operational contexts. However several questions remain unanswered like these relating to the way in which the ensemble should be set up. In other words, which criteria should be adopted to guarantee that the ensemble results will always be superior to those of any individual member? By means of mathematical formalism the paper tries to address this problem.

## 1. Introduction

The properties of ensembles have been demonstrated in various situations and case studies and often in the scientific literature we read the *mantra*: "*... the performance of ensemble of models is shown to be (systematically) superior to that of individual models*". However, although the results from those case studies are undisputable evidence of the fact that the technique works, the above mentioned conclusions relate to heuristic considerations that are confined to the cases analyzed. In this context, the ensemble practice relies on what we could define *phenotypical model distinction*. Models differ for a limited number of modules or simply for the data used; the differentiation of a common model *genotype* occurs whenever the model is adopted or used in a specific *modeling environment* (modeling group, modeling application). In most of the cases the ensemble practice brings together models that show no substantial difference and that are available since they survived the natural selection of individual model evaluation. Therefore one may ask: is it automatically guaranteed that the ensemble performance is superior to the one of the individual members? Is it always the case?

To deal with such generally posed issues we will try to make use of mathematical formalism for describing multi-model ensemble systems. This will allow us to find some basic properties of such systems, which can be deduced from general characteristics of statistical distributions of the ensemble members.

D.G. Steyn and S.T. Rao (eds.), *Air Pollution Modeling and Its Application XX*,
DOI 10.1007/978-90-481-3812-8, 

## 2. The Results

In the article [2] a simple formula for mean square error (*msqe*) was presented to explain the advantage of the multi-model ensemble system for long-term ozone simulations in comparison with a single model approach, namely:

$$msqe = (1 + \frac{1}{m})\sigma^2 + b^2 \tag{1}$$

The formula (1) is valid under the assumption that statistical distributions of model results and observations are independent and identical. The latter assumption is obviously a simplification as the models differ in terms of used parameterizations or numerical concept. Nevertheless it clearly demonstrates that *msqe* for the ensemble (after bias correction) is always less than that of any single model (m = 1). Starting from this, we would like to give a slightly deeper look at the analysis based on statistical characteristics of *msqe*. We will focus on simple one-dimensional case i.e. when the simulation results can be described by a *scalar-valued random variable* for each model (for instance when multi-model ensemble is applied at a single point in space and time), however analogous formulas can be obtained for the multi-dimensional case i.e. when the problem is described by a *vector-valued random variable* [1].

Let us then assume that by using a set of *m* atmospheric dispersion models we get *m* simulations of the concentration of an unspecified substance at some point in space and time together with measurements. Both model data and observations are characterized by some estimation of uncertainty, which we formally represent by *random variables* $x_j$, $j = 1,\ldots,m$, where $x_j$ corresponds to data produced by model *j*, and analogously for the observations by *random variable y*. Each $x_j$ has statistical distributions characterized by probability density functions (pdf) with bias and variance. We consider two cases: when the models are not correlated (i.e. $E\{x_1, x_2\} = E\{x_1\}E\{x_2\}$ where $E\{\}$ is the expectation value) or correlated.

We assume that the multi-model ensemble results are represented by a normalized linear combination of model results which we denote by *X*, namely:

$$X = \sum_j \alpha_j x_j, \quad \sum_j \alpha_j = 1, \ \alpha = [\alpha_1,\ldots,\alpha_m]^T \tag{2}$$

Assuming that the models and measurements are un-correlated (i.e. random variables *X* and *y* are un-correlated) we can express *msqe* as:

$$msqe = V(X - y) + (E(X - y))^2 = V(X) + V(y) + b^2, \quad b = E(X - y) \tag{3}$$

where *b* is the ensemble bias and *V* stands for the variance. Furthermore information on model biases allows eliminating bias term from (3). Then one can

pose a general problem of finding linear combination which minimizes *msqe*. The solution is given in Table 1.

**Table 1.** Weights and optimal variances

| Model un-correlated case | Model correlated case |
|---|---|
| $\alpha_k = \frac{\frac{1}{V(x_k)}}{\sum_j \frac{1}{V(x_j)}}, \quad V(X_{opt}) = \frac{1}{\sum_j \frac{1}{V(x_j)}}$ | $\alpha = \frac{K^{-1}l}{(K^{-1}l, l)}, \quad V(X_{opt}) = \frac{1}{(K^{-1}l, l)}$ $l = (1,...,1)^T, \quad (\cdot,\cdot) = dot\ product$ |

$K$ represents covariance matrix i.e. its $ij$-th element is the covariance of $x_i$ and $x_j$. From these formulas one can conclude some basic properties of multi-model ensemble shown in Table 2. In case of correlated models eigenvalues of the covariance matrix $(s_1,\ldots,s_m)$ play the role of variances $V(x_j)$ – the basic properties are analogous. It is easy to find an example showing that the ensemble mean can produce worse results than the best individual model, while optimal combination always overperforms any single model [1]. The last implications in Table 2 show which conditions ensure that the ensemble mean produces better *msqe* than any single model.

**Table 2.** Basic properties of multi-model ensembles

| Model un-correlated case | Model correlated case |
|---|---|
| $\frac{V(x_1)}{m} \le V(X_{opt}) \le \frac{V(x_m)}{m}, V(x_1) \le \ldots \le V(x_m)$ | $\frac{s_1}{m} \le V(X_{opt}) \le \frac{s_m}{m}, s_1 \le \ldots \le s_m$ |
| $V(X_{opt}) \le \min\{V(x_1), \frac{V(x_m)}{m}\}$ | $V(X_{opt}) \le \min\{V(x_1), \frac{s_m}{m}\}$ |
| $\frac{V(x_m)}{V(x_1)} \le m+1 \Rightarrow V(X_{mean}) \le V(x_1)$ | $\frac{s_m}{s_1} \le m \Rightarrow V(X_{mean}) \le s_1$ |

## 3. Conclusions

First of all by choosing appropriate combination of model results we can find an optimal representative of the ensemble that after bias correction minimizes *msqe* and ensemble will not be deteriorated even by a model with a big variance. Secondly general estimations for the optimal variance and msqe have been obtained showing that multi-model ensemble oveperforms any single model. Thirdly we have shown which condition guarantees that the ensemble mean gives more accurate results than any individual model. This is expressed in the terms of the ratio between

highest and lowest variances or eigenvalues of the appropriate covariance matrix. And finally the same ratio can be considered as an indicator of the *coherence* of the multi-model ensemble. The biggest the ratio is, the highest disagreement among the models in estimating the uncertainty can be observed.

## References

Potempski S Galmarini S (2009) Est modus in rebus: Analytical properties of the multi-model ensembles. Accepted in Atmos. Chem. Phys. Discuss.

Van Loon M et al. (2007) Evaluation of long-term ozone simulations from seven regional air quality models and their ensemble. Atmos. Environ. 41, pp. 2083–2097.

## 4. Question and Answers

**Sarah Lu:** Is the ensemble approach used in NWP applicable to atmospheric dispersion models?

**Answer:** There are many elements that can readily be transfer from one discipline to the other, namely indexes, cluster methodologies. I do not think that the actual methodologies used in NWP for the generation of ensembles (breeding vectors or singular vectors) is applicable to CTM as in general the chemical transformation , even when starting from different initial conditions will tend to converge to the same solution of chemical equilibrium. Never the less the use weather scenarios produced by NWP can be used to take into account the variability of weather patterns and represent automatically a source of variability to be used for the creation of the CTM ensemble.

**Bernard Fisher:** Have you considered different ways of weighting individual model results with the ensemble (apart from a weighted average)? I think that the averaging depends on the decision (trade off, precautionary etc.)

**Answer:** In the absence of experimental evidence and working with pure forecast I could agree with you, although finding a weighting technique that take those elements into account could lead to complicated situation. In the presence of experimental evidence, weighting techniques exist like Bayesian Model Averaging, which allow the use of all existing information to improve the ensemble analysis and give direction on the models that, in forecast mode, should be considered leaders of the ensemble performance. It should be also added that this is also related to the metrics used (like msqe), which should reflect the purpose of the modelling. For different metrics different optimal ensemble representatives can be found.

**Steve Hanna:** Would it help to use second order closure in the models and therefore directly predict the uncertainty (pdf) in addition to the mean?

**Answer:** This is a technique that we have used to transform emission uncertainty into concentration uncertainty (see Galmarini et al., ACP, 2008). Unfortunately that could work only for uncertainties relating to surface-atmosphere interaction where the boundary layer and its turbulence act as system for the transfer of surface information to the upper atmospheric levels.

**Peter Builtjies:** Could we use the fact that in most cases the ensemble/average has a higher correlation than the single model as information about 'stable' and more uncertain model aspects?

**Answer:** To answer your question you would need to gather precise evidence and in formation. However you would agree with me that we are lacking fundamental research on ensemble behaviours. It is clear by now that the ensemble produces a results that compensate for opposite behaviours of individual models, however being a practice, based on heuristic approaches, it does not guarantee of maximum exploitability neither gives hints on which pre-requisite a model should have to produce yet a better result. A theoretical base would help greatly in that setting the boundaries of applicability of the practice and ingredients for its improvements.

**Iversen Trond:** I tend to disagree with you that combining mediocre model results into ensemble is not a valid strategy compared to improving the models. I think it well established theory that as long as the ensemble does not sample the entire uncertainty space, any added, bias-free, ensemble member will improve the ensemble beyond the single ensemble member.

**Answer:** Well it depends on what we need with mediocre, and how bad is bad enough. Your argument would be correct in principle if the members would be independent. We know that our models are not independent at all and they may all be biased toward a specific solution that would be closer to reality but still further than it could be if we could get more clear idea on what it means being independent, estimate the level of dependency, get to know the impact of the dependency on the final result. I find paradoxically that from one side efforts and resources are invested in model development, extremely detailed process modelling, getting our models as deterministic as possible but then we do not care on the quality of their results and their impact of an ensemble because finally averaging will sort all out.

# 4.6 Clustering Analysis of Air Quality Model Performance

**Christopher Fung[1], Paul Yau[1], Connie Lam[2], Philip Yu[2], and Linda Yu[1]**

[1]Hong Kong Environmental Protection Department, 33/F Revenue Tower, 5 Gloucester Road, Hong Kong Special Administrative Region, China

[2]Department of Statistics and Actuarial Science, University of Hong Kong, Pokfulum, Hong Kong

**Abstract** A model performance evaluation approach based on matching clusters was developed to provide a first indication of an air quality modeling system's performance. Observed weather, modeled weather, observe air quality, modeled air quality parameters are clustered and the optimum number of clusters chosen. These sets of clusters are then compared against each other to determine the performance of the individual modules and also how well the modeling system can reproduce the relationship that exists between meteorology and air quality measurements. An index is used to quantify the matches between the different clusters. Change in the values of this index resulting from changes in the system (formulation, input data …etc.) can be interpreted as real improvements or deteriorations of the modeling system's performance.

**Keywords** Air quality modeling system, clustering, performance, evaluation

## 1. General Framework

The performance of a photochemical air quality modelling system depends on the accuracy of each module – emissions, meteorology and transport and chemistry. Yet, the amount of outputs of these modules can be so voluminous that it is often difficult to determine from them whether the system has indeed 'improved' after some measures have been taken to that effect.

Figure 1 gives a schematisation of an approach based on clustering to overcome the difficulty with overwhelming data. Treating emissions as the quasi-steady unknown, the approach recognises that there are recurrent weather patterns which give 'clusters' in the weather parameters. These 'weather clusters' also affect air pollution in distinctive ways through three dimensional transport, availablity of sun light, etc. giving air quality clusters. On the other hand, air quality responds to factors other than meteorology, e.g. spatial and temporal distribution of emissions. By first clustering observed weather parameters (Box 1) and air quality parameters

D.G. Steyn and S.T. Rao (eds.), *Air Pollution Modeling and Its Application XX*,
DOI 10.1007/978-90-481-3812-8, © Springer Science + Business Media B.V. 2010

(Box 2) separately, then doing the same with the output of the meteorological and transport and chemistry module (Boxes 3 and 4) in an air quality modelling system and then comparing the observed and modelled clusters, a synoptic view of the performance of each module can be quantified (Boxes 7 and 8). By further determining the correlation between the observed meteorological and air quality clusters (Box 5), one gets an understanding of the degree to which air quality is determined by meteorology. Repeating the same analyses of cluster correlation for the two corresponding simulation modules (Box 6) would determine if the model can mimick this aspect of the air pollution phenomenon. All these statistical information (Lower right box) would together give a first indication of where performance improvements are needed and determine whether the modelling system, after incorporating some 'intended improvements', has moved in the desired direction.

## 2. Assumptions and Methodology Development

The spatial extent of this analysis cannot be too large for the basic homogeniety assumption to hold, i.e. for the weather parameters to be meaningfully clustered, the area should be influenced by the same synoptic meteorological feature 'simultaneously', hence an area of less than 100 km each way would be appropriate. Hourly data would serve as basic input, but given the spatial scale considered and the diurnal solar forcing, the hourly data from all the monitoring stations within the analysed area are averaged over a day and served as the basic input for clustering. Given the relatively large number of parameters involved in both meteorology and air quality (over 10 each), a long enough period (5 years or more) should be used. The stations were judiciously chosen after inspecting the data. Then standard cleansing and imputation of missing and dubious data were performed on the data set.

Two issues are to be addressed for basic clustering: (1) the best clustering method, and (2) the optimum number of clusters (the number of clusters used in each of culster boxes – 1–4 in Fig. 1 – can be determined independently, hence different). The best clustering approach is determined by trying different methods (hierarchical, K-means, hybrid of the preceding) and judging their performace by a 'correlation coefficient between actual and ideal similarity matrices' (Tan et al., p 542–543, http://www-users.cs.umn.edu/~kumar/dmbook/index.php) and the silhouette coefficient based on cluster cohension and separation (Tan et al., p 536–541). The K-means method was determined to have produced the best clustering results and is adopted for all clustering. The upper limit of cluster number is guided by subjective understanding of weather and air quality patterns which suggests a number less than 10 or so. The optimum number of cluster is then determined from the inflection point in the sum of squared distance (total distance of all points in parameter space from respective cluster centres) versus cluster number plots.

The goodness of the match between clusters (Boxes 5–8 in Fig. 1) is then calculated from the Cramer's V index (based on Chi-square $\chi^2$ statistic, http://www.stats-consult.com/tutorial-10/tutorial-10.htm). This index would vary between 0 and 1 with 1 indicating perfect match between two sets of clusters.

## 3. Applications to an Air Quality Modeling System

The PATH (Pollutants in the Atmosphere and their Transport over Hongkong) air quality modelling system comprises MM5 as the meteorological driver, SAQM as the transport and chemistry module, with the emission data distributed temporally, spatially and speciated by EMS-95. Usually four domains, each with 49 × 49 horizontal grids, are run in a nested fashion (grid spacing of 40.5, 13.5, 4.5 and 1.5 km) with the finest resolution domain covering all of Hong Kong. Data from 10 meteorological stations out of a total of 27 and the 11 air quality monitoring stations were used for clustering observations. Model output from corresponding grids in the 1.5 km resolution model domain are used for model clustering. Only ground level (first layer of model) parameters are used. The parameters used in meteorological clustering are wind speed, wind direction, temperature, relative humidity, pressure, cloud percent, mixing height (calculated), maximum mixing height (calculated), rainfall and radiation (not available in model); and that for air quality are: RSP, $NO_2$, NO, $O_3$, $SO_2$, CO, FSP, $NO_2/NO$, $NO_X/SO_2$, oxidants ($O_3$ + $NO_2$) and FSP/RSP. Ten years (1997–2006) of observations and 6 years (2000–2005) of modelled data are used in this analysis. The emission data used for the 6 years of model simulations is fixed at 2003.

## 4. Clustering Results and Discussions

The optimal numbers of clusters for Boxes 1–4 are 7, 7, 6, 10, respectively. Some selected general characteristics of the observed weather clusters are shown in Table 1 for illustration. In terms of time of occurrences, there are distinct summer (3 – high temperature, low pressure and southerly flow), winter (4 – opposite of 3 and low relative humidity; 1 – easterly flow), year-round easterly flow (2 – light winds, 5 – strong winds), and heavy summer rain (7 – southerly flow and low pressure) ... etc.

The values of the Cramer's V index between these modules (Boxes 5–8) show that the modelled meteorological clusters match their observed counterpart (Box 7 – 0.513, see Table 2 for the correspondences between these clusters) better than that for air quality (Box 8 – 0.328) as is to be expected given that imperfect meteorological modelling would propogate its errors to the air quality modelling results. The Cramer's V values for the modelled meteorology versus air quality clusters (Box 6 – 0.440) is higher than that of the observed (Box 5 – 0.295). While the goal for module performance enhancement is to increase the Cramer's V value in

Boxes 7 and 8, the goal for overall system performance improvement would be to minimise the difference between Boxes 5 and 6 regardless which is higher. Given that there are factors other than meteorology – most notably the spatial and temporal emissions distribution – that shape the air quality picture in reality, the Cramer's V for observation (Box 5) should be less than 1. On the other hand, the modelling system could be over-idealising the emissions (e.g. fixed in space with only periodic temporal variations), thus producing a stronger correlation between meteorology and air quality. The direction for improvement is thus pointed out.

The above comparison of clusters is based on 'free' clustering in that each set of cluster in Boxes 1–4 is determined independently. However, if the goal is to diagnose by how much the model deviate from reality, then one should determine how well the model outputs fit in the clusters defined by observations. This raises another issue. In 'forcing' the model outputs into the observed clusters, depending on the shape of data set, the performance statistics could be strongly 'disfavoured' or 'favoured' by systematic biases for some parameters. In fact, when forcing is applied to evaluate the modelled meteorology and air quality, the Cramer's V value increases for the former (0.548 vs. 0.513) and decreases for the latter (0.292 vs. 0.328). But once we have 'forced' the clustering, it also makes sense to correct for the systematic biases to isolate the residual discrepancy. Table 1 shows model systematic under-prediction of rainfall and cloud amount. But one can go further by recognising that there are also cluster-specific systematic biases, e.g. rainfall under-prediction can range between 12% and 95% depending on the cluster. When these biases are corrected for in the cluster definitions for forced clustering of the meteorological data, the Cramer's V are: 0.535 with overall bias correction, and

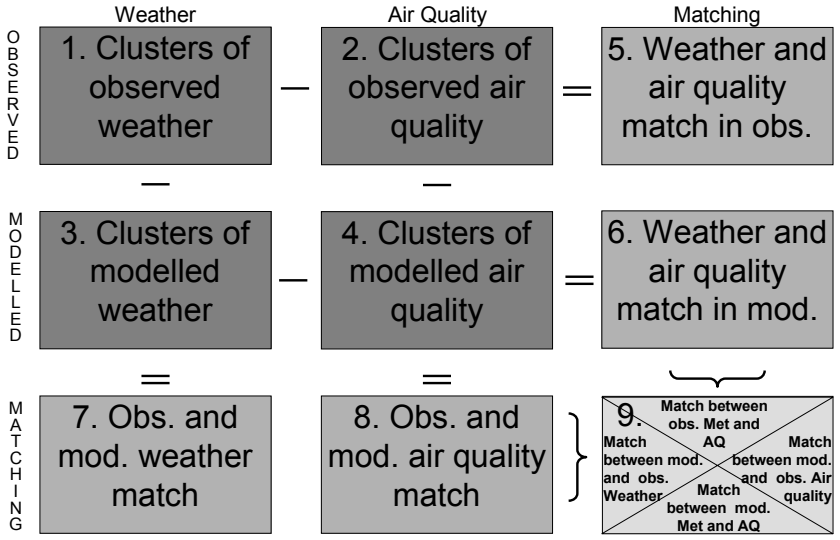


**Fig. 1.** Schematic of Analysis Approach

0.561 with cluster-specific bias correction, versus 0.548 without any correction. The indefinite results (improvement and deterioration) from the two bias corrections here testify to the complexity of the overall pattern which is not easily amenable to simple dissections, but must be viewed as a whole as in this initial attempt.

**Table 1.** Selected cluster characteristics of obs. meteorological data

| *Cl.* | *#Obs.* | *WS m/s* | *WD deg* | *Temp C* | *RH %* | *Pres mb* | *Cld %* | *Rain cm/day* |
|---|---|---|---|---|---|---|---|---|
| 1 | 887 | 3.2 | 75 | 18.3 | 80.1 | 1017.5 | 0.64 | 0.059 |
| 2 | 774 | 2.5 | 95 | 25.6 | 80.0 | 1010.7 | 0.59 | 0.079 |
| 3 | 695 | 3.0 | 209 | 27.3 | 82.9 | 1006.7 | 0.67 | 0.174 |
| 4 | 553 | 4.1 | 23 | 15.6 | 64.4 | 1020.9 | 0.55 | 0.042 |
| 5 | 484 | 5.5 | 89 | 24.1 | 82.0 | 1011.5 | 0.75 | 0.182 |
| 6 | 214 | 3.2 | 121 | 25.0 | 91.1 | 1007.0 | 0.87 | 1.655 |
| 7 | 45 | 4.2 | 159 | 24.7 | 93.1 | 1004.8 | 0.92 | 4.923 |
| Obs. Mean | | 3.5 | 88 | 22.4 | 79.3 | 1013.0 | 0.65 | 0.252 |
| Model Mean | | 3.3 | 57 | 20.8 | 80.9 | 1000.8 | 0.38 | 0.112 |

**Table 2.** Match between observed and modelled meteorological clusters

| | | *Observed clusters* | | | | | | |
|---|---|---|---|---|---|---|---|---|
| *Mod clus* | | *1* | *2* | *3* | *4* | *5* | *6* | *Total* |
| | *1* | 180 | 224 | 119 | 4 | 6 | 0 | 533 |
| | *2* | 155 | 10 | 269 | 27 | 8 | 1 | 470 |
| | *3* | 30 | 0 | 46 | 317 | 3 | 5 | 401 |
| | *4* | 1 | 317 | 20 | 0 | 1 | 0 | 339 |
| | *5* | 176 | 15 | 82 | 3 | 11 | 1 | 288 |
| | *6* | 46 | 0 | 10 | 38 | 25 | 11 | 130 |
| | *7* | 6 | 0 | 2 | 14 | 3 | 3 | 28 |
| *Total* | | 594 | 566 | 548 | 403 | 57 | 21 | 2,189 |

## 5. Question and Answers

**Question:** You left open the question if you would prefer to force the model or let the model generate its own patterns. In a comparison of GCM output with reanalysis data, we chose the second approach. Do you have a recommendation for an appropriate choice? When the bias is low, forcing seems a good approach, but if the biases are high I would definitely let the model generate its own patterns.

**Answer:** Free and forced clustering should theoretically reveal different things – the pattern and the overall performance, respectively. One way to test this theoretical understanding is to correct for the bias in the model output and see if the match between the observed and modeled clusters improves. And the bias can be corrected in two ways: scale the model output by the ratio of the averaged observed value to modeled value for each parameter or scale by the average value

observed value to modeled value for each parameter or scale by the average value for each parameter of each cluster. One would expect the performance to improve from the first (cruder) correction to the second (finer) correction. Yet as pointed out in the last part of the paper, when we tried these two corrections with the meteorological module, the match between modeled and observed clusters improves in one and deteriorates in the other relative to the case without any bias correction. We are still in the process of understanding such behaviour.

**Question:** How are *parameters* (wind, temperature, mixing depth … etc.) *selected* for use in cluster analysis? Is there any *systematic* approach that has been used?

**Answer:** We try to look at the match between output of an air quality modeling system and observation as a whole with the matches of individual modules as part of the analysis. As such, consideration of both meteorological and air quality parameters to be used should not be done separately as meteorological parameters and air quality parameters. Since one step in this technique is to maximize the match between observed meteorology and air quality clusters (Box 5 in Fig. 1) as a bench mark for the modeling system, whatever we think may enhance such match is considered. One example is the trial inclusion of mixing height, a derived meteorological parameter which has implications on air pollution concentration. Another example is the trial inclusion of composite parameters like photochemical smog ($O_3 + NO_2$) in air quality which may respond better to meteorological forcing than the individual pollutants on the averaging time scale used here. As such, there is no a priori way to determine the best list of parameters, as this will vary from place to place given its dependence on the peculiar combination of pollutants in conjunction with the climate. Guided by our initial understanding of the air quality phenomenon, we will test different combinations of meteorological and air quality parameters and then combine the two to determine which combination of meteorological and air quality lists of parameters will produce the best match in the observation data. The list of meteorological and air quality parameters (separate) will be adopted.

# 4.7 An Application of Lagrangian Particle Model with Chemical Reactions to Power Plant Pollution Dispersion in Complex

**Stefano Alessandrini[1] and Enrico Ferrero[2]**

[1]ERSE (Enea Ricerca Settore Elettrico), via Rubattino 54, Milano

[2]Università del Piemonte Orientale, via Teresa Michel, 11, Alessandria, Italy

## 1. Introduction

A modeling system based on the regional atmospheric model RAMS (Pielke et al., 1992) and the Lagrangian particle model SPRAY (Tinarelli et al., 2000) is adopted to forecast the concentration of pollutants around the CERCS power plant, situated in a complex terrain area of Spain. To calculate also the $NO_2$ concentration, we introduced in the Lagrangian dispersion model an hybrid Lagrangian-Eulerian scheme for chemical reactions between nitrogen oxides an ozone including the $NO_2$ photolysis. This new model was tested in controlled conditions in a previous work (Alessandrini and Ferrero, 2009). It is worth noticing that the small distance of the air quality stations from the power plant stacks gives the possibility to study also the cases where the plume has not still reached the photochemical equilibrium condition. In these situations the photochemical algorithm used shows considerably important advantages compared to more simple approaches generally adopted. The results of the simulations carried out using the modeling system are presented analyzing some particularly interesting episodes. The comparison between the predicted and measured concentrations of all the emitted substances shows the ability of the chemical scheme to account for the short term turbulent dispersion.

## 2. The Chemical Model

Following Chock and Winkler (1994a, b) chemistry and dispersion are treated separately and sequentially, each particle (n) released by the source may bring mass of different substances. At each time step the particle position $X^{(n)}(t)$ is updated using the stochastic model equation, then the concentrations of each substance is calculated in a fixed Eulerian grid and the chemistry is updated.

Formation of $NO_2$ occurs when NO is emitted in an atmosphere containing $O_3$. During the daytime, photo-dissociation of $NO_2$ by absorption of ultra-violet

D.G. Steyn and S.T. Rao (eds.), *Air Pollution Modeling and Its Application XX*,
DOI 10.1007/978-90-481-3812-8, © Springer Science + Business Media B.V. 2010

radiation leads to the production of NO and $O_3$. The chemical reactions considered by our model are:

$$NO + O_3 \xrightarrow{k} NO_2 + O_2 \qquad NO_2 + O_2 + h\nu \xrightarrow{J} NO + O_3$$

where $k$ depends on temperature and is around 0.4 $ppm^{-1}s^{-1}$ while $J$ depends on solar radiation and ranges between 0, during the night, and 0.4 $min^{-1}$ in the full sunlight. The discretized form of the chemical equation is (for NO and similarly for the other compounds):

$$\left\langle c_{NO}(\mathbf{x}_j, t_1)\right\rangle = \left\langle c^*_{NO}(\mathbf{x}_j, t_1)\right\rangle - k\Delta t\left\langle c^*_{NO}(\mathbf{x}_j, t_1)\right\rangle\left\langle c^*_{O_3}(\mathbf{x}_j, t_1)\right\rangle + j\Delta t\left\langle c^*_{NO_2}\left(x_j, t_1\right)\right\rangle$$

where * indicates the concentration in the cells after the turbulent dispersion but before the chemical reaction. In the case of $O_3$ deficit of concentration was introduced as described in Alessandrini and Ferrero (2009). Then the mass of the different substances were redistributed to each particle in the cell.

## 3. Segregation Parameterization

In order to simulate the chemical reaction in a turbulent flow on a time scale less than the typical equilibrium scale the cross covariance term between the concentration fluctuation $< c_A' c_B' >$ of the two compounds participating to the reaction should be accounted for. The contribution of this term is often referred as "segregation" and $\alpha = \dfrac{< c_A' c_B' >}{< c_A > \cdot < c_B >}$ is the segregation coefficient.

Looking at the Brown and Bilger (1998) wind tunnel measurements the covariance term seems to experience an exponential decay with the distance. Thus a new parameterization for the segregation coefficient (Alessandrini and Ferrero, 2009) was obtained as a function of the downstream distance, "x", by performing a best fit of the experimental data presented in Brown and Bilger (1998):

$$\alpha = -0.71 e^{-0.12\frac{x}{N_D x_s}}$$

where $x_s$ is the stoichiometric distance (the distance where the mixing ratio of the plume becomes equal to the background mixing ratio) and $N_D$ the Damköhler number (which represents the ratio between the time scales of turbulence and chemical reactions). In this work we have adapted this parameterization to a real atmospheric dispersion case. For $x_s$ the constant values 5,000 m was assumed and $N_D$, estimated from the chemical and turbulence parameters, was set to 0.22.

## 4. Numerical Simulations

The power plant of CERCS is situated inside a very narrow valley in the west part of Spain 100 km far from Barcellona inside the Pirenaic Mountains.

The modeling system consists in a coupled model based on the regional atmospheric model RAMS 6.0 and the Lagrangian particle model SPRAY. The two models are interfaced by MIRS code, which uses the RAMS outputs to calculate the boundary layer and turbulence parameters for the Lagrangian dispersion model SPRAY not directly provided by the circulation model. The forecast of the hourly 3D wind and turbulence fields for the 2 day simulation period (6–7 February 2006) has been carried out by RAMS-MIRS using three nested grids driven by the ECMWF global model analysis fields as boundary condition. The dispersion simulations were performed by SPRAY on a domain corresponding to the smallest RAMS grid of 22 × 22 km$^2$ centered on the stack (120 m high) with a horizontal resolution of 500 m. A variable time step scheme has been used for the Lagrangian particles displacement while the chemical reactions time step was set equal to 30 s. The cells for the concentrations computation have been set equal to 100 × 100 × 50 m$^3$ and constant all over the domain. The reaction rates $k$ and $J$ were computed every hour using the following equations (IUPAC 2005 and Parrish et al., 1983):

$$k = 3.1 \cdot 10^3 \cdot \exp(-1450/T)\,;\; J = 0.01305 \cdot \exp(-0.36/\cos(\alpha))\,,$$

where T is the air temperature, computed by RAMS, and α is the complementary of the solar elevation angle. The ozone background concentration have been set variable, equal to the hourly $O_3$ concentration measured by an EMEP (http://tarantula.nilu.no/projects/ccc/emepdata.html) background station located 50 km far from CERCS plant. An air quality station located 1 km far from the stack measures the NO and $NO_2$ hourly average concentrations used for the comparison with the model results. For sake of comparison two kinds of simulations have been carried out activating ("segr") or not ("no segr") the segregation parameterization.

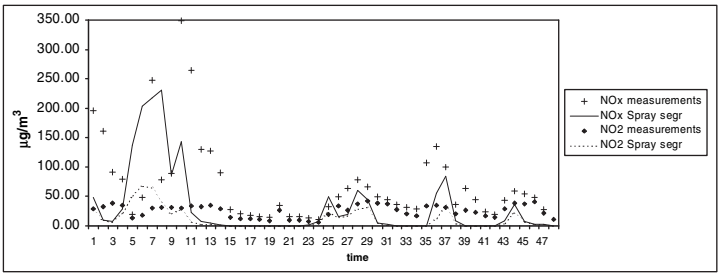


**Fig. 1.** $NO_2$, NOx hourly average concentrations measured and simulated by Spray (segr) simulation during the period 6–7 February 2006

In Fig. 1 $NO_2$, $NO_x$ hourly average concentrations measured and simulated by Spray ("segr") during the period 6–7 February 2006 are compared. Beside the difficulty in evaluating the chemical model performances because measured and simulated $NO_x$ concentrations rarely agree at the same time, it can be observed that Spray generally reproduces the $NO_x$ measurements trend. However, when the values of $NO_x$ are similar, the $NO_2$ simulated values are very close to the measured ones. A useful comparison is shown in Fig. 2, where $NO_x$ against $NO_2/NO_x$ concentrations, concerning measured data, Spray "segr" and Spray "no segr" simulation results, during the nocturnal hours, are depicted. As a matter of fact, being in these cases the ozone background concentrations almost constant, the $NO_2/NO_x$ measured values depend only on the $NO_x$ measured values, especially for high $NO_x$ values, where only the 10–20% of NO emitted has been transformed in $NO_2$ due to the oxidation reaction with $O_3$. The effect of the segregation parameterization yields to a slowing down of the oxidation reaction that otherwise would produce much more $NO_2$ and consequently higher $NO_2/NO_x$ levels at the station location.

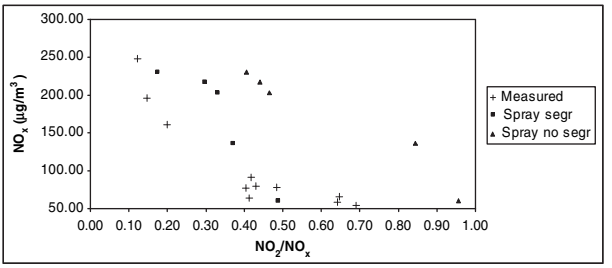


**Fig. 2.** $NO_x$ against $NO_2/NO_x$ measured, Spray "segr", and Spray "no segr" concentrations during nocturnal hours

**Acknowledgments** This work has been financed by the Research Fund for the Italian Electrical System under the Contract Agreement between CESI RICERCA and the Ministry of Economic Development – General Directorate for Energy and Mining Resources stipulated on June 21, 2007 in compliance with the Decree n.73 of June 18, 2007.

## References

Alessandrini S. and E. Ferrero, 2009, A hybrid Lagrangian-Eulerian model for reacting pollutant dispersion in non-homogeneous non-isotropic turbulence, Physica A, 388. pp. 1375–1387

Brown R. J. and R. W. Bilger, 1998: Experiments On A Reacting Plume–1. Conventional Concentration Statistics, Atmospheric Environment, 32, No. 4, pp. 611–628

Chock D. P., Winkler S. L., 1994a: A particle grid air quality modeling approach, 1. Dispersion aspect, Journal of Geophysical Research, 99 D1, 1019–1031.

Chock D. P., Winkler S. L., 1994b: A particle grid air quality modeling approach, 2. Coupling with Chemistry, Journal of Geophysical Research, 1994, 99 D1, 1033–1041.

IUPAC 2005 Evaluated kinetic and photochemical data for atmospheric chemistry- IUPAC subcommittee on gas kinetic data evaluation for atmospheric chemistry. July 2005 web version http://www.iupac-kinetic.ch.cam.ac.uk/index.html

Parrish D.D., Murphy P.C., Albritton D.L., Fehsenfeld F.C. 1983. The measurements of the photodissociation rate of NO2 in the atmosphere, Atmospheric Environment Vol. 17, n°7, 1365–1379

Pielke R. A., Cotton W. R., Walko R. L., Tremback C. J., Lyons W. A., Grasso L. D., Nicholls M. E., Moran M. D., Wesley D. A., Lee T. J., Copeland J. H. (1992) A Comprehensive Meteorological Modeling System RAMS. Meteorology and Atmospheric Physics, 49, 69–91.

Tinarelli G., Anfossi D., Bider M., Ferrero E. and Trini Castelli S. (2000) A new high performance version of the Lagrangian particle dispersion model SPRAY, some case studies, Air Pollution Modelling and its Applications XIII, S.E. Gryning and E. Batchvarova eds., Plenum Press, New York, 23

# 4.8 Tropospheric Ozone in Regional Climate-Air Quality Simulations over Europe: Future Climate and Sensitivity Analysis

**E. Katragkou[1], P. Zanis[2], I. Tegoulias[2], and D. Melas[1]**

[1]Laboratory of Atmospheric Physics, School of Physics, Aristotle University of Thessaloniki, Greece

[2]Department of Meteorology-Climatology, School of Geology, Aristotle University of Thessaloniki, Greece

**Abstract** In this work we present results of regional climate-air quality simulations over Europe performed for the future decade 2041–2050 (2040s) and the control decade 1991–2000 representative of the present climate. Summer ozone mostly decreases in the mid-century decade by about 0.8–1.2 ppb over continental Europe and the Mediterranean Basin, with the exception of the Balkan Peninsula, Adriatic and Black Sea and southern Iberian Peninsula in the area around Gibraltar, where average surface ozone increases by about 0.5–0.8 ppb. Ozone decrease can be mainly attributed to decreasing incoming solar radiation, which is mostly seen over France, England and northern continental Europe. Average temperature increases in the southern and northern parts of Europe, but not more than 1 K, and remains unchanged or even slightly decreases over France and England. Temperature change spatial patterns follow closely the changes in atmospheric circulation as indicated by 500 hPa geopotential high differences. Biogenic emissions follow temperature and radiation changes, thus increasing in Mediterranean countries and decreasing over northern Europe. However, sensitivity studies in our simulations suggest that ozone formation is not sensitive to organic compounds of biogenic origin, therefore, changes in biogenic emissions due to climate change do not impact on surface ozone.

**Keywords** Climate change, regional climate models, air quality

## 1. Introduction

Tropospheric ozone ($O_3$) is an important trace gas with well documented adverse effects on human health, agriculture and natural ecosystems. Global change, including change in climate and anthropogenic emissions, is expected to impact on many key atmospheric species and tropospheric ozone is certainly one of them (IPCC, 2007). Most modeling studies agree that the 21st century climate change will increase regional ozone pollution. The basic reasons were reported to be the

D.G. Steyn and S.T. Rao (eds.), *Air Pollution Modeling and Its Application XX*,
DOI 10.1007/978-90-481-3812-8, © Springer Science + Business Media B.V. 2010

increase in frequency of stagnation episodes and robust increase of temperature which affects ozone either through PAN chemistry or through increased biogenic emissions (Jacob and Winner, 2009). Ozone increases are found to be mostly in the range of 1–10 ppb depending on the future decades and the region examined, the climate scenario which is adopted and the model system used. It is not easy to separate the effects of different meteorological parameters on air quality in the real atmosphere because the interaction between them is complex and there are several feedback mechanisms. A holistic approach is to study the impact of climate change on air quality which is a far more complicated task involving climate change, feedbacks with climate-dependent biogenic emissions and changes in future anthropogenic emission trends.

This paper presents a modeling system of a regional climate model off-line coupled to a regional chemistry transport model used for the assessment of present and future air quality. In the current study it is assumed that there are no changes in future emissions and the background species. Constant anthropogenic emissions and chemical boundary conditions are used for the present and future decades. Differences in tropospheric surface ozone can thus attributed only to climate change.

## 2. Modeling System

The modeling system applied to simulate climate/air quality over Europe is RegCM/CAMx. RegCM was originally developed at the National Centre for Atmospheric Research (NCAR) and has been mostly applied to studies of regional climate and seasonal predictability. The air quality model simulations were performed with the Comprehensive air quality model with extensions (CAMx) version 4.40 (www.camx.com). CAMx is off-line coupled to RegCM with a fortran-based code we developed, reading the basic meteorological parameters from RegCM (wind, temperature, water, cloud/rain, pressure and vertical diffusivity) and exporting them to CAMx-ready format. The spatial resolution of CAMx was set to 50 × 50 km. The domain's vertical profile contains 12 layers of varying thickness. Layer 1 is 36 m deep and the uppermost layer is 1.2 km thick and extends to about 6.5 km. Top and lateral boundary conditions were kept constant corresponding to a clean atmosphere. The chemistry mechanism invoked is Carbon Bond version 4 (CB4). This mechanism includes 117 reactions – 11 of which are photolytic – and up to 67 species (37 gasses, 12 radicals and up to 18 particulates). Calculation of emissions is presented in detail in Krueger et al., 2008. We shortly mention that biogenic emissions are calculated on-line using temperature and radiation data from RegCM and anthropogenic emissions are taken from the EMEP database for the reference year 2000.

The runs presented in this work cover the time slice 1991–2000 and 2040–2050. RegCM was forced by the ECHAM5 global circulation model for the simulations covering the two time-slices. ECHAM5 run under the IPCC A1B scenario to provide forcing for the future decade.

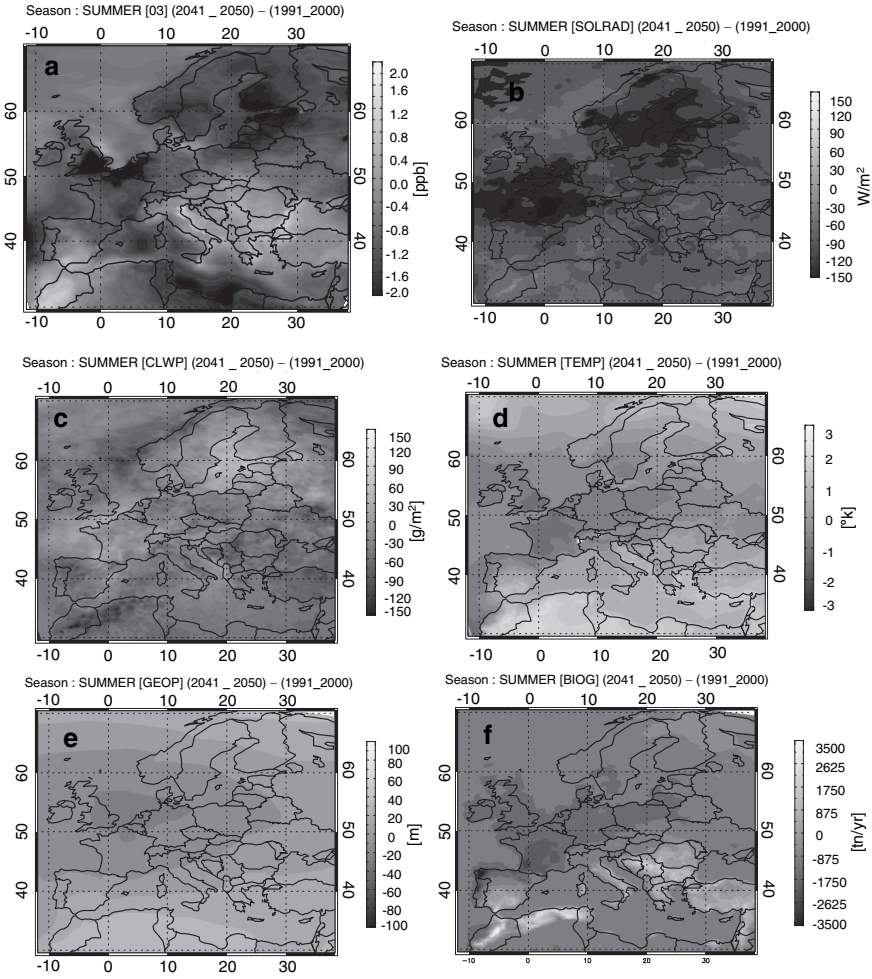


**Fig. 1.** All panels show averaged differences between the future (2041–2050) and present decade (1991–2000) corresponding to the summer season.

(a) Differences of average surface ozone
(b) Differences of average incoming solar radiation
(c) Differences of average cloud liquid water path
(d) Differences of average surface temperature
(e) Differences of 500 hPa geopotential height
(f) Differences of biogenic emissions

## 3. Results

Figure 1 shows changes in surface ozone and various meteorological parameters between the future and the present simulation. The results are averaged over the

whole decadal time slice and are presented only for the summer season. Changes in ozone are depicted in Fig. 1a: ozone mostly decreases over Europe with the exception of the Balkan Peninsula, Adriatic Sea and the area around Gibraltar. Decrease of ozone can be, at least partly, explained by the decrease of solar radiation which is shown in Fig. 1b. The most intense decrease is seen over France, eastern Atlantic and the Baltic Sea, where ozone is mainly lower.

Changes in solar radiation can in turn be explained by changes in cloudiness (Fig. 1c). Cloud liquid water path is used here as an index of cloudiness. A qualitative comparison of Fig. 1b and c shows that in regions where cloudiness increases, solar radiation mostly decreases.

Temperature increases are in the range of 1–1.5 K (Fig. 1d). The areas mostly affected are south and north Europe while central Europe remains relatively unaffected. The temperature in France and England even decreases slightly. The spatial patterns of temperature change follow closely those of the changes in 500 mb geopotential height (Fig. 1e). The later forms a low over England and the North Sea where the minimum of temperature is also located. The geopotential height is used as an index of atmospheric circulation and seems to be strongly modulating the temperature fields.

Finally, Fig. 1f shows changes in biogenic emissions, which in our calculations are temperature and radiation dependent. Biogenic emissions increase in the mid-century decade over the Balkan Peninsula and southern Iberian Peninsula, but decrease over the rest continental Europe. Organic compounds of biogenic origin, the most important being isoprene, are known ozone precursors. Normally, it is expected that change in emissions of organic compounds of biogenic origin affect ozone production. However, sensitivity studies (not shown here) suggest that $O_3$ formation in our modeling system is NOx sensitive, thus such small changes of biogenic emissions are not affecting surface ozone.

**Acknowledgments** This work has been funded by the European Community's Sixth Framework Programme as part of the project CECILIA (Central and Eastern Europe Climate Change Impact and Vulnerability Assessment) under Contract No. 037005. This work was awarded with the 1st EURASAP Award (European Association for the Science of Air) in the 30th ITM NAT/SPS International Technical Meeting on Air Quality Modeling and its Applications.

## References

Climate Change 2007 – The Physical Science Basis Contribution of Working Group I to the Fourth Assessment Report of the IPCC (ISBN 978 0521 88009-1).

Jacob D.J, Winner D.A. (2009) Effect of climate change on air quality, Atmopsheric Environment, 43, p. 51–63.

Krueger, B. E. Katragkou, I. Tegoulias, P. Zanis, D. Melas, E. Coppola, S. Rauscher, P. Huszar, T. Halenka (2008) Regional photochemical model calculations for Europe concerning ozone levels in a changing climate, Quarterly Journal of the Hungarian Meterological Service, 112, 3–4.

## 4. Questions and Answers

**Question:** I am surprised to see increased biogenic emissions in most of your study region, although future increased temperatures and reduced precipitation should reduce biogenic emission in many areas. This is caused by a fairly simple pure-temperature based biogenic response to the model. (Christian Reuten)

**Answer:** The biogenic emissions in our modeling system are temperature and radiation dependent. As temperature and radiation increase in the future climate biogenic emissions increase. Biogenic emissions in more sophisticated emission models are dependent on several other parameters, which were, however, not included in the current study.

**Question:** Did you include changes in vegetation cover in future? (S. Adreani-Askoyoglou)

**Answer:** No, vegetation cover change was not included in the current modelling study. We solely investigated the impact of changes in meteorological parameters due to climate change on surface ozone.

**Question:** Do you have an idea if this pattern of change in solar radiation in ECHAM5 is also seen in other IPCC Models? (W. Lefebvre)

**Answer:** The global circulation model ECHAM5 was used in the current study only to force the regional climate model RegCM3, which we are actually using.

# 4.9 An Investigation of High Summertime Ozone Level in Istanbul with MM5/CMAQ Modeling System

**Ulaş İm[1], Selahattin İncecik[2], Kostandinos Markakis[3], Tayfun Kındap[4], Anastasia Poupkou[3], Orhan Yenigün[1], M. Talat Odman[5], Sema Topçu[2], Mete Tayanç[6], and Dimitros Melas[3]**

[1]Bogazici University, Institute of Environmental Sciences, Bebek, Istanbul, Turkey

[2]Istanbul Technical University, Department of Meteorology, Maslak, Istanbul, Turkey

[3]Aristotle University of Thessaloniki, Laboratory of Atmospheric Physics, Thessaloniki, Greece

[4]Istanbul Technical University, Eurasia Institute of Earth Sciences, Maslak, İstanbul, Turkey

[5]Georgia Institute of Technology, School of Civil and Environmental Engineering, Atlanta, GA, USA

[6]International Cyprus University, Nicosia, Cyprus

**Abstract** In this study a modeling system consisting of PSU-NCAR MM5 and CMAQ model has been applied to a summertime high ozone period in Istanbul, Turkey in the framework of COST-728 Action. A comprehensive anthropogenic and model – ready emission inventory was developed for the first time to make detailed air quality simulations possible in the region. Although the system is still being tested and developed, the first results were very satisfactory. The model performances are evaluated by comparing the model prediction to the measurements. The results show that the predicted ozone concentrations are close to the measured data at semi urban station of the city. But model predictions are underestimated at a background station on Büyükada (Princess Island) due to its location. The statistical evaluations of the model results showed that the modeling system was capable of capturing the temporal resolution as well as the magnitudes, reasonably well.

## 1. Introduction

Istanbul with approximately 13 million inhabitants is one of the significant megacities in the world. High emissions of NOx and VOCs concurrent with high radiation and temperature in ozone season lead to elevated ozone concentrations. Topçu and Incecik (2002, 2003) reported ozone concentrations higher than 100 μg $m^3$. Im et al. (2006, 2008) studied the long term ozone levels in Istanbul. Anteplioğlu et al. (2003, 2003) investigated the local circulations enhancing the ozone levels in Istanbul. Within the COST-728 and TUJJB projects, new ozone and ozone precursor measurement stations was designed and established to investigate the temporal

D.G. Steyn and S.T. Rao (eds.), *Air Pollution Modeling and Its Application XX*,
DOI 10.1007/978-90-481-3812-8, © Springer Science + Business Media B.V. 2010

and spatial dynamics of ozone production in the Istanbul area by measurement and modeling. In this project Istanbul urban plume was modeled using MM5 meteorological model and CMAQ chemistry and transport model.

## 2. Materials and Methods

### 2.1. Area of investigation

The city of Istanbul is in the inner most domains situated at 41°N and 29°E. The Bosporus channel separates the European part from its counterpart in Asia Minor. The total area of the two parts of the city is about 5,712 $km^2$. In the framework of this study of a COST 728 Action, three air quality stations are operated on the Asian side of the city measuring hourly ozone and NOx concentrations. Kandilli air quality station (125 m asl) is situated above the Bosporus and is located at the Kandilli Observatory garden. There are no major emission sources within a few kilometers. Kandilli is considered as a semi-rural surrounding of Istanbul. Büyükada air quality station (200 m asl) is situated at the crest of Prince Island of Istanbul. There are no emissions sources including motor vehicles in the island. It's about 20 km south of the mainland. Büyükada is considered as representative for the background station of Istanbul. Finally, a traffic station is operated on a busy motorway on the Asian side of the city, which is also in the vicinity of various residential and industrial activities.

### 2.2. Model description

Hourly ozone and NOx measurements are used in order to determine high ozone days in İstanbul. Data, common from all three stations goes back to January, 2008. Although the measurements showed that the ozone concentrations were below the national limit of 240 $\mu gm^{-3}$, for the air quality modeling purpose, a 5-day episodic period was chosen, where the ozone concentrations made the maximums in both station (Fig. 1).

#### 2.2.1. Meteorological modeling

The PSU/NCAR Mesoscale Modeling System (MM5) is a non-hydrostatic and limited area model. The MM5 is designed to predict the meteorological fields. In this study, the meteorological fields were generated using MM5 V3.7 mesoscale meteorological model. Three nested domains were used to reach a horizontal resolution of 2 km in the İstanbul area (Fig. 2): 199 × 175 grids of 30 km resolution covering Europe, 181 × 202 grids of 10 km resolution covering the Balkan area, and finally, 136 × 111 grids of 2 km resolution covering the Istanbul area (Fig. 1). The vertical resolution of the model covered 37 sigma levels. The meteorological data was obtained from NCEP on 1° resolution for a 10-day period, starting from

June, 10, 2008 to June 20, 2008. First 3 days of the simulations were considered as spin up period for the model. The physical options used for the model were Mix Phase for moisture scheme, KF2 for cumulus scheme, MRF for PBL scheme and RRTM for radiation scheme.

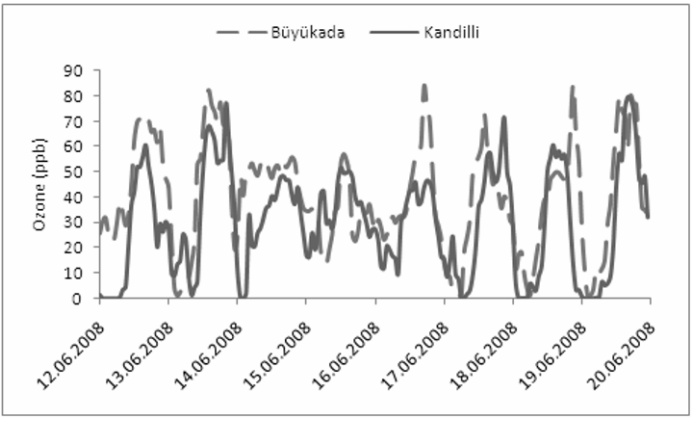


**Fig. 1.** Ozone concentrations measured at Büyükada, Kandilli and DMO air quality stations during the simulation period

### 2.2.2. Emissions

The European emissions were spatially distributed on a 163 × 150 grid system of 30 km resolution and Balkan emissions were distributed on a 140 × 155 grid system of 10 km resolution, with both domains covering 20 vertical layers. Anthropogenic emissions included 11 gaseous/particulate species and 23 VOC species provided from Visschedijk et al. (2005). A domain of 92 × 57 grids for the Istanbul emission data was generated covering various emissions categories from the EMEP sectors. This is the first comprehensive and model – ready emission inventory developed for the city and covers 17 gaseous/particulate species and 23 VOC species.

### 2.2.3. CMAQ model

The Community Multiscale Air Quality (CMAQ) model (version 4.6) is an Eulerian type air quality model which simulates the atmospheric and surface processes affecting the transport, transformation and deposition of air pollutants (Byun and Ching, 1999). The boundary and initial conditions were provided from the default CMAQ files. The chemical mechanism used for the gaseous species was CB-IV, whereas AERO4 was employed as the aerosol mechanism, which includes the sea-salt emissions.


**Fig. 2.** The modeling domain configurations

## 3. Results

The modeling exercise was conducted for a 10-day period between 10 and 19 June, 2008. The results from both MM5 and CMAQ are evaluated using a number of statistical measures. The statistical results presented in Table 1 shows that MM5 and CMAQ reproduced the observations fairly well. The predictions underestimated the observations for both models as expected, except for the ozone levels at Büyükada station (Fig. 3). This may result from the meteorology due to the topography. The location of the Büyükada station with an approximately 200 m is the highest crest point in the Marmara Sea where under the influence of high wind speeds. However, due to the data limitation to evaluate the MM5 model for this station, it was not possible have a solid idea on the error coming from meteorology. The differences between models predicted ozone levels and observations may

**Table 1.** Statistical evaluation of MM5 and CMAQ models

| MEASURES | MM5 | | | CMAQ | |
|---|---|---|---|---|---|
| | T2 | U10 | V10 | Kandilli | Büyükada |
| Correlation | 0.81 | 0.51 | 0.67 | 0.55 | 0.26 |
| Bias | –2.4 | –1.7 | –0.4 | –3.09 | 6.85 |
| RMSE | 2.9 | 2.3 | 1.9 | 19.90 | 24.16 |
| IOA | 0.74 | 0.11 | 0.75 | 0.66 | 0.45 |

originate from a number of factors including the absence of biogenic emissions, various activity data, temporal and chemical profiles and emission factors used in development of the high resolution emission inventory for Istanbul.

## 4. Conclusions

A high resolution MM5/CMAQ air quality modeling system was used for simulating ozone concentrations for Istanbul for a 10-day period in June 2008. From the study we can conclude that these results demonstrate applicability of using MM5-CMAQ modeling system for air quality simulations in Istanbul. Furthermore, there were a number of limitations and that the work is ongoing; the system produced agreeable results for the ozone levels in the region. For the future studies, the biogenic emissions are going to be implemented to the system. On the other hand, sensitivity analyses are to be done.

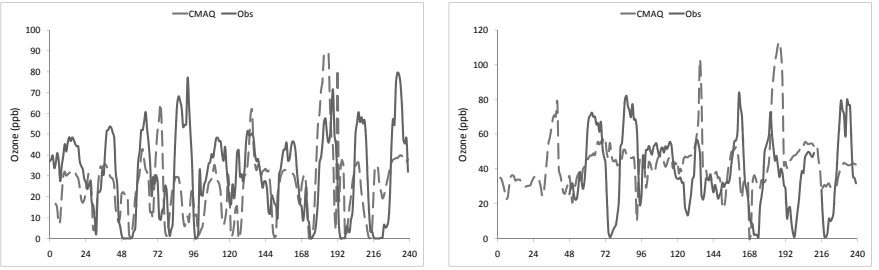


(a) (b)

**Fig. 3.** Comparison of CMAQ results with observations at (a) Kandilli and (b) Büyükada air quality stations (*dashed lines* show model results)

**Acknowledgments** This study is supported by the TUBITAK (COST 728 Action) with a project no. 105Y005 and partly supported by TUJJB project no. TUJJB – TUMEHAP – 03 – 06.

## References

Anteplioğlu U (2000). Modeling of surface ozone with UAM: a case study for Istanbul', Ph.D. Thesis, Istanbul Technical University.

Anteplioğlu, Topçu S., İncecik S. (2003) An Application of a photochemical model for urban airshed in İstanbul, Journal of Water, Air & Soil Pollution: Focus, 3; 53–64.

Anteplioğlu, U, S. İncecik, S. Topçu, 2003, Model study with MM5 and CAMx in Istanbul area during high ozone days, (invited paper) International Symposium on Clean Environment, 21–22 November, Cheonan, Korea, 11–15, Nov. 2003

Byun D.W and Ching J.K.S. (1999). Science Algorithms of the EPA Models-3CMAQ Modeling System. Washington, DC.USEPA.

Im U Tayanç M Yenigün O (2006) Analysis of Major Photochemical Pollutants with Meteorological Factors for High Ozone Days in Istanbul, Turkey. Water, Air, and Soil Pollution, 175; 335–359.

Im U Tayanç M Yenigün O (2008) Interaction patterns of major photochemical pollutants in Istanbul, Turkey. Atmospheric Research. 89; 382–390.

Topçu S., Kahya c., İncecik S., Ercan S. G., Basar U. G. 2005. Review of surface ozone and its precursors in urban atmosphere of Istanbul, Turkey for 2002–2003. Proceedings of Air Quality Management at Urban, Regional and Global Scales, Volume 3, 1083–1093.

Visschedijk, A.J.H., Zandveld, P.Y.J., Denier van der Gon, H.A.C.A., 2007. High Resolution Gridded European Emission Database for the EU Integrate Project GEMS, TNO-report 2007-A-R0233/B.

# 4.10 The Ability of Mesoscale Models to Predict Vertical Profiles

**E. Batchvarova[1] and S.-E. Gryning[2]**

[1]NIMH, Bulgaria Academy of Sciences, Sofia, Bulgaria

[2]Risoe DTU, Roskilde, Denmark

**Abstract** In the manuscript it is argued that examination of model performance should be based on profiles and that the traditional evaluation based on surface measurements at one level easily can be misleading. A model can perform very well near the surface, suggesting good performance, but poorly at 100 meters. When comparing model results and measurements, it is important to emphasize that excellent model performance does not require an excellent match with measurements. The representativeness of the measurements should be taken into account. These points are discussed and argued in the manuscript with examples drawn from a recent model evaluation effort.

**Keywords** Atmospheric boundary layer, Models' evaluation methods, Vertical profiles, Tall meteorological masts, Flux measurements, Representativeness of measurements

## 1. Introduction

As part of the COST 728 action (Enhancing Mesoscale Meteorological Modelling Capabilities for Air Pollution and Dispersion Applications) a major model comparison and evaluation exercise is carried out.

One of the cases covers Central and Northern Europe in February and March 2003, when several PM10 episodes were observed. The predictions of several models were shown to differ widely by Stern at al. (2008). Detailed analysis of meteorological conditions in the same paper pointed out large differences in the boundary layer height used in the chemical models.

Although the boundary-layer height plays a central role for the PM10 predictions by chemical transport models and is often an output parameter from meso-scale meteorological models, the way it is obtained is not transparent. Therefore when modeled and measured heights of the boundary layer are compared it is often not clear if the values are based on the same definitions.

This problem can be examined by evaluating the vertical profiles of meteorological parameters, such as wind speed and direction, humidity, temperature. In

D.G. Steyn and S.T. Rao (eds.), *Air Pollution Modeling and Its Application XX*,
DOI 10.1007/978-90-481-3812-8, © Springer Science + Business Media B.V. 2010

the area of the case study three sites were identified where extensive vertical profile measurements are performed. Specific runs with the same boundary conditions and set-up were performed with several models and profile data were stored. In this type of evaluation, the representativeness of the measurements of the vertical profile becomes an important issue.

## 2. Representativeness

The natural variability in the measurements – also called representativeness – depends on the state of the atmosphere and the averaging time of the measurements. Here we evaluate a model by assuming that the model prediction of a given parameter represents the average (representative) value. Then the uncertainty due. to the natural variability of the measurements is added as error bars on the results from the model simulation. The actual measurement represents one realization only; if the measurement is inside the error bar then it is within the expected natural variability of the model prediction.

Thus, the model evaluation method is used to associate the uncertainty that arises from the natural variability in the atmosphere for the parameter in question – in this paper we take wind speed as example – but the method is applicable for other parameters as well. The standard deviation in the measurements of the wind speed $\sigma_{u,T}$ depends on the averaging time $T$ of the measurements. Under stationary conditions and for an the integration time scale $T$ much longer than the integral time scale $\tau$, Tennekes (1973) suggests:

$$\sigma_{u,T} \approx 2\sigma_u \, \tau/\mathrm{T}$$

where $\sigma_u$ is the standard deviation of the fluctuating wind speed.

An applied method proposed by Sreenivasan et al. (1978) to determine the standard deviation of the wind speed for a given averaging time is used here:

$$\sigma_{u,T} = \sqrt{12}\sqrt{\frac{z}{T\,u}}u$$

It can be seen that the standard deviation $\sigma_u$ increases with height and decreases with averaging time. The method can also be applied to other parameters, for example, the sensible heat flux. It is interesting to note that the higher the moments the larger the standard deviation. Thus, a longer averaging time is required for a higher order moment if the same standard deviation is aimed as for mean value or lower order moment.

The assumption of stationarity is typically not fulfilled in the atmosphere due to the daily variation of the insolation, but can be fulfilled in wind tunnel modeling. However, this deficit is a principal problem as stationarity is also a basic assumption in the Reynolds decomposition of fluxes, which is fundamental for all RANS

models. The fundamental issue is discussed in Gryning and Batchvarova (2005) and with special emphasis in urban area in Gryning and Batchvarova (2009).

## 3. Measurements and Models

Meteorological measurements from the Falkenberg site of Richard Assmann Observatorium near Lindenberg, Germany, has been used. The site is covered with grass; it is equipped with a 98 m high meteorological tower as well as a 12 m mast. Here measurements of wind speed at 98 and 10 m height are used.

The following model results are used here: Cosmo, MM5 run by two groups and WRF. The main point of the study is to demonstrate the method. Results from 1 day only are shown, and therefore caution should be taken on conclusions concerning the individual models.

In Figs. 1 and 2 the wind speed at 100 and 10 m are shown. The line shows the model prediction. The full circles show the measurements and the error bars represent the standard deviation of the measurements due to natural variability for a given averaging time, in this case 30 min. It can be seen that the error bars are larger at 100 m than 10 m height, because the error bars increases both as function of height and wind speed.

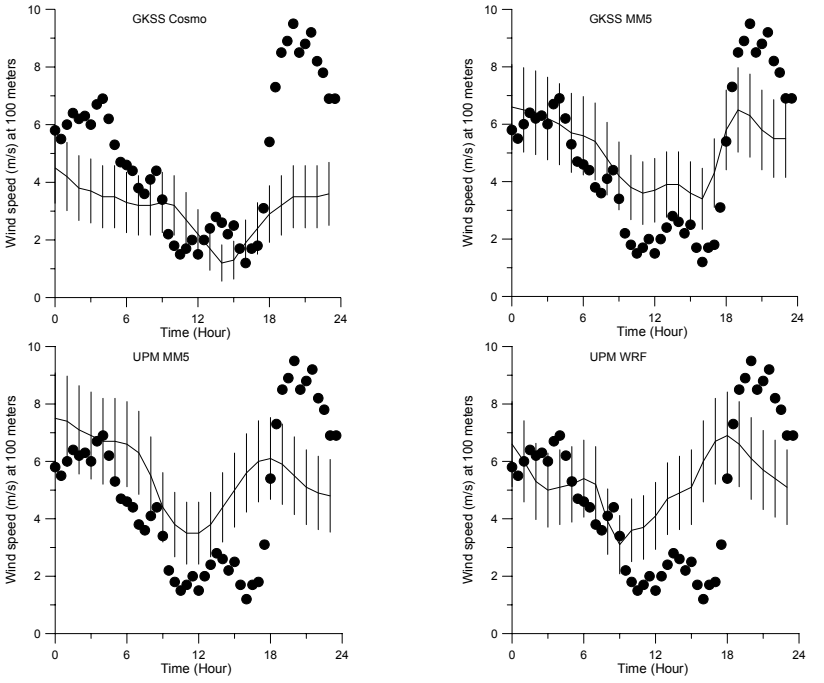


**Fig. 1.** Wind speed at 100 m height, explanation is given in the text

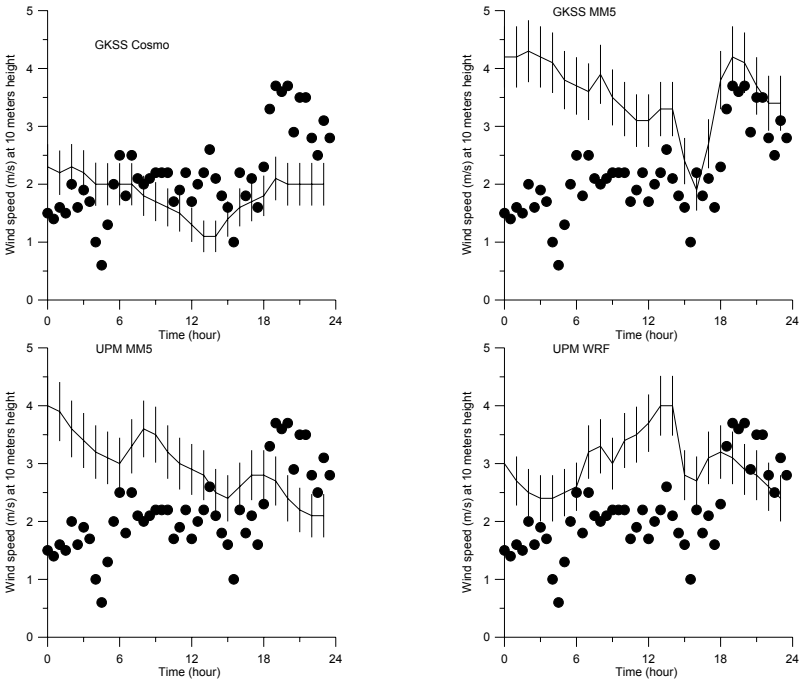


**Fig. 2.** Wind speed at 10 m height, explanation is given in the text

It can be seen (Fig. 1) that at the 100 m level for three of the models the predictions fall inside the representativeness bars of the measurements in the morning. However for the same period at the 10 m level (Fig. 2), the model prediction is higher than the measurements and the measurements are outside the range of the predictability.

It is thus interesting to note that an evaluation study solely at the 100 m level would suggest good agreement, but including the 10 m level would show that the prediction of the profile is not good, emphasizing the importance of performing the evaluation on profiles and not single level measurements.

## 4. Conclusions

- Progress in model developments is based on comparison with data.
- It is essential to evaluate the models on profile measurements, not just traditional surface measurements.
- The representativeness of the measurements should be taken into account in any model evaluation against measurements.

- The representativeness is a function of the length scale of turbulence (height in the surface layer) and averaging time of the measurements (as a first rough approximation).
- A good model performance does not require exact match with data.
- In other words a model cannot be improved if the measurements fall within the statistical range defined by the representativeness.

**Acknowledgments** The data from Lindenberg are provided through the CEOP/GEWEX BALTEX (Baltic Sea Experiment) database and it is a pleasure to acknowledge the Deutscher Wetterdienst (DWD) – Meteorologisches Observatorium Lindenberg/Richard Assmann Observatorium who originally provided the measurements for the data base. The work is part of collaboration within COST 728 – V. Mathias and M. Quante from GKSS (Germany) and R. San Jose from UPM (Spain) are acknowledged for model results. The study is supported by the Danish Council for Strategic Research, Sagsnr 2104-08-0025 and the EU FP7 Marie Curie Fellowship VSABLA.

## References

Gryning, S.-E.; Batchvarova, E., Strengths/weaknesses of laboratory/field and numerical data. In: Proceedings. International workshop on quality assurance of microscale meteorological models, Hamburg (DE), 28–29 Jul 2005. Schatzmann, M.; Britter, R. (eds.), (European Science Foundation, Brussels, 2005) p. 85–93.

Gryning S.-E. and Batchvarova E. 2009 Measuring Meteorology in Urban Areas – Some progress and many problems In proceedings: Meteorological and Air Quality Models for Urban Areas. Exeter (UK) May 3–4 2007. Baklanov, A., Grimmond, S,, Mahura, A. and Athanassiadou M., Springer, Dordrecht, Heidelberg, London, New York.

Sreenivasan K.R., Chambers A.J. and R.A. Antonia, 1978: Accuracy of moments of velocity and scalar fluctuations in the atmospheric surface layer, *Boundary-Layer Meteorology, 14, 341–359.*

Stern R., Builtjes P., Schaap M., Timmermans R., Vautard R., Hodzic A., Memmesheimer M., Feldmann H., Renner E., Wolke, R., Kerschbaumer A. 2008. A model inter-comparison study focussing on episodes with elevated PM10 concentrations, Atmos. Env., 42, 4567–4588.

Tennekes H. and Lumley J.L. 1972. A first course in turbulence. MIT Press, Cambridge, Mass. 300 pp.

## 5. Question and Answers

**Kurt Fedra:** Does anybody use vertical data from airplanes start/landings.

**Answer:** Yes, but such data represent instantaneous slanted vertical profiles and are therefore not suitable for this type of data analysis.

**Christian Reuten:** The error bars on the model results cannot be representative of the uncertainty of the model output. If they were, there would be more variability in model results from hour to hour.

**Answer:** The mean curve is the ensemble average and the error bars are not the uncertainties of the model results but those of the observations.

# 4.11 AQMEII: A New International Initiative on Air Quality Model Evaluation

**S. Trivikrama Rao[1], Kenneth Schere[1], Stefano Galmarini[2], and Douw Steyn[3]**

[1]Atmospheric Modeling and Analysis Division, National Exposure Research Laboratory, United States Environmental Protection Agency, Research Triangle Park, NC, USA

[2]Joint Research Centre, Institute for Environment and Sustainability – European Commission, Ispra, Italy

[3]The University of British Columbia, Vancouver, BC, Canada

**Abstract** We provide a conceptual view of the process of evaluating regional-scale three-dimensional numerical photochemical air quality modeling systems, based on an examination of existing approaches to the evaluation of such systems as they are currently used in a variety of applications. A framework for model evaluation is introduced to provide a context for the evaluation process. The objectives of the model evaluation process include: determining the suitability of a modeling system for a specific application; distinguishing between the performance of different models through confidence-testing of model results; and guiding further model development. The evaluation framework includes methods for *operational, diagnostic, dynamic, and probabilistic* model evaluation. Also discussed is a new effort, the Air Quality Model Evaluation International Initiative (AQMEII), in which some of the new ideas in model evaluation are applied to air quality modeling systems being used in North American and Europe, to assess the utility of the techniques and to compare and contrast model evaluation results among different models on both sides of the Atlantic Ocean. An AQMEII Workshop was conducted in April 2009 in Stresa, Italy to discuss model evaluation concepts and establish collaborative model application and evaluation projects.

## 1. Introduction

Regional-scale three-dimensional numerical photochemical air quality simulation models (AQMs) are being used for air quality management decisions and for short-term forecasting of air quality in many nations around the globe. To build confidence in the model estimates, a model must be critically evaluated to assess whether it is properly simulating the spatial and temporal features on the scales resolved by the model. The evaluation also assesses whether the physical and chemical processes are simulated correctly in the model, leading to proper model response to changes in meteorology and emissions, the principal classes of inut data required by AQMs. To this end, a renewed examination is needed to establish

D.G. Steyn and S.T. Rao (eds.), *Air Pollution Modeling and Its Application XX*,
DOI 10.1007/978-90-481-3812-8, © Springer Science + Business Media B.V. 2010

the best methods for assessing the performance of regional-scale AQMs. Motivated by discussions at a model evaluation Workshop in 2007, sponsored by U.S. EPA and the American Meteorological Society (AMS), a new framework for regional-scale air quality model evaluation is introduced.

## 2. Model Evaluation Framework

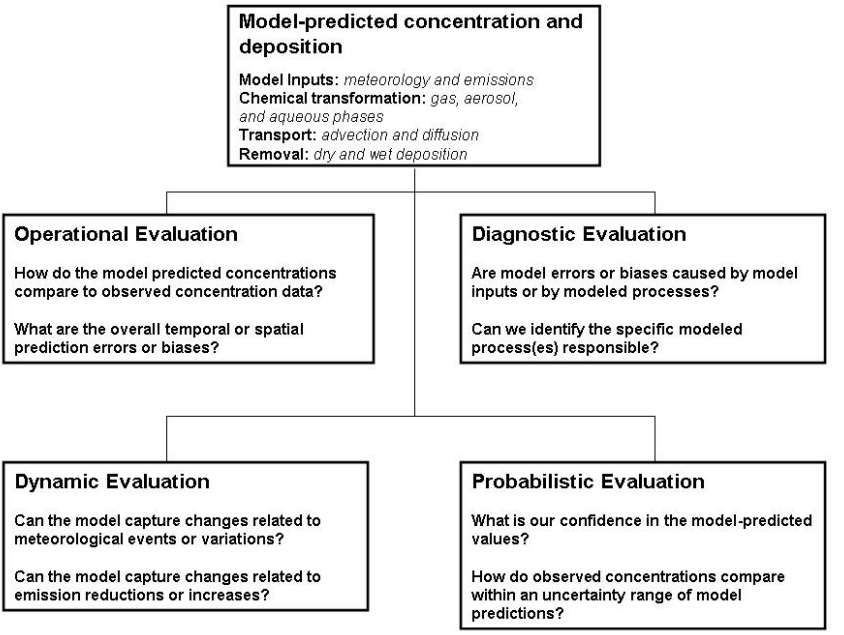


**Fig. 1.** The framework components of air quality model evaluation

As shown in Fig. 1, the framework consists of four components for regional-scale air quality model evaluation. **Operational Evaluation** characterizes how well model predictions compare to observations for specific time periods and conditions. Key questions to consider as part of operational evaluation include: (1) what statistical metrics and graphical depictions are most useful in assessing air quality model performance? and (2) how can point measurements and volume-averaged model predictions be reconciled in terms of spatial and temporal scales? In **Diagnostic Evaluation,** we determine how the performance of the model could be improved through complementary process-based analysis of modeled and measured values. Specific model processes or data are evaluated with the goal of attribution of model errors. Figure 2 is an example of a diagnostic study that used inverse modeling of ammonia ($NH_3$) to update the emissions inventory used in the

Community Multiscale Air Quality (CMAQ) model to improve model predictions of aerosol nitrate, $NO_3$ (Gilliland et al., 2003).

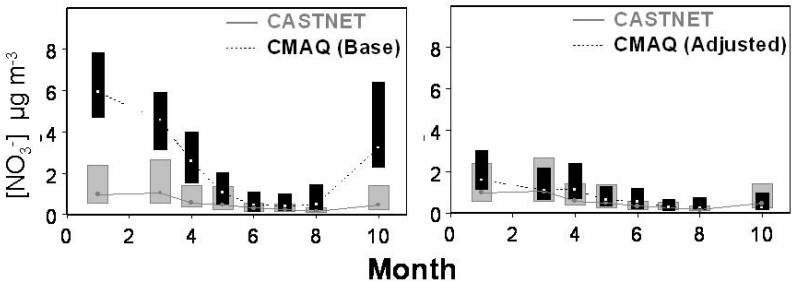


**Fig. 2.** CMAQ model ambient $PM_{2.5}$ nitrate estimates and CASTNET observations before (left) and after (right) top-down estimates of $NH_3$ emissions

**Dynamic Evaluation** characterizes how well the model captures observed changes in air quality induced by changes in emissions and/or meteorology. Some of the challenges involved in dynamic evaluation include distinguishing between meteorological and emissions signals in the model results and determining the relevant space/time scales on which to conduct these evaluations. Assessing the emissions signal is particularly challenging, as anthropogenic source emissions tend to change slowly over time (years), except for weekday/weekend activity differences, and emissions controls implemented over a short period of time.

**Probabilistic Evaluation** transforms deterministic model predictions into probabilistic form, helping to build confidence in the use of air quality models in policy setting. This approach, for example, may characterize the probability of success of an emissions control option in meeting a given air quality objective. One key issue is determining the role of ensemble modeling in probabilistic model use and evaluation (Pinder et al., 2009).

## 3. Air Quality Model Evaluation International Initiative (AQMEII)

Inspired by the emergence of the model evaluation framework and the discussions held at the August 2007 EPA/AMS Workshop, the Air Quality Model Evaluation International Initiative (AQMEII) is now proposed. To start this new collaborative project, a Workshop was held during 27–29 April 2009 in Stresa, Italy, hosted by the European Commission's Joint Research Centre and attended by 50 scientists from North America and Europe. Workshop discussions covered the types of model evaluations contained in the framework and were motivated by key questions (see Fig. 3). The goals of the Workshop included exchanging expert knowledge in regional air quality modeling, identifying knowledge gaps in the science, establishing

model evaluation methods to increase knowledge about relevant processes and support the use of models for policy development, and initiating a coordinated research project on model evaluation/intercomparison. A major outcome from the Workshop was the plan for a near-term North American/European air quality model intercomparison using modeling platforms from both continents, and including aspects of all four types of model evaluations contained in the framework including the demonstration of new methods of evaluation. In addition to this activity, a plan is being developed to establish a long-term vision for maintaining international collaboration in model evaluation and rapidly advancing the science in air quality models. Detailed information on AQMEII and its initiative is available at the website: http://aqmeii.jrc.ec.europa.eu.

| OPERATIONAL EVALUATION | DYNAMIC EVALUATION | PROCESS ORIENTED (DIAGNOSTIC) EVALUATION | PROBABILISTIC EVALUATION |
|---|---|---|---|
| M. Moran (Chair), J. Brandt (Rapporteur), G. Kallos (Provocateur) | P. Builtjes (Chair); K.H. Schluenzen (Rapporteur), C. Hogrefe (Provocateur) | M. Beekmann (Chair), M. Schaap (Rapporteur), K. Schere (Provocateur) | D. Steyn (Chair), R. Vautard (Rapporteur), S. Galmarini (Provocateur) |
| **When evaluating AQ models, how do we determine, represent and present uncertainty?** | | | |
| **How best should we deal with uncertainty in model input and observations when evaluating AQ models?** | | | |
| **What kind of evaluation exercise would you perform in this context that has not yet been performed? Suggestions for new evaluation activities?** | | | |
| **What evaluation results will show that a model is not applicable to a case? Can we opt for falsification rather than validation criteria?** | | | |
| **How can we determine whether an AQ model is appropriate for the context in which it is to be applied?** | | | |

**Fig. 3.** AQMEII Workshop sessions and facilitators and major questions for discussion

**Disclaimer** Although this paper has been reviewed by EPA and approved for publication, it does not necessarily reflect EPA's policies or views.

## References

Gilliland, A.B., R.L. Dennis, S.J. Roselle, T.E. Pierce, 2003: Seasonal $NH_3$ emission estimates for the Eastern United States using ammonium wet concentrations and an inverse modeling method. *J. Geophys. Res.-Atmos.*, **108**, doi: 10.1029/2002JD003063.

Pinder, R.W., R.C. Gilliam, K.W. Appel, S.L. Napelenok, K.M. Foley, A.B. Gilliland, 2009: Efficient probabilistic estimates of surface ozone concentration using an ensemble of model configurations and direct sensitivity calculations. *Environ. Sci. Technol.*, **43**, 2388–2393.

## 4. Questions and Answers

**Question:** Is AQMEII solely focused on regional air quality models?
**Answer:** Initially yes, the focus will be on regional-scale models. Eventually the program may broaden to multi-scale modeling, including regional-to-urban and global-to-regional scale model domains.

**Question:** Is the participation in AQMEII closed?
**Answer:** No, the participation in AQMEII is not closed. In fact, we are encouraging members of the air quality modeling and monitoring communities to participate in AQMEII.

**Question:** Is the IPCC framework for model intercomparison and representation of uncertainty one that our community should do more to emulate?
**Answer:** The IPCC has done an excellent job regarding global climate model evaluation and intercomparison. We need to adapt some of the global modeling community's evaluation techniques to our regional air quality models.

# 4.12 Model Evaluation of Regional Chemistry Transport Models

**Peter Builtjes[1] and Robert Vautard[2]**

[1]TNO Enviroment and Geosciences, Utrecht, The Netherlands

[2]LSCE/IPSL Laboratoire CEA/CNRS/UVSQ, Gif sur Yvette Cedex, France

**Abstract** In Europe, over the last decade several model intercomparison and model evaluation studies have been carried out. Using several models in a model evaluation study has the clear advantage that the model results are not just compared to observations, but that the models are also tested against each other. Model evaluation studies have been performed first for ozone, but more recently also for PM, and the components of PM. In general, the studies have been focused on the overall model performance, without focussing on specific processes. The studies show that most CTM's are capable of simulation ozone concentrations, but that there are still major problems with modelling PM.

**Keywords** Modelling, evaluation

## 1. Introduction

The first step in a model evaluation study should be to define the purpose of the model, to be able to determine whether the model is "fit-for-purpose". In case the model is used to study in detail a specific process like for example in cloud scavenging or dry deposition, then the model evaluation should be process oriented, and will be of a scientific character. The observations used come in that case often from dedicated field campaigns. More operational, and policy oriented model applications ask for an overall model evaluation, and for observations often use is made from existing networks.

Gradually, elements of a model evaluation protocol have been made and tested. As stated, the first step should be to define the purpose of the model. The next step should be to identify the processes required in the model. For example, modelling the CH4-concentration over an extended period does not require that a module for aerosol chemistry is included in the model. Further, the horizontal and vertical resolution, and the time scale should be defined.

Concerning the input data like meteorology and emissions, it should be decided whether these data are considered as "correct", or whether they should be evaluated separately. In most European model evaluation studies the emissions are

D.G. Steyn and S.T. Rao (eds.), *Air Pollution Modeling and Its Application XX*,
DOI 10.1007/978-90-481-3812-8, © Springer Science + Business Media B.V. 2010

taken as they are, and the meteorological input is not evaluated separately. Recently, more attention is given to the impact of the meteorological input data on the results of the CTM's, like in the European initiative COST-728 (see also Stern et al., 2008; de Meij et al., 2009).

The common practice in model evaluation studies is that off-line models, where meteorological information/models is used as input to CTM's, are evaluated. Gradually, more and more online models are being developed, in which the chemical modules are an integrated part of the meteorological models, which enables the calculation of feedback mechanisms (Baklanov and Korsholm, 2007). The approach of the evaluation of such on-line models, as for example WRF-CHEM, is not fully clear yet ( Grell et al., 2005).

Concerning observations, the quality assurance, and especially their spatial representativity should be determined.

By comparing model results with observations, the first step should be by visual inspection of various plots of observations against model results. Subsequently, appropriate statistical methods should be used, see for example (Hanna et al., 1996; Boylan and Russel, 2006). Ideally, a threshold should be given before the model evaluation starts, stating that when the model performance is such that the results are below the threshold, the model results are considered to be inadequate. As an example Boylan and Russel (2006) and Sartelet et al. (2007) have defined a performance goal for aerosol modelling. This goal is reached when the model has reached the highest expected accuracy. The performance criterion is the goal for an acceptable accuracy. They propose that for PM10 and its components the performance goal for mean fractional bias is <50%, and the performance criterion is <75%. For mean fractional error these values are respectively <30% and <60%.

In a model evaluation study also sensitivity runs should be defined and carried out.

During a model evaluation, it should be kept in mind that the total model uncertainty is made up by the sum of the input data uncertainty + the model uncertainty + the variability. The variability, caused by atmospheric turbulence and meandering, is a part of the uncertainty contained in the observations which can not be decreased. More so, especially the emission data also have an associated inherent uncertainty which can not be decreased; country mean, yearly averaged VOC-emissions can never be more accurate than +/– 30% (Borrego, 2009).

## 2. Model Intercomparison and Model Evaluation

One of the first European regional scale model intercomparison and model evaluation studies has been carried out by Hass et al. (1997). Four photochemical models, i.e. EMEP, EURAD, REM-3 and LOTOS were evaluated for an 8 day ozone episode in August, 1990. The results showed that the models were capable to simulate the daily pattern of $O_3$-concentrations within 10–30% of the observations. The results of this study have later been used in one of the first papers concerning an ensemble approach by Delle Monache and Stull (2003).

The growing computer capacity enabled model evaluation studies over longer periods. Roemer et al. (2003) performed a study where ten different photochemical CTM's participated in modelling the summer of 1997. The results gave a correlation coefficient averaged over 30 selected stations between modelled and observed daily maximum ozone of about 0.75. Hass et al. (2003) carried out a study with six aerosol CTM's, focussing on the year 1995. It was shown that the models calculate $SO_4$, $NO_3$ and $NH_4$ within a range of a factor 2 from the observations.

In a further study, van Loon et al. (2004) with seven CTM's, determined the model performance over 1999 and 2001 for $O_3$, NO, $NO_2$ and $SO_2$, the aerosol components $SO_4$, $NO_3$, $NH_4$ and total PM10 and wet deposition fluxes. In general, similar conclusions were found as in the previous studies. The models are capable of modelling $O_3$ well, and do show some skill in modelling the secondary inorganic aerosol components. However, the models do severely underestimate the observed PM10 concentrations.

In a recent study five European CTM's were tested for a period of about 80 days in February–April, 2003, with elevated PM10 and PM2.5 observations., Stern et al., 2008. It was again shown that the current modelling systems are unable to simulate well higher PM10 and PM2.5 levels.

It should be noted that these European model evaluation studies are focussed on operational models, and use mostly monitoring data for the comparison with calculated concentrations.

## 3. Ensemble Approaches as Aspect of Model Evaluation

The concept of the ensemble approach is based on the situation that different CTM's give different results, without being able to determine which model is better, or even why a model would be better. Because models contain different parameterisations, which are all equally valid, models give different results.

The ensemble approach in weather forecasting has already a long tradition, although in weather forecasts often only one model is used, but with uncertainties in the parameterisations. The ensemble forecast of ECMWF is based on 50 members. The ensemble approach with CTM's is based on using different CTM's, and different meteorological input data. In general, the emission data are identical for the different models.

As stated, the first example of an ensemble approach can be found in Delle Monache and Stull (2003).

McKeen et al. (2005) used seven CTM's for forecasting ozone. It was shown, as in the study by Delle Monache and Stull, that the ensemble based on the mean of the participating models has a significantly better temporal correlation to the observed daily maximum 1-h average and maximum 8-h average than any individual model. Similar results are found by van Loon et al. (2007). Vautard et al. (2008) analysed the ensemble of seven models for $O_3$, $NO_2$ and secondary

inorganic aerosols, showing also in this case the overall behaviour of a better performance of the ensemble, than of any single model.

The reason of this result is the cancelling out of uncorrelated uncertainty and errors. Where it is difficult to improve a single model, the improvement in modelling can be achieved by using the ensemble approach.

Future work of the ensemble approach could be in the direction of weighting the different models based on their separate performance, and by analysing in more detail the resulting probability density functions, the spread of the results of the different models.

## 4. Data Assimilation as Aspect of Model Evaluation

Although by the ensemble approach the overall modelling performance can be improved, aspects like the underprediction of PM can not be removed. To improve the performance of CTM's, the combination of observations and model results by data assimilation is a challenging possibility. Active data assimilation, like 4D-var and Kalman-Filtering combines in fact information from three different sources: from the model, from observations and from the current best estimate, including errors, of the concentration field (Carmichael et al., 2007). Although by data assimilation models are in principle not improved, the sensitivity of the different processes and parameterisations can be determined, and the model performance is improved by incorporating the knowledge and information contained in observations.

Data assimilation is a valid approach to create a better model system (Denby et al., 2008).

## 5. Concluding Remarks

Chemistry Transport Models, their meteorological drivers and emission input data will always be an imperfect representation of the real atmosphere and its chemical composition. Although some consider models as a second reality, they are just a model. Models will never determine what is happing in the real world. In other words, climate change is not caused by climate models.

**Acknowledgments** Part of this study had been performed in the framework of COST-728.

## References

Baklanov, A., Korsholm, U.: On-line integrated meteorological and chemical transport modelling: advantages and prospectives. In: Proc. 29 th ITM on Air Pollution Modelling and its Application. Aveiro. Portugal.

Borrego, C. et al., 2009 Estimation of modelling uncertainty according to the EU air quality legislation: the Air4EU Berlin case, submitted Atm. Env.
Boylan, J.W., A.G. Russel, 2006. PM and light extinction model performance metrics, goals, and criteria for three-dimensional air quality models. Atm.Env. 40, 4947–4957
Carmichael, G.R. et al., 2007 Predicting air quality: current status and future direction. Proc. 29th ITM on Air Pollution Modelling and its Application, Aveiro, Portugal.
Delle Monache, L and R.B. Stull, 2003. A comparison of regional oxidant model output with observed ozone data. Atm.Env. 37, 3469–3474
Denby, B. et al., 2008. Comparison of two data assimilation methods for assessing PM10 exceedances on the European scale.Accepted for publication Atm.Env.
Grell, G.A. et al., 2005 Fully coupled "online" chemistry within the WRF model. Atm.Env. 39 (37), 6957–6975
Hanna, S.R., G.E. Moore, M.E. Frenau, 1996 Evaulation of photochemical grid models using data from the Lake Michigan Ozone Study. Atm. Env. 30, 9, 3265–3279
Hass, H. et al., 1997 Comparison of model results obtained with several European regional air quality models. Atm.Env. 31, 19, 3259–3279
Hass, H. et al., 2003 Results and intercomparison from the European regional scale modelling systems-Aerosol modelling, EUROTRAC-ISS Rep.
Loon, M. van et al., 2004 Model intercomparison in the framework of the review of the unified EMEP-model. TNO-Rep. R2004/282
Loon, M. et al., 2007 Evaluation of long term ozone simulations from seven regional scale air quality models and their ensemble average. Atm.Env. 41, 2083–2097
Meij, A. de, et al., 2009 The impact of MM5 and WRF meteorology over complex terrain on CHIMERE model calculations. Accepted for publication ACP.
McKeen, S.A. et al., 2005 Assesment of an ensemble of seven real-time ozone forecasts over eastern North America during the summer of 2005. J. of Geoph. Res. 110 ( D21), D21307
Roemer, M. et al., 2003 Ozone trends according to ten different dispersion models. EUROTRAC-ISS Rep.
Sartelet, K.N. et al., 2007. Simulation of aerosols abd gas-phase species over Europe with the Polyphemus system, Part 1-Model-to-data comparison for 2001. Atm.Env. 41, 6111–6118
Stern, R.M. et al., 2008. A model intercomparison study focussing on episodes with elevated PM10 concentrations. Atm.Env. doi:10.1016/j.atmosenv.2008.01.068.
Vautard, R. et al.: Skill and uncertainty of a regional air quality model ensemble. Accepted for publication, Atm.Env. (2008)

## 6. Questions and Answers

**S.T. Rao:** Can we agree to use the term model evaluation instead of model validation from here on?

**Answer:** Yes, we can agree, especially because from early on in these kind of studies the term evaluation has been used most often.

**S.T. Rao:** AQ-models cannot perform any better than met.models which assimilate observations. So, can we think of using met.model's performance as the target level for AQ-models performance?

**Answer:** This is a valid remark, and I think we can follow that line for AQ-models. It would be interesting to use also chemical data assimilation in this respect.

**J. Bartnicki:** One important application of the model for decision making purpose is the calculation of source-receptor relations. Do you have any suggestion how this type of model application can be evaluated?

**Answer:** There are several possibilities to evaluate the model response to emission changes, although only to a limited extent. A possibility is to analyse the weekend efffect- when emissions are reduced-, or specific situations as the fast changes in emissions after the fall of the wall, or the reduced emissions in summertime.

**S. Lu:** Your talk adresses how to use observations-via model evaluation- to improve models. The interaction should be two-way, the modelling community can feedback to the measuering community on how to set up/configure observations network to improve our understanding.

**Answer:** I do agree with you. Especially by using data assimilation techniques like Ensemble Kalman Filtering, you can in an objective way determine the impact that a certain number of stations have on the determination of an overall air quality field, and in this way determine the optimal lay-out of a network.

**S. Galmarini:** Can we assume that the evaluation classification recently discussed at an EPA-workshop and within AQMEII can become a common working platform for the North American and European modelling communities?

**Answer:** Yes, we can. In my opinion this classification in operational, diagnostic, dynamic and probabilistic model evaluation is very usefull, and we should use it in the future to direct our actions and studies. And I am looking forward to work together with you on this subject.

# 4.13 Improving Low-Level Wind Field Forecast over Coastal Regions with a Mesoscale Boundary Layer Model Forced with Local Observations and Regional Operative Forecasts, Examples of Lagrangian Trajectories

**Guillermo J. Berri**

Department of Atmospheric and Oceanic Sciences (University of Buenos Aires), and National Research Council (CONICET) of Argentina

**Abstract** A primitive equation mesoscale boundary layer model –MBLM- has been especially developed for forecasting the low-level wind field over coastal regions. The model high horizontal resolution allows representing the small scale features and the land-river surface temperature contrast over coastal regions of complex geometry. The model can be forced with observations as well as with regional operative forecasts. The model surface wind climatology reproduces very well the observed winds at five weather stations of the La Plata River region of South America. A 6-month test period of 12-hour surface wind forecast obtained by forcing the MBLM model with regional operative forecasts produces significantly smaller errors than those of the regional forecast model itself.

The La Plata River in South America is an extended water surface –300 km long and between 50 and 200 km wide- that creates the appropriate conditions for low-level atmospheric circulations with sea-land breeze characteristics, which are a dominant factor of the local weather and climate. In general, regional operative forecast models have insufficient horizontal resolution for the appropriate representation of the small scale features of the daily cycle of low-level winds over a region with a complex geometry of the river-land temperature contrast. A mesoscale boundary layer model –MBLM- is used to simulate the high-resolution low-level wind field over the La Plata River region (see Fig. 1).

The dry and hydrostatic model has three forecast equations for the horizontal wind components and potential temperature perturbation, respectively, and three diagnostic equations for the vertical motion, total pressure and pressure perturbation. For more details about the model formulation and the numerical method of solution, please refer to Berri and Nuñez (1993). The model has been validated over the La Plata River region during a 25-year period by comparing the low level wind climatology calculated by model with the local surface wind observations at five weather stations in the region. The model climatology is calculated as the ensemble result of a series of 24-h forecasts initialized at 0900 local standard time

D.G. Steyn and S.T. Rao (eds.), *Air Pollution Modeling and Its Application XX*,
DOI 10.1007/978-90-481-3812-8, © Springer Science + Business Media B.V. 2010

(LST). Each forecast is obtained by forcing the model with a different upper and lower boundary condition defined from the local observations of five surface weather stations and one upper air station.

At the lower boundary, a surface heating function defines the daily cycle of the river-land temperature contrast which takes into account the geometry of the coasts and confines the temperature gradient into a narrow band along the river shores. The MBLM low-level wind field climatology of a 25-year period presents a good agreement with the observed one. The averaged relative RMSE calculated at five weather stations across the region is 35% for wind direction and 21% for wind speed (Berri, 2007). Figure 2 shows the averaged relative RMSE as a function of local standard time. The errors in wind speed are almost constant while the errors in wind direction show more dependence with time of the day and are larger during the nighttime hours.

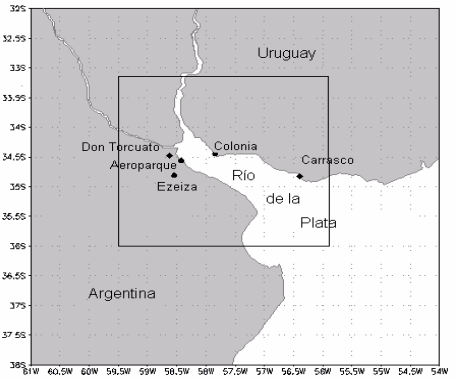


**Fig. 1.** Location of La Plata River region in South America. The inner rectangle is the model domain

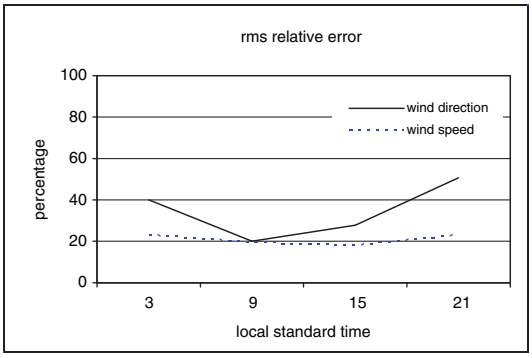


**Fig. 2.** Averaged relative RMSE as a function of local standard time

**Table 1.** Comparison of MBLM and Eta model errors for surface wind predictions

| Model errors | 0900 LST | | 1500 LST | | 2100 LST | |
|---|---|---|---|---|---|---|
| | HR (%) | RMSE (m $s^{-1}$) | HR (%) | RMSE (m $s^{-1}$) | HR (%) | RMSE (m $s^{-1}$) |
| MBLM | 32 | 3.2 | 50 | 3.5 | 41 | 3.6 |
| Eta | 79 | 5.6 | 82 | 6.8 | 85 | 6.5 |

A test was conducted over a 6-month period forcing the MBLM with the Eta model outputs in order to produce operative daily forecasts (Sraibman and Berri, 2009). Two accuracy measures are used: the hit rate (HR) or percentage of cases with agreement in the wind direction sector (45° sectors), and the root-mean-squared error (RMSE) of the horizontal wind components. The BLM surface wind forecasts are always more accurate, since its averaged hit rate is three times greater and its averaged RMSE is one half smaller than the Eta forecasts (see Table 1). Despite the large errors in the surface winds displayed by the Eta forecasts, its 850 hPa winds and surface temperature forecasts are able to drive the BLM model to obtain surface winds forecasts with smaller errors than the Eta model.

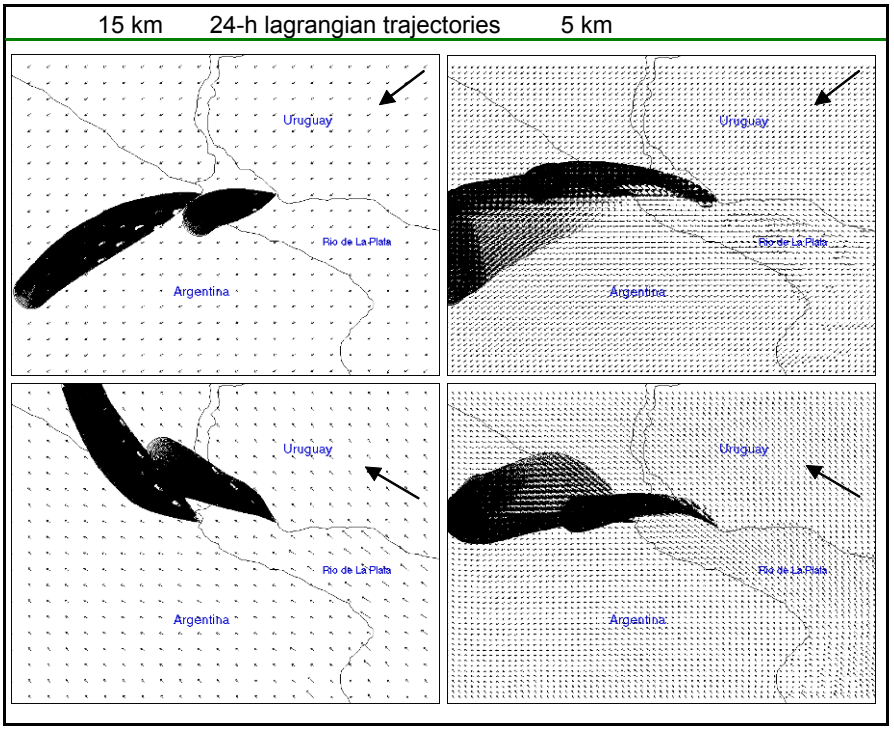


**Fig. 3.** 24-h lagrangian trajectories from two simulated continuous point sources. Left (right) panels are run at 15 km (5 km) horizontal resolution. The thick arrow on the upper right corner indicates the regional scale wind of the experiment

Lagrangian trajectories from point sources across the region calculated with the MBLM model outputs reveal the complexity of low-level circulations over the of the La Plata River region.

Figure 3 presents 24-h lagrangian trajectories that simulate the smoke plumes from two continuous point sources in the region. The example aims at showing the dependence of trajectories on horizontal model resolution. The left panels are obtained by running the model at 15 km resolution, hereinafter referred to as low-resolution or LR. The right panels correspond to a similar experiment at 5 km resolution, referred to as high-resolution or HR. In each case, two experiments are conducted with regional scale winds from different sectors (but same wind speed) that remain constant throughout the integration. The upper panels correspond to northeasterly wind and the lower panels correspond to southeasterly wind, indicated by the thick arrow on the upper right corner of each panel. The LR case shows clearly different lagrangian trajectories that develop downwind the regional scale flow, i.e. northwestward and southwestward from the sources, respectively. Instead, the HR case displays lagrangian trajectories that look alike closer to the sources and differ only at longer distances. Also, the HR trajectories are clearly longer than the LR trajectories. The HR experiments reveal the importance of the local thermal forcing on the low level circulation that despite the change in the regional scale wind direction, forces smoke plume trajectories strongly influenced by the local conditions.

## References

Berri G.J. and M.N. Nuñez (1993) Transformed shoreline–following horizontal coordinates in a mesoescale model: A sea–land breeze case study, J. Appl. Meteorol., 5, 918–928 pp.

Berri G.J. (2007) Using a mesoscale boundary layer model forced with local observations to define the low-level wind field climatology over the La Plata River region, II Encontro Meteorologia Sul do Brasil, Florianopolis, Brasil, June 2007.

Sraibman L. and G.J. Berri (2009) Low level wind forecast over La Plata River region with a mesoscale boundary layer model forced by regional operational forecasts, Boundary Layer Meteorology, 130, 3, 407–422, DOI 10.1007/s10546-009-9350-1

# 4.14 Multi-model Versus EPS-Based Ensemble of Atmospheric Dispersion Predictions: A Quantitative Assessment

**S. Galmarini[1], S. Potempski[1], F. Bonnardot[2], A. Jones[3], and L. Robertson[4]**

[1]European Commission – DG Joint Research Centre, Institute for Environment and Sustainability, Via E. Fermi 2749, 21027, Ispra, VA, Italy

[2]METEOFRANCE, Dir. Prod., Serv./Environ., 42 av. Coriolis, 31057 Toulouse, France

[3]Met Office, FitzRoy Road, Exeter EX1 3PB, UK

[4]Swedish Meteorological and Hydrological Institute (SMHI), SE-601 76 Norrköping, Sweden

**Abstract** Several techniques have been developed over the last decade for the ensemble treatment of atmospheric dispersion model predictions. Among them two have received most of the attention, the multi-model and the Ensemble Prediction System (EPS) modeling. In the paper we compare both approaches with the help of statistical indicators, using simulations performed for ETEX-1 tracer experiment. Both ensembles are also compared against measurement data.

## 1. Introduction

The main difference between multi-model and EPS-based ensembles is the way how the ensemble members are created. The multi-model approach relies on model simulations produced by different atmospheric dispersion models using meteorological data produced by potentially different weather prediction systems. The EPS-based ensemble is generated by running a single atmospheric dispersion model with the ensemble weather prediction members. The difference between the two methods is motivated by the different emphasis that each of them puts on different aspects of model uncertainty and how probabilistic forecast should be used. While the EPS-based method concentrates on the influence of various equally probable weather scenarios on the dispersion produced by one dispersion model, the multi-model considers different answers from multiple sources that include both the uncertainty in the weather predictions and the one that originates from the use of different modeling approached to atmospheric dispersion modeling. The case analyzed is the ETEX-1 release chosen for the abundance of measurements collected and the wide range of studies performed on it in the past. For the specific case the ECMWF EPS system was re-run. The two ensembles have been treated statistically and compared.

D.G. Steyn and S.T. Rao (eds.), *Air Pollution Modeling and Its Application XX*,
DOI 10.1007/978-90-481-3812-8, © Springer Science + Business Media B.V. 2010

## 2. Evaluation and Comparison of Multi-Model and EPS-Based Ensembles

In the simulations the EPS of ECMWF was used to drive long-range atmospheric dispersion models. It consisted of 51 members: one control run and 50 others for which perturbed initial conditions are applied. For ETEX-1 we had three different EPS datasets, corresponding to the analysis times made 64, 40 and 16 h before the beginning of the release, which we denote shortly as –64, –40 and –16 meteorological datasets. As dispersion models we used operational model of our institutions (MATCH, MEDIA, NAME, FLEXPART). For each model the representatives of the set of simulations driven by 51 members of ECMWF-EPS were created as the combinations of model results, namely 50th, 75th, 100th percentiles of the distribution of model predicted values plus the averages. As multi-model ensemble we used 25 model results available in the ENSEMBLE system. These models are different operational long-range atmospheric dispersion systems applied routinely by national weather or environmental centers in case of the release of harmful volatile substances. The models make use of the national weather forecasts but in this case re-analyzed meteorological data were applied eventually with additional use of mesoscale weather prediction models. The same ensembles i.e. 50th, 75th, 100th percentiles and the average of models results were determined.

To evaluate all the created ensembles we apply a number of statistical indicators.

First we analyzed ROC (Receiver Operating Characteristic) graph where as an event we defined the exceedance of the threshold $1 \times 10^{-10}$ g/m$^3$. All the ensembles had low false positive rates (all below 6% with the average 1.3%) but true positive rate varies from 30% to 98% (with the average of 72%). This shows that in general models produced only a little number of false alarms but in few cases the predictions of true alarms was not very good. The comparison based on Euclidian distance showed that the multi-model simulations performed equally well as the best EPS-based simulations. It can be also seen that, simulations based on the newest meteorological data (–16) performed better than those using older data (however –40 based were not better than –64 ones). The best results were produced by the 100% models which suggests that the models mostly under-predicted the concentration. This was confirmed by investigating the Talagrand diagrams. We calculated also accuracy which is generally very high (94–99%) and again both type of ensembles produced similar scores (actually multi-model median had the highest score).

For other evaluation we computed the maximum and the root square errors for all ensemble datasets. Again multi-model median got the best scores for the global root square error, but the average models produced similar results to the medians. It can be observed that for global root square error averages of the EPS-based ensembles have better scores than their medians, while for multi-model ensemble the situation is opposite. These differences however, are small.

For further investigation we calculated also other indicators, namely: FMS (figure of merit in space), FA2, FA5 (factors of 2 and 5), FOEX (factor of excess) and the bias.

Analysis of FMS, FA2 and FA5 shows that the multi-model median slightly over-performed the other ensemble sets. However FOEX is much better for 75th-percentiles, which is the consequence of the already mentioned under-prediction. On the other hand all the biases are positive and the lowest for the medians and averages.

The most important part of the analysis was the verification of the results on the maps. In particular we analyzed space overlap for time integrated concentration at the end of simulation time against measurement for the threshold $1 \times 10^{-10}$ g/m$^3$. First of all it can be seen that the simulations based on older meteorological datasets performed worse than the ones driven by newer weather forecasts. The multi-model median has higher score for space overlap by few percents than the best EPS-based ensemble medians and it seems that the shape of the plume generated by multi-model median is closer to measurement than for EPS-based ensemble median.

One should keep in mind however, that multi-model simulations were driven by re-analyzed meteorological fields. Thus the conclusion can be also like that: the atmospheric dispersion system based on the EPS meteorological data has capabilities similar to the models utilizing meteorological data from the re-analysis.

## 3. Conclusions

Summarizing the analysis we can conclude that:

- In principle there is an overall equivalence in the prediction capacities of the two techniques.
- The multi-model median in a number of aspects over-performed other representations of the ensembles.
- Taking into account that in this analysis we considered multi-model simulations based on re-analyzed meteorological fields while the EPS-based ones used normal forecasts, the systems using EPS also demonstrated strong capabilities.
- In general the median can be considered as a rational choice to represent the ensemble, although the average particularly for EPS-based ensemble could be equally good.

Taking into account these conclusions an interesting suggestion could be to combine these two approaches i.e. to create multi-model ensembles based on EPS meteorological data. The advantage of this type of methodology is such that one can easy obtain uncertainty information (like variance) from EPS-based simulations for each model and then try to make an optimal combination of models results using these uncertainties.

# 4.15 Assessment of CALPUFF for Modeling Winter-Time $PM_{10}$ in Christchurch, New Zealand

**Vicky Lucas**

Environment Canterbury, 58 Kilmore Street, P.O. Box 345, Christchurch 8140, New Zealand

**Abstract** Christchurch, in New Zealand's South Island, has $PM_{10}$ concentrations in winter that exceed the WHO 24-hour guidelines. CALPUFF has been used to model the distribution of $PM_{10}$ concentrations across the city of Christchurch during winter 2005 and 2006. CALMET was shown to effectively develop the terrain induced surface flows that affect Christchurch on light-wind evenings. The modeling of wintertime $PM_{10}$ in the city was verified against measured data at two sites. The model captured diurnal variability well but daily values were generally too high, although the long term averages were shown to be within 10% of the measured values. The model was able to predict high pollution days with reasonable skill, with a rank correlation of 0.63 to 0.80.

**Keywords** CALPUFF, CALMET, particulate matter

## 1. Background

Christchurch is the largest city in New Zealand's South Island, home to 350,000 people. The city has generally good air quality with respect to gaseous pollutants such as ozone and sulfur dioxide, but in wintertime the city experiences $PM_{10}$ (particulate matter of less than 10 μm) concentrations that exceed the 2005 World Health Organization 24-h guidelines of 50 $\mu g/m^3$. Between May and August 2006 the city exceeded the guideline value on 27 days. City-wide emission inventories indicate that the main emission of winter $PM_{10}$ is from burning wood to heat homes. The 2006 inventory indicated that on a cold winters' day 76% of the mass of $PM_{10}$ emitted was by domestic wood burning, 11% by motor vehicles and the remaining 13% was emitted by industrial activities [4].

Environment Canterbury is the local government body responsible for air quality in Christchurch. The development of modeling that captures patterns of ambient $PM_{10}$ is helpful for investigating ways of improving air quality and thereby informing policy decisions. The first step is to develop and verify the model.

D.G. Steyn and S.T. Rao (eds.), *Air Pollution Modeling and Its Application XX*,
DOI 10.1007/978-90-481-3812-8, 

## 2. Meteorology, Modeling and Air Quality Data

Christchurch is on the edge of the Canterbury Plains which descend gently from the foothills of the Southern Alps over a distance of 70 km to the sea. The city is bounded to the east by the Pacific Ocean and on the south by Banks Peninsula, a collection of extinct volcanoes rising steeply to about 400–900 m (Fig. 1). Christchurch experiences high concentrations of $PM_{10}$ on winter evenings when cold air drainage from the Plains results in light winds from the west-northwest [2], concurrently there are down slope flows from the southern hills. Therefore, whilst Christchurch itself is flat, the winds and dispersion can be affected by terrain induced flows.

The localized terrain induced flows were simulated using the meteorological processor, CALMET [3]. CALMET is driven by surface and upper air meteorological data. The surface synoptic data were extracted from the national climate database [5]. No representative upper air data are available for Canterbury, therefore TAPM [1] (The Air Pollution Model) was used to produce point vertical profiles. Figure 1 illustrates how CALMET can combine surface observations (Christchurch airport, Kyle Street and Lincoln) and, on a winter night with low wind speeds, effectively develop the down slope flows around the hills of Banks Peninsula.

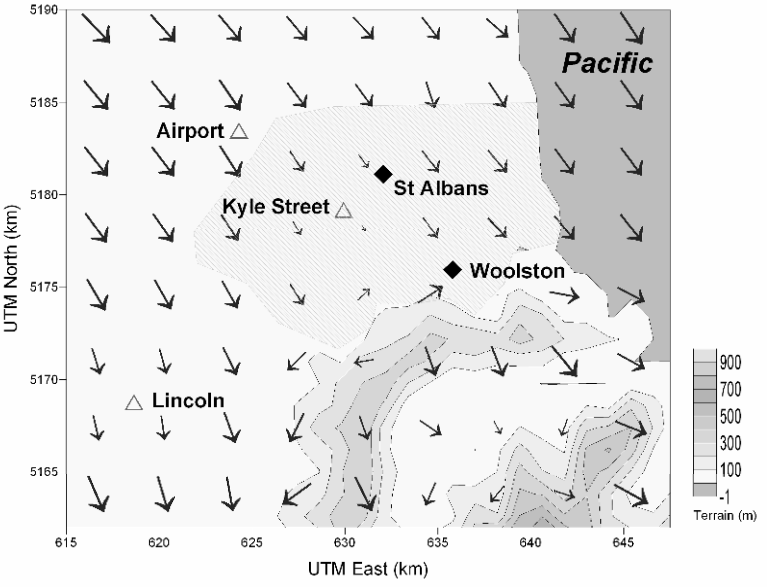


**Fig. 1.** CALMET representation of Christchurch surface winds, 00:00 NZST 10 July 2006. The triangles are meteorological surface observation stations, the *diamonds* are air quality monitoring sites and the shading is the built-up area of Christchurch. Christchurch airport wind speed 340° 0.5 m/s

The $PM_{10}$ dispersion modeling used CALPUFF (version 6.263) forced with CALMET fields; both domains were 120 by 120 km on a 1.2 km grid centered on the city. Area sources were used to represent home heating and vehicle emissions, and industrial stacks were included as point sources. The 'slug' rather than 'puff' dispersion option was used since output concentrations were required from sites within area emission sources. The input hourly diurnal pattern for sources was typical for a cold winters' day [4], therefore, whilst different zones of the city had different diurnal patterns and individual stacks had hourly varying patterns, an identical pattern was repeated every day of the CALPUFF run. The model run was for May to the end of August 2006.

The main air quality reporting site for the city, and one that typically experiences the greatest number of days in excess of 50 $\mu g/m^3$, is in the residential suburb of St Albans (Fig. 1). A second site is located at Woolston, near to an industrial area. $PM_{10}$ is measured continuously with a TEOM FDMS; St Albans has temporal data coverage of greater than 98% and Woolston of over 90%. These two sites provided the verification data for the CALPUFF modeling results.

## 3. Results and Conclusions

The CALPUFF modeled concentrations have good qualitative agreement with observations on both an hourly and 24-hourly basis. Fig. 2. shows a period of 2 weeks in June 2006, the model successfully simulating the diurnal variability, with concentrations peaking strongly in the late evening. The period encompasses a range of dispersion scenarios, including low wind speeds and dawn frosts for the first 6 days, followed by snow during the early hours of the 12 June, a frost on the 14 June and milder, breezier conditions in the end of the period. The false modeled peak in concentrations around midnight on 12 June coincides with what had been a mild evening, the mean daily temperature on the 11 June was 13°C and potentially the emissions from home heating would be low. The use of a fixed diurnal emission pattern representing a typical cold winters' day is likely to lead to a bias in overestimating concentrations.

The relationship between modeled and measured 24-h averaged concentrations was investigated for all days of 8°C or lower May to August 2005 and 2006 (Fig. 3. These lower temperature days were chosen to reflect that the emission inventory focuses on a cold winters' day. The Spearman rank correlation coefficient was 0.80 for St Albans and 0.63 for Woolston. The model tended to predict higher concentrations than were measured. The long term average measured concentration at St Albans for June and July 2005 and 2006 was 49 $\mu g/m^3$ and the modeled 53 $\mu g/m^3$, at Woolston the measured average was 41 $\mu g/m^3$ and the modeled 37 $\mu g/m^3$.

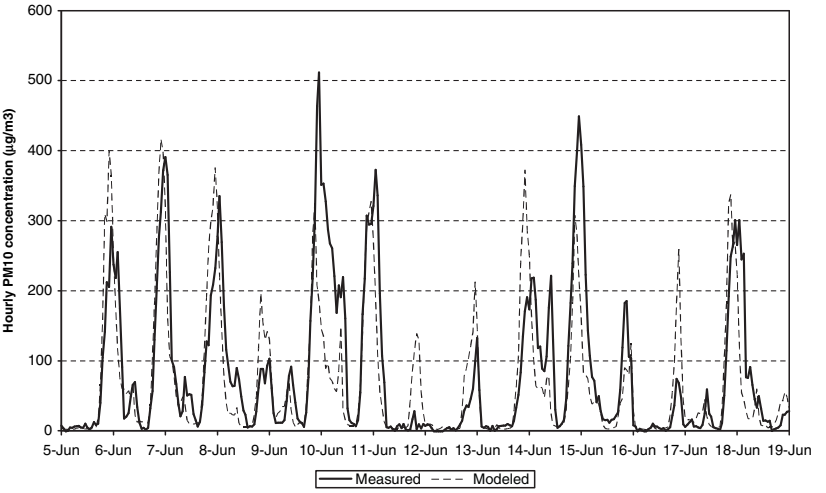


**Fig. 2.** St Albans hourly $PM_{10}$ concentrations ($\mu g/m^3$) 00:00 NZST 5th to 00:00 19th June 2006, modeled and measured concentrations

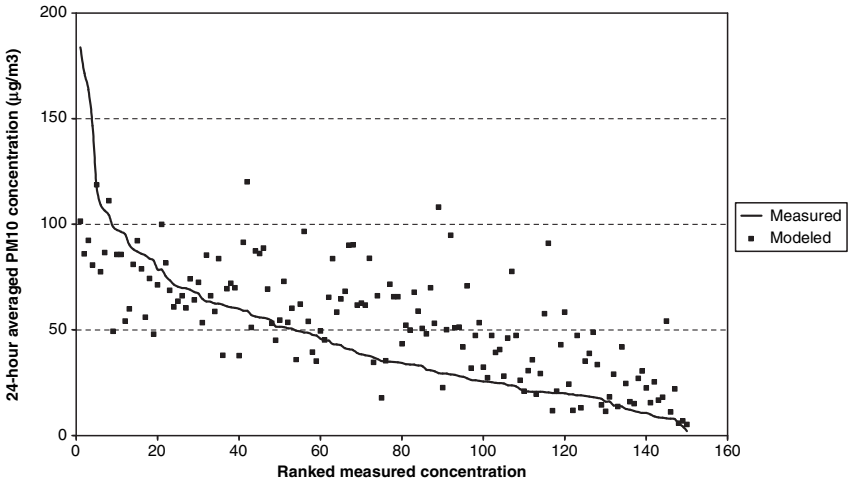


**Fig. 3.** St Albans measured daily $PM_{10}$ ($\mu g/m^3$) in rank order (line) and the corresponding modeled concentrations (points). Spearman rank correlation coefficient 0.80. May–August 2005 and 2006, days 8°C or lower

CALMET has been shown to effectively develop the terrain induced surface flows that affect Christchurch on light-wind evenings. The CALPUFF modeling of wintertime $PM_{10}$ in the city has been verified against measured data at two sites and whilst daily values are generally too high, the model captures diurnal variability

well and is able to predict high pollution days with reasonable skill. Some of the overprediction of concentrations may be due to the emission inventory data used, since it only focuses on establishing emissions for a typically cold winters' day, potentially overestimating emissions from home heating on mild winter days.

## References

Hurley, P.: TAPM V4. Part 1: Technical Description. CSIRO Marine and Atmospheric Research Paper 25. ISBN 978-1-921424-71-7 (2008)

Kossman, M., Sturman, A.P.: The surface wind field during winter smog nights in Christchurch and coastal Canterbury, New Zealand. International Journal of Climatology **24**, 93–108 (2004)

Scire, J.S., Robe, F.R., Fernau, M.E., Yamartino, R.J.: A User's Guide for the CALMET Meteorological Model (V5). Earth Tech, Inc., Concord, MA (1998)

Smithson, J.: Inventory of emissions to air in Christchurch, 2006. Environment Canterbury Technical Report R08/70. ISBN 978-1-86937-885-1 (2008)

Surface meteorological data source: National Institute of Weather and Atmospheric Research http://cliflo.niwa.co.nz/ accessed 1 Feb 2009

# 4.16 Satellite Based Investigations of Day-of-Week Variation in $NO_x$ Emissions

**Ashley Ray Russell[1], Lukas Valin[1], Simon Schmutz[2], Pascal Tay[2], and Ron Cohen[1]**

[1]Department of Chemistry, University of California, Berkeley, CA, USA

[2]Swiss Federal Institute of Technology, Institute for Atmospheric and Climate Science, Zurich, Switzerland

**Abstract** In the state of California, mobile sources account for more than 50% of $NO_x$ emissions. Regulation focusing on passenger vehicles has led to dramatic reductions in total $NO_x$ emissions. Heavy-duty diesel vehicle emissions have, in contrast, not decreased and therefore represent a growing fraction of total $NO_x$ emissions. A pronounced weekend effect, marked by a substantial decrease in measured $NO_2$ on weekends when compared with measurements on weekdays has been observed in some urban areas of the state due to variation in the activity patterns of these two types of vehicles. We examine this weekend effect using observations from the Ozone Monitoring Instrument (OMI). We developed a high resolution ($5 \times 5$ km$^2$) average of the OMI observations that permits a detailed view of spatial variations in emissions with day of week. Comparison of the observations to emission inventories suggests opportunities for improvements and for assessing differences between San Joaquin Valley and South Coast Air Basins.

**Keywords** OMI, Satellite, Day-of-week, NOx, Emissions, Urban

## 1. Introduction

We use satellite observations from the Ozone Monitoring Instrument (OMI) aboard the Aura satellite to monitor variation of $NO_2$ columns with day of week. In the state of California, mobile sources account for a large majority of $NO_x$ emissions. Regulation aimed at reducing these emissions has to date focused primarily on light-duty passenger vehicles yielding a relative increase in the importance of heavy duty diesel truck $NO_x$ emissions. The 'weekend effect' is the name given to the trend in regional $NO_x$ levels in which we see a substantial decrease in weekend concentrations relative to weekday levels. In California, this is due mainly to the different activity patterns of these two mobile source types.

D.G. Steyn and S.T. Rao (eds.), *Air Pollution Modeling and Its Application XX*,
DOI 10.1007/978-90-481-3812-8, © Springer Science + Business Media B.V. 2010

We use the OMI standard product from October 2004 to August 2008 (Bucsela, 2006). Data chosen for analysis has been filtered to exclude pixels with a cloud fraction exceeding 0.2. We take advantage of OMI's 16-day repeat pattern and use an area-weighted averaging, binning to a 0.025° × 0.025° grid. In Fig. 1a we show OMI $NO_2$ columns for one summer day and in Fig. 1b, the area-weighted average summer concentration over 3 years. In Fig. 2 we show average weekday and weekend concentrations of $NO_2$ across California for summers 2005–2008. Both panels show elevated concentrations of $NO_2$ in and around highly populated areas.

We compare OMI tropospheric column concentrations with observations from a network of ground monitoring sites maintained by the California Air Resources Board (CARB). We focus on summer observations because the $NO_2$ lifetime is shorter in the summer so we can expect the column to be more representative of surface emissions on that day. Figure 3 shows the average day of week patterns observed by OMI and the CARB sites for three regions of interest; the San Francisco Bay Area, the South Coast, and the San Joaquin Valley air basins. On average, we see Saturday and Sunday concentrations that are 27% and 40% lower than weekday values, respectively.

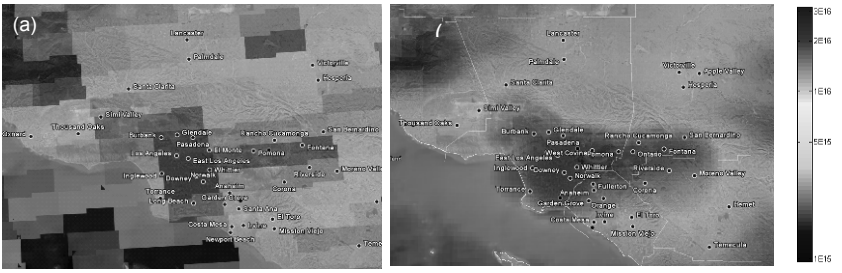


**Fig. 1.** (a) Tropospheric column $NO_2$ concentrations (molecules/cm$^2$) from OMI over the South Coast region of California from August 1, 2008. (b) OMI tropospheric $NO_2$ columns averaged over summer months (June–August) for the years 2005–2008 at 0.025° resolution

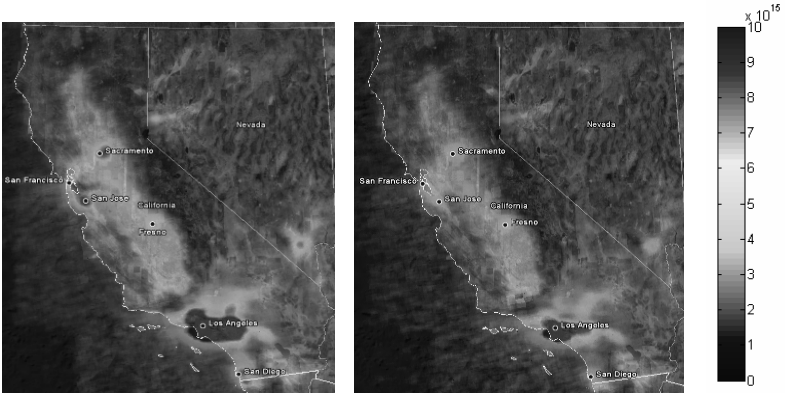


**Fig. 2.** Average OMI tropospheric $NO_2$ column concentrations (molecules/cm$^2$) for (a) weekdays (Tuesday–Friday) and (b) weekends (Saturday–Sunday) for June–August 2005–2008

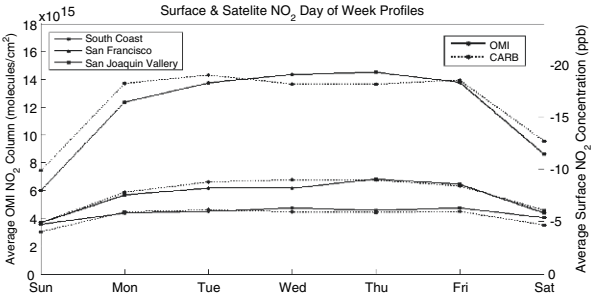


**Fig. 3.** Average day of week $NO_2$ profiles from OMI (solid) and CARB monitoring sites (dashed) for summer 2005–2007 in the South Coast, San Francisco Bay Area, and San Joaquin Valley air basins of California

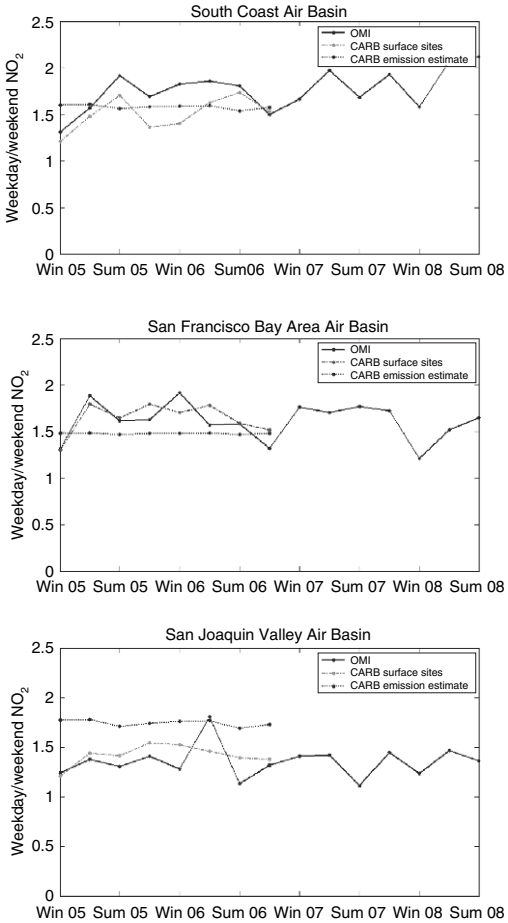


**Fig. 4.** The ratio of weekday to weekend $NO_2$ concentrations from OMI, CARB ground monitoring sites, and CARB emission estimates for (a) the South Coast, (b) the San Francisco Bay Area, and (c) the San Joaquin Valley air basins

We further utilize OMI observations in order to test current emissions estimates used for guiding policy initiatives in California. CARB's emissions inventory divides emissions into source type but includes no day-of-week dependence on emissions. Harley et al. have shown, however, that there is a strong day of week dependence on mobile source emissions with diesel activity being largely confined to weekdays (2005). We use traffic activity data from the EMission FACtors (EMFAC) model, off-road activity data from the NONROAD model (Janssen, 1999) and on-road activity data from Chinken et al. (2002) to compare observations of the weekend effect with current emission inventory estimates.

Figure 4 shows the resultant ratio of weekday to weekend $NO_2$ concentrations from OMI, CARB monitoring sites, and CARB emission estimates for the three regions of interest. For all three cases, a positive slope (South Coast = +0.07, San Francisco = +0.04; San Joaquin Valley = +0.01) indicates that OMI is capturing the increasing relative importance of weekday diesel $NO_x$ emissions. There is excellent agreement between OMI tropospheric $NO_2$ columns and CARB surface measurements, particularly in summers. In the South Coast region, the California Air Resources Board's emission inventory agrees well with OMI and surface measurements. In the San Francisco Bay and San Joaquin Valley regions, however, emissions estimates are inconsistent with observations. This disagreement indicates that there exists some error either in the quantitative estimate of the emissions or in our understanding of how they vary with day of week.

**Acknowledgments** This work was supported by NASA (grant NNX08AE566) and CARB (grant 06-328).

## References

Bucsela EJ, Celarier EA, Wenig MO, Gleason JF, Veefkind JP, Boersma KF, Brinksma EJ (2006) Algorithm for NO2 vertical column retrieval from the ozone monitoring instrument. IEEE Transactions on Geoscience and Remote Sensing 44:1245–1258.

Chinkin LR, Coe DL, Funk TH, Hafner HR, Roberts PT, Ryan PA (2003) Weekday versus weekend activity patterns for ozone precursor emissions in California's South Coast air basin. Air & Waste Manage. Assoc. 53:829–843.

Harley RA, Marr LC, Lehner JK, Giddings SN (2005) Changes in motor vehicle emissions on diurnal to decadal time scales and effects on atmospheric composition. Environ. Sci. Technol. 39:5356–5362.

Janssen et al. (1999) Weekday and weekend day temporal allocation of activity in the NONROAD model. Report prepared for the U.S. Environmental Protection Agency, Office of Mobile Sources by Nonroad Engine Emission Modeling Team, NR-015.

# 4.17 Application of Wavelet Filters in an Evaluation of Photochemical Model Performance

**P.S. Porter[1], C. Hogrefe[2], E. Gégo[3], K. Foley[4], J.M. Godowitch[4], and S.T. Rao[4]**

[1]University of Idaho, Idaho Falls, ID, USA

[2]ASRC, University at Albany, Albany, NY, USA

[3]GEGO and Associates,

[4]Atmospheric Modeling Division U S Environmental Protection Agency

## 1. Introduction

Air quality model evaluation can be enhanced with time-scale specific comparisons of outputs and observations. For example, high-frequency (hours to 1 day) time scale information in observed ozone is not well captured by deterministic models and its incorporation into model performance metrics lead one to devote resources to stochastic variations in model outputs. In this analysis, observations are compared with model outputs at seasonal, weekly, diurnal and intra-day time scales. Filters provide frequency specific information that can be used to compare the strength (amplitude) and timing (phase) of observations and model estimates.

## 2. Methods and Time Series

### 2.1. Modeling system

Model outputs were produced by MM5-v3.7.2., CMAQ-v4.5.1., CB4 and aero3 set to simulate the time period 1988–2005 (Hogrefe et al., 2009). The domain was the northeastern U.S. at a grid of 12 × 12 km. Emissions included NEI 1990, 1996–2001, OTC2002, and OTC2009, processed by SMOKE.

### 2.2. Observations

Observations (ozone concentrations and meteorological variables) used for time series examples were recorded by the *Clean Air Status and Trends Network* (CASTNET, www.epa.gov/castnet/data/metdata/) operated by the Environmental Protection Agency's Clean Air Markets Division. CASTNET sites are located in mostly rural and remote areas such as national parks and monuments. Illustration

D.G. Steyn and S.T. Rao (eds.), *Air Pollution Modeling and Its Application XX*,
DOI 10.1007/978-90-481-3812-8, © Springer Science + Business Media B.V. 2010

of weekly variation in ozone was demonstrated with ozone data from the EPA's air quality system (www.epa.gov/ttn/airs/airsaqs/detaildata/downloadaqsdata.htm).

CASTNET sites and CMAQ grid cells at Abington, CT (ABT147) and Shenandoah National Park, VA (SHN418) were chosen for purposes of illustration. ABT is downwind of the New York City urban area. SHN is a high altitude site (elev. 1,073 m).

### 2.3. Low pass filter (KZ)

A low-pass filter (iterative moving average where high frequencies are damped and low frequencies are unaltered) was used to define the trend (KZ(k = 3 iterations, q = 182 days) and intra-day (original − KZ(k = 3 iterations, q = 1 h)) time scales (Zurbenko, 1986; Rao and Zurbenko, 1994). An advantage of the KZ over other linear filters is its ease of application when some observations are missing: missing values are ignored and a mean is computed from whatever values are present. Endpoints of time series (as well as the edges of gaps) are not properly filtered and are therefore clipped when presented.

### 2.4. Wavelet filter

The KZFT(q,k,w) wavelet is a Fourier transform (FT) version of the KZ (Zurbenko and Porter, 1998). The KZFT is given by:

$$\mathbf{Y_t = \frac{1}{2q+1} \sum_{k=-q}^{+q} exp(-\,i\ 2\ \pi\ \omega\ k) \cdot X_{t+k}} \qquad \mathbf{(1)}$$

where q is the half-window size and k is the number of iterations, T is a frequency of interest, and 'i' is $(-1)^{1/2}$. The real part of the filtered time series, $Y(Y_t)$, is a bandpass component centered at frequency T, and $|(Y_t)|$ is the instantaneous amplitude of Y(t).

Cross-correlations do not adequately describe relationships among different periodic processes. Any two time series with seasonal (or diurnal) variation will tend to be highly correlated when adjusted for phase difference. As such, it's better to compare amplitudes and phases. Consider the following conceptual model for seasonal variation:

$$\mathbf{Q_{se} = A_t \cdot \cos\left(\frac{2\pi t}{p} + ph_t\right)} \qquad \mathbf{(2)}$$

where $Q_{se}$ is seasonal variation in a process Q at time t, $A_t$ is the amplitude of seasonal variation at time t, p is the period (1 year) and $ph_t$ is the phase at time t. Seasonal phase is calculated from (Bloomfield, 2000):

$$\mathbf{ph_t = \Im\left[\ln \frac{Y_t \cdot exp(-i \cdot 2 \cdot \pi \cdot t \cdot \omega)}{abs(Y_t \cdot exp(-i \cdot 2 \cdot \pi \cdot t \cdot \omega))}\right]} \qquad \mathbf{(3)}$$

and can be thought of as the day of the year that a process reaches a maximum. An estimate of $A_t$ is the modulus of the wavelet filtered time series. Phase ($ph_t$) and amplitude ($A_t$) of seasonal ozone are typically low frequency processes.

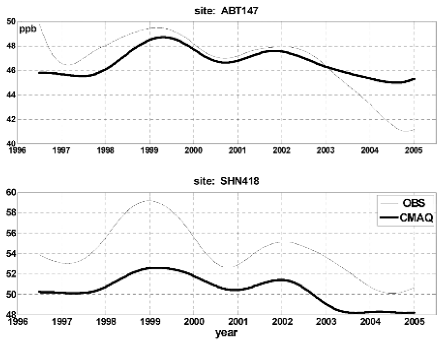


**Figure 1.** Observed and modeled trend (low-frequency variation) at ABT and SHN

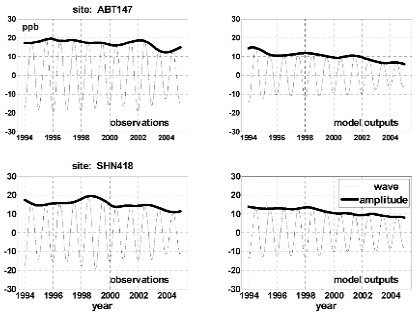


**Figure 2.** Observed and modeled seasonal variation at ABT and SHN

## 3. Results and Discussion

### 3.1. Observed and modeled ozone by time scale

Low-frequency ozone variation (trend) was defined with a low-pass filter (Fig. 1). The trend is captured by CMAQ (R = 0.79 and 0.89 at ABT147 and SHN418, respectively).

Observed and CMAQ seasonal wavelets and their amplitude for ABT and SHN are shown in Fig. 2. Correlations between observed and CMAQ seasonal variation (0.97 and 0.99 at ABT and SHN, respectively), for the most part measure phase differences.

Among the meaningful measures of agreement between observations and model outputs are the correlation between seasonal amplitudes (0.71 and 0.76 at ABT147 and SHN418, respectively) and the phase difference (Fig. 3). CMAQ is out of phase with observations, sometimes by more than 10 days. The CMAQ phase has trended downward since 1999 at both sites (seasonal maximum coming earlier).

Ozone seasonal amplitude is modulated in part by meteorology (Fig. 4). The dotted lines in Fig. 4 are linear combinations of meteorological variables that include temperature, solar radiation, relative humidity and wind speed. The most significant covariates are wind speed and solar radiation at ABT and SHN, respectively.

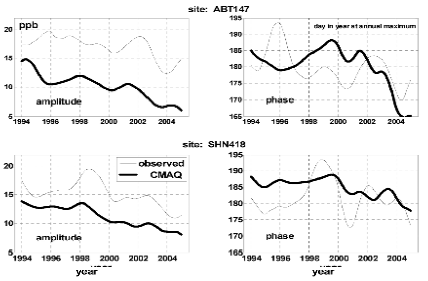


**Figure 3.** Observed and modeled seasonal amplitude and phase at ABT and SHN

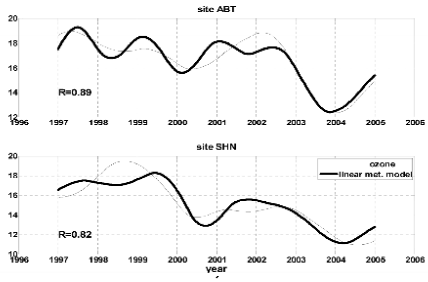


**Figure 4.** Seasonal amplitude and linear meteorological model for ABT and SHN

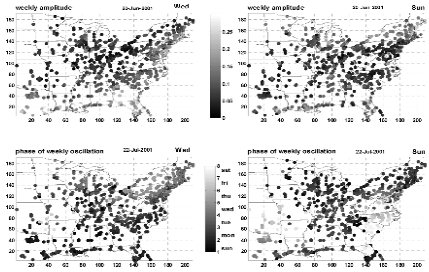


**Figure 5.** ABT weekly amplitude (log of ppb) a) 20 June and b) 22 July and weekly phase c) 20 June d) 22 July

Weekly amplitude and phase at ABT, shown across the eastern US for two different times in 2001 (Fig. 5) illustrate widely varying temporal and spatial properties of weekday/weekend ozone fluctuation.

Observed and CMAQ diurnal amplitude and phase are compared in Figs. 6 and 7. Observed diurnal amplitude at ABT is greater than that of CMAQ. During the 18 years that were modeled, the average diurnal phase difference between observations and CMAQ is zero (cross-correlations between observations and model peak at zero lag). However, there are times (as in Fig. 7) when the two are out of phase.

As with seasonal processes, correlations between observed and CMAQ diurnal variation (0.91 and 0.76 at ABT147 and SHN418, respectively), mostly reflect phase differences (Fig. 6), while observed/model amplitude correlation (0.79 and 0.41) measure the extent to which the model correctly gauges changes in diurnal forcings (Fig. 7). Observation/model agreement was poor at intraday time scales (<11 h, R 0.26 and 0.19 at ABT and SHN, respectively), reflecting, in part, the model's inability to simulate stochastic variation like measurement instrument noise.

## 4. Summary

Wavelet analysis provides frequency specific information about observations and model outputs that can be useful in model evaluation. Differences in the strength (amplitude) between observations and model were illustrated for low-frequency (trend) and intra-day variation, while differences in both strength and timing (phase) were illustrated for seasonal, weekly and diurnal processes. Modulation of seasonal and diurnal ozone occurs at low frequencies (3–5 years for seasonal and 1 year for diurnal processes) and can be tied to low frequency variation in meteorological variables. Wavelet analysis of weekly variation can be used to identify spatial/temporal variation in weekday/weekend ozone air quality.

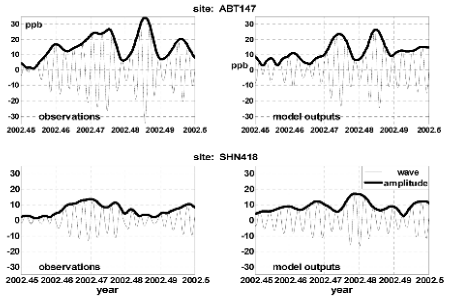


**Figure 6.** Observed and modeled diurnal variation at ABT and SHN

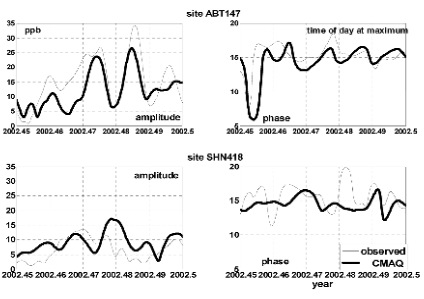


**Figure 7.** Observed and modeled diurnal amplitude and phase at ABT and SHN

**Acknowledgments and Disclaimer** Christian Hogrefe gratefully acknowledges partial support for this work through a research fellowship from the Oak Ridge Institute for Science and Education (ORISE). The model simulations in this paper were supported by National Oceanic and Atmospheric Administration award NAO40AR4310185185, but the paper has not been subjected to its required peer and policy review. Therefore, the statements, findings, conclusions, and recommendations are those of the authors and do not necessarily reflect the views of the sponsoring agency and no official endorsement should be inferred. This work constitutes a contribution to EPA's Air Quality Program. Although it has been reviewed by EPA and approved for publication, it does not necessarily reflect their policies or views.

## References

Bloomfield, P. 2000. Fourier Analysis of Time Series: An Introduction. Wiley-Interscience; 2nd ed.

CASTNET. 2006. Annual Report. prepared by MACTEC Engineering and Consulting, Inc. for the USEPA Clean Air Markets Division, Washington, D.C.

Hogrefe, C., Lynn, B., Goldberg, R., Rosenzweig, C., Zalewsky, E., Hao, W., Doraiswamy, P., Civerolo K., Ku, J., Sistla, G., and P.L. Kinney. 2009. A combined model–observation approach to estimate historic gridded fields of PM2.5 mass and species concentrations. Atmospheric Environment 43: 2561–2570

Rao, S.T., and I.G. Zurbenko. 1994. “Detecting and tracking changes ozone air Quality”, J. Air & Waste Manage. Assoc., 44: 1089

Zurbenko, I.G. 1986. The Spectral Analysis of Time Series. North Holland

Zurbenko I., Porter. P.S. 1998. Construction of high resolution wavelets, IEEE Journal of Signal Processing, vol. 65, pp. 315–327.

# 4.18 Influence of Concentration-Response Temporal Metrics on Control Strategy Optimization

**Daniel S. Cohan[1], Antara Digar[1], and Michelle L. Bell[2]**

[1]Department of Civil and Environmental Engineering, Rice University, Houston, TX 77005, USA

[2]School of Forestry and Environmental Studies, Yale University, New Haven, CT 06511, USA

**Abstract** Epidemiological studies differ as to the temporal averaging periods that govern air pollutant health impacts, and the presence of threshold concentrations at which impacts begin to occur. Here, we investigate how alternate temporal metrics and thresholds for ozone concentration-response functions could influence the optimization of control strategies for health benefits. A photochemical model is applied with direct sensitivity analysis to simulate the responsiveness of ozone to potential regional and point source emissions controls in a summertime air pollution episodes in Georgia. The relative health benefits of various control options are assessed by linking the DDM sensitivity results with population and applying alternate temporal metrics for ozone health impacts. We assess how these metrics influence the relative health impacts of alternate control options.

**Keywords** Ozone health effects, temporal metrics, decoupled direct method, sensitivity analysis

## 1. Introduction

Air quality management aims to achieve two interrelated yet distinct objectives: attainment of ambient standards, and protection of public health. In the development of state implementation plans (SIPs), policy-makers in U.S. states have typically focused on how to achieve National Ambient Air Quality Standards (NAAQS) in the most expedient and cost-effective manner, without explicit quantification of health benefits. An implicit assumption in these efforts is that regulatory attainment will be sufficiently protective of human health, since the U.S. Clean Air Act mandates that NAAQS be set so as to protect human health with an "adequate margin of safety."

Recent work has explored how health implications could be explicitly considered in the development of air quality attainment plans (Cohan et al., 2007). Some epidemiological studies suggest that no clear thresholds exist for air pollution health effects, and that health benefits may result from air quality improvements beyond the NAAQS requirements (Bell et al., 2006) Consideration of health impacts

D.G. Steyn and S.T. Rao (eds.), *Air Pollution Modeling and Its Application XX*,
DOI 10.1007/978-90-481-3812-8, © Springer Science + Business Media B.V. 2010

may be especially influential in multi-pollutant planning due to the tradeoffs and co-benefits between controls for each pollutant (Chestnut et al., 2006). However, such efforts are complicated by lack of clarity as to which temporal metric is best suited for assessing the health benefits of controls. Epidemiological studies in the scientific literature have applied a wide variety of temporal averaging periods (e.g., 1-h, 8-h, daily, or annual average) and threshold values in developing concentration-response functions for air pollutant health effects. For ozone, the choice of a temporal metric may influence health effect magnitude and trend estimates (Stedman and Kent, 2008) and shift which emissions scenario is perceived to most impact human health (Bell et al., 2005).

Here, we investigate how alternate temporal metrics and thresholds for ozone concentration-response functions could influence the optimization of control strategies for health benefits. The work presented here is a preliminary component of a broader study that is exploring how uncertainties in control costs, photochemical sensitivities, and concentration-response functions can be jointly considered to inform the development of air quality attainment strategies.

## 2. Methods

The modeling approach was designed to simulate the health implications that could be considered in the development of a state-level ozone attainment plan. Photochemical sensitivity modeling was conducted with the Community Multi-scale Air Quality (CMAQ) model version 4.5 (Byun and Schere, 2006) with the CB-IV chemical mechanism. Meteorology and emissions inputs were developed and evaluated by the Visibility and Improvements State and Tribal Association of the Southeast (VISTAS) (Morris et al., 2007). VISTAS applied MM5 to simulate meteorological conditions for 2002; here we focus on the period May 30-June 6, 2002 (first 2 days discarded for model initialization). Emissions are from VISTAS' Year 2009 projections (projected from a 2002 base inventory), with updates to Georgia emissions projections based on Georgia Environmental Protection Division's (GA EPD) SIP modeling.

Sensitivity analysis was conducted with the decoupled direct method (DDM) in CMAQ (Dunker, 1984). First-order DDM sensitivity coefficients $S_{i,j}^{(1)}$ represent the responsiveness of pollutant $i$ to an incremental change in input $j$. A sensitivity coefficient of $S_{i,j}^{(1)}$ = y ppb indicates that an x% reduction in $j$ would yield an (xy/100) ppb reduction in $i$.

Sensitivities were simulated to emissions from three regions: "Atlanta," defined as the 20-county ozone non-attainment region; "Macon," defined as a 7-county region centered on the city of Macon; and Plant Scherer, the largest $NO_x$ emitting power plant in Georgia in the projected emissions inventory.

Sensitivity results were processed based on one of the following temporal metrics, each of which has been the basis of some ozone health studies:

*1-h max:* Sensitivity at time of maximal hourly ozone for each cell and day.

*8-h max:* Sensitivity averaged over 8-h interval with maximal ozone. This metric was evaluated for cells exceeding 75 or 85 ppb ozone thresholds (corresponding to new and old US ozone standards), or for all cells (no threshold).

*24-h:* Sensitivity averaged over entire day.

## 3. Results

The sensitivity of ozone to emissions from various source regions and categories was evaluated on a variety of temporal metrics on a ppt/ton-per-day basis to enable comparison between sources of different sizes (Table 1). Within each of the no-threshold temporal metrics, the per-ton impacts of all of the regional $NO_x$ sources are similar. $NO_x$ from the power plant has a slightly smaller per-ton impact, likely reflecting that the altitude and intensity of its plume inhibits ground-level ozone formation. The densely vegetated southeastern U.S. experiences high biogenic VOC emissions, so sensitivities to anthropogenic VOCs are minimal.

**Table 1.** Sensitivity of ground-level ozone to emissions (ppt/tpd), averaged over the episode for all cells exceeding the ozone threshold. The population-weighted metric (ppm-persons/tpd) integrates over population of each cell

| | **Emissions (t/day (tpd))** | **1-h (all)** | **8-h (all)** | **8-h ($O_3 \geq$ 85 ppb)** | **8-h ($O_3 \geq 75$ ppb)** | **24-h (all)** |
|---|---|---|---|---|---|---|
| **Average # of gridcells** | | 9,310 | 9,310 | 83 | 520 | 9,310 |
| **Sensitivity of ozone (ppt/tpd) to** | | | | | | |
| Atlanta all NOx[a] | 346 | 2.10 | 1.91 | 8.57 | 5.35 | 1.08 |
| Atlanta mobile NOx | 206 | 2.16 | 1.98 | 8.59 | 5.48 | 1.14 |
| Atlanta point NOx[a] | 10 | 2.15 | 1.89 | 8.26 | 5.23 | 1.08 |
| Macon all NOx[a] | 52 | 1.84 | 1.79 | 1.38 | 2.43 | 1.23 |
| Plant Scherer NOx | 46 | 1.56 | 1.37 | 1.26 | 2.46 | 0.94 |
| Atlanta all VOC[a] | 467 | –0.08 | –0.08 | –0.01 | –0.14 | –0.05 |
| **Population-weighted impact (ppm-persons/tpd)** | | | | | | |
| Atlanta all NOx [a] | 346 | 159 | 138 | 34 | 61 | 33 |
| Atlanta mobile NOx | 206 | 163 | 145 | 35 | 62 | 41 |
| Atlanta point NOx [a] | 10 | 143 | 124 | 29 | 55 | 46 |
| Macon all NOx [a] | 52 | 84 | 74 | 3 | 14 | 55 |
| Plant Scherer NOx | 46 | 99 | 70 | 3 | 16 | 52 |
| Atlanta all VOC [a] | 467 | –1 | –1 | 1 | 1 | –1 |

[a]Excluding power plant and biogenic emissions

Applying an ozone threshold strongly impacts the relative importance of the regional emissions. A large portion of the grid cells modeled to exceed the ozone thresholds are within the Atlanta region. Thus, a concentration-response metric that includes a threshold would place much greater importance on reducing Atlanta emissions. Although strong regional differences appear when thresholds are applied, source categories within a region (e.g., mobile and non-EGU point sources in Atlanta) continue to have nearly identical per-ton impacts.

Integrating the sensitivity impacts over population (Year 2000 Census) further accentuates the regional differences while maintaining parity of source categories within a region. The Atlanta region has the highest population density in Georgia, so Atlanta emissions have the greatest per-ton impact on a population-weighted basis. Note that whereas Atlanta and Macon $NO_x$ have roughly equal per-ton impacts on spatially-averaged, no-threshold bases, they differ by an order of magnitude when both a threshold and population-weighting are considered.

## 4. Conclusions

For the scenario considered here, the temporal duration of a concentration-response metric would likely have little bearing on the prioritization of control strategies for SIP development. Application of a threshold or population weighting enhances the importance of controls in the most polluted and populated regions, but does not substantially affect prioritization within a region.

This scenario was somewhat unusual in that ozone was almost entirely $NO_x$-limited and insensitive to VOC. It is possible that temporal metrics could play a bigger role in ranking $NO_x$ and VOC control measures in more transitional regions. The sensitivity of ozone to $NO_x$ typically turns strongly negative at night, so 24-h metrics would likely enhance the importance of VOCs relative to $NO_x$.

**Acknowledgments** Funding for this research was provided by EPA STAR Grant R833665. Photochemical model inputs were provided by the Georgia Environmental Protection Division. Neither U.S. EPA nor GA EPD has reviewed this manuscript.

## References

Bell ML, Hobbs BF, et al. (2005) Metrics matter: Conflicting air quality rankings from different indices of air pollution, *J Air Waste Manage*, *55*(1), 97–106.

Bell ML, Peng RD, et al. (2006) The exposure-response curve for ozone and risk of mortality and the adequacy of current ozone regulations, *Environ. Health Perspect.*, *114*(4), 532–536.

Byun DW, and Schere KL (2006) Review of the governing equations, computational algorithms, and other components of the Models-3 Community Multiscale Air Quality modeling system, *Applied Mechanics Review*, *59*, 51–77.

Chestnut LG, Mills DM, et al. (2006) Cost-benefit analysis in the selection of efficient multipollutant strategies, *J Air Waste Manage*, *56*(4), 530–536.

Cohan DS, Boylan JW, et al. (2007) An integrated framework for multipollutant air quality management and its application in Georgia, *Environ Manage*, *40*(4), 545–554.

Dunker AM (1984) The decoupled direct method for calculating sensitivity coefficients in chemical kinetics, *J. Chem. Phys.*, *81*(5), 2385–2393.

Morris RE, Koo B, et al. (2007) Technical Support Document for VISTAS Emissions and Air Quality Modeling to Support Regional Haze SIPs, 244 pp.

Stedman JR, and Kent AJ (2008) An analysis of the spatial patterns of human health related surface ozone metrics across the UK in 1995, 2003 and 2005, *Atmos Environ*, *42*(8), 1702–1716.

# Chapter 5 Aerosols in the atmosphere

Chairperson: A.I. Miranda

Rapporteur: S. Douglas

D.G. Steyn and S.T. Rao (eds.), *Air Pollution Modeling and Its Application XX*,
DOI 10.1007/978-90-481-3812-8_5, © Springer Science + Business Media B.V. 2010

# 5.1 Atmospheric Organic Particulate Matter: Revisiting Its Sources, Properties and Impacts

**Spyros N. Pandis[1,2], Neil M. Donahue[2], and Allen L. Robinson[2]**

[1]Department of Chemical Engineering, University of Patras, Patra, GR 26500, Greece

[2]Center of Atmospheric Particle Studies, Carnegie Mellon University, Pittsburgh, PA, USA

**Abstract** An overview of the development of our understanding of the sources, formation mechanisms, physical and chemical transformations of atmospheric organic aerosol (OA) is presented. Until recently, organic particulate material was simply classified as either primary or secondary with the primary component being treated in models as nonvolatile and inert. However, this oversimplified view fails to explain the highly oxygenated nature of ambient OA, the relatively small OA concentration gradients between urban areas and their surroundings, and the concentrations of OA during periods of high photochemical activity. A unifying framework for the description of all components based on their volatility distribution (the volatility basis set) can be used for the treatment of a wide range of processes affecting organic aerosol loadings and composition in the atmosphere. These processes include direct organic particle and vapor emissions, chemical production of organic PM from volatile precursors, chemical reactions (aging) in all phases, as well as deposition of both particles and vapors and chemical losses to volatile products. The combination of this new framework with the recent results of laboratory studies can resolve some of the discrepancies between OA observations and laboratory results.

**Keywords** Secondary organic aerosol, PMCAMx, Volatility basis set

## 1. Revisiting the Main Assumptions about Primary Organic Aerosol

Primary Organic Aerosol (POA) has been traditionally assumed to be non-volatile and non-reactive in atmospheric aerosol models. Even if these assumptions are used today by the great majority of Chemical Transport Models (CTMs) and are integral parts of most mental models of the system, it has been clear for decades that neither is correct in many cases. Most measurements of ambient organic PM concentrations were accompanied by serious negative (particle evaporation after collection on the filter) and/or positive artifacts (vapor adsorption on the filter), providing strong hints about the semi-volatile nature of organic aerosol.

D.G. Steyn and S.T. Rao (eds.), *Air Pollution Modeling and Its Application XX*,
DOI 10.1007/978-90-481-3812-8, © Springer Science + Business Media B.V. 2010

It has long been recognized that certain primary compounds were semivolatile. Polycyclic Aromatic Hydrocarbons (PAHs) have received special scrutiny because of their known toxicity; they range from completely volatile Napthalene to completely condensed Coronene, with intermediate molecular weight compounds occurring significantly in both phases. The semi-volatile character of many other ambient organics (Fraser et al., 1997, 1998) and sources (Schauer et al., 1999) has also been addressed extensively. However, the overall contribution of semivolatile material to ambient POA has not been comprehensively addressed until recently.

For more than 20 years, dilution samplers have been used to measure POA emission factors. Development of these samplers was motivated by the semivolatile character of primary emissions; specifically upon heating. Initial studies focused on the effect of temperature on partitioning. Only modest amounts of dilution (about 100×) are required to reduce the temperature of the exhaust to ambient levels, which dramatically increases the amount of POA because of the strong dependence of vapor pressure on temperature. More recent experiments have demonstrated that POA emission factors decrease when the aerosol is isothermally diluted (Lipsky et al., 2006). Both of these changes are expected based on partitioning theory.

Although some primary emissions are clearly semivolatile, most CTMs have treated them as non-volatile. The implicit assumption is that the partitioning measured using a dilution sampler is representative over the full range of atmospheric conditions simulated by the model, and that the semi-volatile primary mass is a small fraction of the total POA.

It is also reasonable to expect that the organic aerosol compounds will react with atmospheric oxidants like the OH radical, $O_3$, $NO_3$, etc. leading to chemical changes. Limited studies of the heterogeneous chemistry of POA components and realistic POA have confirmed that these reactions are quite efficient in transforming POA to other compounds. At the same time, the POA components that evaporate after dilution as they move away from their sources will react in the gas-phase, forming products with lower volatility that can condense back in the particulate phase (Robinson et al., 2007). Both of these pathways oxidize primary emissions, forming oxygenated organic aerosol (OOA).

At this point the traditional simple framework and corresponding definitions of POA and SOA have broken down. Is the OA formed from a compound that starts its atmospheric life in the particulate phase, evaporates, reacts in the gas phase and then condenses primary or secondary? Further confusion arises because traditionally ‘primary’ and ‘secondary’ refer to the aerosol mass, and not the specific chemical compounds making up that mass.

## 2. The Volatility Basis Set as a Unifying Framework

The need to treat the volatility of primary OA, the formation of secondary organic aerosol (SOA), the reactions of both primary and secondary OA components, and

the need to model the aging of semi-volatile compounds all motivated the development a new framework for the description of all OA components and their reactions. This framework blurs the distinction between the traditional primary and secondary organic aerosol, providing a more realistic picture of the behavior of atmospheric organic aerosol. Given the increased complexity of the system, the tens of major OA sources, and the hundreds of SOA precursors the framework should also result in computationally efficient modules for CTMs, so that the simulation of OA could still be tractable.

Donahue et al. (2006) proposed using fixed logarithmically-spaced saturation concentrations bins: the volatility basis set (VBS). The volatility bins are separated by powers of 10, typically ranging from 0.01 to $10^6$ μg $m^{-3}$ at 298 K, and they shift with temperature according to the Clausius-Clapeyron equation. The purpose of this article is not to review the state of organic aerosol science but rather to view that science through the unifying lens of the VBS. Specifically, we seek to show how the VBS provides a concise platform to address semi-volatile emissions, SOA formation, and organic aerosol aging in a single, self-consistent framework.

### 2.1. OA component partitioning

Following the work of Pankow (1994), the partitioning of a constituent i between the vapor phase and a condensed phase with mass concentration $C_{OA}$ can be described by a partitioning coefficient, $\xi_i$. If one assumes that the organic solution is ideal (or that the activity coefficients are approximately constant in the range of conditions of interest, pseudo-ideal solution) and the compounds involved have similar molecular weights then the fraction of this compound in the condensed phase is given by the following simple saturation curve:

$$\xi_i = \frac{1}{1 + \left(C_i^* / C_{OA}\right)} \tag{1}$$

where $C_i^*$ is the effective saturation concentration of the compound (the inverse of a Pankow type partitioning coefficient). C* is simply a semi-empirical property that describes partitioning of a complex mixture. Because the C* values are semi-empirical, they are assumed to effectively include activity coefficients of the mixture; however, a limitation is that those activity coefficients are assumed to be roughly constant under atmospheric conditions.

The salient features of Eq. 1 are as follows:

(a). 50% of the material is in each phase when $C^* = C_{OA}$.

(b). Within about one order of magnitude on either side of this equipartition point the response curve is roughly linear.

(c). Beyond this linear region almost all of the material is in one phase or the other, mostly in the condensed phase for $C^* < 0.1\ C_{OA}$ and mostly in the vapor phase for $C^* > 10\ C_{OA}$.

(d). Changing the total organic mass concentration $C_{OA}$ will cause the partitioning to change. Consequently, partitioning close to a point source is very different from partitioning in the remote marine atmosphere.

The phase partitioning of a complex mixture can be accurately described by lumping material into volatility bins separated by an order of magnitude (at 298 K). This is not only convenient; it is a nearly optimal distribution. We refer to these bins as the volatility basis set (VBS). Details are in Donahue et al. (2006).

For the majority of this discussion we shall consider a VBS consisting of nine bins, starting at C* = 0.01 μg $m^{-3}$ and ranging up to $10^6$ μg $m^{-3}$. Typical atmospheric $C_{OA}$ levels are between 1 and 100 μg $m^{-3}$. To facilitate and standardize discussion, we propose three sub classes within this range:

*Low Volatility Organic Compounds* (LVOCs): C* = {0.01, 0.1} μg $m^{-3}$. These compounds are mostly in the condensed phase in all but the most remote (and warm) parts of the atmosphere.

*Semi-Volatile Organic Compounds* (SVOCs): C* = {1, 10, 100} μg $m^{-3}$. Significant fractions of these compounds will be found in both phases under typical conditions.

*Intermediate Volatility Organic Compounds* (IVOCs): C* = {$10^3$, $10^4$, $10^5$, $10^6$} μg $m^{-3}$. These compounds are almost entirely in the gas phase, but they comprise an enormous number of difficult to measure compounds and (probably) a small but important fraction of the total atmospheric burden, as we shall see later.

There are two more classes outside the VBS range:

*Volatile Organic Compounds* (VOCs): C* > $10^6$ μg $m^{-3}$. The vast majority of emissions and routinely measured organics fall in this traditional category. These are typically represented explicitly or with lumped compounds in gas-phase chemistry mechanisms.

*Nonvolatile Organic Compounds* (NVOCs): C* < 0.01 μg $m^{-3}$. These compounds reside always in the particulate phase. They can be placed in the first bin (0.01 μg $m^{-3}$) of the VBS.

### 2.2. Emissions

The view of emissions we present here differs markedly from the conventional view: POA emissions have traditionally been viewed as non-volatile material in both emission inventories and models, and we now understand that the majority of these emissions fall in the SVOC and IVOC range of the VBS. POA emissions have always been modeled as purely non-volatile. This is in part because emissions measurements have traditionally been limited by the signal-to-noise of filter weight measurements or chromatographic characterization of individual compounds. Only very recently have primary emissions measurements been extended down to ambient mass loadings, and in every case examined to date the majority of material in the condensed phase under typical sampling conditions has evaporated by the time the emissions have been diluted to ambient conditions.

This new understanding is based on multiple, independent lines of evidence, including: measured changes in partitioning of primary particulate emissions from diesel and woodsmoke upon isothermal dilution (Lipsky and Robinson, 2006; Shrivastava et al., 2006); volatility-based chromatography of primary emissions samples (Hildemann et al., 1991); similar volatility-based measurements of urban samples (Fraser et al., 1997, 1998). The bottom line is that all emissions with $C^* > 1$ μg $m^{-3}$, corresponding roughly to a saturation mixing ratio greater than 0.1 ppbv, will be found, at least partially, in the gas phase under typical ambient conditions. These constitute 50–90% of the emissions that have traditionally been modeled as non-volatile POA.

### 2.3. Chemical production of organic aerosol

Chemical production involves both reactions of VOCs that generate lower-volatility products in the ('traditional' SOA formation), and reactions within the VBS. Traditional SOA precursors such as α-pinene and toluene have very high $C^*$ ($10^7$ or $10^8$ μg $m^{-3}$). The oxidation of these precursors result in a set of products, which can be schematically represented as

$$\text{VOC} + \text{oxidant} \rightarrow a_1 P_1 + a_2 P_2 + \ldots a_9 P_9$$

where $a_i$ are the set mass yields for products distributed over the VBS. This reaction is almost never an elementary reaction, but rather the left-hand-side represents the (initial) rate-limiting step of a reaction sequence, where subsequent reactions leading to the VBS products will be some combination of rapid gas-phase radical reactions and rapid condensed-phase reactions. As a consequence, the yields $a_i$ may be functions of $NO_x$ levels, temperature, relative humidity, etc. The current state of SOA research is summarized in an excellent recent review by Kroll and Seinfeld (2008). The VBS can help modelers simply address several facets of SOA chemistry, including mass balance, dependence on ambient conditions ($NO_x$, RH, UV, T), and ongoing aging.

It is clear that the VBS includes thousands of organic compounds in both the vapor and condensed phases, and that these compounds will continue to react while they reside in the atmosphere (Robinson et al., 2006). These reactions constitute "chemical aging", or reactions within the VBS. These reactions will almost certainly make products with altered volatility. Mechanisms based on explicit product representation or even multiple surrogates, develop a profusion of products when multiple generation reactions are treated. However, then volatility alone is considered, reactions within the VBS simply redistribute material from one bin to another. This greatly simplifies aging parameterizations, provided that the appropriate aging parameters can be constrained.

Most of the material in the VBS, both in the atmosphere and in most experiments, exists in the vapor phase. Partitioning theory demands this, and experiments on both growth and evaporation confirm it. The vast majority of SOA experiments show increasing mass fractions with increasing aerosol mass concentrations, and as predicted by partitioning theory (Pankow, 1994) in Eq. 1. Likewise, both

isothermal dilution (Grieshop et al., 2007; Lipsky and Robinson 2006) and thermal denuder measurements (An et al., 2007) show that SOA particles shrink when the driving force of mass transfer favors evaporation, again strongly implying the subsequent presence of vapors.

These VBS vapors are likely important precursors for additional chemical production of OA. The vapors produced by SOA experiments will be partially oxidized compounds. On the other hand, vapors from primary emissions will be highly reduced. In either case, we can be absolutely certain that these vapors will react in the atmosphere. They will react in the gas phase with the OH radical in the very least, and quite rapidly. Most of these compounds have a large number of $CH_2$ groups, and such compounds typically have rate constants $k_{OH}$ near $3 \times 10^{-11}$ $cm^3$ $molec^{-1}$ $s^{-1}$ (Seinfeld and Pandis, 2006), giving an atmospheric lifetime of approximately 8 h for $10^6$ OH $cm^{-3}$. It is also likely that the OH uptake coefficient to particles is close to unity, which would also result in a condensed-phase lifetime for organics of a day or so. Shrivastava et al. (2008) have described the chemical aging of the vapors in the VBS assuming a reaction of the form:

$$POA_n(g) + OH \rightarrow OPOA_{n-1}(g)$$

where $POA_n(g)$ is the gas-phase concentration of the components in the n*th* volatility bin of the VBS and $OPOA_n(g)$ is the gas-phase concentrations of an oxidized component in the $(n-1)$*th* volatility bin. This reaction (with rate constant $k_{OH}$) assumes that each oxidation step reduces the volatility of the compounds by one order of magnitude. This formulation with the definition of POA and OPOA surrogate components allows the simulation of the concentration of both the fresh POA and its oxidized products and the direct comparison of the results to those of the AMS: the POA should correspond to the HOA, while the sum of the OPOA and the traditional SOA should correspond to the OOA. More complicated reaction schemes are possible including reactions that increase the volatility of the VBS components (Donahue et al., 2006).

## 3. Revisiting the Sources of Organic Aerosol

The volatility basis set described above has recently been implemented into the regional CTM PMCAMx to investigate the effects of partitioning and aging of primary emissions and multigenerational processing of traditional SOA precursors on urban and regional OA levels in the Eastern US (Shrivastava et al., 2008; Lane et al., 2008). Figure 1 shows average predicted ground-level organic aerosol and vapor concentrations during July 14–28 2001 and January 2002. Details of the modeling are described in Shrivastava et al. (2008).

This more physically realistic representation implemented reveals that ambient organic aerosols are a highly-dynamic system dominated by both variable gas-partitioning and chemical evolution. The majority of the traditionally defined POA emissions evaporate, substantially reducing the predicted POA concentrations.

Figure 1a shows that in the summertime POA concentrations are only significant near heavily urbanized areas. In the summer, photochemical aging of these evaporated emissions creates large amounts of regional OPOA (Fig. 1b). Wintertime simulations show a somewhat larger fraction of the primary organics partitioning into the particle phase (Fig. 1d) and less production of OPOA (Fig. 1e) due to the combination of lower temperatures and oxidant levels.

The substantial evaporation of existing POA is due to multiple factors. Although dilution samplers are used to measure POA emission factors, a large fraction of the low-volatility organics has been misclassified as POA because these samplers are often operated at unrealistically high concentrations that are orders of magnitude higher than typical ambient levels. This biases gas-particle partitioning towards the particle phase relative to atmospheric conditions (Lipsky and Robinson, 2006; Shrivastava et al., 2006). Interestingly, the same problem exists in many of the chamber SOA data sets, which were collected at unrealistically high OA concentrations. This underscores the need for future source tests (and chamber experiments) to be conducted at atmospherically relevant temperatures and concentrations. In addition, quartz filters used to measure POA concentrations collect a substantial amount of organic vapors (positive artifact) during source tests (Lipsky and Robinson, 2006). The net effect of these two problems is that POA emission factors greatly overestimate the amount of POA that exists at typical atmospheric conditions. The aging of evaporated POA reduces its volatility, and shifts its partitioning into the condensed phase. The net result is the production of significant amount of oxidized OA.

Explicit accounting of partitioning and aging of primary emissions only has a modest effect on the total amount of OA (much less than a factor of 2 throughout the domain) relative to a traditional model that assumes POA is non-volatile (Robinson et al., 2007). The change is modest because CTMs based on traditional emission inventories already contain substantial amounts of low-volatility organics, albeit misclassified as POA. For misclassified emissions, the effects of partitioning and aging partly offset each other, resulting in modest changes to the total OA concentrations but substantial increases in the fractional contribution of oxidized OA. If one only accounts for partitioning and aging of the existing primary emissions, the predicted OA levels are lower than the traditional model. In order to create additional OA, one must add emissions to the inventory above and beyond the existing POA emissions. The limited available data suggests that the traditional inventories underestimate the emissions of low volatility organic vapors by a factor of 2–3. Accounting for these emissions has the potential to increase predicted OA concentrations by 10–50%. Therefore this mechanism has the potential to help close the gap between model predictions and ambient observations.

A more significant change associated with the revised framework for primary emission is the primary-oxidized OA split. Accounting for partitioning aging shifts the split towards oxidized OA throughout the domain; this brings model predictions into much better agreement with the ambient AMS data. Sensitivity analysis reveals that the PMCAMx cannot predict the high levels of observed oxidized OA unless a substantial fraction of the existing non-volatile primary emissions evaporate

and react. Therefore, it helps resolve the inconsistencies between the ambient observations and model predictions that motivated the latest round of the debate regarding the oxidized-primary OA split.

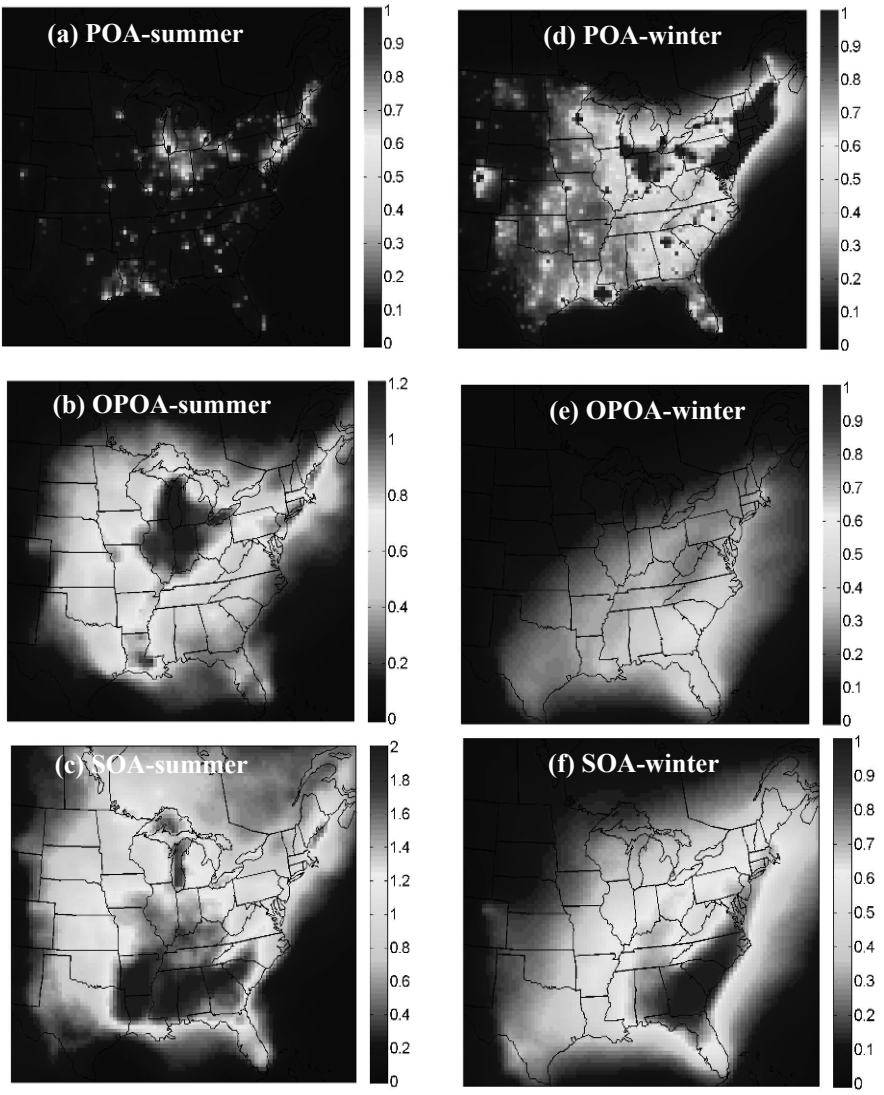


**Fig. 1.** Predictions of average ground-level organic aerosol and vapor concentrations during July 2001 and January 2002: (a) primary organic aerosol during July, (b) oxidized primary organic aerosol during July, (c) secondary organic aerosol formed from traditional precursors during July, (d) primary organic aerosol during January, (e) oxidized primary organic aerosol during January, and (f) secondary organic aerosol formed from traditional precursors during January

## References

An, W.J., Pathak, R.K., Lee, B.-H., Pandis, S.N., 2007. *J. Aerosol. Sci.*, 38:305–314.

Donahue, N.M., Robinson, A.L., Stanier, C.O., Pandis, S.N., 2006. *Environ. Sci. Technol.*, 40:2635–2643.

Fraser, M.P., Cass, G.R., Simoneit, B.R.T., Rasmussen, R.A., 1997. *Environ. Sci. Technol.*, 31:2356–2367.

Fraser, M.P., Cass, G.R., Simoneit, B.R.T., Rasmussen, R.A., 1998. *Environ. Sci. Technol.*, 32:1760–1770.

Grieshop, A., Donahue, N.M., Robinson, A.L., 2007. *Geophys. Res. Lett.*, 34, L14810, doi: 10.1029/2007GL029987.

Hildemann, L.M., Mazurek, M.A., Cass, G.R., Simoneit, B.R.T., 1991. *Environ. Sci. Technol*., 25:1311–1325.

Kroll, J.H., and Seinfeld, J.H., 2008. *Atmos. Environ.*, **42**, 3593–3624.

Lipsky, E.M., Robinson, A.L., 2006. *Environ. Sci. Technol*., 40:155–162.

Pankow, J.F., 1994. *Atmos. Environ*., 28:185.

Robinson, A.L., Donahue, N.M., Rogge, W.F., 2006. *J. Geophys. Res*., 111.

Robinson, A.L., Donahue, N.M., Shrivastava, M.K., Weitkamp, E.A., Sage, A.M., Grieshop, A.P., Lane, T.E., Pierce, J.R., Pandis, S.N., 2007. *Science*, 315:1259–1262.

Schauer, J.J., Kleeman, M.J., Cass, G.R., Simoneit, B.R.T., 1999. Environ. Sci. Technol., 33:1578–1587.

Seinfeld, J.H., Pandis, S.N., 2006. Atmospheric Chemistry and Physics: From Air Pollution to Climate Change, 2nd edition, J. Wiley, New York.

Shrivastava, M., Lane, T.E., Donahue, N.M., Pandis, S.N., Robinson, A.L., 2008. J. Geophys. Res., 113, D18301, doi:10.1029/2007JD009735.

Shrivastava, M.K., Lipsky, E.M., Stanier, C.O., and Robinson, A.L., 2006. Environ. Sci. Technol., 40:2671–2677.

# 5.2 Validation of Coupled Regional Climate Chemistry Simulation in CECILIA EC FP6 Project

**Tomas Halenka, Peter Huszar, and Michal Belda**

Charles University, Department of Meteorology and Environment Protection,
V Holesovickach 2, 180 00 Prague, Czech Republic

**Abstract** The coupling of regional climate model and chemistry/aerosol model has been performed recently in the Department of Meteorology and Environmental Protection, Faculty of Mathematics and Physics, Charles University in Prague, for the EC 6FP Project QUANTIFY and finally for EC 6FP Project CECILIA. One objective of the latter, aiming to study climate change impacts in Central and Eastern Europe based on very high resolution simulations using regional climate models (RCM) in 10 km grid, is dealing with climate change impacts on and interaction to air quality. Chemistry is solved by model CAMx which is coupled to model RegCM, as the first step the distribution of pollutants is simulated off-line for long period in the model couple. The results of "perfect" boundary condition run driven by ERA40 reanalysis are validated against the observations in the region. Some sensitivity runs are performed as well.

**Keywords** Regional climate modeling, air-quality modeling, long term validation

## 1. High Resolution Coupling of Chemistry and Climate

In the assessment of climate change impacts, the information on climate change at regional to local scale is fundamental which Global Circulation Models (GCMs) cannot reproduce reasonably well. Thus, dynamical downscaling, i.e., nesting of a higher resolution limited area model (or Regional Climate Model, RCM) within the GCM becomes the most convenient tool considering processes significantly affected by topography and land use of the region for this kind of studies. This is especially true when estimating the impacts of climate change on air-quality. In the region of Central and Eastern Europe (CEE) the need for high resolution studies is particularly important with respect to complex terrain of the territory, that is why 10 km resolution has been introduced in the EC FP6 project CECILIA. The main aim of the project dealing with climate change impacts and vulnerability assessment in targeted areas of CEE is the application of regional climate modelling studies at a resolution of 10 km for local impact studies in key sectors of the region. The project is covering studies on hydrology, water quality and

D.G. Steyn and S.T. Rao (eds.), *Air Pollution Modeling and Its Application XX*,
DOI 10.1007/978-90-481-3812-8, 

water management, agriculture and forestry as well as air quality issues in urban and industrialized areas (e.g. Black Triangle – a polluted region around the common borders of the Czech Republic, Poland and Germany).

The concentration of air pollutants is affected by both anthropogenic and climate factors. A main issue is the emission of primary pollutants as well as of precursors of secondary pollutants coming either from anthropogenic activities or natural sources. In this study the anthropogenic emission are kept at the values of year 2000 to study climate effect; although for present climate experiment it would me more correct to use actual emission data for better comparison to observation, it would increase the complexity of the study, while for future it would be difficult to extract anthropogenic changes from the scenarios. Then, chemistry and transport depend on changing climate conditions. Long range transport to the target regions is taken into account by simulation for the whole Europe using RCM with the resolution of 50 × 50 km. These simulations are used to constrain nested higher resolution runs (10 × 10 km) for a smaller domain focusing in CEE both for present and future climate. Here we are aiming the validation of the simulation, the key species are ozone, sulphur and nitrogen as well as PM.

Regional climate in this study is simulated using model RegCM while chemistry and transport are solved by model CAMx. The model RegCM was originally developed and further improved by Giorgi et al. (1999) or later see e.g. in Pal et al. (2007). For more details on the use of the model see Elguindi et al. (2006). CAMx is an Eulerian photochemical dispersion model developed by ENVIRON Int. Corp. (Environ, 2006). In version 4.40 CAMx is used for air quality modeling here, with CB-IV gas phase chemistry mechanism option, wet deposition of gases and particles. It uses mass conservative and consistent transport numerics in parallel processing. It allows for integrated "one-atmosphere" assessments of gaseous and particulate air pollution over many scales ranging from sub-urban to continental. CAMx simulates the emission, dispersion, chemical reactions and removal of pollutants in the troposphere by solving the pollutant continuity equation for each chemical species on a system of nested three-dimensional grids.

## 2. Simulation Results and Comparison to Observations

The pre-processor utility was developed which provides the meteorological fields generated by RegCM to drive CAMx transport, dry/wet deposition and through the temperature, radiation and humidity chemical reactions as well. In addition to above mentioned problem with availability of actual emissions there are problems with the anthropogenic emission inventories resolution, at this stage emissions from EMEP 50 × 50 km database are interpolated. Biogenic emissions of isopren and monoterpenes are calculated as a function of 2 m temperature, global radiation and land-use by Guenther et al. (1993, 1994). We use 23 vertical σ-levels reaching up to 70 hPa at 10 km of resolution for RegCM configuration, the same horizontal

grid for CAMx. Initial and boundary conditions are taken from 50 km resolution run for whole Europe by Krueger et al. (2008) or Katragkou et al. (2009). In our setting CB-IV chemistry mechanism is used (Gery et al., 1989). As the first step, the distribution of pollutants is simulated off-line for time slice of 10 years, period of 1991–2000 driven by reanalysis ERA40 is used for validation of the model run against the observation from selected stations.

Example of monthly average ozone concentration comparison is presented in Fig. 1 in terms of Taylor diagram with sensitivity test to precipitation bug. Reasonable agreement can be seen, but deeper insight into the behaviour of the outputs can be seen from time series of the ozone concentration presented in Fig. 2. Clearly, even

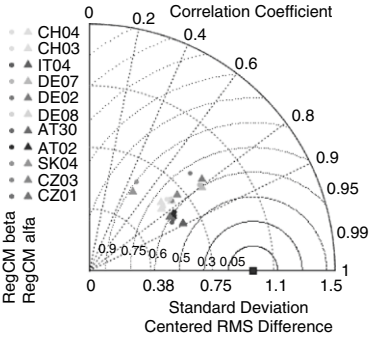


**Fig. 1.** Monthly average of ozone concentration, Taylor diagram of two versions of RegCM (beta – high resolution precipitation bug corrected) against observations, 1991–2000, ERA40 driven

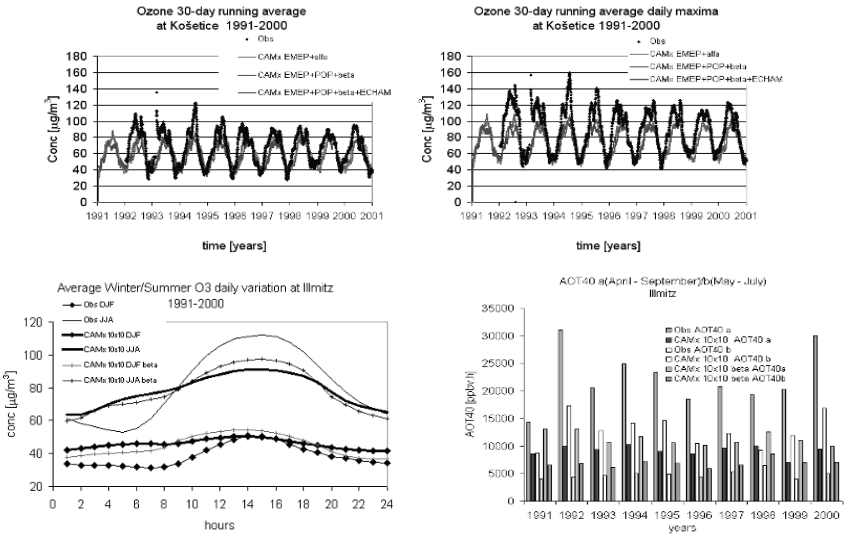


**Fig. 2.** Ozone characteristics from different model versions compared to observation at station Kosetice (above) and Illmitz (bottom) for 1991–2000

the version with corrected high resolution precipitation bug is underestimating daily variations, and reliability of reproducing some other parameters like AOT40 is not so high. Underestimation of the ozone concentration by the model especially during warm season appears for most stations of the Central Europe. Basically, high resolution runs brings slight improvement of the results for most of selected stations. Problems with emission data could probably account for these deviations at least partially.

**Acknowledgments** This work is supported in framework of EC FP6 STREP CECILIA (GOCE 037005), partially by EC FP6 Integrated project QUANTIFY (GOCE 003893) as well as under local support of the grant of Programme Informacni spolecnost, No. 1ET400300414 and Research Plan of MSMT under No. MSM 0021620860.

## References

Elguindi, N., X. Bi, F. Giorgi, B. Nagarajan, J. Pal, F. Solmon, S. Rauscher, A. Zakey, 2006: RegCM Version 3.1 User's Guide. PWCG Abdus Salam ICTP.

ENVIRON Corp., 2006: CAMx Users' Guide, version 4.40

Gery, M.W., G.Z. Whitten, J.P. Killus, and M.C. Dodge. 1989: A Photochemical Kinetics Mechanism for Urban and Regional Scale Computer Modeling. J. Geophys. Res., 94, 925–956.

Giorgi, F., X. Bi, Y. Qian, 2002: Direct radiative forcing and regional climatic effects of anthropogenic aerosols over East Asia: A regional coupled climate-chemistry/aerosol model study. J. Geophys. Res., 107, 4439, doi:10.1029/2001JD001066.

Giorgi, F., Y. Huang, K. Nishizawa and C. Fu, 1999: A seasonal cycle simulation over eastern Asia and its sensitivity to radiative transfer and surface processes. Journal of Geophysical Research, 104, 6403–6423.

Guenther, A.B., Zimmerman, P.R., Harley, P.C., Monson, R.K., and Fall, R., 1993: Isoprene and monoterpene rate variability: model evaluations and sensitivity analyses, J. Geophys. Res., 98, No. D7, 12609–12617.

Guenther, A., Zimmerman, P., and Wildermuth, M., 1994: Natural volatile organic compound emission rate estimates for U.S. woodland landscapes, Atmospheric Environment, 28, 1197–1210.

Katragkou, E., P. Zanis, I. Tegoulias, D. Melas, 2009: Tropospheric ozone in regional climate-air quality simulations over Europe: Future climate and sensitivity analysis. Proceedings 30th NATO/SPS International Technical Meeting on Air Pollution Modelling and its Application.

Krüger B. C., E. Katragkou, I. Tegoulias, P. Zanis, D. Melas, E. Coppola, S. Rauscher, P. Huszar and T. Halenka, 2008: Regional decadal photochemical model calculations for Europe concerning ozone levels in a changing climate, Quarterly J. of the Hungarian Meteorol. Service, Idojaras, 112, 3–4, 285–300.

Pal, J. S., F. Giorgi, X. Bi, N. Elguindi, F. Solmon, X. Gao, S. A. Rauscher, R. Francisco, A. Zakey, J. Winter, M. Ashfaq, F. S. Syed, J. L. Bell, N. S. Diffenbaugh, J. Karmacharya, A. Konaré, D. Martinez, R. P. da Rocha, L. C. Sloan, and A. L. Steiner, 2007: Regional Climate Modeling for the Developing World: The ICTP RegCM3 and RegCNET. Bull. Amer. Meteorol. Soc., 88, 9, 1395–1409.

## 3. Questions and Answers

**S. Andreani-Aksoyoglu:** Why did you choose Chaumont station which is an elevated site? There are many more stations where measurements are available.

**Answer:** We selected a few EMEP stations for the first validation study with respect to the availability of data covering full decade 1991–2000 for most pollutants. Some of them are elevated sites which can bring different behavior of values measured, however, even for higher altitudes the validation makes sense. We are including more stations into the comparison subsequently.

**D. Yin:** Did you consider changes of green-house-gases and land-use in A1B (that are in GCM simulations) when you downscaled ERA40 using RegCM?

**Answer:** The changes of $CO_2$ are considered in climate simulation, but the emissions of antropogenic pollutants (ozone precursors) are kept constant at year 2000 level to see just the effect of climate change. Similarly, there are no changes of land-use included as well. However, the biogenic emissions are changing as depending on climate variables.

**G. Kallos:** What is the extra information you recovered from your exercise that is not already in the ECHAM runs? Your domains simply are influenced by the lateral boundary conditions of ECHAM so you just simply modify the ECHAM results by utilizing local emissions.

**Answer:** That is what we aim when doing dynamical downscaling. Sure, it is expected to have the results strongly driven by global model (or driving one in case of multiple nesting) including long range transport, but the purpose is to get local features imposed by local higher resolution emission data and, of course, high resolution topography and land-use effects, which can be seen in our simulations.

# 5.3 Cloud Processing of Gases and Particles in Urban-Industrial Plumes: Comparison of Several Models

**W. Gong[1], J. Zhang[1], S.-W. Kim[2], M. Leriche[3], G. Frost[2], G.A. Grell[2], C. Mari[3], S. McKeen[2], J.-P. Pinty[3], P. Tulet[4], A.M. Macdonald[1], and W.R. Leaitch[1]**

[1]Science and Technology Branch, Environment Canada, Downsview, ON, Canada

[2]NOAA/ESRL & CIRES, University of Colorado, Boulder, CO, USA

[3]LA/CNRS, Université Paul Sabatier, Toulouse, France

[4]CNRM/GAME, Météo-France, Toulouse, France; also at LACy, Université de la Réunion, La Réunion, France

**Abstract** Several regional/meso-scale chemical transport models are applied to a case study of cloud processing of urban-industrial plumes. The study case is based on airborne measurements made in and below stratocumulus downwind of Chicago during the ICARTT field campaign in summer 2004. Model simulations of cloud microphysics, trace gases and aerosol particle concentrations are compared with aircraft observations.

## 1. Introduction

Clouds play an important role in the processing and cycling of chemicals in the atmosphere. Modeling the effects is challenging due to the temporal and spatial scales and the variety of processes and clouds. As part of the Seventh World Meteorological Organization (WMO) International Cloud Modeling Workshop (Morrison et al., 2009), three regional/meso-scale models (WRF-CHEM of NOAA/Environmental Science Research Laboratory, MesoNH of Laboratoire d'Aerologie/Centre National de la Recherche Scientifique, and AURAMS of Environment Canada) are applied to simulate a case of cloud processing of urban-industrial plumes downwind Chicago. On August 10, 2004, during ICARTT (Fehsenfeld et al., 2007), the National Research Council of Canada Convair 580 sampled in and below cumulus and stratocumulus clouds over Michigan ahead of an advancing cold front. The sampling (including trace gases, aerosol physics and chemistry, and cloud microphysics and chemistry: Hayden et al., 2008) was conducted along two north-south lines: one ca. 200 km east of Chicago (~86 W) and a second ca. 200 km further east (~84 W). Multiple plumes from the Chicago area were encountered across the aircraft sampling lines both in and below cloud. The observations indicate chemical processing by the clouds.

D.G. Steyn and S.T. Rao (eds.), *Air Pollution Modeling and Its Application XX*,
DOI 10.1007/978-90-481-3812-8, © Springer Science + Business Media B.V. 2010

## 2. Participating Models and Simulation Setup

AURAMS is a multi-pollutant, regional air-quality modeling system with size segregated and chemically speciated representation of aerosols (see Gong et al., 2006; McKeen et al., 2007; Smyth et al., 2008). The AURAMS version 1.4 was applied in a cascading fashion from 42 to 15 to 2.5-km resolutions, by one-way nesting; the two coarser resolution runs (42 and 15 km) were carried out for the entire ICARTT period (July 7–August 19, 2004) and the 2.5-km resolution case, focused over the flight area, was run for August 10, 2004. The anthropogenic emission files were prepared from the 2005 U.S. and Canadian and 1999 Mexican inventories using version 2.3 of the SMOKE emission processing system (http://www.smoke-model.org/index.cfm).

**MesoNH:** The MesoNH model (Mesoscale Non-Hydrostatic atmospheric model) was jointly developed by CNRM (Météo France) and Laboratoire d'Aérologie (CNRS) (Lafore et al., 1998). MesoNH simulates small scale (LES type) to synoptic scale and can be run in a two-way nested mode involving up to eight nesting stages. Several parameterizations have been introduced and, in particular, for gaseous chemistry (Tulet et al., 2003), aerosols chemistry (Tulet et al., 2006) and cloud chemistry (Leriche et al., in preparation). Model runs at 15- and 2.5-km resolutions in two-way nesting were carried out, the former from 12 Z August 9 to 0 Z August 11, 2004 and the latter from 0 Z August 10 to 0 Z August 11, 2004. The emission input was prepared from a combination of POET and GEIA inventories at $1° \times 1°$ resolution.

**WRF-CHEM:** The Weather Research and Forecasting (WRF) Chemistry model is based upon the non-hydrostatic WRF community model developed at NCAR (National Center for Atmospheric Research) in collaboration with several research institutes and universities (http://www.wrf-model.org). Details of WRF/CHEM can be found in Grell et al. (2005) and Fast et al. (2006). The simulations were carried out using WRF/CHEM version 3.1 at 27-km resolution, for the eastern U.S., from August 8 to August 10, 2004. WRF-CHEM simulations at 3-km resolution are also being pursued. The emissions were prepared from the U.S. EPA 1999 National Emission Inventory with updated NOx and $SO_2$ emission rates from selected U.S. power plants to their summer 2004 levels (Frost et al., 2006).

## 3. Results and Discussions

Modeled cloud processing of gases and aerosols depends critically on the ability to predict cloud microphysics fields (Zhang et al., 2007). Modeled liquid water content (LWC) is compared with the aircraft in-situ measurements sampled through stratocumulus clouds along the two N-S lines. The models at high resolution (e.g., Fig. 1a, GEM, AURAMS meteorological driver model, at 2.5 km) are able to capture the observed spatial heterogeneity in LWC. The in-situ comparison

(Fig. 1b) shows that all models have skills in predicting LWC, while the LWC from MesoNH (2.5 km) compares better with the observations.

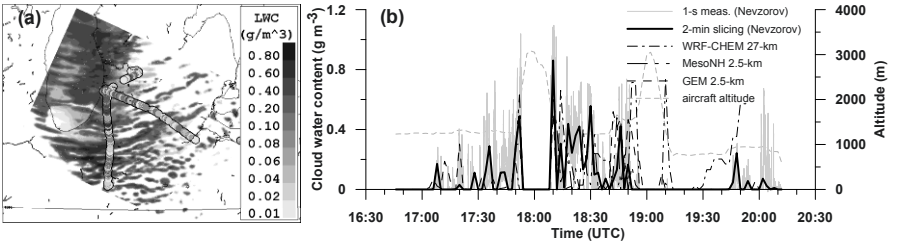


**Fig. 1.** Modeled cloud compared with observation. (a). AURAMS LWC at ~1,400 m (msl) overlaid with aircraft LWC measurement from FLT 16; (b). in-situ comparison between modeled and observed LWC along the flight track

Modeled CO, $NO_2$, $O_3$, $SO_2$, $H_2O_2$, and particle sulfate have been compared with aircraft observations. Figure 2 shows the comparisons of $SO_2$ and particle sulfate.

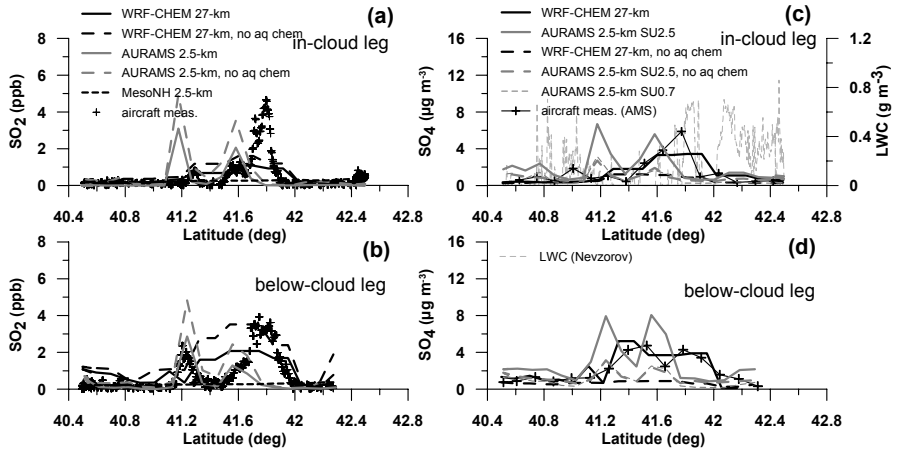


**Fig. 2.** Model-observation comparison of $SO_2$ (a, b) and particulate $SO_4$ (c, d) for FLT 16 (along 86.1 W): top panel – in-cloud leg, bottom panel – below-cloud leg

The 2.5-km AURAMS reproduces the observed plumes reasonably well but with an apparent spatial shift. The emission data used in the MesoNH simulation is inadequate, missing important sources in the area. New simulations with more up-to-date NA emission inventory data are being pursued. The 27-km WRF-CHEM is able to capture the broader structure of the plumes. Both AURAMS and WRF-CHEM were run with aqueous-phase chemistry turned off as a sensitivity test, and the modeled sulfate concentrations are significantly lower (Fig. 2c, d).

## 4. Conclusions

The present preliminary analysis shows that all models have reasonable skills in predicting cloud amount and LWC compared with the observations at model-equivalent resolutions. Predicted sulfate concentrations are within the range of the observations and mostly from aqueous-phase production. The model results shown here are very preliminary as all models are undergoing improvements on process representations and emission updates. New simulations with more detailed and quantifiable comparisons are the subject of continued work.

## References

Fast J.D. et al. (2006): Evolution of ozone, particulates, and aerosol direct radiative forcing in the vicinity of Houston using a fully coupled meteorology-chemistry-aerosol model, J. Geophys. Res., 111, D21305, doi:10.1029/2005JD006721.

Fehsenfeld F.C. et al. (2007): International Consortium for Atmospheric Research on Transport and Transformation (ICARTT): North America to Europe – Overview of the 2004 summer field study, J. Geophys. Res., 111, D23S01, doi:10.1029/2006JD007829.

Frost, G.J., et al. (2006): Effects of Changing Power Plant Emissions on Ozone in the Eastern United States, J. Geophys. Res., Vol. 111, D12306, doi:10.1029/2005JD006354.

Gong W. et al. (2006): Cloud processing of gases and aerosols in a regional air quality model (AURAMS). Atmos. Res., 82, 248–275.

Grell G.A. et al. (2005): Fully coupled "online" chemistry within the WRF model, Atmos. Environ., 39, 6957-6975, doi:10.1016/j.atmosenv.2005.04.027.

Hayden, K.L. et al. (2008): Cloud processing of nitrate, J. Geophys. Res., 113, D18201, doi:10.1029/2007JD009732.

Lafore J., et al. (1998): The meso-nh atmospheric simulation system, part i, Adiabatic formulation and control simulations, Ann. Geophys., 16, 90–109.

McKeen S., et al. (2007): Evaluation of several real-time PM2.5 forecast models using data collected during the ICARTT/NEAQS 2004 field study. J. Geophys. Res., 112, D10S20, doi:10.1029/2006JD007608.

Morrison H. et al. (2009): Seventh WMO International Cloud Modeling Workshop, to appear in BAMS.

Smyth S.C., et al. (2009): A comparative performance evaluation of the AURAMS and CMAQ air quality modelling systems. Atmos. Environ., 43, 1059–1070.

Tulet P., et al. (2003): Description of the Mesoscale Nonhydrostatic Chemistry model and application to a transboundary pollution episode between northern France and southern England, J. Geophys. Res., 108 (D1), 4021, doi:10.1029/2000JD000301.

Tulet, P., et al. (2006): Orilam-soa: A computationally efficient model for predicting secondary organic aerosols in 3d atmospheric models, J. Geophys. Res., 111, doi:10.1029/2006JD 007152.

Zhang J. et al. (2007): Evaluation of modeled cloud properties against aircraft observations for air quality applications, J. Geophys. Res., 112, D10S16, doi:10.1029/2006JD007596.

## 5. Questions and Answers

**Jim Sloan:** Did you drive AURAMS with GEM or with WRF?
**Answer:** With GEM (Global Environmental Multiscale – the Canadian operational weather forecast model).

# 5.4 Development of NCEP Global Aerosol Forecasting System: An Overview and It Applications for Improving Weather and Air Quality Forecasts

**Sarah Lu[1], Ho-Chun Huang[1], Yu-Tai Hou[1], Youhua Tang[1], Jeff McQueen[1], Arlindo da Silva[2], Mian Chin[2], Everette Joseph[3], and William Stockwell[3]**

[1]NOAA/NWS/NCEP Environmental Modeling Center, Camp Springs, MD 20746, USA

[2]NASA Goddard Space Flight Center, Greenbelt, MD 20771, USA

[3]Howard University, Washington, DC 20059, USA

**Abstract** The National Centers for Environmental Prediction (NCEP) Environmental Modeling Center (EMC) is developing global aerosol forecasting and assimilation capabilities to improve the treatment of radiation feedback in the numerical weather predictions and to provide aerosols boundary conditions for the regional air quality forecast system. This paper present two impact studies: (1) the impact of lateral aerosol boundary conditions on aerosol air quality forecasts, and (2) the impact of improved aerosol treatment on medium range weather forecasts.

**Keywords** Aerosols, lateral boundary condition, aerosol-radiation feedback

## 1. Introduction

The NCEP Global Forecast System/Global Data Analysis System (GFS/GDAS) is the decision support system used by NOAA for medium range weather predictions. The forecast model, GFS, is a global spectral model with the state-of-the-science physical parameterizations (Moorthi et al., 2001) and the analysis system, GDAS, uses the Gridpoint Statistical Interpolation (GSI) scheme (Wu et al., 2002). Climatology-derived aerosol distributions are currently used in the GFS radiation module and background aerosol conditions are assumed in the GSI radiative transfer scheme. Consequently the effect of aerosols on radition, clouds, and convection are poorly represented in the GFS and the effects of aerosol attenuation on radiance are yet to be quantified in the GSI.

The NCEP EMC is developing global aerosol forecasting and assimilation capabilities in GFS/GSI by incorporating prognostic aerosols (the GOCART model, Chin et al., 2002) in GFS and assimilating global aerosol information in GSI. This NOAA/NCEP-NASA/GSFC-Howard University collaborative project

D.G. Steyn and S.T. Rao (eds.), *Air Pollution Modeling and Its Application XX*,
DOI 10.1007/978-90-481-3812-8, © Springer Science + Business Media B.V. 2010

aims to improve the treatment of radiation feedback in the GFS forecasts and to provide aerosols boundary conditions for the regional air quality forecast system. Results of two impact studies are presented, including (1) the impact of lateral aerosol boundary conditions on aerosol air quality forecasts, and (2) the impact of improved aerosol treatment on medium range weather forecasts.

## 2. Impact of Dynamic Boundary Conditions on Regional Air Quality Forecasts

Under a NOAA-EPA partnership, NOAA is undertaking the responsibility to develop and maintain the National Air Quality Forecasting (AQF) system (Davidson et al., 2000). The AQF system is based on EPA Community Multi-scale Air Quality (CMAQ) model driven by meteorological forecasts from NCEP North American Meso (NAM) Model. Static lateral boundary conditions are currently used. During Texas Air Quality study 2006, model inter-comparison team found all seven regional air quality models missed elevated PM events, due to trans-Atlantic Saharan dust storms. These events are re-visited here, using dynamic boundary conditions provided from dust-only off-line GFS-GOCART system. Figure 1 shows the observed and modeled surface PM2.5 over an AIRNOW station at Texas. The incorporation of long-range dust transport via lateral BCs leads to significant improvements in model forecasts.

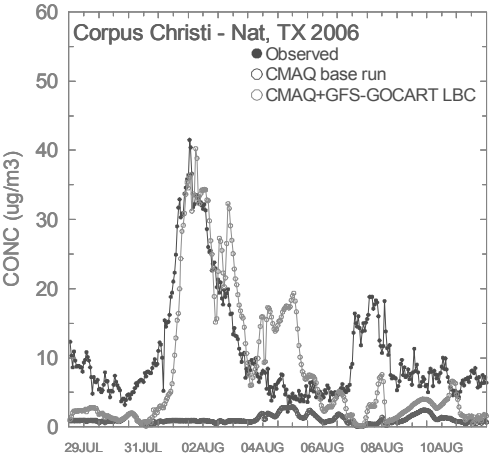


**Fig. 1.** Surface PM2.5 time series from the CMAQ-NAM forecasts with static BCs (in black open circle) and dynamics BCs (in grey open circle), verified against AIRNOW observations (in filled circle) at Corpus Christi, Texas, during 2006/07/29 to 2006/08/11 period

## 3. Impact of Aerosols on Medium Range Weather Forecasts

Two GDAS experiments for the 2006 summer period were conducted. The control run uses the operational aerosol scheme (based on the OPAC climatology, Hess et al., 1998) and the experimental run treats aerosols as passive tracers, updated every 6 h from GEOS4-GOCART in-line simulations. This impact assessment study uses GEOS4-GOCART aerosol dataset as the proxy of our own GFS-GOCART simulations. Overall the experimental run with more realistic representation of aerosols (direct effect only) show neutral to positive impact on GFS medium range weather forecasts. Figure 2 shows temperature biases and RMS errors in North America region, verified against radiosonde observations. Approximately 10% reduction in temperature biases is found in the troposphere (up to 750 mb) for both 24- and 48-h forecasts.

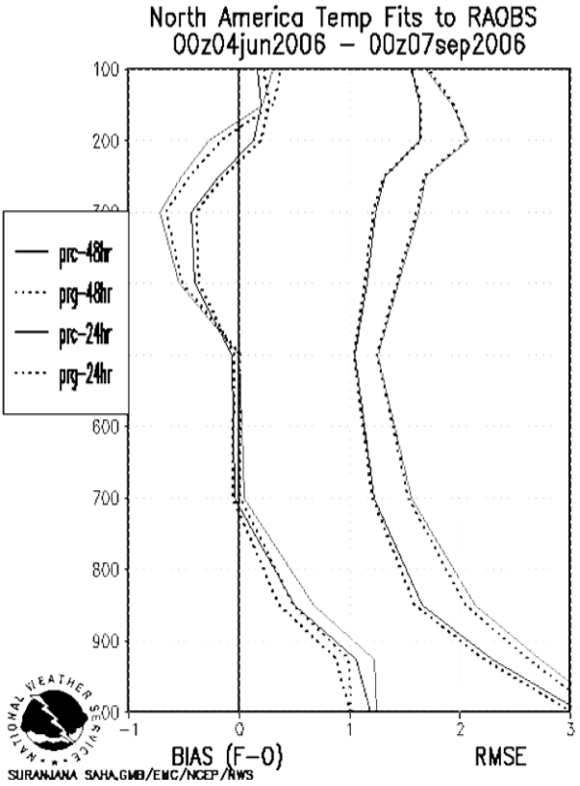


**Fig. 2.** Vertical profiles of temperature biases and RMS errors in North America region, verified against radiosonde observations for both 24-h (in black) and 48-h forecasts (in grey) for climatological-aerosol run (solid lines) and time-varying aerosol run (dotted lines)

## 4. Conclusions

NCEP recently initializes the efforts to develop global aerosol forecasting and assimilation capabilities via NOAA/NCEP-NASA/GSFC-Howard University collaborations. Two impact studies are presented in this paper. First, dust simulations from off-line GFS-GOCART system are used as lateral aerosol BCs for NCEP AQF (an experimental configuration). The incorporation of dynamic LBCs significantly improved the PM forecasts for the 2006 summer episode. Second, results of GDAS experiments for the 2006 summer period are presented. Change in model forecasts arises from the direct radiative effects. The verification against analysis and observations indicates a neutral-to-positive impact due to improved treatment of aerosols.

**Acknowledgments** The authors thank the funding support from NOAA-NASA-DOD Joint Center for Satellite Data Assimilation, NOAA NWS Air Quality program, and NASA Applied Science program.

## References

Chin, M., Ginoux, P., Kinne, S., Torres, O., Holben, B. N., Duncan, B. N., Martin, R. V., Logan, J. A., Higurashi, A., Nakajima, T. (2002). Tropospheric aerosol optical thickness from the GOCART model and comparisons with satellite and sunphotometer measurements, *J. Atmos. Sci.*, 59, 461–483.

Davidson, P. M., Seaman, N., Schere, K., Wayland, R. A., Hayes, J. L., Carey, K. F. (2004). National air quality forecasting capability: First steps toward implementation. Preprints, *Sixth Conf. on Atmos. Chem.,* Ameri. Met. Soc., Seattle, WA, 12–16 Jan. 2004, Paper J2.10.

Hess, M., Koepke, P., Schult, I. (1998). Optical properties of aerosols and clouds: The software package OPAC, *Bull. Am. Meteor. Soc*., 79, 831–844.

Moorthi, S., Pan, H.-L., Caplan, P. (2001). Changes to the 2001 NCEP Operational MRF/AVN Global Analysis/Forecast System, *NOAA Technical Bulletin No. 484*, 14 pp, Available at NOAA/NWS/NCEP, Camp Springs, MD.

Wu, W.-S., Purser, R. J., Parrish, D. F. (2002). Three-dimensional variational analysis with spatially inhomogen.

# 5.5 Chemical Composition Change of Aerosols Along Long-Range Transport Paths

**M. Astitha[1,2], C. Spyrou[1], G. Kallos[1], H.A.C. Denier van der Gon[3], A.J.H. Visschedijk[3], and J. Lelieveld[2,4]**

[1] University of Athens, School of Sciences, Faculty of Physics, Department of Environmental Physics-Meteorology, Atmospheric Modeling and Weather Forecasting Group, University Campus, Bldg. PHYS-V, Athens 15784, Greece

[2] Energy, Environment and Water Research Centre, The Cyprus Institute, Athalassa Campus, Nicosia, Cyprus

[3] TNO Built Environment and Geosciences, Laan van Westenenk 501, P.O. Box 342, 7300 AH Apeldoorn, The Netherlands

[4] Max Planck Institute for Chemistry, Becherweg 27, 55128 Mainz, Germany

**Abstract** The chemical composition of atmospheric aerosols is influenced by a variety of physical-chemical interactions with the gas phase depending on ambient conditions. Following the model development presented during the previous 29th NATO/SPS meeting, where the third generation pollutants were introduced in a regional chemical transport model, improvements in the heterogeneous uptake of gases at the surface of dust particles have been implemented as presented in this work. Our main objective is to analyze these improvements in view of long-range transport paths. It is shown that after 2–10 days the aerosols constitute a mixture of natural and anthropogenic species, of which the chemical characteristics substantially deviate from the freshly emitted particles.

**Keywords** Aerosols, dust, heterogeneous chemistry, long-range transport

## 1. Introduction

Changes in the chemical composition of atmospheric aerosols can occur through a variety of physical and chemical mechanisms. These encompass homogeneous and heterogeneous reactions and mixing of pollutants of different physical state and origin (gas and particulate, natural and anthropogenic). The aerosol chemical composition is altered during transport, known as "aging" from externally to internally mixed aerosols. Continuous model development is needed to realistically represent the complex physico-chemical processes and assess the changes in the chemical composition of the transported aerosols. The first steps of this development were presented during the previous 29th NATO/SPS Meeting.

D.G. Steyn and S.T. Rao (eds.), *Air Pollution Modeling and Its Application XX*,
DOI 10.1007/978-90-481-3812-8, © Springer Science + Business Media B.V. 2010

The continued model development and the introduction of new features in the models SKIRON/Dust and CAMx (Environ, 2006) form the basis of the study presented in this paper. Specifically, desert dust production is treated using an 8-size bin distribution scheme (Zender et al., 2003) and the CAMx preprocessing system has been updated in accordance with the new size sections of dust. The dust composition, in particular the particle alkalinity, affects the ability of the particles to take up gases like nitric acid and in turn, the uptake of strong acids affects the mobility and availability of cations. Information on the mineralogy of dust sources (Claquin et al., 1999) helps to model the interactions with nitrates at the surface of dust particles in the chemical transport model CAMx. This presentation addresses several of the processes that alter the chemical composition of aerosols due to interactions among different pollutants in a wide region around the Mediterranean, which is affected by long-range transport during August 2005.

## 2. Methodology

To address the above mentioned objectives, the modelling systems SKIRON/Dust modelling system and the Comprehensive Air Quality Model with Extensions-CAMx (Environ, 2006) were used, both as updated versions with additions and improvements in the aerosol schemes (Astitha and Kallos, 2008). The most important improvement in the CAMx model has been the reformulation of the heterogeneous uptake of $HNO_3$ on desert dust and the use of a new emission inventory (Visschedijk and Denier van der Gon, 2005) in the simulations performed.

The heterogeneous reactions on dust particles include the uptake of sulfur dioxide (production of sulfate), nitrogen dioxide (production of nitrate), ozone (destruction of ozone) and nitric acid (production of nitrate). The relevant algorithms and uptake coefficients used can be found in detail in Astitha et al. (2007) and in Astitha and Kallos (2008). In order to improve the nitric acid uptake on the dust, changes have been made in the parameterization that describes the chemical reactions on the particle surface. According to laboratory experiments, the reaction-uptake of the other gases on the dust particles is limited to the surface. When dust includes significant amounts of calcite ($CaCO_3$) the nitric acid can react with the bulk of the particle and is not limited to uptake at the surface (Grassian, 2002). Based on the mineralogy of the dust sources in the region (North and Central Africa) (Claquin et al., 1999; Y. Balkanski, personal communication, 2008), we consider a mean mass fraction of calcite in the dust and then limit the uptake of nitric acid at the dust surface, accordingly.

The anthropogenic emission data for Europe were developed at the Netherlands Organization for Applied Scientific Research (TNO). The species included were $CH_4$, $NO_x$, $NH_3$, $SO_2$, NMVOC, CO, PM10 and PM2.5 both for the area and point sources. The year of reference was 2000 and the horizontal analysis $0.25° \times 0.125°$ longitude-latitude. More information on the inventory can be found in Visschedijk and Denier van der Gon (2005). Shipping emissions are from the

EMEP database and for the rest of the domain (Africa, Arabian Peninsula, etc.) the anthropogenic emissions are from the Global Emission Inventory database GEIA. An algorithm was developed for the gridding of the emissions, using an appropriate interpolation technique in order to combine all the mentioned inventories. The simulation period is 1–30 August 2005, with a horizontal resolution of 0.24° × 0.24° for the SKIRON/Dust and 0.5° × 0.25° for the CAMx model.

## 3. Aerosol Chemical Composition: Discussion

Emphasis is given to desert dust, sea salt, nitrates and sulfates. The aerosols enter the domain during the 30 days of the simulation, following different paths and having highly variable concentrations depending on the distance from the sources. Aerosols transported to the Central Atlantic Ocean from the African Continent and the Mediterranean Sea during summer are mostly of primary nature and third generation pollutants (Fig. 1a–d). Furthermore, anthropogenic aerosols in the form of sulfates and nitrates are significant in the area while their concentrations are highest in the European Region (Fig. 1e, f).

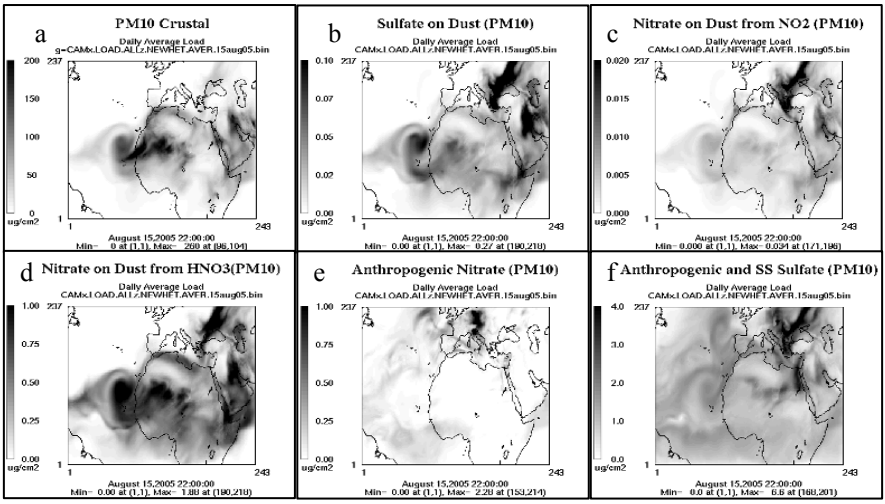


**Fig. 1.** Daily average load of anthropogenic and natural aerosols (μg/cm ) after 15 days of simulation with the CAMx model

The third generation aerosols, which come from the combination of anthropogenic gases ($HNO_3$, $NO_2$, $SO_2$) and natural particles (dust), are traveling towards the Central Atlantic as well as Eastern Europe and the Mediterranean (Fig. 1b–d). In the case of nitrate formation on the dust surface, the comparison between observations and model results indicates an improvement of the model performance. As indicated in Fig. 2, anthropogenic nitrate compared to the observations (denoted as *PNO3*, blue line) has a rather poor correlation. When introducing the nitrate on dust (denoted as *DNO3*, green line) the correlation is better and so is the comparison

between observed values and the sum of anthropogenic and third generation nitrate (denoted as *sum*, red line). This corroborates that the changes in the description of the aerosol chemical composition during the atmospheric transport of pollutants can improve the model performance.

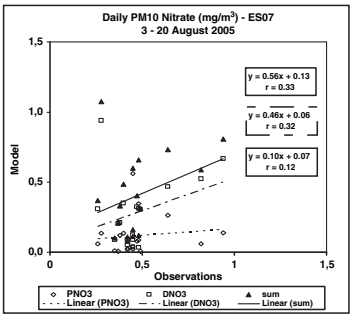


**Fig. 2.** Comparison between observed and simulated nitrate concentration at the EMEP station ES07 (Visnar) in Spain

**Acknowledgments** The authors would like to thank Professor G. Carmichael for his help and comments on the procedure used for the heterogeneous chemical reactions. This work has been supported by the European Union 6th Framework Program CIRCE IP, contract #036961.

## References

Astitha M, Kallos G, Katsafados P, Mavromatidis E (2007) Heterogeneous chemical processes and their role on particulate matter formation in the Mediterranean Region. Proceedings of the 29th NATO/CCMS ITM, Aveiro, Portugal, pp 503–513. ISBN 978-1-4020-8451-5.

Astitha M, and G, Kallos (2008) Gas-phase and aerosol chemistry interactions in South Europe and the Mediterranean Region, *Env. Fluid Mech.*, DOI: 10.1007/s10652-008-9110-7.

Claquin T, M Schulz, YJ Balkanski (1999) Modeling the mineralogy of atmospheric dust sources. *J. Geophys. Res.*, 104 (D18):22243–22256.

Environ (2006) User's Guide to CAMx v4.31, prepared by ENVIRON Inter. Corp., Novato, CA.

Grassian V (2002) Chemical reactions of nitrogen oxides on the surface of oxide, carbonate, soot, and mineral dust particles: Implications for the chemical balance of the troposphere, *J. Phys. 25 Chem. A*, 106(6), 860–877.

Visschedijk AJH and HAC Denier van der Gon (2005) Gridded European anthropogenic emission data for NOx, $SO_2$, NMVOC, $NH_3$, CO, PM10, PM2.5 and $CH_4$ for the year 2000, TNO B&O-A Rapport 2005/106, 2nd version Nov 2005.

Zender CS, H Bian, D Newman (2003) Mineral Dust Entrainment and Deposition (DEAD) model: Description and 1990s dust climatology, *J. Geophys. Res.-Atmos.*, 108, D14.

## 4. Questions and Answers

**James Kelly:** How confident are you in the uptake coefficient used for $HNO_3$ on dust?

**Answer:** The uptake coefficients are highly uncertain as they depend on the atmospheric conditions and the material itself. In this work we have chosen a value from the work of Tang et al. (2004) and Zhang and Carmichael (1999) and currently we have implemented the relevant value proposed by IUPAC for mineral dust. Performing sensitivity tests with different uptake coefficients is a way to assess the model response to such uncertain values for the uptake coefficients.

# 5.6 Impact of Saharan Dust on Precipitation Chemistry in Croatia

**Kornelija Špoler Čanić[1], Iva Kavčič[2], and Zvjezdana Bencetić Klaić[2]**

[1]Meteorological and Hydrological Service, Zagreb, Croatia

[2]Department of Geophysics, Faculty of Science, University of Zagreb, Zagreb, Croatia

**Abstract** The aim of this research was to examine Saharan dust transport over the Mediterranean towards Croatia. We analyzed several episodes of mud rain during the period 2001–2005 on two mountainous, background sites. The mud rains related to Saharan dust outbreaks were identified using Earth Probe/Total Ozone Mapping Spectrometer (TOMS) aerosol index (AI) data and backwards trajectories. The mud rains were characterized by higher calcium concentrations and pH values. In addition, we investigated the contribution of mud rains to the annual total calcium deposition.

**Keywords** Aerosol index, TOMS, trajectories, calcium, pH

## 1. Introduction

The Sahara is the world's largest source of aeolian desert dust (Middleton and Goudie, 2001). The dust can be entrained over large areas in dust storms, transported over thousands of kilometers and then deposited downwind. Saharan dust has a major influence on soil characteristics, oceanic productivity and air chemistry. Thus, Saharan dust is the subject of considerable scientific interest (e.g. Goudie, 2009).

Saharan dust can be removed from the atmosphere by dry or wet deposition. The latter is also known as the mud rain, and such events we examined in this work. Mud rains are frequent over southern Europe and they have been reported since ancient times. However, few investigations have dealt with this phenomenon in Croatia. The most comprehensive one is the work of Lisac (1973), where meteorological, chemical and mineralogical aspects of one mud rain event were analyzed.

In this work we tried to determine the frequency of mud rains over Croatia during the period 2001–2005 and their influence on precipitation chemistry. In order to detect mud rain events we used AI, backwards trajectories and precipitation chemistry analysis.

D.G. Steyn and S.T. Rao (eds.), *Air Pollution Modeling and Its Application XX*,
DOI 10.1007/978-90-481-3812-8, © Springer Science + Business Media B.V. 2010

Previous study of precipitation chemistry in Croatia (Špoler Čanić et al., 2009) had shown significant increase of the trend of the annual volume weighted averages (VWA) of calcium concentration after 1995. It was associated with the post-war recovery. Nevertheless, Löye-Pilot et al. (1986) have shown that only calcium concentration and pH value are consistently affected by Saharan dust in rain water. In addition, some researchers (e.g. Goudie and Middleton, 1992) have shown that dust storm occurrence increased. For those reasons, the observed increase in calcium concentration could be due to more frequent mud rains. Therefore, in this work we also investigated the contribution of mud rains to the above mentioned increase in calcium concentration.

## 2. Data and Methods

### 2.1. Sampling sites

We analyzed episodes of mud rain over Croatia for two mountainous, background sites (Fig. 1). Those sites are parts of Co-operative Programme for the Monitoring and Evaluation of the Long-Range Transmission of Air Pollutants in Europe (EMEP) network. The Site 1 (1594 m) is situated in a protected area (i.e. the National Park Northern Velebit). The nearest pollution sources are in industrial area of the city of Rijeka, about 60 km north-westward. The Site 2 (988 m) is situated in the Nature Park Medvednica and about 10 km far from the city of Zagreb.

### 2.2. Precipitation data

In this work we used the data from the daily bulk precipitation samples collected during the period 2001–2005 at Site 1 (676 samples) and 2 (555 samples). The samples were collected in open polyethylene buckets in accordance with the precipitation measurement protocol, from 07:00 to 07:00 CET. In precipitation samples pH values and electrical conductivity were measured, as were concentrations of main ions. Analysis details are given in Špoler Čanić et al. (2009).

### 2.3. Aerosol index (AI)

AI was used for mud rains identification. AI is a measure of how much the wavelength dependence of backscattered UV radiation from an atmosphere containing aerosols differs from that of a pure molecular atmosphere. Therefore, AI represents an ideal tool for monitoring intensity and pathway of desert dust on daily basis (Herman et al., 1997). The daily maps and data of AI were downloaded from: http://toms.gsfc.nasa.gov. The resolution of the AI data over globe is 1.25° in longitude and 1.00° in latitude.

### 2.4. Backwards trajectories

Origins of air parcels that arrived at the two receptor points (Sites 1 and 2) have been identified using the two-dimensional backwards trajectories downloaded from http://www.emep.int. Backwards trajectories are calculated by tracking an air parcel every 2 h for 96 h backwards in time, four times per day (at 00, 06, 12 and 18 h UTC). The trajectory calculation was based on the wind fields at 925 hPa of PARLAM-PS model at $50 \times 50$ km$^2$.

### 2.5. Mud rain event detection

Mud rains associated with Saharan dust intrusions over Croatia were identified on the basis of daily data of AI. When the points closest to the both sampling sites simultaneously had AI > 0.7 then the daily maps of AI and backwards trajectories were investigated for the possible Saharan source. In the end precipitation chemistry analysis was carried out.

## 3. Results

Mud rains occurred in 22 dust outbreaks during the period 2001–2005. The majority of them (17) were between April and July. In all cases calcium concentration was higher then annual volume weighted average (VWA) and pH was greater than 5.

Trend analyzes of calcium concentrations VWA showed increasing trends for both, all precipitation samples and samples without the mud rain.

Compared to Site 2, the mud rains at Site 1 were more frequent, and they were accompanied with higher calcium concentrations and pH values.

Considering entire investigated period, the most intensive episode with highest AI occurred in April 2002. Figure 1 shows Saharan dust transport over Mediterranean towards Croatia on 12 April 2002. The backwards trajectories (Fig. 1c, d) for Site 1 and 2 also point to Saharan area as a source region.

## 4. Conclusions

The influence of mud rains on VWA concentrations of calcium in precipitation in Croatia was negligible. This is in accordance with previous research where significant increasing trends of the annual VWA of calcium in precipitation at Croatian sampling sites was associated with the post-war recovery. The spatial changes of mud rain chemistry in Croatia were influenced by topography and distance from Sahara.

To test applicability of the present approach in detecting mud rains when the visual inspection of samples is omitted, further research of the longer time period is necessary.

**Acknowledgments** Our work was supported by the Croatian Ministry of Science, Education and Sport (grants No. 004-1193086-3036, No. 037-1193086-2771 and No. 119-1193086-1323) and EMEP4HR project number 175183/S30 provided by the Research Council of Norway. We thank the NASA/GSFC/TOMS group for the use of aerosol index data.

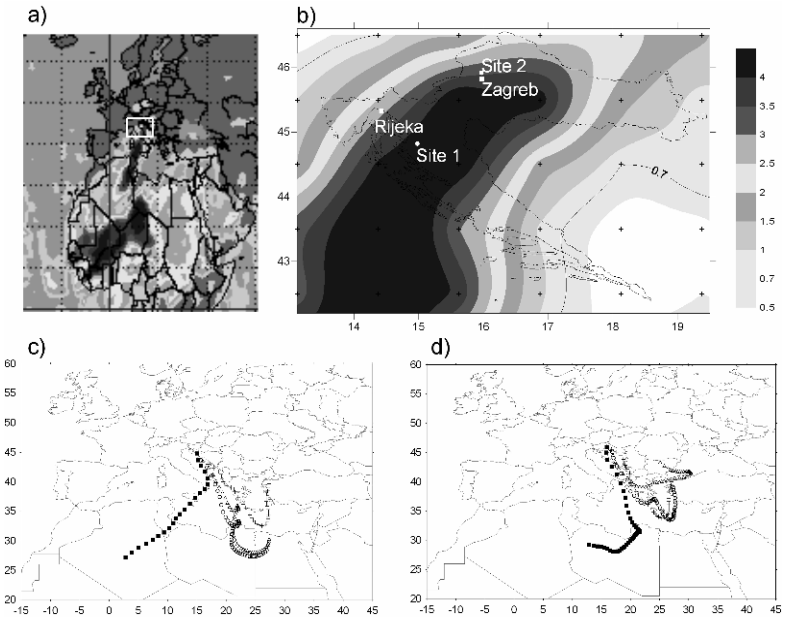


**Fig. 1.** (a) TOMS map of AI for 12 April 2002. Strong Saharan plume over Mediterranean towards Croatia is indicated by a white square. (b) Distribution of AI over Croatia. Small black crosses represent horizontal resolution of AI data. (c) and (d) Backwards trajectories for Site 1 and 2, respectively. Trajectories are calculated four times per day at: 00 (+), 06 (Δ), 12 (°), and 18 h (■) UTC

## References

Goudie, A.S.: Dust Storms: Dust storms: Recent developments, J. Environ. Manage., 90, 89–94 (2009)

Goudie, A.S., Middleton, N.J.: The changing frequency of dust storms through time, Climatic Change, 20, 197–225 (1992)

Herman, J.R., Bhartia, P.K., Torres, O., Hsu, C., Seftor, C., Celarier, E.: Global distribution of UV-absorbing aerosols from Nimbus 7/TOMS data, J. Geophys. Res., 102, 16911–16922 (1997)

Lisac, I.: A contribution to the knowledge of occurrence of dusty rain in Yugoslavia (in Croatian), Hidrografski godišnjak, 113–128 (1973)

Löye-Pilot, M.D., Martin, J.M., Morelli, J.: Influence of Saharan dust on the rain acidity and atmospheric input to the Mediterranean, Nature, 321, 427–428 (1986)
Middleton, N.J., Goudie, A.S.: Saharan Dust: sources and trajectories, Trans. Inst. Br. Geogr., 26, 165–181 (2001)
Špoler Čanić, K., Vidič, S., Klaić, Z.B.: Precipitation chemistry in Croatia during the period 1981–2006, J. Environ. Monit., 11, 839–851 (2009)

# 5.7 A Multiphase Chemistry Model to Study Biophysicochemical Processes in Clouds

**N. Chaumerliac, L. Deguillaume, and Y. Long**

LaMP/CNRS, Université Blaise Pascal, Clermont-Ferrand

## 1. Introduction

Since several years, significant efforts have been made by the scientific community to understand and characterize the tropospheric chemistry. The evaluation of multiphase chemistry versus the overall tropospheric chemistry and its role in the Earth's radiative budget is challenging because the physical nature and reactivity of condensed phases are still poorly known.

Modelling studies attempted to understand the overall role of cloud chemistry in global climate studies, but our knowledge on the details of cloud chemistry is still incomplete. For this, process models make it possible to simulate various reaction pathways for given chemical species within clouds, complex interactions between microphysical, chemical, radiative, and dynamic processes, and the influence of environmental parameters on multiphase chemistry.

The structure of the numerical models allows sensitivity analyses to be carried out for example, on dubious parameters. An integrated approach using modelling tools including laboratory data and field observations could help to improve our understanding of these complex processes.

## 2. Model Description

The M2C2 model is composed of two modules which can be coupled together: (1) a multiphase chemistry model initially developed by Leriche et al. (2000, 2001) and updated in Leriche et al. (2003) and Deguillaume et al. (2004) and (2) a two-moment warm microphysical scheme module predicting the number concentration of cloud droplets and raindrops and the mixing ratio of cloud water and rainwater categories. The microphysical module also considers the cloud droplets nucleation process (Leriche et al., 2007). The dynamical framework of the model is an air parcel with entrainment.

The chemistry included in the chemical module is explicit: the detailed chemistry of $H_xO_y$, chlorine, carbonates, $NO_y$, sulphur, the oxidation of organic volatile compounds (VOCs) with one carbon atom (Leich et al., 2003), the chemistry of transition metal ions for iron, manganese and copper (Deguillaume et al., 2004) is

D.G. Steyn and S.T. Rao (eds.), *Air Pollution Modeling and Its Application XX*,
DOI 10.1007/978-90-481-3812-8, © Springer Science + Business Media B.V. 2010

included in the aqueous chemical mechanism. The exchange of chemical species between the gas phase and the aqueous phase is considered following Schwartz (1986).

## 3. Theoretical Studies on Transition Metal Ion Chemistry

These theoretical studies allow evaluating the role of TMI chemical reactions on, for instance, the concentrations of radicals ($HO_x$) and also on pollutants such as nitric acid, VOCs, sulphate (Deguillaume et al., 2004; Deguillaume et al., 2005a).

Sensitivity analysis allows evaluating cloud chemistry pathways that are still uncertain such as for example the Fenton reaction which is commonly considered as source of OH radicals (Deguillaume et al., 2005b).

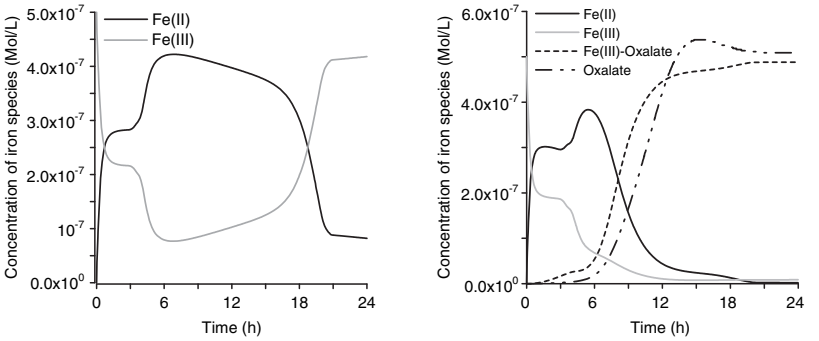


**Fig. 1.** Iron speciation including C1 chemistry (left handside), including C2 chemistry (right handside)

The organic chemistry has been extended to two atom carbon chemistry (C2) (Herrmann et al., 2005). This mechanism is evaluated following an idealistic scenario describing remote conditions with simplified microphysics (duration: 24 h; LWC: 0.3 g/m$^3$; T°: 288.15 K, P: 1,000 hPa and the droplet radius: 10 μm). In Fig. 1, we observe that including C2 chemistry results in a change in Fe(II)/Fe(III) speciation due to the continuous production of oxalate resulting from the oxidation of VOCs with C2 compounds. Indeed, the Fe(III) species is complexed by oxalate and then less iron is available for the $H_xO_y$ chemistry (Deguillaume et al., 2005b). Therefore, the C2 mechanism leads to a depletion of the OH and nitrate radical concentrations (mainly because of VOCs degradation), to an aqueous organic species production (methanol, oxalic acid, acetic acid) and an increase of gaseous and aqueous $H_2O_2$.

## 4. New Developments in Biophysicochemistry

Several studies have shown that primary biological aerosol (PBA) represent a significant fraction of air particulate matter and hence affect the microstructure and water uptake of aerosol particles (Möhler et al., 2007; Bauer et al., 2008). Moreover, airborne micro-organisms, namely fungal spores and bacteria, can transform chemical constituents of the atmosphere by metabolic activity. Recent studies have emphasized the viability of bacteria and metabolic degradation of organic substances in cloud water (Amato et al., 2007; Deguillaume et al., 2008).

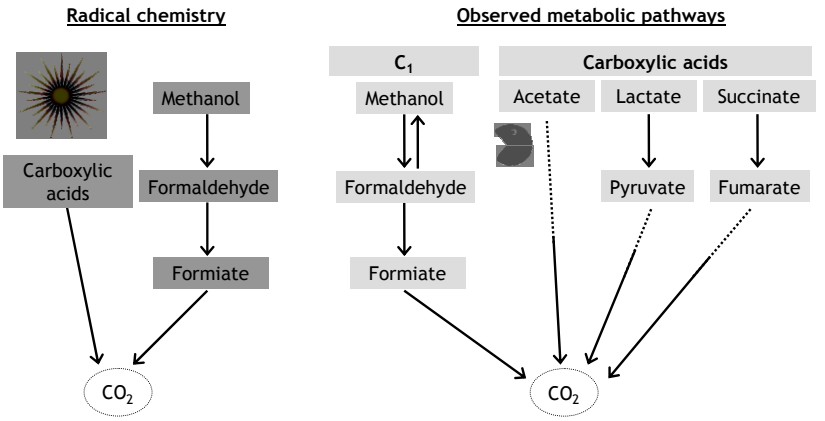


**Fig. 2.** Transformations of organic compounds by photochemical pathways (on the left side) and by biochemical pathways (on the right side) observed in the laboratory for organic compounds with one carbon atom and for carboxylic acids (Deguillaume et al., 2008)

Figure 2 illustrates the similarities between the radical chemistry within clouds and observed metabolic ways of bacteria collected in cloud water. The degradation of carboxylic acids leads to a final release of $CO_2$ with similar active intermediate molecules.

The M2C2 model is suitable to include explicit photochemistry with biological degradation processes. The objective will be to evaluate the global potential of microorganisms present in cloud water on the degradation of relevant chemical compounds. Those microorganisms will be considered as one category of aerosol particles and kinetic constants of biological degradation will be introduced as a function of environmental conditions and compared with photochemical rates. Laboratory studies are developing biodegradation parameterizations as a function of environmental conditions that will be incorporated in the M2C2 model. In the future, simulations of various cloud events under different environmental conditions will allow us to generalize the effect of microorganisms on cloud photochemistry.

## References

Amato P, Demeer F, Melaouhi A et al. (2007) A fate for organic acids, formaldehyde and methanol in cloud water: their biotransformation by micro-organisms. Atmos. Chem. Phys. 7: 4159–4169.

Bauer H, Schueller E, Weinke G et al. (2008) Significant contributions of fungal spores to the organic carbon and to the aerosol mass balance of the urban atmospheric aerosol. Atmos. Environ. 42(22): 5542–5549.

Deguillaume L, Leriche M, Monod A et al. (2004) The role of transition metal ions on $HO_x$ radicals in clouds: a numerical evaluation of its impact on multiphase chemistry. Atmos. Chem. Phys. 4: 95–110.

Deguillaume L, Leriche M, Desboeufs K et al. (2005a) Transition Metals in Atmospheric Liquid Phases: Sources, Reactivity, and Sensitive Parameters. Chem. Rev. 105: 3388–3431.

Deguillaume L, Leriche M, Chaumerliac N (2005b) Impact of radical versus non radical pathway in the Fenton chemistry on the iron redox cycle in clouds. Chemosphere 60-5: 718–724.

Deguillaume L, Leriche M, Amato P et al. (2008) Microbiology and atmospheric processes: chemical interactions of primary biological aerosols. Biogeosciences 5: 1073–1084.

Herrmann H, Tilgner A, Barzaghi P et al. (2005) Towards a more detailed description of tropospheric aqueous phase organic chemistry: CAPRAM 3.0. Atmos. Environ. 39(23-24): 4351–4363.

Leriche M, Voisin D, Chaumerliac N et al. (2000) A model for tropospheric multiphase chemistry: application to one cloudy event during the CIME experiment. Atmos. Environ. 34-(29-30): 5015–5036.

Leriche M, Chaumerliac N, Monod A (2001) Coupling quasi-spectral microphysics with multiphase chemistry: a case study of a polluted air mass at the top of the Puy de Dôme mountain (France). Atmos. Environ. 35-32: 5411–5423.

Leriche M, Deguillaume L, and Chaumerliac N (2003) Modeling study of strong acids formation and partitioning in a polluted cloud during wintertime. J. Geophys. Res. 108-D14 : 4433.

Leriche M, Curier RL, Deguillaume L et al. (2007) Numerical quantification of sources and phase partitioning of chemical species in cloud: Application to wintertime anthropogenic air masses at the Puy de Dôme station. J. Atmos. Chem. 57-3: 281–297.

Möhler O, DeMott PJ, Vali G et al. (2007) Microbiology and atmospheric processes: The role of biological particles in cloud physics. Biogeosciences 4: 1059–1071.

Schwartz S (1986) Mass-transport considerations pertinent to aqueous phase reactions of gases in liquid-water clouds. Chemistry of Multiphase Atmospheric Systems, NATO ASI Ser., vol. G6, Springer-Verlag, New York.

# 5.8 Planning of Experimental Campaigns to Estimate Atmospheric Particles Emission from Diffuse Sources Using an Inverse Modelling Technique

**B. Aceña[1], F. Martín[1], E. Monfort[2], and I. Ceslades[2]**

[1]Atmospheric Pollution Unit. CIEMAT. Avda. Complutense, 22. 28040 Madrid, Spain

[2]Instituto de Tegnología Cerámica-AICE. Universitat Jaume I. Castellón. Spain

**Abstract** This contribution describes a method for determining particles emissions in industrial environments caused by the dusty nature of the raw materials used in the industrial manufacture.

The methodology used to estimate $PM_{10}$ and $PM_{2.5}$ emission rates is based on an inverse modelling technique, which uses a Lagrangian Puff model. In this study we propose a methodology and describe the strategies adopted to carry out three experimental campaigns to estimate PM10 and PM2.5 emissions from diffuse sources produced during the activities of cement manufacture, steel and ceramic.

## 1. Introduction

The idea of this methodology is basically to use the measured concentrations of the pollutant (PM10 and PM2.5) downwind and close to the emission area and a dispersion model fed with meteorological data, to determine which emission data, used in the dispersion model, provide modelled concentrations that best fit the observations.

Since the amount of particles emitted depends on a variety of technological factors (nature of the material, particle size, moisture content, sequence of operations, type of machinery used, etc.), meteorological factors (wind speed and direction, precipitation, atmospheric stability) and location of the activities in the corresponding industry, the correct application of the proposed methodology (optimization) needs a suitable planning of the measurement campaign (time of the year to carry out the intensive campaign, number and sampling locations, etc.) for every industrial site considered.

D.G. Steyn and S.T. Rao (eds.), *Air Pollution Modeling and Its Application XX*,
DOI 10.1007/978-90-481-3812-8, © Springer Science + Business Media B.V. 2010

## 2. Methodology

### 2.1. Experimental campaign

An experimental campaign will be carried out with at least two high time resolution monitors located downwind the solid bulk handling areas and a meteorological tower.

For planning the experimental measurement campaigns (time of the year and sampling locations), the meteorological situation and associated wind field in the study area will be previously evaluated. During the campaign, the emission-generating activities will be annotated closely, in order to enable a further detailed study of the operations involved in every time period.

### 2.2. Emission estimate method

A high resolution Gaussian dispersion model called the MELPUFF-microscale (Martín et al., 2007; Aceña et al., 2002) was used. This is a Lagrangian Puff model that can estimate the contribution of every emitted puff at selected locations where monitors are continuously recording particle concentrations. A first run is done assuming a prescribed and identical and constant emission rate (1 g/puff and 1 puff/min) during the selected period. With this run, the relative contribution of each puff "j" at point "i" (Monitor location) and time "k". ($R_{i,j,k}$) is computed.

The measured concentration of a pollutant ($Co_{i,k}$) at a given point "i" and time "k" may be expressed as a linear combination of the contributions of each theoretical emitted puff "j", by the expression: $C_{i,j} = \sum a_j R_{i,j,k}$

Where $a_j$ is amount of pollutant emitted in each puff "j" from the source area. This is an equation system being $a_j$ the unknowns. The equation system is usually over determined (more equations than unknowns variables). The next scheme shows the structure of this equation system. A multi-regression technique is applied to solve the over determined system of linear equations.

| **Monitor i** | **Puff j** | **Time k** | **Concentration.** | | | | | |
|---|---|---|---|---|---|---|---|---|
| **1** | **1** | **1** | $C_{11}$ | $a_1R_{111}$ | **0** | **0** | …… | **0** |
| **1** | **2** | **2** | $C_{12}$ | $a_1R_{112}$ | $a_2R_{122}$ | **0** | ……. | **0** |
| **1** | **3** | **3** | $C_{13}$ | $a_1R_{113}$ | $a_2R_{123}$ | $a_3R_{133}$ | ……. | **0** |
| ……. | ……. | ……. | …… | ……. | ……. | ……. | ……. | ……. |
| **1** | **n** | **n** | $C_{1n}$ | $a_1R_{11n}$ | $a_2R_{12n}$ | $a_3R_{13n}$ | ……. | $a_nR_{1nn}$ |
| **1** | | | | | | | | |
| ……. | | ……. | …… | ……. | ……. | ……. | ……. | ……. |
| **1** | | **m** | $C_{1m}$ | **0** | **0** | …… | ……. | $a_nR_{1nm}$ |

## 3. Results

In order to evaluate the response of the applied model, the concentration levels obtained with the continuous samplers and the concentration levels estimated with the mathematical model will be compared for the same period of time at the selected sampling points.

**Acknowledgments** This study has been financed by the Spanish Ministry of Science and Technology in the frame of the National Plan for Scientific Research, Development and Technological Innovation, reference REN2003-08916-C02-01.

## References

Directive 96/61/EC of the Council of 24 September 1996 concerning integrated pollution prevention and control.

Aceña, B., I. Palomino, F. Martín and M. Palacios, 2002. Application of the MELPUFF model to air quality assessment in the industrial area of Huelva (Spain). Int. J. of Environment and Pollution, Vol. 18, No. 2, pp. 171–180.

F. Martín, M. Pujadas, B. Artiñano, F. Gómez-Moreno, I. Palomino, N. Moreno, A. Alastuey, X. Querol, J. Basora, J.A. Luaces, A. Guerra, Estimates of atmospheric particle emissions from bulk handling of dusty materials in Spanish Harbours. Atmospheric Environment (2007), doi:10.1016/j.atmosenv.2006.12.003.

# 5.9 Coupled Time-Integration of Chemical and Aerosol Dynamical Processes by Using Multirate Implicit-Explicit Schemes

**Ralf Wolke, Martin Schlegel, Elmar Filaus, Oswald Knoth, and Eberhard Renner**

Leibniz Institute for Tropospheric Research (IfT), Permoserstrasse 15, 04303 Leipzig, Germany

**Abstract** The application of suitable time integration schemes is especially important for highly dynamical problems like atmospheric aerosol processes. Usually, classical time integrators take the same time step over the complete domain and for all components. Consequently, the model regions and the components with the strictest time step restrictions dictate this global time step. Opposed to this, multirate schemes are employed to adapt the time step locally, so that slower components take longer and fewer time steps, which can reduce the computational costs substantially. In the paper, a new class of time integration schemes is proposed which combines the multirate approach with implicit-explicit (IMEX) methods. These schemes are applied for block-structured grids with different horizontal resolutions as well as the coupling between aerosol dynamical and gas phase chemical processes in the chemistry-transport model COSMO-MUSCAT.

**Keywords** Chemistry transport modeling, aerosol dynamics, time integration scheme, multirate method

## 1. Introduction

In contrast to processes in the nature which perform in a coupled manner, these are decoupled in numerical approaches using the "operator splitting" scheme. In chemistry-transport models, such decoupling is often applied between the particular transport processes (diffusion, advection in the different space directions), the aerosol-dynamical transformations, the phase transfer and the chemical conversions in gaseous and liquid phase. Then, the resulting splitting error can be kept small only in the case of small time steps. For instance, changes in the aerosol population or gas phase concentrations after a "long" transport time step can completely destroy the thermodynamic balance in the grid cell, especially in regions with large dynamic activity. Implicit-explicit (IMEX) schemes, which integrate the system in a coupled

D.G. Steyn and S.T. Rao (eds.), *Air Pollution Modeling and Its Application XX*,
DOI 10.1007/978-90-481-3812-8, © Springer Science + Business Media B.V. 2010

manner by controlling stability and treated the stiff parts of the system implicitly, offer a promising opportunity to avoid splitting errors and perform larger time steps.

Furthermore, the advection part is usually integrated explicitly in time, where the time step is constrained by a locally varying Courant–Friedrichs–Lewy (CFL) number. In realistic scenarios there are usually regions of interest such as urban areas which have to be examined more closely than surrounding regions. Therefore the spatial grid in these regions is refined. Thus the smallest cell or more exactly the cell with the smallest characteristic time determines the global advection time step. Multirate schemes exploit the different time scales of the processes by using different time steps for the subsystems. They can be employed to alter the time step locally, leading to a significant reduction of computational cost. Such multirate strategies have been developed since the 1980s when Osher and Sanders (1983) introduced a simple multirate time integration scheme. Later, the approach was refined by increasing the accuracy of multirate schemes based on explicit Runge-Kutta methods (Constantinescu and Sandu, 2007). The generic recursive multirate Runge-Kutta scheme RFSMR ("Recursive Flux Splitting Multirate") has been developed for the advection equation by Schlegel et al. (2009). It preserves the linear invariants of the system and is of third order accuracy when applied to certain explicit Runge-Kutta methods as base method. Furthermore, it can be easily adapted to an arbitrary number of temporal refinement levels. The approach borrows ideas from an IMEX splitting scheme introduced by Knoth and Wolke (1998), where explicit Runge-Kutta methods are combined with an arbitrary implicit time integrator. Due to the method properties, it may not only be applied to a splitting of spatial domains with different time step restrictions, but also on a splitting of different processes, e.g. advection, chemical reactions and aerosol dynamics.

In the paper, we combine the RFSMR approach with adapted IMEX schemes for improving the numerical efficiency. An adaptive step size control as well as the use of different explicit and implicit integration schemes is taken into account. The accuracy and numerical efficiency of the implemented multirate methods are analyzed for the coupled model system COSMO-MUSCAT (Wolke et al., 2004; Hinneburg et al., 2009) and a set of selected artificial and real-life scenarios. In the investigations, an extended version of the modal aerosol model M7 (Vignati et al., 2004) is used for the treatment of aerosol processes. Furthermore, the gas phase mechanisms RACM with 73 species and over 200 reactions is applied in this study. The results are discussed in comparison to simulations using "operator splitting" approaches.

## 2. The Multirate IMEX Approach

From the mathematical point of view, air quality models base on mass balances which can be described by systems of time-dependent, three-dimensional advection-diffusion-reaction equations (given in flux form)

$$\frac{\partial c}{\partial t} + div(\vec{v}\rho\frac{c}{\rho}) = div(K\rho\,\nabla\frac{c}{\rho}) + R(c;T,q) + Q_c - \sum_{m}^{modes} k_t^m\,(c - c_{Eq}^*(a^m)) \quad (1)$$

$$\frac{\partial a^m}{\partial t} + div(\vec{v}\rho\frac{a^m}{\rho}) = div(K\rho\,\nabla\frac{a^m}{\rho}) + P^m(a;T,q) + Q_a{}^m + k_t^m\,(c - c_{Eq}^*(a^m)) \quad (2)$$

for all modes $m$. Here $c$ is the vectors of gas phase concentrations. The vectors $a^m$ denote the component masses and the particle number of mode $m$. The wind vector $\vec{v}$, the density ρ, the temperature $T$, and the humidity $q$ have been provided by the meteorological code. The terms $R$, $Q$, and $P^m$ stand for the chemical reactions in the gas phase, the emissions, and the aerosol dynamical transformations (e.g., coagulation). The parameters $k_t^m$ denote the mass transfer coefficients and $c_{Eq}^m$ stands for the equilibrium saturation of the particles in mode $m$. Note that gas and particle phase are only coupled by the last term which describes the phase transfer.

After spatial discretization this system can be written as a system of ordinary differential equations (ODEs) of the form

$$c' = f_{Hor}^{Slow}(t,c) + f_{Hor}^{Fast}(t,c) + f_{Vert}(t,c) + f_{Phase}(t,c,a) + f_{Chem}(t,c) \quad (3)$$

$$a' = f_{Hor}^{Slow}(t,a) + f_{Hor}^{Fast}(t,a) + f_{Vert}(t,a) + f_{Phase}(t,a,c) + f_{Phys}(t,a) \quad (4)$$

The time step restrictions imposed by the different terms on the right hand side may differ by several orders of magnitude. In chemistry-transport models, stiffness is expected especially for the fast chemical and aerosol dynamical terms, whereas the horizontal transport part is usually characterized by moderate changing courses. The behaviour of vertical exchange is varying from slow to fast depending on the dynamics of the atmosphere. Therefore, as extension to the scheme implemented in MUSCAT (Wolke and Knoth, 2000), the singlerate Runge-Kutta method applied for the horizontal transport integration is replaced by multirate schemes where the step sizes are restricted only by the local CFL numbers. The stiff chemistry, aerosol dynamics and all vertical transport processes are integrated in a coupled manner. This integration can be performed by higher order explicit schemes or, again, by an IMEX scheme where the vertical transport is treated explicitly. In both cases, multirate techniques can be applied again. Special care must be taken in regard to time step selection and the partitioning for parallel execution.

## 3. Numerical Tests

The efficiency of the multirate schemes is analyzed for more “theoretical” advection problems and one real scenario. Here the model system COSMO-MUSCAT was applied in a nested hierarchy with the superior control by the global reanalysis

data of GME. The runs are performed with the uniform COSMO resolutions of approximately 16 km (N1: Europe), 8 km (N2: Germany) and 2.8 km (N3: Saxony). In all domains MUSCAT uses block-structured grids with three different horizontal resolutions. For instance, the innermost region of interest covers an area of 240 × 156 km (Saxony) with variable resolution between 2.8 and 0.7 km, where the finest grid was arranged around the city of Dresden. The simulation was performed for 1 week in October 2006.

The tests for the advection problems confirm that the modified version of MUSCAT, implementing our improved multirate IMEX scheme, calculates results that are comparable to the results of the singlerate version. Small differences were only observable near to the boundaries between blocks with different time levels. The coupling between aerosol dynamics and gas phase chemistry using the multirate IMEX approach works well for the real scenario and allows larger coupling time steps. The computational costs can be reduced significantly in all three domains. The study show the potential of multirate IMEX schemes to reduce calculation cost. An additional effect is the reduced communication between different partitions.

**Acknowledgments** The work was supported by the DFG, the ZIH Dresden and the NIC Jülich. Furthermore, we thank the DWD Offenbach for good cooperation.

## References

Constantinescu EM, Sandu A (2007) Multirate timestepping methods for hyperbolic conservation laws. J. Sci. Comput. 33:239–278

Hinneburg D, Renner E, Wolke R (2009) Formation of secondary inorganic aerosols by power plant emissions exhausted through cooling towers in Saxony. Env. Sci. Pollut Res. 16:25–35

Knoth O, Wolke R (1998) An explicit-implicit numerical approach for atmospheric chemistry-transport modeling. Atmos. Env. 32:1785–1797

Osher S, Sanders R (1983) Numerical approximations to nonlinear conservation laws with locally varying time and space grids. Math. Comput. 41:321–336

Schlegel M, Knoth O, Arnold M, Wolke R (2009). Multirate Runge-Kutta schemes for advection equarions. J. Comput. Appl. Math. 226:345–357

Vignati E., Wilson J, Stier P (2004) M7: An efficient size-resolved aerosol microphysics module for large-scale aerosol transport models. J. Geophys. Res. 109, D22202, doi: 10.1029/2003 JD004485.

Wolke R, Hellmuth O, Knoth O, Schröder W, Heinrich B, Renner E (2004) The chemistry-transport modeling system LM-MUSCAT: Description and CityDelta applications. In:Air Pollution Modeling and its Applicaton XVI, 427–439. Kluwer Academic/Plenum Publisher

Wolke R, Knoth O (2000) Implicit-explicit Runge-Kutta methods applied to atmospheric chemistry-transport modelling. Environmental Modelling and Software, 15:711–719

# Chapter 6 Interactions between air quality and climate change

Chairperson: E. Renner

Rapporteur: Y. Zhang

D.G. Steyn and S.T. Rao (eds.), *Air Pollution Modeling and Its Application XX*,
DOI 10.1007/978-90-481-3812-8_6, © Springer Science + Business Media B.V. 2010

# 6.1 Interactions Between Climate and Air Quality

**A.M. Fiore, H. Levy II, Y. Ming, Y. Fang, and L.W. Horowitz**

National Oceanic Atmospheric Administration Geophysical Fluid Dynamics Laboratory (NOAA GFDL), NJ, USA

**Abstract** We present two examples of air pollutant contributions to climate forcing. First, oxidation of the potent greenhouse gas methane produces tropospheric ozone, another greenhouse gas and the primary constituent of ground-level smog. Methane emission controls are thus a "win-win" strategy for jointly addressing air quality and climate goals, particularly given the availability of low-cost emission control options. Second is the "win-lose" case of aerosol sulfate, where decreases improve air quality but lead to additional warming due to decreased scattering of solar radiation. We highlight the potential for aerosols to change the hydrologic cycle and key aspects of how climate change may affect air quality, underscoring a need for evaluating chemistry-climate models with observed relationships between meteorology and air pollutants to build confidence in future projections.

## 1. Introduction

Ground-level smog, detrimental to human health and vegetation, is pervasive in populated world regions. In the United States, over 150 million people live in counties exceeding air quality standards for ozone ($O_3$) or particulate matter (aerosols), the two major smog constituents (U.S. EPA, 2008). These air pollutants also influence climate, with tropospheric $O_3$ the third most important greenhouse gas after carbon dioxide ($CO_2$) and methane ($CH_4$), and aerosols exerting a net cooling influence (Forster et al., 2007).

The major precursors to $O_3$ that fuel rapid photochemical build-up of $O_3$ during regional air pollution episodes are non-methane volatile organic compounds (NMVOC) and nitrogen oxides ($NO_x$), whereas the global burden of tropospheric $O_3$ is most sensitive to $NO_x$ and $CH_4$ (e.g., Fiore et al., 2002). As $CH_4$ and $O_3$ together are estimated to have contributed nearly half as much radiative forcing from 1750 to 2005 as $CO_2$ (Forster et al., 2007), controls on $CH_4$ emissions could help to slow greenhouse warming (Hansen et al., 2000). Since $CH_4$ oxidation (in the presence of $NO_x$) contributes to the formation of tropospheric $O_3$ (Crutzen, 1973), including in surface air (Fiore et al., 2002), such controls would also decrease $O_3$ pollution. In contrast, decreasing tropospheric $O_3$ through $NO_x$ controls is relatively climate-neutral due to opposing influences on $O_3$ and $CH_4$ (e.g., Fuglestvedt et al., 1999), and the forcing from pre-industrial to present is small for $O_3$ precursor emissions of NMVOC, carbon monoxide (CO) and $NO_x$ compared to $CH_4$ (Shindell et al., 2005).

D.G. Steyn and S.T. Rao (eds.), *Air Pollution Modeling and Its Application XX*,
DOI 10.1007/978-90-481-3812-8, 

Depending on composition, aerosols can heat or cool the atmosphere by absorbing or scattering solar radiation ("direct effects"). For example, the overall impact of absorption by black carbon is atmospheric warming, whereas sulfates cool by scattering solar radiation back to space. By interacting with the hydrologic cycle and changing cloud properties, aerosols also affect transmission of both solar and terrestrial radiation ("indirect effects"). The overall impact of aerosols is believed to be a cooling influence, estimated to offset ~75% of the positive radiative forcing from $CO_2$ from 1750 to 2005, though large uncertainties surround these estimates (Forster et al., 2007).

Since warm temperatures and stagnant air masses are conducive to $O_3$ pollution episodes, changes in climate will likely affect air quality. A variety of modeling approaches have been applied to project how local air quality will respond to climate change: sensitivity studies in which individual meteorological parameters are perturbed (e.g., Steiner et al., 2006); using observed historical correlations between meteorological variables and air quality indices to statistically downscale predictions of future meteorology from climate models (e.g., Holloway et al., 2008); and dynamical downscaling, which links a suite of climate and atmospheric chemistry models from global to regional scales (e.g., Hogrefe et al., 2004). In an analysis of studies examining how a warmer climate will influence air pollution at northern mid-latitudes, Jacob and Winner (2009) conclude that projected increases in temperature and stagnation will exacerbate $O_3$ pollution in urban areas, particularly in the northeastern United States and southern and central Europe, regions where climate models show consistency in predicted meteorological changes (Christenson et al., 2007). Studies of the aerosol response to climate change disagree in sign, reflecting discrepancies in model projections for changes in precipitation frequency and ventilation in many polluted regions (Christenson et al., 2007; Jacob and Winner, 2009 and references therein).

We present two examples of air pollutants influencing climate: (1) $CH_4$ and $O_3$, and (2) sulfate and black carbon aerosols, including potential impacts of aerosols on precipitation. We then briefly review the key processes through which climate is expected to affect air quality, mainly focusing on the more widely studied $O_3$ response to climate change (Jacob and Winner, 2009). Finally, we suggest steps towards building confidence in model simulations of these processes.

## 2. Air Pollutants Influence Climate: Methane, Ozone, and Aerosols

Methane is relatively well-mixed in the troposphere, reflecting its lifetime of approximately a decade. In contrast to the $O_3$ precursors currently regulated to abate $O_3$ pollution ($NO_x$, NMVOC, and CO), the contribution from $CH_4$ to surface $O_3$ is fairly uniform globally, though largest in high-$NO_x$ polluted regions (Fiore et al., 2002, 2008). A multi-model study indicates that this result is robust, with a 20% decrease in global $CH_4$ abundances yielding roughly a 1.2 ppb decrease over

populated regions in the northern hemisphere (Fig. 1; Fiore et al., 2009). As $CH_4$ is not currently regulated for air quality, its contribution to surface $O_3$, along with that from foreign (and natural) emissions of the other $O_3$ precursors, is typically considered part of the "background". While combined reductions of $NO_x$, NMVOC, and CO within a region are more effective than equivalent percentage reductions of $CH_4$ at decreasing surface $O_3$ within that same region, "background" surface $O_3$ responds roughly equivalently to foreign anthropogenic emission reductions of $CH_4$ and $NO_x$+NMVOC+CO (Fig. 2).

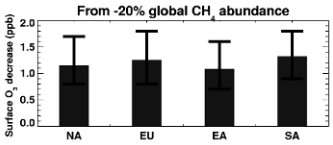


**Fig. 1.** Decrease in surface $O_3$ (ppb) resulting from a 20% decrease in global $CH_4$ abundances (from 1,760 to 1,408 ppb) in 18 global or hemispheric chemical transport models over continental-scale source regions: North America (NA; 15–55°N, 60–125°W), Europe (EU; 25–65°N; 10°W–50°E), East Asia (EA; 15–50°N; 95–160°E) and South Asia (SA; 5–35°N; 50–95°E) (Fiore et al., 2009). Model ensemble mean (blue) and range across individual models (black lines) are shown

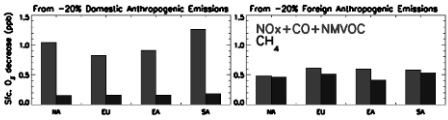


**Fig. 2.** Model ensemble surface $O_3$ decrease (ppb), annually and spatially averaged over the regions in Fig. 1 from 20% decreases in anthropogenic emissions of $NO_x$ + CO + NMVOC (red) versus 20% decreases in anthropogenic $CH_4$ (blue). Influence of each source region on surface $O_3$ within the same region (termed "domestic"; left panel). Sum of the $O_3$ responses to emission changes within the three foreign source regions; these components are generally considered to be "background" $O_3$ (right panel) (Adapted from Figure 3 of Fiore et al. 2009)

The availability of low-cost options suggests that $CH_4$ emission controls are feasible for jointly addressing climate and $O_3$ air quality goals (West and Fiore, 2005). Full-chemistry transient simulations (2005–2030) in the GFDL MOZART-2 global tropospheric chemistry model indicate that cost-effective $CH_4$ controls (at a marginal cost of ~$15/t $CO_2$ equivalent) would offset the positive climate forcing from $CH_4$ and $O_3$ that would otherwise occur from increases in $NO_x$ and $CH_4$ emissions in the baseline CLE (Current Legislation) scenario (Fig. 3a; Fiore et al., 2008). Cost-effective controls (scenario B in Fig. 3) are sufficient to decrease the incidence of $O_3$ events above 70 ppb in the model to below the number of occurrences in 2005 over Europe in summer; over the United States, only the simulation where $CH_4$ is set to pre-industrial levels ($CH_4$-700) achieves this result, reflecting differences in regional projections for $NO_x$ emissions under the baseline scenario (Fig. 3b; Fiore et al., 2008). In all cases, however, $CH_4$ reductions decrease $O_3$ relative to the 2030 CLE baseline scenario.

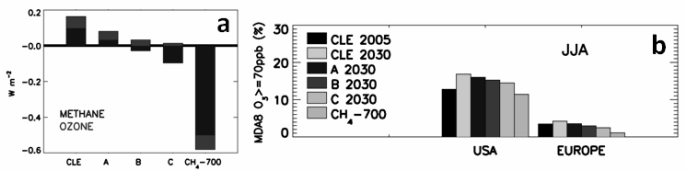


**Fig. 3.** (a) Adjusted radiative forcing (W m$^{-2}$) in 2030 versus 2005 due to changes in tropospheric $CH_4$ (blue) and $O_3$ (red) calculated with the GFDL AM2 radiative transfer model following Naik et al. (2007), and (b) percentage of model grid-cell days in the GFDL MOZART-2 model with daily maximum 8-h average (MDA8) $O_3 \geq 70$ ppb in summer (June–July–August) over the United States (62.5–127.5°W; 24–52°N) and Europe (10°W–50°E; 35–70°N), under the baseline emissions scenario (CLE; global emissions of $CH_4$, $NO_x$, CO, and NMVOC change by +29%, +19%, –10% and +3%, respectively) and with decreases in anthropogenic $CH_4$ emissions by 2030 of 75 (A), 125 (B; cost-effective with available technologies), and 180 (C; requires development of additional control technologies) Tg year$^{-1}$, and in a simulation with pre-industrial $CH_4$ concentrations (700 ppb). Non-$CH_4$ $O_3$ precursors follow the CLE scenario for 2030 in all simulations (Adapted from Table 4 and Figure 12 of Fiore et al. 2008)

Levy et al. (2008) find significant climate impacts by the year 2100 in the GFDL CM2.1 climate model due to decreasing emissions of sulfur dioxide ($SO_2$; to 35% of 2000 levels by year 2100), the precursor of sulfate aerosol, and increasing emissions of black carbon (scaled to CO emission projections) according to the A1B "marker" scenario. In the second half of the 21st century, these projected changes in emissions of short-lived species contribute substantially to the total predicted surface temperature warming for the full A1B scenario: 0.2°C in the Southern Hemisphere, 0.4°C globally, and 0.6°C in the Northern Hemisphere. We consider only the direct radiative effect of aerosols, which has been shown to add linearly to the radiative effect of greenhouse gases (e.g., Gillett et al., 2004), with similar climate responses to their forcings (Levy et al., 2008). In Fig. 4 we present the radiative forcing and surface temperature change in boreal summer between the 2090s and the 2000s due to the changes in emissions of short-lived gases and aerosols. Note that the largest temperature changes occur over the continental United States, Southern Europe and the Mediterranean, which do not coincide with the regions of strongest emission changes and radiative forcing (Southern and Eastern Asia).

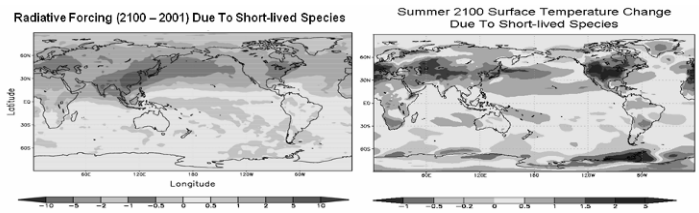


**Fig. 4.** Radiative forcing (W m$^{-2}$; left) and surface temperature change (°C; right) during boreal summer resulting from changes in short-lived species from the 2000s (2001–2010 average) to the 2090s (2091–2100 average) in the GFDL CM2.1 model following an SRES A1B emission scenario (Levy et al., 2008) (Adapted from Levy et al. 2008)

The equilibrium thermal and hydrological responses to the total aerosol effects (i.e., direct, semi-direct and indirect effects) are studied in a version of the GFDL AM2.1 atmosphere general circulation model (AGCM) that includes a prognostic treatment of aerosol-cloud interactions (Ming et al., 2007), coupled to a mixed layer ocean model (Ming and Ramaswamy, 2009). The pre-industrial to present-day increases in aerosols lead to a substantial reduction in the global mean surface temperature (1.9 K), with the strongest cooling over the Northern Hemisphere mid- and high latitudes (Fig. 5a). This is accompanied by a significant reduction in precipitation north of the equator, and an increase to the south (Fig. 5b). The combined response to aerosols and radiatively active gases (i.e., greenhouse gases) deviates considerably from the linear addition of the individual responses when aerosol indirect effects are included. The results indicate that the large shift in tropical precipitation is driven primarily by the spatially non-uniform aerosols.

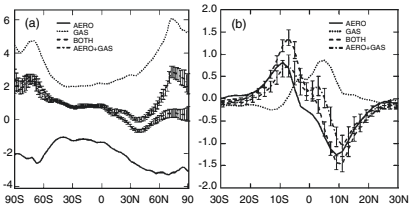


**Fig. 5.** Zonal mean differences (present – pre-industrial) in (a) surface temperature (K) and (b) precipitation (mm day$^{-1}$) in response to aerosols (AERO), radiatively active gases (GAS) and both (BOTH). For reference is the arithmetic sum of AERO and GAS. Figure is from Ming and Ramaswamy (2009)

## 3. Influence of Climate Change on Surface $O_3$

Observational analyses indicate that weather strongly modulates ambient surface $O_3$ levels from day to day, with many techniques developed over the past decades to remove this influence in order to evaluate the success of $O_3$ abatement strategies (e.g., Porter et al., 2001). The number of high-$O_3$ events can vary by as much as a factor of 10 from year to year, largely driven by fluctuations in meteorology (Leibensperger et al., 2008). Of all meteorological variables, temperature typically correlates most strongly with high-$O_3$ events (e.g., Jacob and Winner, 2009). This correlation largely reflects three key processes: ventilation of surface air, with higher temperatures associated with stagnant air (e.g., Jacob et al., 1993); local $O_3$ production chemistry, in particular the thermal dependence of PAN decomposition (e.g., Sillman and Samson, 1995); temperature-sensitive biogenic emissions, most notably isoprene (e.g., Guenther et al., 2006). Increases in other emissions such as wildfires and air-conditioning use in response to higher temperatures may further amplify the $O_3$ response. Other meteorological changes in a warmer world (e.g., convective activity, cloud distributions, humidity, mixing depths) might act as a negative feedback (e.g., Jacob and Winner, 2009 and references

therein). Spatial variations in $NO_x$ and isoprene-emitting vegetation will influence the local sensitivity of $O_3$ to temperature (and other meteorological variables such as humidity), as has been shown to occur within broad U.S. regions (e.g., Lin et al., 2001; Camalier et al., 2007) and on more local scales (e.g., Steiner et al., 2006).

To our knowledge, the ability of global chemistry-climate models to reproduce observed correlations between temperature (or any meteorological index) and air quality metrics has not been evaluated. For example, Fig. 6 shows observed $O_3$-temperature correlations at four U.S. sites, identified as "regionally representative" on the basis of seasonal variations in surface $O_3$ (Reidmiller et al., 2009). We suggest that the regional variations in slope reflect differences in the processes contributing to the $O_3$-temperature relationship and that these types of relationships should be used to evaluate chemistry-climate models. A second test would be to examine how well models capture the relationship between a decreasing frequency of migratory cyclones and increasing high-$O_3$ events, as determined from a recent observational analysis for the northeastern U.S. (Leibensperger et al., 2008). The decreasing frequency of cyclones in this region is associated with a northward shift in storm tracks (Fig. 7), a robust feature across climate models forced with increasing greenhouse gases (Christenson et al., 2007).

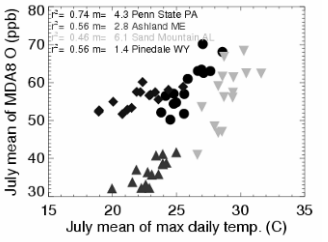


**Fig. 6.** Regional variability in the relationship between July mean daily maximum 8-h average (MDA8) $O_3$ (ppb) vs. July mean daily max temperature (°C) from 1989 to 2004 at selected U.S. CASTNet sites in the northeast (Penn State, PA), far northeast (Ashland, ME), southeast (Sand Mountain, AL), and western (Pinedale, WY) U.S.

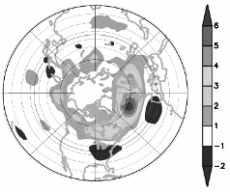


**Fig. 7.** Poleward shift in northern hemisphere summertime storm tracks in the GFDL CM2.1 climate model (Delworth et al., 2006), diagnosed from differencing the root mean square of 2–10 day bandpass filtered 500 hPa geopotential heights (m) between 100-year simulations corresponding to a pre-industrial control experiment and a 1% $year^{-1}$ $CO_2$ increase to doubling

*Priorities for future work.* To build confidence in our understanding as represented in chemistry-climate models, observational constraints are crucial, not only for $O_3$ and temperature, but also for the processes driving their strong correlation. Critical to this effort is the availability of long-term, high quality measurements of relevant species. Complementing routine measurements of $O_3$, PM, and weather variables with species such as formaldehyde (a proxy for isoprene), $NO_x$, and PAN could help to determine the relative importance of the various climate-driven impacts on air quality. In particular, large uncertainties exist in our understanding of isoprene oxidation chemistry, especially in low-$NO_x$ regions (e.g., Horowitz et al., 2007).

Additional work is needed to place climate-driven changes in the context of potentially larger changes to air quality induced through trends in land use and anthropogenic emissions, both locally and globally (e.g., Avise et al., 2009; Chen et al., 2009). While global increases in humidity in a warmer world will likely decrease background $O_3$ in surface air (e.g., Murazaki and Hess, 2006), future increases in global anthropogenic emissions may extend the $O_3$ season (e.g., Fiore et al., 2002). A lengthening of the pollution season may also occur in a warmer climate independently of global emission changes (e.g., Racherla and Adams, 2006).

**Acknowledgments** We thank S. Howard and J. Swall (EPA) for providing daily MDA8 $O_3$ and temperature from the CASTNet sites, and M. Evans (U Leeds), A. Steiner (U Michigan), and C. Wiedinmyer (NCAR) for insightful conversations.

## References

Avise, J., J. Chen, B. Lamb et al. (2009) Attribution of projected changes in summertime U.S. ozone and PM2.5 concentrations to global changes. Atmos. Chem. Phys. 9:1111–1124.

Camalier, L., W. Cox, P. Dolwick (2007) The effects of meteorology on ozone in urban areas and their use in assessing ozone trends. Atmos. Environ. 41:7127–7137.

Chen, J., J. Avise, B. Lamb et al. (2009) The effects of global changes upon regional ozone pollution in the United States. Atmos. Chem. Phys. 9:1125–1141.

Christenson, J.H. et al. (2007) Regional Climate Projections. In: Solomon, S. (Ed.), Climate Change 2007: The Physical Science Basis. Contribution of Working Group I to the Fourth Assessment Report of the Intergovernmental Panel on Climate Change. Cambridge University Press, Cambridge, United Kingdom and New York, NY, USA.

Crutzen, P. (1973) A discussion of the chemistry of some minor constituents in the stratosphere and troposphere. Pure Appl. Geophys., 106–108:1385–1399.

Delworth, T., A. Rosati, R.J. Stouffer et al. (2006) GFDL's CM2 Global Coupled Climate Models. Part I: Formulation and simulation characteristics. J. Clim. 19(5): 643–674.

Fiore, A.M., D.J. Jacob, B.D. Field et al. (2002) Linking ozone pollution and climate change: The case for controlling methane. Geophys. Res. Lett. 29, 1919.

Fiore, A.M., J.J.West, L.W. Horowitz et al. (2008) Characterizing the tropospheric ozone response to methane emission controls and the benefits to climate and air quality. J. Geophys. Res. 113, D08307.

Fiore, A.M., F.J. Dentener, O. Wild et al. (2009) Multimodel estimates of intercontinental source-receptor relationships for ozone pollution, J. Geophys. Res., 114, D04301.

Forster, P. et al. (2007) Changes in Atmospheric Constituents and in Radiative Forcing. In: Solomon, S. (Ed.), Climate Change 2007: The Physical Science Basis. Contribution of Working Group I to the Fourth Assessment Report of the Intergovernmental Panel on Climate Change. Cambridge University Press, Cambridge, United Kingdom and New York, NY, USA.

Fuglestvedt, J.S. et al. (1999) Climatic forcing of nitrogen oxides through changes in tropospheric ozone and methane: Global model studies, Atmos. Environ. 33: 961–967.

Gillett, N.P., M.F. Wehner, S.F.B. Tett, A.J. Weaver (2004) Testing the linearity of the response to combined greenhouse gas and sulfate aerosol forcing, Geophys. Res. Lett. 31, L14201.

Guenther, A., T. Karl, P. Harley et al. (2006) Estimates of global terrestrial isoprene emissions using MEGAN. Atmos. Chem Phys. 6, 3181–3210.

Hansen, J., M. Sato, and R. Ruedy (2000) Global warming in the twenty-first century: An alternative scenario. Proc. Natl. Acad. Sci. 97:9875–9880.

Hogrefe, C., et al. (2004) Simulating changes in regional air pollution over the eastern United States due to changes in global and regional climate and emissions, J. Geophys. Res. 109, D22301.

Holloway, T., S. N. Spak, D. Barker et al. (2008), Change in ozone air pollution over Chicago associated with global climate change, J. Geophys. Res., 113, D22306.

Horowitz, L.W., A.M. Fiore, G.P. Milly et al. (2007) Observational constraints on the chemistry of isoprene nitrates over the eastern United States. J. Geophys. Res. 112, D12S08.

Jacob, D.J., J.A. Logan, G.M. Gardner et al. (1993) Factors regulating ozone over the the United States and its export to the global atmosphere. J. Geophys. Res. 98:14,817–14,826.

Jacob, D.J. and D.A. Winner (2009), Effect of climate change on air quality, Atmos. Environ., 43, 51–63.

Leibensperger, E. M., L. J. Mickley, D. J. Jacob (2008) Sensitivity of U.S. air quality to mid-latitude cyclone frequency and implications of 1980–2006 climate change. Atmos. Chem. Phys. 8:7075–7086.

Levy, H. II, M.D. Schwarzkopf, L. Horowitz et al. (2008) Strong sensitivity of late 21st century climate to projected changes in short-lived air pollutants, J. Geophys. Res., 113, D06102.

Lin, C.-Y.C., D.J. Jacob, A.M. Fiore (2001) Trends in exceedances of the ozone air quality standard in the continental United States, 1980–1998. Atmos. Environ. 35:3217–3228.

Ming, Y., V. Ramaswamy, L.J. Donner et al. (2007) Modeling the interactions between aerosols and liquid water clouds with a self-consistent cloud scheme in a general circulation model. J. Atmos. Sci., 64, 1189–1209.

Ming and Ramaswamy (2009) Nonlinear climate and hydrological responses to aerosol effects. J. Clim., in press.

Murazaki and P. Hess (2006) How does climate change contribute to surface ozone change over the United States? J. Geophys. Res., 111, D05301.

Naik, V., D. Mauzerall, L. Horowitz et al. (2007). On the sensitivity of radiative forcing from biomass burning aerosols and ozone to emission location. Geophys. Res. Lett. 34, L03818.

Porter, P.S., S.T. Rao, I.G. Zurbenko, et al. (2001) Ozone Air Quality over North America: Part II—An analysis of Trend Detection and Attribution Techniques. JAWMA 51:283–306.

Racherla, P.,N. and P.J. Adams (2006) Sensitivity of global tropospheric ozone and fine particulate matter concentrations to climate change, J. Geophys Res., 111, D24103, doi:10.1029/3005JD006939.

Reidmiller, D.R., A.M. Fiore, D.A. Jaffe et al. (2009) The influence of foreign vs. North American emissions on surface ozone in the U.S., submitted to Atmos. Chem. Phys.

Shindell, D.T., G. Faluvegi, N. Bell, G.A. Schmidt (2005) An emissions-based view of climate forcing by methane and tropospheric ozone. Geophys. Res. Lett. 32, L04803.

Sillman, S., and P.J. Samson (1995), Impact of temperature on oxidant photochemistry in urban, polluted rural and remote environments, J. Geophys. Res., 100 (D6), 11,497-11,508.

Steiner, A. L., Tonse, S., Cohen, R. C., Goldstein, A. H., Harley, R. A.(2006), Influence of future climate and emissions on regional air quality in California, J. Geophys. Res., 111, D18303.

U.S. EPA, National Air Quality Status and Trends through 2007, EPA-454/R-08-006, November 2008, available at http://www.epa.gov/air/airtrends/2008/report/TrendsReportfull.pdf.
West, J.J. and A.M. Fiore (2005) Management of tropospheric ozone by reducing methane emissions. Environ. Sci. & Technol. 39(13): 4685–4691

## 4. Questions and Answers

**Katarzyna Juda-Rezler:** I would like to ask you for a comment about (future) precipitation role on air quality. In our simulation with coupled RCM-CTM for Poland, we obtained increased precipitation and decreased PM concentration. Could you comment on that?

**Answer:** We have not yet analyzed the PM or precipitation response in our study in any detail and we are not sure that the modest summertime increase in PM just shown is statistically significant. We would not have been surprised to find just what you found. However, we do seem to have a slight increase in summertime PM2.5 and a decrease in precipitation [not shown] over central Europe, though neither looks like it will be statistically significant. We are just beginning to examine the climate behavior of our new chemistry-climate model.

**K. Fedra:** Does that not suggest we should look into adaptation, robustness, resilience rather than (NBR) impossible prediction?

**Answer:** The speaker's answer, speaking as a private citizen, is that his bet is on adaptation because of the political and technical complexity of identifying the long-term climate change signal, particularly the regional signal in the presence of short-term natural climate variability. The speaker would also note that, in his opinion, by far the biggest uncertainties are in our ability to project future emissions, rather than our ability to model the chemical-climate system.

# 6.2 A Methodology for Determining the Impact of Climate Change on Ozone Level in an Urban Area

**Martin Cope, Sunhee Lee, Bill Physick, Debbie Abbs, Kim Nguyen, and John McGregor**

Centre for Australian Weather and Climate Research, Private Bag No. 1 Aspendale Victoria, Australia 3195

**Abstract** In this paper we present a methodology that has been used to give an insight into the impact of climate change on ozone levels in Sydney in 20 and 50 years time. The methodology comprises a dynamical downscaling system which takes 200 km resolution global climate simulations and through a two stage process, generates 3 km resolution mesoscale meteorological and trace gas concentration fields over populated areas.

The system was assessed for Sydney and was found to perform well in the prediction of the historical ozone climatology, mesoscale meteorology and peak ozone concentrations. The system was used to downscale an A2 climate scenario for 2021–2030 and 2051–2060. Although the simulated ozone climatology did not change significantly, increases in ambient temperature and the resultant increases in ozone precursor concentrations and photochemical transformation rates lead to increases in the frequency and magnitude of peak ozone concentrations and health impacts.

The tools that were developed and assessed in this project are intended to provide a capability which can aid policy makers in formulating long term air pollution policies where the impact of climate change has to be considered. However, when applied for this purpose, it is recommended that the system be operated in an ensemble mode whereby a range of model projections are generated and an estimate of likelihood can be calculated. It is further recommended that the system be enhanced to consider the formation and fate of fine particles (primary and secondary) as this air pollutant is generally considered to cause the largest air quality related health impacts in Australia.

**Keywords** Climate change, ozone projection, dynamic downscaling system, IPCC-A2 scenario

D.G. Steyn and S.T. Rao (eds.), *Air Pollution Modeling and Its Application XX*,
DOI 10.1007/978-90-481-3812-8, © Springer Science + Business Media B.V. 2010

## 1. Introduction

The primary objective of this project was to demonstrate a methodology that is able to give estimates of ozone concentrations under climate change conditions for any period or location in Australia, and to specifically give an insight into the impact of climate change on ozone levels in Sydney in 20 and 50 years time. Ten year periods were chosen for detailed high-resolution chemical transport simulations (1996–2005 [decade 1], 2021–2030 [decade 2] and 2051–2060 [decade 3]) in order to enable the inter-annual variability in ozone climate to be addressed. A second objective was to estimate the decrease of emissions which may be needed to maintain ozone levels below National Environment Protection Measures (NEPM) standards where 1-h peak ozone concentration is 100 ppb and 4-h peak of 80 ppb with an allowable exceedence of 1 day/year.

## 2. Description of the Modelling System

The downscaling system set up for this project consists of nesting an urban/regional atmospheric transport and chemistry model (TAPM–CTM) with 3-km inner grid spacing, into the regional meteorological fields (60-km grid spacing) generated by the stretched grid atmospheric model (CCAM) which in turn is nudged towards global-scale meteorological fields generated by the CSIRO–Mk3 Global Climate System Model. CSIRO–Mk3 and CCAM were forced by one of a family of A2 Special Report on Emissions Scenarios (SRES). CCAM is formulated on a conformal-cubic grid which covers the globe, but can be stretched to provide higher resolution in an area of interest. Because of its higher resolution, CCAM is, in principle, able to generate more accurate climate predictions over Australia, with particular emphasis on the Sydney region. CCAM was integrated for the period 1961–2100 for the purposes of the current study and meteorological boundary conditions suitable for use with TAPM–CTM were generated for the period 1996–2005, 2021–2030 and 2051–2060.

Emission inventories for on-road mobile source, industrial, commercial and domestic emissions for the Sydney Greater Metropolitan Region (GMR) were provided by NSW Department of Environment and Climate Change. Emissions from natural sources ($NO_x$ from bacterial activity in soils; VOC emissions from plants) were modelled internally in CTM.

## 3. System Performance for the Decade of 1996–2005

An important component of this project is an assessment of the capability of the dynamic downscaling system to reproduce the observed fields of the relevant

environmental variables with a level of skill which justifies the use of the system for undertaking climate projection modelling for future decades. A detailed analysis of changes in the important field related to ozone climatology such as temperature, wind field and ventilation rate, is discussed in Cope et al. (2008).

Because model performance for ozone represents a test of the fully coupled system, it is not possible to eliminate the possibility of error compensation (or enhancement) due to biases in individual components of the system (i.e. emissions, meteorology or chemistry). However our previous experience in modelling photochemical smog production in Sydney suggests that the ability to simulate the correct mesoscale flows is the most significant factor in determining whether elevated concentrations of ozone will be correctly simulated by the chemical transport model simulation for Sydney.

The majority of the modelled concentrations lie within 30% of the observed concentrations from 16 monitoring stations. While overall the model has a tendency to over-predict the lower percentile concentrations and to under-predict the upper percentile concentrations, there is an excellent level of agreement between the modelled and observed 50th, 75th, 80th and 100th percentile peak daily 1-h ozone concentrations. With respect to the peak daily 4-h ozone concentrations, the detailed performance is slightly worse than the daily peak 1-h ozone performance.

## 4. Projections

This section discusses the projected changes in peak ozone concentration for a climate projection based on the A2 SRES emission scenario. In interpreting the results in this section it must be noted that they correspond to downscaling based on a single climate (A2) emissions scenario.

### 4.1. Projection with current emission levels

This section presents ozone change for decade 2 and decade 3 for a scenario in which the emissions are fixed at 1996–2005 values. In the case of the second decade, the majority of the changes in 1-h peak ozone from the first decade concentrations are projected to vary in the range −5 to +10 ppb, with the majority of the changes being positive. In the case of the third decade the majority of the 99th percentile 1-h concentrations are calculated to increase, with increases of up to 15 ppb calculated. Recall that violation of the NEPM goals for ozone occurs when more than one exceedence per year is recorded. The number and spatial extent of the 4-h ozone exceedences are projected to increase in the second and third decades.

### 4.2. Projections with A2 scenario and emission reductions

SRES emission estimates for the OECD90 region under the A2-ASF scenario for the year 2050 indicates a 33.3% increase of NOx, 16.2% increase of VOC and 12.4% decrease of CO from the 2000 emissions. TAPM-CTM was run for the decade 3 with the GMR anthropogenic emissions inventory scaled by these factors. The results show that the number of exceedence cell-days decreases slightly (4%) compared to the base case 2051–2060 scenario for 1-h average ozone and increase slightly (7%) for the 4-h average ozone. The mixed result for 1- and 4-h ozone likely reflects the response of the modelled chemistry to increasing $NO_x$ concentrations.

To investigate the level of reduction required to achieve compliance with the NEPM standards for ozone in the GMR for the climate change scenario, it was attempted for the decade 3 meteorological scenario by selecting months from this decade which contain the ten highest 4-h ozone concentrations and then running emission reduction scenarios in which all anthropogenic precursor emissions were uniformly reduced by 40% and 70%. The projection with a 40% reduction in anthropogenic precursor concentrations is estimated to reduce peak 1-h ozone by 17% and peak 4-h ozone by 8% compared to the base case 2051–2060 scenario. A 70% reduction is estimated to reduce peak 1- and 4-h ozone by 36% and 25%, respectively. These results support the statement above that the 4-h ozone is more challenging to reduce than the 1-h concentrations. The results also suggest that an equal reduction strategy for all of the precursors may not be optimal given that peak ozone concentrations are still modelled to exceed the NEPM standards even for emission reductions of 70%.

## 5. Limitations and Future Directions

(1) As noted earlier, this study is based on a single A2 SRES emissions scenario and a small suite of GMR anthropogenic emission scenarios. An important area of future work lies in the generation of ensembles of downscaling results based on alternative IPCC SRES emission scenarios, based on the climatologies of different GCMs, and potentially based on different downscaling methodologies. (2) The current project did not take account for bushfire impacts on ozone and aerosols. With the likely increase in bushfires, their impact should be considered in future ozone and climate impact modelling. (3) Changes in background ozone and other precursor species concentrations due to climate change and due to increases in global emission should be considered in future work. (4) This project is restricted to the consideration of gas phase processes. For future work, fine particles should be included since the largest air pollution health impacts and health costs in Australia are associated with fine particles.

**Acknowledgments** We'd like to acknowledge the Federal Department of Environment, Water, Heritage and the Arts for providing funding in support of this project. We would also like to acknowledge Suzanne Quigley and Charles Xu and for providing air quality data, the GMR motor vehicle emissions inventory and also much helpful advice during the course of this project.

## References

Cope, ME, Lee, S, Physick, B, Abbs, D, Nguyen, K & McGregor, J (2008) 'A methodology for determining the impact of Climate Changes on Ozone Levels in Urban Area', Final CARP 11 report to the Federal Department of Environment, Water, Heritage and the Arts, Australia.

## 6. Questions and Answers

**Question:** When introducing electric cars where does the (supposedly no polluting) electricity comes from?

**Answer:** For the scenario that petrol fuelled passenger cars are replaced by pure electric cars, it is assumed that their batteries will be recharged by renewable green energy such as power generated by solar panel and wind turbine.

**Question:** How was synoptic typing performed and how representable are synoptic patterns?

**Answer:** The method (based on Yanal 1993) is grid based and uses a correlation analysis to group together days which have similar mean sea level pressure (MSLP) patterns. The methodology involves multiple passes through a data set of gridded MSLP. (1) Cycle through each day in the MSLP data set calculating the Pearson product-moment ($r_{xy}$) for every other day in the data set. Consider 2 days to have similar synoptic patterns if $r_{xy} > 0.7$. (2) The day which has the greatest number of matches is designated as "key day 1". This day and all days having similar synoptic patterns are removed from the data set and step 1 is repeated to identify "key day 2". (3) Repeat 1 and 2 until all of the key days have been identified. (4) Once the key days have been identified, a second pass is undertaken and all days in the data set are again correlated with each key day. (5) In a third pass, any remaining days which are unclassified are again correlated with the key days and are assigned to a key day if $r_{xy} > 0.5$. It was undertaken for days in the period 1996–2005 where peak 1-h ozone concentrations exceeded 100 ppb. In the case of the observed ozone data set, days were first filtered to remove instances where bushfire smoke may have influenced ozone production. Once a set of days had been generated, a data base of NCEP 00 UTC MSLP fields were analysed to generate the key days. The pattern analysis was also run for the modelled data set and then matched with the observed key day patterns. For key day 1, observed pattern represent 55% while modeled pattern represents 40%. For key day 2, observed pattern

represents 17% while modeled pattern represents 28%. For key day 3, observed pattern represents 14% while modeled pattern represents 13%. The results showed the modelling system has done reasonably well in matching the observed synoptic categories.

# 6.3 Air Quality: Meteorology Interaction Processes in the ICLAMS Modeling System

**G. Kallos, S. Solomos, and J. Kushta**

University of Athens, School of Physics,

Atmospheric Modeling and Weather Forecasting Group, 15784 Athens, Greece

**Abstract** In order to study processes and feedbacks between air pollution and climate a new Integrated Community Limited Area Modeling System – ICLAMS has been developed. ICLAMS is an enhanced version of the Regional Atmospheric Modeling SystemRAMS.6.0. It includes submodels for the dust and sea salt cycles, gas and aqueous phase chemistry and gas to particle conversion. All these processes are directly coupled with meteorology. The system has been developed to study air pollution transport and transformation processes in the Greater Euro-Mediterranean Region and East Atlantic. This area is well known for its regional characteristics where the mixture of different age of anthropogenic air pollutants with Saharan dust and sea salt may lead to the formation of new particles with different characteristics. In this presentation, we demonstrate the transport and transformation processes at various spatiotemporal scales and discuss implications related to aerosol composition and their impacts on cloud formation and on radiation. The new modeling tool is applied in studies related to air quality and climate in the Mediterranean, North Africa and Atlantic Ocean.

## 1. Introduction

Natural-born and anthropogenic aerosols have profound impacts on the thermodynamic and radiative energy budgets of the Earth [1] and also on human health [2]. Desert dust and sea-salt spray are considered to be the main components of natural-born aerosol. Anthropogenic pollutants consist mainly of black carbon, sulphates, nitrates, ozone and carbon oxides. Continuous research on aerosol emission and removal mechanisms as well as on their contribution to atmospheric procedures is essential for weather and climate. Aerosols change the optical properties of the atmosphere and redistribute the radiation fluxes between earth and sun (direct aerosol effect). They can also serve as efficient Cloud Condensation Nuclei (CCN) and Ice Nuclei (IN) thus changing the microphysical and radiative properties of the clouds (indirect aerosol effect). The above effects of aerosol in regional and local weather cannot be easily resolved by the available modeling tools. However, the ability to forecast severe weather phenomena such

D.G. Steyn and S.T. Rao (eds.), *Air Pollution Modeling and Its Application XX*,
DOI 10.1007/978-90-481-3812-8, 

as dust storms, convective thunderstorms, intense lightning and hurricanes is strongly connected to understanding and modeling such effects. The present work focuses on the feedbacks between air pollution and meteorology. Under certain weather conditions such processes must be adequately resolved because they affect the removal processes and therefore define the air pollution levels. The role of tropospheric aerosols in atmospheric processes and implications on air quality is examined for a test case over Eastern Mediterranean.

## 2. Model Description

ICLAMS has been developed by the Atmospheric Modeling and Weather Forecasting Group at the University of Athens (AMWFG), in order to be used as a research and forecasting tool for air pollution and climate applications at the framework of CIRCE project. The new developed modeling system is based on RAMS6.0 [3]. ICLAMS capabilities have been extended with the addition of a detailed air-quality scheme including desert-dust [4], sea-salt spray [5] and anthropogenic pollutants parameterization, online coupled with gas and aqueous phase chemistry modules. The chemical component of the model constitutes of the gas and aqueous chemistry module and the gas-particle interaction module. The gas chemistry module is based on the chemistry mechanism SAPRC99. The photochemical scheme uses basic formulations and it is directly coupled with the radiation scheme of RAMS. The aqueous chemistry module deals with the chemical processes that take place inside a cloud. For the gas-aerosol processes the ISORROPIA mechanism is incorporated into the model. The original lookup table approach of cloud droplet nucleation in RAMS has been replaced by the FNS (Fountoukis-Nenes-Seinfeld) cloud droplets nucleation formulation [6, 7]. The rest of the microphysics package remains the same as in original RAMS model.

The main mechanisms through which particles and gas pollutants are removed from the atmosphere are the dry and wet deposition. Dry deposition velocities are calculated from gravitational settling and surface resistances. Wet deposition mechanism is responsible for the larger amount of natural and anthropogenic pollutants removal, especially away from the sources and is strongly connected to the precipitation process. The parameterization scheme for the wet deposition describes the removal of the particles from the atmosphere through in-cloud and below-cloud scavenging. ICLAMS has been used for studying effects of dust and seasalt on cloud formation in the Mediterranean.

## 3. Results and Discussion

Aged air masses usually contain increased numbers of CCN. For the greater Mediterranean area, CCN are often composed of a mixture of several species such as sulphate coated or salt coated mineral dust particles, sea-salt particles and secondary particles from anthropogenic pollutants [8]. Such particles exhibit higher hygroscopicity and play important role in cloud formation and precipitation. The cloud droplet activation parameterization in ICLAMS is properly designed for air-quality applications since it allows the aerosol species to explicitly interact with the model physics and dynamics. Proper handling of aerosol properties and aerosol-cloud interactions in the model leads into remarkable improvement in precipitation estimation (Fig. 1) and consequently in wet deposition and air quality analysis (Fig. 2).

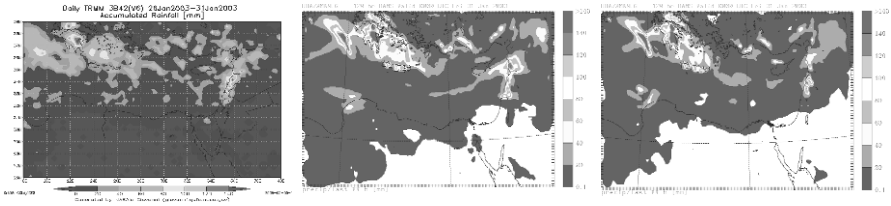

**Fig. 1.** 120 h accumulated precipitation (mm) (26–31January 2003). (a) TRMM Satellite observations (b) model results with aerosol meteorology interaction and (c) model results without aerosol meteorology interaction

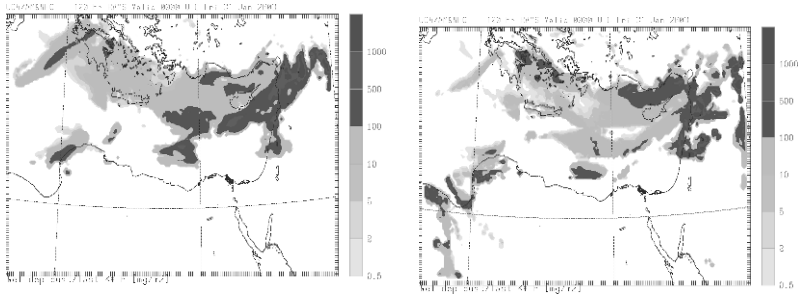

**Fig. 2.** 120 h model accumulated dust wet deposition (mg/m$^2$) (26–31 January 2003). (a) Aerosol particles are treated as passive tracers. (b) Aerosol meteorology interaction

When utilizing aerosol chemistry, the sulfates are higher in the areas where there are significant emissions of $SO_2$ and slightly smaller when the $SO_2$ availability is limited (Fig. 3a). This is a result of the formation of additional aerosols from $H_2SO_4$ which depends on $SO_2$. The $SO_2$ concentrations are lower in the presence of clouds when the aerosol module is utilized (Fig. 3b). This happens due to the adjustment of the gas and vapor phase concentrations of $SO_2$ in order to be in equilibrium with the aerosol phase. The available $SO_2$ in the atmosphere reacts with hydroxyl radical to produce $HO_2$ and sulfates. Hence it is an indicator

of the available OH radicals in the atmosphere. The more $SO_2$ leads to less OH which in turn affects ozone production cycle (Fig. 3c). The smaller ozone concentrations in presence of higher $SO_2$ concentrations indicate a signal of this interaction.

## 4. Conclusions

Features that cannot be accurately captured by the conventional meteorological and air quality models are adequately described with the new model development (direct coupled system). ICLAMS includes a robust parameterization package of atmospheric processes and feedbacks between air quality and meteorology. The application of the above algorithms leads into a more accurate and versatile modelling tool for air quality and climatic forcing research.

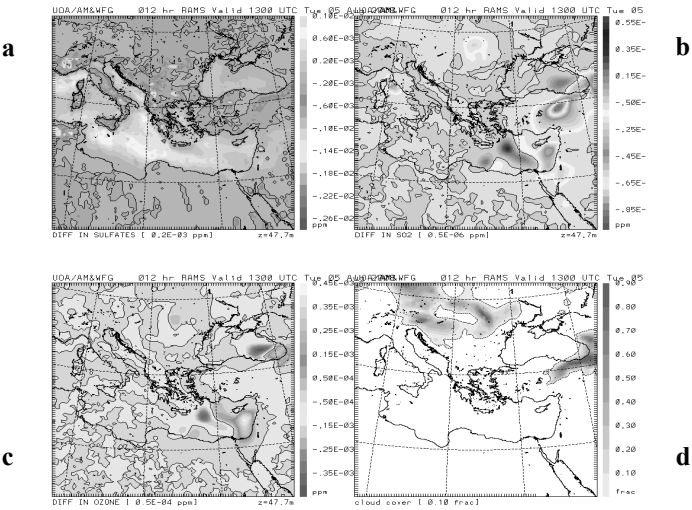


**Fig. 3.** Differences in concentrations (ppm) of (a) sulfates, (b) $SO_2$, and (c) ozone expressed as $[C_{\text{aerosol chemistry}} - C_{\text{only gas chemistry}}]$ and d) cloud cover on 5 August 2008 at 13:00 UTC

**Acknowledgments** We would like to thank Dr. A. Nenes for kindly providing the cloud nucleation routines and Dr. C. J. Tremback for his support during the new code development. This work was supported by the EU 6th Framework Program CIRCE IP, contract# 036961 and EUROCONTROL Research Studentship Agreement no CO6/22048ST

## References

Andreae MO and Rosenfeld D (2008): Aerosol-cloud-precipitation interactions, Part 1, The nature and sources of cloud-active aerosols: Earth Science Reviews, 89, 13–41

Mitsakou and co-authors (2008): Saharan dust levels in Greece and received inhalation doses, Atmos. Chem. Phys., 8, 7181–7192

Cotton WR and co-authors (2003): RAMS 2001: Current status and future directions. Meteoro. and Atmos Phys 82, 5–29.

Kallos G and co-authors (2009): Ten-year operational dust forecasting – Recent model development and future plans, IOP Earth and Environmental Science

Gong SL (2003): A parameterization of sea-salt aerosol source function for sub- and super-micron particles , Global Biochemical Cycles, 17(4),1097

Nenes A and JH Seinfeld (2003): Parameterization of cloud droplet formation in global climate models, J. Geophys. Res., 108, 4415

Fountoukis C and A Nenes (2005): Continued Development of a Cloud Droplet Formation Parameterization for Global Climate Models J. Geophys. Res., 110, D11212

Astitha and G Kallos (2008): Gas-phase and aerosol chemistry interactions in South Europe and the Mediterranean Region. Env. Fl. Mech.

# 6.4 Assessing Impacts of Aerosol Processes on Equilibrium Climate Sensitivity

**Trond Iversen[1,2], Alf Kirkevåg[1], Øyvind Seland[1], Jens Debernard[1], Jon Egill Kristjansson[2], and Corinna Hoose[2]**

[1]Norwegian Meteorological Institute, Oslo, Norway

[2]Department of Geosciences, University of Oslo, Oslo, Norway

**Abstract** We study possible climate impacts of anthropogenic aerosols by modeling their atmospheric life-cycles, and parameterizing their extinction of solar radiation and interactions with clouds. We have developed and implemented such schemes in the global atmospheric climate model CAM3 of the National Centre for Atmospheric Research (NCAR). We present results from CAM-Oslo coupled to a slab ocean. Equilibrium climate response, assuming different aerosol properties, are estimated as the change in equilibrium values of surface air temperature and precipitation due to changed atmospheric content of $CO_2$ or aerosol production. Feed-back processes with aerosols are discussed, along with effects of an added background cloud droplet number concentration (cdnc), and how $CO_2$-induced climate change may influence aerosols.

**Keywords** Aerosols, climate change, equilibrium climate sensitivity

## 1. Introduction and Model Tool

Indirect effects of aerosols and feedback effects of clouds contribute large uncertainty to calculated climate projections (Stainforth et al., 2005; Solomon et al., 2007). Modeling the cooling effects of aerosols is a major source of uncertainty in estimates of climate sensitivity to forcing (Andréa et al., 2005; Figure 2.20 in Forster et al., 2007), implying a risk of a stronger 21st century warming than anticipated from greenhouse gases alone. The uncertainty in climate sensitivity is therefore important when assessing possible anthropogenic climate change.

We have calculated atmospheric life-cycling and physico-chemical properties of aerosols on-line in the global community atmospheric model 3 (CAM3) of the National Center for Atmospheric Research (Collins et al., 2006). This model version is named CAM-Oslo. Size-distributed composition and numbers are estimated based on primary particle production of sea-salt, mineral dust, and nucleated sulphate ($SO_4$), and condensation, coagulation, and aqueous production involving

D.G. Steyn and S.T. Rao (eds.), *Air Pollution Modeling and Its Application XX*,
DOI 10.1007/978-90-481-3812-8, © Springer Science + Business Media B.V. 2010

$SO_4$, black carbon (BC), and particulate organic matter (POM). POM includes natural secondary organic aerosols. Results have recently been published (Seland et al., 2008; Kirkevåg et al., 2008; Storelvmo et al., 2008; Seland and Iversen, 2007). Here we diagnose cloud droplet number concentrations (cdnc) from aerosol activation, but prognostic cdnc is underway. CAM-Oslo is coupled to a slab-ocean with ocean fluxes calibrated to maintain preseny-day surface temperatures. This system is used to estimate equilibrium climate response.

**Table 1.** Experiments identified by aerosol emissions (PI = pre-industrial, PD = present-day) and $CO_2$ concentrations (unit ppm: 355 = 1 × $CO_2$; 580 = 1.63 × $CO_2$; 710 = 2 × $CO_2$). Selected key long-term global results are: T = surface air temperature, P = precipitation, Cl = fractional cloudiness, LWP = liquid water path, τ = atmospheric life-time, "Aq $SO_2$-ox" is the in-cloud percentage of $SO_2$ oxidized to sulphate. AOD is the aerosol optical depth at 350–640 nm

| Experiment | T K | P $mmd^{-1}$ | Cl $10^{-2}$ | LWP $g\ m^{-2}$ | Aq. $SO_2$ -ox % | τ $SO_4$ d | τ BC d | τ POM d | τ SS d | τ DU d | AOD $10^{-3}$ |
|---|---|---|---|---|---|---|---|---|---|---|---|
| 1a) PI, 355 | 290.6 | 3.10 | 60.90 | 106.4 | 87.30 | 3.35 | 6.86 | 6.98 | 0.247 | 2.07 | 91.4 |
| 1b) PD, 355 | 288.5 | 2.92 | 60.27 | 113.9 | 85.16 | 3.78 | 6.80 | 7.35 | 0.256 | 2.20 | 130.7 |
| 1c) PD, 580 | 290.5 | 3.04 | 60.92 | 115.6 | 85.15 | 3.73 | 6.66 | 7.20 | 0.250 | 2.21 | 128.4 |
| 2a) PI, 355 | 288.5 | 2.93 | 60.02 | 127.3 | 86.92 | 3.58 | 6.86 | 6.96 | 0.257 | 2.20 | 96.2 |
| 2b) PD, 355 | 287.0 | 2.80 | 59.52 | 129.5 | 84.77 | 3.97 | 6.89 | 7.37 | 0.265 | 2.29 | 138.1 |
| 2c) PI, 710 | 291.2 | 3.07 | 60.75 | 131.3 | 87.12 | 3.50 | 6.86 | 6.93 | 0.248 | 2.21 | 94.3 |
| 2d) PD, 580 | 289.1 | 2.92 | 60.18 | 132.9 | 84.83 | 3.88 | 6.77 | 7.23 | 0.255 | 2.28 | 133.3 |
| 2e) PD, 710 | 289.9 | 2.96 | 60.41 | 134.2 | 84.64 | 3.89 | 6.76 | 7.21 | 0.253 | 2.31 | 132.6 |

## 2. Experiments and Results

The aerosols force the climate system by influencing solar radiation and clouds. Our experiments, as defined in Table 1, are intended for estimating the response on atmospheric dynamics, SST, and sea-ice. Experiments are 30 years long and approximate radiative equilibrium is assumed at the top of the atmosphere for years 15–30. Result statistics from this period are discussed. Experiments 1 are pre-calibrated with the standard prescribed aerosols in NCAR CAM3, whilst experiments 2 are pre-calibrated with our own present-day aerosols. Therefore, all experiments 1 have a slight positive bias since the PD conditions differ slightly from the conditions used when calibrating the ocean fluxes. There is a tendency that aerosol life-times are short when precipitation is high and v.v., but since precipitation may increase in areas with small aerosol loading this is not always the case. In experiments 2, a background cloud droplet number concentration (cdnc) of 3 $cm^{-3}$ over oceans and the Antarctic and 17 $cm^{-3}$ over continents is added.

Table 2 shows summary results for equilibrium climate responses to external forcing produced by changing $CO_2$-concentrations or aerosol emissions. Rows 1–3 concern the effect of aerosol changes from pre-industrial times; rows 4–5 the effect of increasing $CO_2$ by 63%, rows 6 and 7 the effect of $CO_2$-doubling, and row 8 the effect of a combined 63% increase in $CO_2$ and an aersol change from PI to PD. In Fig. 1 more details are shown for the results in rows 5 and 8.

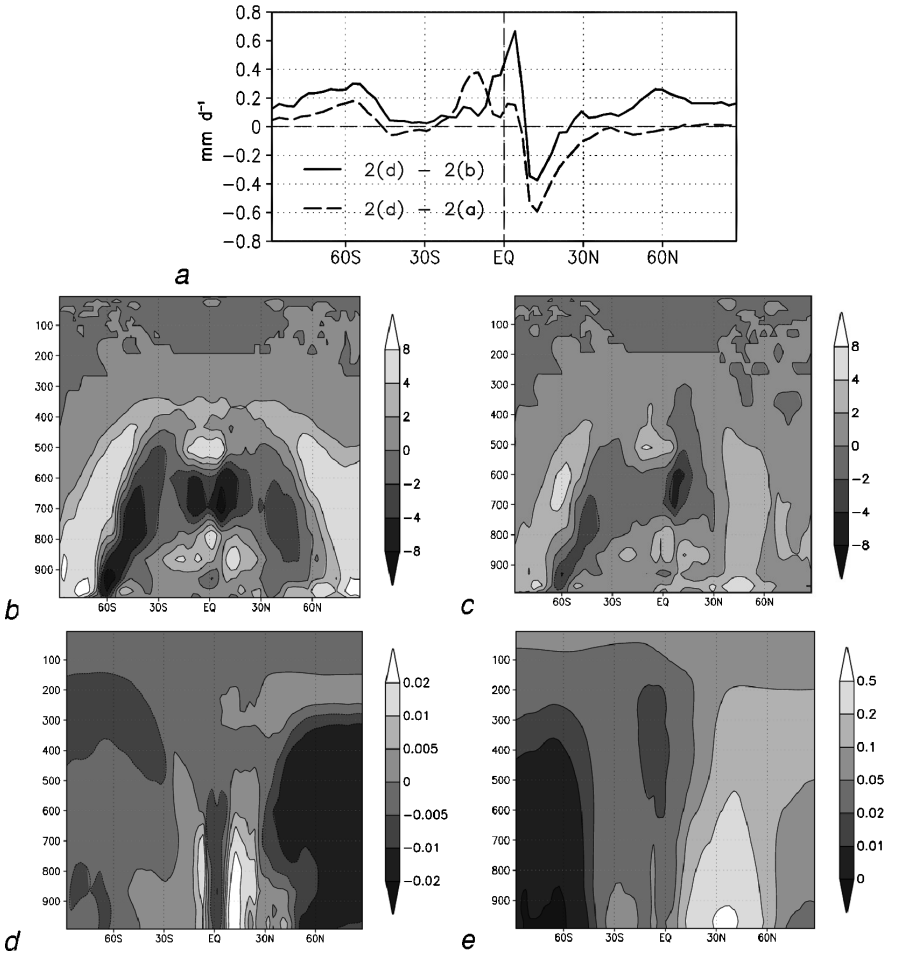


**Fig. 1.** Equilibrium climate response to two sets of external forcing shown for zonal average daily precipitation, mm $d^{-1}$ (a); Cloud liquid water mass mixing ratio, ppm (b, c); $SO_4$ mass mixing ratio, ppb (d, e). Continuous curve in (a) and plots to the left (b, d) show effects of a 63% $CO_2$ increase with present-day aerosol emissions (PD); Dashed curve in (a) and plots to the right (c, e) show effects of a combined 63% $CO_2$ increase and aerosol emissions change from PI to PD

**Table 2.** Estimated equilibrium climate response to increments in $CO_2$ or aerosols obtained by taking differences between experiments defined in Table 1. The brackets in column no.2 define the increments causing response. The numbers define levels or increments of $CO_2$ (ppm), whilst aerosol levels or increments are defined by the letters PI (pre-industrial) and PD (present-day). In the bottom row both $CO_2$ and aerosols are changed. Absolute changes are shown for temperature, precipitation, cloud fraction, and liquid water path; relative changes are shown for atmospheric life-time of aerosol species, both relative and absolute changes are shown for aerosol optical depth (AOD). Rows 5 and 8 are associated with examples in Fig. 1

| Experiment | Increment | ΔT K | ΔP mm/d | ΔCl $10^{-2}$ | Δ LWP g/m2 | Δτ $SO_4$ % | Δτ BC % | Δτ POM % | Δτ SS % | Δτ DU % | Δ AOD % $10^{-3}$ |
|---|---|---|---|---|---|---|---|---|---|---|---|
| 1a)–1b) | [PI – PD], 355 | 2.09 | 0.178 | 0.63 | –7.52 | –11.4 | 0.9 | –5.1 | –3.3 | –5.8 | –30.06 –39.3 |
| 2a)–2b) | [PI – PD], 355 | 1.50 | 0.131 | 0.50 | –2.29 | –9.7 | –0.4 | –5.6 | –3.0 | –3.9 | –30.31 –41.9 |
| 2c)–2e) | [PI – PD], 710 | 1.34 | 0.114 | 0.34 | –2.83 | –10.0 | 1.4 | –3.8 | –2.0 | –4.4 | –29.30 –38.4 |
| 1c)–1b) | PD, [580–355] | 1.99 | 0.113 | 0.65 | 1.69 | –1.4 | –1.9 | –2.1 | –1.7 | 0.3 | –1.72 –2.3 |
| 2d)–2b) | PD, [580–355] | 2.06 | 0.120 | 0.66 | 3.39 | –2.3 | –1.7 | –1.8 | –3.8 | –0.3 | –3.45 –4.8 |
| 2e)–2b) | PD, [710–355] | 2.85 | 0.160 | 0.89 | 4.62 | –2.0 | –1.8 | –2.1 | –4.5 | 0.8 | –3.94 –5.4 |
| 2c)–2a) | PI, [710–355] | 2.69 | 0.143 | 0.73 | 4.08 | –2.4 | 0.0 | –0.3 | –3.5 | 0.4 | –2.01 –1.97 |
| 2d)–2a) | [PD, 580 – PI, 355 ] | 0.56 | –0.011 | 0.16 | 5.68 | 8.2 | –1.3 | 4.0 | –0.8 | 3.7 | 38.54 37.41 |

## 3. Concluding Remarks

In short we conclude as follows. (1) Whilst aerosol changes since PI largely counteract the effects of $CO_2$-increases, there are potentially important exceptions for precipitation in the subtropics and in the southern extra-tropics. (2) Adding an unaccounted cdnc-level strongly reduces the effects of aerosols on climate. A pre-requisite for estimating climate effects of anthropogenic aerosols is therefore that the natural conditions are accurately modelled. (3) A $CO_2$-increase shortens the atmospheric life-time of aerosols due to increased precipitation in major aerosol emission regions. This life-time reduction is larger for present-day (PD) aerosol emissions than for pre-industrial (PI). The aerosol cooling effect is thus reduced by the $CO_2$-increase as a feedback causing nonlinear reinforcement of the $CO_2$ driven global warming.

**Acknowledgments** This work is partly financed by the Research Council of Norway (NorClim and IPY Polarcat) and the EU project EUCAARI. The work is granted computer time by the Norwegian Research Council's Programme for Supercomputing. The authors are grateful for support and discussions with P. J. Rasch at NCAR and S. Ghan at PNNL.

## References

Andreae, M. O., Jones, C. D. and Cox, P. M. (2005) Strong present-day aerosol cooling implies a hot future. *Nature* **435**, 1187–1190.

Collins,W. D., Rasch, P. J., Boville, B. A., Hack, J. J., McCaa, J. R. and co-authors (2006) The Formulation and Atmospheric Simulation of the Community Atmospheric Model Version 3 (CAM3). *J. Climate* **19**, 2144–2161.

Forster, P., Ramaswamy, V., Artaxo, P., Berntsen, T., Betts, R. and co-authors. (2007) Changes in Atmospheric Constituents and in Radiative Forcing. In: *Climate Change 2007: The Physical Science Basis. Contribution of Working Group I to the Fourth Assessment Report of the Intergovernmental Panel on Climate Change* (Eds Solomon, S., Qin, D., Manning, M., Chen, Z., Marquis, M., Averyt, K. B., Tignor, M. and Miller, H. L.). Cambridge University Press, Cambridge, United Kingdom and New York, NY, USA.

Kirkevåg, A., Iversen, T., Seland, Ø., Debernard, J. B., Storelvmo, T. and Kristjansson,J.E. (2008) Aerosol-cloud-climate interactions in the climate model CAM-Oslo, *Tellus* **60A**, doi: 10.1111/j.1600-0870.2008.00313.x.

Seland, Ø and Iversen, T. (2007) Causes for spread between global models w.r.t. Lifetime and distribution of particulate sulphate. *Developments in Environmental Science*, **6,** (C. Borrego and E. Renner; Eds.). Elsevier Ltd. /DOI:10.1016/S1474-8177(07)06511-4.

Seland, Ø., Iversen, T., Kirkevåg, A. and Storelvmo, T. (2008) Aerosol climate interactions in the CAM-Oslo atmospheric GCM and investigation of associated basic shortcomings. *Tellus* **60A**, doi: 10.1111/j.1600-0870.2008.00318.x.

Storelvmo, T., Kristjansson, J.E., Lohmann, U. Iversen, T., Kirkevåg, A. and Ø. Seland (2008) Modeling the Wegener-Bergeron-Findeisen process – implications for aerosol indirect effects. *Environ. Res. Lett.* **3**. 045001. doi:10.1088/1748-9326/3/4/045001.

Solomon, S., D. Qin, M. Manning, and co-authors (2007) Technical Summary. In: *Climate Change 2007: The Physical Science Basis. Contribution of Working Group I to the Fourth Assessment Report of the Intergovernmental Panel on Climate Change* [Solomon, S., D. Qin, M. Manning, Z. Chen, M. Marquis, K.B. Averyt, M. Tignor and H.L. Miller (eds.)]. Cambridge University Press, Cambridge, United Kingdom and New York, NY, USA.

Stainforth, D. A., Aina, T., Christensen, C.., Collins, M., Faull, N. Frame, D.J., Kettleborough, J.A., Knight, S., Martin, A., Murphy, J.M., Piani, C., Sexton, D., Smith, L.A., Spicer, R.A., Thorpe, A.J., and Allen, M.R. (2005) Uncertainty in predictions of the climate response to rising levels of greenhouse gases. *Nature* **433**, 403–406.

# 6.5 Modelling the Impact of Climate Changes on PM Levels in Poland

**Katarzyna Juda-Rezler[1], Wojciech Trapp[2], and Magdalena Reizer[1]**

[1]Faculty of Environmental Engineering, Warsaw University of Technology, Warsaw, Poland

[2]Air Protection Unit of Ekometria, Gdańsk, Poland

**Abstract** For assessing the impacts of climate changes on PM levels we adopted, for the first time in Poland, the modelling system built with the CAMx model coupled with the RegCM3 regional climate model. The simulations were performed with very high resolution of 10 km for the modelling area of Central-Eastern Europe, centered over Poland. The modelling system was evaluated for the entire 2000 year of reference for which detailed emissions database was created. The predictions of $PM_{10}$ concentrations by the RegCM3/CAMx driven by the ECHAM5 global circulation model were of similar quality to those of the RegCM3/CAMx driven with the ERA40 global atmospheric reanalysis dataset. We obtained the NMSE in the predictions of annual $PM_{10} \leq 0.35$ and the IA > 0.5. Next the system was forced by the output of the ECHAM5 for the simulations covering present day and near future decadal time-slices. The anthropogenic emissions were kept unchanged. The results obtained suggest that the changes in $PM_{10}$ concentrations induced by climate changes in near future will be small to moderate and will not exceed –4.5 to 1.5 $\mu g/m^3$ for the Central-Eastern Europe.

**Keywords** Air quality modelling, Climate change, Particulate matter, Model evaluation, Poland

## 1. Introduction

Particulate matter (PM) and ozone ($O_3$) have currently become critical pollutants worldwide, with respect to human health and environment. Increased levels of $O_3$ and fine particulates ($PM_{2.5}$) can cause severe respiratory and cardiovascular diseases and increase the risk of death. Understanding the possible impacts of climate changes on future air quality is of key importance. Changes in climate and anthropogenic emissions of primary PM and its precursors are expected in the 21st century (IPCC, 2007).

In Poland particulate pollution is presently posing the most serious air pollution problem. The wintertime air pollution episodes due to PM occur in many urban

D.G. Steyn and S.T. Rao (eds.), *Air Pollution Modeling and Its Application XX*,
DOI 10.1007/978-90-481-3812-8, © Springer Science + Business Media B.V. 2010

locations. The most severe episodes were registered in January–February 2006, when $PM_{10}$ levels were extremely high, exceeding the EU daily limit value even 14 times. The highest daily $PM_{10}$ level equalled to 680 $\mu g/m^3$, while hourly levels reached up to 1,000 $\mu g/m^3$ (Juda-Rezler, 2006).

The main goal of this work is to assess the impact of climate changes on future air quality in Poland, with emphasis to PM levels. In Europe few operational regional chemistry transport models (CTM) are used for simulating PM. Model evaluation studies show that most models severely underestimate the observed $PM_{10}$ levels. In a recent PM modelling study performed for Northern Germany by Stern et al. (2008), five European CTM's were tested for a winter-spring period of 2003 with elevated $PM_{10}$ and $PM_{2.5}$ observations. It was shown that the current modelling systems are unable to simulate correctly higher $PM_{10}$ and $PM_{2.5}$ levels.

In this paper we are presenting results of PM simulations over Poland for reference year 2000 of present day as well as for near future decade. We implemented the modelling system consisting of CAMx model driven off-line by the regional climate model RegCM3.

## 2. Materials and Methods

The modelling system was built at Warsaw University of Technology (WUT modelling system) by coupling off-line Regional Climate Model RegCM3 with chemical-transport model CAMx and emission model EMIL developed at WUT.

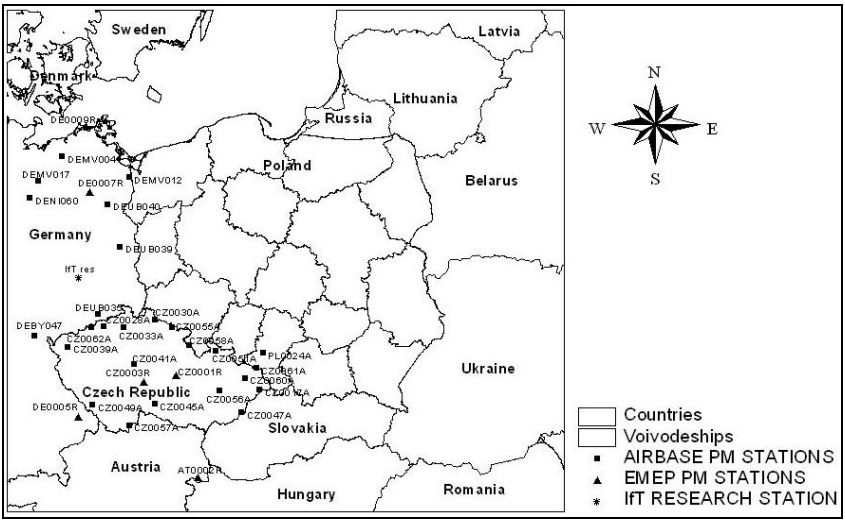


**Fig. 1.** The modelling domain with $PM_{10}$ rural background monitoring stations

The established modelling domain is centred over Poland (52.00°N, 19.30°E) and covers a part of Central-Eastern Europe (Fig. 1) on a grid with 120 × 109 points and a 10 km resolution. The map projection is Lambert conformal. The domain vertical profile contains 12 layers of varying thickness, extending up to 450 hPa.

The RegCM3 model of ICTP (International Centre for Theoretical Physics) with Grell convective scheme and Fritsch and Chappell closure assumption was applied. Beta version (RegCM3-β) developed for refined high resolution applications (Pal et al., 2007) was implemented. The air quality was simulated by the Comprehensive air quality model with extensions CAMx (version 4.40) from ENVIRON (http://www.camx.com).

The emission model EMIL (EMIssion modeL) was developed for Poland and coupled with RegCM3-β and CAMx models. Based on detailed emission sources inventory composed for reference year 2000 in 1 × 1 km resolution, meteorological data and terrain characteristics, the model generates $PM_{10}$, $PM_{2.5}$, $SO_2$, $NO_x$, $NH_3$ and NMVOC emissions from Large Combustion Plants (LCP) as well as gridded area emissions with 10 km resolution. The data on population density, sector-specific activity, fuel demand and characteristics as well as sector-dependent Polish specific emission factors were gathered. For the quantification of $NO_x$, NMVOC and PM emissions, the method proposed by Krüger et al. (2008) was used. For temporal distribution of emissions the EMIL model applies sector-specific monthly, daily and hourly emission factors.

Anthropogenic emissions for the parts of modelling domain not belonging to Poland were calculated with the emission model based on the UNECE/EMEP database for the year 2000, available in 50 km EMEP grid resolution. For every emission sector data were distributed to 10 km Lambert grid resolution (see Krüger et al., 2008 for details).

Two emission databases were prepared: (1) with all data introduced to CAMx as gridded emissions, and (2) with separate introduction of elevated point emissions. For the present study we applied the version 1 of the database (EMIL-v.1).

CAMx is coupled off-line to RegCM3-β with a FORTRAN-based code interface, which calculates all the meteorological fields required by CAMx as well as biogenic emissions. The boundary conditions (BC) were obtained from the results of European simulations performed within the framework of the EU project CECILIA (http://www.cecilia-eu.org): chemical BC – from 50 km RegCM3/CAMx; meteorological BC – from 25 km RegCM3 driven by ECHAM5.

## 3. Results

### 3.1. Simulations for the 2000 year of reference

For validation purposes RegCM3-β/EMIL-v.1/CAMx system was run for the entire 2000 year using two different meteorological forcing to constrain RegCM3-β: the ERA40 global atmospheric reanalysis dataset and the output from the ECHAM5

global circulation model. These two runs will be referred to hereafter as ERA and ECHAM runs, respectively.

Both runs were compared and validated for $PM_{10}$ concentrations using observation from the EMEP (http://www.emep.int) and EIONET-Airbase (http:// air-climate. eionet.europa.eu) databases. Only rural background stations fulfilling $PM_{10}$ data completeness requirements were considered. It should be noted, that the distribution of $PM_{10}$ sites in the domain is very uneven: for Poland there was only one $PM_{10}$ site in 2000 (see Fig. 1).

The validation results are given in Table 1. They indicate quite satisfactory overall model performance for both runs. Modelling system driven by ECHAM5 performs at least as well as does standard retrospective modelling (ERA run). In general the system tends to underestimate long-term observations.

**Table 1.** Validation results of modelling system for ERA and ECHAM runs for reference year 2000

| Statistical measures<br>Number of stations, N = 33 | RegCM3-β/EMIL-v.1/CAMx | |
|---|---|---|
| | ERA run | ECHAM run |
| NMB – Normalized Mean Bias (%) | 33.74 | 35.21 |
| NMSE – Normalized Mean Square Error | 0.35 | 0.31 |
| IA – Index of Agreement | 0.51 | 0.58 |
| Predictions within factor 2 of the observations (%) | 78.80 | 75.80 |

During winter season the modelling system is performing better than in spring/ summer seasons. It is also able (in opposite to the CTM's tested in recent study by Stern et al., 2008) to capture quite well the high concentrations. This is most likely a result of detailed emission inventory employed in the EMIL model.

### 3.2. Simulations for present day and near future climate

A satisfactory validation of ECHAM run of WUT modelling system allow for using this system with predictions of future climate. Two decadal time-slices: present day (1991–2000) and near future (2041–2050) were simulated, with all model parameterizations and anthropogenic emissions remained unchanged. For the future decade the ECHAM5 model was forced by the SRES-A1B IPCC scenario.

The results presented in Fig. 2 show that annual mean $PM_{10}$ concentrations in near future are close to these for present day.

For the Central-Eastern Europe the differences do not exceed –4.5 to 1.5 $\mu g/m^3$. The highest decrease in $PM_{10}$ levels are expected in Eastern Poland as well as in Belarus, Northern Ukraine and great part of Lithuania.

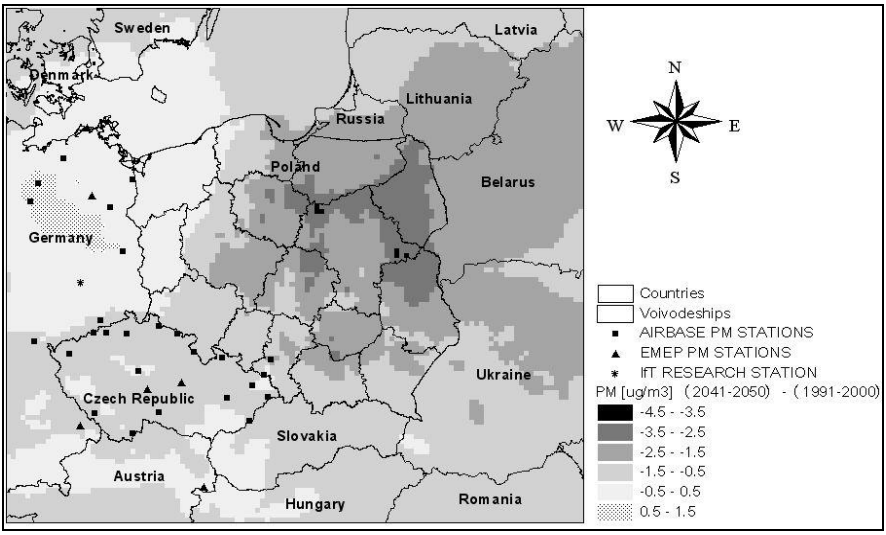


**Fig. 2.** Differences in annual $PM_{10}$ concentrations between present day (1991–2000) and near future (2041–2050) time-slices

## 4. Conclusions

The overall performance of RegCM3-β/EMIL-v.1/CAMx modelling system is quite satisfactory, with statistical measures similar for ECHAM and ERA runs. The system is underpredicting observations, however it is able to capture elevated $PM_{10}$ levels quite well. We believe that this is a result of detailed emission inventory and country-specific emission factors employed in the emission model.

The $PM_{10}$ levels predicted for near future decade (2041–2050) show small to moderate differences compared to present day decade (1991–2000). These results suggest that impacts of climate changes on $PM_{10}$ levels in near future will not be significant and that the concentrations will slightly decrease for the majority of Central-Eastern Europe. It is very likely that this decrease is due to increased precipitation in near future time-slice.

Future work will focus on determining the cause of $PM_{10}$ underpredictions as well as poor model performance for spring/summer. Also we will employ the EMIL-v.2 emission model with elevated point sources.

**Acknowledgments** This work was supported by the Central and Eastern Europe Climate Change Impact and Vulnerability Assessment Project (CECILIA), financed by EU 6. FP Contract GOCE 037005 to Warsaw University of Technology, Warsaw, Poland.

## References

IPCC, 2007: Climate Change 2007. The Physical Science Basis, 996 pp., Cambridge Univ. Press, New York, 2007.

Juda-Rezler, K., 2006: Assessing the Winter Time Air Pollution in Cracow (Poland) in Relation with Possible Influences on Human Health and Cultural Heritage. *Pol. J. Env. Stud.*, **15 (5c)**, 123–128.

Krüger, B.C. et al., 2008: Regional photochemical model calculations for Europe concerning ozone levels in a changing climate. *Q. J. Hung. Meteor. Serv.,* **112**, No. 3–4, 285–300.

Pal, J. S. et al., 2007: Regional climate modelling for the developing world: The ICTP RegCM3 and RegCNET. *B. Am. Meteorol. Soc*., **88**, 1395–1409.

Stern, R.M. et al., 2008 : A model intercomparison study focussing on episodes with elevated PM10 concentrations. *Atmos. Env.*, **42**, 4567–4588.

## 5. Questions and Answers

**S. Andreani-Aksoyoglu:** We had very high PM concentrations in January–February 2006 as you had in Poland. Is it possible that some part of PM came from Poland? Did you look at some trajectories?

**Answer:** No, we did not look at trajectories. However, this high winter PM concentrations in Poland were mainly due to extremely low air temperatures (up to −27°C) which had caused intensive heating of houses by burning coal (as well as wastes probably) in domestic sector. Thus, as it was “low emission” it is almost impossible that this emission was transported to Switzerland.

# 6.6 Regional Climate Change Impacts on Air Quality in High Resolution

**Tomas Halenka, Peter Huszar, and Michal Belda**

Charles University, Department of Meteorology and Environment Protection,
V Holesovickach 2, 180 00 Prague, Czech Republic

**Abstract** The coupling of regional climate model and chemistry/aerosol model has been performed recently on the Department of Meteorology and Environmental Protection, Faculty of Mathematics and Physics, Charles University in Prague, for the EC 6FP Project QUANTIFY and finally for EC 6FP Project CECILIA. One objective of the latter, aiming to study climate change impacts in Central and Eastern Europe based on very high resolution simulations using regional climate models (RCM) in 10 km grid, is dealing with climate change impacts on air quality. Chemistry is solved by model CAMx which is coupled to model RegCM. As the first step, the distribution of pollutants is simulated off-line for four time slices of 10 years in the model couple. Period of 1991–2000 driven by reanalysis ERA40 is used for validation whereas control run 1991–2000 driven by global model ECHAM5 is used for comparison basis and estimate of systematic error imposed by GCM, future time slices 2041–2050 and 2091–2100 provide the information on climate change impact on future air quality. The comparison to the driving simulations in 50 km resolution shows the benefit of high resolution runs in more detailed description of emissions and surface processes.

**Keywords** Regional climate modeling, air-quality modeling, climate change impact on air quality

## 1. High Resolution Modelling and Air Quality

In many applications, particularly related to the assessment of climate-change impacts, the information on surface climate change at regional to local scale is fundamental and that is Global Circulation Models (GCMs) can hardly reproduce reasonably well. Thus, dynamical downscaling, i.e., nesting of a fine scale limited area model (or Regional Climate Model, RCM) within the GCM is the most convenient tool taking into account processes critically affected by topography and land use at high resolution in this kind of studies and especially when aiming

D.G. Steyn and S.T. Rao (eds.), *Air Pollution Modeling and Its Application XX*,
DOI 10.1007/978-90-481-3812-8, © Springer Science + Business Media B.V. 2010

the interactions of climate and air-quality issues. In the region of Central and Eastern Europe (CEE) the need for high resolution studies is particularly important, that is why 10 km resolution has been introduced in the EC FP6 project CECILIA. The main aim of the project dealing with climate change impacts and vulnerability assessment in targeted areas of CEE is the application of regional climate modelling studies at a resolution of 10 km for local impact studies in key sectors of the region. The project is covering studies on hydrology, water quality and water management, agriculture and forestry as well as air quality issues in urban and industrialized areas (e.g. Black Triangle – a polluted region around the common borders of the Czech Republic, Poland and Germany).

The concentration of air pollutants depends on both anthropogenic and climate factors. However, in this study the anthropogenic emission are kept for all the time slices at the values of year 2000 to study climate effects. Longer range transport to the target regions is taken into account from simulation for the whole Europe using RCM with the resolution of 50 × 50 km. These simulations are used to constrain nested higher resolution runs (10 × 10 km) focusing in CEE both for present and future climate. The key species are ozone, sulphur, nitrogen and PM, which have a central role in tropospheric chemistry as well as the strong health impacts.

It is now well established that climatically important (radiatively active) gases and aerosols can have substantial climatic impact trough their direct and indirect effects on radiation, especially on regional scales (Qian and Giorgi, 2000; Qian et al., 2001; Giorgi et al., 2002). To study these effects requires coupling of regional climate models with atmospheric chemistry/aerosols to assess the climate forcing to the chemical composition of the atmosphere and its feedback to the radiation, eventually other components of the climate system. In this study climate is calculated using model RegCM while chemistry is solved by model CAMx. The model RegCM was originally developed and further improved by Giorgi et al. (1999) or later see e.g. in Pal et al. (2007). For more details on the use of the model see Elguindi at al. (2006).

CAMx is an Eulerian photochemical dispersion model developed by ENVIRON Int. Corp. (Environ, 2006). In version 4.40 CAMx is used for air quality modeling here, with CB-IV gas phase chemistry mechanism option, wet deposition of gases and particles. It uses mass conservative and consistent transport numerics in parallel processing. It allows for integrated “one-atmosphere” assessments of gaseous and particulate air pollution (ozone, PM2.5, PM10, air toxics) over many scales ranging from sub-urban to continental. CAMx simulates the emission, dispersion, chemical reactions and removal of pollutants in the troposphere by solving the pollutant (eulerian) continuity equation for each chemical species on a system of nested three-dimensional grids. These processes are strongly dependent on the meteorological conditions, therefore CAMx requires meteorological input from a NWP model or RCM for successful run.

## 2. Settings and Results

Meteorological fields generated by RegCM drive CAMx transport and dry/wet deposition. Briefly, a preprocessor utility was developed which takes RegCM's outputs and convert them to fields and formats accepted by CAMx. There are problems with the anthropogenic emission inventories available, at this stage emissions from EMEP 50 × 50 km database are interpolated. Biogenic emissions of isopren and monoterpenes are calculated as a function of 2 m temperature, global radiation and land-use by Guenther et al. (1993, 1994). We use 23 vertical $\sigma$-levels reaching up to 70 hPa at 10 km of resolution for RegCM configuration, the same horizontal grid for CAMx. Initial and boundary conditions are taken from 50 km resolution run for whole Europe by Krueger et al. (2008) or Katragkou et al. (2009). In our setting CB-IV chemistry mechanism is used (Gery et al., 1989). As the first step, the distribution of pollutants is simulated off-line for four time slices of 10 years in the model couple. Period of 1991–2000 driven by reanalysis ERA40 is used for validation whereas control run 1991–2000 driven by global model ECHAM5 is used for comparison and estimate of systematic error imposed by GCM, future time slices 2041–2050 and 2091–2100 provide the information on climate change impact on future air quality.

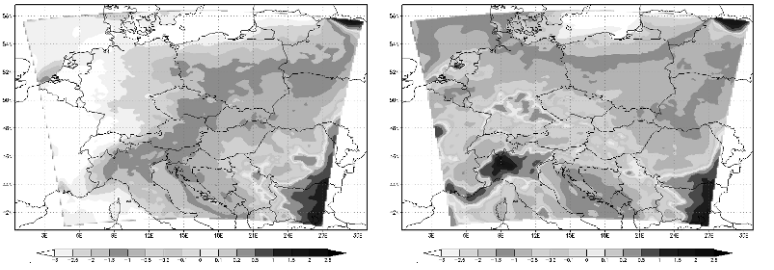

**Fig. 1.** Climate change impact on summer season ozone concentration (in ppbv) in terms of the difference for 2041–2050 period (left panel) and 2091–2100 period (right panel) against the control period 1991–2000

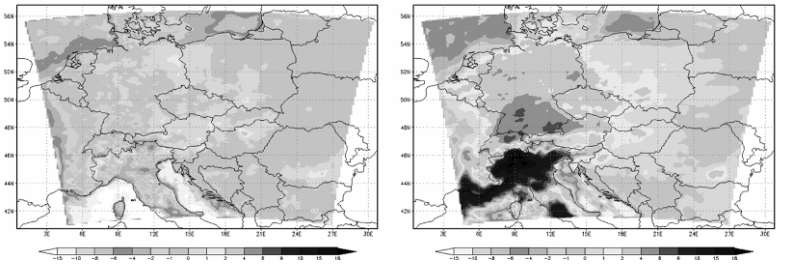

**Fig. 2.** Climate change impact on number of days with 8-h ozone concentration above the threshold of 120 μg in terms of the difference for 2041–2050 period (left panel) and 2091–2100 period (right panel) against the control period 1991–2000

Examples of the high resolution integration for all the time slices are presented in Fig. 1 for selected species. There is much more local features seen in these simulations compare to less resolution run (not shown), especially for ozone the effect of high resolution land use which provides basis for biogenic emission computation is well pronounced in the concentration fields, even more in summer (with respect to limited extent not shown again). The development of the impact on air quality can be seen not only in term of the concentration changes but e.g. in terms of number of days with exceedance of certain threshold shown in Fig. 2.

**Acknowledgments** This work is supported in framework of EC FP6 STREP CECILIA (GOCE 037005), partially by EC FP6 Integrated project QUANTIFY (GOCE 003893) as well as under local support of the grant of Programme Informacni spolecnost, No. 1ET400300414 and Research Plan of MSMT under No. MSM 0021620860.

## References

Elguindi, N., X. Bi, F. Giorgi, B. Nagarajan, J. Pal, F. Solmon, S. Rauscher, A. Zakey, 2006: RegCM Version 3.1 User's Guide. PWCG Abdus Salam ICTP.

ENVIRON Corp., 2006: CAMx Users' Guide, version 4.40

Gery, M.W., G.Z. Whitten, J.P. Killus, and M.C. Dodge. 1989: A Photochemical Kinetics Mechanism for Urban and Regional Scale Computer Modeling. J. Geophys. Res., 94, 925–956.

Giorgi, F., X. Bi, Y. Qian, 2002: Direct radiative forcing and regional climatic effects of anthropogenic aerosols over East Asia: A regional coupled climate-chemistry/aerosol model study. J. Geophys. Res., 107, 4439, doi:10.1029/2001JD001066.

Giorgi, F., Y. Huang, K. Nishizawa and C. Fu, 1999: A seasonal cycle simulation over eastern Asia and its sensitivity to radiative transfer and surface processes. Journal of Geophysical Research, 104, 6403–6423.

Guenther, A.B., Zimmerman, P.R., Harley, P.C., Monson, R.K., and Fall, R., 1993: Isoprene and monoterpene rate variability: model evaluations and sensitivity analyses, J. Geophys. Res., 98, No. D7, 12609–12617.

Guenther, A. , Zimmerman, P., and Wildermuth, M., 1994: Natural volatile organic compound emission rate estimates for U.S. woodland landscapes, Atmospheric Environment, 28, 1197–1210.

Katragkou, E., P. Zanis, I. Tegoulias, D. Melas, 2009: Tropospheric ozone in regional climate-air quality simulations over Europe: Future climate and sensitivity analysis. Proceedings 30th NATO/SPS International Technical Meeting on Air Pollution Modelling and its Application.

Krüger B. C., E. Katragkou, I. Tegoulias, P. Zanis, D. Melas, E. Coppola, S. Rauscher, P. Huszar and T. Halenka, 2008: Regional decadal photochemical model calculations for Europe concerning ozone levels in a changing climate, Quarterly J. of the Hungarian Meteorol. Service, Idojaras, 112, 3–4, 285–300.

Pal, J. S., F. Giorgi, X. Bi, N. Elguindi, F. Solmon, X. Gao, S. A. Rauscher, R. Francisco, A. Zakey, J. Winter, M. Ashfaq, F. S. Syed, J. L. Bell, N. S. Diffenbaugh, J. Karmacharya, A. Konaré, D. Martinez, R. P. da Rocha, L. C. Sloan, and A. L. Steiner, 2007: Regional Climate Modeling for the Developing World: The ICTP RegCM3 and RegCNET. Bull. Amer. Meteorol. Soc., 88, 9, 1395–1409.

Qian, Y., F. Giorgi, 2000: Regional climatic effects of anthropogenic aerosols? The case of Southwestern China, Geophys. Res. Lett., 27(21), 3521–3524, 10.1029/2000GL011942.

Qian, Y., F. Giorgi, Y. Huang, W.L. Chameides, and C. Luo, 2001: Simulation of anthropogenic sulfur over East Asia with a regional coupled chemistry/climate model. Tellus, Ser. B, 53, 171–191.

# Chapter 7 Air quality and human health

Chairperson: J. Baldasano

Rapporteur: P. Lee

D.G. Steyn and S.T. Rao (eds.), *Air Pollution Modeling and Its Application XX*,
DOI 10.1007/978-90-481-3812-8_7, © Springer Science + Business Media B.V. 2010

# 7.1 Air Pollution and Human Health: From Local to Global Issues

**Bert Brunekreef**

Professor of Environmental Epidemiology, Institute for Risk Assessment Sciences, Utrecht University, The Netherlands, P.O. Box 80176 3508 TD Utrecht, The Netherlands

## 1. Introduction

Air pollution from fossil fuel combustion has been known to affect human health for centuries. More detailed insights developed in the 20th century, as a result of studies prompted by severe air pollution episodes such as those in the Meuse Valley, Belgium in 1930, and London, UK in 1952. In the Meuse Valley, stagnant weather conditions prevented local, industry-generated pollutants from dispersing during several days in December 1930 (1). Several dozens of people died suddenly, and the episode attracted worldwide attention. In December 1952, stagnant weather conditions prevented local pollution dominated by coal smoke from dispersing in London, UK. It was initially estimated that some 4,000 people died as a result, but later estimates, taking into account delayed effects in the following months, put the figure at perhaps as high as 10,000 (2). In the second part of the 20th century, pollution abatement measures were taken in many developed countries as a result of these dramatic events, and urban pollution levels declined. Emphasis shifted to secondary pollutants formed in the atmosphere as a result of chemical reactions, notably ozone and fine particles. Many studies have been published on the health effects of these pollutants, showing that day-to-day variations in their levels are associated with adverse health outcomes including mortality even at very low levels of exposure. For ozone, the associations with mortality are a relatively recent finding that was confirmed by three independent reviews (3–5). Associations between particulate matter and health have been reported from many areas (6). This review discussed six dimensions of associations between ambient PM and health: (1) short term exposure and mortality; (2) long term exposure and mortality; (3) time scales of exposure; (4) the shape of the concentration-response function; (5) cardiovascular disease; and (6) biological plausibility.

## 2. Health Effects of Air Pollution in Asia

Although most studies published so far are from developed countries, there is an increasing flow of publications coming from developing parts of the world where

D.G. Steyn and S.T. Rao (eds.), *Air Pollution Modeling and Its Application XX*,
DOI 10.1007/978-90-481-3812-8, 

air pollution levels are often still higher than in developed countries. The remainder of this paper will focus on such studies, notably on studies conducted in Asia.

### 2.1. Health effects of indoor exposure to biomass and coal smoke

It has long been known that indoor exposure to biomass fuel combustion products may be very high in developing countries. Recent reviews include (7). Early reviews (8) drew attention to the fact that, at that time, more than half of the world population was probably exposed to high levels of indoor pollution from biomass burning, with severe consequences. The WHO Global Burden of Disease project recently estimated that in the developing world, 1,619,000 young children die every year from acute respiratory infections worsened by indoor biomass smoke exposure (9). A review focused on acute respiratory infections in children documents the high burden of illness and death from this disease alone in relation to indoor biomass combustion product exposure in developing countries (10). Measurements using state of the art technology have confirmed that indoor PM levels can be extremely high in households using biomass for heating and cooking fuel. Levels of many hundreds of $\mu g/m^3$ have been observed regularly, and such levels are much higher than outdoor PM levels even in highly polluted megacities (11).

Quite recently, it has been shown that rural women living in south China have higher indoor PM exposures than urban women, and have more chronic obstructive pulmonary disease (COPD) as a consequence (12).

### 2.2. Health effects of urban and industrial pollution in Asia

We now come to studies which are more generally about health effects of urban and industrial air pollution on urban populations. As mentioned, the Health Effects Institute Public Health and Air Pollution in Asia program reviewed a large number of pertinent studies from Asia. Most of these were conducted in China, India, South Korea and Japan. Generally, studies from Asia have documented similar adverse health effects of air pollution as studies conducted in Europe and North America, despite large differences in pollution levels and demography. Some recent examples will be discussed below.

Several early time series studies covering the 1989–1990 period in Beijing documented increases in daily mortality and hospital admissions with increasing $SO_2$ and PM levels (measured as TSP) which ranged up to 400 and 900 $\mu g/m^3$, respectively (13). A much more recent study from Shanghai, covering the March 2004–December 2005 period, found evidence of a relationship between daily fluctuations in PM2.5 and all-cause, cardiovascular and respiratory mortality (14). PM2.5 levels were 56 $\mu g/m^3$ on average, and ranged from 8 to 235 $\mu g/m^3$. The authors also investigated the effect of coarse particles with a size range between 2.5 and 10 $\mu m$ and could not demonstrate any effect (14). This observation is in line with a recent review on the topic of coarse PM effects (15). In China, a respiratory health study was conducted in the three cities of Lanzhou, Wuhan and Guangzhou with different air pollution levels. Respiratory health parameters of

parents and children were measured, and significant and strong effects of air pollution, by district, were found on prevalence rates of cough, phlegm, persistent cough and phlegm, and wheeze for both the mothers and the fathers. In addition, the odds ratios increased as ambient total suspended particle concentration increased across the three urban districts (16). There was also a positive and significant association between total suspended particle levels and the adjusted odds ratios for cough, phlegm, hospitalization for diseases, and pneumonia in children. Furthermore, parental smoking status was associated with cough and phlegm, and use of coal in the home was associated only with cough prevalence (17). A study from Beijing found significant associations between $SO_4^{2-}$ concentration and total mortality and mortality due to cardiovascular disease, malignant tumour and lung cancer ($r > 0.50$ in all cases) (18). The correlations were found not only between the current $SO_4^{2-}$ concentration and these mortalities, but also for $SO_4^{2-}$ levels measured up to 12 years prior to death, suggesting long-term effects of air pollution. No significant associations were observed for mortality from respiratory diseases and cerebrovascular diseases ($r = 0.30–0.50$). This study indicates that the concentration of $SO_4^{2-}$ in air is a useful air pollution indicator in areas where coal is used as the main source of energy. Areas with high levels of $SO_4^{2-}$ experienced higher mortality owing to a variety of chronic diseases.

The HEI PAPA project has now produced its first published papers (19–22). In the cities of Hong Kong, Wuhan, Shanghai (all China) and Bangkok, Thailand, PM10, $SO_2$, $NO_2$ and Ozone were all found to be associated with day-to-day variations in mortality, with effect estimates being equal to or larger than those reported from North America and Europe (22). In most analyses, there was little indication of a threshold concentration below which no effects on mortality were seen. Effects were larger in economically more deprived cities (Wuhan and Bangkok) which was attributed to populations being less able to protect themselves from high exposures. In Wuhan, there was also a clear interaction between pollution and temperature, pollution effects being higher on high temperature days (19). Within the Hong Kong population, effects were also shown to be larger for populations living in economically more deprived areas (21).

## 3. Concluding Remarks

Air pollution has negative effects on the health of populations worldwide. New studies from Asia suggest that short-term variations in PM and several gaseous pollutants are associated with short-term variations in mortality, with effect estimates being as high as or higher than those reported from North America or Europe. Studies on effects of long-term exposure to air pollution are still scarce in Asia, and conducting such studies is a priority and a challenge for the near future. A large fraction of the world population lives in China, India and other rapidly developing economies in Asia with associated large increases in energy production and consumption. Air pollution emissions are high, producing widespread

"atmospheric brown clouds" with negative impacts on air quality at very large distances from the main source areas (23). It will be a major challenge to reduce the negative environmental effects of the economic development needed to provide better standards of living in this part of the world.

## References

Nemery B, Hoet PH, Nemmar A. The Meuse Valley fog of 1930: an air pollution disaster. Lancet. 2001 Mar 3;357(9257):704–8.

Bell ML, Davis DL, Fletcher T. A retrospective assessment of mortality from the London smog episode of 1952: the role of influenza and pollution. Environ Health Perspect. 2004 Jan;112(1):6–8.

Bell ML, Dominici F, Samet JM. A meta-analysis of time-series studies of ozone and mortality with comparison to the national morbidity, mortality, and air pollution study. Epidemiology. 2005 Jul;16(4):436–45.

Ito K, De Leon SF, Lippmann M. Associations between ozone and daily mortality: analysis and meta-analysis. Epidemiology. 2005 Jul;16(4):446–57.

Levy JI, Chemerynski SM, Sarnat JA. Ozone exposure and mortality: an empiric bayes metaregression analysis. Epidemiology. 2005 Jul;16(4):458–68.

Pope CA, 3rd, Dockery DW. Health effects of fine particulate air pollution: lines that connect. J Air Waste Manag Assoc. 2006 Jun;56(6):709–42.

Emmelin A, Wall S. Indoor air pollution: a poverty-related cause of mortality among the children of the world. Chest. 2007 Nov;132(5):1615–23.

Chen BH, Hong CJ, Pandey MR, Smith KR. Indoor air pollution in developing countries. World Health Stat Q. 1990;43(3):127–38.

Ezzati M, Kammen DM. The health impacts of exposure to indoor air pollution from solid fuels in developing countries: knowledge, gaps, and data needs. Environ Health Perspect. 2002 Nov;110(11):1057–68.

Smith KR, Samet JM, Romieu I, Bruce N. Indoor air pollution in developing countries and acute lower respiratory infections in children. Thorax. 2000 Jun;55(6):518–32.

Balakrishnan K, Sankar S, Parikh J, Padmavathi R, Srividya K, Venugopal V, et al. Daily average exposures to respirable particulate matter from combustion of biomass fuels in rural households of southern India. Environ Health Perspect. 2002 Nov;110(11):1069–75.

Liu S, Zhou Y, Wang X, Wang D, Lu J, Zheng J, et al. Biomass fuels are the probable risk factor for chronic obstructive pulmonary disease in rural South China. Thorax. 2007 Oct;62 (10):889–97.

Xu X, Gao J, Dockery DW, Chen Y. Air pollution and daily mortality in residential areas of Beijing, China. Arch Environ Health. 1994 Jul-Aug;49(4):216–22.

Kan H, London SJ, Chen G, Zhang Y, Song G, Zhao N, et al. Differentiating the effects of fine and coarse particles on daily mortality in Shanghai, China. Environ Int. 2007 Apr;33(3):376–84.

Brunekreef B, Forsberg B. Epidemiological evidence of effects of coarse airborne particles on health. Eur Respir J. 2005 Aug;26(2):309–18.

Zhang J, Qian Z, Kong L, Zhou L, Yan L, Chapman RS. Effects of air pollution on respiratory health of adults in three Chinese cities. Arch Environ Health. 1999 Nov-Dec;54(6):373–81.

Qian Z, Chapman RS, Tian Q, Chen Y, Lioy PJ, Zhang J. Effects of air pollution on children's respiratory health in three Chinese cities. Arch Environ Health. 2000 Mar-Apr;55(2):126–33.

Zhang J, Song H, Tong S, Li L, Liu B, Wan L. Ambient sulfate concentration and chronic disease mortality in Beijing. Sci Total Environ. 2000 Oct 30;262(1–2):63–71.

Qian Z, He Q, Lin HM, Kong L, Bentley CM, Liu W, et al. High Temperatures Enhanced Acute Mortality Effects of Ambient Particle Pollution in the "Oven" City of Wuhan, China. Environ Health Perspect. 2008;116:1172–8.

Vichit-Vadakan N, Vajanapoom N, Ostro B. The Public Health and Air Pollution in Asia (PAPA) Project: Estimating the Mortality Effects of Particulate Matter in Bangkok, Thailand. Environ Health Perspect. 2008;116:1179–82.

Wong CM, Ou CQ, Chan KP, Chau JK, Thach TQ, Yang L, et al. The Effects of Air Pollution on Mortality in Socially Deprived Urban Areas in Hong Kong, China. Environ Health Perspect. 2008;116:1189–94.

Wong CM, Vichit-Vadakan N, Kan H, Qian Z. Public Health and Air Pollution in Asia (PAPA): A Multicity Study of Short-Term Effects of Air Pollution on Mortality. Environ Health Perspect. 2008;116:1195–202.

Lelieveld J, Crutzen PJ, Ramanathan V, Andreae MO, Brenninkmeijer CAM, Campos T, et al. The Indian Ocean Experiment: Widespread air pollution from South and Southeast Asia. Science. 2001 Feb 9;291(5506):1031–6.

## 4. Questions and Answers

**Christian Reuter:** Increase in life expectancy in US study related to decrease in PM2.5 – could it be other factors?

**Answer:** Investigators tried to adjust for other known factors influencing life expectancy, but only had indirect data on smoking. So further studies are needed to corroborate this finding.

**Katarzyna Juda-Rezler:** EU health impact studies are based on US cohort, Pope et al. studies. Is this reasonable?

**Answer:** Whereas there may be differences between Europe and US in terms of pollution and population, both are highly developed regions with similar pollution sources and lifestyles. Also, European cohort studies are starting to emerge that by and large show similar findings.

**M. Sofiev:** Is the association between PM and health effects causal, or could it be due to other pollutants and/or social factors?

**Answer:** In observational studies, there always remains a possibility that other factors are responsible for the associations seen. However, especially the associations between PM and health effects have been re-analyzed and scrutinized likke no others, and there is now much support for causality also from experimental studies.

**Unknown:** PM episodes are clearly associated with increases in mortality, hospital admissions etc; but are these really extra cases or just cases advenced in time by a few days or weeks?

**Answer:** This is called ‘harvesting’, and has received much attention in the epidemiological literature. Generally, it appears that cases are not just advanced by a few days or weeks, but that they are truly extra cases in the timeframe of months or a few years.

# 7.2 Computational Scheme Accounting for Heterogeneous Surface Emissions in CTMs

**Myrto Valari and Laurent Menut**

Laboratoire de Météorologie Dynamique/IPSL 91128 Palaiseau, France

**Abstract** Chemistry transport models (CTMs) have been widely used for urban air-quality forecast over the last 10 years but rarely for human exposure studies or health impact assessment (HIA). Exposure models require information on pollutant concentration at the neighborhood scale (sub-kilometer resolution). High resolution modelling applications may look appealing but their high computational cost makes them inappropriate for this purpose. Spatio-temporal analysis of monitor data is used in most cases in exposure studies (Georgopoulos et al., 2005). On the other hand, traditional HIA methods use area-aggregated monitor data. Not taking into account the spatial variability of pollutant concentrations has been shown to lead to significant bias in health risk estimates in HIA methods (Smith, 1997). It becomes clear that CTMs should adapt to the needs of such studies and provide information on small scale concentration variability.

We applied an emission scheme to the CHIMERE CTM that allows to extract information on the variability of pollutant concentrations at sub-grid scale. The application is based on the split of grid-averaged emission into separate contributions of emitting activities co-existing over the same grid-cell area (e.g. traffic transportation, residential emissions, etc.). Different concentrations are calculated for each emission scenario allowing the evaluation of concentration variability between source-specific areas inside grid-cells. The advantage of the application is that modelled concentrations are directly associated to human-activities during the day and are therefore, easily adapted to human exposure models.

**Keywords** Urban air-quality, heterogeneous emissions, small-scale pollutant variability

## 1. Methodology

In cities people live and move over areas of highly variable pollutant concentration fields. This variability is due, at a large degree, to heterogeneous surface emissions. In common CTMs small scale emission variability is not accounted for since emissions are averaged over grid-cell areas, beforehand. However, grid resolution is of some square kilometers and sub-grid scale effects have been proved to

D.G. Steyn and S.T. Rao (eds.), *Air Pollution Modeling and Its Application XX*,
DOI 10.1007/978-90-481-3812-8, 

modify grid-averaged concentrations leading to biased model results (Krol, 2000). A first approach may be a deterministic downscaling to higher resolution. It has been shown that uncertainties, including emission and meteorological input, accumulate at high resolutions and model error may increase with resolution (Valari and Menut, 2008). Sub-grid scale parametrizations have been proposed to account for the impact of the unresolved scale on Reynolds average fields (Vinuesa and de Arellano, 2005; Galmarini, 2007). However, these applications may model concentration variability but they do not provide direct information on what the 'real' concentration would be over specific areas inside grid-cells.

In the present study we propose a computational scheme that allows the estimation of concentrations over micro-environments inside grid-cells, where specific emission activity dominates. Fractional land-use data were used to divide grid-cell areas into source-specific emission surfaces (e.g. roads, residential districts, parks, etc.). Furthermore, we calculated the contribution of each different emission activity in the grid-averaged flux by using emission data at sub-grid scale. The separate contributions are then mapped on the sub-grid emission surfaces creating a set of emission scenarios. Each scenario is accounted for individually during the CTM simulation leading to a set of concentrations for all of model species. Modelled concentrations, under the influence of each scenario represent concentrations over sub-grid surfaces. The variability of pollutant concentrations around the commonly modelled grid-averaged concentration can be expressed as the standard deviation of the concentrations over the considered micro-environments.

The described methodology is based on the consideration than urban chemistry is faster than the mixing of emissions over grid-cell surfaces. Emitted species over each source-specific surface are therefore, not diluted in the entire grid-cell volume. Air mass is transported from the neighboring cells inside each micro-environment, where it comes in contact with local emissions. Chemical transformations take place before emissions are mixed. This treatment is particularly advantageous in what concerns fast chemical reactions such as NO oxidation by $O_3$. At the urban environment high NOx emissions are released over the traffic network. Under the common CTM assumption of instant and homogeneous mixing $O_3$ consumption in the $O_3$ + NO reaction is overestimated because grid-cell surface is larger than the corresponding emission surface.

The method was validated in an idealized case. It is commonly argued that 1 km is the lower limit of validity for CTMs. In practice, however, and due to the high computational time and uncertainties in input data, the large majority of urban air-quality models run at lower resolution (~3 km). We created a simulation domain of 1 km resolution centered around an emission domain typical of the urban environment. We considered that at 1 km grid-cell size emission surfaces may be represented by a single activity such as traffic, residential, parks or industrial. A first simulation is ran over the domain resolving explicitly emissions variability at 1 km. The obtained variability in modelled concentrations is thus considered to be the maximal variability that a CTM can represent over a city.

At a second stage, we run a simulation over the same domain but at lower resolutions (3, 6 and 12 km). Instead of averaging emission fluxes at the coarser

resolution cells, as is done in the usual CTM modelling, we applied the proposed emission scheme. We thus model pollutant concentrations implicitly over the sub-grid areas assigned as 'roads', 'residential', parks and 'industrial'. The implicit calculation of concentration variability is compared to the explicitly resolved one at all resolutions.

## 2. Results

The comparison showed that for primary emitted species ($NO_2$ and PM10) the emission scheme is able to reproduce concentrations over the sub-grid environments that are very close to the concentrations modelled explicitly at 1 km resolution. The variability represented by the implicit calculation reaches the 90% of the variability resolved by the model at 1 km. For secondary species (i.e. ozone), the implicit calculation underestimates more significantly the variability resolved by the model at 1 km (~70% of the 1 km variability is represented). However, the model is able to dissociate the fast ozone depletion in the traffic environment from a state closer to the photo-stationary equilibrium over the residential micro-environment.

The stability of the calculation, with regards to the model time-step, was tested and it was shown that modelled variability was not affected by this parameter. This means that inside each micro-environment modelled concentrations reach a steady-state before getting mixed to the grid-averaged value. We also tested the effect of the wind speed ant the intensity of turbulence on modelled variability. It was shown that in both cases (implicit and explicit calculation) modelled variability behaved in the same manner towards changes in wind speed and the boundary layer height.

Finally the emission scheme was used in a real-case simulation during the summer 2006 (1 June–31 August) over the city of Paris and model results were compared with measurements. This validation over real data was focused in the comparison of modelled concentrations over the 'traffic' or the 'residential' environments with measurements at stations co-existing inside the same grid-cell and characterized by the local air-quality network as 'traffic' or 'background' respectively. First of all we show that for primary species ($NO_2$ and PM10) the recombination of sub-grid concentrations to a 'grid-averaged' value provides practically the same concentration as the 'usual' model calculation. This means that any the extracted information on concentration variability is a clear 'gain' since the mean concentration remains unaltered. For ozone the difference between the recombined mean concentration and the 'standard' grid-averaged value can go up to 10%. This is due to the non-linear aspect of ozone chemistry.

The comparison of modelled results with measurements showed that the emission scheme is able to generate concentration fluctuations around the grid-averaged value that are in all cases closer to the measurement at the corresponding

micro-environment than the 'standard' model output. An example of this kind of comparison for $NO_2$ is shown in Fig. 1.

## 3. Application in a Human Exposure Study

We ran a 4-years period simulation over Paris region in order to create a long data base of spatially resolved concentration data for use in an exposure study (2001–2004). Apart from the grid-averaged concentration we also modelled the 'residential' and 'traffic' sub-grid scale concentration components. Demographic data on the population of Paris were selected and by means of a Monte-Carlo model we created a simple data-base of human activity patterns. Human activity patterns in this study refer to the time people spend at (a) home, (b) work, and (c) transportation. We then expressed daily averaged human exposure as the weighted sum of three terms: (a) exposure at the place of residence; (b) exposure at the place of work; (c) exposure to traffic, with relative weights the time spent by the individual at each micro-environment. Modelled, grid-averaged concentrations at the grid-cells corresponding to the place of residence and work were used for the evaluation of the first and second terms of the exposure formulation respectively. For the third term of exposure formula we used the 'traffic' component of sub-grid scale concentration.

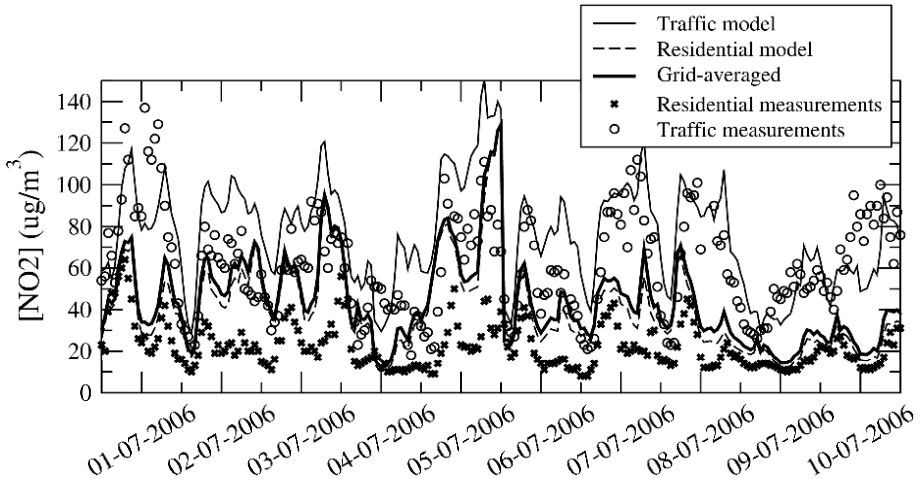


**Fig. 1.** Comparison between modelled and measured $NO_2$ concentrations at a background and a traffic monitor stations

Even if the time people spend in transportation is very low compared to the time spent in the other two micro-environments, the difference between ambient concentration levels is very high. Consequently, even if the relative weight of the traffic exposure term is low it may still play a significant role in the overall, daily

average, exposure. We estimated that not taking into account the 'traffic' exposure term in our data set would lead to an underestimation of exposure to $NO_2$ and PM10 by 5% and 3%, respectively, and an overestimation of exposure to $O_3$ by 2%.

## References

Galmarini, S., J.-F. Vinuesa et A. Martilli 2007: Modelling the impact of sub-grid scale emission variability on upper-air concentration. Atmospheric Chemistry and Physics Discussions, 7(4), 12289–12326.

Georgopoulos, G., Wang, S., Vikram, M., Sun, Q., Burke, J., Vedantham, R., McCurdy, T., and Ozkaynak, O. 2005: A source-to-dose assessment of population exposure to fine PM and ozone in Philadelphia, PA, during a summer 1999 episode, Journal of Exposure Analysis and Environmental Epidemiology, 15, 439–457.

Krol, M. C., Molemaker, M. J. and Guerau de Arellano, J. V. 2000: Effects of turbulence and heterogeneous emissions on photochemically active species in the convective boundary layer, Journal of Geophysical Research, 105, 6871–6884.

Smith, A. 1997: Written statement of testimony before U.S. Senate Subcommittee on Clean Air, Wetlands, Private Property, and Nuclear Safety. Rapport technique, U.S. Government Printing Office, Washington, D.C.

Valari, M. and Menut, L. 2008: Does increase in air quality models resolution bring surface ozone concentrations closer to reality?, Journal of Atmospheric and Oceanic Technology, 25, 1955–1968.

Vinuesa, J.-F. et J. V.-G. de Arellano 2005: Introducing effective reaction rates to account for inefficient mixing in the convective boundary layer. 39: 445–461.

## 4. Questions and Answers

**Massimi Cassiani:** Do effects of non-linear chemical reactions on averaged values explain differences in the model with and without the emission scheme?

**Answer:** Evidently the non-linear chemical transformations is the explanation of the large difference between ozone concentrations modelled with the usual CTM calculation and the implementation of the emission scheme. This becomes clear by the fact that this difference is much smaller for the primary emitted species. After all, those differences is what the authors were after: so that chemistry is better represented inside micro-environments where chemical transformations occur before mixing homogenizes emissions.

**Anthony Dore:** How does uncertainty in mapping emissions depend on the resolution on which emissions are mapped and how confident can you be in the 1 km resolution emissions?

**Answer:** The whole point of the implementation is to minimize uncertainties due to emissions and meteorological input. We did so by avoiding the deterministic downscaling to the 1 km scale so that uncertainties of input are not accumulated

into the final model output. The information of fine scale emissions is treated in a statistical manner as the fraction of the grid-averaged emission that is due to source-specific emissions. In this manner we do not need to locate exactly the emission sources, either to explicitly account for dynamical processes such as eddies in street-canyon structures.

**Bernard Fisher:** Do you have human activity data for Paris in order to do the exposure assessment, which depends on the amount of time people spend in the different micro-environments?

**Answer:** There does not exit a human-activity patterns data base for Paris population at the moment. A simple data-base was created for the purpose of this study, based on demographic data over the region of Paris. Then we coded a Monte-Carlo algorithm that mapped the members of the population over the study domain at the resolution of the CTM, respecting the distribution of the initial demographic data.

# 7.3 Integrated Application of Source Apportionment Tools to Support Development and Implementation of Air Quality Regulations to Protect Public Health

**D. Hammond, T. Watkins, and G. Norris**

Human Exposure and Atmospheric Sciences Division, U.S. Environmental Protection Agency, 109 T.W. Alexander Drive, Research Triangle Park, NC 27711, USA

**Abstract** Air pollution is associated with increased health and ecological effects. A complex mixture of local, urban, and regional sources contribute to air pollution, presenting a challenge to separate sources dispersed across the range of spatial scales. Understanding the relative contribution of these sources is important because recent health studies suggest differences in exposure relationships and health effects for different sources. In addition, air quality management decisions require information on the sources contributing to air pollution to develop effective air pollution control strategies. This paper will describe efforts to identify and quantify sources of air pollution using a multidisciplinary research approach focused on the integrated application of sampling methods, analytical methods, and receptor-based modeling tools.

The application of high time resolution sampling methods, such as the Semi-continuous Elements in Aerosol Sampler (SEAS), provides valuable data for source apportionment. When samples collected are analyzed with high resolution analytical methods, source marker compounds are identified which can be used as inputs to multivariate receptor-based modeling tools, such as Positive Matrix Factorization and Unmix, that provide information to identify relative source contributions. The application of the Air Pollution Transport to Receptor (APTR) model provides additional information regarding the location of sources. APTR has a local component based on nonparametric wind regression and a regional component based on Quantitative Transport Bias Analysis.

This paper will present results from the intensive source apportionment studies conducted in various location in the US, including St. Louis, Missouri, Dearborn, Michigan, and Steubenville, Ohio. The paper will demonstrate how the results of these studies have provided valuable information for air quality management decisions, as well as, information to support development of air quality regulations to protect public health. Finally, the paper will also discuss future efforts to integrate receptor-based approaches with source-oriented models to enhance source apportionment capabilities.

**Keywords** Source-oriented modeling, receptor modeling, source apportionment, air quality

D.G. Steyn and S.T. Rao (eds.), *Air Pollution Modeling and Its Application XX*,
DOI 10.1007/978-90-481-3812-8, © Springer Science + Business Media B.V. 2010

# 1. Introduction

Air quality standards and regulations provide a legal basis to classify pollutant levels in metropolitan areas. Many urban areas have air quality levels that fail to meet the standards established to protect public health and the environment. Broad air monitoring networks have been put in place to understand air quality trends, however, the impacts of specific sources, such as smelters and steel mills, on air quality remain relatively unknown in most areas. Air quality management districts often need additional information on specific sources as a basis for pollution control decisions. In addition, data on specific sources is instrumental to understanding source-specific health impacts. Recently, advanced source apportionment methods have been developed to improve source characterization at the regional, urban and local scale and to reduce uncertainty. This paper will describe how advanced source apportionment techniques have been used in recent studies, how source apportionment results have been applied to support local air quality management decisions, and future directions of source apportionment research.

## 1.1. Receptor-Based Source Apportionment Methods

Receptor-based source apportionment approaches quantify the contributions of various pollution sources to a location of interest. The receptor may be an ambient monitor used primarily for regulatory purposes, an indoor monitor deployed to assess indoor pollutant infiltration, or a personal monitor used to investigate the impacts of microenvironments on personal exposures. Multiple receptor models exist to conduct sources apportionment, including Principal Component Analysis (PCA), Chemical Mass Balance (CMB), and Positive Matrix Factorization (PMF). Numerous studies have successfully employed the aforementioned models to apportion source impacts; however, source apportionment ambiguity continues to be high due to uncertainties associated with sampling methods, laboratory analyses and model use, such as treatment of outliers and error estimations. The US Environmental Protection Agency (EPA) has led research efforts to develop integrated approaches to air quality research focused on advancing the state-of-the-science in laboratory methods, measurements and sampling techniques, and modeling. Through the use of high-time resolution sampling techniques, sensitive analytical methods and sophisticated models, receptor-based source apportionment techniques provide critical air quality data to support the protection of human health.

# 2. Review of Select Source Apportionment Studies

The following discussion provides examples of air quality research that have applied improved techniques to reduce uncertainty in source apportionment.

### 2.1. St. Louis Advanced Monitoring Initiative

The US EPA conducted an air quality study in St. Louis to quantify local, urban and regional sources using a combination of ambient and source sampling (Duvall et al., 2008). The St. Louis Advanced Monitoring Initiative (AMI) project was initiated to assist the State of Missouri and the State of Illinois in developing a State Implementation Plan (SIP) for fine particulate matter ($PM_{2.5}$) in the St. Louis non-attainment area. The St. Louis area is impacted by several industrial point sources, including U.S. Steel Corporation's Granite City Works. As part of the St. Louis AMI project, source samples were collected from Granite City Works along with upwind (Madison Fire House) and downwind (Granite City Fire House) ambient PM and passive PM air samples to support receptor modeling and SIP development for St. Louis. Twelve source profiles were obtained from the Granite City Works to use in the source apportionment analysis. Excess PM mass contributions from specific steelmaking processes, such as casthouse emissions, are identifiable using a combination of facility-specific source profile information and monitoring at upwind and downwind locations. The results indicate that steel processing operations at the Granite City Works contribute greater than 2 $\mu g/m^3$ in excess PM in St. Louis.

### 2.2. Dearborn SEAS Collocated Precision Study

A collocated precision study was conducted by US EPA in collaboration with local partners in Dearborn, Michigan to evaluate the performance of the SEAS sampler in an urban airshed. The objectives of the Dearborn SEAS Collocated Precision Study were to understand spatial gradients of pollutants within heavily industrialized communities, to quantify SEAS $PM_{2.5}$ collocated precision, and to pilot US EPA multi-site hybrid receptor modeling methods. The SEAS is a glass sampler void of denuders that collects gaseous and particulate species (Kidwell and Ondov 2004). The SEAS allows for 15-min air samples which are collected in slurry after preconcentration and subsequently analyzed for trace metals. Figure 1 depicts the relationship between the collocated SEAS instruments (US EPA and Univ. of Michigan) for the Dearborn study. The linear regressions for vanadium indicate consistent agreement between the collocated instruments at low and high

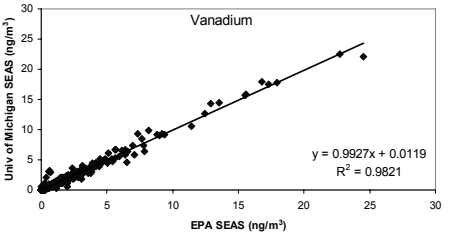


**Fig. 1.** Dearborn collocated SEAS results for vanadium

pollutant levels. Hence, the US EPA will deploy uncollocated SEAS in multiple locations to support future spatial air quality studies and provide high-time resolution data for model evaluation.

### 2.3. Steubenville Source Apportionment Study

Secondary sulfate, a byproduct of coal combustion, is one of the largest contributors to air pollution in urban and rural areas. Research has shown that regional transport of coal combustion emissions originating from the Ohio Valley region contribute significantly to air pollution in the midwest, east and southeast (Keeler et al., 2006). US EPA has conducted research to investigate regional, secondary sulfate dominated $PM_{2.5}$ and mercury emissions from coal-fired power plants to the west and southwest of Steubenville, Ohio. This study has employed multiple receptor modeling techniques and the new APTR hybrid model. APTR results for Steubenville, including the local and urban/regional apportionment, are shown in Fig. 2. The APTR analysis identified a "hot spot" south of the monitoring station near Brilliant, Ohio. Using Google Earth, a coal-fired power plant was identified in the vicinity of the "hot spot". APTR will be used in future studies to examine, quantify, and separate impacts from specific sources in complex airsheds influenced by multiple stationary sources and high traffic roadways.

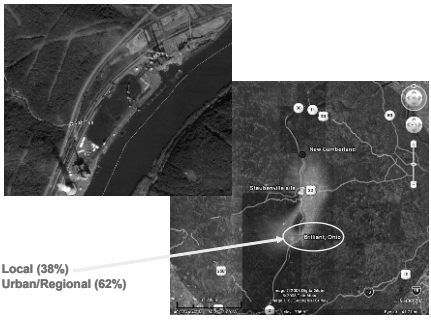


**Fig. 2.** Steubenville APTR Local and Urban/Regional Apportionment (bottom) and the Coal-fired Power Plant south of Steubenville (top) identified in the APTR analysis

## 3. Integrating Receptor- and Source-Based Apportionment Techniques

Source apportionment analyses can also be conducted using source-based approaches which start with a source emission contribution, usually from an inventory, that is input into a chemical transport model which generates an estimated concentration at a location or locations. The integration of receptor- and source-based source can provide increased confidence in source contribution estimates that are needed to

analyze and develop alternative emissions control strategies. One source-based apportionment technique is to run the chemical transport model twice – once with all emissions sources and once with emissions from a particular source category "zeroed-out." The resulting difference in estimated ambient concentrations provides an estimated source contribution at the location of interest. Another source-based apportionment approach is to calculate contributions from source regions using spatially defined sensitivity coefficients calculated by techniques such as the decoupled direct method in 3d (Napelenok et al., 2008) and model adjoints (Hakami et al., 2006). These approaches also account for nonlinearities in the chemical processes of air quality models to better represent source contributions.

## 4. Summary and Conclusions

Air pollution is a known contributor to adverse human health and ecological outcomes. A complex mixture of local, urban, and regional sources contribute to air pollution, presenting a challenge to separate sources dispersed across the range of spatial scales. Understanding the relative contribution of these sources is important because recent health studies suggest differences in exposure relationships and health effects for different sources. In addition, air quality management decisions require information on the sources contributing to air pollution to develop effective air pollution control strategies. Receptor-based source apportionment approaches and hybrid techniques, which incorporate components of receptor- and source-based source apportionment models, are informative tools in the assessment of local, urban and regional air pollution sources and source-specific health impacts. Understanding the spatial gradients of pollutant concentrations in urban centers, the personal exposures of sensitive populations to air pollutants, and the specific contributions to air quality levels of specific sources are key information needs for the development and implementation of effective air quality regulations. Integrated source apportionment techniques show promise to address scientific information gaps to inform air quality management decisions and protect public health.

**Disclaimer** The views expressed in these Proceedings are those of the individual authors and do not necessarily reflect the views and policies of the United States Environmental Protections Agency (EPA). Scientists in the EPA have prepared the EPA sections and those sections have been reviewed in accordance with EPA's peer and administrative review policies and approved for presentation and publication.

## References

Duvall RM, Norris GA, Willis RD, Turner JR, Kaleel R, Sweitzer T. 2008. St. Louis Advanced Monitoring Initiative (AMI) Project: Source Sampling and Ambient Monitoring Study Design. 27th Annual Conference of the American Association for Aerosol Research, October 20–24, 2008, Orlando, Fl.

Hakami A, Seinfeld JH, Chai TF, Tang YH, Carmichael GR, Sandu A 2006. Adjoint sensitivity analysis of ozone nonattainment over the continental United States. Environ Sci & Technol, 40,12 3855–3864

Keeler GJ, Landis MS, Norris GA, Christianson EM, Dvonch JT. 2006. Sources of Mercury Wet Deposition in Eastern Ohio, USA, Environ. Sci. Technol., 40, 5874–5881.

Kidwell CB, Ondov JM. 2004. Elemental analysis of sub-hourly ambient aerosol collections, Aerosol Science and Technology, 38, 1–14.

Napelenok SL, Pinder RW, Gilliland AB, Martin RV. 2008. A method for evaluating spatially-resolved NOx emissions using Kalman filter inversion, direct sensitivities, and space-based NO2 observations, Atmospheric Chemistry and Physics (ACP), 8, 5603–5614.

# 7.4 Estimates of Personal Exposure to $NO_2$ Using Ambient Concentrations and Activity Data

**Bill Physick, Jennifer Powell, Martin Cope, Kate Boast, and Sunhee Lee**

CSIRO Marine and Atmospheric Research, PB1, Aspendale, Victoria, 3195, Australia

**Abstract** This paper presents results from a study to investigate the extent to which $NO_2$ data from ambient network monitoring, air quality modelling, or a combination of both, can improve estimates of personal exposure across a city. As it is not practical to measure the personal exposure of every individual, a common assumption in most epidemiological studies for urban areas has been that people are exposed to a spatially-homogenous pollutant, ignoring variations in concentrations across an airshed and in various micro-environments.

Our conceptual model of an individual's personal exposure to $NO_2$ is based on time-weighted sums of exposure in the microenvironments of home, transit and work. Personal exposure in each microenvironment is linked to ambient concentration by indoor-outdoor concentration ratios. To allow us to both develop and evaluate the model, we designed a measurement program involving volunteers across Melbourne wearing personal passive samplers. Participants also wore additional samplers for sub-periods of each 48-hour exposure, at home, at work and in transit. Diaries were designed to record details of time and activities in each microenvironment, especially those associated with cooking and ventilation.

Three methods of estimating indoor-outdoor ratios and three approaches to calculating ambient exposure were evaluated. For estimation of the personal exposure to $NO_2$ of a large number of people, it is recommended that best results would be obtained with the I/O ratio calculated from a mass balance method. This requires participants to record daily gas cooking periods and approximate house age, although a simpler but slightly less accurate method dependent only on the existence or not of a gas cooking appliance also produces satisfactory results. The recommended method for calculating the required ambient outdoor concentration is to use values from the network monitor nearest to a person's microenvironment. Evaluation statistics were considerably poorer for a commonly-used method whereby each person is assigned the same ambient concentration, taken to be the mean concentration across all network monitors.

**Keywords** Personal exposure, passive $NO_2$ samplers, spatial variation, indoor-outdoor concentration ratio

D.G. Steyn and S.T. Rao (eds.), *Air Pollution Modeling and Its Application XX*,
DOI 10.1007/978-90-481-3812-8, © Springer Science + Business Media B.V. 2010

## 1. A Conceptual Model for Personal Exposure and the Measurement Program

This paper presents results from a study to investigate the extent to which $NO_2$ data from ambient network monitoring, air quality modelling, or a combination of both, can improve estimates of personal exposure across a city. We link ambient and personal exposure via an indoor-outdoor (I/O) ratio, and follow the approach outlined in Monn (2001) in which total personal exposure (PE) to a particular pollutant is estimated by weighting exposures in different microenvironments ($C_i$) according to the time spent in each microenvironment ($t_i$). Such an approach is based on easy-to-use time-activity diaries. Algebraically, this is expressed as

$$PE = \sum_{i=1}^{n} C_i t_i \Big/ \sum_{i=1}^{n} t_i \,. \tag{1}$$

To allow us to both develop and evaluate the above model, we designed a measurement program involving volunteers across Melbourne (Australia) wearing small Ferm-type passive gas samplers (about 2.5 cm diameter) attached to chest clothing (Keywood et al., 1998). The study was done for a total of four separate 2-day events, in April 2007, May 2006, May 2007 and June 2006. These times of year were chosen for the stable light-wind conditions, in order to maximize concentrations and the spatial variation in concentrations across the city and suburbs. The $NO_2$ data (cumulative) were gathered by between 15 and 17 volunteers wearing the personal samplers for each of the 2-day periods and maintaining a diary of their activities over these periods. Both working and non-working participants were included in the study. All participants were non-smokers and no dwellings with unflued gas heaters were used.

Participants wore two sets of $NO_2$ passive samplers at all times, each set containing two samplers to enable precision checking to be done. One set was worn at all times throughout the 48-h period and the second set depended on which microenvironment (home, work or transit between work and home) was being experienced. When in none of the above environments, volunteers wore a set of samplers labelled ‘other’ for their second set. ‘Other’ included such activities as shopping, visiting friends, attending the cinema etc. When not being worn, a sampler was closed by returning it to a canister fitted with a lid. An additional pair of samplers was placed outside a participant’s home and workplace and opened only while the volunteer was in that environment. In this way, ratios of indoor to outdoor concentrations were obtained. For vehicles, a sampler was placed on the mirror-side of the side mirror to enable ratios of in-car to out-car concentrations.

Activity diaries were kept by each person, noting times of arrival and exit in the different environments. At home, details of heating and cooking appliances and usage times were recorded, as were age of house, materials, floor area and volume. Open doors and windows were also noted. The infiltration rate (ventilation rate of a house in a closed-up state) was measured for five selected houses using a $CO_2$ release method similar to that described in Dunne et al. (2006).

## 2. Findings

Methodologies for estimating personal exposure that were evaluated in this study included three approaches to calculating ambient exposure and three methods of estimating indoor-outdoor ratios. Ultimately it is hoped that our recommended methodology can be used in epidemiological studies where pollutant exposure of many subjects needs to be estimated. To this end, we introduced two simplifications. Firstly, following our finding that the major personal exposure components occur in the home and work environments, we omitted the transit environment from our model. Secondly, recognising the practicalities of an epidemiological study, we assumed that all participants were at home between 1800 Eastern Standard Time (EST) and 0800 EST, and at work between 0800 EST and 1800 EST.

Estimates of personal exposure for each participant were calculated as a time-weighted sum of the mean ambient concentrations during the home and work periods, scaled by respective I/O concentration ratios. Ambient $NO_2$ exposures for each person for these periods were obtained by three methods:

- Concentrations at the *nearest monitor* in the EPA Victoria ambient monitoring network to home or work were assigned
- Concentrations at the home and workplace were assigned from the gridded hourly $NO_2$ concentrations obtained by *blending* modelled and EPA Victoria monitored data

Details of this blending approach using simulations from a complex air quality model can be found in Physick et al. (2007). In epidemiological studies, the exposure assigned to all urban dwellers over a period is often the mean pollutant concentration for that period, averaged over all monitors in the urban monitoring network. For comparison with our two methodologies above, we also evaluated a third approach to estimating ambient concentration:

- For each event, the *mean concentration across all monitors* in the network was assigned to each participant

Home indoor-outdoor ratios were calculated from two methods for computing indoor $NO_2$ concentrations, developed from the measurement program. These methods can be summarised as:

- *Mass balance*. Applying the steady state mass balance equation, the indoor $NO_2$ concentration is calculated using activity and house characteristics with an outdoor (ambient) concentration. Then it is straightforward to calculate the I/O ratio.
- *Gas cooking*. One of two indoor-outdoor ratios is assigned to each home according to whether a gas cooking appliance is installed (0.67) or not (0.47). These mean values are obtained from measurements in the current study.
- Also, the use of *measured indoor-outdoor concentration ratio* averaged across all homes for each participant was evaluated.
- *Mean measured ratio*. The I/O ratio used is the mean value from all homes measured in this study (0.57).

For the workplace, a constant indoor-outdoor ratio was used for all workplaces and was the mean value measured in the study (0.74).

When used in Eq. 1, nearly all combinations led to personal exposure estimates in good agreement with the measured 48-h personal exposure values, especially by the criterion that a prediction method is deemed to be valid if the root mean square error (RMSE) is less than the standard deviation of the measurements. Importantly, the standard deviations predicted by these spatial-variation techniques match well with the variation seen in the measurements. However there was a hierarchy of skill amongst the methods. For example, the two methods that assign an I/O ratio according to home characteristics consistently produced better statistical results than that which assigns the same *mean ratio* to everyone. The *mass balance* method was more accurate than the *gas cooking* method, especially for the RMSE and correlation statistics.

As far as the three approaches for calculating the ambient outdoor concentration are concerned, the *blended* approach led to better personal exposures than the *nearest monitor* approach with respect to RMSE and correlation, but was slightly inferior for mean value and standard deviation. However, results from both were more than satisfactory. All statistics were poor for the method in which the personal exposure was calculated by assigning to each participant the *mean monitor concentration* scaled by the mean measured ratio, and this approach is clearly inferior to the techniques developed in this project. It must also be remembered that there is no exposure variation between participants using this *mean monitor concentration* method, whereas the standard deviation predicted by the spatial variation techniques matched well the variation seen in the measurements.

## 3. Summary and Discussion

Our research has identified a simple $NO_2$ personal exposure methodology that could be widely applied, without the need for access to air quality models and with only minimum information from respondents. It is recommended that best results would be obtained with the I/O ratio calculated from a *mass balance* method. This requires participants only to record daily gas cooking periods and approximate house age. For simplicity's sake, the recommended method for calculating the required ambient outdoor concentration is to use the *nearest monitor* approach instead of the *blended* approach.

Strictly speaking, the findings can only be related at this stage to $NO_2$ and to the existing EPA Victoria monitoring network, although it is expected that the methodology would also be valid for cities with monitoring networks of similar density to that of Melbourne. Our sample size for $NO_2$ was necessarily limited to a total of 24 volunteers, with between 15 and 17 participating in each of the 4 events. However our methodologies showed skill for each event, as well as for the combined data set involving 59 samples. Repetition of our work, ideally in another city and with a higher number of participants, is highly desirable and would

strengthen the findings of this project. More participants would also widen the variety of homes, workplaces and even ages.

**Acknowledgments** We are most grateful to the participants in this study who gave freely of their time and carried out their often-complex tasks in a most capable manner, and to the Environment Protection Authority of Victoria who provided ambient monitoring data. The project was funded by the Australian Government Department of Environment, Water, Heritage and the Arts under the Clean Air Research Programme and by CSIRO's Preventative Health Flagship.

## References

Keywood MD, Beer T, Ayers GP et al. (1998) The use of passive gas samplers to monitor personal exposure to environmental pollutants. Clean Air 32(3):32–36.

Dunne E, Kirstine WV, Galbally IE et al. (2006) A study of gaseous indoor air quality for a Melbourne home. Clean Air and Environmental Quality 40(3): 45–51.

Monn C (2001) Exposure assessment of air pollutants: a review on spatial heterogeneity and indoor/outdoor/personal exposure to suspended particulate matter, nitrogen dioxide and ozone. Atmos Environ 35:1–32

Physick WL, Cope ME., Lee S et al. (2007) An approach for estimating exposure to ambient concentrations. J Expos Sci and Enviro Epidemiol 17:76–83.

## 4. Questions and Answers

**Question:** How do the air quality model-based exposures compare with the in-vivo measurements?

**Answer:** The comparison is not as good as hoped for. This is what prompted us to develop the hourly-gridded fields consisting of observations from the EPAV monitoring network blended into the air-quality fields. As discussed in the paper, exposures calculated from these blended fields agree well with the measured values. We think that the purely modelled exposures are not as good because of limitations in the emissions inventory, as the meteorology for all four events was modelled well.

**Question:** Have you distributed some passive samplers as controls, e.g. placing them next to a continuous monitor or keeping one at home 24 × 7?

**Answer:** The first kind of control has been carried out previously, placing samplers near the inlet of monitors, and showed difference errors of less than 10% on average. Also, every participant carried two samplers for each environment and the difference between the two was less than 5%. Some participants were at home (moving between indoors and outdoors) for the duration of an experiment, and the mean concentration of their permanent outdoor sampler was greater than their personal sampler, due to indoor concentrations being smaller. It should also be mentioned that across all participants, the weighted

sum of $NO_2$ concentration (ppb) from the samplers worn in each micro-environment against the concentration from the personal sampler worn at all times returned a value for $r^2$ of 0.94 with a mean bias of 0.4 ppb.

# 7.5 Examining the Impact of Regional-Scale Air Quality Regulations on Human Health Outcomes

**V.C. Garcia[1], E. Gego[2], R. Jones[3], S. Lin[3], C.I. Pantea[3], S.T. Rao[1], and Adrienne Wootten[4]**

[1]Atmospheric Modeling and Analysis Division, U.S. Environmental Protection Agency, Raleigh, NC, USA

[2]GEGO and Associates, Idaho Falls, ID, USA

[3]New York State Department of Health, Albany, NY, USA

[4]North Carolina State University, Raleigh, NC, USA

**Abstract** The $NO_x$ State Implementation Plan Call was issued by the U.S. Environmental Protection Agency to reduce the emissions of nitrogen oxides from the electric power sector to curtail the regional transport of the secondarily-formed pollutant, ozone. As emission control actions often come at a significant economic cost, it is important to understand whether such regulations have reduced air pollution and improved public health and the environment as originally anticipated. In this paper, we examine the relationships among meteorological transport patterns, ozone concentration levels and respiratory-related hospital admissions across New York State using trajectory analysis and other spatial and statistical approaches. Preliminary results from this analysis are presented in the paper.

**Keywords** Air quality, air pollution and health, air pollution, transport

## 1. Introduction

The Clean Air Act requires that the U.S. Environmental Protection Agency (EPA) set National Ambient Air Quality Standards for pollutants considered harmful to public health and the environment. Previous research has shown that high ambient ozone concentrations are harmful to humans (e.g., Bell et al., 2005; Ito et al., 2005). While ozone is not directly emitted, the formation and distribution of ozone is driven by chemical reactions involving nitrogen oxides ($NO_x$) and Volatile Organic Compounds (VOCs), as well as interactions with meteorological factors. NOx and the secondarily formed ozone can be transported downwind, contributing to pollutant levels at locations much farther from the emission sources, potentially impacting human health in downwind areas. As a result, the $NO_x$ State Implementation Plan (SIP) Call was issued by the EPA to reduce the transport of ozone.

D.G. Steyn and S.T. Rao (eds.), *Air Pollution Modeling and Its Application XX*,
DOI 10.1007/978-90-481-3812-8, 

This study investigates methods to characterize the transport of ozone from the Ohio River Valley (ORV) region, a major source area experiencing significant emission reductions resulting from the NOx SIP Call, into a domain encompassing New York State (NYS). Back-trajectories were performed from several sites within this domain across eight summers (1999–2006) to identify predominant meteorological patterns. These meteorological patterns were investigated for associations with ozone concentrations and respiratory-related hospital admissions. This paper presents the preliminary results from this analysis.

## 2. Approach

Daily maximum 8-h ozone concentrations were calculated from hourly measurements for the summers (June 1 through August 31) of 1999 through 2006 obtained from the EPA's Air Quality System database (http://www.epa.gov/oar/data/aqsdb.html) and the Clean Air Status and Trends Network (http://www.epa.gov/castnet/ ). Daily 8-h maximum ozone concentrations were interpolated to provide estimates for each county to coincide with the hospital admissions data. Back trajectories from selected sites were computed using the HYSPLIT (HYbrid Single-Particle Lagrangian Integrated Trajectory) model (Draxler and Hess, 1997) for 48 h back in time, producing a total of 736 trajectories for each site. Health data for the summers of 1999 through 2006 were obtained from the NYS Statewide Planning and Research Cooperative (SPARCS). These data included daily hospital admissions for respiratory-related diseases, including asthma, chronic bronchitis, chronic obstructive pulmonary disease (COPD), emphysema, and pneumonia and influenza.

## 3. Discussion and Results

The transport of ozone into NYS was examined by performing back-trajectories during the summers of 1999 through 2006 at selected sites in Albany (Fig. 1), Buffalo, New York City (NYC) and southwestern NYS. Based on these back-trajectories, each day was categorized as having a wind flow pattern originating from the ORV or not originating from the ORV (Fig. 2). These days were then matched to the corresponding daily maximum 8-h ozone concentrations and daily respiratory-related hospital admissions. In addition, ozone concentrations and hospital admissions were examined before the implementation of the NOx SIP Call (1999–2000) and after the implementation of the NOx SIP Call (2004–2006).

The results of this analysis indicate that the mean levels for ozone concentrations and respiratory-related hospital admissions were significantly higher for those days when the sites were downwind from the ORV versus those days that the sites were not downwind from the ORV. In addition, the mean levels for ozone concentrations were found to be significantly higher before the implementation of

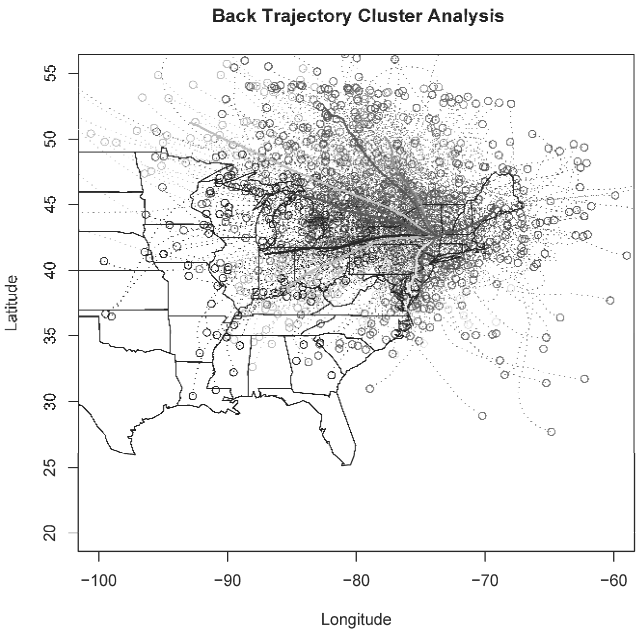


**Fig. 1.** Example of back-trajectories performed for selected sites (Albany, NY shown here) for summers of 1999–2006 (dashed lines), clustered into 12 major meteorological patterns (solid lines)

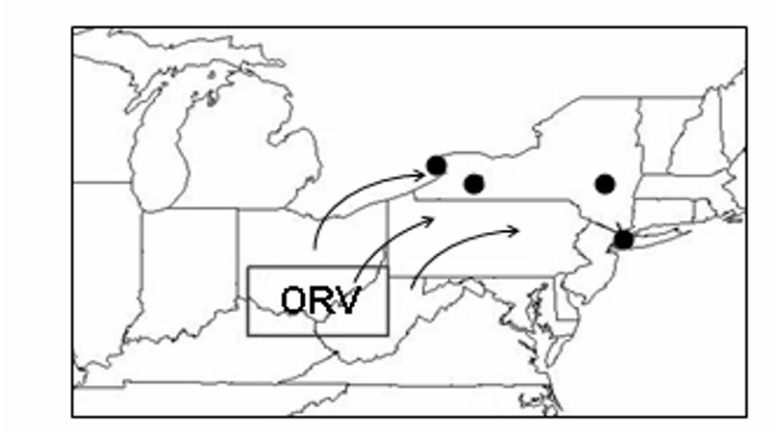


**Fig. 2.** Rectangle shows Ohio River Valley as defined for this study. Arrows indicate wind direction for downwind sites. From left to right, circles represent approximate location of Buffalo, the southwestern site, Albany and NYC

the NOx SIP Call versus after the implementation of the NOx SIP Call. Furthermore, there were fewer extreme ozone events after the implementation of the NOx SIP Call as compared to before the implementation of the NOx SIP Call,

particularly for those days that the wind originated from the ORV. While there was not a significant difference in the mean hospital admissions before and after the implementation of the NOx SIP Call , a crude analysis using a cumulative distribution function for the southwestern site indicates that a decrease in ozone concentrations is associated with a decrease in hospital admissions at the higher ozone percentiles (>75%). Because of many confounding factors (e.g., temperature, human behavior), the health signal associated with the implementation of the NOx SIP Call will be difficult to discern at best. This study presents a promising approach for identifying such impacts through the use of meteorological conditions as an indicator of exposure.

**Acknowledgments** The authors wish to thank Jim Godowitch, Kristen Foley and Jenise Swall for their contributions to this study. Although this work was reviewed by EPA and approved for publication, it may not necessarily reflect official Agency policy.

## References

Bell ML, Dominici F, Samet JM (2005) A meta-analysis of time-series studies of ozone and mortality with comparison to the national morbidity, mortality, and air pollution study. *Epidemiol* 16(4):436–45.

Ito K, De Leon SF, Lippmann M (2005) Associations between ozone and daily mortality: analysis and meta-analysis. *Epidemiol* 16(4):446–57.

Draxler RR, ess GD (1997) Description of the HYSPLIT_4 Modeling System, NOAA Technical Memorandum ERL ARL-224, NOAA Air Resources Laboratory, Silver Spring, MD, http://www.arl.noaa.gov/ready/hysplit4.html.

## 4. Questions and Answers

**Question:** Try to include other time varying determinants of hospital admission in the analysis.

**Answer:** This paper presents a preliminary analysis on the use of meteorological conditions as a variable in examining associations between transported pollution and respiratory-related hospital admissions. A full epidemiology study with other time varying determinants of hospital admissions is also being performed in a companion study (see paper entitled “Impact of the NOx SIP Call on Respiratory Hospitalizations in New York State”).

# 7.6 Impact of the NOx SIP Call on Respiratory Hospitalizations in New York State

**Shao Lin[1], Rena Jones[1], Cristian Pantea[1], Valerie C. Garcia[2], S.T. Rao[2], Syni-An Hwang[1], and Nancy Kim[1]**

[1]New York State Department of Health, Albany, NY, USA

[2]Atmospheric Modeling and Analysis Division, U.S. Environmental Protection Agency, Raleigh, NC, USA

## 1. Background/Objectives

Asthma is a serious public health problem in New York State (NYS), affecting 8.4% (370,000) children and 7.6% (more than 1.1 million) adults.[1] Asthma burden in New York's urban areas is consistently higher than the national average, with marked differences in prevalence and severity by socio-economic strata.[2] Poor air quality from traffic pollution and other sources has consistently been linked to asthma morbidity. More specifically, nitrogen oxides, criteria pollutants which serve as a precursor to ozone, have been implicated as a player in respiratory irritation.[3]

This study investigated whether the U.S. Environmental Protection Agency-mandated NOx State Implementation Plan (NOx SIP) in NYS, aiming to reduce nitrogen oxide emissions from major sources during the summer months, had an impact on hospitalizations for asthma and other respiratory illnesses. More specifically, hospital admissions due to respiratory diseases (1997–2006) were compared during the period before the legislation, during the period of partial NOx SIP implementation, and post-implementation.

## 2. Methods

### 2.1. Population

Several existing data sources were used: (1) the Statewide Planning and Research Cooperative System (SPARCS) is a legislatively mandated database, maintained by the NYS Department of Health, of hospital discharges from all hospitals in the NYS (excluding psychiatric and federal hospitals); and (2) ozone concentrations kriged to the center-point of a 12 km horizontal grid structure. Ozone data was provided by the EPA and incorporated air quality data from AIRS, CASTNet and NAPS monitoring systems, which span the entire Northeastern U.S. and parts of Canada.

D.G. Steyn and S.T. Rao (eds.), *Air Pollution Modeling and Its Application XX*,
DOI 10.1007/978-90-481-3812-8, © Springer Science + Business Media B.V. 2010

All residents of NYS were included in the analysis. Health outcomes included hospitalizations for respiratory disease, years 1997–2006. Specifically, respiratory diseases included the following principal diagnoses based on the International Classification of Disease, 9th Revision (ICD-9): bronchitis (491), emphysema (492), asthma (493), and chronic obstructive pulmonary disease (496). In addition, for children ages 0–4 years, a diagnosis of acute bronchitis and bronchiolitis (466) and bronchitis, not specified as acute or chronic (490) were also included because they are common respiratory diseases among very young children and the symptoms are difficult to distinguish from asthma at this age. The control admissions included hospitalizations for gastrointestinal diseases (009) and accidental falls (E880-E888).

Monthly, seasonal, and yearly respiratory hospital admission rates during the study period were calculated. The rates of seasonal and yearly hospital admissions for combined disease categories were compared across three different time periods. Based on the actual timing of the regulation, these periods were defined as follows: (1) 1997–2000 (pre-NOx regulation or baseline); (2) 2001–2003 (partial-NOx SIP implementation); and (3) 2004–2006 (post-NOx SIP or post implementation).

Periodic trends in respiratory hospitalizations during the three NOx time periods (baseline, partial-implementation and post-implementation) were compared by geographic region, race/ethnicity, gender, age, and disease sub-groups. We then calculated the percent change in average daily respiratory admissions partial- and post- implementation compared to the average daily admissions during the baseline period.

### 2.2. Statistical methods

Time series models using an intervention analysis approach were used to investigate the temporal trends for the three NOx study periods. ARIMA models were used to examine the change in average daily ozone levels, respiratory hospitalizations, and their relationship during the summer months (June–August) between each of the time periods, after adjusting for day-of-the-week, temperature, secular trend, and other temporal/seasonal effects. The temporal/seasonal effects included a long term trend indicator variable for capturing the baseline, partial implementation and post implementation effect, as well as a separate indicator variable capturing the seasonal trend of summertime effect during these periods. In addition, the respiratory analysis included terms for holidays and day-of-the-week to control for their potential confounding effects. The autocorrelation of the residuals were investigated at various lags. The final model was determined when it included sufficient orders of autocorrelations and moving averages such that the model residuals contained no signal beyond random variation. Following passage of these autocorrelation tests, statewide and region-specific time series models were estimated separately for ambient ozone concentrations and respiratory admissions. To examine the intervention effect, the baseline time period was compared against the partial and post implementation periods. Analyses were stratified by eight NYS regions as defined by the NYS Department of Environmental Conservation (DEC), including: Long Island, New York City (NYC) Metro, Lower Hudson, Upper

Hudson, Adirondack, Central, Eastern Ontario and Western region. All analyses were conducted using SAS v. 9.2 and the criterion for statistical significance was $\alpha = 0.05$.

## 3. Results

Daily average ozone declined during the summer months of the post-implementation period (compared to baseline) in all regions of NYS. Adjusted modeling analysis showed evidence of regional differences in these summertime declines; the south-western Long Island and NYC Metro regions experienced the greatest declines (4.79% and 3.15%, respectively), while in the rest of the regions ozone levels showed declines in the range of 1.32–2.54%. In contrast, daily average temperature generally increased for all NYS regions during these time periods.

Post-implementation respiratory admissions did not follow such clear patterns as ambient ozone levels. Hospitalizations declined in the southwestern regions of the state during the post-implementation time period, but across all regions of NYS the greatest reduction in respiratory admissions occurred during the fall and winter months. Adjusted summertime respiratory admissions in the Lower Hudson region declined non-significantly by 5.28% (95% CI: −11.56, 1.44), in the Central region by 1.29 (95% CI: –6.00,3.66) and in the Western region by 2.21 (95% CI: –7.24,3.09). Conversely, daily respiratory admissions increased in each of the other regions, from 0.24% to 9.5% (Fig. 1). This result is particularly interesting as we hypothesize that the greatest impact of the NOx SIP Call will occur in the southern regions of NYS due to prevalent wind patterns that transport ozone from the Ohio River Valley.

| Region | Percent change estimate | Percent change lower 95% CI | Percent change upper 95% CI |
|---|---|---|---|
| Adirondack | 9.50 | 0.08 | 19.80 |
| Central | –1.29 | –6.00 | 3.66 |
| Eastern Ontario | 3.77 | –3.18 | 11.23 |
| Long Island | 0.24 | –3.86 | 4.52 |
| Lower Hudson | –5.28 | –11.56 | 1.44 |
| Upper Hudson | 1.02 | –4.95 | 7.36 |
| Western | –2.21 | –7.24 | 3.09 |

**Fig. 1.** Summertime NOx intervention effect on daily respiratory admissions in upstate regions, post-implementation (2004–2006) compared to baseline (1997–2000). Note that the three southern regions of interest (Central, Lower Hudson and Western) show a negative percent change in respiratory admissions (although not significant) as compared to the other regions

Stratified analyses showed greater reductions in admissions in NYC, among those aged 0–4 years old, and whites than among upstate, other age groups, and other racial/ethnic groups (data not shown). In contrast, admissions for the control diseases, gastroenteritis and accidental falls, were higher during the post-implementation period compared to baseline (data not shown).

## 4. Conclusion

Preliminary findings show significant reductions in ozone concentrations during the summer season after the NOx SIP Call went into effect. However temperatures increased across these same time periods, indicating that the ozone reductions are not related to temperature. Although not significant, analyses identified reductions in admission rates during the fall and winter season in all NYS regions following the NOx SIP call, after controlling for multiple confounding factors. The findings also identified that the intervention effect has regional differences that may be accounted for by the NOx implementation which reduced ozone transport from neighboring states into the southern portions of NYS. Further studies will examine the potential effects of NOx SIP call on sensitive sub-populations, effects by urbanicity, and relationships based on meteorological and windflow patterns.

## References

New York State Department of Health. National Asthma Survey - New York State Summary Report. 2007.

Lin S, Fitzgerald E, Hwang SA, Munsie JP, Stark A. Asthma hospitalization rates and socioeconomic status in New York State (1987–1993). *J Asthma.* 1999 May;36(3):239–51.

Kampa M, Castanas E. Human health effects of air pollution. *Environ Pollut.* 2008 January;151(2):362–7.

## 5. Questions and Answers

**D. Bert:** Accountability studies are very important but also difficult to do when changes in pollution as a result of regulatory actions are gradual?

**Answer:** The challenges can be overcome but they require careful thought and very targeted study designs. We agree that determining the impact of a regulation is extremely difficult. The signal associated with a change in emissions is embedded within the overall health endpoint that is confounded by other factors. We believe multiple approaches will be needed to discern this signal using a “weight of evidence” approach. This paper presents one approach for such an analysis.

# 7.7 Spatial Mapping of Air Quality Trends in Europe

**Bruce Denby, Ingrid Sundvor, and Massimo Cassiani**

Norwegian Institute for Air Research (NILU), P.O. BOX 100, 2027 Kjeller, Norway

**Abstract** This paper investigates the spatial mapping of air quality trends in Europe. Such spatially distributed maps provide information for policy making and for understanding the spatial character of air quality trends. Previous trend studies have concentrated on individual, or groups of, monitoring sites, looking at the average trends of these. In this study use is made of statistical interpolation methods that combine observed and modeled data in an optimized way, in this case using residual log-normal kriging with multiple linear regression, to produce annual maps of air quality indicators for ozone (AOT40) and annual mean $SO_2$ in the period 1996–2005. Trends in these maps are then calculated and their significance and uncertainty are assessed. The methodology is effectively used for mapping $SO_2$ trends to a significant level in most of Europe. However, trends in AOT40 are less clearly defined since the uncertainty is generally of the same order as the calculated trends. A general north to south gradient in AOT40 trends can be seen, negative trends in the UK and Scandinavia but positive trends in the Mediterranean.

## 1. Introduction

This paper investigates the spatial mapping of air quality trends in Europe, in particular the mapping of ozone (AOT40) and annual mean $SO_2$. Previous trend studies have concentrated on individual, or groups of, monitoring sites, looking at the average trends of these. In this study European wide maps of air quality trends are produced.

To provide full spatial coverage of air quality some form of interpolation of the measurement data is required. However, the spatial and temporal coverage of the measurement data alone is generally insufficient for providing maps of sufficient quality for a long enough period (10 years). Alternatively, good spatial coverage is available from air quality models but these have also been shown to misrepresent the trends in air quality data (e.g. Solberg et al., 2009).

To improve the mapping of air quality, statistical interpolation methods may be used (e.g. Denby, 2008a, b; Horálek et al., 2007). These methods combine observations, air quality models and other supplementary data to provide maps of air quality, as well as maps of uncertainty, on an annual (or daily) basis. By applying these methods to the available measurement and modeling data the best estimate of the spatial distribution of the air quality can be achieved. In this study

D.G. Steyn and S.T. Rao (eds.), *Air Pollution Modeling and Its Application XX*,
DOI 10.1007/978-90-481-3812-8, 

sta-tistical interpolation methods are applied to annual monitoring (AirBase) and modeling (EMEP) data to produce individual yearly maps of AOT40 and annual mean $SO_2$ for the years 1996–2005. These maps are then assessed to determine both the spatial distribution and the uncertainty of the 10 year trend. A number of sensitivity tests are carried out. This paper provides a summary of a more extensive report from Denby at al. (2008a).

## 2. Methodology

To spatially map trends in air quality a number of steps are needed. For each year, from 1996 to 2005, maps of AOT40 and annual mean $SO_2$ are produced at a spatial resolution of 25 km using statistical interpolation methods that combine both monitoring (AirBase, 2008) and modeling (EMEP) data (Solberg et al., 2009). Residual log-normal kriging, after multiple linear regression, is the statistical interpolation method employed (Denby et al., 2008b; Horálek et al., 2007).

For each grid point in the maps trends are calculated, producing maps of air quality trends. Both linear regression and Sen's method (Sen, 1968) are applied.

For each year and at each grid point an uncertainty is determined using the residual kriging variance. Monte Carlo methods are used to determine the uncertainty in the trend by randomly sampling the kriging variance. For each random sample set a trend is determined and the standard deviation of the ensemble of resulting trends is used to indicate the uncertainty in the mean trend.

A range of sensitivity studies are carried out concerning the influence of station selection, trend assessment methodology and interpolation methodology. Details concerning these sensitivity studies can be found in Denby et al. (2008a).

## 3. Modeled and Observed Trends

In Fig. 1 the modeled (EMEP) and observed trends in the station averaged AOT40 and annual mean $SO_2$ concentrations are shown. From this it can be seen that the modeled and observed trends for AOT40 are opposite in sign, whilst the modeled and observed trends for $SO_2$ are of the same sign but the modeled con-centrations, and trends, are around 40% less in magnitude than those observed. These differences make the use of only models, to study trends, inappropriate. By applying the statistical interpolation method for each year of data the general observed trends will be followed and the spatial distribution will be represented.

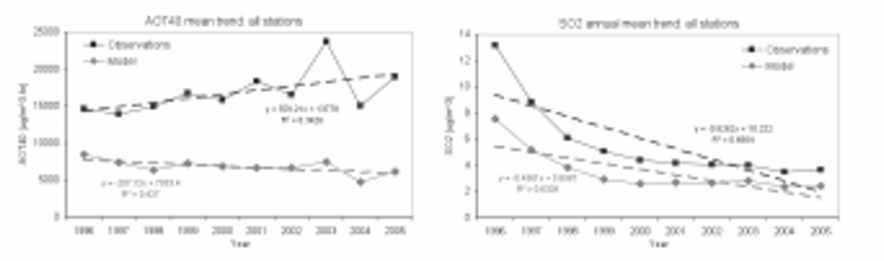


**Fig. 1.** Trends of the mean observed and modeled AOT40 (left) and annual mean $SO_2$ (right) using all available stations

## 4. Spatially Mapped Trends

In this paper we report results where all available stations have been used for the mapping, i.e. no station selection has been carried out. In Figs. 2 and 3 maps showing trends, and their relative uncertainty, are presented for both AOT40 and annual mean $SO_2$ using the above methodology.

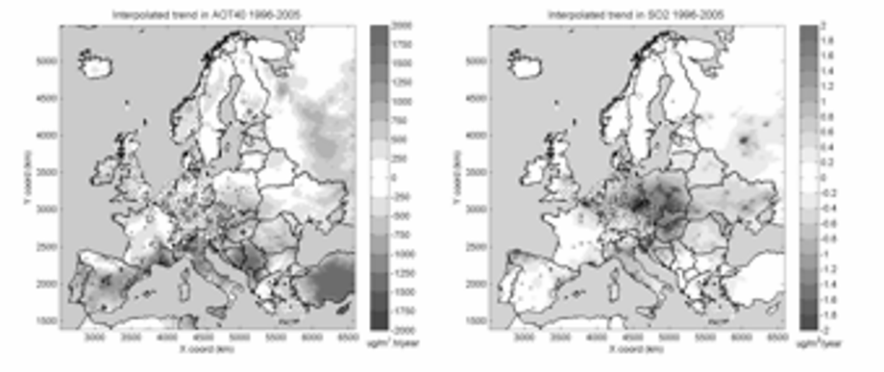


**Fig. 2.** Maps showing the estimated trend for AOT40 (left) and $SO_2$ (right) for the years 1996–2005. Also shown for comparison are the station trends. Circles with color indicate stations with at least 8 years of data and crosses other stations with less than 8 years of data

The spatial trends in AOT40 (Fig. 2, left) indicate a general north–south gradient in AOT40, with negative trends in the UK and Scandinavia but positive trends in the Mediterranean region.

In general there is a lack of data in the South-eastern regions of Europe. The uncertainty assessment carried out (Fig. 3) reflects this. Trend maps are found to be, to some extent, sensitive to the selection of observational data.

There are few areas in the AOT40 trend maps with trends greater than their estimated uncertainty. There are large areas in the $SO_2$ trend maps with negative trends greater than their estimated uncertainty.

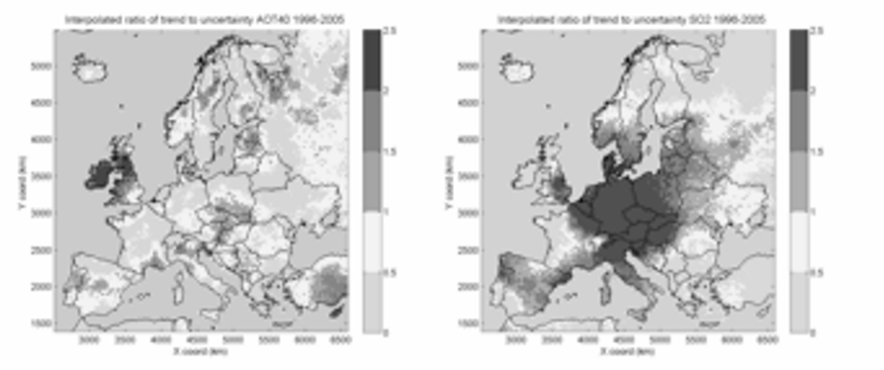

**Fig. 3.** Maps showing the ratio of the absolute trend to the standard deviation of the trend for AOT40 (left) and annual mean $SO_2$ (right) for the years 1996–2005. The standard deviation of the trend is calculated using Monte Carlo methods

**Acknowledgments** This work was carried out by the European Topic Centre on Air and Climate Change on behalf of the European Environment Agency.

## References

AirBase (2008), European air quality database. http://airbase.ionet.europa.eu/

Denby, B., I. Sundvor P. de Smet, and F. de Leeuw (2008a) Preliminary assessment report on the spatial mapping of air quality trends for Europe. ETC/ACC Technical Paper 2008/3. http://air-climate.eionet.europa.eu/reports/ETCACC_TP_2008_3_spatial_trends_scoping

Denby B., M. Schaap, A. Segers, P. Builtjes and J. Horálek (2008b). Comparison of two data assimilation methods for assessing PM10 exceedances on the European scale. Atmos. Environ. 42, 7122–7134.

Horálek J., P. Kurfürst, P. de Smet, F. de Leeuw, R. Swart, T. van Noije, B. Denby and J. Fiala (2007) Spatial mapping of air quality for European scale assessment. ETC/ACC Technical Paper 2006/6. http://air-climate.eionet.europa.eu/reports/ETCACC_TechnPaper_2006_6_Spat_AQ

Sen, P. K. (1968), 'Estimates of the regression coefficient based on Kendall's tau', J. American Statist. Assoc. 63, 1379–1389.

Solberg S., J. Horalek, J. E. Jonson, S. Larssen, F. de Leeuw (2009). Assessment of ground-level ozone within the EEA Member Countries with focus on long-term trends. First draft of an ETC/ACC technical report, in preparation.

## 5. Questions and Answers

**Douw Steyn:** We usually consider discrete fields that are constant in time (for the interpolation). Indeed we should not ignore the temporal variation.
**Answer:** Though it is possible to include the temporal dimension into interpolations we do not do this, and since we are looking for trends in time we do not see the advantage of this either.

**S.T. Rao:** Do you see any indication for differences in the trend (observed compared to emissions).
**Answer:** The trend in reported ozone precursor emissions is negative, on average in Europe, which is not found in the observations, on average. $SO_2$ emission trends reflect the trends in concentrations, at least qualitatively if not exactly quantitatively.

**Question:** Is there consistency in what the world is seeing.
**Answer:** Not in the case of ozone, and also not generally for PM.

**Peter Builtjes:** Emissions are claimed to be reduced, but reality may not yet substantiate this.

# 7.8 The Influence of Chemistry-Transport Model Scale and Resolution on Population Exposure Due to Aircraft Emissions from Three Airports in the United States

**Saravanan Arunachalam[1], Bok Haeng Baek[1], Hsiao-Hsien Hsu[2], Binyu Wang[1], Neil Davis[1], and Jonathan I. Levy[2]**

[1]Institute for the Environment, University of North Carolina at Chapel Hill, 137 E. Franklin St., #645, Chapel Hill, NC 27599-6116, USA

[2]Harvard School of Public Health, Department of Environmental Health, Landmark Center 4th floor West, 401 Park Drive, Boston, MA 02215, USA

**Abstract** Understanding the impact of aviation emissions on air quality is becoming more important due to the projected growth in aviation transport and decrease in emissions from other anthropogenic sources. Atmospheric chemistry-transport models are often used to determine the marginal impact of emissions on air quality and public health, but the uncertainties related to modeling assumptions are rarely formally characterized from the perspective of public health impact calculations. In this study, we estimate the incremental contribution of commercial aviation emissions to air quality near three U.S. airports – Atlanta Hartsfield, Chicago O'Hare, and Providence T.F. Green – using the Community Multiscale Air Quality Model (CMAQ), a comprehensive chemistry-transport air quality model. To evaluate the significance of model resolution and geographic scales of influence, we ran a one-atmosphere version of CMAQ (with air toxics) at 36- and 12-km resolutions, and calculated the total population exposure per unit emissions at various distances from each airport. Total population exposure per unit emissions was systematically higher for air toxics with increased model grid resolution, and the distance at which most of the population exposure was estimated varied by compound and airport. A 108 × 108 km domain centered on the airport captured most population exposure for reactive gases (e.g., formaldehyde) at airports with high nearby population density, but more than half of the fine particulate matter ($PM_{2.5}$) exposure occurred outside of a 324 × 324 km domain centered on the airport, given contributions from secondary formation. Our findings provide insight about the model resolution and spatial scales necessary for population risk assessment from airports and other combustion sources, and demonstrate the robustness of risk-based prioritization across multiple grid resolutions.

D.G. Steyn and S.T. Rao (eds.), *Air Pollution Modeling and Its Application XX*,
DOI 10.1007/978-90-481-3812-8, © Springer Science + Business Media B.V. 2010

## 1. Introduction

Aircrafts and airport sources emit a variety of pollutants, but limited studies have quantified their contributions using comprehensive air quality models. From a population risk perspective, there are questions about the ideal spatial domain and resolution for chemistry-transport modeling. Although the largest domain and finest resolution would be desired in principle, there are logistical and computational constraints, and it is important to know over what spatial domain most of the population exposure occurs, and whether this depends on the model resolution. Even with the application of a complex model such as CMAQ, multiple modeling choices can be made that will influence the model run-time and complexity, with unclear implications for health impact estimates. High-resolution modeling (with smaller or nested grid cells) represents the theoretical optimum but is more computationally demanding and requires more refined emissions data, and it is unclear whether such modeling is necessary in a given decision context. The optimal spatial domain and resolution may differ across pollutants as well as across airports.

## 2. Modeling Approach

In this study, we consider emissions from commercial aircraft activities from three airports in the U.S. – Hartsfield-Atlanta International Airport (ATL, Georgia), Chicago O'Hare International Airport (ORD, Illinois), and T.F. Green Airport (PVD, Rhode Island). We included 73 commercial aircraft types for ATL, 109 for ORD, and 144 for PVD. Emissions Dispersion Modeling System (EDMS) emissions of criteria pollutants and air toxics were generated for each of the airports. To provide realistic representations of all emissions from aviation and airport-related sources, we developed EDMS2Inv [1], an interface to the Sparse Matrix Operator Kernel Emissions (SMOKE) modeling system, to process hourly emission inventory outputs from EDMS to create emissions inputs to CMAQ. The CMAQ model application has a varying vertical resolution from the surface to 50 millibars (about 18 km). There are a total of 22 layers, with the first 15 layers spanning 10,000 ft, where aircraft emissions are provided. There is thus a significant spatial enhancement in the vertical representation of aviation emissions in the vicinity of the airports during the Landing and Takeoff (LTO) cycle.

To characterize exposures, we performed MM5-SMOKE-CMAQ modeling with and without airport emissions at 36 × 36 km and 12 × 12 km resolutions. We used CMAQ in a one-atmosphere mode, to include treatment of ozone, $PM_{2.5}$ and air toxics. Recent risk prioritization work indicated that health risks would be dominated by $PM_{2.5}$ and that cancer risks from air toxics would be most influenced by formaldehyde and 1,3-butadiene with contributions from acetaldehyde and benzene, arguing for their inclusion in this analysis [2]. Additional details of the

modeling and the model evaluation against observed data can be seen elsewhere [3].

CMAQ outputs are largely characterized in our analysis using intake fractions (iFs), to elucidate the emissions-to-exposure relationship in a form relevant for population health risk estimation. The quantitative definition of iF is

$$iF_j = \Sigma_i(P_i \Delta C_{ij})*BR/Q_j$$

where $iF_j$ is the intake fraction for exposure to pollutant j, $P_i$ refers to the population in geographic area i, $\Delta C_{ij}$ (in $\mu g/m^3$) is the change in ambient concentration at geographic area i related to emissions $Q_j$, and BR is a nominal population breathing rate (assumed to be 20 $m^3$/day). Of note, BR is divided back out in a risk calculation, so this assumption is only included to ensure that iFs are unitless measures. We estimate iFs for all modeled air toxics and calculate total population exposure for primary and secondary $PM_{2.5}$, given the challenge of extracting iF values for secondary $PM_{2.5}$ constituents based on CMAQ outputs.

## 3. Results

In Fig. 1, we present iFs for air toxics and cumulative population exposure for $PM_{2.5}$. We present values at increasing distance from each airport using 36- and 12-km resolution CMAQ results, and we include secondary formation in the estimated concentrations. Findings demonstrate systematically higher iF values using 12-km resolution and for less reactive pollutants, with clear influences of population centers. Most national-scale population exposure is captured within 612 × 612 km domains surrounding each airport (95–100% across all air toxics and model resolutions), although less so for secondary byproducts and where large populations are found just outside of these domains (e.g., for PVD). In contrast, for $PM_{2.5}$, while most of the total population exposure for primary constituents is found within this domain (96% with 36-km and 98% with 12-km resolution), the corresponding values are 60% and 64% for the secondary constituents that dominate public health impacts. More than half of the population exposure to air toxics is observed within a 108 × 108 km domain surrounding each airport, but for $PM_{2.5}$, half of the total population exposure occurs outside of 324 × 324 km domains surrounding each airport. In part because of the larger domain necessary to capture $PM_{2.5}$ population exposure, model resolution has less of an influence on $PM_{2.5}$ population exposure estimates than for air toxics.

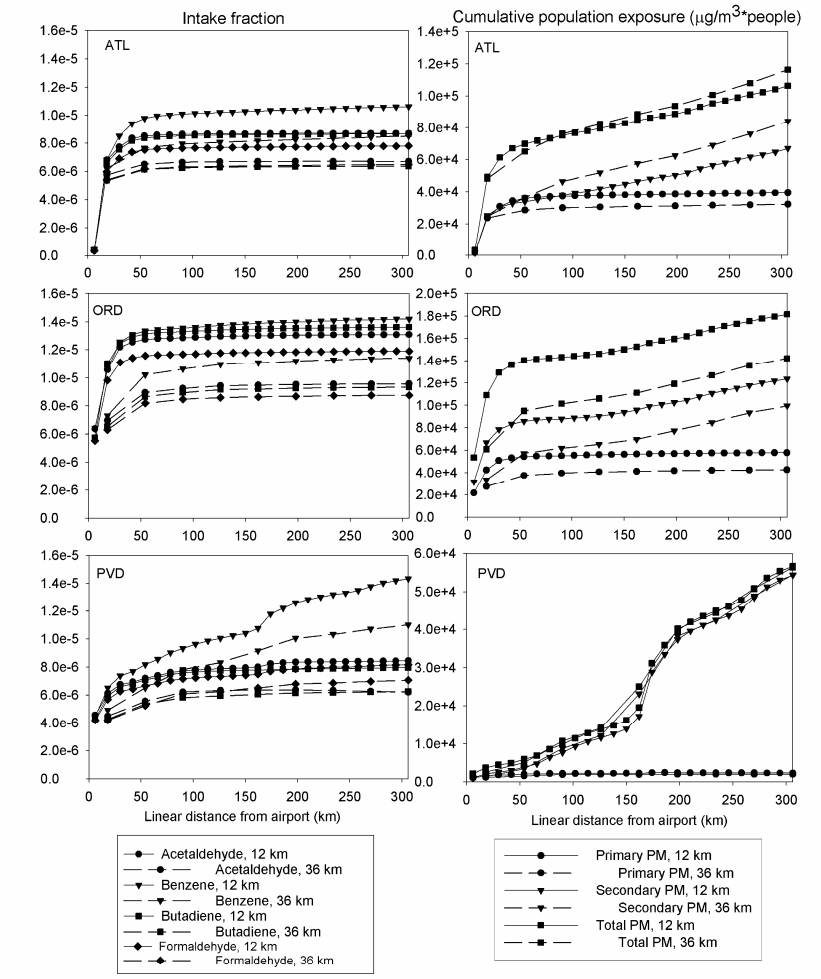


**Fig. 1.** Intake fractions for selected air toxics (left) and cumulative population exposure for $PM_{2.5}$ (right) at increasing distances from the three airports

## 4. Discussion

Our results demonstrate the applicability of CMAQ for estimating population exposures to air toxics and $PM_{2.5}$ associated with aircraft emissions, and reinforce that high-resolution modeling is necessary for reactive compounds while large domain modeling is important for secondarily-formed pollutants.

**Acknowledgments** This work was funded by PARTNER under grants to UNC and Harvard University. The Air Quality project is managed by Dr. Mohan Gupta. Any opinions, findings,

and conclusions or recommendations expressed in this material are those of the author(s) and do not necessarily reflect the views of PARTNER and its sponsors. PARTNER is funded by FAA, NASA, and Transport Canada.

## References

Baek, B.H., et al. (2007). *Development of an Interface for EDMS*, In Proceedings of the 16th Annual Emissions Inventory Conference – "Emissions Inventories: Integration, Analyses and Communication", Raleigh, NC, May 2007.

Levy, J.I., H-H Hsu, and S. Melly (2008). *High Priority Compounds Associated With Aircraft Emissions*, Report No. PARTNER-COE-2008-008, October 2008. Available at: http://web.mit.edu/aeroastro/partner/index.html

Arunachalam, S., et al. (2008). *An Improved Method to Represent Aviation Emissions in Air Quality Models and their Impacts on Air Quality,* In Proceedings of the 13th Conference on Aviation, Range and Aerospace Meteorology, New Orleans, LA, January 2008.

# 7.9 Temporal Trends of PCDDs/Fs in Ambient Air in Seoul, Korea

**Yong-suk Choi[1], Min-young Kim[1], Seok-won Eom[1], and Seoung-gu Ahn[2]**

[1]Waste engineering team, Seoul Metropolitan Government Public Health and Environment Research Institute, Sechogu Yangjaedong 202-3, Seoul 137-130, Korea

[2]Professor, Department of Environmental Engineering, University of Seoul, Dongdaemungu Jeonnongdong 90, Seoul 130-743, Korea

**Abstract** The aim of this study was to determine dioxin levels and to assess temporal trends of the atmospheric content of these pollutants in Seoul. Moreover, patterns of PCDDs/Fs isomers have been investigated and the relationship between the level of dioxin in ambient air and seasonal fluctuation was investigated. Ambient air monitoring for dioxin in Seoul has been conducted continuously over the 7 years: January 2002 through December 2008. An estimated 450 samples in ambient air were collected by PUF air sampler and analyzed for PCDDs/Fs using HRGC-HRMS. I-TEQ values of dioxin in ambient air ranged from 22 to 563 fg I-TEQ/$m^3$ with a mean 142 fg I-TEQ/$m^3$. Our findings show that contemporary PCDDs/Fs levels in ambient air have declined since the 2002s. Special characteristics were found according to the seasonal changes. The PCDDs/Fs levels in this study were higher in the winter compared to the summer.

## 1. Instruction

Polychlorinated dibenzo-*p*-dioxins(PCDDs) and dibenzofurans(PCDFs) are believed to be formed unintentionally by many industrial activities including a variety of thermal processes. Once released into the atmosphere, these toxicants can be transported far from their original sources, and as a result, their presence can be determined in remote areas. Although PCDDs/Fs levels is very low in environment, they have been found virtually in almost all areas of earth and ocean ecosystem.

There are a lot of previous studies that have reported for determining PCDDs/Fs levels in ambient air. Choi et al. (2008) researched PCDDs/Fs levels at three different sites in Hong Kong. The annual average concentrations of PCDDs/Fs congener at three sampling sites were 69.8 ± 44.0 fg WHO-TEQ/$m^3$, 152 ± 1,470 fg WHO-TEQ/$m^3$, 102 ± 71.10 fg WHO-TEQ/$m^3$, respectively. Raun et al. (2005) reported concentrations of 17 dioxins congeners in ambient air in Huston. The annual mean

D.G. Steyn and S.T. Rao (eds.), *Air Pollution Modeling and Its Application XX*,
DOI 10.1007/978-90-481-3812-8, © Springer Science + Business Media B.V. 2010

value was 15 fg I-TEQ/$m^3$ (16 fg WHO-TEQ/$m^3$). The studies also suggested that the fluctuations of PCDDs/Fs levels are correlated with minimum relative humidity, mean temperature, and mean NOx concentration. Abad et al. (2004) monitored PCDDs/Fs levels in ambient air of 28 different sites (rural, urban, suburban and industrial) between 1994 and 2002. The mean of TEQ values in industrial areas, urban and suburban areas and rural areas were 180 fg I-TEQ/$m^3$, 80 fg I-TEQ/$m^3$, 42 fg I-TEQ/$m^3$, respectively. Cheng et al. (2003) reported PCDDs/Fs levels measured in the ambient air range from 0.058 to 0.127 pg-TEQ/$m^3$.

Seoul, the largest city of Korea, has a lot of source of dioxin such as MSWI, a variety of plants, traffic and etc. Recently, many plants have moved out of the city but there still remain lots of sources of dioxin in Seoul. The aim of this study was to determine dioxin levels and to assess temporal trends of the atmospheric content of these pollutants in Seoul. Moreover, patterns of PCDDs/Fs congeners have been investigated and the relationship between the level of dioxin in ambient air and seasonal fluctuation was investigated. Ambient air monitoring for dioxin in Seoul has been conducted continuously over the 7 years: January 2002 through December 2008.

## 2. Sampling and Laboratory Analysis

### 2.1 Sampling

Air samples for dioxin analysis were collected using high-volume air samplers equipped with a quartz fiber filter before the PUF (polyurethane foam). An about 450 samples were collected from January 2002 through December, 2008 at three different sampling locations in Seoul area. Volumetric sampling flow rate was set on 0.8 $m^3$/min.

### 2.2 Analytical Procedure

The 2,3,7,8-substituted congeners of PCDDs/Fs in samples were determined by HRGC/HRMS, according to US EPA method TO-9(1999a), 1613b(1994) and 1668a(1999b). Chromatograms were obtained from Gas chromatography electron impact mass spectrometry (GC-EIMS, a Micromass Autospec Ultima) at a resolution of 10,000(10% valley) in SIM mode.

# 3. Result and Discussion

## 3.1. Seasonal variation and temporal trends

The concentration of PCDDs/Fs in ambient air samples from 2002 through 2008 ranged from 292 to 9,900 fg/m$^3$ with a mean 3,300 fg/m$^3$. The TEQ value of them ranged from 22 to 563 fg I-TEQ/m$^3$ with a mean 142fg I-TEQ/m$^3$. The levels were a bit higher than those of previous studies in urban area but lower than those in industrial areas (Choi et al., 2008; Raun et al., 2005; Abad et al., 2004). The first plot in Fig. 1. indicates monthly variation of PCDDs/Fs in ambient air. There was apparently a tendency which the TEQ value in ambient air was higher in the winter compared to the summer. The PCDDs/Fs concentrations in winter were approximately double compared to those in summer. The trend of higher levels of PCDDs/Fs during colder periods has been recognized by other researchers (Raun et al., 2005; Oh et al., 2001). The seasonal variations of PCDDs/Fs levels are presumed due to the increase in domestic heating, the presence of temperature inversion layer in winter and reaction with $OH^-$ radicals in summer. The second plot shows temporal trends of PCDDs/Fs in ambient air in Seoul. The plot indicated that mean TEQ value of PCDDs/Fs in 2002 was 0.187 fg I-TEQ/m$^3$ and the mean value tends to decline year by year. The level in 2008 was 0.106 fg I-TEQ/m$^3$.

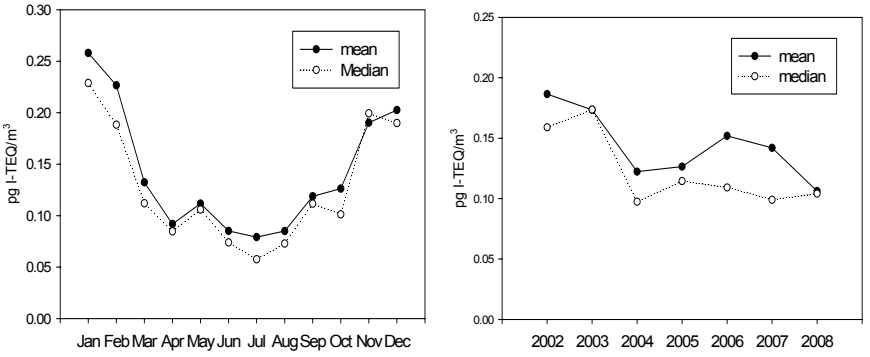


**Fig. 1.** Monthly variation and temporal trends of PCDDs/Fs in ambient air

## 3.2. Congener profile of PCDDs/Fs

The vertical bar chart in Fig. 2 indicates average congener profiles of PCDDs in ambient air. This plot presents a similar pattern with hepta- and octa CDDs/Fs making the major contributions in 2002, 2005, 2008. The ratios of PCDDs/PCDFs in air were from 0.43 to 0.52. Caserini et al. (2004) reported congener pattern of PCDDs/Fs in air in Italy. There was no significant difference of congener pattern

of PCDDs/Fs in their results comparing to those of my study. According to another study released (Raun et al., 2005), the occupation percentage of 1,2,3,4, 6,7,8-HpCDD and OCDD in 17 congener concentration was over 90%.

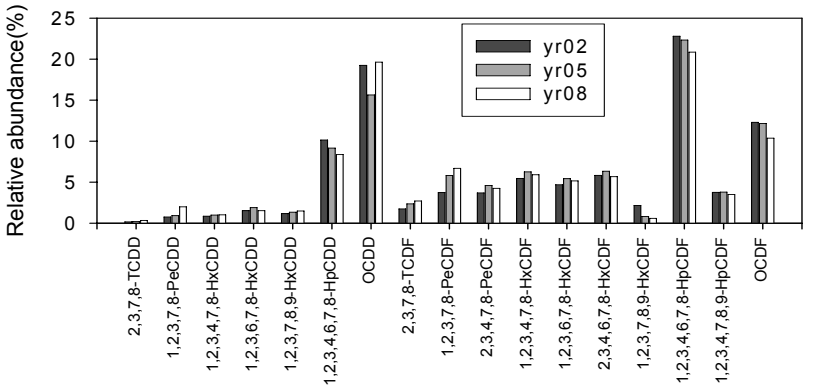


**Fig. 2.** Average congener profiles of PCDDs/Fs in ambient air in 2002, 2005 and 2008

## References

Abad E, Caixach J, Rivera J, Gustems L, Massague G, Puig O (2004) Temporal trends of PCDDs/PCDFs in ambient air in Catalonia(Spain) Science of the Total Environment 334–335, 279–285

Caserini S, Cernuschi S, Giugliano M, Grosso M, Lonati G, Mattanini P (2004) Air and soil dioxin levels at three sites in Italy in proximity to MSW incineration plants. Chemosphere 54, 1279–1287

Cheng PS, Hsu MS, Ma E, Chou U, Ling YC (2003) Levels of PCDD/Fs in ambient air and soil in the vicinity of a municipal solid waste incinerator in Hsinchu. Chemosphere 52, 1389–1396

Choi MPK, Ho SKM, So BKL, Cai Z, Lau AKH, Wong MH (2008) PCDD/F and dioxin PCB in Hong Kong air in relation to their regional transport in the Pearl River Delta region. Chemosphere 71, 211–218

Oh JE, Choi JS, Chang YS (2001) Gas/particle partitioning of polychlorinated dibenzo-*p*-dioxins and dibenzofurans in atmosphere; evaluation of predicting models. Atmospheric Environment 35, 4125–4134

Raun LH, Correa O, Rifai H, Suarez M, Koenig L, (2005) Statistical investigation of polychlorinated dibenzo-*p*-dioxins and dibenzofurans in the ambient air of Houston, Texas. Chemosphere 60, 973–989

# Chapter 8 Special session of California 2000 field study

Chairpersons: R. Fovell
J. Wilczak

Rapporteurs: R. Cohen
D. Yin

D.G. Steyn and S.T. Rao (eds.), *Air Pollution Modeling and Its Application XX*,
DOI 10.1007/978-90-481-3812-8_8, © Springer Science + Business Media B.V. 2010

# 8.1 Central California Ozone Study: Synthesis of Results

**Steven Reynolds[1], Carol Bohnenkamp[2], Ajith Kaduwela[3], Bruce Katayama[4], Evan Shipp[5], James Sweet[6], Saffet Tanrikulu[7], and Stephen Ziman[8]**

[1]Envair, San Rafael, CA, USA

[2]U.S. Environmental Protection Agency, Region 9, San Francisco, CA, USA

[3]California Air Resources Board, Sacramento, CA, USA

[4]Sacramento Metropolitan Air Quality Management District, Sacramento, CA, USA

[5]Shipp Air Quality Consulting, Fresno, CA, USA

[6]San Joaquin Valley Air Pollution Control District, Fresno, CA, USA

[7]Bay Area Air Quality Management District, San Francisco, CA, USA

[8]Ziman Consulting, San Francisco, CA, USA

This paper summarizes key findings of the Central California Ozone Study (CCOS). CCOS is a multi-year program of meteorological and air quality monitoring, emission inventory development, data analysis, and air quality simulation modeling. The objectives of CCOS are: (1) obtain suitable aerometric and emission databases to update, evaluate, and improve model applications for representing urban and regional-scale ozone episodes in central and northern California to meet the regulatory requirements for 1-h and 8-h ozone standards; (2) identify feasible, cost effective, and equitable emission controls to meet 1-h and 8-h ozone standards; (3) determine the contributions of transported and locally generated emissions to ozone formation and the relative benefits of volatile organic compound (VOC) and oxides of nitrogen (NOx) emission controls in upwind and downwind areas; and (4) assess the relative contributions of ozone generated from emissions in one air basin to federal and State exceedances in neighboring air basins. The study domain for CCOS covers all of central California and most of northern California, extending from the Pacific Ocean to east of the Sierra Nevada and from Redding to the Mojave Desert. The selection of this study area reflects the regional nature of ozone exceedances, increasing urbanization of traditionally rural areas, and a need to include all of the major flow features that affect air quality in the study domain.

The CCOS program consists of five main components: (1) development of an overall program plan, with particular emphasis on planning for the field measurement study; (2) conduct of an intensive field monitoring study from 1 June to 2 October 2000; (3) development of the information to support data analyses and air quality modeling; (4) development and evaluation of a suitable photochemical air quality simulation model for the study area; and (5) identifying and evaluating

D.G. Steyn and S.T. Rao (eds.), *Air Pollution Modeling and Its Application XX*,
DOI 10.1007/978-90-481-3812-8, 

emissions controls that will help achieve desired air quality goals in a cost effective manner

Key accomplishments in the planning area include the acquisition of sufficient funding to support a major integrated field measurement, data analysis, and air quality modeling program for ozone for central and northern California. The success of such a complex endeavor hinges on the development of a carefully designed plan for the conduct of each component. This helps assure that information needed in data analysis and modeling efforts is collected at appropriate times and locations. Planning was carried out in two-steps. First, a conceptual plan was developed that clearly delineates the goals and technical objectives of the study, and describes alternative experimental, modeling, and data analysis approaches for addressing the study objectives. After a consensus was reached on the conceptual plan, the second step involved the development of an operational plan for the field measurement study. The operational plan describes the details of the field measurement program in a manner that enabled the large number of participants making the measurements to do so in an effective and coordinated manner.

The summer 2000 field measurement program and the associated meteorological, emissions, and air quality database is a key accomplishment of CCOS. The main elements of this measurement program include: (1) implementation of forecast and decision-making protocols to decide whether or not to declare an Intensive Operating Period; (2) collection of surface-based meteorological data (primarily wind speed, wind direction, temperature, relative humidity, and solar and ultraviolet radiation) from a large array of sites; (3) operation of an array of radar wind profilers (several with RASS), SODARS, and radiosondes to measure meteorological conditions aloft; (4) deployment of a commercial ozonesonde to observe ozone profiles to about 2,000 m AGL; (5) conduct of aloft air quality measurements from fixed towers; (6) measurements of spectrally-resolved actinic flux at three sites and solar radiation measurements at several sites; (7) operation of 186 surface air quality monitoring stations that variously collect measurements of ozone, NOx, CO, and hydrocarbons; (8) expansion of PAMS monitoring of speciated hydrocarbons and carbonyls at 11 sites; (9) implementation of additional surface and aloft measurements designed to increase the understanding of high ozone in the Livermore Valley; (10) coordination of data collection activities with those of the California Regional PM10/PM2.5 Air Quality Study (CRPAQS); (11) operation of five instrumented aircraft to collect data pertaining to boundary conditions along western edge of the modeling domain, intra-valley transport within the San Joaquin Valley by eddies and slope flows, boundary conditions along the northern edge of the modeling domain, and measurements in power plant plumes for use in evaluating the plume-in-grid parameterizations used in air quality models. Upon completion of the field measurement program, the data collected were subject to quality control checks and scrutiny. Quality assurance efforts examined these activities to assure they were carried out in accordance with procedures established at the outset of the program.

Several studies were carried out to develop and improve emissions information. Efforts were devoted to validating databases describing the spatial distribution and identification of vegetation species as well as the leaf area index in natural areas. Process rates and other information from sources emitting more than 10 t/year of any criteria pollutant were reviewed and updated as necessary. Area source emissions methodologies were reviewed and improved where appropriate. Surrogates used to spatially distribute stationary area sources for both base and future year inventories were updated. Stack testing at two large power plants was conducted to better characterize plume parameters and the speciation of pollutant emissions. Day-specific traffic count information was used to develop more accurate estimates of hourly traffic volumes. Gridded emissions estimates were examined in light of ozone precursor measurements in various areas of the study area as a means of checking the quality of the modeling inventory and for identifying the potential need for improvements.

Initial data analysis efforts focused on characterizing the meteorology and air quality that occurred during the summer of 2000. Several additional data analysis efforts were initiated to address other key issues using the CCOS database, including the evaluation of mobile source emissions using remote sensing data, comparisons of the proportions of species derived from ambient and emissions data, and the evaluation of photolysis parameters. Considerable effort has been devoted to developing improved representations of meteorological phenomena through use of the MM5 and more recently the WRF meteorological models.

Historical ambient ozone and precursor trends and have been examined in an effort to better understand how ozone concentrations in central California respond to changes in precursor emissions. Ambient monitoring data confirm that emissions of ozone precursors decreased consistent with inventory estimates of emission trends. Peak ozone concentrations have trended downward in central California, especially within larger urban areas, but have been resistant to change in many downwind locations. The resistance of peak ozone to changes in emissions of ozone precursors is plausibly due to the complex, nonlinear relationship of ozone formation to NMOC and $NO_x$. The ozone and ozone-precursor trends indicate that air-quality management of ozone in central California requires a focus on emissions of ozone precursors within and throughout central California. Ongoing emission reductions will be needed to further reduce peak ozone concentrations, especially where past emission decreases were smallest.

Modeling efforts included a study to improve and evaluate the treatment of reactive plumes from large point sources in a photochemical grid model. A model including an advanced plume-in-grid (PiG) module was applied to one CCOS episode period. Comparisons of modeling results derived both with and without using the PiG module provide insights into the potential importance of such special treatments of large point source plumes in the study area. More recently, a seasonal ozone modeling capability is being developed and evaluated using measurements collected during the summer of 2000. The seasonal modeling is also being used to assess the sensitivity of calculated ozone levels to variations in key input parameters.

CCOS projects are being coordinated with those sponsored by CRPAQS. Though the emphases of these two studies are different (i.e., ozone versus particulate matter), they do share a common study area. Physical and chemical phenomena associated with ozone formation are also germane to particulate air quality issues. Particular attention is being given to developing a broad understanding of ozone and particulate matter air quality phenomena in central California and to identifying appropriate means for effectively achieving air quality goals.

## 1. Questions and Answers

**Wei Zhou:** How representative was 2000 high ozone and meteorology for the California air pollution?

**Answer:** To determine the representativeness of the CCOS episodic periods, a number of statistical approaches were taken that included classifying weather patterns over a medium-length period (13 years), and using CART analyses to establish relationships between weather types and routinely measured meteorological parameters, and sub-basin peak ozone levels. With regards to the CCOS modeling episodes, peak ozone levels in the six Central California sub basins were, for the most part, historically representative of other periods with similar meteorology. Further information can be obtained in the report by Lehrman et al. (2004), *Characterization of the CCOS 2000 Measurement Period*, Final Report (Contract 01-2CCOS), Technical and Business Systems, Inc., Santa Rosa, CA, March 1, 2004. This document is available at http://www.arb.ca.gov/airways/ccos/ccos.htm.

**Ron Cohen:** How well does the modeling system perform at describing so-called non-episode conditions?

**Answer:** Model performance for non-episode conditions is being examined in an ongoing study being conducted by the University of California and Lawrence Berkeley National Laboratory. Regional model simulations for the CCOS domain are being made for the entire summer 2000 period. Analysis of these results will provide insights into how well the modeling system simulates both episode and non-episode conditions.

**Douw Steyn:** Is the data base from this study available for model intercomparison studies such as AQMETI?

**Answer:** The CCOS data base is available for use in model intercomparison studies. Please contact Ajith Kaduwela at the California Air Resources Board for further information.

# 8.2 Meteorological Triggers for Ozone Episodes in Central California

**Ahmet Palazoglu, Angadh Singh, and Scott Beaver**

University of California, Davis, CA, USA

**Abstract** A wind field cluster analysis was performed for the summer ozone seasons (May–October) of 1996–2004 for the Central California domain. The data consisted of hourly surface wind speed and direction measurements collected by a number of surface monitoring networks. For each air basin, we identified days sharing similar diurnal cycles. Each day and basin was categorized among these recurring meteorological patterns associated with distinct 500-hPa conditions. We show how summer air quality is consistently driven by these synoptic (large-scale) influences – anticyclonic and cyclonic weather systems that develop over the Pacific Ocean and the southwestern United States. Two such anticyclonic patterns are shown to trigger the majority of the ozone exceedences. For all Central California air basins, an eastward sweeping ridge of high pressure originating offshore is associated with rapidly building ozone levels. For the inland San Joaquin and Sacramento Valleys, the northward migration of an anticyclone forming over Mojave Desert and/or Four Corners triggers a number of episodes. These episodic scenarios are illustrated by examples demonstrating these meteorological triggers.

**Keywords** CCOS 2000 Field Study, cluster analysis, synoptic meteorology, wind fields

## 1. Introduction

The purpose of this study was to determine the relationship between meteorology and ozone levels throughout the CCOS domain, which includes three major, coupled air basins in non-attainment of ambient ozone regulations: San Francisco Bay Area (SFBA), San Joaquin Valley (SJV), and Sacramento Valley (SV). Robust statistical methods (Beaver and Palazoglu, 2006; Beaver et al., 2008) were applied to routine surface measurements collected from these basins over nine extended summer ozone seasons (May–October of 1996–2004), for 1,656 days. The results were essential for conceptual modeling of Central California summer air quality; ozone numerical modeling and forecasting; air quality planning; categorizing transport potential; designing future field monitoring programs;

D.G. Steyn and S.T. Rao (eds.), *Air Pollution Modeling and Its Application XX*,
DOI 10.1007/978-90-481-3812-8, 

performing meteorologically adjusted trend analyses; and evaluating emissions control strategy efficacy.

## 2. Method

Extensive use was made of cluster analysis techniques. These algorithms identify distinct groups of days sharing similar, recurring boundary layer characteristics. A main goal was to identify conditions allowing 8-h ozone to build to the NAAQS exceedance threshold (85 ppb). First, clustering of wind field measurements identified distinct air flow patterns associated with different ozone source-receptor relationships. Second, clustering of ozone level measurements identified distinct ozone spatial distributions potentially associated with different meteorological conditions. These complimentary clustering methods are commonly referred to as *circulation-to-environment* and *environment-to-circulation* approaches, respectively (Ainslie and Steyn, 2007). We considered data from 9 recent years after reformulated gasoline (RFG) was introduced to California. It is assumed that emissions characteristics during the period were relatively constant, so that patterns isolated by the clusterings largely reflect meteorological variability and day-of-week emissions differences. Clustering a total of 1,656 days since RFG introduction ensures the identified meteorological patterns are representative for use in current and future air quality studies and policy development efforts.

The large size and meteorological complexity of Central California preclude a direct clustering of measurements spanning the entire domain. Instead, independent clusterings were performed for seven subdomains to characterize the regional variability of meteorology and air quality within each. SFBA and SV are each considered as individual subdomains. SJV was subdivided into northern, central, and southern subdomains (N-SJV, C-SJV, and S-SJV, respectively). The remaining subdomains are the Mountain Counties (MC) and Sequoia National Park area (Sequoia). Direct clusterings of MC and Sequoia measurements were not instructive due to highly localized meteorology in these mountainous regions. Thus, their air quality is evaluated in response to the clusterings for SV and SJV, respectively, with which these elevated subdomains are contiguous and meteorologically coupled.

## 3. Results and Discussion

The wind field clustering identified four to seven weather patterns for each subdomain. Such relatively small numbers of clusters are typical of air quality meteorology studies. Forcing the clustering algorithm to yield larger numbers of patterns tends to produce clusters that are too meteorologically similar to capture distinct ozone source-receptor relationships and dispersion patterns. The more

meteorologically complex subdomains had larger numbers of clusters. Meteorological complexity here refers to the degree of interaction between the large-scale pressure gradient and more localized terrain effects to produce the observed flow field. Differences in complexity among the subdomains justify their independent clusterings. SFBA exhibits four clusters and is the least complex. It is directly affected by marine flows of variable strength which nearly always arrive from the Pacific Ocean to the west. Relative to SFBA, SJV has one additional cluster (five total) and is more complex. Bulk flows along the SJV major axis are nearly always oriented from the north, and a number of localized, terrain-induced flow features significantly impact regional air quality. SV exhibits seven clusters and is the most complex. Bulk flows along the SV major axis can be oriented from either the north or south, and localized, terrain-induced flow features significantly impact regional air quality.

The clusters were named according to their dominant upper-level features. Clusters R and H exhibit relatively calm conditions and have the highest ozone pollution potentials. R and H reflect upper-level (500-hPa) ridges and onshore high pressure centers, respectively. This pair of clusters generally has reduced marine air flows through the Carquinez Strait and into the Central Valley, as well as limited vertical dispersion. A variety of ventilated patterns (named using V) exhibit relatively high winds through the Carquinez Strait and have lower ozone pollution potentials. Cluster H/V is a hybrid pattern capturing high winds through Carquinez Strait, limited vertical dispersion, and moderate to high ozone pollution potential, depending on the subdomain. The clusters are seasonally distinct. H and H/V account for more exceedances during the middle of the ozone season, whereas R accounts for more exceedances near the beginning and end of the ozone season. Specific to each subdomain, the clusters are associated with localized flow features which may trigger NAAQS exceedances. These features include: sea breeze activity along the I-680 Corridor and Santa Clara Valley for SFBA; lack of ventilating flows through minor Coast Range gaps such as Altamont Pass for N-SJV; the Fresno Eddy for C-SJV; reversal of flows exiting SJV toward Mojave Desert for S-SJV; and slope flows over the Sierra Range extending over the Sacramento source area for SV.

Two subsequent analyses were applied to the wind field cluster labels to better characterize meteorological impacts on ozone levels. The clusters alone categorize the conditions on a given day in a given subdomain among a small number of idealized patterns. They do not directly account for temporal patterns longer than a single day (i.e., multi-day evolution of episodes) or spatial patterns larger than a single subdomain (i.e., meteorological coupling of connected basins). First, we tracked the day-to-day evolution of weather systems impacting ozone levels by considering multi-day sequences of the daily cluster labels. This sequence analysis distinguished between various episodic scenarios in which stagnating air masses develop. Different scenarios reflect weather systems of onshore (over the Mojave Desert or Four Corners) and offshore (over the Pacific Ocean) origins. Second, a domain-wide synthesis of the clustering and sequencing results was constructed by combining the independent results for all subdomains. Qualitatively, each of the

CCOS subdomains is impacted by similar large-scale meteorological phenomena; however, the timings and sensitivity of ozone levels to these weather patterns vary considerably throughout the CCOS domain.

We observed that summer air quality throughout Central California is consistently driven by synoptic (large-scale) influences – anticyclonic and cyclonic weather systems that develop over the Pacific Ocean and the southwestern United States. Two such anticyclonic patterns were shown to trigger the majority of the ozone exceedences. For all Central California air basins, an eastward sweeping ridge of high pressure originating offshore is associated with rapidly building ozone levels. For the inland SJV and SV, northward migration of an anticyclone forming over Mojave Desert and/or Four Corners triggers a number of episodes.

The ozone clustering was shown to be useful for describing the spatial distribution of ozone within a basin having complex terrain (e.g. SFBA). However, we concluded that it is not very useful for regional ozone analysis. This type of clustering is perhaps simple to implement, but lacks sufficient statistical power to provide further insight into the analysis. Similar discussion is present in Ainslie and Steyn (2007). For SFBA, the clustering was applied to days exceeding the 8-h NAAQS (85 ppb) as well as the new California state 8-h ambient standard (70 ppb). Both clusterings reflected episodes driven by different meteorological conditions, as well as weekend-weekday emissions differences. A key conclusion was that the SFBA exceedances of the 70 ppb standard become more likely for weekdays at locations for which 85 ppb exceedances are not as prevalent.

## References

Ainslie, B. and Steyn, D. G., 2007: Spatiotemporal trends in episodic ozone pollution in the Lower Fraser Valley, British Columbia, in relation to mesoscale atmospheric circulation patterns and emissions. *J. Appl. Meteor. Climatol.*, **46**, 1631–1644.

Beaver, S. and Palazoglu, A., 2006: Cluster analysis of hourly wind measurements to reveal synoptic regimes affecting air quality. *J. Appl. Meteor. Climatol.*, **45**, 1710–1726.

Beaver, S., Palazoglu, A., and Tanrikulu, S., 2008: Cluster sequencing to analyze synoptic transitions affecting regional ozone. *J. Appl. Meteor. Climatol.*, **47**, 901–916.

## 4. Questions and Answers

**Ron Cohen:** Is temperature a sufficient surrogate for high ozone, allowing a much larger dataset for cluster analysis?

**Answer:** Our analysis focused on the wind field, because it directly reveals meteorological processes impacting ozone source-receptor relationships. Using a two-stage approach, synoptic and mesoscale air flow patterns were identified to explain ozone levels. Certainly temperature does affect ozone production for Central California. Statistically, temperature correlates strongly with ozone levels

throughout this region; however, we did not find temperature to add explanatory power to our statistical model based on the wind field. This is because temperature is largely a function of marine penetration through the complex Central California terrain. The degree of marine penetration is already reflected in the wind field, and thus temperature offers little additional information. We have not explored clustering of (scalar) temperature because the algorithm utilized has been tailored for (two-dimensional) wind fields.

**Christian Reuten:** When you talked about the influence of up- and down-slope flows, did you mean slope flows or valley flows?

**Answer:** Both slope flows and valley flows impact ozone levels throughout the Central California valleys. Strong up/down valley flows tend to ventilate the region. Weaker valley flows indicate near-calm and stable conditions that set the stage for ozone exceedances. Under such conditions, the localized slope flows have important influences on ozone source-receptor relationships. Overnight downslope (drainage) flows especially impact fresh emissions during the morning hours. Certain downslope flow features appear to trigger ozone exceedances under near-calm, stable, subsiding conditions.

**Chip Levy:** Will you not consider inter-annual variability of the met triggers you have identified (i.e. ENSO type as well as climate change)?

**Answer:** In this study, we focused on a 15-year period to obtain representative meteorological patterns impacting ozone levels. Certain patterns were associated with conducive conditions under which ozone exceedances become likely. Year-to-year variability in the frequency of such conducive conditions largely determines how many exceedances occur in a given year. We attempted to relate the frequency of conducive conditions with traditional indices for inter-annual variability such as El Nino-Southern Oscillation Index (ENSO) and the Pacific/North American teleconnection pattern (PNA). We found no simple relationship between such indices and the frequency of conducive conditions indicated by the clustering. A follow-up study of the inter-annual variability is indeed being considered. Our method requires extremely high quality data which are difficult to obtain prior to our 15-year study period. We do not believe that a 15-year study period is sufficient to observe climate change trends. Rather, we would consider the climate stable during this 15-year period to assay the degree of natural year-to-year variability in planetary flow patterns. Such a study would provide a baseline for examining future trends due to climate change.

# 8.3 Factors Controlling the Formation of Ozone in the San Francisco Bay Area

**Su-Tzai Soong and Saffet Tanrikulu**

Bay Area Air Quality Management District, San Francisco, CA, USA

## 1. Introduction

Factors controlling the production of ozone in the San Francisco Bay Area (SFBA) were studied using the process analysis module of the CAMx model. This study is a continuation of previous modeling work that was performed as part of the Central California Ozone Study (CCOS). During that study, meteorology of one of the captured ozone episodes (July 29–August 3, 2000) was simulated by Wilczak et al. (2004) using the MM5 model and ozone concentrations were simulated by Soong et al. (2004) using the CAMx model. Both MM5 and CAMx performed well in simulating this episode.

The modeling domain had a 185 × 185 horizontal grid with 4 km resolution, covering most of Central California. A stretching vertical grid spacing was employed in both models with 50 layers in MM5 and 20 layers in CAMx. The thickness of the layer near the surface was 24 m in both models. Initial and boundary conditions of CAMx were specified using surface and upper air observations. A day-specific emissions inventory was generated for the modeling period.

To study the factors controlling the production of ozone in the SFBA, we focused on July 31, 2000, when the 1-h observed maximum ozone concentration reached 126 ppb in Livermore. We hypothesized and investigated three factors that may be controlling ozone production in the SFBA: the VOC-NOx ratio (V/N ratio hereafter), the magnitude of VOC and NOx concentrations, and ambient temperatures.

## 2. Results

The left panel of Fig. 1 shows simulated 1-h ozone concentrations in the SFBA at 1400 PDT on July 31, 2000, when simulated ozone production reached a maximum there. The highest ozone production rate of 20–30 ppb/h was simulated in portions of four counties, Alameda, Contra Costa, Santa Clara and Sonoma (dark areas of right panel of Fig. 1). In the remaining portions of these counties, the production rate was mostly 10–20 ppb/h. Along the northern and western boundaries of the SFBA, the production rate was under 10 ppb/h. In the core areas of San Francisco, Oakland and San Jose, and along some freeways, however, the production rate was negative (white areas).

D.G. Steyn and S.T. Rao (eds.), *Air Pollution Modeling and Its Application XX*,
DOI 10.1007/978-90-481-3812-8, 

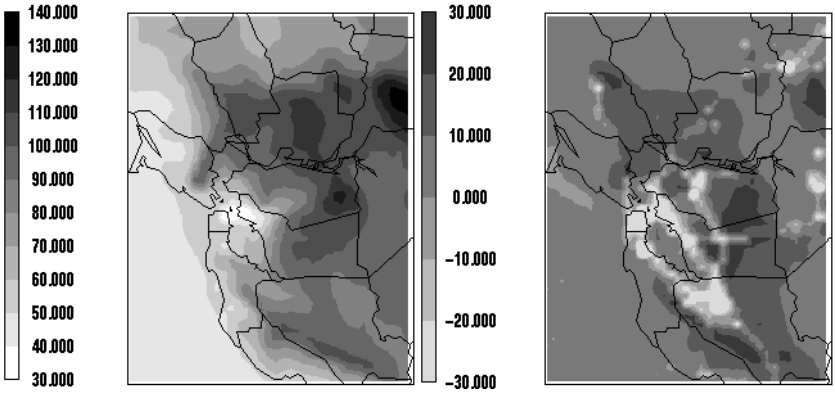


**Fig. 1.** Simulated 1-h ozone concentrations (ppb, left panel) and 1-h net change in ozone concentrations due to chemical processes (ppb/h, right panel) at 1400 PDT on July 31, 2000

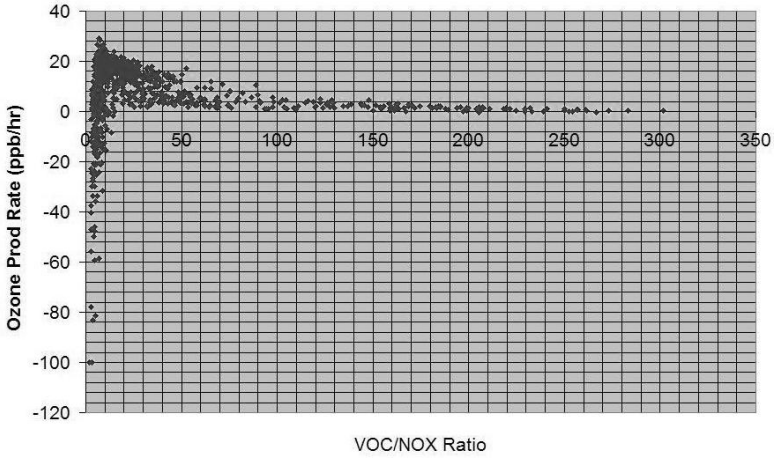


**Fig. 2.** Scatter plot of ozone production rate versus V/N ratio

The locations of maximum ozone and net ozone production areas mostly matched, as expected.

The relationship between ozone production rate and the V/N ratio is shown in Fig. 2. Each point in the figure shows information from a grid cell in the SFBA domain. Ozone production was at a maximum when the V/N ratio was about 7. Ozone production decreased gradually with increasing V/N ratio. In the areas where the V/N ratio was less than 7, the rate of ozone production decreased sharply. These are in general NOx rich areas with a large titration rate of ozone.

The relationship between change in ozone concentration and NOx and VOC concentrations are shown in Table 1. All grid cells with NOx concentrations of 0–4 ppb show net ozone production. Ozone production at these cells increases linearly with increasing NOx concentration. Cells with NOx concentrations of

4–20 ppb predominantly show net ozone production, with 20–60 ppb, predominantly net ozone destruction, and with more than 60 ppb, always net ozone destruction. All grid cells with VOC concentrations 25–50 ppbc show only net ozone production. Note that the minimum VOC concentration in the SFBA was 25 ppbc. Grid cells with VOC concentrations of 50–110 ppbc predominantly show net ozone production, with 110–190 ppbc, predominantly net ozone destruction and with more than 190 ppbc, only net ozone destruction.

Figure 3, a scatter plot of VOC and NOx, shows a regression line for VOC and NOx concentrations. Cells with high VOC and NOx concentrations (near large anthropogenic emission sources) are generally low V/N ratio areas with net ozone destruction. Cells with low VOC and NOx concentrations are high V/N ratio areas with net ozone production.

The horizontal distribution of the V/N ratio in the SFBA is shown in Fig. 4 (left panel). In the San Francisco Bay and areas in the east and south of the Bay, the V/N ratio is less than 6. This is the region where net ozone destruction dominates. There is a large area in the east and a narrow strip of land in the west of this region where the V/N ratio is between 6 and 12. While in the east, net ozone production dominates, net ozone destruction dominates in the west because of cold air temperature, Fig. 4 (right panel).

**Table 1.** The relationship between change in ozone and in NOx and VOC concentrations

| VOC (ppbc) | 25–50 | 50–110 | 111–190 | 190< |
|---|---|---|---|---|
| Change in ozone | Production only | Production dominant | Destruction dominant | Destruction only |
| NOx (ppb) | 0–4 | 4–20 | 20–60 | 60< |

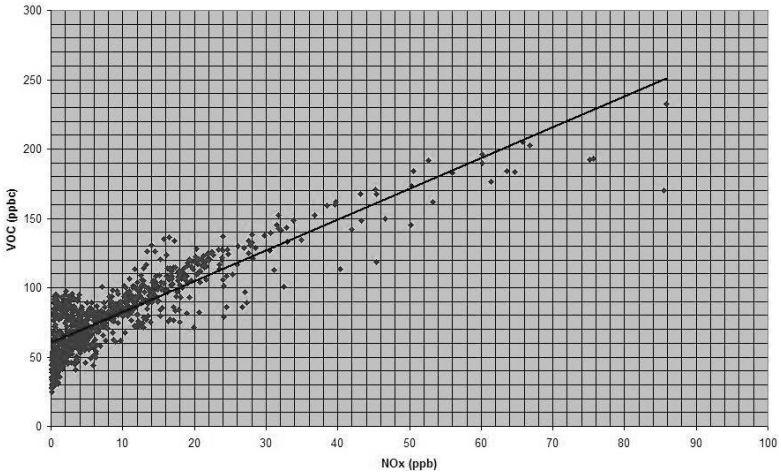


**Fig. 3.** Scatter plot of NOx and VOC with regression line

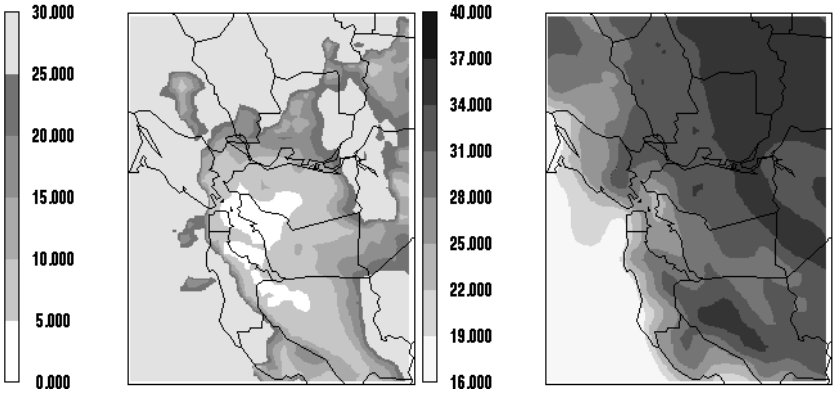


**Fig. 4.** Horizontal distribution of the V/N ratio (left panel) and surface temperature (C, right panel) in the SFBA at 14 PDT on July 31, 2000

We also studied other atmospheric and chemical processes that affect ozone in the SFBA including advection, diffusion, and dry deposition. The effect of advection and diffusion changes from 1 h to the next both in magnitude and direction. Over most of the eastern part of the SFBA, however, dry deposition dominates and removes about 20–30 ppb/h ozone from the atmosphere (not shown).

The conclusions of this paper can be summarized as follows: (1) VOC and NOx are positively correlated in the SFBA, (2) the V/N ratio is negatively correlated with either VOC or NOx, (3) areas of large VOC and NOx concentrations limit ozone production while areas of small VOC and NOx concentrations promote ozone, (4) the V/N ratio that is correlated with peak ozone production is 7, (5) Cold sea surface temperature limits ozone production, (6) the effect of dry deposition is significant.

## 3. Questions and Answers

**Question:** Have the authors considered the inclusion of indicator species (NOy, HCHO/NOy) in the study? Indicator species consider the air mass aging with respect to $O_3$ sensitivity and could provide additional info on $O_3$ formation.

**Answer:** We investigated 37 grid cells in depths where NOx concentrations were around 15 ppb and VOC concentrations were around 100 ppb. Even though these cells had similar NOx and VOC values, and similar VOC/NOx ratios, there were large variations of $O_3$ production over them, ranging from –30 to +25 ppb/h. In these cells, there was no clear correlation between NOy and $O_3$ production or between HCHO/NOy and $O_3$ production. However, there was a slight positive correlation between NOy–NOx and $O_3$ production. There was also a negative correlation between HONO and $O_3$ production. We further investigated the

correlation between each VOC specie and $O_3$ production. About half of the VOC species were positively correlated with $O_3$ production and the remaining half were negatively correlated. The different mix of these species at a given cell determines the positive or negative $O_3$ productions at that cell.

**Question:** Have you computed $Ox/O_3$ to evaluate the effects of photochemical production and titration?

**Answer:** For the same 37 cells discussed in question 1, we did not find a correlation between $Ox/O_3$ and $O_3$ production. But we did find a fairly good negative correlation between $Ox/O_3$ and $O_3$ itself.

# 8.4 Effects of VOC and $NO_x$ Emission Changes on Ozone and Precursor Concentrations in Central California from 1990 to 2004

**Charles L. Blanchard[1], Shelley Tanenbaum[1], Eric Fujita[2], James Wilkinson[3], and David Campbell[2]**

[1]Envair, Albany, CA, USA

[2]Desert Research Institute, Reno, NV, USA

[3]Alpine Geophysics, Eugene, OR, USA

**Abstract** From 1990 to 2004, peak ozone concentrations trended predominantly downward in central California, but the median rate of decrease in the annual 4th-highest peak ozone at 44 trend sites was only 0.3 ppbv per year and trends were statistically significant at only 6 sites. Ambient monitoring data confirm that emissions of ozone precursors decreased at rates consistent with inventory estimates of emission trends (~10 to 50 percent reductions). We examine ten possible hypotheses that might explain why the observed ozone trends did not show larger decreases.

**Keywords** Central California, ozone trends, emission trends

From 1990 to 2004, peak ozone concentrations trended predominantly downward in central California: 36 long-term monitoring sites had downward trends in the annual fourth-highest daily maximum 8-h ozone and eight sites had upward trends. Six downward site trends were statistically significant ($p > 0.05$) for 1990–2004. The rates of progress were greater post-2000 than in the 1990s, and 11 sites showed significant ($p < 0.05$) downward trends for 1990–2007. The median rate of decrease in the annual fourth-highest peak ozone was modest (0.3 ppbv/year from 1990 to 2004 and 0.7 ppbv/year from 1990 to 2007).

We examine ten possible hypotheses that might explain why the observed ozone trends did not show larger decreases. The hypotheses fall into three general categories: (1) emissions-related; (2) exogeneous factors; and (3) the chemistry of ozone formation.

The hypothesis that emissions did not decline is incorrect. Ambient monitoring data confirm that emissions of ozone precursors decreased at rates consistent with inventory estimates of emission trends. The downward trends in mean morning or mid-day concentrations of oxides of nitrogen ($NO_x$), carbon monoxide (CO), and non-methane organic compounds (NMOC) were statistically significant ($p < 0.05$) at 22 of 28 sites, 21 of 25 sites, and 6 of 7 sites, respectively. Although the

D.G. Steyn and S.T. Rao (eds.), *Air Pollution Modeling and Its Application XX*,
DOI 10.1007/978-90-481-3812-8, 

downward trend in $NO_x$ emissions was not matched by ambient $NO_x$ trends at all monitoring sites, the average ambient $NO_x$ decreases were approximately equal to the inventory trends. For all NMOC sites and most CO monitoring sites, ambient pollutant declines were as large as, or larger than, emission decreases reported in the inventory.

While emissions declined overall, a plausible hypothesis is that ozone precursor emissions and concentrations did not decline enough in some areas experiencing substantial growth and development to produce a significant ozone response in those areas. From 1990 to 2004, domain-wide NMOC, $NO_x$, and CO emissions declined by 33%, 29%, and 52%, respectively. In local (28 × 28 km) areas surrounding ozone-monitoring sites, NMOC and $NO_x$ emissions exhibited declines of approximately 10% to 40%. However, 15 of 44 sites exhibited local $NO_x$ reductions less than 20% and eight sites showed local NMOC reductions less than 20%; six sites showed local emission reductions less than 20% for both NMOC and $NO_x$. The geographical range of the six sites includes much of the northern and central San Joaquin Valley; local NMOC emissions increased at three of the six locations. In Fresno County, the emission inventory indicates that downward trends in $NO_x$ emissions from point sources and from gasoline-engine vehicles were partially offset by upward trends in emissions from diesel-engine vehicles. The lack of change in local emissions in the northern and central San Joquin Valley is a potentially significant factor in the amount of local ozone formation. Ozone decreases, if any, might be expected to result more from regional-scale emission reductions than from the relatively modest local emission changes. Ambient measurements showed no direct and simple correlation between local emission changes and peak ozone trends, however.

Meteorological factors affect peak ozone concentrations and induce year-to-year variations that result in "good" and "bad" ozone years, but do not account for the observed ozone trends. Monitoring data from 1990 to 2004 do not show significant trends in synoptic-scale meteorological conditions, average upper-air (850 mb) temperature, average daily-maximum surface temperature, or season-average background ozone concentrations. Changes in background ozone, temperature, or synoptic-scale meteorological patterns, if any, do not explain the observed spatial variations in ozone trends. The ozone decreases were larger in the southern San Francisco Bay Area, the Sierra Nevada foothills, and the northern San Joaquin Valley than in other parts of central California.

The resistance of peak ozone to substantial (~10–50%) reductions in emissions of ozone precursors is plausibly due to the complex, nonlinear relationship of ozone formation to NMOC and $NO_x$. The ambient monitoring data show that changes occurred in ratios of NMOC/$NO_x$, ratios of various NMOC species, and in average NMOC reactivity from 1994 to 2004. The ambient decreases in total NMOC and sums of species concentrations exceeded 50%. The predominant change was a reduction in species and total NMOC concentrations, though the average reactivity (with OH radical as represented by the $k_{OH}$ rate constants) also declined at some sites post-2000. Mean morning NMOC/$NO_x$ molar ratios declined from ~6:1–8:1 during 1994–1998 to ~4:1–6:1 during 2000–2004. The

emission-inventory ratios averaged approximately 30% lower than the ambient ratios when converted to comparable units. The observed declines in ambient NMOC/$NO_x$ ratios represent shifts toward ratios at which ozone production is less efficient. The trends do not imply a change in the limiting precursor at the urban locations where NMOC was monitored. The differences between the morning (5–8 a.m.) and afternoon (noon–2 p.m. or 4–7 p.m.) ambient NMOC/$NO_x$ ratios generally diminished over time. This change suggests that air masses at the NMOC-monitoring sites were less photochemically aged by mid-day in later years than in earlier years. One possibility is that $NO_x$ was removed less rapidly during later years; another is that some sites may have experienced a relative increase in fresh emissions during mid-day hours. Further study is needed.

The ozone and ozone-precursor trends indicate that management of ozone in central California requires a focus on emissions of ozone precursors within and throughout central California. Ongoing emission reductions will be needed to further reduce peak ozone concentrations. The analyses do not identify where and when peak ozone concentrations might be more effectively managed through reductions of NMOC, $NO_x$, or both. Because the CCOS domain is large and encompasses highly urbanized, rural, undeveloped, and wilderness lands, it is expected that ozone formation is limited by NMOC in some areas and by $NO_x$ in others. Although the analyses are not definitive in this respect, they suggest that emission reductions that continue to maintain low ratios of NMOC/$NO_x$ are more likely to be effective than reductions that cause NMOC/$NO_x$ ratios to increase. Further study is needed to identify the specific reductions of ozone precursors of greatest value within each nonattainment area.

**Acknowledgments** The authors greatly appreciate the help provided by many people and especially thank Dar Mims, Dwight Oda, Martin Johnson, Ajith Kaduwela, Larry Larsen, and Cheryl Taylor of the California Air Resources Board, Jim Cordova and Saffet Tanrikulu of the Bay Area Air Quality Management District, and Evan Shipp of the San Joaquin Valley Air Pollution Control District for their assistance with data, emission inventories, statistical methods, and project review.



## Questions and Answers

**Question:** European data indicate declining peak (episode) ozone and increasing background ozone. Can you explain the apparent contradiction between these results and yours?

**Answer:** Data from the National Park Service passive ozone monitoring program suggest an increasing trend in seasonal mean ozone concentrations at some parks in California and Oregon that are not immediately downwind of local emission source regions, specifically, Crater Lake National Park, Lava Beds National Monument, and Point Reyes National Seashore, and so are not necessarily inconsistent with other trend data. The magnitudes of the observed changes at these west-coast parks are not large enough to explain the trends in the annual fourth-highest peak daily 8-h ozone at compliance-monitoring sites in central California, or the spatial variations of the central California peak ozone trends.

**Question:** First, do NMOC include biogenics and has the relative fraction of "controllable" VOC changed? Second, $NO_x$ decrease causes an OH radical increase, so ambient VOC should decrease faster than emissions; is that an explanation for the more rapid decrease of ambient NMOC concentrations than of VOC emissions?

**Answer:** The NMOC data are from the PAMS program's canister samples and continuous measurements, both of which represent total nonmethane organic compounds. Total NMOC includes biogenic compounds that are captured by the sampling methods. However, isoprene is the only individually-measured biogenic compound. Our data do not answer the question of the effect of $NO_x$ on ambient NMOC concentrations and trends. Another possible explanation for the discrepancy between ambient and emissions NMOC trends is that the ambient trends at the seven NMOC monitoring sites may not be representative of the entire domain. The ambient trends were more similar to county-level and multi-county emission trends than to either local (within 28 × 28 km areas around monitors) or domain-wide emission trends.

# 8.5 High-Resolution Meteorological Modeling of California Air Quality Episodes: Model Intercomparison and Validation

**Robert G. Fovell[1], Bruce Jackson[2], and Ajith Kaduwela[2]**

[1]Atmospheric and Oceanic Sciences, University of California, Los Angeles, CA, USA

[2] California Air Resources Board, Sacramento, CA, USA

**Abstract** Mesoscale model simulations of a high ozone summer episode are validated against surface observations, for the purpose of finding optimal configurations to support air quality studies for present and future climates. Issues involving validating temperatures are discussed.

**Keywords** California CCOS 2000 field study, mesoscale model validation

## 1. Introduction

Our understanding of poor air quality episodes, and ability to forecast and mitigate them, depends on proper representation of lower tropospheric meteorology at high resolution. The employment of mesoscale models in this effort is indicated for three reasons. First, insufficient observations, especially above the surface, exist to permit a full understanding of pollution transport. Second, operational models fail to properly capture complex and important topographic and landuse patterns. Finally, the need exists to not only understand past and present events but also anticipate how air quality may respond to regional and large-scale climate change.

Yet, mesoscale models need to be properly tuned and systematically validated. This work employs two such models – the Weather Research and Forecasting (WRF) ARW core and the NCAR/Penn State Mesoscale Model, Version 5 (MM5) – to simulate meteorological conditions during the Central California Ozone Study. This report narrows the focus to model physics selection based on validation against surface observations.

D.G. Steyn and S.T. Rao (eds.), *Air Pollution Modeling and Its Application XX*,
DOI 10.1007/978-90-481-3812-8, 

## 2. Model Description, Initialization and Validation

These simulations employed the most recent versions of WRF (v.3.0.1, v.3.1) and MM5 (v.3.7.4) with three nests telescoping to 4 km resolution. Initializations included three-hourly analyses from the Eta model (ETA) and the North American Regional Reanalysis (NARR), and six-hourly Global Forecast System Final Analyses (FNL). For WRF, simulations were made using the Noah and Thermal Diffusion (TD) land surface models, RRTM/Dudhia and CAM radiation parameterizations, and YSU and MYJ planetary boundary layer (PBL) schemes, with and without analysis nudging. Model tests spanned three platforms (Xeon, Athlon, PowerPC), two operating systems (Linux and Mac OS X) and three compilers (Intel, Portland Group and IBM). Comparable MM5 runs were also made.

We seek accurate representations of PBL temperature, wind and humidity across complex terrain. However, validation data largely consists of hourly observations from Remote Automated Weather Stations (RAWS) and mainly airport-based Automated Surface Observing System (ASOS) sites. For August 1–2, 2000, 140 *representative stations* in the 4 km nest with fewer than 25% of hours missing and post-interpolation elevation discrepancies <200 m were identified (Fig. 1, Table 1).

**Table 1.** Representative station information

| Type | Number of stations | Avg. elevation (m) | Elevation range (m) |
|---|---|---|---|
| ASOS | 39 | 243 | 1–1958 |
| RAWS | 101 | 957 | 5–2679 |
| RAWS subset | 32 | 242 | 5–459 |

## 3. Temperature Diurnal Cycle Assessment

The present analysis focuses on the temperature diurnal cycle for the 24 h period commencing 00Z August 1, from over 50 simulations initialized at variety of times back to 00Z July 31. As winds were light and variable in the absence of large-scale forcing, the boundary layer circulation was sensitively dependent on differential heating reflecting mesoscale landuse and topographic variations, stressing a model's weakest components.

Surprisingly large variation among forecasts of average 2 m temperature for the combined RAWS and ASOS dataset was found (Fig. 2a). Many forecasts evinced a nighttime warm bias and all ostensibly underpredicted temperature the following afternoon; the TD scheme consistently overpredicted 2 m dewpoints (Fig. 2b). However, inspection revealed a substantial difference in forecasts at ASOS and

RAWS sites, such that *simulations characterizing one station type well necessarily handled the other poorly*. After little difference overnight, the average RAWS observation was 4°C warmer than ASOS by local noon (Fig. 2c). Even after adjustment for elevation (Table 1) and timing issues, the former addressed via a 32-station, lower altitude RAWS subset (Fig. 1), a substantial discrepancy between RAWS and ASOS averages remained (Fig. 2c).

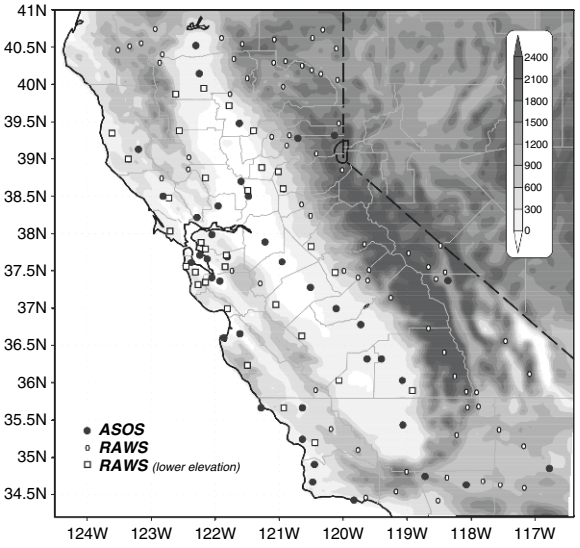


**Fig. 1.** Terrain of 4 km domain with locations of ASOS and RAWS stations shown

This analysis raises questions about these remote, unattended RAWS sites, which appear to permit greater variation in temperature sensor placement height. The most skillful simulation with respect to ASOS stations alone (WRF-55, Table 2) evinced a warm bias overnight for RAWS stations and a pronounced cold bias for the following afternoon (Fig. 2d). This suggests RAWS sensors may be systematically placed too close to the ground, invalidating model physics similarity assumptions. Subsequent analyses involve ASOS stations only.

The WRF-55 simulation, which used WRF v.3.1, was an unnudged 48 h run from 00Z July 31 using the QNSE PBL scheme and CAM radiation. This was one of the few WRF runs that bested MM5 without resorting to nudging. We hoped that skillful WRF simulations could be obtained without that commonly employed technique for model limitation compensation. Further work is needed to determine if this physics combination has wider applicability.

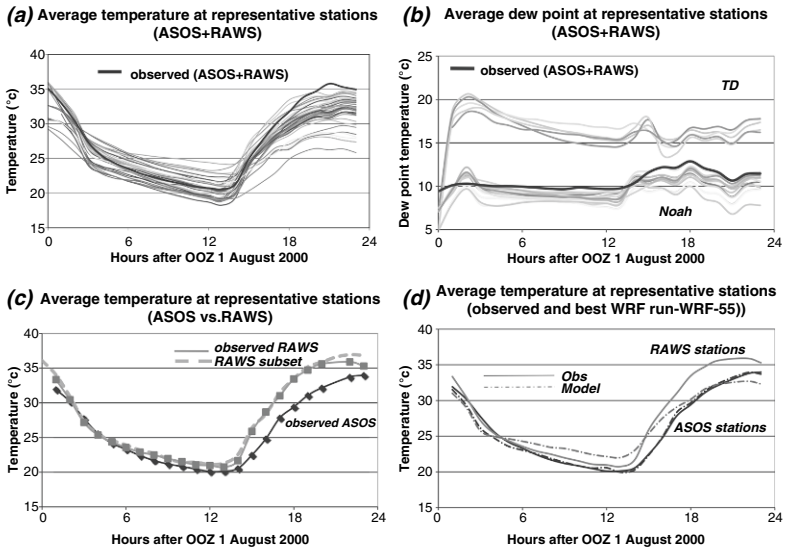


**Fig. 2.** Time series for August 1, 2000, observations and simulations. See text

## 4. Model Physics Issues

Difficulties were encountered in WRF runs with some data sources and physics combinations, manifested as substantial afternoon cold biases. Although the cold bias appeared to develop "bottom-up" from the surface after sunrise on August 1, nudging to the analysis "top-down" from the free atmosphere succeeded in controlling the problem. Figure 3 shows the difference 2 m temperature between unnudged and nudged runs using RRTM and Dudhia radiation. This is a 48 h forecast valid 00Z August 2. In many places, the unnudged forecast is up to 12°C colder than the nudged forecast, which is more skillful relative to the observations.

In the Pacific Northwest, cold biases were negatively correlated with 2 m moisture, suggesting an issue with the land surface model (Fig. 4). Of particular concern for this study, however, were predicted Central Valley temperatures that were, on average, 7°C too low on the afternoon of August 1, even when RAWS stations were excluded. The Central Valley problem appeared as nests were implemented, and thus a longstanding bug in WRF may have been exposed. Both problems were very largely mitigated through the employment of CAM longwave and shortwave radiation, which removed the need for nudging.

## 5. Further Work

This is part of a more extensive assessment of mesoscale model forecast skill in seemingly benign yet deceptively challenging "asynoptic" summertime situations relevant to air quality research and forecasting.

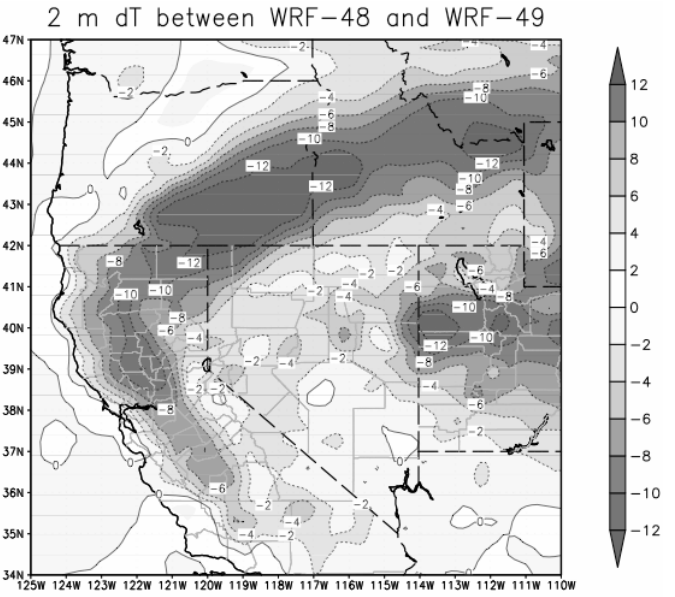


**Fig. 3.** 2 m temperature difference between unnudged run WRF-48 and nudged run WRF-49, both using RRTM/Dudhia radiation for a 48 h forecast valid 00Z August 2. Only part of the 36 km outer domain is shown

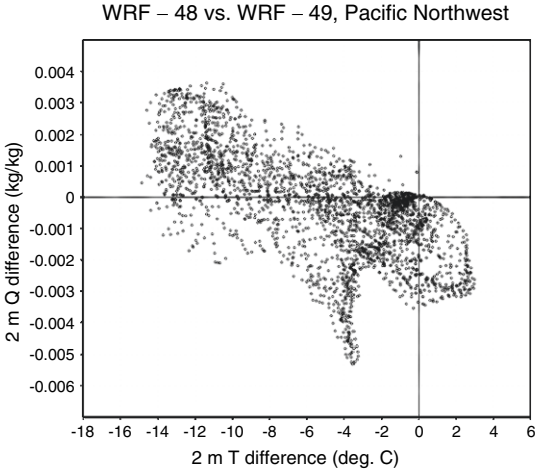


**Fig. 4.** Scatterplot of 2 m temperature (T) and vapor mixing ratio (Q) differences between unnudged run WRF-48 and nudged run WRF-49, for the region north of 42°N in Fig. 3

**Table 2. Temperature forecast skill at ASOS stations for selected model runs.** SSErel is sum of squared temperature error for August 1 relative to best result. Nudging Type 1 excluded PBL winds; Type 2 excluded PBL temperature and moisture; type 3 excluded all three. Two day runs started July 31. Simulations numbered above 50 used WRF v3.1

| Model/run | Days | SSErel | Source | Radiation | Surface | PBL | Nudging |
|---|---|---|---|---|---|---|---|
| WRF-55 | 2 | 1.0 | ETA | CAM | Noah | QNSE | None |
| MM5-10 | 2 | 1.65 | ETA | RRTM | Noah | MRF | None |
| WRF-49 | 2 | 1.95 | ETA | RRTM | Noah | YSU | Type 2 |
| WRF-40 | 1 | 2.59 | ETA | RRTM | Noah | YSU | Type 2 |
| WRF-34 | 1 | 2.60 | ETA | RRTM | TD | YSU | None |
| WRF-28 | 1 | 3.77 | ETA | CAM | Noah | YSU | None |
| MM5-1 | 1 | 4.55 | ETA | CAM | TD | MRF | None |
| WRF-39 | 1 | 4.78 | ETA | RRTM | Noah | MYJ | None |
| WRF-41 | 1 | 5.52 | ETA | RRTM | Noah | YSU | Type 3 |
| WRF-26 | 1 | 6.60 | ETA | RRTM | Noah | YSU | None |
| WRF-32 | 1 | 6.70 | ETA | CAM | Noah | YSU | Type 1 |
| WRF-36 | 1 | 9.08 | ETA | RRTM | TD | YSU | Type 1 |
| WRF-35 | 1 | 10.84 | FNL | RRTM | TD | YSU | None |
| WRF-56 | 2 | 16.28 | ETA | RRTM | Noah | QNSE | None |
| WRF-25 | 1 | 16.43 | NARR | CAM | Noah | YSU | Type 1 |
| WRF-54 | 2 | 20.00 | ETA | RRTM | TD | YSU | None |
| WRF-48 | 2 | 25.00 | ETA | RRTM | Noah | YSU | None |

## 6. Questions and Answers

**Question:** Rutherford would also say that if you need to tune a model, you should have built a better model.

**Answer:** In the presentation, I (RGF) suggested that Ernest Rutherford, famous for opining that "if your experiment needs statistics you should have made a better experiment", might today suggest the same about nudging. I was expressing the opinion that model flaws should be exposed and corrected instead of patched over. That said, I would expect Rutherford would see the value and need for model *tuning*, especially with respect to parameterizations that have many settings each with some degree of uncertainty and range of applicability. I see this as far more justifiable than brute-force nudging.

**Question:** The spatial distribution of cold temperature bias looks as if it could have been caused by a clould shield associated with a synoptic weather system. How well do the model and observed cloud fields agree?

**Answer:** I showed that some physics combinations resulted in dramatic cold 2 m temperature biases in the afternoon that had a propagating component, as revealed in the difference field between unnudged and nudged runs, the latter being more congruent with the observations. The temperature discrepancies

had a pronounced diurnal cycle, and were as large as 10°C in the afternoon of August 1. Satellite pictures reveal isolated, thin clouds did drift across the California Central Valley during the day but this is an unlikely source for so large a cold bias. None of the model runs produced significant cloudiness. That this issue did not occur with other physics combinations points to a likely bug in the WRF model.

**Question:** Does the WRF run that works (i.e., agrees with the observations) do so for the right reason?

**Answer:** Indeed, as theme of my talk was a critical assessment of model performance, I myself raised the question of whether the ostensibly correct forecasts were right for the right reason, so that's an ongoing concern shared by the questioner and myself.

# 8.6 A Mass Consistency Method for Air Quality Modeling over Complex Terrain

**Yongtao Hu, Aika Yano, and M. Talat Odman**

School of Civil and Environmental Engineering, Georgia Institute of Technology, Atlanta, GA 30332-0512

## 1. Introduction

Mass inconsistency in air quality models (AQMs) can be severe particularly over complex terrain. Inconsistencies may originate from meteorological models or may be introduced by using AQMs with grids, time steps, or finite difference forms different from those of the driving meteorological model. Without correction, inconsistencies may lead to instabilities or produce unrealistic air quality fields. In the past, we developed a vertical winds adjustment method to deal with the mass inconsistency [1]. That method we refer to as Method 1 here was strictly mass conservative but required the use of the first-order accurate upwind scheme for vertical advection. In an application to Central California, where the complexity of the terrain is further emphasized by fine grid resolution (4 km), Method 1 resulted in large trajectory deviations and high ozone concentrations near the surface especially at night. Here we developed two new mass consistency methods for air quality modeling over complex terrain.

## 2. Methodology

First, we replace the upwind scheme with the higher-order accurate Bott's scheme [2] for vertical advection (Method 2). The non-linear flux limiters in this scheme necessitate an iterative solution for vertical winds adjustment. Since the iterative solution is assumed to have converged when a small tolerance is met, it is not exact and may introduce very small mass conservation errors. Second, to deal with large trajectory deviations resulting from the use of adjusted vertical winds instead of the winds generated by meteorological models, we developed a hybrid method. This method (Method 3) switches from vertical winds adjustment to concentration renormalization, which is not mass conservative, whenever the required adjustments to wind speed or direction exceed typical uncertainties associated with these parameters. Method 3 provides a compromise between trajectory deviations and mass conservation errors.

D.G. Steyn and S.T. Rao (eds.), *Air Pollution Modeling and Its Application XX*,
DOI 10.1007/978-90-481-3812-8, 

## 3. Results

The three different methods were evaluated by simulating the July 29–August 2, 2000 ozone episode in Central California. The uncertainties in wind speed and direction to be used in Method 3 for switching from vertical winds adjustment to concentration renormalization were determined by comparing the winds generated by the meteorological model with profiler data at 24 locations in Central California.

The more accurate vertical advection scheme in Method 2 resulted in better ozone performance than the upwind scheme in Method 1. The normalized error in hourly-average ozone concentrations was reduced at 71 out of 122 sites, with a reduction of the average error from 56.63% to 49.81% (Table 1). Method 3 effectively limited the trajectory deviations seen both in Method 1 and Method 2. It introduced some mass conservation errors but at a lesser degree than the pure renormalization approach. The normalized error was reduced at 72 out of 122 sites when Method 1 was replaced with Method 3. The average normalized error decreased from 56.63% to 55.16% (Table 1).

In Method 2, the adjusted winds are solved iteratively for each layer using the secant method, starting from the bottom and moving to the top. Another option is the iterative solution of the wind adjustments for all the layers at once, as a system. This may result in better convergence characteristics since in our solution technique, errors may be accumulating as we go from the bottom to the top. This hypothesis was tested by using the Newton-Raphson method for solving the system of nonlinear equations. The simultaneous solution did not improve convergence and resulted in larger wind adjustments.

**Table 1.** Normalized errors (%) for ozone at CCOS sites

| | Method-1 | Method-2 | Method-3 |
|---|---|---|---|
| Average | 56.63 | 49.81 | 55.16 |
| Max | 228.75 | 184.95 | 221.82 |
| Min | 10.97 | 11.17 | 10.75 |
| St. dev. | 39.37 | 31.38 | 37.34 |

## 4. Conclusion

The adjustment of vertical winds helps achieve mass conservation in AQMs. It yields better ozone performance when applied with more accurate vertical advection schemes such as Bott's. However, since those schemes are non-linear, an iterative solution is needed. This introduces small mass conservation errors. Recall that the mass was strictly conserved with the first-order upwind scheme. Both methods introduce trajectory deviations compared to wind fields generated by meteorological models. Therefore we developed a third method which mixes the use of

vertical winds adjustment with concentration renormalization under strong vertical wind shear conditions. Recall that renormalization is not mass conservative therefore some mass conservation errors are introduced but the trajectory deviations are smaller than those seen in pure vertical wind adjustment methods.

**Acknowledgments** This research was supported by the San Joaquin Valleywide Air Pollution Study Agency under contract number 05-4CCOS

## References

Hu, Y., Odman, M.T., Russell, A.G.: Mass conservation in the Community Multiscale Air Quality model. Atmos. Environ. **40**, 1199–1204 (2006).

Bott, A.: A positive definite advection scheme obtained by nonlinear renormalization of the advective fluxes. Mon. Wea. Rev. **117**, 1006–11015 (1989).

## 5. Questions and Answers

**Jim Wilczak:** Are all of the problems with mass consistency completely mitigated by the use of a fully coupled, on-line model that uses identical grids for chemistry and meteorology.

**Answer:** For mass consistency, the models must use the same grids, the same time steps, and the same finite difference forms. Recently, we see more and more applications where meteorology and chemistry-transport models share the same grid. In an on-line model, it is much easier to use the same time steps. In addition, if the density is a prognostic variable in the meteorology model and if the continuity equation and the species continuity equation are discretized using the same finite difference forms (e.g., upwind differencing), then mass consistency should no longer be a problem.

# 8.7 An Investigation of Aloft Model Performance for Two Episodes During the 2000 Central California Ozone Study

**Neil J.M. Wheeler, Kenneth J. Craig, and Stephen B. Reid**

Sonoma Technology, Inc., 1455 N. McDowell Blvd., Petaluma, CA 94954, USA

**Abstract** The Central California Ozone Study (CCOS) was a multi-year program of meteorological and air quality monitoring, emission inventory development, data analysis, and air quality simulation modeling. Photochemical modeling studies were previously carried out using both the Comprehensive Air Quality Model with Extensions (CAMx) and the Community Multiscale Air Quality (CMAQ) model. Performance evaluations of the photochemical modeling have shown that the models tend to underpredict peak ozone concentrations, both at the surface and aloft, and that model performance did not meet traditional goals for ozone. The objective of this study was to understand and improve model performance for ozone and ozone precursors aloft. Data analysis of surface and aloft air quality and meteorological data was used to characterize the episodes studied. Model-to-measurement comparisons of air quality, meteorological, and integrated (e.g., pollutant flux) values, and sensitivity analyses were used to investigate model performance. These analyses suggested that emission estimates, particularly for wildfires, and regional transport and recirculation of ozone aloft through model's boundaries may account for a significant portion of the underprediction of ozone concentrations.

**Keywords** Air quality, ozone, California, model performance, CCOS, CAMx, CMAQ

## 1. Introduction

The Central California Ozone Study (CCOS) was a multi-year program of meteorological and air quality monitoring, emission inventory development, data analysis, and air quality simulation modeling. Photochemical modeling studies have been carried out using both the Comprehensive Air Quality Model with Extensions (CAMx) (ENVIRON International Corporation, 2004) and the Community Multiscale Air Quality (CMAQ) model (National Exposure Research Laboratory, 1999). Early performance evaluations of the photochemical modeling have shown that

D.G. Steyn and S.T. Rao (eds.), *Air Pollution Modeling and Its Application XX*,
DOI 10.1007/978-90-481-3812-8, 

the models tend to underpredict peak ozone concentrations both at the surface and aloft and model performance does not meet traditional goals for ozone. Prior modeling efforts in the San Joaquin Valley (SJV) have also shown this tendency. For example, during the SJV Air Quality Study (SJVAQS) – Atmospheric Utility Signatures, Predictions, and Experiments (AUSPEX) Regional Modeling Adaptation Project (SARMAP), ozone concentrations at about 500 m above the surface were underestimated by as much as 60 ppb (Thuillier and Ranzieri, 1995; DaMassa et al., 1996). These performance issues undermine confidence in the models as planning tools and need to be addressed.

While some limited evaluations of model performance aloft have been made, model evaluation studies (e.g., Tesche et al., 2004; San Joaquin Valley Air Pollution Control District, 2004) have focused on the ability to replicate surface-based measurements. Greater attention to assessing aloft model performance using data collected on tall towers, balloon soundings, and instrumented aircraft is needed. This study focused on understanding and improving model performance for ozone and ozone precursors aloft. Understanding model performance both at the surface and aloft allows us to identify critical performance problems, diagnose their causes, and implement changes in the modeling system that will improve its ability to predict the spatial and temporal patterns of observed ozone and thus, increase credibility.

## 2. Methodology

Two ozone episodes and their associated simulations with CAMx were investigated in this study: (1) July 29–August 2, 2000 and (2) September 16–20, 2000. Two simulations were evaluated for the first episode. The first simulation used hybrid meteorology from the Pennsylvania State University/National Center for Atmospheric Research Mesoscale Model version 5 (MM5) and the California Meteorological Model (CALMET) while the second simulation used meteorology from MM5 alone. Only one simulation, based on MM5 meteorology, was evaluated for the second episode.

Extensive analyses of the available air quality and meteorological data were performed to clarify the chemical and physical processes leading to elevated concentrations of ozone aloft and provide the basis for diagnosis of aloft model performance deficiencies. The analyses included descriptive statistics; three-dimensional (3-D) visualization; chemical composition; indicator species ratios; biogenic hydrocarbons; spatial variations in chemical composition; pollutant fluxes; multivariate time series; and transport and mixing height statistics.

Model results were evaluated by comparing measured aloft air quality using traditional model performance statistical and graphic products. These products include peak performance statistics by level, location, and day; bias and error statistics by level, location, and day; scatter plots of observations versus predictions by level and location; quantile-quantile plots; vertical profiles of observed

and predicted ozone and ozone precursor concentrations for balloon soundings and aircraft spirals; time series comparisons of predicted and observed concentrations from transverse aircraft flights and tall towers; and spatial plots of predicted concentrations at selected levels aloft with observations over plotted.

The results of the data analyses and model performance evaluations were used to test 11 widely held hypotheses that have been proposed over the past decade. Some hypotheses were rejected based on the analyses while other hypotheses required additional diagnostic and sensitivity simulations with CAMx to test.

## 3. Findings and Recommendations

Based on the analyses performed, we reached the following key findings.

- Ozone concentrations aloft were observed to be well above background during the two episodes with concentrations exceeding 100 ppb in the upper-mixed layer (below 2 km). During the July–August episode, ozone concentrations between 70 and 80 ppb were observed to persist in deep layers above 3 km for multiple days.
- Aloft ozone were generally underpredicted by CAMx when observed concentrations were greater than 70 ppb and overpredicted when observed concentrations were less than 50 ppb. While CAMx explained more than 75% of the variance in observations in the first 100 m above the surface. it explained less than 50% of the variance in observations at altitudes above 1 km agl.
- Mass flux analysis of the CAMx results based on hybrid meteorology (MM5-CALMET) showed that domain-wide ozone mass was dominated by contributions from the model's top boundary. Further analysis indicated that the hybrid meteorology introduced artificial areas of convergence resulting in localized loss of mass through the top boundary. Analysis of mass fluxes with MM5 meteorology indicated that circulations near the southern model boundary may have resulted in the loss of ozone aloft through that boundary and thus, the size of the modeling domain may be too small.
- Maximum afternoon temperatures predicted for the September episode appeared to be biased low, which could impact peak ozone production.
- Improvements in MM5 meteorology, vertical resolution in the model, photolysis rates at high elevations, nighttime mixing processes, and plume rise for wildfires did not significantly improve aloft ozone model performance.
- The current state of knowledge about the contributors to wildfire emissions (e.g., location, size, fuels, consumption, time rate-of-change, speciation, and plume rise) is uncertain and it may be several years before the fire science community will be able to provide better estimates of fire emissions for the air quality modeling community.

- The CAMx modeling was performed using the most recent draft emission inventory available at the time the study was initiated. However, several issues were noted with that inventory and it has been revised significantly since then. Studies to reconcile emission inventories with measurements in the CCOS region indicate an underestimation of total non-methane organic compound to oxides of nitrogen (TNMOC:$NO_x$) emission ratios in southern SJV. Biogenic emissions were significantly different between the July–August and September episodes.

Based on these findings, we recommend that (1) an updated emission inventory be implemented and used in the CCOS air quality modeling; (2) the CCOS modeling domain be nested within a larger regional 12-km domain; (3) research on wildfire emissions from the fire science community be monitored for improvements in emission rates, temporalization, spatial allocation, speciation, and plume rise; and (4) temperature biases in the SJV during the September 2000 episode should be investigated further.

**Acknowledgments and Disclaimer** The work described in this paper was funded by the San Joaquin Valleywide Air Pollution Study Agency (SJVAPSA) and managed by Dr. Ajith Kaduwela of the California Air Resources Board (CARB). The authors would like to thank Dr. Kaduwela and the members of the CCOS Technical Committee for their suggestions and guidance over the course of the project. The statements and conclusions in this paper are those of the authors at Sonoma Technology, Inc. and not necessarily those of the CARB, the SJVAPSA, its Policy Committee, their employees, or their members. The mention of commercial products, their source, or their use in connection with the material reported herein is not to be construed as actual or implied endorsement of such products.

## References

DaMassa J., Tanrikulu S., Magliano K., Ranzieri A.J., and Niccum L. (1996) Performance evaluation of SAQM in Central California and attainment demonstration for the August 3–6, 1990 ozone episode. Report prepared by Technical Support Division, California Air Resources Board, Sacramento, CA, February.

ENVIRON International Corporation (2004) User's guide to the Comprehensive Air Quality Model with Extensions (CAMx). Version 4.00. Prepared by ENVIRON International Corporation, Novato, CA, January.

National Exposure Research Laboratory (1999) Science algorithms of the EPA Models-3 Community Multiscale Air Quality (CMAQ) modeling system. Report prepared by the National Exposure Research Laboratory, Research Triangle Park, NC, EPA/600/R-99/030 (peer reviewed), March.

San Joaquin Valley Air Pollution Control District (2004) San Joaquin Valley Air Basin plan demonstrating attainment of federal 1-hour ozone standards. October.

Tesche T.W., McNally D.E., Wilkinson J.G., Jeffries H.E., Kumra Y., Emery C., Yarwood G., and Souten D.R. (2004) Evaluation of the 16–20 September 2000 ozone episode for use in 1-hr SIP development in the California Central Valley. Draft final report prepared by Alpine Geophysics, LLC, Ft. Wright, KY, February.

Thuillier R.H., and Ranzieri A. (1995) SARMAP–Lessons Learned. Air &Waste Management Association's International Specialty Conference, San Diego, CA, 7–12 November 1993, Regional Photochemical Measurement and Modeling Studies, Volume 3, Other Topics Related to Regional Studies, A.J. Ranzieri and P.A. Solomon, eds., Air & Waste Management Association, Pittsburgh, PA.

## 4. Questions and Answers

**Saffet Tanrikulu, Bay Area Air Quality Management District**: David Parrish at NOAA is publishing a paper that indicates the high ozone layer is from large scale transport, not from local sources.

**Answer:** Parrish's paper proposes a mechanism and presents evidence of the transport of ozone aloft over the northern California coast into the northern Sacramento Valley. His research indicates that this transport from aloft accounts for 58 ppbv of the ozone on days when the ozone concentrations exceed 75 ppbv. In our analysis of the CCOS data we did review the ozone soundings from Trinidad Head used by Parrish and found concentrations aloft were in the range of 40–60 ppbv during the episodes studied while ozone soundings in the southern Sacramento Valley and San Joaquin Valley showed concentrations greater than 80 ppbv in a layers up to 6 km above the ground. Therefore, we concluded that while transported ozone contributed to higher concentrations, it alone could not explain the measured values, and that local or regional ozone production was important under those conditions. We hypothesized that this production was a result of wildfires. It should be noted that Parrish did not demonstrate that the ozone concentrations aloft at Trinidad Head were a result of long ranger transport and that intensive aloft measurement studies over California indicate that regional transport may contribute to the high ozone values seen aloft along the California coast.

**Ron Cohen, University of California at Berkeley:** Is there any evidence that the surface CO is from wildfires?

**Answer:** Measurements of CO near fires was not a primary monitoring objective during CCOS so the available CO measurements were in urban and suburban areas with existing traffic-related CO issues. Our review of those sites indicated no unusual values during the fires. However, there were higher than usual nighttime ozone concentrations at monitoring sites in the foothills and higher elevations during the fires.

# 8.8 Evaluation of Toxic Air Contaminants in the San Francisco Bay Area: Regional Modeling

**Philip T. Martien[1], Saffet Tanrikulu[1], Yiqin Jia[1], David Fairley[1], Cuong Tran[1], Jeff Matsuoka[1], Henry Hilken[1], Chris Emery[2], Ed Tai[2], and Greg Yarwood[2]**

[1]Bay Area Air Quality Management District, San Francisco, CA, USA

[2]ENVIRON International Corporation, Novato, CA, USA

## 1. Introduction

In 2004, Bay Area Air Quality Management District (BAAQMD) initiated the Community Air Risk Evaluation (CARE) program to estimate and reduce health risks associated with exposure to outdoor toxic air contaminants (TAC) within the San Francisco Bay Area (Bay Area, see Fig. 1). Information gathered through a variety of technical studies has guided the development of measures to reduce TAC in areas with high health risk. This extended abstract summarizes regional toxics modeling and model evaluation conducted to support the CARE program.

To produce inputs for regional toxic modeling, we generated meteorological fields for winter and summer periods in 2000 using the MM5 mesoscale meteorological model (Grell et al., 1994) and an emissions inventory for year 2005 using methods described in a companion report (Martien et al., 2009). Initial and boundary conditions were set using available observations as a guide. The horizontal grid resolution of both meteorological and air quality models was 4 by 4 km.

Modeling inputs were supplied to the CAMx air quality model (ENVIRON, 2006) to predict concentrations of toxic compounds. Some toxic contaminants, such as diesel PM, were treated as inert compounds. Other contaminants, such as formaldehyde and acrolein, underwent chemical reactions in the atmosphere. They were both directly emitted and formed secondarily from other pollutants. Reactive chemistry simulations used the SAPRC99 chemical mechanism to predict ozone and radical concentrations, and applied the reactive tracer chemical mechanism compiler (RTCMC; Emery et al., 2008) to predict trace toxic compounds. Predicted concentrations were compared to measurements from a network of TAC monitoring sites (Martien et al., 2009).

To estimate health risks, predicted pollutant concentrations were weighted by unit risk factors for cancer-causing compounds – such as benzene – or normalized by reference exposure levels for compounds that produce non-cancerous, chronic and acute heath effects – such as acrolein. Total excess cancer risk was estimated by from cancer-risk-weighted concentrations of five species that collectively represent

D.G. Steyn and S.T. Rao (eds.), *Air Pollution Modeling and Its Application XX*,
DOI 10.1007/978-90-481-3812-8, 

more than 95% of the region-wide risk-weighted emissions: diesel particulate matter (diesel PM), 1,3-butadiene, benzene, formaldehyde, and acetaldehyde.

## 2. Modeling Results and Evaluation

Figure 1 shows simulated annual average diesel PM concentrations, a major contributor to regional cancer risk from air pollutants. Annual average concentrations of diesel PM were estimated from weighted averages of simulated results from one summer and one winter month. Annual average concentrations over 6 $\mu g/m^3$ were predicted in the Bay Area's urban core; populated areas along freeways had concentrations in the range of 1–4 $\mu g/m^3$. Diesel PM simulations were found to be well correlated with elemental carbon (EC) measurements collected via the IMPROVE method, though differences (not shown) suggest that other sources of EC are important, particularly in the wintertime.

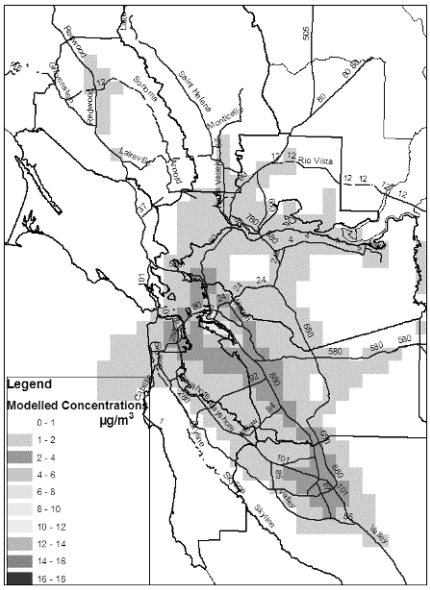


**Fig. 1.** Simulated annual average diesel PM concentrations with county boundaries, air district boundaries, and major roadways

Annual concentrations and health risk from reactive gaseous toxic contaminants were estimated from two, week-long (one summer, one winter) reactive chemistry simulations. Estimated annual concentrations of gaseous toxics were compared to observations (Fig. 2). Simulated concentrations of benzene, 1,3-butadiene, formaldehyde, and acetaldehyde were generally smaller than measured values,

though differences were often not statistically significant. Simulated acrolein concentrations were significantly lower than observed values.

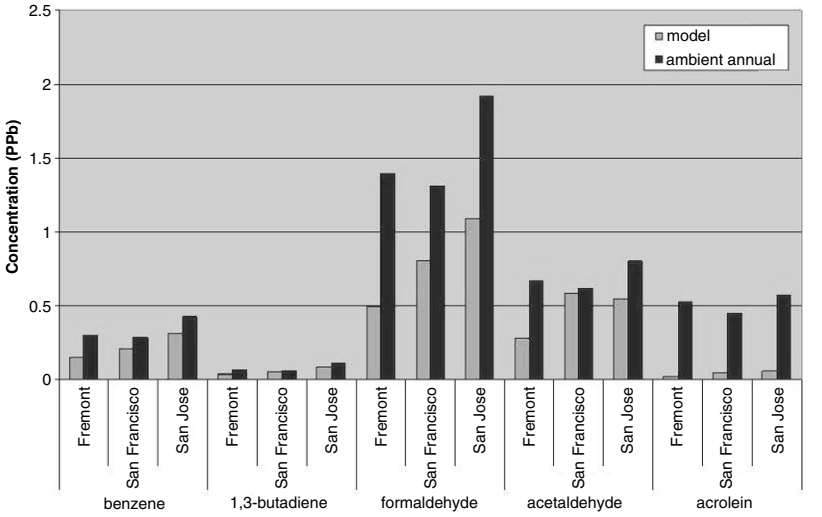


**Fig. 2.** Model-observation comparisons

## 3. Cancer Risk Evaluation

Excess cancer risk from the five compounds listed above was estimated by multiplying annual average concentrations for each compound by their unit risk factors and summing the resulting values across all compounds. The results were expressed as the number of excess cancer incidents per million people, assuming a 70-year lifetime exposure (Fig. 3). In many of the populated areas of the Bay Area, the number of excess cancers ranged from 200 to 500 per million, with higher numbers near major freeways and large maritime ports.

## 4. Summary and Conclusion

For the first time, simulations were performed for the Bay Area to estimate regional concentrations of TAC and associated cumulative health risks. Using 2005 emissions estimates, excess cancer risk from TAC ranged from 200 to 500 per million for most populated areas of the Bay Area, with higher values in urbanized areas. More than 95% of the regional potential cancer risk from TAC was estimated to be from diesel PM and four other compounds. Predicted concentrations were found to be consistent with measured data, except for acrolein,

for which predictions were significantly lower than observations. Modeling results are being used by the CARE program to help guide the District's mitigation effort.

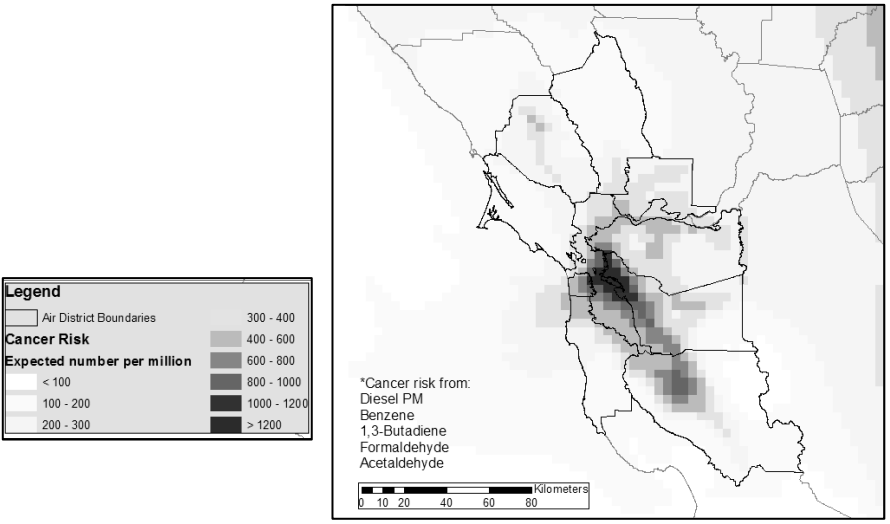


**Fig. 3.** Estimated excess cancer risk (per million) from toxic air contaminants in the Bay Area

## References

Grell, G.A.; Dudhia, J.; Stauffer, D.R. *A description of the fifth-generation Penn State/NCAR mesoscale model (MM5)* 1994. NCAR Technical Note, NCAR/TN-398+STR.

Martien, P. et al., 2009. "Evaluation of Toxic Air Contaminants in the San Francisco Bay Area: Regional Emissions and Ambient Observations." International Technical Meeting on Air Pollution and its Application, San Francisco, CA, May 18–22, 2009.

ENVIRON International Corp. User's Guide to the Comprehensive Air Quality Model with Extensions (CAMx) Version 4.30, 2006. See http://www.camx.com (Accessed Mar. 2008)

Emery, C., et al. "Modeling chemically reactive air toxics in the San Francisco Bay Area using CAMx." 7th Annual CMAS Conference, Chapel Hill, NC, Oct. 6–8, 2008.

# 8.9 Source Apportionment of Wintertime Secondary Organic Aerosol During the California Regional Particulate Matter Study

**Jianjun Chen[1], Qi Ying[2], and Michael J. Kleeman[1]**

[1]Department of Civil and Environmental Engineering, University of California, Davis, CA 95616, USA

[2]Zachry Department of Civil Engineering, Texas A&M University, College Station, TX 77843, USA

**Abstract** The quantity and origin of secondary organic aerosol (SOA) formation in the San Joaquin Valley from December 15, 2000 to January 7, 2001 were studied using the UCD/CIT air quality model with the Caltech Atmospheric Chemistry Mechanism (CACM). Average SOA concentration across the entire SJV was 1.4 μg/m$^3$, which accounted for approximately 20% of predicted organic aerosol. Major SOA sources in the SJV were solvent uses (28% of SOA), catalytic gasoline engines (25% of SOA), wood smoke (16% of SOA), non-catalyst gasoline engines (13% of SOA), and other anthropogenic sources (11% of SOA). This study highlighted the importance of considering SOA formation during wintertime periods in the SJV.

**Keywords** CRPAQS, Secondary organic aerosol, UCD/CIT

## 1. Introduction

The San Joaquin Valley (SJV) in the southern portion of California's Central Valley is one of the largest $PM_{2.5}$ non-attainment areas in the US [1]. Organic aerosol (OA) is one of the most important constituents of $PM_{2.5}$ in the SJV [1]. OA consists of primary organic aerosol (POA) and secondary organic aerosol (SOA). While the importance of SOA has been recognized and modeled extensively during photochemical events, the formation of SOA under wintertime conditions has only received limited attention. The purpose of this work is to study SOA formation and source contributions in the SJV between December 15, 2000 and January 7, 2001. This episode is part of the California Regional Particulate Air Quality Study (CRPAQS), which was designed to improve our understanding of the causes of excessive PM levels in central California [1].

D.G. Steyn and S.T. Rao (eds.), *Air Pollution Modeling and Its Application XX*,
DOI 10.1007/978-90-481-3812-8, 

## 2. Model Description

The UCD/CIT air quality model is used in this study with the Caltech Atmospheric Chemistry Mechanism (CACM) that has been expanded to perform source apportionment of SOA [2]. Semi-volatile organic compounds predicted by CACM are allowed to partition to both the organic and aqueous phases of particles to form SOA. The modeling domain covers the Central Valley of California and is horizontally divided into 8 × 8 km cells, with 95 grid cells in each direction. Meteorological fields were generated using the objective analysis method. Hourly emissions used in the study are based on the emission inventory of 4 km spatial resolution generated by the California Air Resources Board (CARB) that were aggregated spatially to be consistent with the 8 km modeling grid. In order to perform SOA source apportionment, VOCs emissions were grouped into nine source categories: solvent use, wood smoke, diesel engines, catalyst gasoline engines, non-catalyst gasoline engines, gasoline disposal and storage, high sulfur fuel combustion, other anthropogenic sources, and the biogenic source.

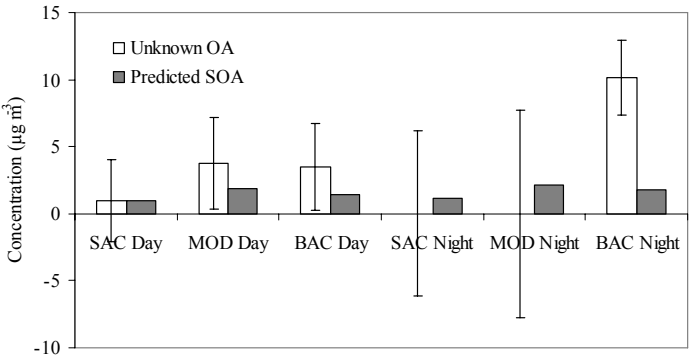


**Fig. 1.** Comparison of the average predicted SOA with the average "unknown" OA for daytime (day, 1000-1800PST) and nighttime hours (night, 2000-0800PST) at Sacramento (SAC), Modesto (MOD), and Bakersfield (BAC)

## 3. Model Results

Figure 1 compares SOA concentrations predicted by the UCD/CIT/CACM model to the concentration of "unknown" OA described by Kleeman et al. [3]. The "unknown" OA was calculated as the difference between the measured total OA and the primary OA identified by a molecular marker source apportionment technique. Comparisons are made at the urban locations of Sacramento, Modesto, and Bakersfield spanning a north-south transect of the SJV for both daytime (1000-1800 PST) and nighttime (2000-800 PST) hours. Error bars for "unknown" OA concentrations reflect the uncertainty in the molecular marker source

apportionment technique. The predicted SOA concentration in the current model simulation matches the calculated "unknown" OA using molecular markers at all sites and times except during nighttime hours at Bakersfield, which may indicate an under-prediction of SOA concentrations at this time and location. Under prediction of SOA formation is not surprising given that our current understanding of SOA formation is far from complete [4].

The predicted SOA accounts for approximately 20% of the predicted OA averaged across the entire SJV, indicating the importance of considering the best available estimates of wintertime SOA in regional model calculations. Urban locations are dominated by POA and so predicted SOA only accounts for approximately 5% of total OA at urban locations such as Fresno and Bakersfield. However, predicted SOA can constitute up to 50% of predicted OA at certain rural locations within the SJV and along the coastlines north of San Francisco (SF).

**Table 1.** Source apportionment of SOA at selected locations in Central California between December 25, 2000 and January 7, 2001[a]

| Sources | FRES[b] | ANG[b] | BAC[b] | SJV[b] |
|---|---|---|---|---|
| Initial/boundary conditions | 0.014 | 0.009 | 0.008 | 0.009 |
| Solvent use | 0.776 | 0.664 | 0.469 | 0.376 |
| Wood smoke | 0.401 | 0.322 | 0.244 | 0.212 |
| Diesel engines | 0.030 | 0.043 | 0.027 | 0.022 |
| Non-catalyst gasoline engines | 0.312 | 0.303 | 0.204 | 0.173 |
| Catalyst gasoline engines | 0.611 | 0.610 | 0.432 | 0.332 |
| Gasoline storage and disposal | 0.045 | 0.042 | 0.032 | 0.023 |
| High sulfur fuel combustion | 0.010 | 0.032 | 0.011 | 0.027 |
| Other anthropogenic sources | 0.212 | 0.242 | 0.236 | 0.147 |
| Biogenic source | 0.026 | 0.016 | 0.018 | 0.030 |
| Total SOA | 2.463 | 2.284 | 1.680 | 1.351 |

[a]Unit in $\mu g\ m^{-3}$

[b]FRES: Fresno; ANG: Angiola; BAC: Bakersfield; SJV: average of the entire SJV

Table 1 gives the total SOA concentrations and SOA source contributions predicted by the UCD/CIT/CACM model for Fresno, Angiola, Bakersfield, and the entire SJV averaged between December 25, 2000, and January 7, 2001. Angiola is a rural location within the SJV in contrast to urban locations such as Fresno and Bakersfield. However, major sources for SOA formation are fairly consistent among these locations. Solvent use, catalyst gasoline engines, wood smoke, non-catalyst gasoline engines, and other anthropogenic sources are major SOA contributors, accounting for ~28–32%, ~25–27%, ~14–16%, ~12–13%, and ~9–14% of SOA formation, respectively. Contributions from the remaining sources are minor, accounting for only ~5–8% of the SOA.

## 4. Conclusions

The quantity and origin of SOA formation in the SJV between December 15, 2000 and January 7, 2001 were predicted using a state of the science SOA formation mechanism. While the majority of predicted OA in the SJV during the winter episode was of primary origin, SOA concentrations were not negligible. Averaged over December 25, 2000 to January 7, 2001, the dominant sources of SOA in the SJV were solvent use (28%), catalyst-gasoline engines (25%), wood smoke (16%), non-catalyst gasoline engines (13%), and other anthropogenic sources (11%).

**Acknowledgments** We would like to thank Robert Griffin for helpful comments. This research was supported by the California Air Resources Board and the San Joaquin Valleywide Air Pollution Study Agency under contract 2000-05PM. The statements, opinions, findings, and conclusions of this paper are those of the authors and do not necessarily represent the views of the California Air Resources Board.

## References

Chow JC, Chen LWA, Watson JG et al. (2006) $PM_{2.5}$ chemical composition and spatiotemporal variability during the California Regional $PM_{10}$/$PM_{2.5}$ Air Quality Study (CRPAQS). Journal of Geophysical Research. doi:10.1029/2005JD006457

Kleeman MJ, Ying Q, Lu J et al. (2007) Source apportionment of secondary organic aerosol during a severe photochemical smog episode. Atmospheric Environment 41: 576–591.

Kleeman MJ, Riddle SG, Robert MA et al. (2009) Source apportionment of fine ($PM_{1.8}$) and ultrafine ($PM_{0.1}$) airborne particulate matter during a severe winter pollution episode. Environmental Science & Technology 43: 272–279.

Kroll JH, Seinfeld JH (2008) Chemistry of secondary organic aerosol: Formation and evolution of low-volatility organic in the atmosphere. Atmospheric Environment 42: 3593–3624.

## 5. Questions and Answers

**Question:** Saffett Tanrikulu at Bay Area Air Quality Management District stated that the SJV acts as a source of nitrate aerosol to the Bay Area. He stated that the highest concentrations in the SJV and the Bay Area occur during periods of northward flow.

**Answer:** These trends were not evident in the current episode. Each region produces most of its own nitrate and we were confident in our model results.

**Question:** Ron Cohen from UC, Berkeley asked if any of the unknown OC at Angiola could be related to agricultural sources.

**Answer:** This was certainly a possibility. However, we also had unknown sources of NOx and elemental carbon at Angiola that suggested an anthropogenic influence.

# 8.10 Long-Term One-Atmosphere CMAQ Modeling in Central California: Model Performance Evaluation

**James T. Kelly[1], Kathleen Fahey[2], and Ajith Kaduwela[1,3]**

[1]Planning and Technical Support Division, Air Resources Board, California Environmental Protection Agency, Sacramento, CA, USA

[2]Science and Technology Team, Northeast States for Coordinated Air Use Management (NESCAUM), Boston, MA, USA

[3]Department of Land, Air, and Water Resources, University of California at Davis, CA, USA

**Abstract** Techniques for evaluating model performance for long-term (i.e., annual) air quality simulations are needed for use in regulatory modeling applications. This study applies numerous evaluation techniques to results of a 14-month simulation in California. Traditional evaluation approaches are shown to be useful for defining model performance criteria and providing an overview of model performance. Spectral decomposition methods and evaluations of spatial correlations can isolate temporal and spatial scales with characteristic model performance. Mechanistic and chemical-ratio evaluations indicate needs for model process development. Future work will focus on combining the various evaluation techniques into a single cohesive model evaluation framework.

**Keywords** CRPAQS, long-term evaluation, Kolmogorov-Zurbenko filter

## 1. Introduction

As state regulatory bodies develop implementation plans to reach goals dictated by the US EPA's Regional Haze Plan and National Ambient Air Quality Standards (NAAQS) for $PM_{2.5}$ and ozone, a need exists for reliable chemical transport modeling to assess effects of emissions controls on pollutant concentrations. The focus of such modeling efforts has recently shifted from short-term pollution episodes to long-term simulations that elucidate seasonal and regional differences in pollutant concentrations. Long-term modeling is required to construct mutually beneficial control strategies for pollutants whose concentrations become elevated under different environmental conditions (e.g., $PM_{2.5}$ and ozone). In central California, the annual $PM_{2.5}$ NAAQS is restrictive in the sense that attainment of the 24-h standard does not ensure attainment of the annual standard. Thus annual modeling is an imperative for this region. A suite of accepted model performance

D.G. Steyn and S.T. Rao (eds.), *Air Pollution Modeling and Its Application XX*,
DOI 10.1007/978-90-481-3812-8, © Springer Science + Business Media B.V. 2010

metrics exist for episodic simulations, but a comparable set of metrics for long-term simulations remains elusive. This report outlines key aspects of model performance evaluation using a 14-month California simulation as an example. Traditional evaluation techniques are discussed along with infrequently used approaches possibly more appropriate for long-term simulations.

## 2. Model Application

A 14-month simulation (December 1999–January 2001) was conducted with CMAQv4.6 for a California domain (Fig. 1) with 12- × 12-km horizontal grid cells and 15 vertical layers. Meteorological inputs were generated from simulations with the mesoscale meteorological model (MM5), and emissions were prepared internally at the California Air Resources Board. Gas-phase chemistry followed the SAPRC99 mechanism; aerosol processes were modeled with the AE4 module.

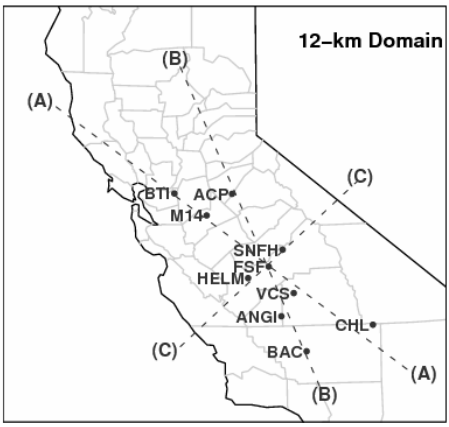


**Fig. 1.** Simulation domain with observation sites and San Joaquin Valley transects

## 3. Approaches for Model Performance Evaluation

*Traditional techniques*. Model performance has traditionally been evaluated using statistical measures of bias and error based on grid-cell average predictions matched in space and time with observations from sites in the domain. These statistical measures concisely summarize aspects of general model performance, and goals for acceptable performance can be defined in terms of statistical quantities. Visually, model performance is often examined using scatter and time-series plots of pollutant concentration. An example of such a plot for our simulation is given in Fig. 2. Despite their usefulness, statistical performance measures provide limited information on the accuracy of individual parameterizations of atmospheric processes.

Moreover, evaluations focused on absolute concentration may not be ideal for determining a model's ability to predict a relative change in pollutant concentration corresponding to an emission change.

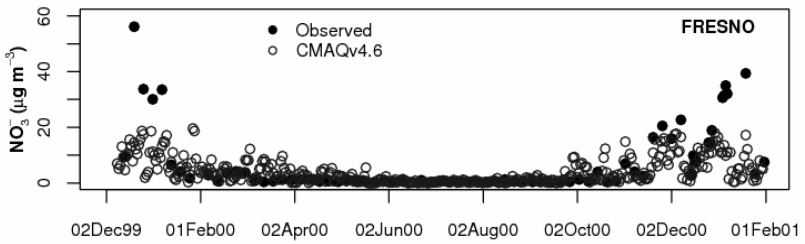


**Fig. 2.** Modeled and simulated daily average $PM_{2.5}$ nitrate concentration at FSF site

*Ratios and indicators*. Estimates of the relative change in pollutant concentration associated with a change in emissions are used in developing plans for attaining air quality standards. Therefore predictions of pollutant ratios and photochemical indicators should be evaluated in addition to absolute concentration. In Fig. 3, the ratio of $PM_{2.5}$ nitrate to total inorganic concentration is compared with observations. Performance for the nitrate ratio differs from that for absolute nitrate concentration (Fig. 2). In Fig. 4, predictions of an indicator of photochemical regime are compared with observations. For much of the simulation, the model correctly predicts ozone-to-$NO_X$ ratios of less than 15.

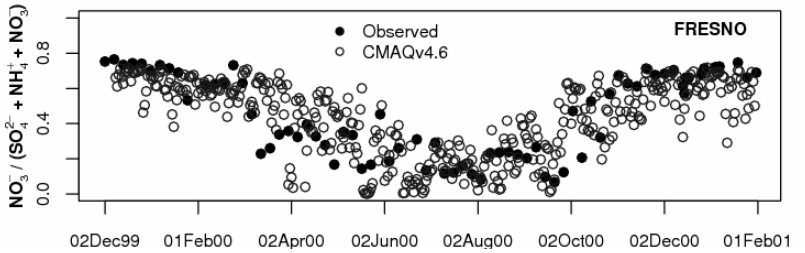


**Fig. 3.** Modeled and simulated daily average $PM_{2.5}$ nitrate ratio at FSF site

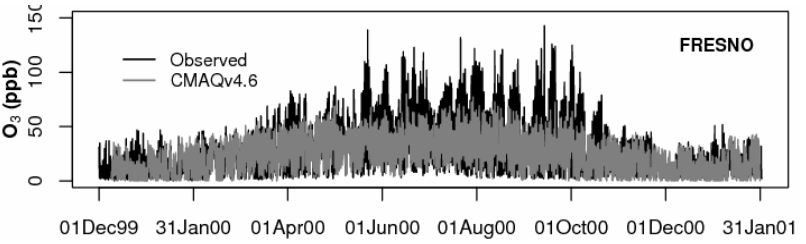


**Fig. 4.** Modeled and simulated hourly ozone-to-$NO_X$ ratio at FSF site

*Temporal evaluation*. For long-term simulations, a model's ability to represent processes that occur on a wide range of time scales must be evaluated. This ability is obscured in plots of hourly values over an annual period (e.g., Fig. 4). Spectral decomposition methods can often separate contributions with different characteristic frequencies. Such methods enable key time scales to be identified so that performance evaluations can focus on those scales. The long-term component of hourly $PM_{2.5}$ measurements is shown with predictions in Fig. 5.

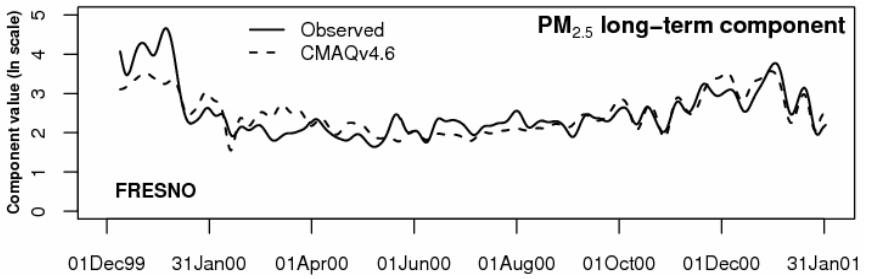


**Fig. 5.** Modeled and simulated long-term component (>about 21 days) of $PM_{2.5}$ at FSF site

*Subsets and spatial evaluation*

For a given simulation, a variety of data subsets can be defined based on, for example, surface elevation, meteorological conditions, land use, etc. Performance evaluations should demonstrate that a model adequately simulates conditions for subsets associated with poor air quality. The ability of a model to predict the spatial distribution of pollutants should also be evaluated. In Fig. 6, average nitrate predictions are compared with observations along transect (A)–(A) of Fig. 1 for a subset of months in 1999 and 2000 with high $PM_{2.5}$ concentration. Model performance is not consistent along this transect.

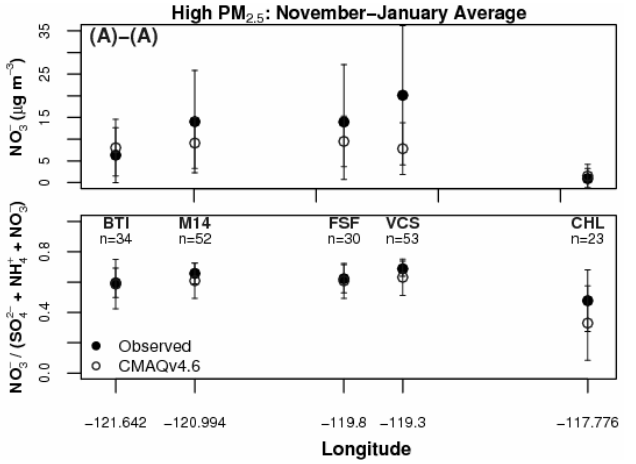


**Fig. 6.** Modeled and simulated average $PM_{2.5}$ nitrate and nitrate ratio along Fig. 1 transect

*Intensive observational periods*. Non-routine measurements (e.g., vertical profiles, precursors, etc.) are occasionally available from field campaigns. Such observations are usually short term and tailored to specific study objectives, and so they cannot form the basis of general long-term evaluations. However, non-routine measurements enable evaluation of model parameterizations at a level of detail not possible with routine network observations. Comparisons of predicted particle size distributions with impactor measurements from a field study in California are shown in Fig. 7. Predicted distribution peak heights are in reasonable agreement with observations, but modeled distributions are too wide and incorrectly indicate a significant portion of the accumulation mode at aerodynamic diameter >2.5 μm.

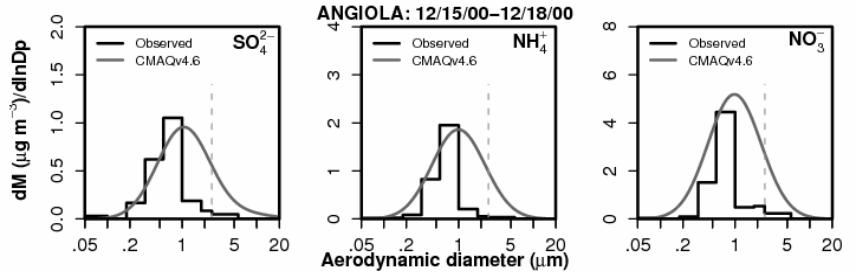


**Fig. 7.** Modeled and simulated particle size distribution at ANGI site

# 8.11 Evaluating CMAQ Particulate Matter Simulations in Central Valley California with Ground and Airborne LIDAR Observations

**Dazhong Yin[1], Bruce Jackson[1], and Ajith Kaduwela[1,2]**

[1]Planning and Technical Support Division, Air Resources Board, California Environmental Protection Agency, Sacramento, CA, USA

[2]Department of Land, Air, and Water Resources, University of California at Davis, CA, USA

**Abstract** Models-3/Community Multi-scale Air Quality (CMAQ) model particulate matter (PM) simulations for February 11-18 in the Central Valley California were evaluated against ground-based PM2.5 observations and the United Stated (US) Environmental Protection Agency (EPA) Advanced Monitoring Initiative (AMI) field campaign aerosol optical depth (AOD) data. The comparisons showed that the modeled AOD peaks corresponding to the observed peaks well, although the modeled AOD values were generally smaller than the observations. The modeled surface PM2.5 concentrations showed different temporal variation trend than that of the AOD sometimes. The modeled hourly dry PM2.5 (with which water components excluded) compared better with the Beta Attenuation Monitors observations than modeled PM2.5 including water contents.

**Keywords** Particulate matter, aerosol optical depth, air quality modeling, model evaluation

California's Central Valley is one of the largest PM2.5 and PM10 non-attainment areas in the United States (Chow et al., 2006). In this study, we used EPA's Models-3 Community Multi-scale Air Quality (CMAQ) 4.6 (Byun and Ching, 1999) to simulate particulate matter (PM) in Central California from February 10 to February 18, 2007. The results were compared with surface PM2.5 and aerosol optical depth (AOD) observations from a High Spectral Resolution LIDAR (HSRL) onboard a NASA B200 King Air aircraft. In the simulations, two chemical mechanisms, Carbon Bond (CB) 05 (Yarwood et al., 2005) and the Statewide Air Pollution Research Center (SAPRC) 99 (Carter, 2000) were used. We used aerosol module AERO4 (Binkowski and Roselle, 2003) in CMAQ. Emissions were for the year 2005. We assume there are no significant emission changes from 2005 to 2007. Meteorological conditions were simulated with MM5 3.7.4 (Grell et al., 1994). Two level nesting domains, one 36 km and the other 12 km, were employed in a one-way nesting model run. There were 30 vertical model layers from the ground

D.G. Steyn and S.T. Rao (eds.), *Air Pollution Modeling and Its Application XX*,
DOI 10.1007/978-90-481-3812-8, 

to 100 mb level. The lowest half sigma level was about 15 m above the ground. The 12 km domain MM5 output was used as the input to the CMAQ system.

Between February 11 and February 18, 2007, NASA King Air flew seven times in the Central Valley. The flight paths (Fig. 1) are along the city corridor and/or highways I-5 and US-99. The paths are very similar between flights. This ensures AOD measurements capture day to day variations. Surface PM2.5 and meteorological observations at sites located in cities such as Sacramento, Stockton, Fresno, and Bakersfield (Fig. 1) were available for our model evaluation.

We used an empirical approach to calculate modeled AOD from CMAQ modeled PM concentrations. To consider effects of hygroscopic particles, the humidity adjustment factors used in the Regional Haze Guideline Documents were applied to sulfate, nitrate, ammonium, and sea salt derived PM mass (Malm et al., 1994).

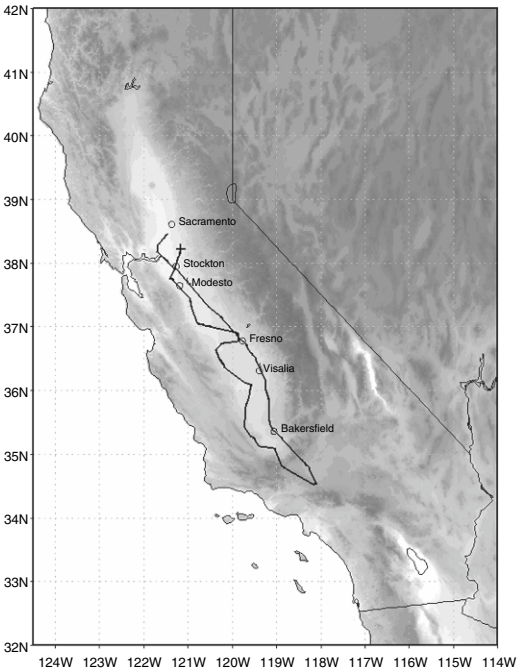


**Fig. 1.** Path of the NASA King Air flight on February 11, 2007 in the Central Valley. The paths of the other flights are similar

The observed AOD (Fig. 2) shows that the aerosol loadings in the atmosphere gradually built up from February 11 to February 16. The maximal observed AOD value was about 0.1 on February 11. It reached about 0.35 on February 15 and February 16. On the 17th and 18th, the values reduced to about 0.2. Two distinctive weather systems occurred in the region during this period. From the 11th to 13th, the Central Valley experienced a cold front passage and the control of the low pressure behind it. Starting from the 14th, a high pressure system gradually moved in and up to the 16th, a typical Great Basin High established. On the 17th

and 18th, although the Great Basin High was still there, another cold system started moving into Washington, Oregon and northern California. The observed large AOD values were mostly in the southern portion of the Central Valley, in the areas between Fresno and Bakersfield.

The modeled AOD values from CMAQ with CB05 and SAPRC99 show few differences between them. With the exception of February 11 and a couple of points on February 16, the modeled AOD values were smaller than the observed ones. The modeled peak values usually corresponded well to the observed peaks near Fresno and Bakersfield. Some of the peak values were very close to the observed ones. However, the modeled peaks were sharper than the measured peaks. This may be due to the unrealistically abrupt change of emissions from one model grid cell to another in the urban areas near Fresno and Bakersfield. The modeled meteorological fields on these days were fairly good.

The surface observed PM2.5 (Fig. 3) in the valley has a similar trend of the HSRL AOD until February 17, 2007. The concentrations gradually ramped up from the 11th to the 15th and 16th, especially at the sites in southern San Joaquin Valley. With the exception of Fresno, after the 16th, the observed PM2.5 at other sites in southern San Joaquin Valley stayed at the high level of the 16th. Sacramento,

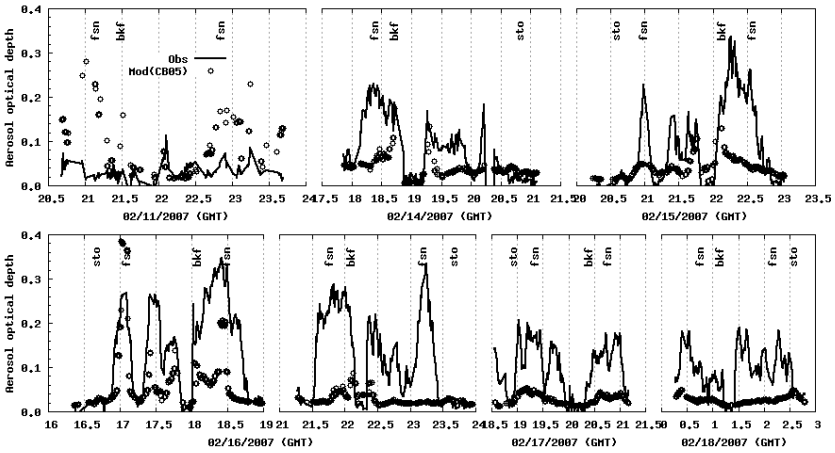


**Fig. 2.** Comparison of HSRL observed AOD and modeled AOD. Stockton (sto), Fresno (fsn), Bakersfield (bkf) are marked to show the values close to these sites

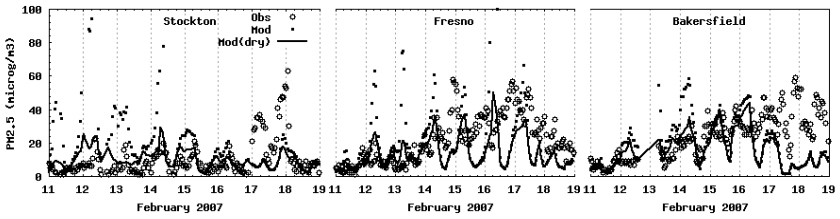


**Fig. 3.** Comparison of hourly BAM PM2.5 and CMAQ/CB05 modeled PM2.5 at three sites in the Central Valley. The modeled dry PM2.5 does not include water contents (Time in PST)

Stockton, and Modesto actually had higher PM2.5 concentrations. This indicates that surface PM conditions can have a different temporal trend than AOD.

Differences of model surface PM2.5 from CMAQ/CB05 and CMAQ/SAPRC99 were seen with some PM2.5 species. CMAQ/CB05 ammonia and nitrate were obviously larger than CMAQ/SAPRC99 values, but CMAQ/SAPRC99 SOA and sulfate were larger than CMAQ/CB05 values. The total surface CMAQ/CB05 PM2.5 was larger than CMAQ/SAPRC PM2.5, although the difference was not significant. Between modeled surface PM2.5 and modeled PM2.5 with no water contents (dry PM2.5), the model dry PM2.5 was much closer to the observations throughout the sites in the valley. The CMAQ simulated PM2.5 water component seems unrealistically high. PM2.5 observations were from Beta Attenuation Monitors (BAM). Typical operation protocols for BAM specify heating of the inlet line to a temperature about 30°C in order to reduce relative humidity to below 60% (Chung et al., 2001). However, in winter time, relative humidity in the valley can be 100% for a sustaining period of time. The BAM PM2.5 observations do not have all the water contents in PM2.5. Based on this study, the CMAQ modeled dry PM2.5 seems to be what should be used in a model evaluation against BAM hourly observations. The model dry PM2.5 concentrations were close to the observed PM2.5 except on the 17th and 18th. Analyses showed that biases of the modeled meteorological conditions contributed significantly to the discrepancies on these 2 days.

**Acknowledgments** The authors would like to thank Jay Al-Saadi, James Szykman at the NASA for providing the HSRL data. The airplane field study in the Central Valley was sponsored by the US EPA under the Advance Monitoring Initiative.

## References

Binkowski FS, Roselle SJ (2003) Models-3 Community Air Quality (CMAQ) model aerosol component, 1. Model description. Journal of Geophysical Research, 108(D6), 4183, doi:10.1029/2001JD001409.

Byun DW, Ching JKS (1999) Science algorithms of the EPA Models-3 Community Multiscale Air Quality (CMAQ) modeling system. Rep. EPA-600/R-99/030, US EPA, US Government Print. Off., Washington, D.C.

Carter WPL (2000) Implementation of the SAPRC-99 chemical mechanism into the models-3 framework. Report to the US EPA.

Chow JC, Chen ALW et al. (2006) PM2.5 chemical composition and spatiotemporal variability during the California Regional PM10/PM2.5 Air Quality Study(CRPAQS). Journal of Geophysical Research, 111, D10S04, doi:10.1029/2005JD006457.

Chung A., Chang DPY et al. (2001) Comparison of real-time instruments used to monitor airborne particulate matter. Journal of Air & Waster Management Association, 51, 109–120.

Grell G, Dudhia J et al. (1994) A description of the fifth-generation Penn State/NCAR mesoscale model (MM5). NCAR/TN-398+STR, 117p.

Malm WC, Sisler JF et al. (1994) Spatial and seasonal trends in particle concentration and optical extinction in the United States. Journal of Geophysical Research, 99, D1, 1347–1370.

Yarwood G, Rao, ST et al. (2005) Updates to the Carbon Bond chemical mechanism: CB05. Final Report to the US EPA, RT-0400675, December 8, 2005.

# 8.12 Post-2000 Air Quality Studies in California: ARCTAS-CA 2008 and 2010 CalNex

**Ajith Kaduwela[1,2], Chenxia Cai[1], Eileen McCauley[3], Ronald Cohen[4], Donald Blake[5], Hanwant Singh[6], and David Parrish[7]**

[1]Planning and Technical Support Division, Air Resources Board, California Environmental Protection Agency, Sacramento, CA, USA

[2]Department of Land Air and Water Resources, University of California, Davis, CA, USA

[3]Research Division, Air Resources Board, California Environmental Protection Agency, Sacramento, CA, USA

[4]Departments of Chemistry and Earth and Planetary Sciences, University of California, Berkeley, CA, USA

[5]Departments of Chemistry and Earth System Science, University of California, Irvine, CA, USA

[6]Atmospheric Science Branch, National Aeronautics and Space Administration, Ames Research Center, Moffett Field, CA, USA

[7]Chemical Sciences Division, National Oceanic and Atmospheric Administration, Boulder, CO, USA

## 1. Introduction

California has a rich history of air quality studies conducted over more than 3 decades. The most recent and comprehensive air quality studies to date in northern California are the Central California Ozone Study [1] (CCOS) and the California Regional PM10/PM2.5 Air Quality Study (CRPAQS) that took place in the year 2000. Results of these air quality studies were used in developing State Implementation Plans (SIPs) for the northern California region. Recent comprehensive air quality studies in the southern California region are the Southern California Ozone Study (SCOS) of 1997, Multiple Air Toxics Exposure Study II (MATES-II) during 1998–1999, and MATES-III [2] during 2004–2006. Results of these studies were used in developing SIPs for the southern California region.

Of the several small-scale air quality studies conducted in California since 2000, the 2008 California portion of the **A**rctic **R**esearch of the **C**omposition of the **T**roposphere from **A**ircraft and **S**atellites [3] (ARCTAS-CARB 2008) is particularly significant. Prior to the ARCTAS deployment in Canada, NASA conducted a series of flights in collaboration with scientists from the California Air Resources

D.G. Steyn and S.T. Rao (eds.), *Air Pollution Modeling and Its Application XX*,
DOI 10.1007/978-90-481-3812-8, © Springer Science + Business Media B.V. 2010

Board (CARB). These flights, already configured for the ARCTAS mission, examined California's atmosphere to better understand the chemical dynamics of smog and greenhouse gases over the state. During these flights, various organizations produced both meteorology and air quality forecasts to assist flight-path planning. We will discuss the accuracy of these forecasts with respect to the large-scale features observed.

Four science flights were conducted in California during the 18–24 June 2008 period. The two-dimensional flight paths for those flights are shown in Fig. 1. The flights on June 18 and 24 focused on characterizing photochemistry, emissions and boundary conditions (both inflow and outflow) in southern California. The flight on June 20 attempted to characterize the photochemistry and emissions in central California including the Bay Area. Inflow boundary conditions for photochemical modeling were the focus of the June 22nd flight.

A large number of chemical species (both inorganic and organic) were measured during these flights using various measurement methods. Most of these chemical species, especially the free radicals, are not measured at routine groundbased measurement sites. We will demonstrate how these additional measurements are useful for understanding the chemical regimes of various air parcels.

## 2. Model Application

The month of June 2008 was simulated using CMAQ v4.6 [4] for a modeling domain that includes all of California with 4 × 4 km horizontal grid cells and 30 vertical layers. Meteorological inputs were generated from simulations with the mesoscale meteorological model [5] (MM5) with analysis nudging but without observational nudging. Emissions were prepared internally at the California Air Resources Board. The base year for emissions was 2002, and emissions were projected to 2005 assuming no appreciable emission changes in California between 2005 and 2008. Gas-phase chemistry was simulated using the SAPRC99 mechanism [6], and aerosol processes were simulated with the AE4 module. We consider these simulation results to be preliminary. A more rigorous simulation will be conducted in the near future using emissions projected to 2008 from a 2005 base year, MM5 simulations with observational nudging, and a more detailed version of the SAPRC99 chemical mechanism that explicitly models several additional measured species.

We will present a comparison of the results of preliminary meteorology/airquality modeling with measurements aloft by aircrafts as well as those at the ground monitoring stations.

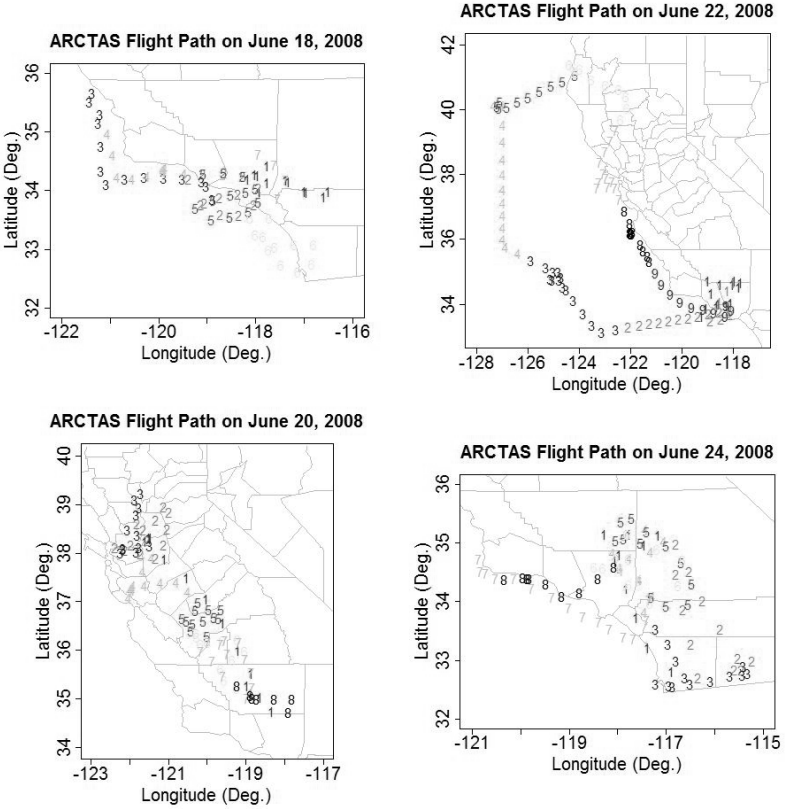


**Fig. 1.** Two-dimensional flight paths for the four ARCTAS flights in California. The numerical plot characters in each panel indicate the wall-clock hour during the flight in 5 min intervals

## 3. 2010 CalNex

ARCTAS-CARB 2008 was conducted as a pilot study to assist the design of an air quality study planned for California (Cal) in 2010 to investigate the nexus (Nex) between air quality and global climate change (2010 CalNex). The design of 2010 CalNex is guided by a set of science questions [7] that are oriented toward basic science, policy, or both. The current plan [7] calls for several instrumented aircrafts, an instrumented ship, a network of upper air meteorology and ozone measurements, and at least two "super sites." The number of individual chemical species measured by aircrafts, ship, and at the super sites is expected to be comparable to that measured during ARCTAS-CA 2008. One of the major goals of 2010 CalNex is improving meteorology and photochemical models. This goal will be achieved by measuring specific species/parameters that provide direct insights into atmospheric processes. We will present the overall design of 2010 CalNex within the context of lessons learned during ARCTAS-CARB 2008.

**Acknowledgments** Meteorology simulations were conducted at ARB by Dr. Dazhong Yin and Dr. Kemal Gürer. Authors thank the entire ARCTAS Science Team for their excellent contributions to the ARCTAS-CA 2008 (http://www.espo.nasa.gov/arctas/participants.php).

**Disclaimer** This paper has been reviewed by the staff of the California Air Resources Board and has been approved for publication. Approval does not signify that the contents necessarily reflect the views and policies of the California Air Resources Board, nor does mention of trade names or commercial products constitute endorsement or recommendation for use.

## References

More information on CCOS and CRAPQS (collectively known as Central California Air Quality Studies) can be found at www.arb.ca.gov/airways/

More information on the MATES series, conducted by the South Coast Air Quality Management District, is found at www.aqmd.gov/news1/2005/matesiiifactsheet.html

More information on ARCTAS, including the California portion, can be found at http://www-air.larc.nasa.gov/missions/arctas/arctas.html

More information on 2010 CalNex project can be found at http://www.arb.ca.gov/research/fieldstudy2010/fieldstudy2010.htm

Byun, D. and Schere, K.L., Review of the Governing Equations, Computational Algorithms, and Other Components of the Models-3 Community Multiscale Air Quality (CMAQ) Modeling System, *Appl. Mech. Rev.* 59, 51, 2006.

Carter, W.P.L., 2000. Implementation of the SAPRC-99 chemical mechanism into the models-3 framework. Report to the United States Environmental Protection Agency http://www.cert.ucr.edu/~carter/absts.htm#s99mod3

Grell, A.G., J. Dudhia, and D.R. Stauffer, 1994: A description of the fifth-generation Penn State/NCAR mesoscale model (MM5). NCAR Technical Note NCAR/TN 398+STR.

## 4. Questions and Answers

**Question:** Is your NOx simulation as bad as you explained?

**Answer:** The agreement between the simulation and measurements presented were typical of that reported previously for California and other areas. The simulated NOx concentrations were generally lower than those observed by the aircraft. This is expected as the simulation is not able to represent NOx plumes very realistically since all NOx emissions in a 4 × 4 km two grid cell would be diluted instantaneously into that grid cell. But, the locations of most NOx peaks were represented well in the simulation. That indicates that the emissions inventory has major NOx sources in the correct places. The simulation may not improve unless we include the plume-in-grid treatment for NOx sources, but California does not have major NOx sources that warrant the plume-in-grid treatment.

**Question:** Why were you not seeing high ozone concentrations due to wildfire plumes?

**Answer:** First, the simulations presented did not include wildfire emissions. Second, it appears that wildfires in California did not have high NOx concentrations at the time of the measurement. But, wildfires were strong emitters of volatile organic compounds (VOC). It is possible that the lack of NOx resulted in low concentrations of ozone. But, further analyses of measurements are needed to exclude other plausible explanations.

# Author Index